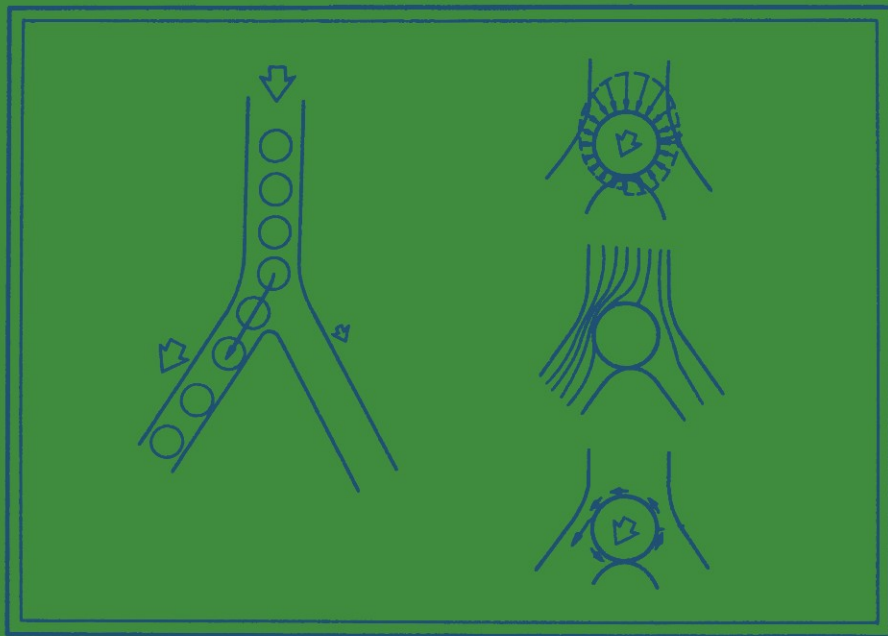


Y. C. Fung

Biomechanics

Mechanical Properties of Living Tissues



Springer Science+Business Media, LLC

Y. C. Fung

Biomechanics

**Mechanical Properties
of Living Tissues**



Springer Science+Business Media, LLC

Y. C. FUNG

Professor of Applied Mathematics
and Engineering Sciences/Bioengineering
University of California, San Diego
La Jolla, CA 92093
USA

Library of Congress Cataloging in Publication Data

Fung, Yuan-cheng, 1919–
Biomechanics.

Bibliography: p.

Includes index.

1. Tissues. 2. Biomechanics. 3. Rheology
(Biology) I. Title. [DNLM: 1. Biomechanics. QT34 F981b]
QP88.F87 **599.01'852** **80-16532**

With 244 illustrations.

All rights reserved.

**No part of this book may be translated or reproduced in any form without
written permission from Springer Science+Business Media, LLC.**

© 1981 by Springer Science+Business Media New York
Originally published by Springer-Verlag New York Inc. in 1981

9 8 7 6 5 4 3 2 1

ISBN 978-1-4757-1754-9 **ISBN 978-1-4757-1752-5 (eBook)**
DOI 10.1007/978-1-4757-1752-5

*Dedicated to
Chia-Shun Yih,*



*and
Luna, Conrad, and
Brenda Fung*



Preface

The motivation for writing a series of books on biomechanics is to bring this rapidly developing subject to students of bioengineering, physiology, and mechanics. In the last decade biomechanics has become a recognized discipline offered in virtually all universities. Yet there is no adequate textbook for instruction; neither is there a treatise with sufficiently broad coverage. A few books bearing the title of biomechanics are too elementary, others are too specialized. I have long felt a need for a set of books that will inform students of the physiological and medical applications of biomechanics, and at the same time develop their training in mechanics. We cannot assume that all students come to biomechanics already fully trained in fluid and solid mechanics; their knowledge in these subjects has to be developed as the course proceeds. The scheme adopted in the present series is as follows. First, some basic training in mechanics, to a level about equivalent to the first seven chapters of the author's *A First Course in Continuum Mechanics* (Prentice-Hall, Inc. 1977), is assumed. We then present some essential parts of biomechanics from the point of view of bioengineering, physiology, and medical applications. In the meantime, mechanics is developed through a sequence of problems and examples. The main text reads like physiology, while the exercises are planned like a mechanics textbook. The instructor may fill a dual role: teaching an essential branch of life science, and gradually developing the student's knowledge in mechanics.

The present volume is the first in a series. In this book the mechanical properties of biological materials are discussed. This will be followed by a forthcoming volume devoted to the mechanics of circulation and respiration.

Yet biomechanics at the level of current research cannot be bound by elementary mathematics. To develop the subject fully, advanced methods in continuum mechanics would have to be used. These more advanced topics,

perhaps accessible only to students with suitable training in fluid and solid mechanics, are presented in a third volume, *Advanced Biomechanics*.

To strike a balance between biological and physical topics in a single course is not easy. Biology contains a great deal of descriptive material, whereas mechanics aims at quantitative analysis. The need to unify these topics sometimes renders the text nonuniform in style, stressing a mathematical detail here and describing an anatomy there. This nonuniformity is more pronounced at the beginning, when the necessary background material has to be introduced.

A special word needs to be said about the exercises. Students of mechanics thrive on exercises. We must constantly try to formulate and solve problems. Only through such practice can we make biomechanics a living subject. I do not wish to present this book as a collection of solved problems. I wish to present it as a way of thinking about problems. I wish to illustrate the use of mechanics as a simple, quantitative tool. For this reason many problems for solution are proposed in the text; some are used as a vehicle to inform the readers of some published results, others are intended to lead the reader to new paths of investigation. I followed this philosophy even at the very beginning by presenting some problems and solutions in the Introductory Chapter 1. I think colleagues who use this as a textbook would appreciate this, because then they can assign some problems to the students after the first lecture.

With our limited objective, this book does not claim to be a compendium or handbook of current information on the selected topics, nor a review of literature. For those purposes a much larger volume will be needed. In this volume we develop only a few topics that seem related and important. A comprehensive bibliography is not provided; the list of references is limited to items quoted in the text. Though the author can be accused of quoting papers and people familiar to him, he apologizes for this personal limitation and hopes that he can be forgiven because it is only natural that an author should talk more about his own views than the views of others. I have tried, however, never to forget mentioning the existence of other points of view.

Biomechanics is a young subject. Our understanding of the subject is yet imperfect. Many needed pieces of information have not yet been obtained; many potentially important applications have not yet been made. There are many weaknesses in our present position. For example, the soft tissue mechanics developed in Chapter 7, based on the concept of quasilinear viscoelasticity and pseudo-elasticity, may someday be replaced by constitutive equations that are fully nonlinear but not too complex. The blood vessel mechanics developed in Chapter 8 is based on a two-dimensional average. Our discussion of the muscle mechanics in Chapter 9–11 points out the deficiency in our present knowledge on this subject. An alternative to Hill's model is presented. I was hoping that by the time this book went to print the experimental work to validate the alternative model would have been completed; but this was not the case; and the fading memory approach

remained just an idea. In Chapter 12 we discussed the constitutive equations for growth or resorption of tissues under stress. This is a subject of universal importance in the study of every living tissue; but only on bone do we have some quantitative information on this topic. It is safe to predict that the study of the constitutive equations for growth or resorption will be a great theme for biomechanics in the future. These equations have immediate applications to the art of surgery, orthopedics, orthodontics, orthoptics, body building, and athletic training. Basically they distinguish biomechanics from all other branches of mechanics. It is for the purpose of conveying this sense of growth and change that we devoted long passages on blood circulation in the bone in Chapter 12. All this means that I expect rapid progress in our subject in the future.

I wish to express my thanks to many authors and publishers who permitted me to quote their publications and reproduce their figures and data in this book. I wish to mention especially Professors Sidney Sabin, Evan Evans, Harry Goldsmith, Jen-shih Lee, Wally Frasher, Richard Skalak, Andrew Somlyo, Salvatore Sutera, Andrus Viidik, Joel Price, Savio Woo, and Benjamin Zweifach who supplied original photographs for reproduction.

This book grew out of my lecture notes used at the University of California, San Diego over the past ten years. To the students of these classes I am grateful for discussions. Much of the results presented here are the work of my colleagues, friends, and former students. Professors Sidney Sabin, Benjamin Zweifach, Marcos Intaglietta, Arnost and Kitty Fronek, Wally Frasher, Paul Johnson, and Savio Woo provided the initial and continued collaboration with me on this subject. Drs. Jen-shi Lee, Pin Tong, Frank Yin, John Pinto, Evan Evans, Yoram Lanir, Hyland Chen, Michael Yen, Donald Vawter, Geert Schmid-Schoenbein, Peter Chen, Larry Malcom, Joel Price, Nadine Sidrick, Paul Sabin, Winston Tsang, and Paul Zupkas contributed much of the material presented here. The contribution of Paul Patitucci to the numerical handling of data must be especially acknowledged. Dr. Yuji Matsuzaki contributed much to my understanding of flow separation and stability. Professor Zhuong Feng-Yuan read the proofs and made many useful suggestions. Eugene Mead kept the laboratory going. Rose Cataldi and Virginia Stephens typed the manuscript. To all of them I am thankful.

Finally, I wish to thank the editorial and production staffs of Springer-Verlag for their care and cooperation in producing this book.

La Jolla, California

Yuan-Cheng Fung

Contents

Chapter 1

Introduction: A Sketch of the History and Scope of the Field	1
1.1 What Is Biomechanics?	1
1.2 Historical Background	1
1.3 What's in a Name?	6
1.4 Mechanics in Physiology	7
1.5 What Contributions Has Biomechanics Made to Health Science?	10
1.6 Our Method of Approach	12
References	21

Chapter 2

The Meaning of the Constitutive Equation	22
2.1 Introduction	22
2.2 Stress	22
2.3 Strain	26
2.4 Strain Rate	31
2.5 Constitutive Equations	32
2.6 The Nonviscous Fluid	33
2.7 The Newtonian Viscous Fluid	33
2.8 The Hookean Elastic Solid	35
2.9 The Effect of Temperature	37
2.10 Materials with More Complex Mechanical Behavior	38
2.11 Viscoelasticity	41
2.12 Response of a Viscoelastic Body to Harmonic Excitation	47
2.13 Use of Viscoelastic Models	50
2.14 Methods of Testing	56
References	61

Chapter 3	
The Flow Properties of Blood	62
3.1 Blood Rheology: An Outline	62
3.2 The Constitutive Equation	68
3.3 Laminar Flow of Blood in a Tube	72
3.4 Speculation on Why Blood Viscosity Is the Way It Is	80
3.5 Fluid-Mechanical Interaction of Red Blood Cells with a Solid Wall	89
3.6 Coagulation	91
3.7 Medical Applications of Blood Rheology	93
References	98
Chapter 4	
Red Blood Cells and Their Deformability	101
4.1 Introduction	101
4.2 Human Red Cell Dimensions and Shape	104
4.3 The Extreme-Value Distribution	108
4.4 The Deformability of Red Blood Cells (RBC)	112
4.5 Theoretical Considerations of the Elasticity of Red Cells	114
4.6 Cell Membrane Experiments	122
4.7 Elasticity of the Red Cell Membrane	132
4.8 The Red Cell Membrane Model	135
References	136
Chapter 5	
The Rheology of Blood in Microvessels	139
5.1 Introduction	139
5.2 Apparent Viscosity and Relative Viscosity	139
5.3 Effect of Size of the Blood Vessel on the Apparent Viscosity of Blood: The Fahraeus-Lindqvist Effect	146
5.4 The Distribution of Suspended Particles in Fairly Narrow Rigid Tubes	149
5.5 The Motion of Red Cells in Tightly Fitting Tubes	150
5.6 Inversion of the Fahraeus-Lindqvist Effect in Very Narrow Tubes	156
5.7 Hematocrit in Very Narrow Tubes	159
5.8 Theoretical Investigations	167
References	172
Chapter 6	
Bio-viscoelastic Fluids	174
6.1 Introduction	174
6.2 Methods of Testing and Data Presentation	177
6.3 Protoplasm	181
6.4 Mucus from the Respiratory Tract	182
6.5 Saliva	186

6.6 Cervical Mucus and Semen	187
6.7 Synovial Fluid	188
References	194

Chapter 7 Bio-viscoelastic Solids

7.1 Introduction	196
7.2 Some Elastic Materials	197
7.3 Collagen	203
7.4 Thermodynamics of Elastic Deformation	214
7.5 Behavior of Tissues Under Uniaxial Loading	219
7.6 Quasi-linear Viscoelasticity of Soft Tissues	226
7.7 Incremental Laws. The Concept of Pseudo-elasticity	238
7.8 Biaxial Loading Experiments on Soft Tissues	242
7.9 Description of Three-Dimensional Stress and Strain States	245
7.10 The Constitutive Equation of Skin	248
7.11 Generalized Viscoelastic Relations	253
7.12 The Complementary Energy Function: Inversion of the Stress-Strain Relationship	253
References	257

Chapter 8 Mechanical Properties of Blood Vessels

8.1 Introduction	261
8.2 Correlation of the Mechanical Properties of a Vessel with the Content and Structure of Its Material Composition	262
8.3 The Behavior of Arteries Under Uniaxial Loading	267
8.4 Stresses in Arteries Under Biaxial Loading	276
8.5 Mathematical Representation of the Pseudoelastic Stress-Strain Relationship	277
8.6 Dynamic Testing: Wave Propagation	282
8.7 Arterioles	284
8.8 Capillary Blood Vessels	286
8.9 Veins	290
8.10 Long Term Response to Stress	295
References	298

Chapter 9 Skeletal Muscle

9.1 Introduction	302
9.2 The Functional Arrangement of Muscles	303
9.3 The Structure of Skeletal Muscle	305
9.4 The Sliding Element Theory of Muscle Action	308

9.5 Single Twitch and Wave Summation	308
9.6 Contraction of Skeletal Muscle Bundles	309
9.7 Hill's Equation for Tetanized Muscle	310
9.8 Hill's Three-Element Model	316
9.9 Other Approaches	324
References	327
Chapter 10	
Heart Muscle	329
10.1 Introduction: The Difference Between Myocardial and Skeletal Muscle Cells	329
10.2 Properties of Unstimulated Heart Muscle	333
10.3 The Behavior of Active Myocardium	342
10.4 Active Muscle at Shorter Length with Negligible Resting Tension	343
10.5 Stimulated Papillary Muscle at Lengths at Which Resting Tension Is Significant	350
10.6 Heart Muscle Mechanics and Whole Heart Behavior	351
References	353
Chapter 11	
Smooth Muscles	355
11.1 Types of Smooth Muscles	355
11.2 The Contractile Machinery	358
11.3 Rhythmic Contraction of Smooth Muscle	360
11.4 The Property of a Resting Smooth Muscle: Ureter	365
11.5 Resting Smooth Muscle: Taenia Coli	371
References	381
Chapter 12	
Bone and Cartilage	383
12.1 Mechanical Properties of Bone	383
12.2 Bone as a Living Organ	389
12.3 Functional Adaptation of Bone	392
12.4 Blood Circulation in Bone	397
12.5 Cartilage	400
12.6 Viscoelastic Properties of Articular Cartilage	401
12.7 The Lubrication Quality of Articular Cartilage Surfaces	406
References	413
Author Index	
	417
Subject Index	
	425

CHAPTER 1

Introduction: A Sketch of the History and Scope of the Field

1.1 What Is Biomechanics?

Biomechanics is mechanics applied to biology. The word “mechanics” was used by Galileo as a subtitle to his book *Two New Sciences* (1638) to describe force, motion, and strength of materials. Through the years its meaning has been extended to cover the study of the motions of all kinds of particles and continua, including quanta, atoms, molecules, gases, liquids, solids, structures, stars, and galaxies. In a generalized sense it is applied to the analysis of any dynamic system. Thus thermodynamics, heat and mass transfer, cybernetics, computing methods, etc., are considered proper provinces of mechanics. The biological world is part of the physical world around us and naturally is an object of inquiry in mechanics.

Biomechanics seeks to understand the mechanics of living systems. It is an ancient subject and covers a very wide territory. In this book we concentrate on physiological and medical applications, which constitute the majority of recent work in this field. The motivation for research in this area comes from the realization that physiology can no more be understood without biomechanics than an airplane can without aerodynamics. For an airplane, mechanics enables us to design its structure and predict its performance. For an organ, biomechanics helps us to understand its normal function, predict changes due to alterations, and propose methods of artificial intervention. Thus diagnosis, surgery, and prosthesis are closely associated with biomechanics.

1.2 Historical Background

To explain what our field is like, it is useful to consider its historical background. Since science and scientists have always been concerned with the world of living things, it is natural that biomechanics has roots which reach

back to the dawn of civilization. Of the ancient philosophers, Aristotle (384–322 B.C.) was an eloquent speaker for the connection between “physics”—which for him was a general description of the universe—and the study of living things. His writings cover the whole area of knowledge, and as a whole were deeply influenced by his biological studies. We quote the following translation by Singer in *A Short History of Scientific Ideas to 1900* (1959, p. 40) from Aristotle’s great work *On the Parts of Animals*:

Of things constituted by nature, some are ungenerated, imperishable, eternal; others subject to generation and decay. The former are excellent beyond compare and divine, but less accessible to knowledge. The evidence that might throw light on them, and on the problems which we long to solve respecting them, is furnished but scantily by our senses. On the other hand, we know much of the perishable plants and animals among which we dwell. We may collect information concerning all their various kinds, if we but take the pains.

Yet each department has its own peculiar charm. The excellence of celestial things causes our scanty conceptions of them to yield more pleasure than all our knowledge of the world in which we live; just as a mere glimpse of those we love is more to us than the grandest vista. On the other side we may set the certitude and completeness of our knowledge of earthly things. Their nearness and their affinity to us may well balance the loftier interest of things of heaven, that are the objects of high philosophy.

But of a truth every realm of nature is marvellous. It is told that strangers, visiting Heraclitus and finding him by the kitchen fire, hesitated to enter. “Come in, come in,” he cried, “the gods are here too.” So should we venture on the study of every kind of creature without horror, for each and all will reveal something that is natural and therefore beautiful. [Somewhat paraphrased.]

We may not agree with him as to which subject is easier to study, but we must agree that the physical world and the biological world are equally beautiful. However, the modern development of mechanics received its impetus mainly from engineering, and to most engineers today biomechanics sounds like a new subject. But if we look at the following slate of names of those who contributed significantly to biomechanics, we have to admit that this field has been alive all along.

- Galileo Galilei (1564–1642)
- William Harvey (1578–1658)
- René Descartes (1596–1650)
- Giovanni Alfonso Borelli (1608–1679)
- Robert Boyle (1627–1691)
- Robert Hooke (1635–1703)
- Leonhard Euler (1707–1783)
- Thomas Young (1773–1829)
- Jean Poiseuille (1799–1869)
- Herrmann von Helmholtz (1821–1894)

Adolf Fick (1829–1901)

Diederik Johannes Korteweg (1848–1941)

Horace Lamb (1849–1934)

Otto Frank (1865–1944)

Balthasar van der Pol (1889–1959)

A brief account of the contributions of these people may be of interest. William Harvey, of course, is credited with the discovery of blood circulation. He made this discovery in 1615. Having no microscope, he never saw the capillary blood vessels. This should make us appreciate his conviction in logical reasoning even more deeply today because, without the capability of seeing the passage from the arteries to the veins, the discovery of circulation must be regarded as “theoretical.” The actual discovery of capillaries was made by Marcello Malpighi (1628–1694) in 1661, 45 years after Harvey made the capillaries a logical necessity.

A contemporary of William Harvey was Galileo. You remember that Galileo was a student of medicine before he became famous as a physicist. He discovered the constancy of the period of a pendulum, and used the pendulum to measure the pulse rate of people, expressing the results quantitatively in terms of the length of a pendulum synchronous with the beat. He invented the thermoscope, and was also the first one to design a microscope in the modern sense in 1609, although rudimentary microscopes were first made by J. Janssen and his son Zacharias in 1590.

Young Galileo's fame was so great and his lectures at Padua so popular that his influence on biomechanics went far beyond his personal contributions mentioned above. According to Singer (*History*, p. 237), William Harvey should be regarded as a disciple of Galileo, though he himself might not be aware of it. Harvey studied at Padua (1598–1601) while Galileo was active there. By 1615 he had attained to a conception of the circulation of the blood. He published his demonstration in 1628. The essential part of his demonstration is the result not of mere observation but of the application of Galileo's principle of measurement. He showed first that the blood can only leave the ventricle of the heart in one direction. Then he measured the capacity of the heart, and found it to be two ounces.* The heart beats 72 times a minute, so that in one hour it throws into the system $2 \times 72 \times 60$ ounces = 8640 ounces = 540 pounds! Where can all this blood come from? Where can it all go? He concludes that the existence of circulation is a necessary condition for the function of the heart.

Another colleague of Galileo, Santorio Santorio (1561–1636), a professor of medicine at Padua, used Galileo's method of measurement and philosophy to compare the weight of the human body at different times and in different circumstances. He found that the body loses weight by mere exposure, a process which he assigned to “insensible perspiration.” His experiments laid

* We know today that the resting cardiac output is very close to one total blood volume per minute in nearly all mammals.

the foundation of the modern study of “metabolism.” (See Singer, *History*, p. 236.)

The physical discoveries of Galileo and the demonstrations of Santorio and of Harvey gave a great impetus to the attempt to explain vital processes in terms of mechanics. Galileo showed that mathematics was the essential key to science, without which nature could not be properly understood. This outlook inspired Descartes, a great mathematician, to work on physiology. In a work published posthumously (1662 and 1664), he proposed a physiological theory upon mechanical grounds. According to Singer, this work is the first important modern book devoted to the subject of physiology. Descartes did not have any extensive practical knowledge of physiology. On theoretical grounds he set forth a very complicated model of animal structure, including the function of nerves. Subsequent investigations failed to confirm many of his findings. These errors of fact caused the loss of confidence in Descartes’ approach—a lesson that should be kept in mind by all theoreticians.

Other attempts a little less ambitious than Descartes’s were more successful. Giovanni Alfonso Borelli (1608–1679) was an eminent Italian mathematician and astronomer, and a friend of Galileo and Malpighi. His *On Motion of Animals (De Motu Animalium)* (1680) is the classic of what is variously called the “iatrophysical” or “iatromathematical” school *ιατρός*, Gr., physician). He was successful in clarifying muscular movement and body dynamics. He treated the flight of birds and the swimming of fish, as well as the movements of the heart and of the intestines.

Robert Boyle studied the lung and discussed the function of air in water with respect to fish respiration. Robert Hooke gave us Hooke’s law in mechanics and the word “cell” in biology to designate the elementary entities of life. His famous book *Micrographia* (1664) has been reprinted by Dover Publications, New York (1960). Leonhard Euler wrote a definitive paper in 1775 on the propagation of waves in arteries. Thomas Young, who gave us the Young’s modulus of elasticity, was a physician in London. He worked on the wave theory of light while he was concerned with astigmatism in lenses and in color vision. Poiseuille invented the mercury manometer to measure the blood pressure in the aorta of a dog while he was a medical student, and discovered Poiseuille’s law of viscous flow upon graduation.

To von Helmholtz (Fig. 1.2:1) might go the title “Father of Bioengineering.” He was professor of physiology and pathology at Königsberg, professor of anatomy and physiology at Bonn, professor of physiology at Heidelberg, and finally professor of physics in Berlin (1871). He wrote his paper on the “law of conservation of energy” in barracks while he was in military service fresh out of medical school. His contributions ranged over optics, acoustics, thermodynamics, electrodynamics, physiology, and medicine. He discovered the focusing mechanism of the eye and, following Young, formulated the trichromatic theory of color vision. He invented the phakoscope to study the changes in the lens, the ophthalmoscope to view the



Figure 1.2:1 Portrait of Hermann von Helmholtz. From the frontispiece to *Wissenschaftliche Abhandlungen von Helmholtz*. Leipzig, Johann Ambrosius Barth, 1895. Photo by Giacomo Brogi in 1891.

retina, the ophthalmometer for measurement of eye dimensions, and the stereoscope with interpupillary distance adjustments for stereo vision. He studied the mechanism of hearing and invented the Helmholtz resonator. His theory of the permanence of vorticity lies at the very foundation of modern fluid mechanics. His book *Sensations of Tone* is popular even today. He was the first to determine the velocity of the nerve pulse, giving the rate 30 m/s, and to show that the heat released by muscular contraction is an important source of animal heat.

The other names on the list are equally familiar to engineers. The physiologist Fick was the author of Fick's law of mass transfer. The hydrodynamicists Korteweg (1878) and Lamb (1898) wrote beautiful papers on wave propagation in blood vessels. Frank worked out a hydrodynamic theory of circulation. Van der Pol (1929) wrote about the modeling of the heart with nonlinear oscillators, and was able to simulate the heart with four Van der Pol oscillators to produce a realistic looking electrocardiograph.

This list perhaps suffices to show that there were, and of course are, people who would be equally happy to work on living subjects as well as inanimate objects. Indeed, what a scientist picks up and works on may depend a great deal on chance, and the biological world is so rich a field

that one should not permit the opportunities there to slip by unnoticed. The following example about Thomas Young may be of interest to those who like to ponder about the threads of development in scientific thought. When he tried to understand the human voice, Thomas Young turned to the mechanics of vibrations. Let us quote Young himself (from his “Reply to the *Edinburgh Reviewers*” (1804), see *Works*, ed. Peacock, Vol. i, pp 192–215):

When I took a degree in physic at Göttingen, it was necessary, besides publishing a medical dissertation, to deliver a lecture upon some subject connected with medical studies, and I choose for this Formation of the Human Voice, . . . When I began the outline of an essay on the human voice, I found myself at a loss for a perfect conception of what sound was, and during the three years that I passed at Emmanuel College, Cambridge, I collected all the information relating to it that I could procure from books, and I made a variety of original experiments on sounds of all kinds, and on the motions of fluids in general. In the course of these inquiries I learned to my surprise how much further our neighbours on the Continent were advanced in the investigation of the motions of sounding bodies and of elastic fluids than any of our countrymen. And in making some experiments on the production of sounds, I was so forcibly impressed with the resemblance of the phenomena that I saw to those of the colours of thin plates, with which I was already acquainted, that I began to suspect the existence of a closer analogy between them than I could before have easily believed.”

This led to his ‘Principle of Interferences’ (1801) which earned him lasting fame in the theory of light. How refreshing are these remarks! How often do we encounter the situation “at a loss for a perfect conception of what . . . was.” How often do we leave the vague notions untouched!

1.3 What’s in a Name?

Biomechanics is mechanics applied to biology. We have explained in Sec. 1.1 that the word “mechanics” has been identified with the analysis of any dynamic system. To people who call themselves workers in applied mechanics, the field includes the following topics:

Stress and strain distribution in materials

Constitutive equations which describe the mechanical properties of materials

Strength of materials, yielding, creep, plastic flow, crack propagation, fracture, fatigue failure of materials; stress corrosion

Dislocation theory, theory of metals, ceramics

Composite materials

Flow of fluids: gas, water, blood, and other tissue fluids

Heat transfer, temperature distribution, thermal stresses

Mass transfer, diffusion, transport through membranes

Motion of charged particles, plasma, ions in solution
Mechanisms, structures
Stability of mechanical systems
Control of mechanical systems
Dynamics, vibrations, wave propagation
Shock, waves, and waves of finite amplitude

It is difficult to find any organ in any animal that does not involve some of these problems.

On the other hand, how did the word biology come about? The term *biology* was first used in 1801 by Lamarck in his *Hydrogéologie*, (see Merz, *History*, p. 217). Huxley, in his *Lecture on the Study of Biology*, [South Kensington (Dec. 1876), reprinted in *American Addresses*, 1886, p. 129] gave the following account of the early history of the word:

About the same time it occurred to Gottfried Reinhold Treviranus (1776–1837) of Bremen, that all those sciences which deal with living matter are essentially and fundamentally one, and ought to be treated as a whole; and in the year 1802 he published the first volume of what he also called *Biologie*. Treviranus's great merit lies in this, that he worked out his idea, and wrote the very remarkable book to which I refer. It consists of six volumes, and occupied its author for twenty years—from 1802 to 1822. That is the origin of the term “biology”; and that is how it has come about that all clear thinkers and lovers of consistent nomenclature have substituted for the old confusing name of “natural history,” which has conveyed so many meanings, the term “biology,” which denotes the whole of the sciences which deal with living things, whether they be animals or whether they be plants.

In the present volume, we address our attention particularly to continuum mechanics in physiology. By physiology we mean the science dealing with the normal functions of living things or their organs. Originally the term had a much more broad meaning. William Gilbert (1546–1603), personal physician to Queen Elizabeth, wrote a book (1600) called *On the Magnet and on Magnetic Bodies and Concerning the Great Magnet, the Earth, a New Physiology*, which was the first major original contribution to science published in England (Singer, *History*, p. 188). It earned the admiration of Francis Bacon and of Galileo. Note the last word in the title, “physiology.” The word *physiologia* was, in fact, originally applied to the material working of the world as a whole, and not to the individual organism.

1.4 Mechanics in Physiology

In Sec. 1.2 we listed a slate of giants in applied mechanics. We can equally well list a slate of giants in physiology who clarified biomechanics. For example, following William Harvey (1578–1658), we have

Marcello Malpighi (1628–1694)
Stephen Hales (1677–1761)

Otto Frank (1865–1944)

Ernest Henry Starling (1866–1926)

August Krogh (1874–1949)

Archibald Vivian Hill (1886–1977)

To outline their contributions, we should remember that there are great ideas which, when perfectly understood, seem perfectly natural. The idea of blood circulation is one of them. Today we no longer remember what William Harvey had to fight against in 1615 when he conceived the principle of blood circulation. There was the great Galen, whose medical teachings had been accepted and unquestioned for 15 centuries. There was the fact that no connection between arteries and veins had ever been seen. There was the fact that the arterial and venous bloods do look different. To fight against these and other difficulties, Harvey took the quantitative method promulgated by Galileo. He concluded that the existence of circulation is a necessary condition for the function of the heart. All other difficulties were temporarily put aside. Thus Harvey won, illustrating at once the principle that a crucial argument can be settled by a detailed quantitative analysis.

There was much more to be discovered after Harvey. For example, it was not clear how blood completes the circulation. Of this, James Young (1930 p. 1) wrote:

It has often been observed, by men ill-versed in the history of scientific developments, that great new ideas, when developed, might easily have been inferred from others accepted long before. For example, when Erasistratos has told us that the heart's valves ensure a one-way course of the blood, and that all the blood of the body can be driven out by the opening of one artery by aid of the *horror vacui*, and Celsus has informed us that the heart is a muscular viscus, one might have inferred the circulation of the blood without waiting for Harvey. Even so one might imagine that Harvey, to complete his system, might have inferred the presence of definite vessels of communication between the arteries and the veins instead of an indefinite soakage through the "porosities of the tissues." But he did not do so, nor did any one else for thirty years of keen discussion. The discovery of the capillaries was reserved for the work of Malpighi, who was trying to clear his views about the structure of the lungs.

Marcello Malpighi (1628–1694) communicated his discovery in two letters addressed to Alfonso Borelli in 1661. Let us quote him from his second letter, [see Young's translation (1930)]:

In the frog lung owing to the simplicity of the structure, and the almost complete transparency of the vessels which admits the eye into the interior, things are more clearly shown so that they will bring the light to other more obscure matters

Observation by means of a microscope reveals more wonderful things than those viewed in regard to mere structure and connection: for while

the heart is still beating the contrary (i.e., in opposite directions in the different vessels) movement of the blood is observed in the vessels—though with difficulty—so that the circulation of the blood is clearly exposed

Thus by this impulse the blood is driven in very small arteries like a flood into the several cells, one or other branch clearly passing through or ending there. Thus the blood, much divided, puts off its red colour, and, carried round in a winding way, is poured out on all sides till at length it may reach the walls, the angles, and the absorbing branches of the veins

What better introduction to pulmonary circulation is there! With the anatomy known, biomechanical analysis can begin.

Of the other people in the list, Stephen Hales (Fig. 1.4:1) is the man who measured the arterial blood pressure in the horse, and correlated it to hemorrhage. He made wax casts of the ventricles at the normal distending pressure in diastole and then measured the volume of the cast to obtain an estimate of the cardiac output. With his measurements he was able to estimate the forces in ventricular muscle. He measured the distensibility of the aorta and used it to explain how the intermittent pumping of the heart can be converted to a smooth flow in the blood vessels. The explanation was that the distension of the aorta functions like the air chamber in a fire engine, which converts intermittent pumping into a steady jet. (This word was rendered as *Windkessel* in the first German translation of his book; hence the famous theory by that name). He introduced the concept of



Figure 1.4:1 Stephen Hales.

peripheral resistance in blood flow, and showed that the main site of this resistance was in the minute blood vessels in the tissue. He even went further to show that hot water and brandy have vasodilatation effects.

Otto Frank worked out a hydrodynamic theory of circulation. Starling proposed the law for mass transfer across biological membrane and clarified the concept of water balance in the body. Krogh won his Nobel prize on the mechanics of microcirculation. Hill won his Nobel prize on the mechanics of the muscle. Their contributions form the foundation on which biomechanics rests.

1.5 What Contributions Has Biomechanics Made to Health Science?

Most biomechanics work aims at increasing basic knowledge about living systems and any artificial interventions thereof. Any serious projects in bioengineering, except those which are well understood, need advanced basic understanding. For example, prosthetic heart valves are now commonplace; but a need exists for improving their service life, minimizing blood trauma, eliminating undesirable blood–artificial-material–interaction, and simplifying anticoagulation managements. To achieve these improvements in a second generation of valves, one must understand the flow of blood in the heart, through the valves, and in the aorta. To study this flow one requires all the modern resources. It requires the same kind of attention engineers have given to the development of airplanes and rockets. Indeed it has been the aeronautical engineers' experience that significant advances in design are virtually always brought about by fundamental advances in fluid and solid mechanics, and that the most effective training one can give to a student is to teach him/her the fundamentals.

Can we name some points of concentration of current biomechanics? Some topics can certainly be listed.

A. Clinical Problems in the Cardiovascular System

1. Prosthetic heart valve.
2. Heart assist devices, such as the left ventricle assist pump, the aortic balloon pump, body acceleration synchronized with heart beat, peripheral cuffs, and diastolic counterpulsation.
3. Extracorporeal circulation. Heart-lung machine. Hemodialysis machine.
4. Heart replacement.
5. Postoperative trauma, pulmonary edema, and atelectasis.
6. Arterial pulse wave analysis.
7. Ultrasound applications. Phonoangiography. Turbulent noise analysis. Pseudo-sound generation at arteriosclerotic constrictions in arteries.

B. Quantitative Physiology

1. Systems analysis of physiology.
2. Rheology of biological tissues, such as blood, muscles, bones, connective tissues, and artificial implantable materials.
3. Analysis of fluid transfer across biological membranes and blood vessels.
4. Diffusion analysis such as pulmonary function, and indicator dilution method.
5. Interfaces. Surfactants in the lung. Thrombogenic tendency of blood on artificial implantable materials. Recent work shows that platelet action and thrombosis on interfaces are shear stress dependent, thus projecting mechanics to the foreground of this important problem.
6. Microcirculation. Biomechanics has contributed to every aspect of microcirculation research. Perhaps it is a historical accident, but physiologists and mechanics researchers have cooperated throughout the development of this branch of science.

C. Additional Applications

Surgery. Biomechanics of injury and the healing of surgical wounds are topics of great importance. New surgical procedures such as arterio-venous reversal and attachment of implantable mechanical devices are studied.

Implantable Artificial Materials. Materials for prosthesis require a detailed study of their mechanical properties and biocompatibility.

Orthopedics, Orthosis, Orthodontics. Mechanics of bone and cartilage. Reaction of bone to stress resulting either in growth or reabsorption. Joint lubrication. Joint replacement. Orthopedic implants.

Artificial Limb. Design of artificial limb is a classical objective of biomechanics.

Artificial Internal Organs. Renal replacement. Artificial kidney. Artificial heart. Other organs. Here an infinitely large vista is open in front of us.

Wheelchairs and Beds. Chairs to enable disabled patients to function as normally as possible. Use of back muscle, eye movement, or voice to steer and control such chairs. Design of beds to minimize trauma of bed-bound patients.

Occupational Safety and Health. Examples are: mechanics of pulmonary function testing, detection of black lung disease, mechanics of exercises and athletics.

Highway Safety. Head injury research. Seat belt research. Impact analysis. Safety of internal organs. Design of cars from the point of view of protecting the passengers.

Flight Safety. Vibration and impact of human bodies. Human tolerance to acceleration. Man's reaction to environment such as zero gravity, high heat, low heat, or low oxygen atmosphere.

Flying and Swimming in Nature. Flagellar motion. Microbial locomotion. Swimming. Flight of insects and birds.

Design of Socially Acceptable Monitoring Instruments. Instruments to meter and record a variety of parameters such as blood pressure, heart rate, respiration rate, electrocardiograms, and electromyograms, to be carried or worn by patients in a socially acceptable way over a long period of time.

Unexciting Research into Necessary Equipment [H. S. Wolff (1973) calls this Project URINE]. This needs no explanation, but it does need promotion. In this field talented persons can make tremendous contributions to society.

Every one of these topics can make a significant contribution to the welfare of human beings and provide extremely rewarding careers for bioengineers.

1.6 Our Method of Approach

In the tradition of physics and engineering, our approach to the study of problems in biomechanics consists of the following steps:

1. Study the morphology of the organism, anatomy of the organ, histology of the tissue, and the structure and ultrastructure of the materials in order to know the geometric configuration of the object we are dealing with.
2. Determine the mechanical properties of the materials or tissues that are involved in a problem. In biomechanics this step is often very difficult, either because we cannot isolate the tissue for testing, or because the size of available tissue specimens is too small, or because it is difficult to keep the tissue in the normal living condition. Furthermore, biological tissues are often subjected to large deformations, and the stress-strain relationships are usually nonlinear and history dependent. The nonlinearity of the constitutive equation makes its determination a challenging task. Usually, however, one can determine the mathematical form of the constitutive equation of the material quite readily, with certain numerical parameters left to be determined by physiological experiments named in steps 6 and 7 below.
3. On the basis of fundamental laws of physics (conservation of mass, conservation of momentum, conservation of energy, Maxwell's equations, etc.) and the constitutive equations of the materials, derive the governing differential or integral equations.
4. Understand the environment in which an organ works in order to obtain meaningful boundary conditions.

5. Solve the boundary-value problems (differential equations with appropriate boundary conditions) analytically or numerically.
6. Perform physiological experiments that will test the solutions of the boundary-value problems named above. If necessary, reformulate and resolve the mathematical problem to make sure that the theory and experiment do correspond to each other, i.e., that they are testing the same hypotheses.
7. Compare the experimental results with the corresponding theoretical ones. By means of this comparison, determine whether the hypotheses made in the theory are justified, and, if they are, find the numerical values of the undetermined coefficients in the constitutive equations.
8. Explore practical applications of the theory and experiments.

It is clear that the interaction between theory and experiment must be iterative. In successive investigations one hopes that the process converges, and an understanding of the problem is achieved both qualitatively and quantitatively. With such an understanding, one is then ready to predict with confidence any changes in the behavior of the organ when some boundary conditions or material properties are changed, thus approaching the objectives of deductive medicine and bioengineering.

The most serious frustration to a biomechanics worker is usually the lack of information about the constitutive equations of living tissues. Without the constitutive laws, no analysis can be done. On the other hand, without the solution of boundary value problems the constitutive laws cannot be determined. Thus, we are in a situation in which serious analyses (usually quite difficult because of nonlinearity) have to be done for hypothetical materials, in the hope that experiments will yield the desired agreement. If no agreement is obtained, new analyses based on a different starting point would become necessary.

It is for this reason that we emphasize the constitutive equations in this book. All biological solids and fluids are considered. Among the biofluids blood is treated in greater detail. Among biosolids the blood vessels, muscles, bone, and cartilage are given special attention. I give smooth muscles a separate chapter because of their extreme importance, although we really know very little about them. Vigorous research is being done on smooth muscles. It is hoped that by the time a second edition of this book is to be issued we would have nailed down the constitutive equations for smooth muscles.

Problems

- 1.1** To practice the use of free-body diagram, consider the problem of analyzing the stress in man's back muscles when he does hard work. Figure P1.1 shows a man shoveling snow. If the snow and shovel weigh 10 kg and have a center of gravity located at a distance of 1 m from the lumbar vertebra of his backbone, what is the moment about that vertebra?

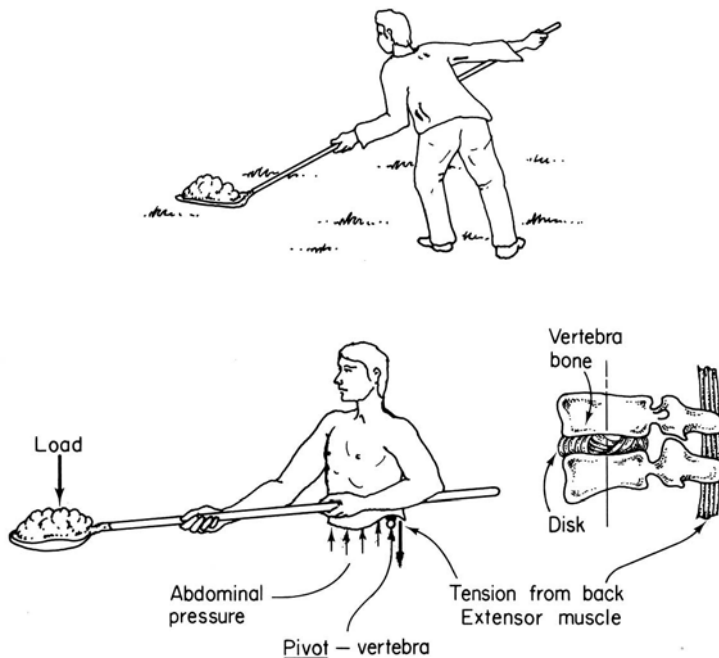


Figure P1.1 Analysis of the stress in man's back muscle as he shovels snow.

The construction of a man's backbone is sketched in the figure. The disks between the vertebrae serve as the pivots of rotation. It may be assumed that the intervertebral disks cannot resist rotation. Hence the weight of the snow and shovel has to be resisted by the vertebral column and the muscle. Estimate the loads in his back muscle, vertebrae, and disks.

Lower back pain is such a common affliction that the loads acting on the disks of patients were measured with strain gauges in some cases. It was found that no agreement can be obtained if we do not take into account the fact that when one lifts a heavy weight, one tenses up the abdominal muscles so that the pressure in the abdomen is increased. A free-body diagram of the upper body of a man is shown in Fig. P1.1. Show that it helps to have a large abdomen and strong abdominal muscles.

See Ortengren et al. (1978) for in vivo measurements of disk and intra-abdominal pressures.

1.2 Compare the bending moment acting on the spinal column at the level of a lumbar vertebra for the following cases:

- A secretary bends down to pick up a book on the floor (i) with her knees straight and (ii) with her knees bent.
- A water skier skis (i) with her arms straight and (ii) with elbows hugging her sides.

Discuss these cases quantitatively with proper free-body diagrams.

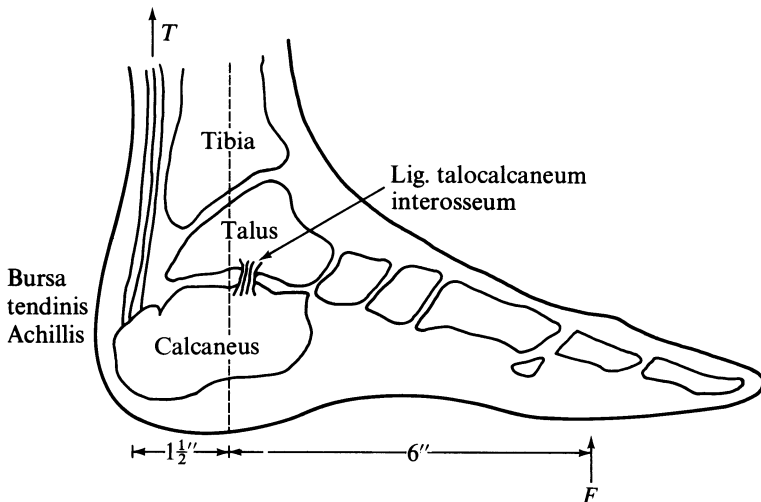


Figure P1.3 The bones and tendons of a foot.

1.3 Consider the question of the strength of human tissues and their margins of safety when we exercise. Take the example of the tension in the Achilles tendon in our foot when we walk and when we jump. The bone structure of the foot is shown in Fig. P1.3. To calculate the tension in the Achilles tendon we may consider the equilibrium of forces that act on the foot. The joint between the tibia and talus bones may be considered as a pivot. The strength of tendons, cartilages, and bones can be found in Yamada's book (1970).

Solution. Assume that the person weighs 150 lb and that the dimensions of the foot are as shown in the figure. Let T be the tension in the Achilles tendon. Refer to Fig. P1.3. We see that the balance of moments requires that

$$T \times 1.5 = 75 \times 6,$$

which gives $T = 300$ lb. If the cross-sectional area of the Achilles tendon is $\frac{1}{4}$ in.², then the tensile stress is

$$1200 \text{ lb/in.}^2 \quad \text{or} \quad 1200/14.19 \text{ kg/cm}^2 = 846 \text{ g/mm}^2.$$

This is the stress acting in the Achilles tendon when one is poised to jump but remaining stationary. To actually jump, however, one must generate a force on the feet larger than the body weight. Equivalently, one must generate a kinetic energy initially. At the highest point of his jump the initial kinetic energy is converted to the potential energy. Thus

$$mgh = \frac{1}{2}mv^2,$$

where m is the mass of the body, g is the gravitational acceleration, h is the height of jump measured at the center of gravity of the body, and v is the initial velocity of jump measured at the center of gravity of the body.

If the person weighs 150 lb, and the height of jump h is 2 ft, then

$$v^2 = 2 \times 32.2 \times 2 = 128.8 \quad \text{or} \quad v = 11.3 \text{ ft/sec.}$$

To do this jump, one must bend the knees, lowering the center of gravity, then suddenly jump up. During this period, the only external forces acting are gravity and the forces acting on the soles. The impulse imposed on the feet must equal to the momentum gained during this period. Let F be the additional force on the feet, and t be the time interval between the instant of initiation of the jump and the instant leaving the ground, then the impulse is $F \cdot t$ and the momentum is mv , and we have

$$Ft = mv.$$

How long t is depends on the gracefulness of the jump. Some experimental results by Miller and East (1976) show that t may be about 0.3 sec. Let us assume that $t = 0.3$ sec. Then, since $mg = 150$ lb,

$$F = \frac{150 \times 11.3}{32.2 \times 0.3} = 175 \text{ lb.}$$

Thus, if the person uses both feet in this jump the total force acting on each foot is $(175 + 150)/2 = 162$ lb. Correspondingly, the tension in the Achilles tendon is $162 \times (6/1.5) = 650$ lb. The stress is, again assuming a cross-sectional area of 0.25 in.^2 , $650/(0.25) = 2600 \text{ lb/in.}^2$ or 1.83 kg/mm^2 .

How strong are our tendons? From Yamada's book, Table 70, p. 100, we have the value $5.6 \pm 0.09 \text{ kg/mm}^2$ for the ultimate tensile stress for the calcaneal (Achilles) tendon in the age group 10 to 29 years. Comparing the computed stress of 1.83 kg/mm^2 with the ultimate stress, we see that the factor of safety is quite small. Such a small factor of safety is compatible with life only because the living organism has an active self-repairing and self-renewal capability.

- 1.4** Consider a thin-walled spherical balloon made of uniform material and having a uniform wall thickness (Fig. P1.4). When it is inflated with an internal pressure p , the radius of the sphere is R and the tension in the wall is T per unit length. Derive

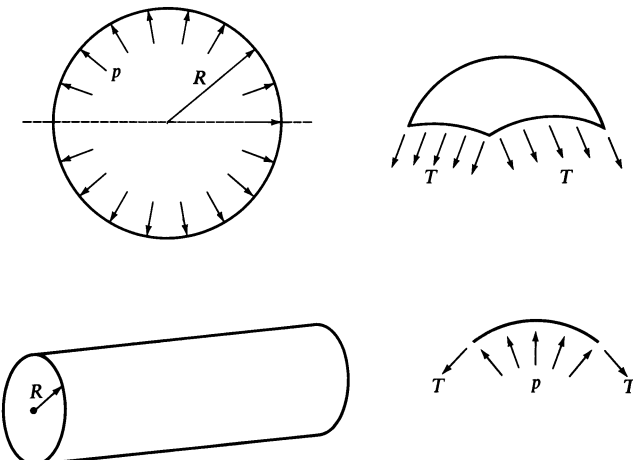


Figure P1.4 A thin-walled spherical balloon and a circular cylindrical shell subjected to internal pressure.

the condition of equilibrium:

$$p = \frac{2T}{R} \quad (1)$$

Consider next a circular cylindrical tube inflated with an internal pressure p to a radius R . Show that the circumferential tension per unit length, T (the so called hoop tension), is related to p and R by

$$p = \frac{T}{R} \quad (2)$$

Resistance to bending of the wall is assumed to be negligible.

Notes on the Law of Laplace

Equations (1) and (2) are known as the law of Laplace. Engineers may be surprised at the prominent role played by this law in physiology. Originally, it referred to a relationship between the surface pressure, the surface tension, and the curvature of a liquid surface. Consider the surface of a liquid column in a capillary tube standing in a bath. On assuming that the surface tension is constant in every direction, the law of Laplace reads:

$$p = T \left(\frac{1}{r_1} + \frac{1}{r_2} \right), \quad (3)$$

in which p denotes the pressure acting on the surface, T is the surface tension, and r_1, r_2 are the principal radii of curvature of the surface. Equations (1)–(3) have been applied to the analysis of a variety of biological problems, such as the cell membrane strength, the distensibility of blood vessels, and the deformability of red blood cells.

If the membrane tension in the wall is not the same in every direction, or if the wall is not very thin, then Eq. (3) is not applicable. A more general result is the following: Consider a curved membrane with principal radii of curvature r_1 and r_2 . Let the principal axes of the membrane stress resultants be coincident with the principal radii of curvature, so that the tension in the directions of the principal curvatures $1/r_1$ and $1/r_2$ be T_1 and T_2 , respectively. Then there is no shear stress resultant in these directions. Hence, when the membrane is subjected to an internal pressure p_i and an external pressure p_o , the equation of equilibrium is

$$p_i - p_o = \frac{T_1}{r_1} + \frac{T_2}{r_2}. \quad (4)$$

This equation is valid as long as the membrane is so thin that bending rigidity can be neglected. It is valid even if the membrane is made of an inelastic

material. If $T_1 = T_2$, then Eq. (4) reduces to Eq. (3). If $T_1 = T_2$ and $r_1 = r_2$, then Eq. (4) reduces to Eq. (1). When $T_1 = T$ and $1/r_2 = 0$, then Eq. (4) reduces to Eq. (2) for an arbitrary value of membrane tension T_2 in the axial direction of the cylinder. For a thin membrane only the pressure difference counts, hence $p_i - p_o$ can be replaced by p .

Equations (1)–(4) do not apply to thick-walled shells such as the heart and the arteries. (The ratio of the wall thickness to the inner radius of the heart, the veins, large arteries, and arterioles are, respectively, about 25%, 3%, 20%, and 100%.) In thick-walled shells the stress is not uniformly distributed in the wall. A more detailed analysis is necessary. In the case of a thick-walled circular cylinder, the solution was obtained by Lamé and Clapeyron in 1833 (see Todhunter and Pearson, 1886, 1960, Vol. 1, Sec, 1022). It is known that the circumferential stress in the wall tends to be concentrated toward the inner wall. However, when the circumferential stress is integrated throughout the thickness of the wall, an equation of equilibrium can be obtained that resembles Eqs. (3) and (4), namely,

$$T_1 = h\langle\sigma_\theta\rangle = p_i r_i - p_o r_o \quad (5)$$

Here $h = r_o - r_i$ denote the wall thickness, $\langle\sigma_\theta\rangle$ denotes the average of the circumferential stress σ_θ , T_1 is the circumferential stress resultant, and r_i, r_o are the inner and outer radii of the cylinder, respectively. Since this is an equation of equilibrium, it can be derived directly from statics as follows. Draw a free-body diagram for half of a circular cylinder with unit length in the axial direction. The total force radially outward due to internal pressure is $p_i \cdot 2r_i \cdot 1$; that due to external pressure is $-p_o \cdot 2r_o \cdot 1$. The total force due to the circumferential stress σ_θ is $2T_1h = 2\langle\sigma_\theta\rangle \cdot h \cdot 1$. Since in a cylinder the axial forces have no influence on the balance of forces in the radial direction, we obtain the equation of equilibrium in the radial direction, Eq. (5), immediately.

Equation (5) reduces to Eq. (2) in the case of a thin-walled cylinder, and is valid even if the cylinder is made of nonhomogeneous, nonlinear, inelastic material. It is applicable to finite deformation as long as r_i, r_o represent the final radii.

Similarly, a consideration of the longitudinal equilibrium of a circular cylinder with closed ends leads directly to the equation

$$T_2 = h\langle\sigma_x\rangle = \frac{p_i r_i^2 - p_o r_o^2}{r_o + r_i}, \quad (6)$$

where T_2 is the longitudinal membrane stress. To derive Eq. (6), we note that on a free-body diagram which includes an end of the cylinder, the axial force due to internal pressure is $\pi r_i^2 p_i$, that due to the external pressure is $-\pi r_o^2 p_o$, whereas the resultant axial force in the wall is equal to the mean stress $\langle\sigma_x\rangle$ multiplied by the area $\pi r_o^2 - \pi r_i^2$, or the product of the membrane stress T_2 and the circumference $\pi(r_i + r_o)$. The vanishing of the sum of all axial forces leads to Eq. (6).

An entirely analogous consideration of a spherical shell yields the average circumferential stress

$$T = h\langle\sigma_\theta\rangle = \frac{p_i r_i^2 - p_o r_o^2}{r_o + r_i}, \quad (7)$$

which again reduces to Eq. (1) in the case of a very thin shell. Equations (5)–(7) are valid for arbitrary materials.

It may be interesting to comment on the history of the law of Laplace itself. It is generally recognized that Thomas Young obtained this law earlier than Laplace. According to Merz (1965), Young presented a derivation of this formula, based entirely on the existence of surface tension, to the Royal Society on the 20th of December, 1804, in a *Memoir on the cohesion of the fluids*. In December, 1805, Laplace read before the Institute of France his theory of capillary attraction, in which the formula was derived on the basis of a special hypothesis of molecular attraction. In a supplement to his memoir, which appeared anonymously in the first number of the *Quarterly Review* (1809, no. 1, p. 109) Young, evidently annoyed that some of his results had been reproduced without acknowledgment, reviewed the treatise of Laplace and said: “The point on which M. Laplace seems to rest the most material part of his claim to originality is the deduction of all the phenomena of capillary action from the simple consideration of molecular attraction. To us, it does not appear that the fundamental principle from which he sets out is at all a necessary consequence of the established properties of matter; and we conceive that this mode of stating the question is but partially justified by the coincidence of the results derived from it with experiment, since he has not demonstrated that a similar coincidence might not be obtained by proceeding on totally different grounds” (Merz, 1965, p. 20).

This historical incident is interesting in that it shows how precariously fame rests. It also exhibits an age-old conflict in the scientific method of approach. Young’s derivation was phenomenological, quite general, and had few assumptions, but was regarded by many as “abstract.” Laplace’s derivation was complicated, and was based on a special assumption about molecular attraction, yet was accepted by many. Even today, such a divergence of approach is encountered again and again. To some, a formula is “understood” when it is derived from a molecular model, however imperfect. To others, the abstract (mathematical and phenomenological) approach is preferred.

Problems

- 1.5** Palpation is used commonly to estimate the internal pressure in an elastic vessel such as a balloon, artery, eyeball, or aneurysm. But when we palpate, what are we measuring? The pressure? Or the resultant force? Show that in general the force or pressure acting on the finger will be affected by the tension in the vessel wall. Show also, however, that if you push just so much that the membrane (vessel wall) is flat

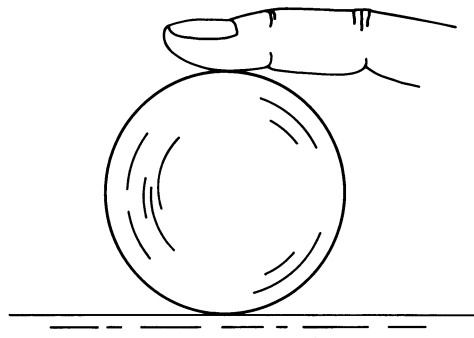
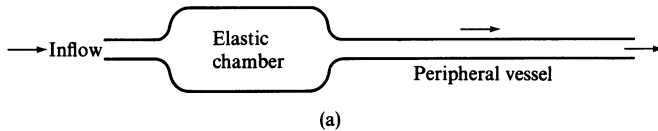


Figure P1.5 Palpation of a blood vessel.

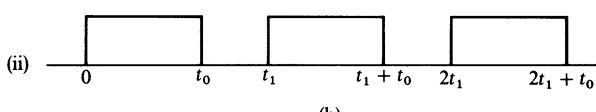
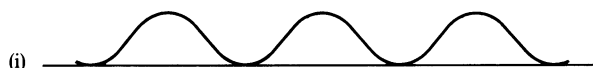
(has infinitely large radius of curvature), then you feel exactly the internal pressure in the vessel. The tacit assumption made in this analysis is that the resistance to bending of the wall is negligible. See Fig. P1.5.

- 1.6** The simplest theory of the cardiovascular system is the *Windkessel* theory proposed by Otto Frank in 1899. The idea was stated earlier by Hales (1733) and Weber (1850). In this theory, the aorta is represented by an elastic chamber, and the peripheral blood vessels are replaced by a rigid tube of constant resistance. See Fig. P1.6(a). Let \dot{Q} be the inflow (cm^3/sec) into this system from the heart. Part of this inflow is sent to the peripheral vessels, and part of it is used to distend the elastic chamber. If p is the blood pressure (pressure in the aorta or elastic chamber), the flow in the peripheral vessel is equal to p/R , where R is called peripheral resistance. For the elastic chamber, its change of volume is assumed to be proportional to the pressure. The rate of change of the volume of the elastic chamber with respect to time t is therefore proportional to dp/dt . Let the constant of proportionality be written as K . Show that on equating the inflow to the sum of the rate of change of volume of the elastic chamber and the outflow p/R , the differential equation governing the pressure p is

$$\dot{Q} = K \frac{dp}{dt} + \frac{p}{R}. \quad (1)$$



(a)



(b)

Figure P1.6 (a) A simple representation of the aorta. (b) Some pulse waves.

Show that the solution of this differential equation is

$$p(t) = \frac{1}{K} e^{-t/(RK)} \int_0^t \dot{Q}(\tau) e^{\tau/(RK)} d\tau + p_0 e^{-t/(RK)}, \quad (2)$$

where p_0 is the value of p at time $t = 0$. Using this solution, discuss the pressure pulse in the aorta as a function of the left ventricle contraction history $\dot{Q}(t)$ (i.e., the pumping history of the heart). Discuss in particular the condition of periodicity and the steady-state response of the aorta to a periodically beating heart. This equation works remarkably well in correlating experimental data on the total blood flow \dot{Q} with the blood pressure p , particularly during diastole. Hence in spite of the simplicity of the underlying assumptions, it is quite useful.

Note: The derivation of Eq. (1) is already outlined in the statement of the problem. For the last part, it would be interesting to discuss the solutions when $\dot{Q}(t)$ is one of the idealized periodic functions shown in Fig P1.6(b):

$$\dot{Q}(t) = a \sin^2 \omega t. \quad (3)$$

$$\begin{aligned} \dot{Q}(t) &= a \{ [\mathbf{1}(t) - \mathbf{1}(t - t_0)] + [\mathbf{1}(t - t_1) - \mathbf{1}(t - t_1 - t_0)] \\ &\quad + [\mathbf{1}(t - 2t_1) - \mathbf{1}(t - 2t_1 - t_0)] + \dots \\ &= \sum_{n=\infty}^{\infty} a [\mathbf{1}(t - nt_1) - \mathbf{1}(t - nt_1 - t_0)]. \end{aligned} \quad (4)$$

- 1.7 Show that the action of the air chamber in a hand-pumped fire engine is governed by the same equations as those of Problem 1.6. Hence the name *Windkessel*.

References

- Galileo Galilei (1638) *Discorsi e Dimostrazioni matematiche, intorno à due nuove Scienze, Attenenti alla Mecanica & i Movimenti Locali*. Elzevir, Leida. Translated into English by H. Crew and A. de Salvio under the title *Dialogues Concerning Two New Sciences*. MacMillan, London, 1914. Reissued by Dover Publications, New York, 1960.
- Merz, J. T. (1965) *A History of European Thought in the Nineteenth Century*. Dover Publications, New York (reproduction of first edition, W. Blackwood & Sons, 1904).
- Miller, D. I. and East, D. J. (1976) In *Biomechanics V-B*, P. V. Komi (ed.) University Park Press, Baltimore, 1976, pp. 65–72.
- Ortengren, R., Andersson, G., and Nachemson, A. (1978). In *Biomechanics VI-B*, E. Asmussen and K. Jorgensen (eds.) University Park Press, Baltimore, pp. 159–166.
- Singer, C. J. (1959) *A Short History of Scientific Ideas to 1900*. Oxford University Press, New York.
- Todhunter, I., and Pearson, K. (1960) *A History of the Theory of Elasticity, and of the Strength of Materials from Galilei to Lord Kelvin*. Cambridge University Press (1886, 1893); Dover Publications, New York.
- Wolff, H. S. (1973) Bioengineering—a many splendored thing—but for whom? In *Perspectives in Biomedical Engineering*, Proceedings of a symposium, Kenedi, R. M. (ed.). University Park Press, Baltimore, pp. 305–311.
- Yamada, H. (1970) *Strength of Biological Materials*. Williams and Wilkins, Baltimore (translated by F. G. Evans).
- Young, J. (1930). Malpighi's "de Pulmonibus." *Proc. Roy. Soc. Med.* **23**, Part 1, 1–14.

CHAPTER 2

The Meaning of the Constitutive Equation

2.1 Introduction

In the biological world, atoms and molecules are organized into cells, tissues, organs, and individuals. The object of study of this book is at the animal, organ, and tissue level. *The smallest volume we shall consider contains a very large number of atoms and molecules.* In such a volume it is convenient to consider the material as a continuum.

Many important biological phenomena occur at the continuum level. Thus, gametes swim, cilia beat, the heart contracts, the arteries pulsate. To understand these phenomena, we must understand the forces that cause or are caused by the motion. Thus we must know how to describe the motion and deformation of the body, and how the forces are transmitted in the body. The method of continuum mechanics offers a scientific treatment of these forces and deformations.

While the reader is referred to standard works on continuum mechanics for a more detailed presentation, we shall outline very briefly the concepts, definitions, and notations we shall use in this work.

2.2 Stress

If we want to determine the strength of a tendon, we can test a large or small specimen. A large specimen can sustain a large force, a smaller specimen can take only a small force. Obviously, the size of the test specimen is incidental; only the force relative to the size is important. Thus, we are led to the concept that it is the stress (force per unit cross-sectional area) that is related to the strength of the material.

Let the cross-sectional area of a tendon be A , and let the force that acts in the tendon be F . The ratio

$$\sigma = F/A \quad (1)$$

is the *stress* in the tendon. In the International System of Units (SI units), the basic unit of force is the *newton* (N) and that of length is the *meter* (m). Thus the basic unit of stress is *newton per square meter* (N/m^2) or *pascal* (Pa, in honor of Pascal). $1\text{ MPa} = 1\text{ N/mm}^2$. A force of 1 N can accelerate a body of mass 1 kg to 1 m/sec^2 . A force of 1 dyne (dyn) can accelerate a body of mass 1 gram to 1 cm/sec^2 . Hence, $1\text{ dyn} = 10^{-5}\text{ N}$. Some conversion factors are listed below:

$$1\text{ pound force} \doteq 4.448\text{ N}$$

$$1\text{ pound per square inch (p si)} \doteq 6894\text{ N/m}^2 = 6.894\text{ kPa}$$

$$1\text{ dyn/cm}^2 \doteq 0.1\text{ N/m}^2 = 0.1\text{ Pa}$$

$$1\text{ atmosphere} \doteq 1.013 \times 10^5\text{ N/m}^2 = 1.013\text{ bar}$$

$$1\text{ mm Hg at } 0^\circ\text{C} \doteq 133\text{ N/m}^2 = 1\text{ torr} \sim \frac{1}{8}\text{ kPa}$$

$$1\text{ cm H}_2\text{O at } 4^\circ\text{C} \doteq 98\text{ N/m}^2; 1\text{ inch H}_2\text{O} \sim \frac{1}{4}\text{ kPa}$$

$$1\text{ poise (viscosity)} = 0.1\text{ N sec/m}^2.$$

More generally, the concept of stress expresses the interaction of the material in one part of the body on another. Consider a material continuum B occupying a spatial region V (Fig. 2.2:1). Imagine a small surface element of area ΔS . Let us draw, from a point on ΔS , a unit vector* v normal to ΔS . Then we can distinguish the two sides of ΔS according to the direction of v . Let the side to which this normal vector points be called the positive side. Consider the part of material lying on the positive side. This part exerts a force ΔF on the other part, which is situated on the negative side of the normal. The force ΔF depends on the location and size of the area

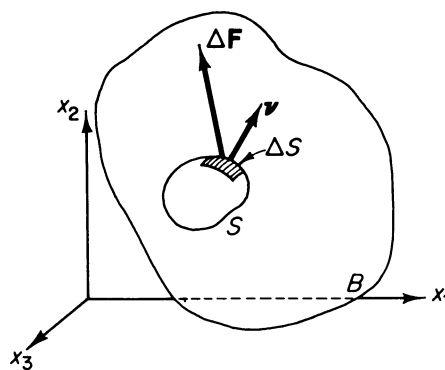


Figure 2.2:1 Stress principle.

* All vectors are printed in bold face in this book.

and the orientation of the normal. We introduce the assumption that as ΔS tends to zero, the ratio $\Delta F/\Delta S$ tends to a definite limit, dF/dS , and that the moment of the force acting on the surface ΔS about any point within the area vanishes in the limit. The limiting vector will be written as

$$\overset{v}{T} = d\mathbf{F}/dS, \quad (2)$$

where a superscript v is introduced to denote the direction of the normal v of the surface ΔS . The limiting vector $\overset{v}{T}$ is called the *traction*, or the *stress vector*, and represents the force per unit area acting on the surface.

The general notation for stress components is as follows. Consider a little cube in the body (replacing S in Fig. 2.2:1 by a cube, as shown in Fig. 2.2:2). It has 6 surfaces. Erect a set of rectangular cartesian coordinates x_1, x_2, x_3 . Let the surface of the cube normal to x_1 be denoted by ΔS_1 .

Let the stress vector that acts on the surface ΔS_1 be T . Resolve the vector T into three components in the direction of the coordinate axes and denote them by $\tau_{11}, \tau_{12}, \tau_{13}$. Then $\tau_{11}, \tau_{12}, \tau_{13}$ are the stress components acting on the small cube. Similarly, we may consider surfaces $\Delta S_2, \Delta S_3$ perpendicular to x_2 and x_3 , the stress vectors acting on them, and their components in x_1, x_2, x_3 directions. We can arrange the components in a square matrix:

	Components of Stresses		
	1	2	3
Surface normal to x_1	τ_{11}	τ_{12}	τ_{13}
Surface normal to x_2	τ_{21}	τ_{22}	τ_{23}
Surface normal to x_3	τ_{31}	τ_{32}	τ_{33}

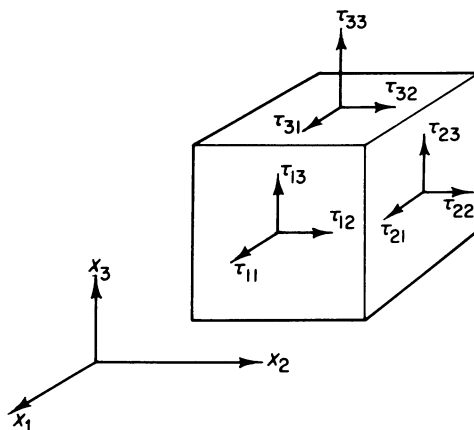


Figure 2.2.2 Notations of stress components.

This is illustrated in Fig. 2.2:2. The components τ_{11} , τ_{22} , τ_{33} are called *normal stresses*, and the remaining components τ_{12} , τ_{13} , etc., are called *shearing stresses*.

It is important to emphasize that a stress will always be understood to be the force (per unit area) that the part lying on the positive side of a surface element (the side on the positive side of the outer normal) exerts on the part lying on the negative side. Thus, if the outer normal of a surface element points in the positive direction of the x_2 axis and τ_{22} is positive, the vector representing the component of normal stress acting on the surface element will point in the positive x_2 direction. But if τ_{22} is positive while the outer normal points in the negative x_2 axis direction, then the stress vector acting on the element also points to the negative x_2 axis direction (see Fig. 2.2:3).

Similarly, positive values of τ_{21} , τ_{23} will imply shearing stress vectors pointing to the positive x_1 , x_3 axes if the outer normal agrees in sense with the x_2 axis, whereas the stress vectors point to the negative x_1 , x_3 directions if the outer normal disagrees in sense with the x_2 axis, as illustrated in Fig. 2.2:3.

We now give without proof four important formulas concerning stresses. [See Y. C. Fung (1977) *A First Course in Continuum Mechanics*, for detailed derivations and proofs.] First, it can be shown that knowing the components τ_{ij} , we can write down at once the stress vector acting on any surface with unit outer normal vector v whose components are v_1 , v_2 , v_3 . This stress vector is denoted by $\overset{v}{T}$, with components $\overset{v}{T}_1$, $\overset{v}{T}_2$, $\overset{v}{T}_3$ given by Cauchy's formula,

$$\overset{v}{T}_i = v_1 \tau_{11} + v_2 \tau_{21} + v_3 \tau_{31}. \quad (3)$$

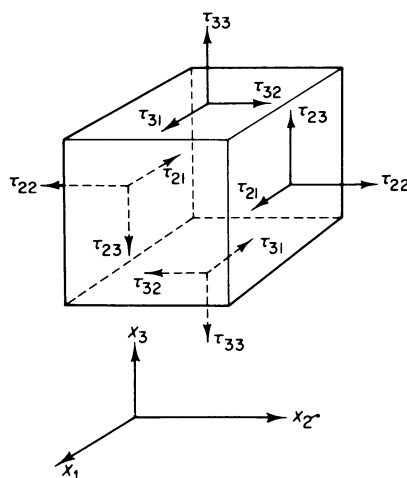


Figure 2.2:3 Senses of positive stress components.

Next, for a body in equilibrium, the stress components must satisfy the differential equations

$$\begin{aligned}\frac{\partial \tau_{11}}{\partial x_1} + \frac{\partial \tau_{21}}{\partial x_2} + \frac{\partial \tau_{31}}{\partial x_3} + X_1 &= 0, \\ \frac{\partial \tau_{21}}{\partial x_1} + \frac{\partial \tau_{22}}{\partial x_2} + \frac{\partial \tau_{23}}{\partial x_3} + X_2 &= 0, \\ \frac{\partial \tau_{31}}{\partial x_1} + \frac{\partial \tau_{32}}{\partial x_2} + \frac{\partial \tau_{33}}{\partial x_3} + X_3 &= 0,\end{aligned}\quad (4)$$

where X_1, X_2, X_3 are the components of the body force (per unit volume) acting on the body. Third, the stress tensor is always symmetric:

$$\tau_{12} = \tau_{21}, \quad \tau_{23} = \tau_{32}, \quad \tau_{31} = \tau_{13}. \quad (5)$$

Finally, let a system of rectangular cartesian coordinates x_1, x_2, x_3 be transformed into another such system x'_1, x'_2, x'_3 by the transformation

$$x'_k = \beta_{ki}x_i \equiv \beta_{k1}x_1 + \beta_{k2}x_2 + \beta_{k3}x_3, \quad (k = 1, 2, 3) \quad (6)$$

where β_{ki} denotes the direction cosine of the x'_k axis with respect to the x_i axis. Then the stress components are transformed according to the tensor transformation law:

$$\tau'_{km} = \tau_{ji}\beta_{kj}\beta_{mi}. \quad (7)$$

In these formulas, the summation convention of the index is used: any repetition of an index in a single term means summation over that index. For example, Eq. (7) stands for

$$\begin{aligned}\tau'_{km} &= \beta_{k1}\beta_{m1}\tau_{11} + \beta_{k1}\beta_{m2}\tau_{12} + \beta_{k1}\beta_{m3}\tau_{13} + \beta_{k2}\beta_{m1}\tau_{21} + \beta_{k2}\beta_{m2}\tau_{22} \\ &\quad + \beta_{k2}\beta_{m3}\tau_{23} + \beta_{k3}\beta_{m1}\tau_{31} + \beta_{k3}\beta_{m2}\tau_{32} + \beta_{k3}\beta_{m3}\tau_{33}\end{aligned}$$

for any combination of $k = 1, 2$, or 3 , and $m = 1, 2$, or 3 .

2.3 Strain

Deformation of a solid that can be related to stresses is described by strain. Take a string of an initial length L_0 . If it is stretched to a length L as shown in Fig. 2.3:1(a), it is natural to describe the change by dimensionless ratios such as L/L_0 , $(L - L_0)/L_0$, $(L - L_0)/L$. Use of dimensionless ratios eliminates the absolute length from consideration. The ratio L/L_0 is called the *stretch ratio* and is denoted by the symbol λ . The ratios

$$\varepsilon = \frac{L - L_0}{L_0}, \quad \varepsilon' = \frac{L - L_0}{L} \quad (1)$$

are *strain measures*. Either of them can be used. Numerically, they are different. For example, if $L = 2$, $L_0 = 1$, we have $\varepsilon = 1$, $\varepsilon' = \frac{1}{2}$. We shall have

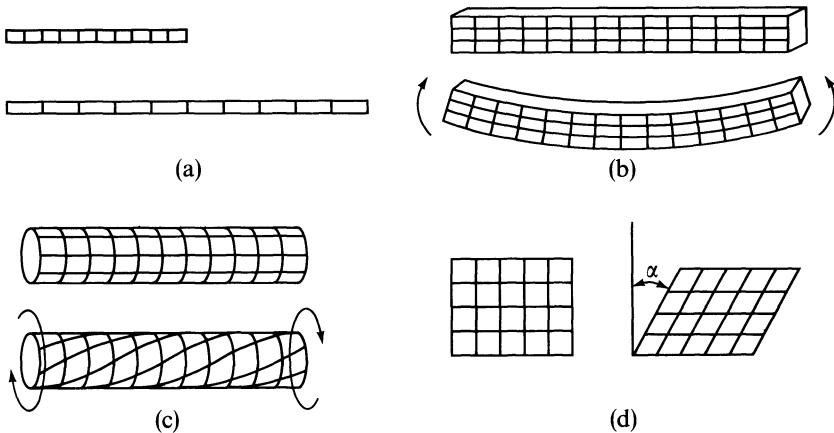


Figure 2.3:1 Patterns of deformation.

reasons (to be named later) also to introduce the measures

$$e = \frac{L^2 - L_0^2}{2L^2}, \quad \mathcal{E} = \frac{L^2 - L_0^2}{2L_0^2}. \quad (2)$$

If $L = 2$, $L_0 = 1$, we have $e = \frac{3}{8}$, $\mathcal{E} = \frac{3}{2}$. But if $L = 1.01$, $L_0 = 1.00$, then $e \doteq 0.01$, $\mathcal{E} \doteq 0.01$, $\varepsilon \doteq 0.01$, and $\varepsilon' \doteq 0.01$. Hence in infinitesimal elongations all the strain measures named above are equal. In finite elongations, however, they are different.

To illustrate shear, consider a circular cylindrical shaft as shown in Fig. 2.3:1(c). When the shaft is twisted, the elements in the shaft are distorted in a manner shown in Fig. 2.3:1(d). In this case, the angle α may be taken as a strain measure. It is more customary, however, to take $\tan \alpha$, or $\frac{1}{2} \tan \alpha$, as the *shear strain*; the reasons for this will be elucidated later.

The selection of proper strain measures is dictated basically by the stress-strain relationship (i.e., the constitutive equation of the material). For example, if we pull on a string, it elongates. The experimental results can be presented as a curve of the tensile stress σ plotted against the stretch ratio λ , or strain e . An empirical formula relating σ to e can be determined. The case of infinitesimal strain is simple because the different strain measures named above all coincide. It was found that for most engineering materials subjected to an infinitesimal strain in uniaxial stretching, a relation like

$$\sigma = Ee, \quad (3)$$

is valid within a certain range of stresses, where E is a constant called *Young's modulus*. Equation (3) is called *Hooke's law*. A material obeying Eq. (3) is said to be a *Hookean material*. Steel is a Hookean material if σ lies within certain bounds that are called *yield stresses*. Corresponding to Eq. (3), the relationship for a Hookean material subjected to an infinitesimal shear strain is

$$\tau = G \tan \alpha, \quad (4)$$

where G is another constant called the *modulus of rigidity*. The range of validity of Eq. (4) is again bounded by yield stresses. The yield stresses in tension, in compression, and in shear are generally different.

Deformations of most things in nature are much more complex than those discussed above. We therefore need a general method of treatment. Let a body occupy a space S . Referred to a rectangular cartesian frame of reference, every particle in the body has a set of coordinates. When the body is deformed, every particle takes up a new position, which is described by a new set of coordinates. For example, a particle P located originally at a place with coordinates (a_1, a_2, a_3) is moved to the place Q with coordinates (x_1, x_2, x_3) when the body moves and deforms. Then the vector \mathbf{PQ} or, \mathbf{u} , is called the *displacement vector* of the particle (see Fig. 2.3:2). The components of the displacement vector are, clearly,

$$u_1 = x_1 - a_1, \quad u_2 = x_2 - a_2, \quad u_3 = x_3 - a_3. \quad (5)$$

If the displacement is known for every particle in the body, we can construct the deformed body from the original. Hence, a deformation can be described by the displacement field. Let the variable (a_1, a_2, a_3) refer to any particle in the original configuration of the body, and let (x_1, x_2, x_3) be the coordinates of that particle when the body is deformed. Then the deformation of the body is known if x_1, x_2, x_3 are known functions of a_1, a_2, a_3 :

$$x_i = x_i(a_1, a_2, a_3) \quad (i = 1, 2, 3). \quad (6)$$

This is a transformation (mapping) from a_1, a_2, a_3 to x_1, x_2, x_3 . We assume that the transformation is one-to-one; i.e., the functions in Eq. (6) are single-

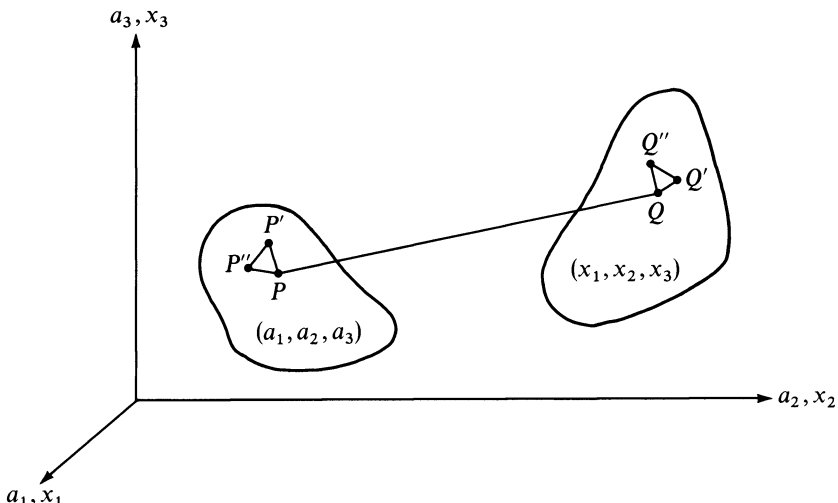


Figure 2.3:2 Deformation of a body.

valued, continuous, and have a unique inverse,

$$a_1 = a_i(x_1, x_2, x_3), \quad (7)$$

for every point in the body.

A rigid-body motion induces no stress. Thus, the displacements themselves are not directly related to the stress. To relate deformation with stress we must consider the stretching and distortion of the body. For this purpose, it is sufficient if we know the change of distance between any arbitrary pair of points.

Consider an infinitesimal line element connecting the point $P(a_1, a_2, a_3)$ to a neighboring point $P'(a_1 + da_1, a_2 + da_2, a_3 + da_3)$. The square of the lengths ds_0 of PP' in the original configuration is given by

$$ds_0^2 = da_1^2 + da_2^2 + da_3^2. \quad (8)$$

When P and P' are deformed to the points $Q(x_1, x_2, x_3)$ and $Q'(x_1 + dx_1, x_2 + dx_2, x_3 + dx_3)$, respectively, the square of the length ds of the new element QQ' is

$$ds^2 = dx_1^2 + dx_2^2 + dx_3^2. \quad (9)$$

By Eqs. (6) and (7), we have

$$dx_i = \frac{\partial x_i}{\partial a_j} da_j, \quad da_i = \frac{\partial a_i}{\partial x_j} dx_j. \quad (10)$$

Hence, on introducing the Kronecker delta, δ_{ij} , which has the value 1 if $i = j$, and zero if $i \neq j$, we may write

$$ds_0^2 = \delta_{ij} da_i da_j = \delta_{ij} \frac{\partial a_i}{\partial x_l} \frac{\partial a_j}{\partial x_m} dx_l dx_m, \quad (11)$$

$$ds^2 = \delta_{ij} dx_i dx_j = \delta_{ij} \frac{\partial x_i}{\partial a_l} \frac{\partial x_j}{\partial a_m} da_l da_m. \quad (12)$$

The difference between the squares of the length elements may be written, after several changes in the symbols for dummy indices, either as

$$ds^2 - ds_0^2 = \left(\delta_{\alpha\beta} \frac{\partial x_\alpha}{\partial a_i} \frac{\partial x_\beta}{\partial a_j} - \delta_{ij} \right) da_i da_j, \quad (13)$$

or as

$$ds^2 - ds_0^2 = \left(\delta_{ij} - \delta_{\alpha\beta} \frac{\partial a_\alpha}{\partial x_i} \frac{\partial a_\beta}{\partial x_j} \right) dx_i dx_j. \quad (14)$$

We define the strain tensors

$$E_{ij} = \frac{1}{2} \left(\delta_{\alpha\beta} \frac{\partial x_\alpha}{\partial a_i} \frac{\partial x_\beta}{\partial a_j} - \delta_{ij} \right), \quad (15)$$

$$e_{ij} = \frac{1}{2} \left(\delta_{ij} - \delta_{\alpha\beta} \frac{\partial a_\alpha}{\partial x_i} \frac{\partial a_\beta}{\partial x_j} \right), \quad (16)$$

so that

$$ds^2 - ds_0^2 = 2E_{ij} da_i da_j, \quad (17)$$

$$ds^2 - ds_0^2 = 2e_{ij} dx_i dx_j. \quad (18)$$

The strain tensor E_{ij} was introduced by Green and St.-Venant and is called *Green's strain tensor*. The strain tensor e_{ij} was introduced by Cauchy for infinitesimal strains and by Almansi and Hamel for finite strains and is known as *Almansi's strain tensor*. In analogy with terminology in hydrodynamics, E_{ij} is often referred to as *Lagrangian* and e_{ij} as *Eulerian*.

E_{ij} and e_{ij} thus defined are tensors. They are symmetric; i.e.,

$$E_{ij} = E_{ji}, \quad e_{ij} = e_{ji}. \quad (19)$$

An immediate consequence of Eqs. (17) and (18) is that $ds^2 - ds_0^2 = 0$ implies $E_{ij} = e_{ij} = 0$ and vice versa. But a deformation in which the length of every line element remains unchanged is a rigid-body motion. Hence, the necessary and sufficient condition that a deformation of a body be a rigid-body motion is that all components of the strain tensor E_{ij} or e_{ij} be zero throughout the body.

If the components of displacement u_i are such that their first derivatives are so small that the squares and products of the partial derivatives of u_i are negligible compared with the first order terms, then e_{ij} reduces to *Cauchy's infinitesimal strain tensor*,

$$\varepsilon_{ij} = \frac{1}{2} \left(\frac{\partial u_j}{\partial x_i} + \frac{\partial u_i}{\partial x_j} \right). \quad (20)$$

In unabridged notation, writing u, v, w for u_1, u_2, u_3 and x, y, z for x_1, x_2, x_3 , we have

$$\begin{aligned} \varepsilon_{xx} &= \frac{\partial u}{\partial x}, & \varepsilon_{xy} &= \frac{1}{2} \left(\frac{\partial u}{\partial y} + \frac{\partial v}{\partial x} \right) = \varepsilon_{yx}, \\ \varepsilon_{yy} &= \frac{\partial v}{\partial y}, & \varepsilon_{xz} &= \frac{1}{2} \left(\frac{\partial u}{\partial z} + \frac{\partial w}{\partial x} \right) = \varepsilon_{zx}, \\ \varepsilon_{zz} &= \frac{\partial w}{\partial z}, & \varepsilon_{yz} &= \frac{1}{2} \left(\frac{\partial v}{\partial z} + \frac{\partial w}{\partial y} \right) = \varepsilon_{zy}. \end{aligned} \quad (21)$$

In the infinitesimal displacement case, the distinction between the Lagrangian and Eulerian strain tensor disappears, since then it is immaterial whether the derivatives of the displacements are calculated at the position of a point before or after deformation.

It is important to visualize the geometric meaning of the individual strain components. The illustrations shown in Fig. 2.3:3 will be helpful. For greater details the reader is referred to the *First Course*, pp. 129–142.

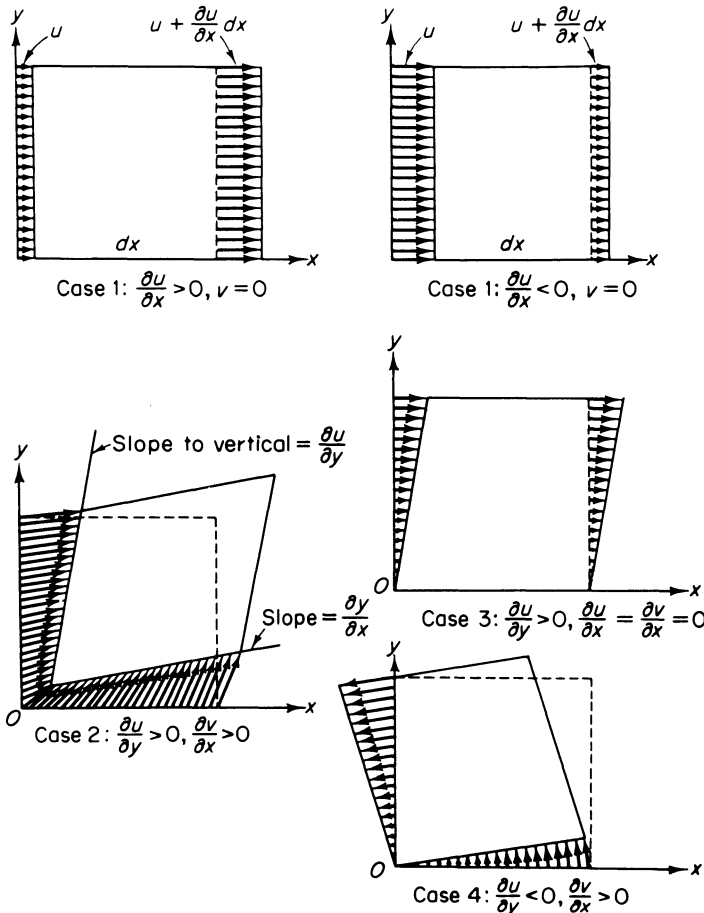


Figure 2.3:3 Deformation gradients and interpretation of infinitesimal strain components.

Note that our definition of the shear strains ϵ_{xy} , ϵ_{yz} , ϵ_{zx} given in Eq. (21) makes ϵ_{ij} as defined in Eq. (20) a *tensor*. Only when ϵ_{ij} is a tensor can the tensor transformation law such as Eq. (7) of Sec. 2.2, the tensor equations (17), (18), and the constitutive equations presented in Secs. 2.6–2.8 be valid. In older engineering mechanics books the shear strains are defined as twice as large as those defined in Eq. (21). This difference should be borne in mind in reading engineering literature.

2.4 Strain Rate

For fluids in motion we must consider the velocity field and the rate of strain. If we refer the location of each fluid particle to a frame of reference O-xyz; then the field of flow is described by the velocity vector field $\mathbf{v}(x, y, z)$,

which defines the velocity at every point (x, y, z) . In terms of components, the velocity field is expressed by the functions

$$u(x, y, z), \quad v(x, y, z), \quad w(x, y, z),$$

or, if index notations are used, by $v_i(x_1, x_2, x_3)$.

For continuous flow, we consider the continuous and differentiable functions $v_i(x_1, x_2, x_3)$. To study the relationship of velocities at neighboring points, let two particles P and P' be located instantaneously at x_i and $x_i + dx_i$, respectively. The difference in velocities at these two points is

$$dv_i = \frac{\partial v_i}{\partial x_j} dx_j, \quad (1)$$

where the partial derivatives $\partial v_i / \partial x_j$ are evaluated at the particle P . Now

$$\frac{\partial v_i}{\partial x_j} = \frac{1}{2} \left(\frac{\partial v_i}{\partial x_j} + \frac{\partial v_j}{\partial x_i} \right) - \frac{1}{2} \left(\frac{\partial v_j}{\partial x_i} - \frac{\partial v_i}{\partial x_j} \right). \quad (2)$$

If we define a *strain rate tensor* V_{ij} and a *vorticity tensor* Ω_{ij} as

$$V_{ij} \equiv \frac{1}{2} \left(\frac{\partial v_i}{\partial x_j} + \frac{\partial v_j}{\partial x_i} \right), \quad (3)$$

$$\Omega_{ij} \equiv \frac{1}{2} \left(\frac{\partial v_j}{\partial x_i} - \frac{\partial v_i}{\partial x_j} \right), \quad (4)$$

then Eq. (1) becomes

$$dv_i = V_{ij} dx_j - \Omega_{ij} dx_j. \quad (5)$$

It is evident that V_{ij} is symmetric and Ω_{ij} is antisymmetric; i.e.,

$$V_{ij} = V_{ji}, \quad \Omega_{ij} = -\Omega_{ji}. \quad (6)$$

Equation (3) is similar to Eq. (2.3:20). Its geometric interpretation is also similar. Therefore, the analysis of the velocity field is similar to the analysis of an infinitesimal deformation field. Indeed, if we multiply v_i by an infinitesimal interval of time dt , the result is an infinitesimal displacement $u_i = v_i dt$. Hence, whatever we learned about the infinitesimal strain field can immediately be extended to the *rate of change* of strain, with the word *velocity* replacing the word *displacement*.

2.5 Constitutive Equations

The properties of materials are specified by constitutive equations. A wide variety of materials exist. Thus, we are not surprised that there are a great many constitutive equations describing an almost infinite variety of materials. What should be surprising, therefore, is the fact that three simple, idealized, stress-strain relationships give a good description of the mechanical prop-

erties of many materials around us: namely, the nonviscous fluid, the Newtonian viscous fluid, and the perfectly elastic solid. Air, water, and many engineering structural materials can be described by these idealized equations. Most biological materials, however, cannot.

2.6 The Nonviscous Fluid

A *nonviscous fluid* is one for which the stress tensor is of the form

$$\sigma_{ij} = -p\delta_{ij}, \quad (1)$$

where δ_{ij} is the Kronecker delta, which has the value 1 if $i = j$, and zero if $i \neq j$, and p is a scalar called *pressure*. The pressure p in an *ideal gas* is related to the density ρ and temperature T by the *equation of state*

$$\frac{p}{\rho} = RT, \quad (2)$$

where R is the gas constant. For a real gas or a liquid, it is often possible to obtain an equation of state:

$$f(p, \rho, T) = 0. \quad (3)$$

An anomaly exists in the case of an *incompressible fluid*, for which the equation of state is merely

$$\rho = \text{const.} \quad (4)$$

Thus, the pressure p is left as an arbitrary variable for an incompressible fluid.

2.7 The Newtonian Viscous Fluid

A *Newtonian viscous fluid* is a fluid for which the shear stress is linearly proportional to the strain rate. For a Newtonian fluid the stress-strain relationship is specified by the equation

$$\sigma_{ij} = -p\delta_{ij} + \mathcal{D}_{ijkl}V_{kl}, \quad (1)$$

where σ_{ij} is the stress tensor, V_{kl} is the strain rate tensor, \mathcal{D}_{ijkl} is a tensor of viscosity coefficients of the fluid, and p is the *static pressure*. The term $-p\delta_{ij}$ represents the state of stress possible in a fluid at rest (when $V_{kl} = 0$). The static pressure p is assumed to depend on the density and temperature of the fluid according to an equation of state. For a Newtonian fluid we assume that the elements of the tensor \mathcal{D}_{ijkl} may depend on the temperature but not on the stress or the rate of deformation. The tensor \mathcal{D}_{ijkl} , of rank 4, has $3^4 = 81$ elements. Not all these constants are independent. A study of the theoretically possible number of independent elements can be made by examining the symmetry properties of the tensors σ_{ij} , V_{kl} and the symmetry that may exist in the atomic constitution of the fluid.

If the fluid is *isotropic*, i.e., if the tensor \mathcal{D}_{ijkl} has the same array of components in any system of rectangular cartesian coordinates, then \mathcal{D}_{ijkl} can be expressed in terms of two independent constants λ and μ ,

$$\mathcal{D}_{ijkl} = \lambda\delta_{ij}\delta_{kl} + \mu(\delta_{ik}\delta_{jl} + \delta_{il}\delta_{jk}), \quad (2)$$

and we obtain

$$\sigma_{ij} = -p\delta_{ij} + \lambda V_{kk}\delta_{ij} + 2\mu V_{ij}. \quad (3)$$

A contraction of Eq. (3) gives

$$\sigma_{kk} = -3p + (3\lambda + 2\mu)V_{kk}. \quad (4)$$

If it is assumed that the mean normal stress $\frac{1}{3}\sigma_{kk}$ is independent of the rate of dilation V_{kk} , then we must set

$$3\lambda + 2\mu = 0; \quad (5)$$

and the constitutive equation becomes

$$\sigma_{ij} = -p\delta_{ij} + 2\mu V_{ij} - \frac{2}{3}\mu V_{kk}\delta_{ij}. \quad (6)$$

This formulation is due to George G. Stokes, and a fluid that obeys Eq. (6) is called a *Stokes fluid*, for which one material constant μ , the *coefficient of viscosity*, suffices to define its property.

If a fluid is *incompressible*, then $V_{kk} = 0$, and we have the constitutive equation for an incompressible viscous fluid:

$$\sigma_{ij} = -p\delta_{ij} + 2\mu V_{ij}. \quad (7)$$

If $\mu = 0$, we obtain the constitutive equation of the nonviscous fluid:

$$\sigma_{ij} = -p\delta_{ij}. \quad (8)$$

Newton's concept of viscosity may be explained in the simplest case of a shear flow with a uniform velocity gradient as sketched in Fig. 2.7:1. Newton proposed the relationship

$$\tau = \mu \frac{du}{dy} \quad (9)$$

for the shear stress τ , where μ is the coefficient of viscosity. In the centimeter-gram-second system of units, in which the unit of force is the dyne, the unit of μ is called a *poise*, in honor of Poiseuille. In the SI system, the unit of viscosity is newton-second per square meter (Ns/m^2). 1 poise (P) is 10 N s/m^2 .

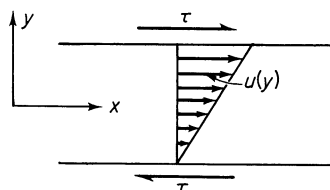


Figure 2.7:1 Newtonian concept of viscosity.

The viscosities of air and water are small, being 1.8×10^{-4} poise for air and 0.01 poise for water at atmospheric pressure and 20°C. At the same temperature the viscosity of glycerine is about 8.7 poise. The viscosity of liquids decreases as temperature increases. That of gases increases with increasing temperature.

2.8 The Hookean Elastic Solid

A *Hookean elastic solid* is a solid that obeys Hooke's law, which states that the stress tensor is linearly proportional to the strain tensor; i.e.,

$$\sigma_{ij} = C_{ijkl} e_{kl}, \quad (1)$$

where σ_{ij} is the stress tensor, e_{kl} is the strain tensor, and C_{ijkl} is a tensor of elastic constants, or moduli, which are independent of stress or strain.

A great reduction in the number of elastic constants is obtained when the material is *isotropic*, i.e., when the elastic properties are identical in all directions. More precisely, isotropy for a material is defined by the requirement that the array of numbers C_{ijkl} has exactly the same numerical values no matter how the coordinate system is oriented. An isotropic material has exactly two independent elastic constants, for which the Hooke's law reads

$$\sigma_{ij} = \lambda e_{xx} \delta_{ij} + 2\mu e_{ij}. \quad (2)$$

The constants λ and μ are called the *Lamé constants*. In the engineering literature, the second Lamé constant μ is practically always written as G and identified as the *shear modulus*.

It will be useful to write out Eq. (2) *in extenso*. With x, y, z as rectangular cartesian coordinates, we have Hooke's law for an isotropic elastic solid:

$$\begin{aligned} \sigma_{xx} &= \lambda(e_{xx} + e_{yy} + e_{zz}) + 2Ge_{xx} \\ \sigma_{yy} &= \lambda(e_{xx} + e_{yy} + e_{zz}) + 2Ge_{yy} \\ \sigma_{zz} &= \lambda(e_{xx} + e_{yy} + e_{zz}) + 2Ge_{zz} \\ \sigma_{xy} &= 2Ge_{xy}, \quad \sigma_{yz} = 2Ge_{yz}, \quad \sigma_{zx} = 2Ge_{zx}. \end{aligned} \quad (3)$$

These equations can be solved for e_{ij} . But customarily, the inverted form is written as

$$e_{ij} = \frac{1+v}{E} \sigma_{ij} - \frac{v}{E} \sigma_{kk} \delta_{ij} \quad (4a)$$

or

$$\begin{aligned} e_{xx} &= \frac{1}{E} [\sigma_{xx} - v(\sigma_{yy} + \sigma_{zz})] & e_{xy} &= \frac{1+v}{E} \sigma_{xy} = \frac{1}{2G} \sigma_{xy}, \\ e_{yy} &= \frac{1}{E} [\sigma_{yy} - v(\sigma_{zz} + \sigma_{xx})], & e_{yz} &= \frac{1+v}{E} \sigma_{yz} = \frac{1}{2G} \sigma_{yz}, \\ e_{zz} &= \frac{1}{E} [\sigma_{zz} - v(\sigma_{xx} + \sigma_{yy})], & e_{zx} &= \frac{1+v}{E} \sigma_{zx} = \frac{1}{2G} \sigma_{zx}. \end{aligned} \quad (4b)$$

The constants E , v , and G are related to the *Lamé constants* λ and G (or μ). E is called *Young's modulus*, v is called *Poisson's ratio*, and G is called the *modulus of elasticity in shear*, or *shear modulus*. They can be written out as follows:

$$\begin{aligned}\lambda &= \frac{2Gv}{1-2v} = \frac{G(E-2G)}{3G-E} = \frac{Ev}{(1+v)(1-2v)}, \\ G &= \frac{\lambda(1-2v)}{2v} = \frac{E}{2(1+v)}, \\ v &= \frac{\lambda}{2(\lambda+G)} = \frac{\lambda}{(3K-\lambda)} = \frac{E}{2G} - 1, \\ E &= \frac{G(3\lambda+2G)}{\lambda+G} = \frac{\lambda(1+v)(1-2v)}{v} = 2G(1+v).\end{aligned}\tag{5}$$

It is very easy to remember Eq. (4). Apply it to the simple block as illustrated in Fig. 2.8:1. When the block is compressed in the z direction, it shortens by a strain:

$$e_{zz} = \frac{1}{E} \sigma_{zz}.\tag{6}$$

At the same time, the lateral sides of the block will bulge out somewhat. For a linear material the bulging strain is proportional to σ_{zz} and is in a sense opposite to the stress: A compression induces lateral bulging; a tension induces lateral shrinking. Hence we write

$$e_{xx} = -\frac{v}{E} \sigma_{zz}, \quad e_{yy} = -\frac{v}{E} \sigma_{zz}.\tag{7}$$

This is the case in which σ_{zz} is the only nonvanishing stress. If the block is also subjected to σ_{xx} , σ_{yy} , as is illustrated in Fig. 2.2:3, and if the material is isotropic and linear (so that causes and effects are linearly superposable), then the influence of σ_{xx} on e_{yy} , e_{zz} and σ_{yy} on e_{xx} , e_{zz} must be the same as the

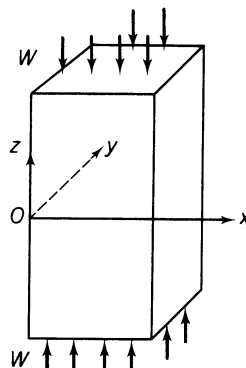


Figure 2.8:1 Stresses in a block.

TABLE 2.8:1

	E (10^6 lb/in. ²)	G (10^6 lb/in. ²)	v	Speed of sound (dilatational wave) (10^3 ft/s)
<i>Metals</i>				
Steels	30	11.5	0.29	16.3
Aluminum alloys	10	3.4	0.31	16.5
Magnesium alloys	6.5	2.4	0.35	16.6
Copper (hot rolled)	15.0	5.6	0.33	16.4
<i>Plastics</i>				
Cellulose acetate	0.22			3.6
Vinylchloride acetate	0.46			5.1
Phenolic laminates	1.23		0.25	8.2
<i>Glass</i>	8	3.2	0.25	
<i>Concrete</i>	4		0.2	

influence of σ_{zz} on e_{xx} , e_{yy} . Hence we have

$$e_{zz} = \frac{1}{E} \sigma_{zz} - \frac{v}{E} \sigma_{xx} - \frac{v}{E} \sigma_{yy}, \quad (8)$$

which is one of the equations of (4). Other equations in (4) can be explained in a similar manner. For shear, the stress σ_{ij} and the strain e_{ij} ($i \neq j$) are directly proportional.

Table 2.8:1 gives the average values of E , G , and v at room temperature for several engineering materials that are approximately isotropic.

2.9 The Effect of Temperature

In the preceding sections, the constitutive equations are stated at a given temperature. The viscosity of a fluid, however, varies with temperature (think of the motor oil in your car) as does the elastic modulus of a solid. In other words, D_{ijkl} in Eq. (2.7:1) and C_{ijkl} in Eq. (2.8:1) are functions of temperature and are coefficients determined under an isothermal experiment (with temperature kept uniform and constant).

If the temperature field is variable, Hooke's law must be modified into the *Duhamel-Neumann form*. Let the elastic constants C_{ijkl} be measured at a uniform constant temperature T_0 . Then if the temperature changes to T , we put

$$\sigma_{ij} = C_{ijkl} e_{kl} - \beta_{ij}(T - T_0) \quad (1)$$

in which β_{ij} is a symmetric tensor, measured at zero strains. For an isotropic material, the second order tensor β_{ij} must also be isotropic. It follows that

β_{ij} must be of the form $\beta\delta_{ij}$, hence

$$\sigma_{ij} = \lambda e_{kk}\delta_{ij} + 2Ge_{ij} - \beta(T - T_0)\delta_{ij}. \quad (2)$$

Here λ and G are Lamé constants measured at constant temperature. The inverse can be written as

$$e_{ij} = \frac{1 + \nu}{E} \sigma_{ij} - \frac{\nu}{E} \sigma_{kk}\delta_{ij} + \alpha(T - T_0)\delta_{ij}. \quad (3)$$

The constant α is the *coefficient of linear expansion*.

2.10 Materials with More Complex Mechanical Behavior

Nonviscous fluids, Newtonian fluids, and Hookean elastic solids are abstractions. No real material is known to behave exactly as one of these, although in limited ranges of temperature, stress, and strain, some materials may follow one of these laws accurately. They are the simplest laws we can devise to relate the stress and strain, or strain rate. They are not expected to be exhaustive.

Almost any real material has a more complex behavior than these simple laws describe. Among fluids, blood is non-Newtonian. Household paints and varnish, wet clay and mud, and most colloidal solutions are non-Newtonian. For solids, most structural materials are, fortunately, Hookean in the useful range of stresses and strains; but beyond certain limits, Hooke's law no longer applies. For example, virtually every known solid material can be broken (fractured) one way or another, under sufficiently large stresses or strains; but to break is to disobey Hooke's law. Few biological tissues obey Hooke's law. Their properties will be discussed in the following chapters.

Problems

2.1 Consider deformation of a body. Let the position of a point in the initial (undeformed) configuration of the body be denoted by the position vector \mathbf{a} , with components a_1, a_2, a_3 when referred to a set of rectangular cartesian coordinates. When the body deforms, the position of the point \mathbf{a} is moved to \mathbf{x} , with components x_1, x_2, x_3 . Consider an infinitesimal line element $d\mathbf{a}$ (a vector with components da_1, da_2, da_3) in the initial configuration. This line element is transformed into $d\mathbf{x}(dx_1, dx_2, dx_3)$ in the deformed configuration. Set down the definitions of strains as relationships between $d\mathbf{a}$ and $d\mathbf{x}$.

2.2 A set of rectangular cartesian coordinates x_1, x_2, x_3 is changed into another set x'_1, x'_2, x'_3 , through an orthogonal transformation

$$\begin{aligned} x'_1 &= \beta_{11}x_1 + \beta_{12}x_2 + \beta_{13}x_3, \\ x'_2 &= \beta_{21}x_1 + \beta_{22}x_2 + \beta_{23}x_3, \\ x'_3 &= \beta_{31}x_1 + \beta_{32}x_2 + \beta_{33}x_3, \end{aligned}$$

or

$$x'_1 = \beta_{ij}x_j$$

for short. How do the strain components $e_{11}, e_{22}, e_{33}, e_{12}, e_{23}, e_{31}$ change when the deformation is referred to the new coordinates x'_1, x'_2, x'_3 ? Let the strain components referred to x'_i be denoted by e'_{ij} . Write down the relationship between e'_{ij} and e_{ij} .

- 2.3** Show that the following combinations of strain components $e_{11}, e_{22}, e_{33}, e_{12}, e_{23}, e_{31}$, do not change when the reference coordinates x_1, x_2, x_3 are changed to x'_1, x'_2, x'_3 through the transformation

$$x'_i = \beta_{ij}x_j.$$

$$I_1 = e_{11} + e_{22} + e_{33},$$

$$I_2 = e_{11}e_{22} - e_{12}^2 + e_{22}e_{33} - e_{23}^2 + e_{33}e_{11} - e_{13}^2,$$

$$I_3 = \begin{vmatrix} e_{11} & e_{12} & e_{13} \\ e_{21} & e_{22} & e_{23} \\ e_{31} & e_{32} & e_{33} \end{vmatrix}.$$

Note: The corresponding relationship for the stress tensor is given in *First Course* Sec. 4.4, p. 99.

- 2.4** Give definitions of principal strains and principal axes of deformations. Let e_1, e_2, e_3 be the principal strains. Show that the invariants I_1, I_2, I_3 named in Problem 2.3 have the meaning

$$I_1 = e_1 + e_2 + e_3,$$

$$I_2 = e_1e_2 + e_2e_3 + e_3e_1,$$

$$I_3 = e_1e_2e_3.$$

what are the physical meanings of these invariants? Discuss especially the physical meaning of I_1, I_2, I_3 when the strains e_{ij} are infinitesimal.

- 2.5** Consider a deformation as described in Problem 2.1. Let a line element da have components $da_1 = ds_0, da_2 = 0, da_3 = 0$, i.e., with length ds_0 in the direction of the coordinate axis x_1 . When the body is deformed, the line element da becomes dx (with components $ds, 0, 0$) whose length is ds . The ratio ds/ds_0 is called the *stretch ratio*, and is denoted by λ_1 . Show that the Green's strain component E_{11} is

$$E_{11} = \frac{1}{2}(\lambda_1^2 - 1).$$

Similarly, the other two normal strain components are

$$E_{22} = \frac{1}{2}(\lambda_2^2 - 1), \quad E_{33} = \frac{1}{2}(\lambda_3^2 - 1),$$

where λ_2, λ_3 are stretch ratios referred to coordinate axes orthogonal to x_1 .

If the coordinate axes x_1, x_2, x_3 were principal axes, then E_{11}, E_{22}, E_{33} are principal strains, and $\lambda_1, \lambda_2, \lambda_3$ are principal stretch ratios. Thus, it is seen that the three principal stretch ratios completely define the deformation of a body, provided that the orientations of the principal axes are known.

- 2.6** Review tensor transformation laws. By direct substitution, show that the tensors $\delta_{ij}\delta_{kl}$ and $\delta_{ik}\delta_{jl} + \delta_{il}\delta_{jk}$ are isotropic.

It can be shown (see *First Course*, p. 193), that any isotropic tensor of rank 4 can be represented in the form

$$\lambda\delta_{ij}\delta_{kl} + \mu(\delta_{ik}\delta_{jl} + \delta_{il}\delta_{jk}) + v(\delta_{ik}\delta_{jl} - \delta_{il}\delta_{jk}),$$

where λ , μ , v , are scalars. Hence deduce that the generalized Hooke's Law between stress and strain,

$$\sigma_{ij} = C_{ijkl},$$

can be reduced to the form

$$\sigma_{ij} = \lambda e_{xx}\delta_{ij} + 2\mu e_{ij}$$

if the material is isotropic.

- 2.7** Following the same reasoning as in Problem 2.6, show in detail that if stresses in a viscous fluid are a linear function of the strain rate, and if the fluid is isotropic, then

$$\sigma_{ij} = -p\delta_{ij} + \lambda V_{xx}\delta_{ij} + 2\mu V_{ij},$$

where V_{ij} is the strain rate tensor defined for a velocity field v_1, v_2, v_3 :

$$V_{ij} = \frac{1}{2} \left(\frac{\partial v_i}{\partial x_j} + \frac{\partial v_j}{\partial x_i} \right),$$

and λ and μ are numerical constants.

Explain the meaning of the term p . Why is this term necessary for the constitutive equation of a fluid but is not required (see Problem 2.6) in the constitutive equation of an elastic solid?

- 2.8** Derive Navier-Stokes equations for a Newtonian viscous fluid such as water.
- 2.9** Derive Navier-Stokes equations for a non-Newtonian viscous fluid such as blood.
- 2.10** Although the no-slip boundary condition on a solid wall is well accepted for homogeneous Newtonian viscous fluids such as air, water, and oil; for particulate flow of fluids such as the blood, which contains cellular bodies to the extent of about 45% by volume, one wonders if the no-slip condition applies at the solid-fluid interface. Invent a method to investigate this problem. Design and sketch the apparatus needed for your investigation. Explain in detail why your method would be decisive.
- 2.11** Under strain, an infinitesimal spherical region in the initial state is transformed into an ellipsoid in the deformed state. The principal axes of the ellipsoid are the principal axes of the strain. The ratios of the lengths of principal axes of the ellipsoid to the radius of the sphere are the *principal stretches* $\lambda_1, \lambda_2, \lambda_3$. The ratio of the volume of the infinitesimal body in the deformed state to that in the initial state is

$$\frac{dV}{dV_0} = \lambda_1\lambda_2\lambda_3.$$

Express the volume ratio in terms the principal strains E_1, E_2, E_3 , or e_1, e_2, e_3 , or $\varepsilon_1, \varepsilon_2, \varepsilon_3$ defined in the senses of Green, Almansi, and Cauchy, respectively. Show that

$$\lambda_1^2\lambda_2^2\lambda_3^2 = 8I_3 + 4I_2 + 2I_1 + 1$$

where the I 's are the invariants given in Probs. 2.3 and 2.4, with e standing for Green's strain.

2.11 Viscoelasticity

When a body is suddenly strained and then the strain is maintained constant afterward, the corresponding stresses induced in the body decrease with time. This phenomena is called *stress relaxation*, or *relaxation* for short. If the body is suddenly stressed and then the stress is maintained constant afterward, the body continues to deform, and the phenomenon is called *creep*. If the body is subjected to a cyclic loading, the stress-strain relationship in the loading process is usually somewhat different from that in the unloading process, and the phenomenon is called *hysteresis*.

The features of hysteresis, relaxation, and creep are found in many materials. Collectively, they are called features of *viscoelasticity*.

Mechanical models are often used to discuss the viscoelastic behavior of materials. In Fig. 2.11:1 are shown three mechanical models of material behavior, namely, the *Maxwell model*, the *Voigt model*, and the *Kelvin model* (also called the *standard linear solid*), all of which are composed of combinations of linear springs with spring constant μ and dashpots with coefficient of viscosity η . A *linear spring* is supposed to produce instantaneously a deformation proportional to the load. A *dashpot* is supposed to produce a velocity proportional to the load at any instant. Thus if F is the force acting in a spring and u is its extension, then $F = \mu u$. If the force F acts on a dashpot, it will produce a velocity of deflection \dot{u} , and $F = \eta \dot{u}$. The shock absorber

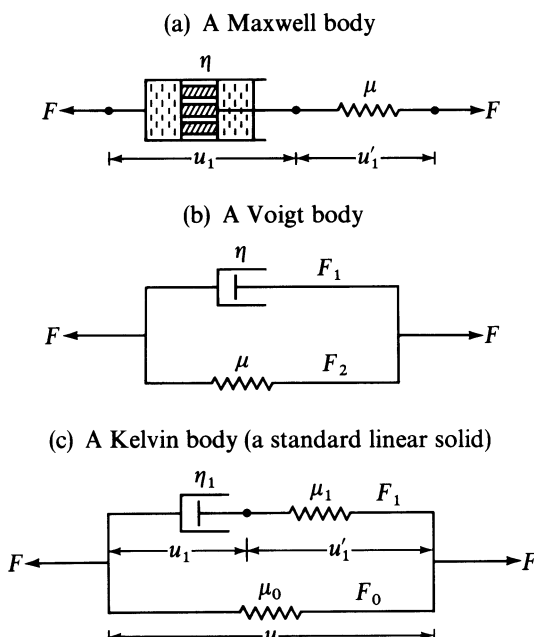


Figure 2.11:1 Three mechanical models of viscoelastic material. (a) a Maxwell body, (b) a Voigt body, and (c) a Kelvin body (a standard linear solid).

on an airplane's landing gear is an example of a dashpot. Now, in a *Maxwell model*, shown in Fig. 2.11:1(a), the same force is transmitted from the spring to the dashpot. This force produces a displacement F/μ in the spring and a velocity F/η in the dashpot. The velocity of the spring extension is \dot{F}/μ if we denote a differentiation with respect to time by a dot. The total velocity is the sum of these two:

$$\dot{u} = \frac{\dot{F}}{\mu} + \frac{F}{\eta} \quad (\text{Maxwell model}). \quad (1)$$

Furthermore, if the force is suddenly applied at the instant of time $t = 0$, the spring will be suddenly deformed to $u(0) = F(0)/\mu$, but the initial dashpot deflection would be zero, because there is no time to deform. Thus the initial condition for the differential equation (1) is

$$u(0) = \frac{F(0)}{\mu}. \quad (2)$$

For the *Voigt model*, the spring and the dashpot have the same displacement. If the displacement is u , the velocity is \dot{u} , and the spring and dashpot will produce forces μu and $\eta \dot{u}$, respectively. The total force F is therefore

$$F = \mu u + \eta \dot{u} \quad (\text{Voigt model}). \quad (3)$$

If F is suddenly applied, the appropriate initial condition is

$$u(0) = 0. \quad (4)$$

For the *Kelvin model* (or standard linear model), let us break down the displacement u into u_1 of the dashpot and u'_1 for the spring, whereas the total force F is the sum of the force F_0 from the spring and F_1 from the Maxwell element. Thus

- | | |
|----------------------|--|
| (a) $u = u_1 + u'_1$ | (b) $F = F_0 + F_1,$ |
| (c) $F_0 = \mu_0 u,$ | (d) $F_1 = \eta_1 \dot{u}_1 = \mu_1 u'_1.$ |
- (5)

From this we can verify by substitution that

$$F = \mu_0 u + \mu_1 u'_1 = (\mu_0 + \mu_1) u - \mu_1 u_1.$$

Hence

$$F + \frac{\eta_1}{\mu_1} \dot{F} = (\mu_0 + \mu_1) u - \mu_1 u_1 + \frac{\eta_1}{\mu_1} (\mu_0 + \mu_1) \dot{u} - \eta_1 \dot{u}_1.$$

Replacing the last term by $\mu_1 u'_1$ and using Eq. (5a), we obtain

$$F + \frac{\eta_1}{\mu_1} \dot{F} = \mu_0 u + \eta_1 \left(1 + \frac{\mu_0}{\mu_1} \right) \dot{u}. \quad (6)$$

This equation can be written in the form

$$F + \tau_e \dot{F} = E_R(u + \tau_\sigma \dot{u}), \quad (\text{Kelvin model}) \quad (7)$$

where

$$\tau_\varepsilon = \frac{\eta_1}{\mu_1}, \quad \tau_\sigma = \frac{\eta_1}{\mu_0} \left(1 + \frac{\mu_0}{\mu_1}\right), \quad E_R = \mu_0. \quad (8)$$

For a suddenly applied force $F(0)$ and displacement $u(0)$, the initial condition is

$$\tau_\varepsilon F(0) = E_R \tau_\sigma u(0). \quad (9)$$

For reasons that will become clear below, the constant τ_ε is called the *relaxation time for constant strain*, whereas τ_σ is called the *relaxation time for constant stress*.

If we solve Eqs. (1), (3), and (7) for $u(t)$ when $F(t)$ is a *unit-step function* $\mathbf{1}(t)$, the results are called *creep functions*, which represent the elongation produced by a sudden application at $t = 0$ of a constant force of magnitude unity. They are:

Maxwell solid:

$$c(t) = \left(\frac{1}{\mu} + \frac{1}{\eta} t\right) \mathbf{1}(t), \quad (10)$$

Voigt solid:

$$c(t) = \frac{1}{\mu} (1 - e^{-(\mu/\eta)t}) \mathbf{1}(t), \quad (11)$$

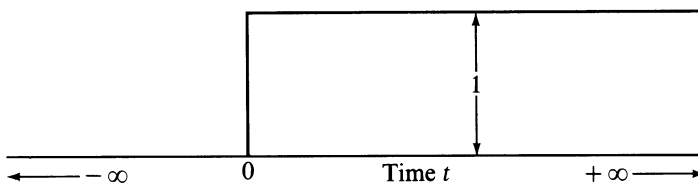
Standard linear solid:

$$c(t) = \frac{1}{E_R} \left[1 - \left(1 - \frac{\tau_\varepsilon}{\tau_\sigma}\right) e^{-t/\tau_\sigma} \right] \mathbf{1}(t), \quad (12)$$

where the unit-step function $\mathbf{1}(t)$ is defined as [see Fig. 2.11:2(a)]

$$\mathbf{1}(t) = \begin{cases} 1 & \text{when } t > 0, \\ \frac{1}{2} & \text{when } t = 0, \\ 0 & \text{when } t < 0. \end{cases} \quad (13)$$

(a) A unit-step function $\mathbf{1}(t)$



(b) A unit-impulse function $\delta(t)$

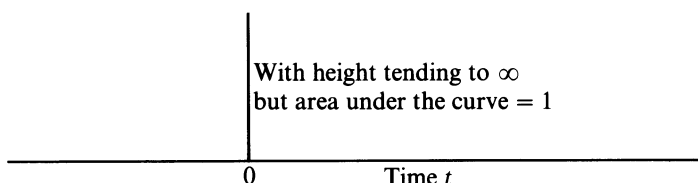


Figure 2.11:2 (a) A unit-step function $\mathbf{1}(t)$. (b) A unit-impulse function $\delta(t)$. The central spike has a height tending to ∞ but the area under the curve remains to be unity.

A body that obeys a load-deflection relation like that given by Maxwell's model is said to be a *Maxwell solid*. Since a dashpot behaves as a piston moving in a viscous fluid, the above-named models are called models of viscoelasticity.

Interchanging the roles of F and u , we obtain the *relaxation function* as a response $F(t) = k(t)$ corresponding to an elongation $u(t) = \mathbf{1}(t)$. The relaxation function $k(t)$ is the force that must be applied in order to produce an elongation that changes at $t = 0$ from zero to unity and remains unity thereafter. They are

Maxwell solid:

$$k(t) = \mu e^{-(\mu/\eta)t} \mathbf{1}(t), \quad (14)$$

Voigt solid:

$$k(t) = \eta \delta(t) + \mu \mathbf{1}(t), \quad (15)$$

Standard linear solid:

$$k(t) = E_R \left[1 - \left(1 - \frac{\tau_\sigma}{\tau_e} \right) e^{-t/\tau_e} \right] \mathbf{1}(t). \quad (16)$$

Here we have used the symbol $\delta(t)$ to indicate the *unit-impulse function or Dirac-delta function*, which is defined as a function with a singularity at the origin (see Fig. 2.11:2(b)):

$$\begin{aligned} \delta(t) &= 0 && (\text{for } t < 0, \text{ and } t > 0), \\ \int_{-\varepsilon}^{\varepsilon} f(t) \delta(t) dt &= f(0) && (\varepsilon > 0), \end{aligned} \quad (17)$$

where $f(t)$ is an arbitrary function, continuous at $t = 0$. These functions, $c(t)$ and $k(t)$, are illustrated in Figs. 2.11:3 and 2.11:4, respectively, for which we add the following comments.

For the Maxwell solid, the sudden application of a load induces an immediate deflection by the elastic spring, which is followed by "creep" of the dashpot. On the other hand, a sudden deformation produces an immediate reaction by the spring, which is followed by stress relaxation

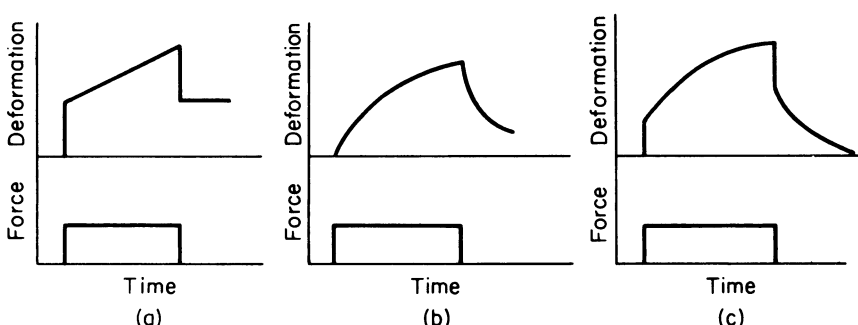


Figure 2.11:3 Creep functions of (a) a Maxwell, (b) a Voigt, and (c) a standard linear solid. A negative phase is superposed at the time of unloading.

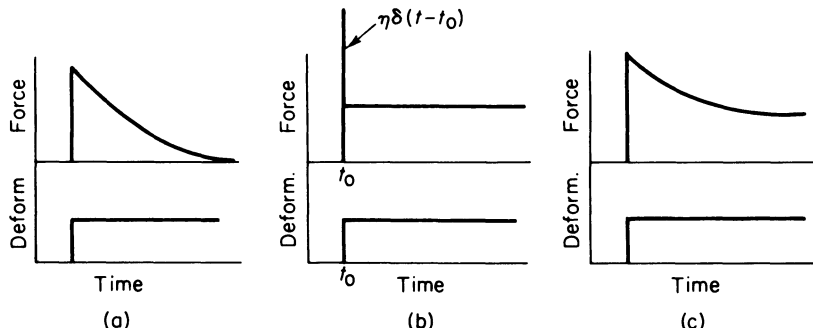


Figure 2.11:4 Relaxation functions of (a) a Maxwell, (b) a Voigt, and (c) a standard linear solid.

according to an exponential law [see Eq. (14)]. The factor η/μ , with the dimension of time, may be called the *relaxation time*: it characterizes the rate of decay of the force.

For the Voigt solid, a sudden application of force will produce no immediate deflection, because the dashpot, arranged in parallel with the spring, will not move instantaneously. Instead, as shown by Eq. (11) and Fig. 2.11:3, a deformation will be gradually built up, while the spring takes a greater and greater share of the load. The dashpot displacement relaxes exponentially. Here the ratio η/μ is again a relaxation time: it characterizes the rate of relaxation of the dashpot.

For the standard linear solid, a similar interpretation is applicable. The constant τ_e is the time of relaxation of load under the condition of constant deflection [see Eq. (16)], whereas the constant τ_σ is the time of relaxation of deflection under the condition of constant load [see Eq. (12)]. As $t \rightarrow \infty$, the dashpot is completely relaxed, and the load-deflection relation becomes that of the springs, as is characterized by the constant E_R in Eqs. (12) and (16). Therefore, E_R is called the *relaxed elastic modulus*.

Maxwell introduced the model represented by Eq. (3), with the idea that all fluids are elastic to some extent. Lord Kelvin showed the inadequacy of the Maxwell and Voigt models in accounting for the rate of dissipation of energy in various materials subjected to cyclic loading. Kelvin's model is commonly called the standard linear model because it is the most general relationship that includes the load, the deflection, and their first (commonly called "linear") derivatives.

More general models may be built by adding more and more elements to the Kelvin model. Equivalently, we may add more and more exponential terms to the creep function or to the relaxation function.

The most general formulation under the assumption of linearity between cause and effect is due to Boltzmann (1844–1906). In the one-dimensional case, we may consider a simple bar subjected to a force $F(t)$ and elongation $u(t)$. The elongation $u(t)$ is caused by the total history of the loading up to the time t . If the function $F(t)$ is continuous and differentiable, then in a

small time interval $d\tau$ at time τ the increment of loading is $(dF/d\tau) d\tau$. This increment remains acting on the bar and contributes an element $du(t)$ to the elongation at time t , with a proportionality constant c depending on the time interval $t - \tau$. Hence, we may write

$$du(t) = c(t - \tau) \frac{dF(\tau)}{d\tau} d\tau. \quad (18)$$

Let the origin of time be taken at the beginning of motion and loading. Then, on summing over the entire history, which is permitted under Boltzmann's hypothesis, we obtain

$$u(t) = \int_0^t c(t - \tau) \frac{dF(\tau)}{d\tau} d\tau. \quad (19)$$

A similar argument, with the role of F and u interchanged, gives

$$F(t) = \int_0^t k(t - \tau) \frac{du(\tau)}{d\tau} d\tau. \quad (20)$$

These laws are linear, since doubling the load doubles the elongation, and vice versa. The functions $c(t - \tau)$ and $k(t - \tau)$ are the *creep* and *relaxation functions*, respectively.

The Maxwell, Voigt, and Kelvin models are special examples of the Boltzmann formulation. More generally, we can write the relaxation function in the form

$$k(t) = \sum_{n=0}^N \alpha_n e^{-tv_n}, \quad (21)$$

which is a generalization of Eq. (16). If we plot the amplitude α_n associated with each characteristic frequency v_n on a frequency axis, we obtain a series of lines that resembles an optical spectrum. Hence $\alpha_n(v_n)$ is called a *spectrum of the relaxation function*. The example shown in Fig. 2.11:5 is a *discrete spectrum*. A generalization to a *continuous spectrum* may sometimes be desired. In the case of a living tissue such as mesentery, experimental results on relaxation, creep, and hysteresis cannot be reconciled unless a continuous spectrum is assumed.

Let us conclude this section by generalizing Eqs. (19) and (20) into tensor equations relating stress and strain tensors of a viscoelastic solid. All we need

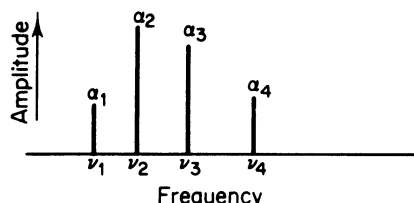


Figure 2.11:5 A discrete spectrum of the relaxation function.

to say here is that if F and u are considered to be stress and strain tensors, then Eqs. (19) and (20) can be considered as constitutive equations of a viscoelastic solid if c and k are tensors defining the creep and relaxation characteristics of the material. We do have to be careful about the time derivatives \dot{F} and \dot{u} if the deformation is large, because then the time derivatives of the components of stress and strain of any material particle (such as the small cubic element shown in Fig. 2.2:3) may depend not only on how fast the element stretches, but also on how fast it rotates. To account for the stress rate (i.e., the rate of change of the stress tensor) in finite deformation turns out to be quite complex.* Hence, for the moment let us limit our consideration to a small deformation, with infinitesimal displacements, strains, and velocities. Under this restriction we can express our idea more explicitly. Let us denote the stress and strain tensors by σ_{ij} and e_{ij} (which are functions of space \mathbf{x} (i.e., x_1, x_2, x_3) and time t .) Then a material is said to be *linear viscoelastic* if $\sigma_{ij}(\mathbf{x}, t)$ is related to $e_{ij}(\mathbf{x}, t)$ by the following convolution integral:

$$\sigma_{ij}(\mathbf{x}, t) = \int_{-\infty}^t G_{ijkl}(\mathbf{x}, t - \tau) \frac{\partial e_{kl}}{\partial \tau}(\mathbf{x}, \tau) d\tau, \quad (22)$$

or its inverse,

$$e_{ij}(\mathbf{x}, t) = \int_{-\infty}^t J_{ijkl}(\mathbf{x}, t - \tau) \frac{\partial \sigma_{kl}}{\partial \tau}(\mathbf{x}, \tau) d\tau. \quad (23)$$

G_{ijkl} is called the *tensorial relaxation function*. J_{ijkl} is called the *tensorial creep function*. Note that the lower limit of integration is taken as $-\infty$, which is to mean that the integration is to be taken before the very beginning of motion. If the motion starts at time $t = 0$, and $\sigma_{ij} = e_{ij} = 0$ for $t < 0$, then Eq. (22) reduces to

$$\sigma_{ij}(\mathbf{x}, t) = e_{kl}(\mathbf{x}, 0+) G_{ijkl}(\mathbf{x}, t) + \int_0^t G_{ijkl}(\mathbf{x}, t - \tau) \frac{\partial e_{kl}}{\partial \tau}(\mathbf{x}, \tau) d\tau, \quad (24)$$

where $e_{ij}(x, 0+)$ is the limiting value of $e_{ij}(x, t)$ when $t \rightarrow 0$ from the positive side. The first term in Eq. (24) gives the effect of initial disturbance: it arises from the jump of $e_{ij}(x, t)$ at $t = 0$. If the strain history contains other jumps at other instants of time, then each jump calls for an additional term similar to the first term in Eq. (24).

2.12 Response of a Viscoelastic Body to Harmonic Excitation

Since biological tissues are all viscoelastic, and since one of the simplest ways to experimentally determine the viscoelastic properties is to subject the material to periodic oscillations, we shall discuss this case in greater detail.

* See Fung (1965), *Solid Mechanics*, p. 448 for details.

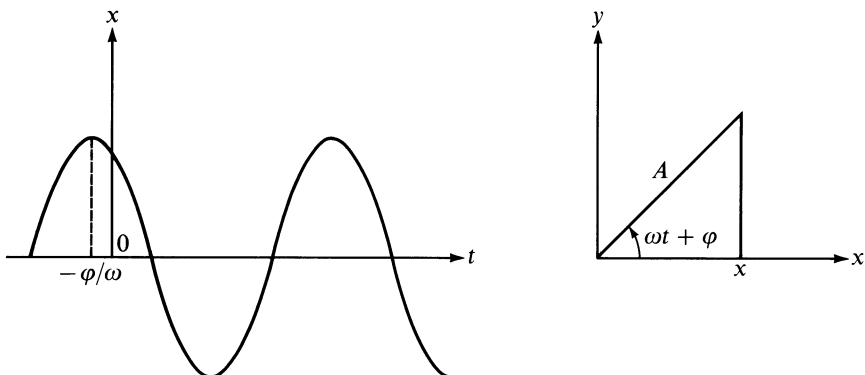


Figure 2.12:1 Complex representation of a harmonic motion.

Consider a quantity x , which varies periodically with frequency ω (radians per second) according to the rule

$$x = A \cos(\omega t + \varphi). \quad (1)$$

This is a *simple harmonic motion*; A is the *amplitude* and φ is the *phase angle*. We may consider x to be the projection of a rotating vector on the real axis (see Fig. 2.12:1). Since a vector is specified by two components, it can be represented by a complex number. For example, the vector in Fig. 2.12:1 can be specified by the components $x = A \cos(\omega t + \varphi)$ and $y = A \sin(\omega t + \varphi)$, and hence by the complex number $x + iy$. But

$$e^{i(\omega t + \varphi)} = \cos(\omega t + \varphi) + i \sin(\omega t + \varphi), \quad (2)$$

so the rotating vector can be represented by the complex number

$$x + iy = Ae^{i(\omega t + \varphi)} = Be^{i\omega t}, \quad (3)$$

where

$$B = Ae^{i\varphi}. \quad (3a)$$

Equation (1) is the real part of Eq. (3), and the latter is said to be the *complex representation* of Eq. (1). B is a complex number whose absolute value is the *amplitude*, and whose polar angle $\varphi = \text{arc tan}(\text{Im } B/\text{Re } B)$ is the *phase angle* of the motion.

The vector representation is very convenient for “composing” several simple harmonic oscillations of the same frequency. For example, if

$$x = A_1 \cos(\omega t + \varphi_1) + A_2 \cos(\omega t + \varphi_2) = A \cos(\omega t + \varphi), \quad (4)$$

then x is the real part of the resultant of two vectors as shown in Fig. 2.12:2.

Now, if the force and displacement are harmonic functions of time, then we can apply complex representation. Let $u = U e^{i\omega t}$. Then by differentiation with respect to t , we have $\dot{u} = i\omega U e^{i\omega t} = i\omega u$. In this case a differentiation

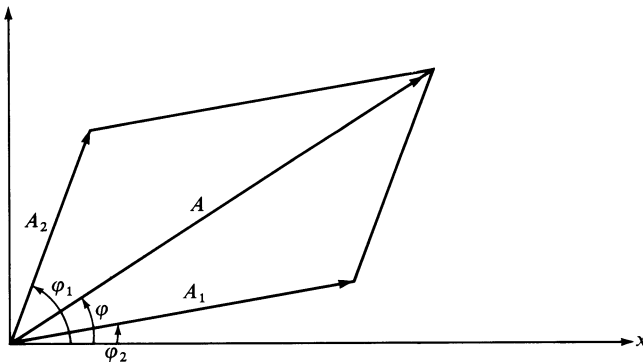


Figure 2.12:2 Vector sum of two simple harmonic motions of the same frequency.

with respect to t is equivalent to a multiplication by $i\omega$. Applying this result to Eq. (1) of Sec. 2.11, we obtain

$$i\omega u = \frac{i\omega F}{\mu} + \frac{F}{\eta}. \quad (5)$$

This can be written in the form

$$F = G(i\omega)u, \quad (6)$$

which is the same as

$$Fe^{i\omega t} = G(i\omega)ue^{i\omega t}, \quad (6a)$$

where $G(i\omega)$ is called the *complex modulus of elasticity*. In the case of the Maxwell body,

$$G(i\omega) = i\omega \left(\frac{i\omega}{\mu} + \frac{1}{\eta} \right)^{-1}. \quad (7)$$

In a similar manner, Eqs. (3), (7), (19), (20), (22), and (23) of Sec. 2.11 can all be put into the form of Eq. (6), and the complex modulus of each model can be derived.

The complex modulus of elasticity of the Kelvin body (standard linear solid), corresponding to Eq. (7) of Sec. 2.11, is

$$G(i\omega) = \frac{1 + i\omega\tau_\sigma}{1 + i\omega\tau_\epsilon} E_R. \quad (8)$$

Writing

$$G(i\omega) = |G|e^{i\delta}, \quad (9)$$

where $|G|$ is the amplitude of the complex modulus and δ is the phase shift, we have

$$|G| = \left(\frac{1 + \omega^2\tau_\sigma^2}{1 + \omega^2\tau_\epsilon^2} \right)^{1/2} E_R, \quad \tan \delta = \frac{\omega(\tau_\sigma - \tau_\epsilon)}{1 + \omega^2(\tau_\sigma\tau_\epsilon)}. \quad (10)$$

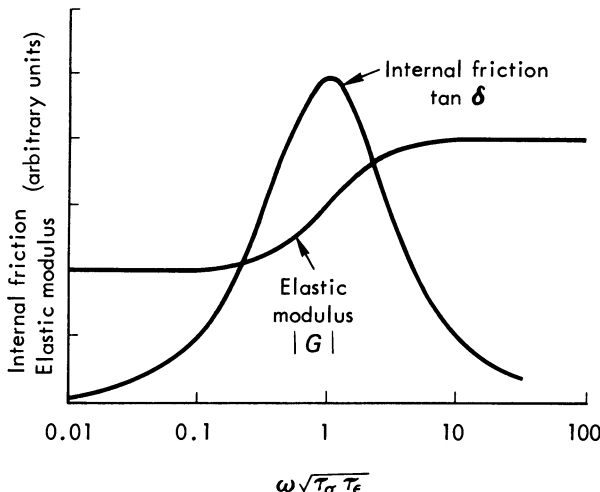


Figure 2.12:3 The dynamic modulus of elasticity $|G|$ and the internal damping $\tan \delta$ plotted as a function of the logarithm of frequency ω for a standard linear solid.

The quantity $\tan \delta$ is a measure of “internal friction.” When $|G|$ and $\tan \delta$ are plotted against the logarithm of ω , curves as shown in Fig. 2.12:3 are obtained. The internal friction reaches a peak when the frequency ω is equal to $(\tau_\sigma \tau_\epsilon)^{-1/2}$. Correspondingly, the elastic modulus $|G|$ has the fastest rise for frequencies in the neighborhood of $(\tau_\sigma \tau_\epsilon)^{-1/2}$.

2.13 Use of Viscoelastic Models

The viscoelastic models discussed in the previous sections are especially useful in biomechanics because biological tissues have viscoelastic features. In the laboratory, it is quite easy to determine the relaxation and creep curves. With suitable testing machines it is also easy to determine the complex modulus of a material subjected to a periodic forcing function. The amplitude and phase angle of the complex modulus can be plotted with respect to the frequency of oscillation. Having determined these curves experimentally, we try to fit them with a model. If a model (i.e., a differential equation such as Eqs. (1), (3), or (7) of Sec. 2.11, or a complex modulus such as that given in Eq. (8) of Sec. 2.12) can be found whose relaxation, creep, hysteresis, and complex modulus agree with the experimental data, then the material tested can be described by this model. Each model contains only a few material constants (such as η_1 , μ_1 , or τ_σ , τ_ϵ , E_R). The reams of experimental curves can then be replaced by a list of these material constants. Furthermore, the constitutive equation can then be used to analyze other problems concerned with the tissue. Many examples of such applications are presented in the chapters to follow.

I am not sure who first drew the model diagrams and wrote down Eqs. (1), (3), and (7) of Sec. 2.11, but the work of the people to whom these models are attributed is well known. James Clerk Maxwell (1831–1879), one of the greatest theoretical physicists of all times, was born in Edinburgh. When he was appointed to the newly founded professorship of experimental physics in Cambridge in 1871, he set about to establish a laboratory to study mechanical properties of matter. The first object of interest was air. He felt that air is viscoelastic. He built a testing machine consisting of two parallel disks rotating relative to each other to measure the viscosity of air. His mathematical description of air is the Maxwell model of viscoelasticity.

Woldemar Voigt (1850–1919) was a German physicist especially known for his work on crystallography. The Voigt model was named in his honor.

William Thomson (Lord Kelvin), 1824–1907, was born in Belfast, Ireland. He was educated at home by his father, James Thomson, a professor of mathematics at Glasgow. In 1846 he himself became a professor in the University of Glasgow. In the period 1848–1851 Thomson worked on the dynamic theory of heat and formulated the first and second laws of thermodynamics, which reconciled the work of Carnot, Rumford, Davy, Mayer, and Joule. In connection with the second law, he searched for supporting evidence in irreversible processes that are revealed in the mechanical properties of matter. He tested metals, rubber, cork, etc., in the form of a torsional pendulum (using these materials as the torsional spring). When the pendulum was set in motion, the amplitude of its oscillations decayed exponentially, and the number of cycles required for the amplitude to be reduced to one-half of the initial value could be taken as a measure of the “internal friction” of the material. Kelvin found that the material behavior can be explained by a model system possessing a spring and a dashpot, in parallel with another spring.

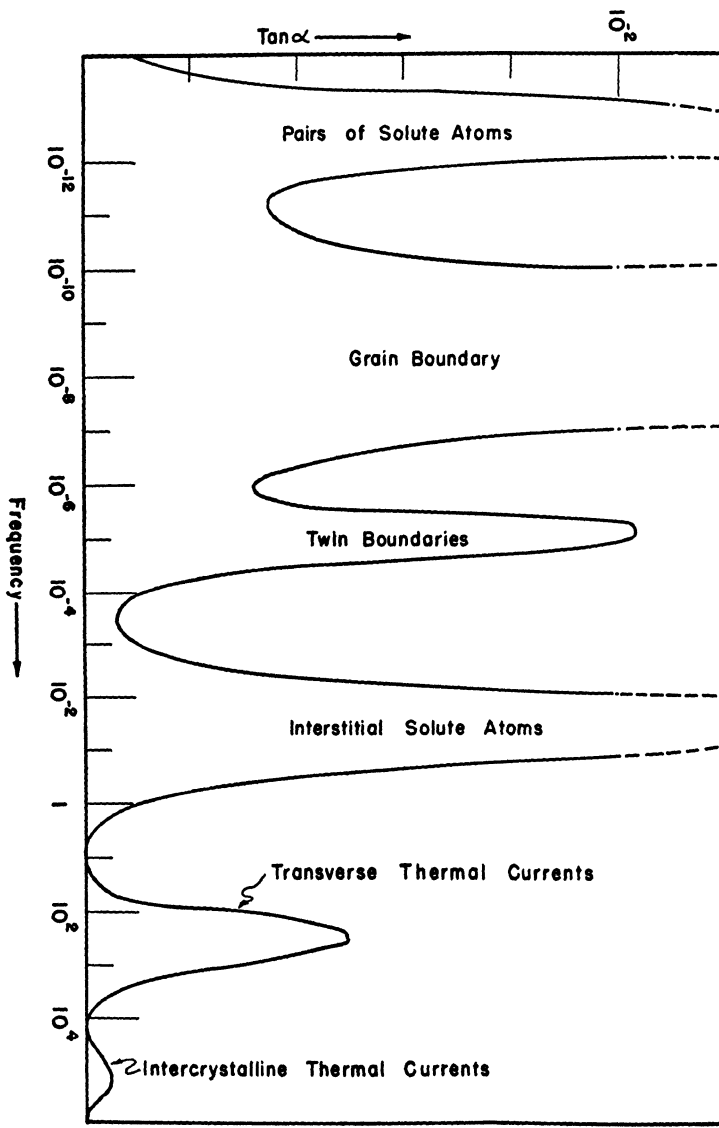
Thus, we see that these models were invented to correlate experimental data on real materials. Further generalization of these models, as is shown in Problems 2.12–2.16, may be necessary to correlate experimental data of a more complex nature.

The question of choosing the right model to fit the experimental data is an important one. Usually the first step is to compare the experimental curves of relaxation, creep, frequency response, and internal friction (complex modulus) with those of the theoretical models, such as those shown in Figs. 2.11:3, 2.11:4, and 2.12:3. If they look alike, then a curve fitting procedure can be used to determine the best constants. If the simple models cannot yield the desired features, then it would be necessary to consider generalized models, such as those listed in Problems 2.12–2.16 infra. Hints are often obtainable from the general character of the theoretical and experimental curves. For example, the generalized Kelvin or Voigt models of order n would have a relaxation function of the type

$$k(t) = a + c_1 e^{-t/\tau_1} + c_2 e^{-t/\tau_2} + \cdots + c_n e^{-t/\tau_n}, \quad (1)$$

which contains n exponential functions. The creep functions would also contain n exponential functions. The imaginary part of the corresponding

complex modulus of elasticity, representing the internal friction, would have n peaks in the frequency spectrum. The real part of the complex modulus, plotted with respect to frequency, would look like a staircase with n steps. If such were the features of the experimental curve, then a generalized linear viscoelastic model of order n is suggested.



A TYPICAL RELAXATION SPECTRUM

Figure 2.13:1 A typical relaxation spectrum of a polycrystalline metal. Reproduced by permission from C. Zener (1948) *Elasticity and Anelasticity of Metals*. University of Chicago Press, Chicago.

A typical internal friction spectrum, i.e., a plot of $\tan \alpha = \text{Im } G / \text{Re } G$ according to Eq. (10) of Sec. 2.12 versus frequency, for a polycrystalline metal is shown in Fig. 2.13:1, from Zener (1948). Each of the peaks is identified with a physical activity in the metal, as indicated in the figure. The largest peak arises from the grain boundaries, where crystals of different orientations meet. When deformation of the metal occurs, the deformations of individual crystals interfere with each other, and the dislocations are transported toward the grain boundary and become accumulated there. This process is irreversible and energy dissipating, leading to anelasticity. A second peak comes from the interstitial solute atoms (e.g., hydrogen) which seek to stay at potential wells and move to different lattice points when the crystal is strained. When the strain fluctuates the solute atoms oscillate and dissipate energy. A third cause is twinning, which is a uniform change in inclination in the bands of the crystal lattice which occurs in metals such as copper. The twin boundaries oscillate with fluctuating strain. Other bands in Fig. 2.13:1 represent other strain-related relaxation phenomena. Thermal current arises because deformations generate heat and because crystals of different orientation generate heat nonuniformly and out of phase with the strain. A magnetic field changes the volume of ferromagnetic material; hence an oscillating magnetic field and strain are other sources of viscoelasticity. Figure 2.13:1 illustrates the case of metals; but by analogy it should lead us to anticipate the existence of a relaxation spectrum for biopolymers and living tissues. Note the extraordinarily wide range of frequency shown on the horizontal axis of Fig. 2.13:1. At the room temperature, it is quite impossible to make experiments over such a wide range of frequencies. Actual tests were done at different temperatures, and the data were converted to room temperature by certain thermomechanical considerations.

It often happens that many relaxation functions of the type of Eq. (1) can fit the relaxation data (because the determination of the constants $c_1, c_2 \dots \tau_1, \tau_2 \dots$ is nonunique and multiple choices are possible). Similarly, many such functions can fit the creep data. Then a choice can be made by demanding that the chosen model be the one that fits *all* the experimental data, including relaxation, creep, hysteresis, amplitude of the complex modulus, and the internal friction spectrum. An example of this is given in Sec. 7.6.

It may happen that none of the models can fit *all* the experimental data. Then we may have to concede that the linearized viscoelasticity theory does not apply at all.

Problems

- 2.12** Consider the generalized Kelvin model of a linear viscoelastic body as shown in Fig. P2.12(a), where μ 's are spring constants and η 's are the viscosity coefficients of the dashpots. Derive (a) the differential equation relating the force F and displacement u , (b), the creep function, and (c), the relaxation function.

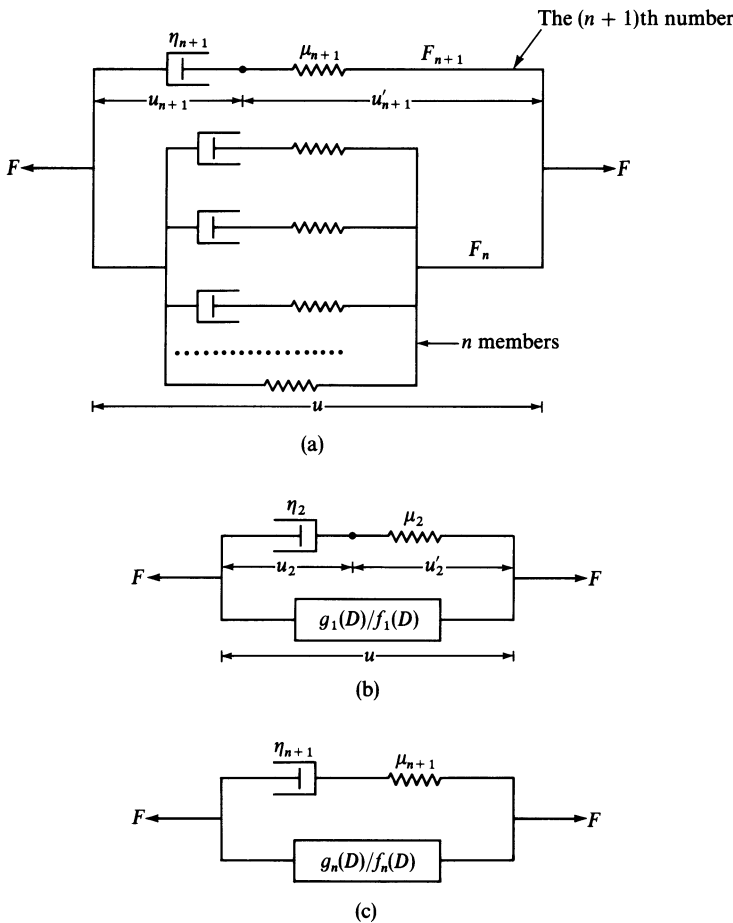


Figure P2.12 A generalized Kelvin body.

Solution. A Kelvin body may be regarded as adding a Maxwell body (see Fig. 2.11:1) in parallel with a spring. A *generalized Kelvin body of order n* is one that has n Maxwell bodies in parallel with a spring. See Fig. P2.12:(a). To derive the differential equation that governs the generalized Kelvin body, note first that if we write d/dt by the symbol D , then Eq. (7) of Sec. 2.11 can be written symbolically as

$$f_1(D)F = g_1(D)u, \quad (1)$$

where

$$f_1(D) = 1 + \frac{\eta_1}{\mu_1}D, \quad g_1(D) = \mu_0 \left(1 + \frac{\eta_1}{\mu_1}D \right) + \eta_1 D. \quad (2)$$

This is the equation for a Kelvin body, or a *generalized Kelvin body of order 1*. We can also write Eq. (1) symbolically as

$$F = \frac{g_1(D)}{f_1(D)} u. \quad (3)$$

Now consider a *generalized Kelvin body of order 2*. This may be represented symbolically as in Fig. P2.12.(b). Compare this with Fig. 2.11:1. We see that they are the same if μ_0 is replaced by $g_1(D)/f_1(D)$, and all subscripts 1 are replaced by subscript 2. Thus we can deduce its differential equation,

$$f_2(D)F = g_2(D)u, \quad (4)$$

with

$$\begin{aligned} f_2(D) &= f_1(D) \left(1 + \frac{\eta_2}{\mu_2} D \right), \\ g_2(D) &= g_1(D) \left(1 + \frac{\eta_2}{\mu_2} D \right) + \eta_2 f_1(D)D. \end{aligned} \quad (5)$$

Finally, consider the *generalized Kelvin body of order $n + 1$* as shown in Fig. P2.12(a). It is equivalent to the symbolic version shown in Fig. P2.12(c). Hence, we can readily write down its differential equation,

$$f_{n+1}(D)F = g_{n+1}(D)u, \quad (6)$$

where

$$\begin{aligned} f_{n+1}(D) &= f_n(D) \left(1 + \frac{\eta_{n+1}}{\mu_{n+1}} D \right), \\ g_{n+1}(D) &= g_n(D) \left(1 + \frac{\eta_{n+1}}{\mu_{n+1}} D \right) + \eta_{n+1} f_n(D)D. \end{aligned} \quad (7)$$

- 2.13** Determine the complex modulus of elasticity of the generalized Kelvin body of order n when it is subjected to a periodic force of circular frequency ω (rad/s).
- 2.14** A *generalized Maxwell body of order n* is one that is composed of a spring and n Voigt bodies connected in series, as illustrated in Fig. P2.14. Determine the differential equation relating the force and displacement of such a body, and the appropriate initial conditions. Derive the complex modulus when the body is subjected to a periodic force of circular frequency ω rad/s.

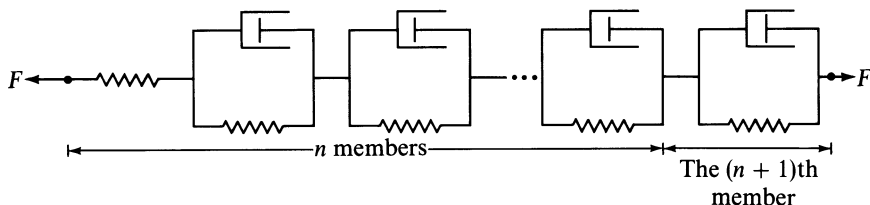


Figure P2.14 A generalized Maxwell body.

- 2.15** If Voigt models were put in series as shown in Fig. P2.15, then since for the i th unit, $F = \mu_i u_i + \eta_i \dot{u}_i$ so that $u_i = (\mu_i + \eta_i D)^{-1} F$, we have

$$u = u_1 + u_2 + \cdots + u_n = \sum_{i=1}^n \frac{1}{\mu_i + \eta_i D} F.$$

Show that the model retains the undesirable feature of the Voigt model: a step displacement calls for an infinitely large force at the instant of step application. This feature is corrected by adding a spring as in the model shown in Fig. P2.14.

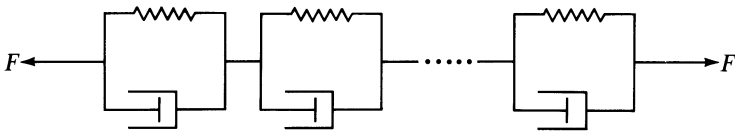


Figure P2.15 Voigt models in series.

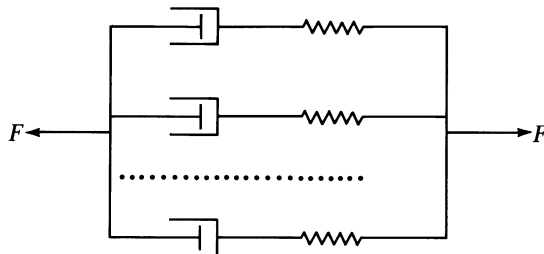


Figure P2.16 Maxwell models in parallel.

2.16 If n Maxwell models are put in parallel as shown in Fig. P2.16, show that

$$F = \sum_{i=1}^n \frac{D}{D/\mu_i + 1/\eta_i} u.$$

This system still has the feature of a Maxwell model: a constant force will produce an infinitely large displacement u when time $t \rightarrow \infty$. This difficulty can be corrected by adding a spring as in the Kelvin model. Compare Fig. P2.16 with Fig. P2.12.

2.14 Methods of Testing

The ideal constitutive equations named above are abstractions of nature. The vast literature of fluid and solid mechanics is based principally on these idealized equations. Behavior of materials in the biological world usually deviates from these simple relationships. It is important to test the materials to determine how closely their mechanical behavior can be represented by simplified constitutive equations.

Testing the mechanical properties of biological materials does not differ in principle from testing industrial materials, except possibly in three aspects: (1) it is seldom possible to get large samples of biological materials; (2) strict attention must be given to keep the samples viable and in a condition as close as possible to that *in vivo*; and finally (3), many materials are nonhomogeneous. These special features usually call for special testing methods and equipment. In this section, only a few methods of testing will be discussed. Others will be presented later when occasions arise.

One of the most popular methods for measuring fluid viscosity uses flow in a long circular cylindrical tube. A standard type, the Ostwald viscometer,

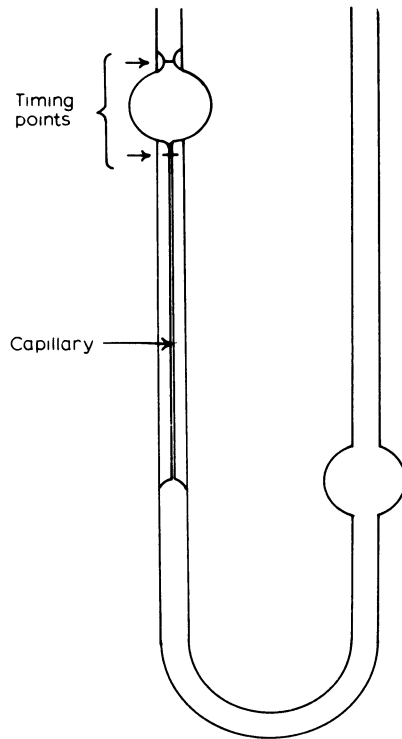


Figure 2.14:1 An Ostwald viscometer.

is shown in Fig. 2.14:1. It is known (see Eq. (8) of Sec. 3.3) that for a Newtonian fluid in a laminar (nonturbulent) flow in such a tube the coefficient of viscosity η is related to the pressure gradient dp/dL , the volume rate of flow \dot{Q} , and the tube radius R by the equation

$$\eta = \frac{\pi R^4}{8\dot{Q}} \frac{dp}{dL}. \quad (1)$$

If pressure is given in dyn/cm^2 , L and R in cm, and \dot{Q} in cm^3/s , then η is in $\text{dyn s}/\text{cm}^2$, or poise. If pressure is given in N/m^2 , or Pascal, and length in m, then η is in $\text{N}\cdot\text{s}/\text{m}^2$. One poise equals $0.1 \text{ Ns}/\text{m}^2$. To use Eq. (1) to calculate η , one must make sure that the flow is laminar, and that the “end effect” is corrected for, i.e., instead of using P/L for dp/dL , where P is the difference of pressures at the ends and L is the length of the “capillary,” one makes corrections for the anomaly at the ends, including the “kinetic energy correction” to allow for the effects of accelerations with the sudden change of radius of the vessel through which the fluid flows. An Ostwald viscometer may be used to test a non-Newtonian fluid (such as blood) to determine the “apparent” viscosity, (see Sec. 5.2 for definition), but methods for correcting the end effects are often unknown for non-Newtonian fluids.

A variation of the microcapillary viscometer useful for small samples is to measure the rate of filling or emptying of a “capillary” (small) tube. In this case, the length of the column of material (L) varies, and the pertinent equations are

$$\text{For filling: } \eta = \frac{t}{L^2} \cdot \frac{PR^2}{4}; \quad (2)$$

$$\text{For emptying: } \eta = \frac{t}{L_0^2 - L^2} \cdot \frac{PR^2}{4}; \quad (3)$$

where t is the time. L_0 is the initial length of the column, and P is the applied pressure differential. Very short columns should be corrected for errors caused by surface tension.

Another popular viscometer is the Couette type, using flow between two coaxial cylinders. An example is shown in Fig. 2.14:2. The outer cylinder (radius R_2), which contains the sample, is rotated at a constant angular speed ω . The inner cylinder (radius R_1) is suspended on a torsion wire centrally within the outer cylinder, so that the material to be tested fills the annular space between the cylinders. The viscosity of the liquid causes a torque to be transmitted to the inner cylinder which can be measured by a transducer. The shear rate is not constant across the gap, but the variation is small if the gap is small. The viscosity for a Newtonian fluid in a Couette viscometer is given by the equation

$$\eta = \frac{M(R_2^2 - R_1^2)}{4\pi\omega h R_1^2 R_2^2}$$

where M is the measured torque, h is the height of the inner cylinder immersed in the liquid, and ω is the angular speed of the outer cylinder.

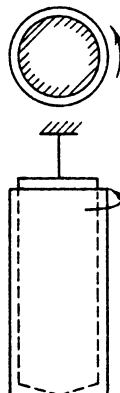


Figure 2.14:2 A Couette viscometer.

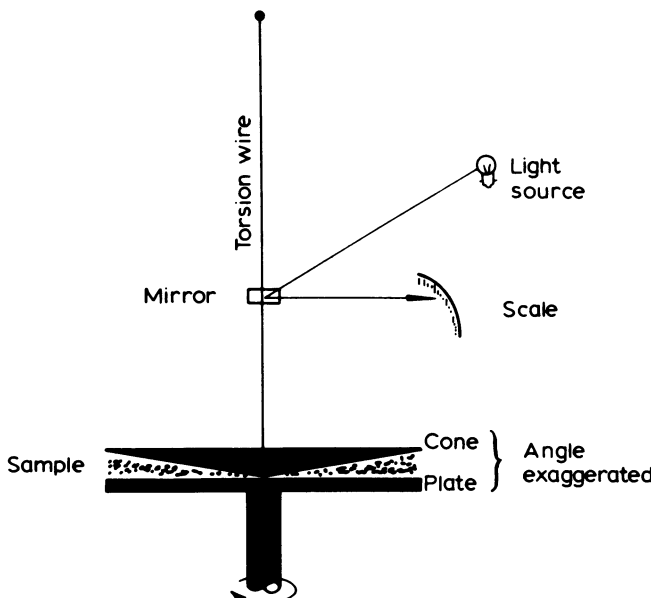


Figure 2.14:3 A cone-plate rheometer.

For higher accuracy and smaller samples, one may use the cone-plate viscometer illustrated in Fig. 2.14:3. The sample occupies the conical space. When the plate rotates, the linear velocity increases with the radial distance; but since the gap also increases linearly with the radius, the shear rate remains constant throughout if the cone remains stationary. One might suppose that the magnitude of the cone angle would not matter; but, for rather complex hydrodynamic reasons, this is not the case, and very flat cones must be used.

The Couette or cone-plate rheometers can be operated not only with a steady rotation at constant speed, but also in an oscillatory mode. The lower cylinder, cone, or plate is caused to oscillate harmonically, and the torque response of the upper member can be recorded. The magnitude and phase relationship between the torque and shear rate will yield the complex modulus of a viscoelastic material (see Sec. 2.12).

A general instrument called Weissenberg's "rheogoniometer" can be used either for rotation or for sinusoidal oscillation, and can operate with either coaxial cylinders or cone-plates. It can measure not only the torque, but also the normal force (the "upthrust") on the upper member. The upthrust, known as the "Weissenberg effect," occurs in certain non-Newtonian fluids when they are sheared. If such a fluid is sheared between two cylinders (in rotation) as in a Couette flow, the fluid will climb up the inner cylinder if it is not totally immersed. The rheogoniometer measures such a thrust; hence, it measures forces "at all angles" (Greek, *gonia*, angle).

There are other types of rheometers that measure complex moduli. In one of these a vertical rod is oscillated sinusoidally within a hollow cylinder containing the material. In another the material is placed between a spherical bob and a concentric hemispherical cup. A third one uses a tuning fork to drive an oscillatory rod in the fluid, either in axial motion or in lateral motion.

Another popular method is that of a falling (or rising) sphere. In the simplest case, a metal or plastic sphere is timed as it falls or rises through a known distance in a liquid. If the liquid is opaque, the passage of the ball can be detected electromagnetically. If the fluid is Newtonian, and the container is much larger than the sphere, and if the Reynolds number is much smaller than 1, then the falling velocity is given by Stokes' formula,

$$v = \frac{2r^2 \Delta \rho g}{9\eta},$$

where v is the velocity of fall, r is the radius of the sphere, $\Delta \rho$ is the difference between the densities of the sphere and of the liquid, and g is the gravitational constant. Unfortunately, this formula does not work if the Reynolds number ($vr\rho/\eta$) is greater than 1, and if the container is not very much larger than the sphere. In the case of a large Reynolds number or a small container, more complex hydrodynamic considerations must be given. Sometimes a sphere rolling or sliding down an inclined plane is used to determine the viscosity of the fluid; in such cases, careful corrections must be made for inertia effects around the sphere. Sometimes a falling sphere apparatus can be modified so that the sphere can be dragged sideways by a magnet. On release, the elastic recovery can be measured.

So far we have mentioned instruments for measuring viscosity or viscoelasticity of fluids. For solid materials there are a number of commercial testing machines available. Generally, the specimen is clamped and stretched or shortened at a specific rate while the force and displacement are both recorded. For biological specimens, the usual problems of small size and the necessity for keeping the specimen viable cause difficulty. Usually it is preferred that no measuring instrument should touch the specimen in the region where deformation is measured.

A noncontact method for three-dimensional analysis of blood vessels *in vivo* and *in vitro* is shown in Fig. 2.14:4. The vessel is soaked in a saline bath at 37°C. The dimensions between markers in the longitudinal and circumferential directions are measured with two closed-circuit television cameras (TV) and two video dimension analyzers (VDA). By rotating the camera, any scene may be selected, and the image can be magnified to any size by introducing different lenses and extension tubes in the camera optics. At a given optical magnification, the resolution of the obtainable measurements is limited primarily by the TV camera. With a quality camera, resolution exceeding 0.1% of full width of the screen is readily attainable. The VDA utilizes the video signal from the TV camera, and forms a DC voltage analog of the distance between two selected points in the scene. The optical

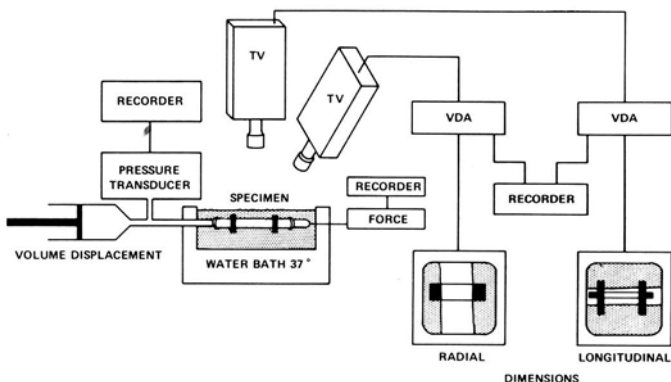


Figure 2.14:4 A noncontact method for three-dimensional analysis of vascular elasticity *in vivo* and *in vitro*. From Fronek, K., Schmid-Schoenbein, G., and Fung, Y. C. (1976) *J. Appl. Physiol.* 40, 634–637.

density of the space between the two points must be sufficiently different from that of the surrounding space. Following acquisition, dimensional changes are automatically tracked. Since the image tube of a standard TV camera is scanned horizontally to form the video signal to be transmitted to the monitor, dimensions measured by an interposed VDA are synchronized along the horizontal axis. The resulting analog voltage, precalibrated in dimensional units of interest, can be displayed on a meter or strip-chart recorder. This noncontact type of optical dimension measurement makes it possible to select any portion of the specimen for study. Because the mechanical properties are influenced by the mounting of the specimen, it is an additional advantage of this approach that a middle portion uninfluenced by the stress disturbances due to clamped ends can be selected for measurement.

References

- Fung, Y. C. (1977) *A First Course in Continuum Mechanics*, 2nd edn. Prentice-Hall, Englewood Cliffs, N.J.
 Fung, Y. C. (1965) *Foundations of Solid Mechanics*. Prentice-Hall, Englewood Cliffs, N.J.

CHAPTER 3

The Flow Properties of Blood

3.1 Blood Rheology: An Outline

Blood is a marvelous fluid that nurtures life, contains many enzymes and hormones, knows when to flow and when to clot, and transports oxygen and carbon dioxide between the lungs and the cells of the tissues. We can leave the study of most of these important functions of blood to hematologists, biochemists, and pathological chemists. For biomechanics the most important information we need is the constitutive equation.

Human blood is a suspension of cells in an aqueous solution of electrolytes and nonelectrolytes. By centrifugation, the blood is separated into *plasma* and *cells*. The plasma is about 90% water by weight, 7% plasma protein, 1% inorganic substances, and 1% other organic substances. The cellular contents are essentially all *erythrocytes*, or *red cells*, with *white cells* of various categories making up less than 1/600th of the total cellular volume, and *platelets* less than 1/800th of the cellular volume. Normally, the red cells occupy about 50% of the blood volume. They are small, and number about 5 million/mm³. The normal white cell count is considered to be from 5000 to 8000/mm³, and platelets from 250 000 to 300 000/mm³. Human red cells are disk shaped, with a diameter of 7.6 μm and thickness 2.8 μm . White cells are more rounded and there are many types. Platelets are much smaller and have a diameter of about 2.5 μm .

If the blood is allowed to clot, a straw-colored fluid called *serum* appears in the plasma when the clot spontaneously contracts. Serum is similar to plasma in composition, but with one important colloidal protein, *fibrinogen*, removed while forming the clot. Most of the platelets are enmeshed in the clot.

The specific gravity of red cells is about 1.10; that of plasma is 1.03. When plasma was tested in a viscometer, it was found to behave like a Newtonian viscous fluid (Merrill et al., 1965a; Gabe and Zatz, 1968), with a coefficient of

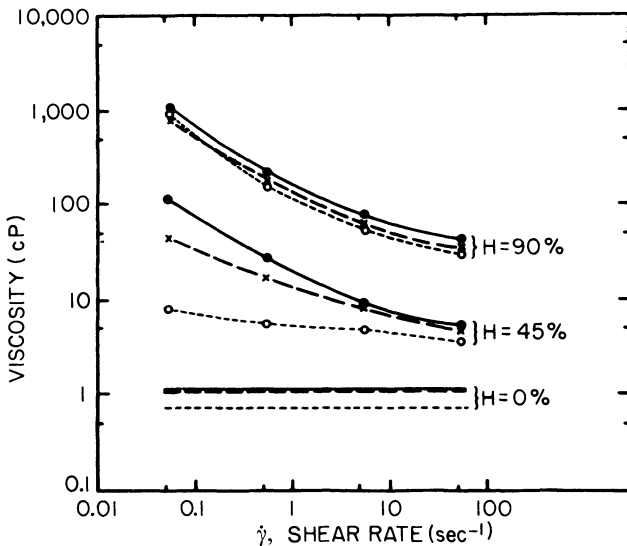


Figure 3.1:1 The viscosity-shear rate relations in whole blood (●—●), defibrinated blood (×—×), and washed cells in Ringer solution (○—○), at 45 and 90% red cell volume concentrations. From Chien et al. (1966), by permission.

viscosity about 1.2 cP (Gregersen et al., 1967; Chien et al., 1966, 1971). When whole blood was tested in a viscometer, its non-Newtonian character was revealed. Fig. 3.1:1 shows the variation of the viscosity of blood with the strain rate when blood is tested in a Couette-flow viscometer whose gap width is much larger than the diameter of the individual red cells. For the curves in Fig. 3.1:1, the shear rate $\dot{\gamma}$ is defined as the relative velocity of the walls divided by the width of the gap. The viscosity of blood varies with the *hematocrit*, H , the percentage of the total volume of blood occupied by the cells. It varies also with temperature (see Fig. 3.1:2) and with disease state, if any.

There is a question about what happens to the blood viscosity when the strain rate is reduced to zero. Cokelet et al. (1963) insist that the blood has a finite yield stress. They say that at a vanishing shear rate the blood behaves like an elastic solid. They deduced this conclusion on the basis that their torque measuring device had a rapid response, and could be used to measure transient effects. They studied the time history of the torque after the rotating bob had been stopped suddenly, and compared the transient response for blood with that for a clay suspension, which is known to have a finite yield stress. They showed that the values deduced from this experiment agreed with a few percent with those obtained by extrapolation of the Casson plot as shown in Fig. 3.1:3. Merrill et al. (1965a) also used a capillary viscometer to see if blood in a capillary could maintain a pressure difference across the tube ends without any detectable fluid flow. Such a pressure difference was detected and found to agree with the yield stress determined by Cokelet's method.

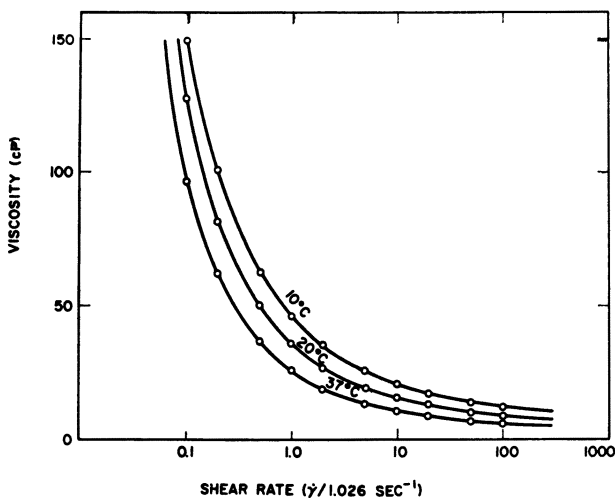


Figure 3.1:2 The variation of the viscosity of human blood with shear rate $\dot{\gamma}$ and temperature for a male donor, containing acid citrate dextrose, reconstituted from plasma and red cells to the original hematocrit of 44.8. From Merrill et al. (1963a, p. 206), by permission.

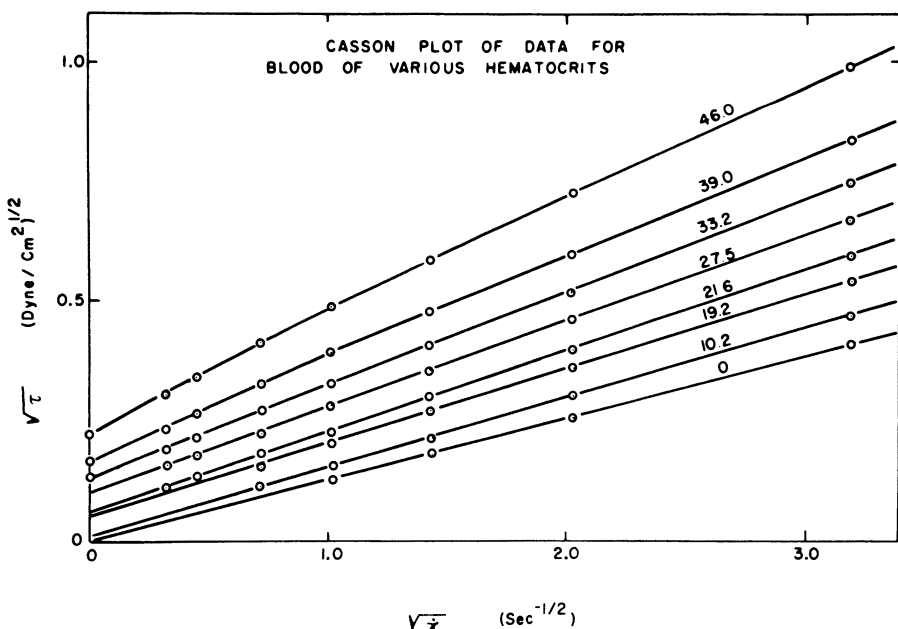


Figure 3.1:3 Casson plot of very low shear rate data for a sample of human blood at a temperature of 25°C. Range of linearity decreases as the hematocrit increases. Plasma is Newtonian. Data from Cokelet et al. (1963), by permission.

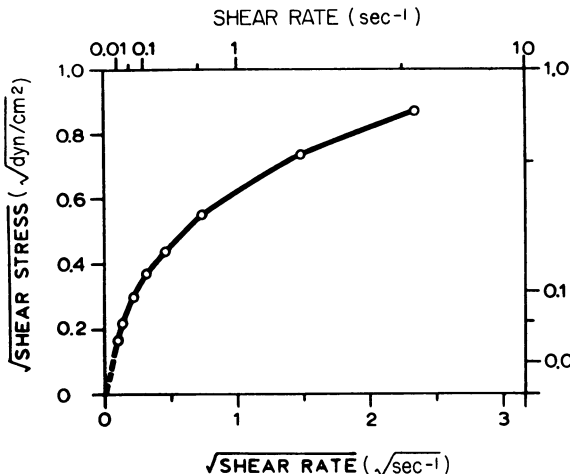


Figure 3.1:4 Casson plot for whole blood at a hematocrit of 51.7 (temp. = 37°C), according to Chien et al. (1966).

It must be understood that by “existence” of a yield stress is meant that no sensible flow can be detected in a fluid under a shearing stress in a finite interval of time (say, 15 min). The difficulty of determining the yield stress of blood as $\dot{\gamma} \rightarrow 0$ is compounded by the fact that an experiment for very small shear rate is necessarily a transient one if that experiment is to be executed in a finite interval of time. For blood the analysis is further complicated by the migration of red cells away from the walls of the viscometer when $\dot{\gamma}$ is smaller than about 1 s^{-1} . Cokelet’s analysis takes these factors into account, and requires considerable manipulation of the raw data (see Cokelet, 1972). If the maximum transient shear stress reached after the start of an experiment at constant shear rate is plotted directly with respect to the nominal shear rate, the result appears as shown in Fig. 3.1:4 by Chien et al. (1966). The differences between the plots of Figs. 3.1:3 and 3.1:4 are caused mainly by the data analysis procedures, and partly reflect the dynamics of the instrument as well as that of the blood state.

The data of Cokelet et al. for a small shear rate, say $\dot{\gamma} < 10 \text{ s}^{-1}$, and for hematocrit less than 40%, can be described approximately by Casson’s (1959) equation

$$\sqrt{\tau} = \sqrt{\tau_y} + \sqrt{\eta\dot{\gamma}} \quad (1)$$

where τ is the shear stress, $\dot{\gamma}$ is the shear strain rate, τ_y is a constant that is interpreted as the yield stress in shear, and η is a constant. The fitting of this equation to experimental data can be seen in Fig. 3.1:3, from which it is clear that for hematocrit below 33% the experimental data points fall quite accurately on straight lines. For higher hematocrit (39% and above), deviations from straight lines are more evident. The yield stress τ_y given by Merrill

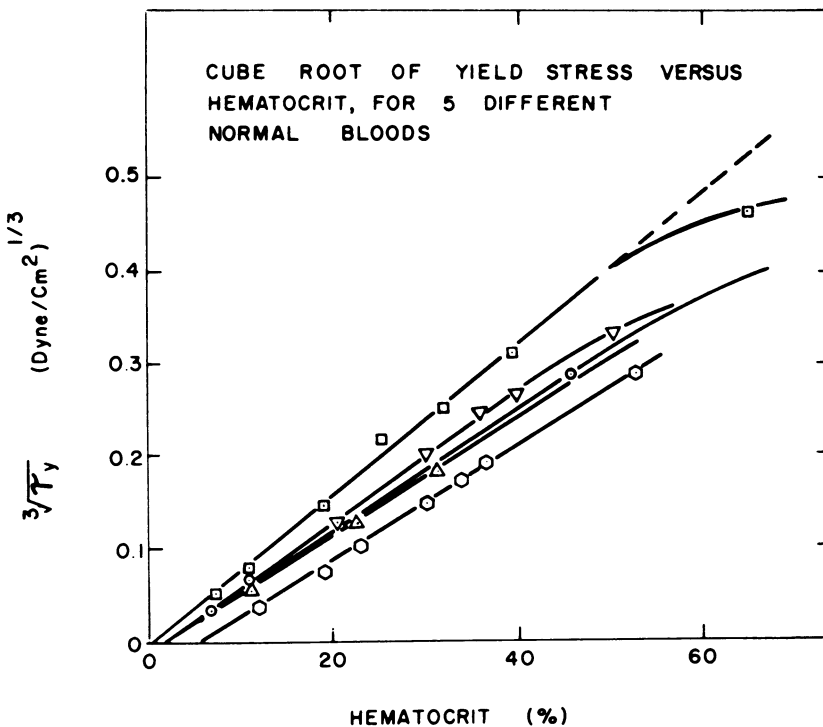


Figure 3.1:5 Variation of the yield stress of blood with hematocrit. Tests on samples with hematocrits less than the applicable abscissa intercept showed no yield stress. From Merrill et al. (1963a), by permission.

et al. (1963) is shown in Fig. 3.1:5. Note that τ_y is very small: of the order of 0.05 dyn/cm^2 , and is almost independent of the temperature in the range 10–37°C. τ_y is markedly influenced by the macromolecular composition of the suspending fluid. A suspension of red cells in saline plus albumin has zero yield stress; a suspension of red cells in plasma containing fibrinogen has a finite yield stress.

At high shear rate, whole blood behaves like a Newtonian fluid with a constant coefficient of viscosity, as is seen in Fig. 3.1:1. In other words, for sufficiently large values of $\dot{\gamma}$ we have

$$\tau = \mu \dot{\gamma} \quad \text{or} \quad \sqrt{\tau} = \sqrt{\mu} \sqrt{\dot{\gamma}}, \quad \mu = \text{const.} \quad (2)$$

As the shear rate $\dot{\gamma}$ increases from 0 to a high value, there is a transition region in which the stress-strain rate relation changes from that described by Eq. (1) to that described by Eq. (2). This is illustrated in Fig. 3.1:6, with data from Brooks et al. (1970). The part of the data to the right of the dashed curve belongs to the Newtonian region, described by Eq. (2); straight regression lines pass through the origin. The part to the left of the dashed curve

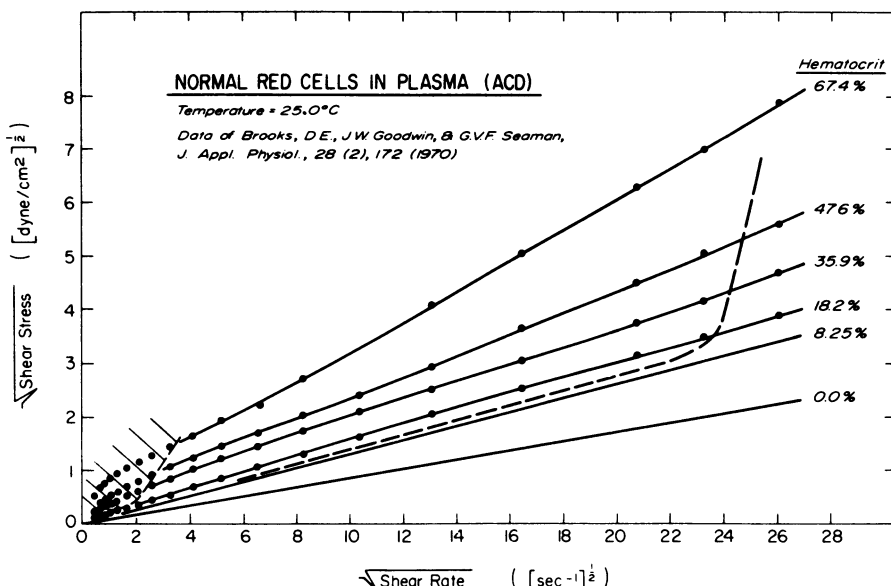


Figure 3.1:6 Casson plot of higher shear rate rheological data for a blood with ACD anticoagulant. The actual data points for plasma and the 8.25% hematocrit red cell suspension are not shown for clarity; these fluids appear to be Newtonian. Viscometer surfaces were smooth. From Cokelet (1972), by permission.

is the non-Newtonian region. The range of validity of Eq. (1) is smaller for higher hematocrit, and the transition region from Eq. (1) to Eq. (2) is larger for higher hematocrit. For hematocrit below 40% at 37°C, Eqs. (1) and (2) can be assumed to merge smoothly.

This outline shows the major features of blood flow in a viscometer of the Couette-flow type. The width of the channel in which blood flows in these testing machines is much larger than the diameter of the red blood cells. The blood is considered as a *homogeneous fluid*. This is a reasonable way to look at the blood when we analyze blood flow in large blood vessels. But all our blood vessels are not so large. In the human body there are about 10^{10} blood vessels whose diameter is about the same as that of the red blood cells, ranging from 4 to 10 μm . These are called the *capillary blood vessels*. When blood flows in capillary blood vessels, the red cells have to be squeezed and deformed, and move in single file. In this case then, it would be more useful to consider blood as a *nonhomogeneous* fluid, of at least two phases, one phase being the blood cells, the other being the plasma. Between large arteries and veins and the capillaries there are blood vessel of varying diameters. At what level can we regard blood as homogeneous? This is a question whose answer depends on the fluid mechanical features that one wishes to examine. Flow of blood in microvessels has many unique features, which will be discussed in Chapter 5.

In the present chapter, we shall first put the experimental results in a form suitable for further analysis. The problem of blood flow in a circular cylindrical tube will be discussed. We shall then turn to the question why blood viscosity behaves the way it does. Through this kind of examination, we will gain some understanding of blood rheology in states of health or disease. We shall conclude this chapter with a discussion of blood coagulation and medical applications of blood rheology.

3.2 The Constitutive Equation

Blood in physiological conditions may be considered as *incompressible*. An isotropic incompressible fluid is Newtonian if its constitutive equation that relates stress to strain rate has the form

$$\sigma_{ij} = -p\delta_{ij} + 2\mu V_{ij}, \quad (1)$$

where

$$V_{ij} = \frac{1}{2} \left(\frac{\partial u_i}{\partial x_j} + \frac{\partial u_j}{\partial x_i} \right), \quad V_{ii} = V_{11} + V_{22} + V_{33} = 0. \quad (2)$$

Here σ_{ij} is the stress tensor, V_{ij} is the strain-rate tensor, u_i is the velocity component, δ_{ij} is the isotropic tensor or Kronecker delta, p is the hydrostatic pressure, and μ is a constant called the *coefficient of viscosity*. The indices i, j range over 1, 2, 3, and the components of the tensors and vectors are referred to a set of rectangular cartesian coordinates x_1, x_2, x_3 . The summation convention is used, so that a repetition of an index means summation over that index, e.g., $V_{ii} = V_{11} + V_{22} + V_{33}$. A fluid obeying Eqs. (1) and (2), with μ a constant, is called an *isotropic incompressible Newtonian fluid*. Note the factor $\frac{1}{2}$ in our definition of strain rate in Eq. (2). This definition makes V_{ij} a tensor. In older books, shear rate is defined as twice this value. Thus $\dot{\gamma}$ of Fig. 3.1:1 is equal to $2V_{12}$ if the coordinate axes x_1, x_2 point at directions parallel and perpendicular to the wall, respectively.

The question arises whether blood obeys Eq. (1). The answer is *yes* if the shear strain rate is sufficiently high, but *no* if the rate is not high enough. When experimental results of blood flow at lower shear rate are reduced, it is found that they do not fit Eq. (1); but in steady flow in larger vessels they do fit a modification of Eq. (1), with a μ that is not a constant, but varies with the strain rate. Thus blood is said to be *non-Newtonian*. Similar experiments do verify, however, that *normal plasma alone is Newtonian*. Therefore the non-Newtonian feature of whole blood comes from the cellular bodies in the blood.

Red blood cells have finite size, can form aggregates, and can be hardened by artificial means. The rheology of whole blood depends, therefore, on the hematocrit, the size of the aggregates, the size of the blood vessel or testing equipment, the hardness of the cells, the viscosity of the plasma, and, if any, the abnormality of the plasma.

How can we generalize the Newtonian equation (1) to accommodate the non-Newtonian behavior of blood? What guidance do we have?

The most important principle we learned from continuum mechanics is that any equation must be tensorially correct, i.e., every term in an equation must be a tensor of the same rank. Thus, if we decide to try an equation of the type of Eq. (1) for blood, with μ a scalar, then μ as a function of the strain rate tensor must be a scalar function of V_{ij} . In other words, μ must be a function of numbers that are derived from V_{ij} . Since we have assumed blood to be isotropic [otherwise Eq. (1) will not apply; see Chapter 2, Sec. 2.7], we see that μ must be a function of the invariants of V_{ij} . Now since V_{ij} is a symmetric tensor, it has three invariants:

$$\begin{aligned} I_1 &= V_{11} + V_{22} + V_{33}, \\ I_2 &= \begin{vmatrix} V_{11} & V_{12} \\ V_{21} & V_{22} \end{vmatrix} + \begin{vmatrix} V_{22} & V_{23} \\ V_{32} & V_{33} \end{vmatrix} + \begin{vmatrix} V_{33} & V_{31} \\ V_{13} & V_{11} \end{vmatrix}, \\ I_3 &= \begin{vmatrix} V_{11} & V_{12} & V_{13} \\ V_{21} & V_{22} & V_{23} \\ V_{31} & V_{32} & V_{33} \end{vmatrix}. \end{aligned} \tag{3}$$

See the author's *First Course*, 2nd edn., p. 99. But we have assumed blood to be incompressible; hence I_1 vanishes. But when $I_1 = 0$, I_2 is negative valued, and it is more convenient to use

$$J_2 = 3I_1^2 - I_2 = \frac{1}{2}V_{ij}V_{ij}. \tag{4}$$

Hence μ must be a function of J_2 and I_3 . From Eq. 4 it is seen that J_2 is directly related to the shear strain rate. For example, if V_{12} is the only non-vanishing component of shear rate, then $J_2 = \frac{1}{2}V_{12}^2$. From experiments described in Sec. 3.1 we know that the blood viscosity depends on the shear rate, hence on J_2 . Whether it depends on I_3 or not is unknown because in most viscometric flows (e.g., Couette, Poiseuille, and cone-plate flows, see Sec. 2.14) I_3 is zero. Thus, we assume that μ is a function of J_2 and propose the following constitutive equation for blood:

$$\sigma_{ij} = -p\delta_{ij} + 2\mu(J_2)V_{ij}. \tag{5}$$

Let us now compare this proposal with experimental results. For the simple shear flow shown in Fig. 2.7:1 in Sec. 2.7, we have the shear rate

$$\dot{\gamma} = \frac{v}{h} = 2 \cdot \frac{1}{2} \left(\frac{\partial v_1}{\partial x_2} + \frac{\partial v_2}{\partial x_1} \right) = 2V_{12}. \tag{6}$$

(Note the factor of 2 due to the difference in the old and the tensorial definition of strain rate as remarked previously.) In this case, all other components V_{ij} vanish, and

$$J_2 = \frac{1}{2}V_{12}^2, \tag{7}$$

so that from Eq. (6),

$$\dot{\gamma} = 2\sqrt{2J_2}, \quad (8)$$

whereas from Eq. (5), we have the shear stress

$$\sigma_{12} = 2\mu(J_2)V_{12} = \mu\dot{\gamma}. \quad (9)$$

It is shown in Sec. 3.1 that in steady flow in larger vessels, the experimental results may be expressed in Casson's equation, Eq. (1) of Sec. 3.1,

$$\sigma_{12} = [\sqrt{\tau_y} + \sqrt{\eta\dot{\gamma}}]^2 \quad (10)$$

in a wide range of $\dot{\gamma}$. Comparing Eqs. (9) and (10), we see that

$$\mu = \frac{[\sqrt{\tau_y} + \sqrt{\eta\dot{\gamma}}]^2}{\dot{\gamma}}. \quad (11)$$

Thus, we conclude that the constitutive equation for blood is, in this range of $\dot{\gamma}$,

$$\sigma_{ij} = -p\delta_{ij} + 2\mu(J_2)V_{ij}, \quad (12a)$$

where

$$\mu(J_2) = [(\eta^2 J_2)^{1/4} + 2^{-3/4}\tau_y^{1/2}]^2 J_2^{-1/2}. \quad (12b)$$

Equation (12) is valid when $J_2 \neq 0$ and sufficiently small. On the other hand, when J_2 is sufficiently large, the experimental results reduce to the simple statement that $\mu = \text{constant}$, so that Eq. (1) applies. The point of transition from Eqs. (12a,b) to the Newtonian equation, $\mu = \text{constant}$, depends on the hematocrit, H (the volume fraction of red blood cells in whole blood). For normal blood with a low hematocrit, $H = 8.25\%$, μ was found to be constant over the entire range of shear rate from 0.1 to 1000 s^{-1} . When $H = 18\%$, the blood appears to be Newtonian when $\dot{\gamma} > 600 \text{ s}^{-1}$, but obeys Eq. (12) for smaller $\dot{\gamma}$. For higher H the transition point increases to $\dot{\gamma} \approx 700 \text{ s}^{-1}$. See Fig. 3.1:6.

The flow rule must be supplemented by another stress-strain relation when the blood is not flowing, i.e., when $V_{ij} = 0$. We know so little about the behavior of blood in this condition, however, that only a hypothetical constitutive equation can be proposed. A Hooke's law, for example, may be suggested, because the stress and strain are both very small. (The "yielding stress," τ_y , in Eq. (11) or (12), is only of the order of 0.05 dyn/cm^2 . The weight of a layer of water 1 mm thick, spreading over 1 cm^2 , produces a compressive stress of 100 dyn/cm^2 !) For a complete formulation, we need another condition, the "yielding condition," to define at what stress level flow must occur. In the theory of plasticity, the yielding condition is often stated in terms of the second invariant of the stress deviation, defined as

$$J'_2 = \frac{1}{2}\sigma'_{ij}\sigma'_{ij}, \quad (13)$$

where

$$\sigma'_{ij} = \sigma_{ij} - \frac{1}{3}\sigma_{kk}\delta_{ij}. \quad (14)$$

Flow or yielding occurs when J'_2 exceeds a certain number K . Thus:

$$V_{ij} = \begin{cases} 0 & \text{if } J'_2 < K, \\ \frac{1}{2\mu} \sigma'_{ij} & \text{if } J'_2 \geq K. \end{cases} \quad (15)$$

The stress-strain law when there is no flow, the yielding condition, and the flow rule together describe the mechanical behavior of the blood.

Other Aspects of Blood Rheology

Actually the rheological properties of blood are more complex than what is portrayed above. If blood is tested dynamically, it can be made to reveal all features of viscoelasticity. Furthermore, the viscoelastic characteristics of blood change with the level of strain and strain history; hence it is *thixotropic*. These complex properties are probably unimportant in normal circulatory physiology, but can be significant when one tries to use blood rheology as a basis of clinical applications to diagnosis of diseases, pathology, or biochemical studies.

Why Do We Need the General Constitutive Equation?

We have obtained with some effort in theoretical reasoning, a constitutive equation for blood that is consistent with our experimental knowledge. Why is this complicated constitutive equation needed? The answer is that Although the simple Casson equation, Eq. (1) of Sec. 3.1, suffices in the analysis of simple problems in which the strain rate tensor can be calculated a priori (without using the constitutive equation), in more complex problems it is insufficient. Casson's equation is all we need in analyzing Poiseuille and Couette flows, for which the shear stress and strain distributions are known from statics and kinematics. But if we wish to analyze the flow of blood at the point of bifurcation of an artery into two branches, or the flow through a stenosis, or the flow in aortic sinus, etc., the stress and strain rate distributions are not known. To analyze these problems, it is necessary to write down the general equations of motion based on an appropriate constitutive equation and solve them. For these problems the general constitutive equation is necessary.

Problems

3.1 Show that, for an incompressible fluid, $I_1 = 0$.

3.2 Thus far we have treated blood as a viscous fluid. This is undoubtedly permissible if blood flows in a steady state condition. But since blood is a suspension of blood

cells in plasma, and the cells are capable of interacting with each other, it is expected that blood will exhibit viscoelastic properties when conditions permit, just like many other polymer solutions. Speculate, on theoretical grounds, on what may be expected in the following situations:

- (a) A volume of blood sits in a condition of stationary equilibrium in a Couette viscometer or in a circular cylindrical tube (Poiseuille viscometer). A harmonic oscillation of very small amplitude is imposed on the blood in the viscometer. What would be the relationship between force and velocity? How would one express the relationship through the method of a complex variable? What is the phase relationship? What do the real and imaginary parts of the complex modulus mean?
- (b) Let the blood in the viscometer flow in a steady state and then superimpose a small harmonic oscillation on the viscometer. How would the complex modulus vary with the steady-state shear gradient?
- (c) Instead of harmonic oscillations of small amplitude as considered above, impose a small step function in velocity (Couette) or pressure gradient (Poiseuille), and discuss the expected response as a function of time.
- (d) If the step function considered in (c) is finite in amplitude, what difference would it make? The change in viscoelastic properties of a material with respect to time after a finite disturbance is called a *thixotropic* change. Thixotropy of blood may be described by a complex modulus of viscosity as a function of time after the initiation of disturbance (e.g., a step function); the modulus being obtained by a superposed small harmonic perturbation. Speculate on the possible thixotropic properties of blood.

Experimental results on the features named above as well as a mechanical and mathematical model of the viscoelasticity of blood expressed in terms of springs and dashpots are discussed by G. B. Thurston, (1979).

3.3 Laminar Flow of Blood in a Tube

Let us consider the flow of blood in a circular cylindrical tube. We shall assume the flow to be *laminar*, that is, *not turbulent*. We shall also assume that the tube is long and the flow is steady, so that the conditions of flow change neither with the distance along the tube, nor with the time. Under these assumptions we can analyze the flow with a simple ad hoc approach, which is presented below.

We shall use polar coordinates for this problem. The polar axis coincides with the axis of the cylinder. See Fig. 3.3:1. The flow obeys Navier-Stokes equations of motion of an incompressible fluid. The boundary condition is that blood adheres to the tube wall (the so-called *no-slip* condition). Since the boundary condition is axisymmetric, the flow is also axisymmetric and the

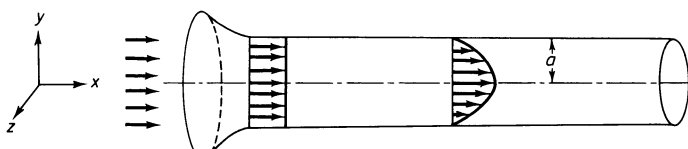


Figure 3.3:1 Velocity profiles in a steady laminar flow into a circular cylindrical tube.

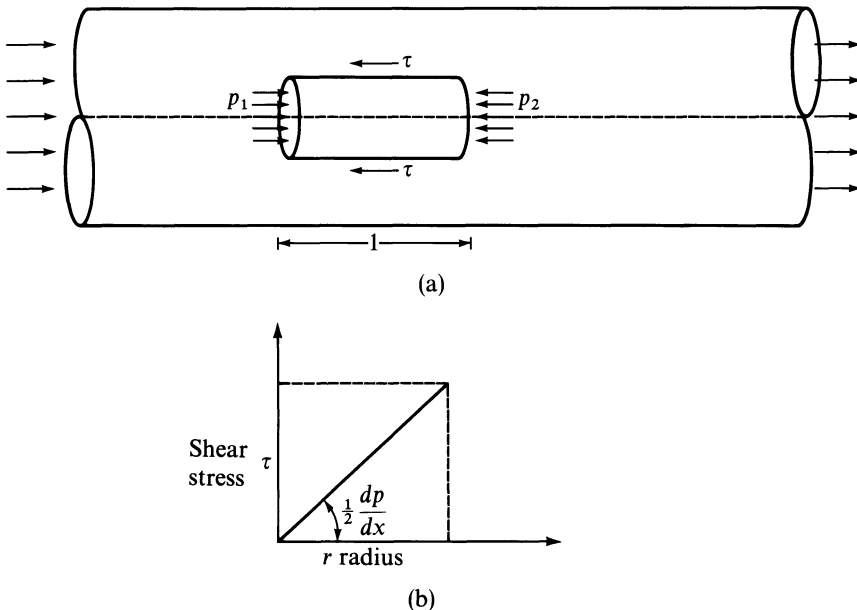


Figure 3.3:2 Steady flow in a long circular cylindrical pipe. (a) A free-body diagram of a centrally located element on which pressure and shear stresses act. (b) Relationship between the shear stress τ and the radial distance r from the axis of symmetry.

only nonvanishing component of velocity is $u(r)$ in the axial direction; $u(r)$ is a function of r alone, and not of x . Isolate a cylindrical body of fluid of radius r and unit length in the axial direction, as shown in Fig. 3.3:2(a). This body is subjected to a pressure p_1 on the left-hand end, p_2 on the right-hand end, and shear stress τ on the circumferential surface. Since $p_1 - p_2 = -1 \cdot (dp/dx)$ acts on an area πr^2 , and τ acts on an area $1 \cdot 2\pi r$, we have, for equilibrium, the balance of forces

$$\tau \cdot 2\pi r = -\pi r^2 \frac{dp}{dx},$$

or

$$\tau = -\frac{r}{2} \frac{dp}{dx} \quad (\text{Stokes, 1851}). \quad (1)$$

This important result is shown in Fig. 3.3:2(b).

Now we must introduce a constitutive equation that relates the shear stress τ to the velocity gradient. Let us first consider a Newtonian fluid.

A Newtonian Fluid

By the definition of Newtonian viscosity, we have

$$\tau = \mu \frac{du}{dr}. \quad (2)$$

A substitution of Eq. (2) into Eq. (1) yields

$$\frac{du}{dr} = -\frac{r}{2\mu} \frac{dp}{dx}. \quad (3)$$

Since the left-hand side is a function of r , the right-hand side must be also. Hence dp/dx cannot be a function of x . But since the fluid does not move in the radial direction, the pressures in the radial direction must be balanced, and p cannot vary with r . Hence the pressure gradient dp/dx must be a constant. Therefore, we can integrate Eq. (3) to obtain

$$u = -\frac{r^2}{4\mu} \frac{dp}{dx} + B, \quad (4)$$

where B is an integration constant. B can be determined by the boundary condition of no-slip:

$$u = 0 \quad \text{when} \quad r = a. \quad (5)$$

Combining Eqs. (4) and (5) yields the solution

$$u = \frac{1}{4\mu} (a^2 - r^2) \frac{dp}{dx}, \quad (6)$$

which shows that the velocity profile is a parabola, as sketched in Fig. 3.3:1.

The rate of flow through the tube can be obtained by integrating velocity times area over the tube cross-section:

$$\dot{Q} = 2\pi \int_0^a u r dr. \quad (7)$$

On substituting Eq. (6) into Eq. (7), we obtain the well-known formula

$$\dot{Q} = \frac{\pi a^4}{8\mu} \frac{dp}{dx}. \quad (8)$$

A division of the rate of flow by the cross-sectional area of the tube yields the mean velocity of flow,

$$u_m = \frac{a^2}{8\mu} \frac{dp}{dx}. \quad (9)$$

Blood, with Viscosity Described by Casson's Equation

If we compute the shear strain rate of the fluid at the tube wall, using the formulas obtained above for a Newtonian fluid, we obtain

$$\left. \frac{du}{dr} \right|_{r=a} = -\frac{1}{2} \frac{a}{\mu} \frac{dp}{dx} \quad \text{from Eq. (3) or (6),} \quad (10)$$

or

$$\left. \frac{du}{dr} \right|_{r=a} = \frac{4u_m}{a} \quad \text{from Eqs. (3) and (9).} \quad (11)$$

If physiological data on u_m , a , μ , and dp/dx are substituted into Eqs (10) and (11), we find that $\dot{\gamma}$ ($=du/dr$ at $r = a$) ranges from 100 to 2000 sec $^{-1}$ in large and small arteries, and 20 to 200 sec $^{-1}$ in large and small veins. Thus in the neighborhood of the blood vessel wall, the shear rate is high enough for the Newtonian assumption to be valid for normal blood. Toward the center of the tube, however, the shear gradient tends to zero, and the non-Newtonian feature of the blood will become more evident.

Let us assume that the blood is governed by Casson's equation, Eq. (1) of Sec. 3.1 or Eq. (12) of Sec. 3.2. We assume that the flow is laminar, uniaxial, axisymmetric, and without entrance effect (far away from the ends of the tube).

Equation (1) is valid for any fluid, hence for blood. The shear stress acting on any cylindrical surface ($r = \text{const.}$) is proportional to r , as shown in Fig. 3.3:2 and reproduced in Fig. 3.3:3. On the wall, the shear stress is τ_w . At a certain point on the stress axis it is τ_y , the yield stress. This corresponds to a radius r_c , shown on the horizontal axis. If the shear stress is smaller than the yield stress, that is, $\tau < \tau_y$ or $r < r_c$, the blood will not flow. If it moves at all it would have to move like a rigid body. Therefore, the velocity profile depends on the relative magnitude of τ_y and τ_w . Now, by Eq. (1),

$$\tau_w = \frac{a}{2} \frac{dp}{dx}, \quad \tau_y = \frac{r_c}{2} \frac{dp}{dx}. \quad (12)$$

Therefore, if $\tau_y > \tau_w$, i.e., $r_c > a$, then there is no flow:

$$u = 0 \quad \text{when} \quad \frac{dp}{dx} < \frac{2\tau_y}{a}. \quad (13)$$

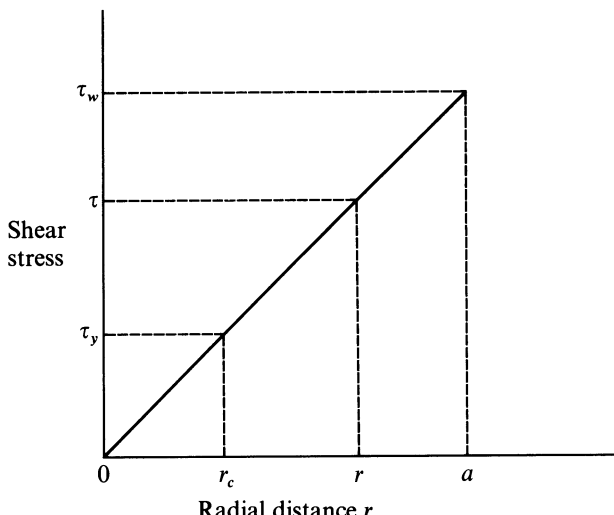


Figure 3.3:3 The relationship between shear stress and radial distance in a steady pipe flow. The shear stress reaches the yields stress of blood τ_y at radial distance r_c .

If $\tau_y < \tau_w$, i.e., $r_c < a$, or

$$\frac{dp}{dx} > \frac{2\tau_y}{a}, \quad (14)$$

then the velocity profile of the flow will be like that sketched in Fig. 3.3:4. In the core, $r < r_c$, the profile is flat. Between r_c and a , Casson's equation applies:

$$\sqrt{\tau} = \sqrt{\eta} \sqrt{\dot{\gamma}} + \sqrt{\tau_y}, \quad (15)$$

η is called *Casson's coefficient of viscosity*. Taking the square root of Eq. (1) and using (15), we obtain

$$\sqrt{-\frac{r}{2} \frac{dp}{dx}} = \sqrt{\tau_y} + \sqrt{\eta} \sqrt{\dot{\gamma}}. \quad (16)$$

Solving for $\dot{\gamma}$, we have

$$\frac{du}{dr} = \dot{\gamma} = \frac{1}{\eta} \left(\sqrt{-\frac{r}{2} \frac{dp}{dx}} - \sqrt{\tau_y} \right)^2 \quad (17)$$

Integrating this equation and using the boundary condition $u = 0$ when $r = a$, we have

$$\int_r^a \frac{du}{dr} dr = u|_a - u|r = \frac{1}{\eta} \int_r^a \left(\sqrt{-\frac{r}{2} \frac{dp}{dx}} - \sqrt{\tau_y} \right)^2 dr, \quad (18)$$

or

$$u = \frac{1}{4\eta} \frac{dp}{dx} [a^2 - r^2 - \frac{8}{3}r_c^{1/2}(a^{3/2} - r^{3/2}) + 2r_c(a - r)] \quad \text{for } (r_c \leq r \leq a). \quad (19)$$

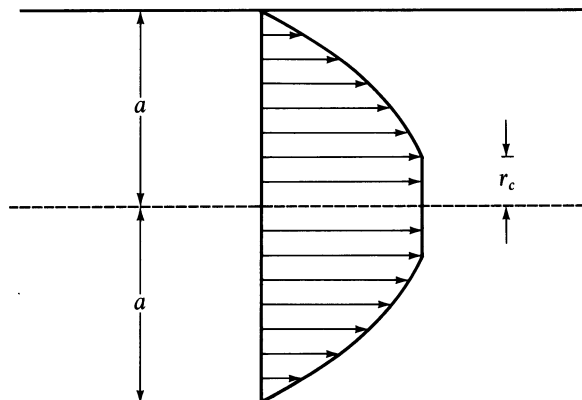


Figure 3.3:4 The velocity profile of laminar flow of blood in a long circular cylindrical pipe.

At $r = r_c$, the velocity u becomes the core velocity u_c :

$$\begin{aligned} u_c &= \frac{1}{4\eta} \frac{dp}{dx} (a^2 - \frac{8}{3}r_c^{1/2}a^{3/2} + 2r_c a - \frac{1}{3}r_c^2) \\ &= \frac{1}{4\eta} \frac{dp}{dx} (\sqrt{a} - \sqrt{r_c})^3 (\sqrt{a} + \frac{1}{3}\sqrt{r_c}). \end{aligned} \quad (20)$$

And for all values of r between 0 and r_c ,

$$u = u_c. \quad (21)$$

The velocity distribution is given by Eqs. (19) and (21) if $r_c < a$, i.e., if Eq. (14) applies; whereas the flow is zero if the inequality sign in Eq. (14) is reversed.

We can now find the rate of volume flow by an integration:

$$\dot{Q} = 2\pi \int_0^a ur dr. \quad (22)$$

Using Eqs. (13), (19), and (21) for appropriate ranges of pressure gradient and radius, we obtain

$$\dot{Q} = \frac{\pi a^4}{8\eta} \left[\frac{dp}{dx} - \frac{16}{7} \left(\frac{2\tau_y}{a} \right)^{1/2} \left(\frac{dp}{dx} \right)^{1/2} + \frac{4}{3} \left(\frac{2\tau_y}{a} \right) - \frac{1}{21} \left(\frac{2\tau_y}{a} \right)^4 \left(\frac{dp}{dx} \right)^{-3} \right]. \quad (23)$$

if $dp/dx > (2\tau_y/a)$; whereas

$$\dot{Q} = 0 \quad \text{if } \frac{dp}{dx} < \frac{2\tau_y}{a}. \quad (24)$$

If we introduce the notation

$$\xi = \left(\frac{2\tau_y}{a} \right) \left(\frac{dp}{dx} \right)^{-1}, \quad (25)$$

then Eq. (23) can be written as

$$\dot{Q} = \frac{\pi a^4}{8\eta} \frac{dp}{dx} F(\xi), \quad (26)$$

where

$$F(\xi) = 1 - \frac{16}{7} \xi^{1/2} + \frac{4}{3} \xi - \frac{1}{21} \xi^4. \quad (27)$$

Equation (26) is similar to Poiseuille's law, but with a modifying factor $F(\xi)$. These results were obtained by S. Oka (1965, 1974). Figure 3.3:5 gives Oka's graph of $F(\xi)$ vs. ξ . It is seen that the flow rate decreases rapidly with increasing ξ . For $\xi > 1$, there is no flow, and $\dot{Q} = 0$. Oka also obtained the interesting result shown in Fig. 3.3:6, that if one plots the square root of \dot{Q} versus the square root of the pressure gradient, one obtains a curve that resembles the flow vs shear stress curve of a Bingham plastic material (See Prob. 3.17, p. 97). Taking the square root on both sides of Eq. (26), expanding

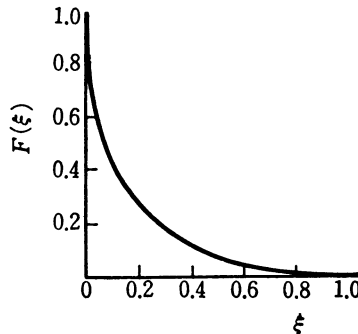


Figure 3.3:5 The function $F(\xi)$ from Eq. (37) of Sec. 3.5, which is the ratio of the flow rate in a tube of a fluid obeying Casson's equation to that of a Newtonian fluid with the same Casson viscosity. The variable ξ is inversely proportional to the pressure gradient; see Eq. (36) of Sec. 3.5. From Oka (1974), by permission.

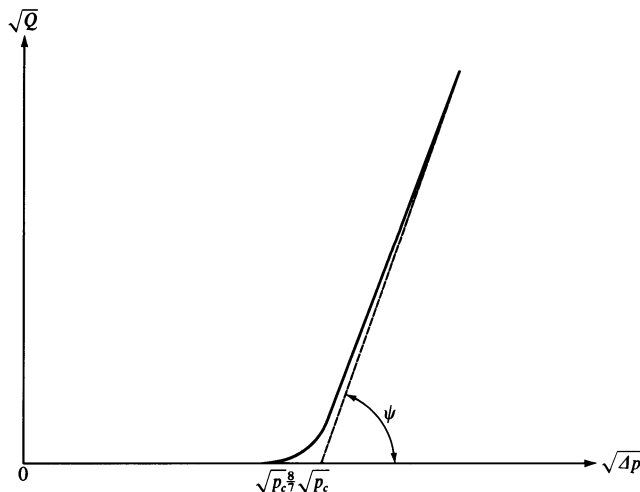


Figure 3.3:6 The relationship between \sqrt{Q} and $\sqrt{\Delta p}$; Q is the flow rate of a fluid obeying Casson's equation, and Δp is the pressure gradient. From Oka (1974), by permission.

the square root of $F(\xi)$ in a power series of $\xi^{1/2}$, and retaining only the first power, one obtains the asymptotic equation

$$\begin{aligned} Q^{1/2} &= \left(\frac{\pi a^4}{8\eta} \right)^{1/2} \left(\frac{dp}{dx} \right)^{1/2} \left(1 - \frac{8}{7}\xi^{1/2} \right) \\ &= \left(\frac{\pi a^4}{8\eta} \right)^{1/2} \left[\left(\frac{dp}{dx} \right)^{1/2} - \frac{8}{7}p_c^{1/2} \right], \end{aligned} \quad (28)$$

where $p_c = 2\tau_y/a$. This is plotted as the dotted line in Fig. 3.3:6. The solid curve is the exact solution. The dotted line is an asymptote whose slope is

$$\tan \psi = \left(\frac{\pi a^4}{8\eta} \right)^{1/2}. \quad (29)$$

These results give complete information on the laminar flow of blood in circular cylindrical tubes.

Problems

3.3 Entry flow of blood into a pipe. So far we have analyzed the condition of flow in a pipe in a region far away from the entry section. At the entry section ($x = 0$), where the pipe is connected to a large reservoir, the velocity profile is uniform, as shown in Fig. 3.3:1. As the distance from the entry section increases, the profile changes gradually to the steady-state profile of a parabola (if the fluid is Newtonian) or the flat-topped parabola of Fig. 3.3:4 (if the fluid is blood). Consider blood. We can trace the change as sketched in Fig. P3.3. At $x = x_1$ the velocity has to change from u_0 at the center to 0 on the wall, where the no-slip condition applies. This creates a high shear-strain gradient at the wall, which has to decrease to zero at the center. At a certain distance δ from the wall is a point where the shear stress is equal to the yield stress of the blood. Beyond $y = \delta$, the velocity profile remains flat. As x increases, δ increases. At $x = x_n$ the velocity profile tends to the steady state, as shown in Fig. 3.3:4.

The layer between the wall and $y = \delta(x)$ is a kind of *boundary layer* of blood flow. It is bounded by a surface on which the shear stress is exactly equal to the yield stress. The rate at which $\delta(x)$ grows with x depends on the Reynolds number of flow N_R . For larger N_R , $\delta(x)$ is thinner and grows slower. When $N_R \rightarrow 0$,

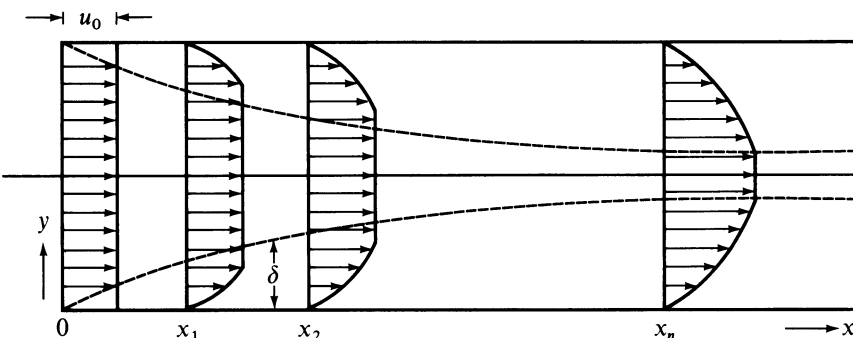


Figure P3.3 Entry flow of blood into a pipe. Dotted lines show the boundary layer of yielding.

the entire tube is at once engulfed in the boundary layer. Give this qualitative picture a mathematical expression, thereby making it a more rigorous theory.

- 3.4** With the constitutive equations of blood presented in Sec. 3.2, derive the equation of motion of blood in a form that is a generalization of the Navier-Stokes equation. Discuss the range of validity of the equations. Discuss any simplification that results if the shear-strain rate is sufficiently high.
- 3.5** When blood is in contact with a solid wall, what would the boundary conditions be? The answer must be consistent with the constitutive equation of the blood. Answer the question theoretically. Consider statistics of the cellular bodies in a manner similar to the kinetic theory of gases and ask what the boundary condition should be. Or introduce a continuum theory of a fluid with microstructure and ask what are the appropriate boundary conditions for that theory.
- 3.6** Reduce the equations you obtained in Problem 3.4 to a dimensionless form. Introduce characteristic length L , characteristic velocity V , dimensionless coordinates $x'_1 = x_i/L$, velocities $u'_1 = u_i/V$, and

$$p' = \frac{p}{\rho V^2}, \quad t' = \frac{Vt}{L}, \quad N_R = \frac{VL\rho}{\mu},$$

where N_R is the Reynolds number.

- 3.7** If laboratory model testing is to be done for blood flow, on what basis would you design the models. A scaled model may be desired to facilitate observations on velocity, pressure, forces, etc. It may be convenient to use water or a polymer fluid as the working fluid in place of blood. Discuss the principles of kinematic and dynamic similarities in model design.

3.4 Speculation on Why Blood Viscosity Is the Way It Is

Since normal plasma is Newtonian, there is no doubt that the non-Newtonian features of human blood come from blood cells. How the red blood cells move when blood flows is the central issue. Some very fine research work has been done on this subject, which throws light on the flow properties of the blood.

It has been known for a long time (Fahreus, 1929) that human red blood cells can form aggregates known as rouleaux (Fig. 3.4:1), whose existence depends on the presence of the proteins fibrinogen and globulin in plasma. (Bovine blood does not form rouleaux.) The slower the blood flows, or rather, the smaller the shear rate, the more prevalent are the aggregates. When the shear rate tends to zero, it is speculated that human blood becomes one big aggregate, which then behaves like a solid. A solid may be viscoelastic or viscoplastic. If the blood aggregate behaves as a plastic solid, then a yield stress exists which can be (but does not have to be) identified with the constant τ_y in Casson's equation [Eq. (1) of Sec. 3.1].

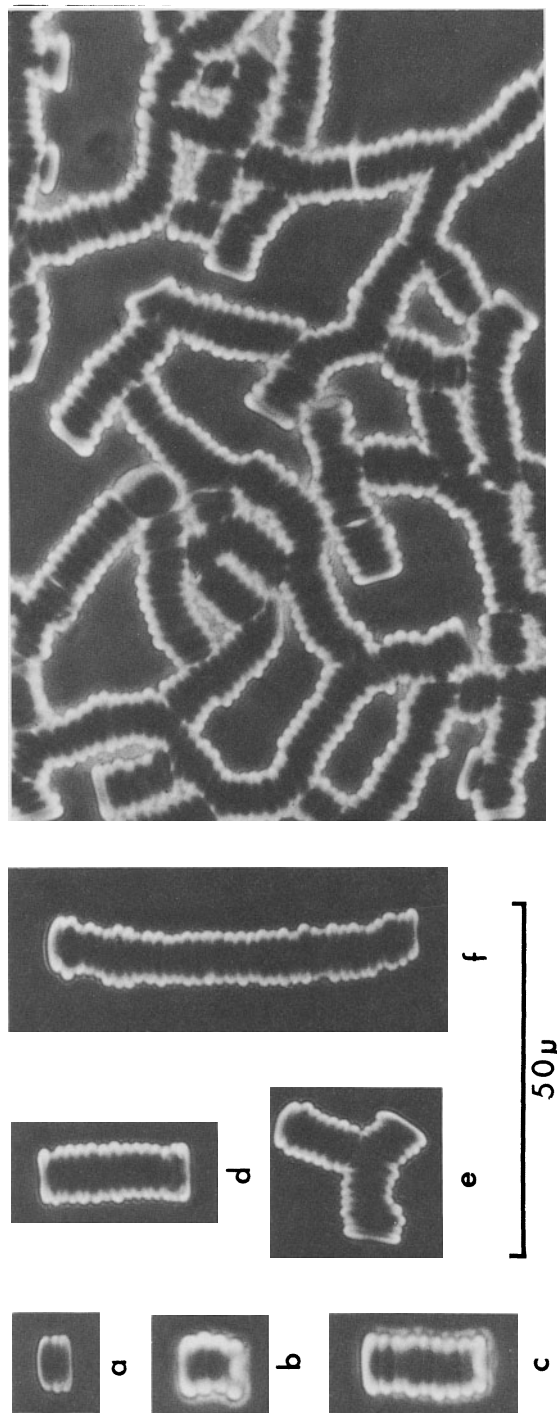


Figure 3.4:1 Rouleaux of human red cells photographed on a microscope slide showing single linear and branched aggregates (left part) and a network (right part). The number of cells in linear array are 2, 4, 9, 15, and 36 in a, b, c, d, and f, respectively. From Goldsmith (1972b), by permission.

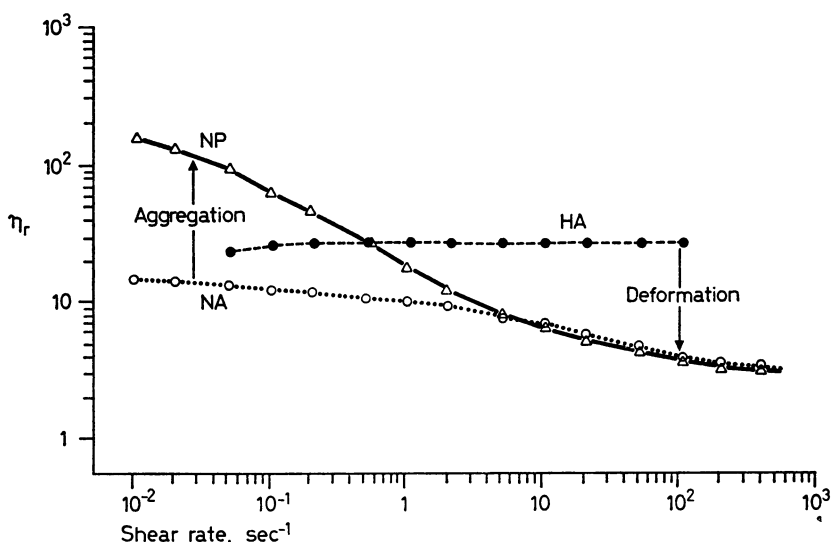


Figure 3.4:2 Logarithmic relation between relative apparent viscosity and shear rate in three types of suspensions, each containing 45% human RBC by volume. Suspending medium (plasma) viscosity = 1.2 cP (0.12 N s m⁻²). NP = Normal RBC in plasma; NA = normal RBC in 11% albumin; HA = hardened RBC in 11% albumin. From Chien (1970), by permission.

When the shear rate increases, blood aggregates tend to be broken up, and the viscosity of blood is reduced. As the shear rate increases further, the deformation of the red cells becomes more and more evident. The cells tend to become elongated and line up with the streamlines. This further reduces the viscosity. The effects of aggregation and deformation of the red cells are well illustrated in Fig. 3.4:2, from Chien (1970). In this figure, the line NP refers to normal blood. The line NA refers to a suspension of normal red blood cells in an albumin-Ringer solution that does not contain fibrinogen and globulins. The tendency toward rouleaux formation was removed in the latter case, and it is seen that the viscosity of the suspension was reduced, even though the viscosity of the albumin-Ringer solution was adjusted to be the same as that of the plasma of the NP case. The third curve, HA, refers to a suspension of hardened red blood cells in the same albumin-Ringer solution. (Red cells can be hardened by adding a little fixing agent such as glutaraldehyde to the solution.) Hence the difference between the NP and NA curves indicates the effect of cell aggregation, whereas that between NA and HA indicates the effect of cell deformation.

The amazing fluidity of human blood is revealed in Fig. 3.4:3, in which the viscosity of blood at a shear rate $> 100 \text{ s}^{-1}$ (at which particle aggregation ceased to be important) is compared with that of other suspensions and

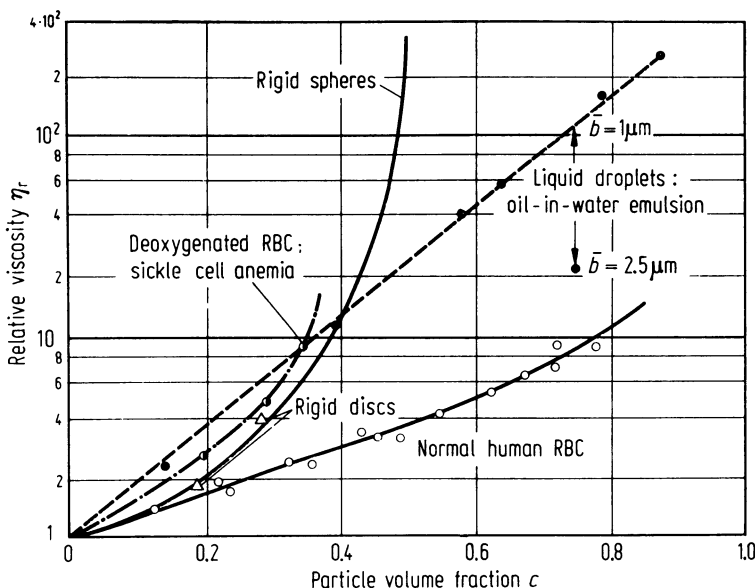


Figure 3.4:3 Relative viscosity of human blood at 25°C as a function of red cell volume fraction, compared to that of suspensions of rigid latex spheres, rigid discs, droplets, and sickled erythrocytes, which are virtually nondeformable. From Goldsmith (1972b) by permission.

emulsions. At 50% concentration, a suspension of rigid spheres will not be able to flow, whereas blood is fluid even at 98% concentration by volume. The much higher viscosity of blood with deoxygenated sickle cells is also shown: it tells us why sickle cell anemia is such a serious disease.

Since in a field of shear flow with a velocity gradient in the y direction the velocity is different at different values of y , any suspended particle of finite dimension in the y direction will tumble while flowing. The tumbling disturbs the flow and requires expenditure of energy, which is revealed in viscosity. If n red cells form a rouleaux, the tumbling of the rouleaux will cause more disturbance than the sum of the disturbances of the n individual red cells. Hence breaking up the rouleaux will reduce the viscosity. Further reduction can be obtained by deformation of the particle. If the particle is a liquid droplet, for example, it can elongate to reduce the dimension in the y direction, thus reducing the disturbance to the flow. A red cell behaves somewhat like a liquid droplet; it is a droplet wrapped in a membrane. These factors explain the reduction of viscosity with increasing shear rate.

Detailed studies of the tumbling and deformation of the red cells and rouleaux in shear flow have been made by Goldsmith and his associates by observing blood flow in tiny circular cylindrical glass tubes having diameters from 65 to 200 μm under a high powered microscope. The tubes lay on a

vertically mounted platform, which was moved mechanically or hydraulically upward as the particles being tracked flowed downward from a syringe reservoir. The cell motion was photographed. Particle behavior at hematocrits $> 10\%$ was studied by using tracer red cells in a transparent suspension of hemolyzed, unpigmented red cells—so-called *ghost cells*. The ghosts were also biconcave in shape, although their mean diameter ($\sim 7.2 \mu$) and volume ($7.4 \times 10^{-11} \text{ cm}^3$) were somewhat smaller than those of the parent red cells.

Figure 3.4:4 shows the tumbling of an 11- and a 16-cell rouleau of red cells in Poiseuille flow at a shear rate $\dot{\gamma} < 10 \text{ sec}^{-1}$ (at shear stress $< 0.2 \text{ dyn cm}^{-2}$). This was observed at very low Reynolds numbers, and in a very dilute suspension.

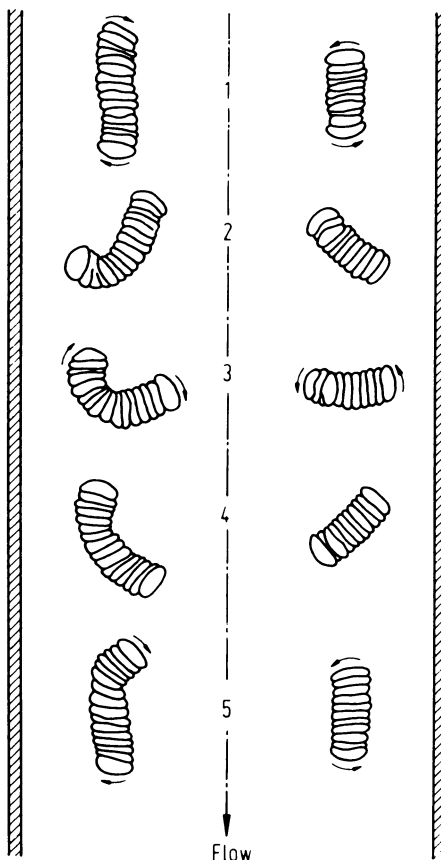


Figure 3.4:4 Rotation of an 11- and a 16-cell rouleau of erythrocytes in Poiseuille flow; $\dot{\gamma} < 10 \text{ sec}^{-1}$. Bending commenced at position 2 where the fluid stresses are compressive to the rouleaux. The longer particle did not straighten out in the succeeding quadrant, in which the stresses in the rouleaux are tensile. From Goldsmith and Marlow (1972), by permission.

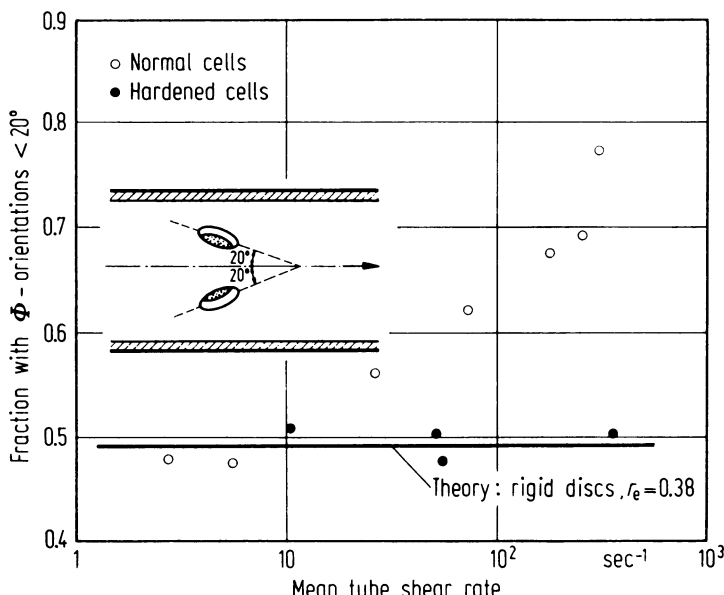


Figure 3.4:5 The increasing fraction of normal red cells (open circles) found in orientation within $\pm 20^\circ$ with respect to the direction of flow as the shear rate is increased in a tube flow. The orientation distribution of hardened cells (closed circles) is independent of the flow speed and radial location in the tube, and agrees with that calculated for rigid discs having an equivalent thickness-to-diameter ratio of $r_e = 0.38$. From Goldsmith (1971), by permission.

The tendency of the deformable red cells to be aligned with the streamlines of flow at higher shear rates is illustrated in Fig. 3.4:5 which refers to observations made in very dilute suspensions in which particle interactions were negligible. It is seen that as the shear rate $\dot{\gamma}$ was increased, more and more cells were found in orientations in which their major axes were aligned with the flow. By contrast, rigid but still biconcave erythrocytes, produced by hardening with gluturaldehyde, continued to show orientations independent of shear rate.

The features shown in Figs. 3.4:4 and 3.4:5 are for isolated red cells or aggregates. Normal blood contains a high concentration of red blood cells,—with a hematocrit ratio (defined as cell volume/blood volume) of about 0.45 in large vessels, and 0.25 in small arterioles or venules. At such a high concentration, the cells crowd each other: no one cell can act alone. Goldsmith's (1972b) observations then show that

1. The velocity profile in the tube is no longer parabolic as in Poiseuille flow;
2. Deformation of the erythrocytes in blood occurs to a degree that is not attributable to shear alone;
3. The particle paths exhibit erratic displacements in a direction normal to the flow.

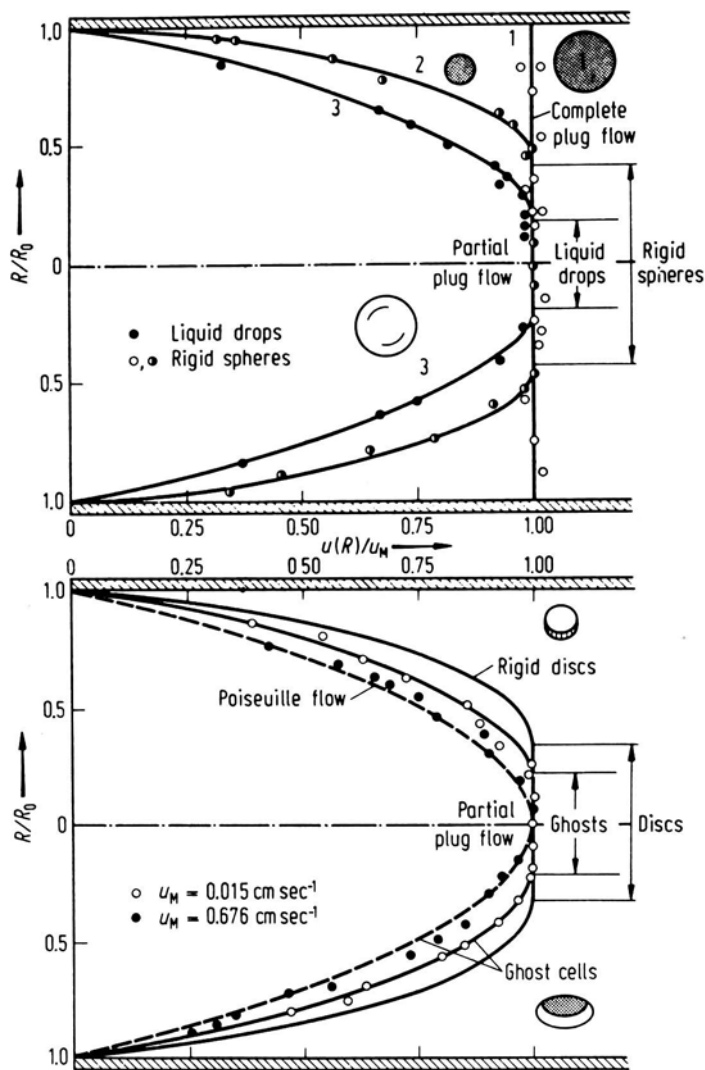


Figure 3.4:6 Comparison of dimensionless particle velocity profiles in 32% suspensions of rigid spheres ($b/R_0 = 0.112$ and 0.056 in curves 1 and 2, respectively) and liquid drops ($b/R_0 = 0.078$, curve 3)—upper part; and between 32% suspensions of rigid discs ($b/R_0 = 0.078$) and ghost cells ($b/R_0 = 0.105$)—lower part. The lines drawn are the best fit of the experimental points; the dashed line is calculated from Eq. (6) of Sec. 3.3 in the form $U(R)/U(0) = 1 - R^2/R_0^2$. Note that by complete plug flow in curve 1 (upper part), we do not imply slip of fluid at the wall. Close to the boundary there must be a steep velocity gradient in the suspending fluid. From Goldsmith (1972b), by permission.

The velocity profiles measured in model systems with ghost cells, as well as rigid discs, liquid droplets, and rigid spheres, are shown in Fig. 3.4:6, and can be explained as follows. In a flow of a homogeneous fluid, the profile is parabolic (Poiseuille flow, shown by a dotted line in the lower panel). If there is a *single* isolated *rigid* sphere in the flow, and if the radius of the sphere b is much smaller than the radius of the tube R_0 , and if the Reynolds number of the flow is smaller than 1, then the spherical particle will translate along a path parallel to the tube axis with a velocity which, except when the particle is very close to the wall, is equal to the velocity of the undisturbed fluid at the same radial distance. As the concentration of rigid spheres is increased, the particle velocity profile remains parabolic, provided that $b/R_0 < 0.04$ and the volume concentration $c < 0.2$. As the concentration c and the particle-tube-radius ratio b/R_0 are increased further, the velocity profile becomes blunted in the center of the tube. Flow in this central region may be called a *partial plug flow*. For a suspension of rigid spheres the velocity profile is independent of flow rate and suspending phase viscosity, and the pressure drop per unit length of the tube is directly proportional to the volume flow rate \dot{Q} . In contrast, flow of a concentrated, monodispersed oil-in-oil emulsion has a velocity profile which is appreciably less blunted than the rigid particle case, at the same values of c and b/R_0 , and moreover, this profile is *dependent* on the flow rate and the suspending phase viscosity. In a given system, the lower the flow rate, and the greater the suspending phase viscosity, the greater was the degree of blunting.

Similar non-Newtonian behavior was exhibited by ghost cell plasma suspensions at concentrations from 20 to 70%. Figure 3.4:6 (lower panel) shows the results obtained at a concentration $c = 0.32$, a mean velocity of flow = 1.04 tube diameters per sec; ($U_M = 0.015 \text{ cm s}^{-1}$); and a tube radius of $36\mu\text{m}$. Upon increasing the mean velocity of flow to 47 tube diameters per sec ($U_M = 0.676 \text{ cm s}^{-1}$), the velocity distribution in the ghost cell suspension became almost parabolic. These features are consistent with the analytical results of Sec. 3.3.

The influence of particle crowding on cell deformation can be expected; but it becomes quite dramatic if we think of the meaning of the curves shown in Fig. 3.4:3. As seen in that figure, the relative viscosity of human blood is considerably lower than that of concentrated oil-in-water emulsions. Are the red blood cells more deformable than the liquid droplets? Are the red cells, in a crowded situation, able to squeeze and move past each other more readily than colliding liquid droplets? The answer is "yes." Direct observation has shown large distortion of red cells and rouleaux at very low shear rates ($\dot{\gamma} < 5\text{s}^{-1}$ or shear stress $< 0.07 \text{ dyn cm}^{-2}$). An example is shown in Fig. 3.4:7, at a cell concentration (hematocrit) $c = 0.5$. The explanation is believed to lie in the biconcave shape of the red cells. In Chapter 4, Sec. 4.3, it is shown that because of the biconcave shape, the internal pressure of an isolated red cell must be the same as the external pressure if the bending rigidity of the cell membrane is negligibly small. Therefore, the cell membrane is unstressed in the normal biconcave configuration.

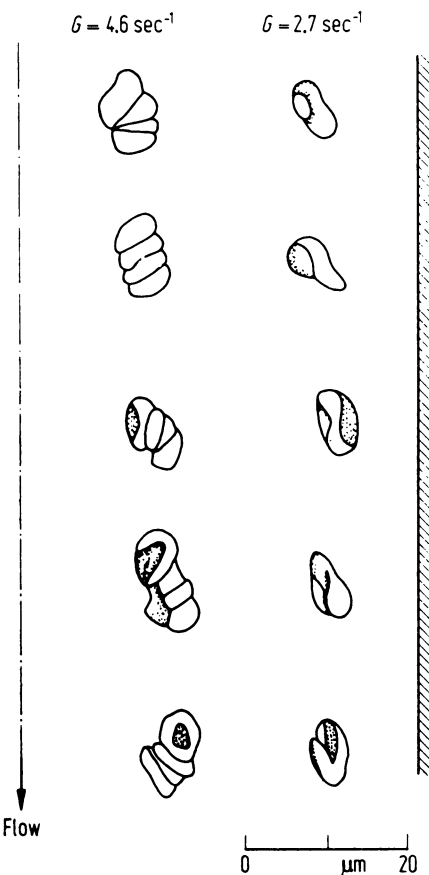


Figure 3.4:7 Tracings from a cine film showing the continuous and irregular deformation of a single erythrocyte and a 4-cell rouleau in a ghost cell suspension, $H = 0.5$. The cell is shown at intervals of 0.4, 0.6, 2.0, and 3.2 s, respectively, in which time the isolated corpuscle would execute just over half a rotation. From Goldsmith (1972a), by permission.

It is shown that such a biconcave cell can deform into an infinite variety of shapes without stretching the cell membrane anywhere in any direction. These large deformations are said to be *applicable deformations* by borrowing a term from the theory of differential geometry. In these applicable deformations the only strain energy needed is used to bend the cell membrane, whose bending rigidity is very small because of the thinness of the membrane (30–70 Å). If, in a crowding situation, the neighboring cells did not permit a red cell to deform in “applicable” manner, then deformation of the cell membrane (usually with no change of area) would be inevitable; but it can be expected that the strain energy needed is quite small compared with any deformation that requires a change of surface area (because for a red cell membrane the Young’s modulus is four orders of magnitude smaller than the modulus for area change; see Chapter 4, Sec. 4.4).

On the other hand, a liquid droplet in emulsion is maintained by surface tension. In a static condition, a droplet must be spherical if the surface tension is uniform. In a shear flow, the droplets become ellipsoidal in shape; whereas in the crowded situation of a concentrated emulsion, large distortion of shape from that of a regular ellipsoid was noted. Such distortion from the spherical shape increases the surface area of the droplet, and hence the surface energy (surface tension is equal to surface energy per unit area). Thus it becomes plausible that the red cell, by packaging into the biconcave shape, is more deformable than a liquid droplet without a cell membrane. It also follows from this discussion that a detailed analysis of the rheology of blood or emulsion at high concentration needs data on the viscosities of the liquids and hemoglobin, as well as on the surface tension and cell membrane elasticity.

The third feature of concentrated particulate flow named above; the erratic sidewise movement of particles, has been recorded extensively by Goldsmith. Such erratic motion is expected because of frequent encounters of a particle with neighboring particles. The particle path therefore, must show features of a random walk. These observations offer a qualitative explanation of the way blood flows the way it does.

3.5 Fluid-Mechanical Interaction of Red Blood Cells with a Solid Wall

It has been pointed out by Thoma (1927) that in a tube flow there seems to be a tendency for the red cells to move toward the axis of the tube, leaving a marginal zone of plasma, whose width increases with increase in the shear rate. There is a layer close to the wall of a vessel that is relatively deficient of suspended material. In dilute suspensions, this “wall effect” has been measured by Goldsmith in the creeping flow regime (Reynolds number $\ll 1$). In emulsions the deformation of a liquid drop results in its migration across the streamlines away from the tube wall. Such lateral movement is not observed with rigid spherical particles; thus the deformability of the particle appears to be the reason for lateral migration.

A similar difference in flow behavior was found between normal red blood cells (RBC) and glutaraldehyde-hardened red cells (HBC), as illustrated in the upper panels of Fig. 3.5:1, which show the histograms of the number-concentration distributions of cells as a function of radial distance, at a section 1 cm downstream from the entry in a tube of $83 \mu\text{m}$ diam. at a Reynolds number about 0.03. Even more striking is the lateral migration in dextran solutions at Reynolds numbers $R_n = 3.7 \times 10^{-3}$ and 9.1×10^{-4} , shown in the lower panels. It is seen that very few cells are present in the outer half of the tube. Dextran solutions have a higher viscosity than Ringer or Ringer-plasma solutions. In dextran solutions the red cells are deformed into ellipsoidlike shapes. Similar observations of flow containing rouleaux of red cells show that rouleaux migrate to the tube axis faster than individual red cells.

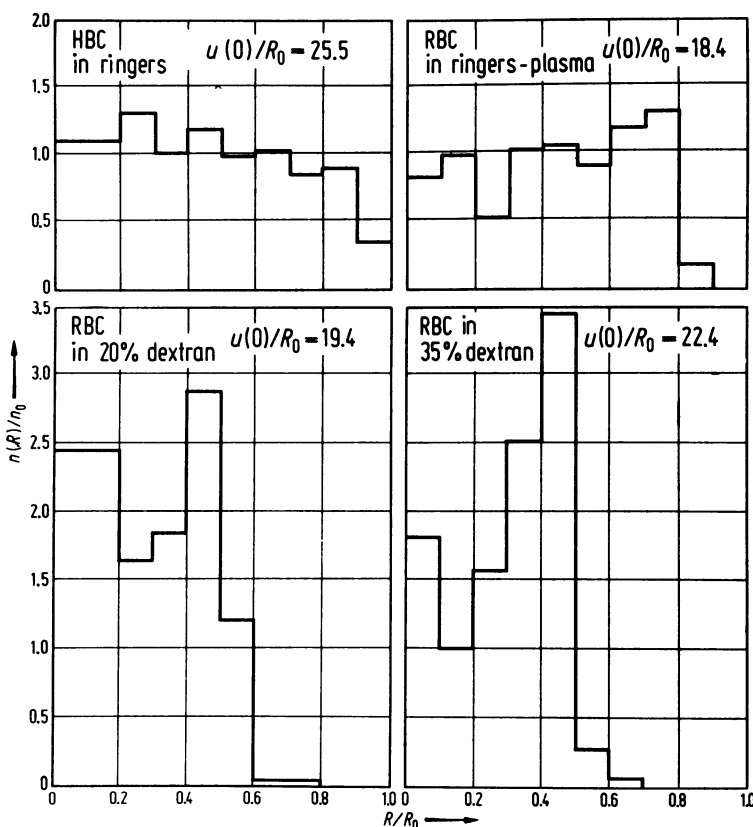


Figure 3.5:1 Number of cells/cm³ suspension, $n(R)$, divided by the syringe reservoir concentration, n_0 , at intervals of $0.1 R_0$, 1 cm downstream from the reservoir; $R_0 = 41.5 \mu\text{m}$, $c = 2 \times 10^{-3}$. The mean tube shear rates $= u(0)/R_0$ were approximately the same in each suspension. If the number distribution were uniform, then $n(R)/n_0 = 1$ at all R/R_0 . From Goldsmith (1972b), by permission.

Inward migration of deformable drops, fibers, and red cells away from the wall in both steady and oscillatory flows has been observed also at higher Reynolds numbers ($R_n > 1$), when the effects of fluid inertia are significant. At $R_n > 1$ nondeformable particles also exhibit lateral migration in dilute suspensions.

When the cell concentration is high, the crowding effect acts against migration away from the wall into the crowded center. Measurements made by Phibbs (1969) in quick-frozen rabbit femoral arteries, by Bugliarello and Sevilla (1971) on cine films of blood flow in glass tube, and by Blackshear et al. (1971) on ghost cell concentration, make it appear unlikely that at hematocrits of 40–45% and normal flow rates, the plasma-rich zone can be much larger than $4 \mu\text{m}$ in vessels whose diameters exceed $100 \mu\text{m}$.

This plasma-rich (or cell-rare) zone next to the solid wall, although very thin, has important effect on blood rheology. In the first place, measurement

of blood viscosity by any instrument which has a solid wall must be affected by the wall layer. The change in cell concentration in the wall layer makes the blood viscosity data somewhat uncertain. Thus we are forced to speak of "apparent" viscosity (see Chapter 5, Sec. 5.1,) rather than simply of the viscosity. It makes it necessary to specify how "smooth" or "serrated" the surface of viscometers must be. In the second place, the smaller the blood vessel is, the greater will be the proportion of area of the vessel occupied by the wall layer, and greater would be its influence on the flow. The low hematocrit in the wall layer lowers the average hematocrit in small blood vessels. And when a small blood vessel branches off from another vessel, it draws more fluid from the wall layer where the hematocrit is low. The result is a lower average hematocrit in the smaller blood vessel; and hence a lower apparent viscosity. This will be discussed in Chapter 5.

3.6 Coagulation

If blood coagulates in the heart or blood vessels of a living organism, the clot is called a *thrombus*, and the process is called *thrombosis*. Thrombosis is, of course, dangerous to life, and nature must make sure that it does not happen. On the other hand, if blood leaves the blood vessel and comes into contact with a foreign surface, a coagulation process is initiated immediately, which seals the wound and saves the organism's life.

The mechanism of blood coagulation is very complex. In principle, it involves polymerization of fibrinogen into fibrin. The key lies in the conversion of prothrombin into an active enzyme, thrombin. There are two pathways for prothrombin activation. An "intrinsic" pathway is activated by contact of blood with surfaces other than normal vascular endothelium. But there is also an "extrinsic" pathway activated by enzymes in tissue juices from damaged tissue. Because of the "extrinsic" process, some hematologists always discard the first small volume of blood taken from a vein for test purposes.

The biochemical reactions of the clotting mechanism have been studied extensively; see Biggs and Macfarlane (1966). By an international agreement a number of proenzymes and enzymes involved in blood clotting are called *factors* and numbered I, II, . . . , XIII. To the beginner the numbers given to the separate factors can be misleading. They number backwards, in reverse order from the sequence of events beginning with the contact with a foreign surface. Thus, the contact factor is numbered XII, VI proved to be a mistake and is omitted, 10 comes in the wrong place, and although most of the factors are proenzymes, one of them is simply calcium, the need for which occurs at more than one stage in the process. Calcium is important; if one takes it away, blood will not clot. If we wish to draw blood freely from an artery or vein, it is only necessary to have it flow into a medium which lacks calcium ion. (This is why blood collecting vessels are treated with oxalate or citrate.)

TABLE 3.6:1 Nomenclature of Blood Clotting Factors

Factors	Other nomenclature or description
Factor I	Fibrinogen
Factor II	Prothrombin
Factor III	Tissue thromboplastin
Factor IV	Calcium
Factor V	Proaccelerin = labile factor = accelerator globulin = Ac-G
Factor VII	Proconvertin = SPCA = serum prothrombin conversion accelerator
Factor VIII	Antihemophilic factor = antihemophilic globulin
Factor IX	Christmas factor, plasma thromboplastin component
Factor X	Stuart-Prower factor = Stuart factor
Factor XI	Plasma thromboplastin antecedent
Factor XII	Hageman factor = contact factor = the fifth plasma thromboplastin precursor
Factor XIII	Fibrin stabilizing factor

Table 3.6:1 lists the factors involved in blood clotting. Biggs and Macfarlene (1966) explain the coagulation process as a cascade of transformations of inactive plasma clotting factors (proenzymes) into the active state (enzymes). At each stage, the product of one reaction triggers the next, and as a biochemical amplifier, leading to the formation of a greater weight of protein than the earlier step. Because a triggering sequence and amplification are necessary for coagulation, an almost total absence of any of these factors will make coagulation extremely slow.

An animal must possess some automatic leak-stopping device in the cardiovascular system in order to avoid bleeding to death as a result of any break in the vascular wall. Of the hemostasis mechanisms, the more obvious ones are (1) coagulation of the blood, (2) agglutination of the platelets, (3) contraction of damaged vessels, and (4) adhesion of the walls of cut vessels as a result of endothelium stickiness.

In biorheology our attention is drawn to the measurement of the course of mechanical changes that occur in the blood while coagulating. The rheological behavior can then be correlated with diseases, or used to develop drugs that either promote or prevent coagulation, or dissolve intravascular clots.

In principle, what we want to measure is the progressive change of a viscous fluid into a viscoelastic solid. The tools needed are the viscometer, rheogoniometer, cone-plate, cone-cone, or coaxial cylinders subjected to oscillatory motions, with provisions to measure the real and imaginary components of viscoelastic moduli. The real clinical demand is that the instrument should be simple, inexpensive, reliable, and need only a small amount of blood sample. A summary of some more popular instruments is given in Scott-Blair (1974). The instrument "thrombelastograph" of Hartert (1968) needs blood sample of only 0.3 ml.

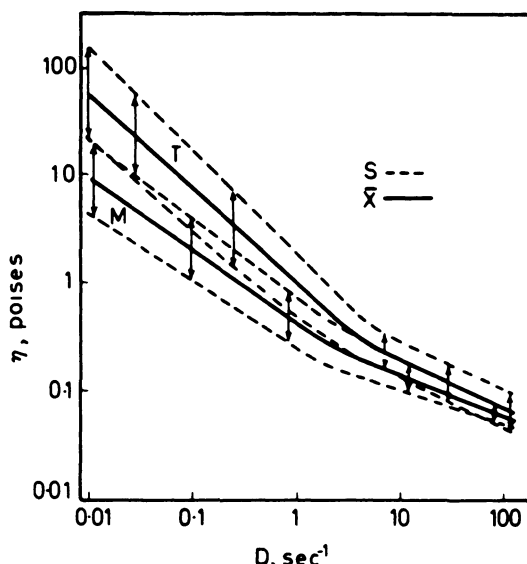


Figure 3.7:1 Arithmetic means (full lines) and one standard deviation (broken lines) of viscosities in normal men (M) and in patients with various thrombotic diseases (T). Viscosity, η , in poises, is plotted against the rate of shear, D , in s^{-1} , on a log-log scale, where \bar{x} is the arithmetic mean, and s is the standard deviation. Experimental data show log-normal distribution. From Dintenfass, (1971), p. 11. by permission.

3.7 Medical Applications of Blood Rheology

The most obvious use of blood rheology in clinical medicine is to identify diseases with any change in blood viscosity. Data collected for this purpose have been presented by Dintenfass in two books (1971, 1976). For our purpose it suffices to cite a few examples. Figure 3.7:1 shows a comparison of Dintenfass' data on the blood viscosity of normal healthy persons and patients with various thrombotic diseases. The diseased persons have higher viscosity. As we have seen in Sec. 3.4, elevation of blood viscosity at low shear rates indicates aggregation, whereas that at high shear rates suggests loss of deformability of the red blood cells. The viscosity change suggests some disease related changes in the blood.

Figure 3.7:2 suggests another aspect of blood rheology. It shows Langsjoen's (1973) result that a reduction of blood viscosity consequent to the infusion of dextran 40 solution in cases of acute myocardial infarction led to a significant improvement in both immediate and long-term survival. Dextran 40 (molecular weight about 40 000) solution dilutes the blood. The physiological effect of hemodilution is not simple, but the changed rheology must be a principal factor. For hemodilution, see Messmer and Schmid-Schoenbein (1972).

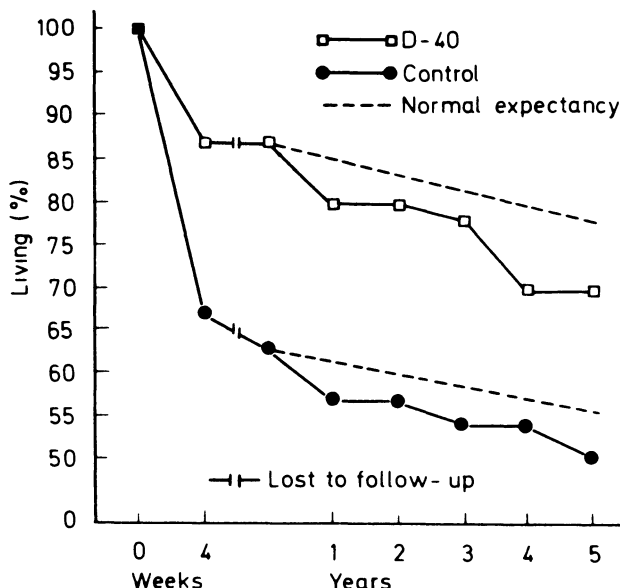


Figure 3.7:2 Survival of patients with acute myocardial infarction after conservative treatment (73 patients) and after treatment by infusion of dextran 40 (65 patients). Survival is recorded as the percentage of the original group. Note that there were more surviving patients in the dextran-treated group after 5 years than in the controls (conservative treatment) after 4 weeks. This gives cogent support to the premise that blood viscosity is an important determinant of myocardial work. Reproduced from Langsjoen, (1973), by permission.

The fluid added to the bloodstream to make up the lost volume of blood due to hemorrhage when a person suffers a wound is called *plasma expander*. Dextran solution is a good expander. The right plasma expander must have the right rheological property.

A second important rheological factor in clinical use is the coagulation characteristics of the blood. An obvious example is the hemophilic patient's difficulty with blood coagulation. On the other hand, hypertension (high blood pressure) and arteriosclerosis seem to correlate with an increase in the elasticity of the thrombi.

A third parameter in clinical use is the *erythrocyte sedimentation rate*. In anticoagulated blood, red cells may still clump together and cause a sedimentation. Fahraeus (1918) first studied this effect seriously. He noticed that blood from pregnant women sedimented faster than that of nonpregnant women, and believed that he might have found a convenient test for pregnancy. However, he soon afterwards found the same more rapid sedimentation in some male patients! It was then established that an increased erythrocyte sedimentation rate served as a good indication for both male and female patients that all was not well, and that quite a variety of conditions, many of them serious, increased the sedimentation rate. This is discussed in considerable detail in Dintenfass (1976).

It is quite clear that blood rheology as discussed in this chapter, referring to flow in vessels much larger than the diameter of red blood cells, reflects the interaction of red cells in bulk of whole blood. The “hyperviscosity” of blood in some disease states reflects the changes in hematocrit, plasma, and red cell deformability. On the other hand, the critical sites of interaction of red blood cells with blood vessels are in the capillary blood vessels. In the microcirculation bed, the deformability of the red cells is subjected to a really severe test. Hence it is expected that the pathological aspects of hyperviscosity will be seen in microcirculation. To pursue this matter, we shall consider the mechanical properties of red cells in the following chapter, and the flow properties of blood in microvessels in Chapter 5.

Problems

- 3.8** Assume that Casson's equation [Eq. (11) of Sec. 3.2] describes the viscosity of blood. Both τ_y and η are functions of the hematocrit. Experimental data (see Fig. 3.1:4) on τ_y may be presented by an empirical formula,

$$\tau_y = (a_1 + a_2 H)^3.$$

For normal blood, we may take $a_1 = 0$, $a_2 = 0.625$, when τ_y is in dyn cm^{-2} and H is a fraction. Experimental data on η can be expressed in many ways. Let us assume that for large blood vessels (Cokelet et al., 1963)

$$\eta = \eta_0 \frac{1}{(1 - H)^{2.5}},$$

where η_0 is the viscosity of the plasma.

For the capillary blood vessels Casson's equation does not hold; but we may assume

$$\mu = \eta_0 \frac{1}{1 - CH}.$$

We may take an average value $C = 1.16$ for pulmonary capillaries (Yen-Fung, 1973) and H in capillaries to be 0.45 times that of the systemic hematocrit in large arteries. The peripheral resistance from capillary blood vessels may be assumed to be a constant fraction of the total peripheral resistance. For the lung this fraction may be as high as $\frac{1}{3}$. For other parts of the body, this fraction is perhaps 15%.

With these pieces of information, let us consider the question “What is the best hematocrit that minimizes the work of the heart while the total amount of oxygen delivered to the tissues of the body remains constant?” Such a question is important in surgery or hemodilution, in deciding the proper amount of plasma expander to use.

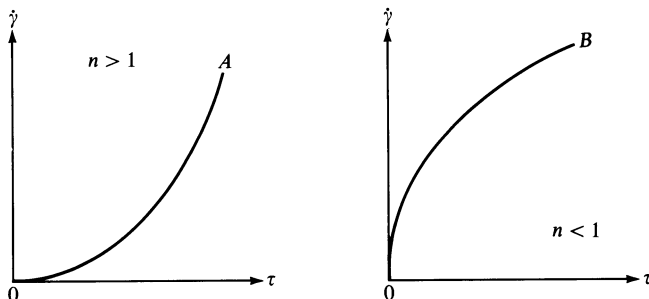
To answer this question we may consider blood flow as a flow in large and small vessels in series. The pressure drop in each segment is equal to the flow times the resistance which is proportional to blood viscosity. The total pressure difference the heart has to create is the sum of the pressure drop of the segments. The rate at which work is done by the heart is equal to the cardiac output (flow) times the pressure difference. The total amount of oxygen delivered to the tissues is proportional to the product of cardiac output and the hematocrit if the lung functions normally.

What would be the optimum hematocrit if the blood pressure is fixed and oxygen delivery is maximized?

- 3.9** The analysis of tube flow given in Sec. 3.3 ignores the radial migration of red cells away from the wall. As discussed in Sec. 3.5, for blood flowing in a tube, the immediate neighborhood of the solid wall is cell free. For blood with a red cell concentration above 0.4 and tube diameter $> 100 \mu\text{m}$, the cell-free layer is about $4 \mu\text{m}$ thick. For a dilute suspension, e.g., at red cell concentration 0.03, the thickness of the cell-free layer is larger (see Fig. 3.5:1). Use the information on the dependence of the constants τ_y and η of the Casson equation on the hematocrit as given in Problem 3.8 to revise the velocity profile and flow rate given in Eqs. (19) and (21) of Sec. 3.3. For this purpose assume the hematocrit to be constant away from the cell-free layer next to the wall. This assumption is quite good at normal hematocrit (0.2–0.5), but is rather poor for very dilute suspensions.
- 3.10** Consider the effect of non-Newtonian features of blood on the Couette flow of blood between concentric circular cylinders. Assume the outer cylinder to rotate, the inner cylinder stationary, Casson's equation to apply, cell-free layers next to solid walls with a thickness of a few (say, $4 \mu\text{m}$), and absence of end effects.
- 3.11** Analyze blood flow in a cone-plate or a cone-cone viscometer analogous to Problem 3.10.
- 3.12** Blood exposed to air will form a surface layer at the interface, which has a specific surface viscosity and surface elasticity, depending on the plasma constitution. In viscometry using a Couette flow or cone-plate arrangement, one must avoid reading the torque due to the surface layer. A *guard ring* was invented to shield the stationary cylinder from the torque transmitted through the surface layer. Propose a design for such a guard ring.
- 3.13** Consider the following thought experiment. Take normal red blood cells and suspend them in an isotonic dextran solution of viscosity η_0 . η_0 can be varied by varying the concentration of dextran. Measure the viscosity at a sufficiently high shear rate $\dot{\gamma}$ so that the influence of cell aggregates is insignificant. Let the viscosity be $\mu = \eta_r \eta_0$, where η_r is the “relative viscosity.” How would η_r vary with η_0 ? η_r reflects the effect of cell deformation. Would the red cells be more readily deformed in a more viscous suspending medium? Or less so? Predict curves of η_r versus $\dot{\gamma}$ for various values of η_0 .
- Note.* Compare your prediction with Chien's (1972) experimental results.
- 3.14** Discuss the pros and cons for several types of viscometers from the point of view of practical laboratory applications (convenience of operation, accuracy of data, amount of fluid samples needed, data reduction procedures, and procedures required for correction of errors).
- 3.15** Consider the flow of a Newtonian viscous fluid in a straight tube of infinite length and a rectangular cross-section, $a \times b$. Derive the equation that governs the velocity distribution in the tube. Express the volume flow rate as a function of the pressure gradient and the dimensions of the cross-section. Obtain results for the specially simple case when $b \gg a$. Then repeat the analysis if the fluid obeys Casson's equation, at least for the case in which $b \gg a$.
- 3.16** A fluid is said to obey a *power law* viscosity if the shear stress τ in a Couette flow is related to the shear rate $\dot{\gamma}$ by the equation

$$\dot{\gamma} = \frac{1}{k} \tau^n, \quad (n > 0). \quad (1)$$

This relationship is illustrated in Fig. P3.16.

Figure P3.16 Power-law viscosity. Curve A, $n > 1$; curve B, $n < 1$.

For a steady flow of an incompressible fluid obeying the power law (1) in a circular cylindrical tube of radius R , show that the axial velocity is

$$u = \frac{1}{2^n(n+1)k} \left(\frac{\Delta p}{L} \right)^n (R^{n+1} - r^{n+1}), \quad (2)$$

where Δp is the difference of pressures at the ends of a tube of length L . The rate of flow (volume) is

$$Q = \frac{\pi R^{n+3}}{2^n(n+3)k} \left(\frac{\Delta p}{L} \right)^n. \quad (3)$$

Let the average velocity be $U = Q/\pi R^2$, then

$$\frac{u}{U} = \frac{n+3}{n+1} \left[1 - \left(\frac{r}{R} \right)^{n+1} \right]. \quad (4)$$

- 3.17** A material is said to be a *Bingham-plastic* if the shear stress τ is related to the shear rate $\dot{\gamma}$ by the equation

$$\dot{\gamma} = \frac{1}{\eta_B} (\tau - f_B) \quad \text{when } \tau > f_B; \quad \text{and} \quad \dot{\gamma} = 0 \quad \text{when } \tau < f_B$$

The stress f_B is called the *yield stress*. The constant η_B is called *Bingham viscosity*. The relation is illustrated in Fig. P3.17.

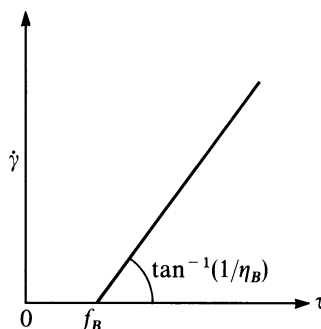


Figure P3.17 Flow curve of a Bingham plastic.

The steady flow of a Bingham plastic in a circular cylindrical tube of length L subjected to a pressure difference Δp can be analyzed in a manner similar to that presented in Sec. 3.5. Show that:

$$(a) \text{ If } \frac{\Delta p}{L} > \frac{2f_B}{R} \quad \text{and} \quad r_B = \frac{2f_B L}{\Delta p}, \quad \text{then}$$

$$u = \frac{\Delta p}{4\eta_B L} (R - r_B)^2 \quad \text{when } (r < r_B),$$

$$= \frac{\Delta p}{4\eta_B L} [R^2 - r^2 - 2r_B(R - r)] \quad \text{when } (r > r_B),$$

$$(b) \text{ If } \frac{\Delta p}{L} < \frac{2f_B}{R}, \text{ then there is no flow: } u = 0.$$

The flow rate is zero if $\Delta p < p_B \equiv 2Lf_B/R$, and is

$$Q = \frac{\pi R^4}{8\eta_B L} \left[\Delta p - \frac{4}{3} p_B + \frac{1}{3} \frac{p_B^4}{(\Delta p)^3} \right] \quad \text{if } (\Delta p > p_B).$$

- 3.18** A plastic material obeying the following relation between the shear stress τ and shear rate $\dot{\gamma}$ is called a plastic of *Herschel-Bulkley* type:

$$\dot{\gamma} = \frac{1}{k} (\tau - f_H)^n \quad \text{if } \tau > f_H, \quad \text{and} \quad \dot{\gamma} = 0 \quad \text{if } \tau < f_H,$$

where k , f_H , and $n > 0$ are constants. The Bingham plastic of Problem 3.17 is a special case in which $n = 1$, whereas the power law of Problem 3.16 is a special case when $f_H = 0$. For the general case, find the velocity distribution in a steady laminar flow of an incompressible Herschel-Bulkley fluid in a circular cylindrical tube.

- 3.19** Discuss the turbulent flow of water in a circular cylindrical tube. Consider the question of the relationship of mean velocity of flow with pressure gradient. Does it remain linear? How is the flow rate related to pressure gradient? Discuss resistance to flow in a turbulent regime.

Note. Many books deal with this subject. See references listed on p. 304 of Fung, *A First Course in Continuum Mechanics*.

References

- Barbee, J. H., and Cokelet, G. R. (1971) *Microvasc. Res.* **3**, 1–21.
 Biggs, R., and Macfarlane, R. G. (1966) *Human Blood Coagulation and Its Disorders*, 3rd ed. Blackwell, Oxford.
 Blackshear, P. L., Forstrom, R. J., Dorman, F. D., and Voss, G. O. (1971) *Fed. Proc.* **30**, 1600–1609.
 Brooks, D. E., Goodwin, J. W., and Seaman, G. V. F. (1970) *J. Appl. Physiol.* **28**, 172–177.
 Bugliarello, G., and Sevilla, J. (1971) *Biorheology* **7**, 85–107.
 Casson, M. (1959) In *Rheology of Disperse Systems*, Mills, C. C. (ed.). Pergamon, Oxford, pp. 84–104.

- Charm, S. E., and Kurland G. S. (1974) *Blood Flow and Micro Circulation*. Wiley, New York.
- Chien, S. (1970) *Science* **168**, 977–979.
- Chien, S. (1972) In *Hemodilution: Theoretical Basis and Clinical Application*, Messmer K., and Schmid-Schoenbein, H. (eds.). Karger, Basel.
- Chien, S., Usami, S., Taylor, M., Lundberg, J. L., and Gregersen, M. I. (1966) *J. Appl. Physiol.* **21**, 81–87.
- Chien, S., Usami, S., Dellenback, R. J., and Gregersen, M. I. (1967) *Science* **157**, 827–831.
- Chien, S., Usami, S., Dellenback, R. J., and Gregersen, M. (1970) *Am. J. Physiol.* **219**, 136–142.
- Chien, S., Luse, S. A., and Bryant, C. A. (1971) *Microvasc. Res.* **3**, 183–203.
- Cokelet, G. R. (1972) In *Biomechanics: Its Foundation and Objectives*. Fung Y. C., Perrone, N., and Anliker M. (eds.) Prentice-Hall, Englewood Cliffs, N. J., pp. 63–103.
- Cokelet, G. R., Merrill, E. W., Gilliland, E. R., Shin, H., Britten, A., and Wells, R. E. (1963) *Trans. Soc. Rheol.* **7**, 303–317.
- Dintenfass, L. (1971) *Blood Microrheology*. Butterworths, London.
- Dintenfass, L. (1976) *Rheology of Blood in Diagnostic and Preventive Medicine*. Butterworths, London.
- Fahraeus, R. (1918) *Biochem. Z.* **89**, 355.
- Fahraeus, R. (1929) *Physiol. Rev.* **9**, 241–274.
- Fahraeus, R., and Lindqvist, R. (1931) *Am. J. Physiol.* **96**, 562–568.
- Fung, Y. C. (1965) *Foundations of Solid Mechanics*. Prentice-Hall, Englewood Cliffs, N.J.
- Fung, Y. C. (1977) *A First Course in Continuum Mechanics*, 2nd ed. Prentice-Hall, Englewood Cliffs, N. J.
- Gabe, I. T., and Zatz, L. (1968) *Biorheology* **5**, 86 (Abstract).
- Goldsmith, H. L. (1971) *Biorheology* **7**, 235–242.
- Goldsmith, H. L. (1972a) In *Progress in Hemostasis and Thrombosis, Vol. I*, Spaet, T.H. (ed.). Grune & Stratton, New York, pp. 97–139.
- Goldsmith, H. L. (1972b) In *Theoretical and Applied Mechanics. Proc. 13th IUTAM Congress 1972*, Becker, E., and Mikhailov, G. K. (eds.). Springer, New York.
- Goldsmith, H. L., and Marlow, J. (1972) *Proc. Roy. Soc. London B* **182**, 351–384.
- Gregersen, M. I., Bryant, C. A., Hammerle, W. E., Usami, S., and Chien, S. (1967) *Science* **157**, 825–827.
- Hartert, H. (1968) In *Hemorheology, Proc. 1st Int Conf., Reykjavik, 1966*, Copley A. L. (ed.), Pergamon, Oxford, p. 335.
- Langsjoen, P. H. (1973) *Bibl. anat.*, No. 11. Karger, Basel, pp. 180–184.
- Larcan, A., and Stoltz, J. F. (1970) *Microcirculation et Hemorheologie*, Masson, Paris.
- Merrill, E. W., Gilliland, E. R., Cokelet, G. R., Shin, H., Britten, A., and Wells, R. E. (1963a) *Biophys. J.* **3**, 199–213.
- Merrill, E. W., Cokelet, G. C., Britten, A. and Wells, R. E. (1963b) *Circulation Res.* **13**, 48–55.
- Merrill, E. W., Benis, A. M., Gilliland, E. R., Sherwood, T. K., and Salzman, E. W. (1965a) *J. Appl. Physiol.* **20**, 954–967.

- Merrill, E. W., Margetts, W. G., Cokelet, G. R., and Gilliland, E. W. (1965b) In *Symposium on Biorheology*, Copley, A. L. (ed.). Interscience, New York, pp. 135–143.
- Messmer, K., and Schmid-Schoenbein, H. (ed.) (1972) *Hemodilution: Theoretical Basis and Clinical Application*. Karger, Basel.
- Oka, S. (1965) In *Symposium on Biorheology*, Copley, A. L. (ed.). Interscience, New York, p. 89.
- Oka, S. (1974) *Rheology—Biorheology*. Syokabo, Tokyo (in Japanese).
- Phibbs, R. H. (1969) In *Hemorheology*, Copley, A. L. (ed.). Pergamon, New York, pp. 617–630.
- Scott-Blair, G. W. (1974) *An Introduction to Biorheology*. Elsevier, New York.
- Thoma, R. (1927) In *Handbuch der biologischen Arbeitsmethoden*, Abderhalden, E. (ed.), Abt. V, Teil 4, II, p. 1103–1258. Urban & Schwarzenburg, Berlin.
- Thurston, G. B. (1972) *Biophys. J.* **12**, 1205–1217.
- Thurston, G. B. (1973) *Biorheology* **10**, 375–381; also, *ibid.* (1976) **13**, 191–199; (1978) **15**, 239–249; (1979) **16**, 149–162.
- Vadas, E. B., Goldsmith, H. L., and Mason, S. G. (1973) *J. Colloid Interface Sci.* **43**, 630–648.
- Whitmore, R. L. (1968) *Rheology of the Circulation*. Pergamon, New York.
- Yen, R. T. and Fung, Y. C. (1973) *J. Appl. Physiol.* **35**, 510–517.

CHAPTER 4

Red Blood Cells and Their Deformability

4.1 Introduction

In the previous chapter we studied the flow properties of blood. In this chapter we turn our attention to the red blood cells. Red blood cells are the gas exchange units of animals. They deliver oxygen to the tissues of all organs, exchange with CO_2 , and return to the lung to unload CO_2 and soak up O_2 again. This is, of course, what circulation is all about. The heart is the pump, the blood vessels are the conduits, and the capillary blood vessels are the sites where gas exchange between blood and tissue or atmosphere takes place.

If one observes human red blood cells suspended in isotonic solution under a microscope, their beautiful geometric shape cannot escape attention (see Fig. 4.1:1; which shows two views of a red blood cell, one a plane view, and one a side view. The cell is disc-shaped. It has an almost perfect symmetry with respect to the axis perpendicular to the disc. The question is often asked: Why are red cells so regular? Why are they shaped the way they are? When red cells grow in the bone marrow, they have nuclei, and their shape is irregular. Then as they mature, they expel their nuclei and enter the blood. They circulate in the body for 120 days or so, then swell into spherical shape and become hemolyzed by macrophages in the spleen. It is strongly suggestive that the red cell's regularity of shape is the consequence of its being circulated, crowded all along the way by other red cells and by capillary blood vessel walls. Every part of its membrane has an equal chance of being stretched, sheared, and worked on as another part. As a consequence, every part becomes equal to another in its mechanical properties. The idea is perhaps analogous to the making of ball bearings in a tumbling machine. The tumbling makes the balls perfect.

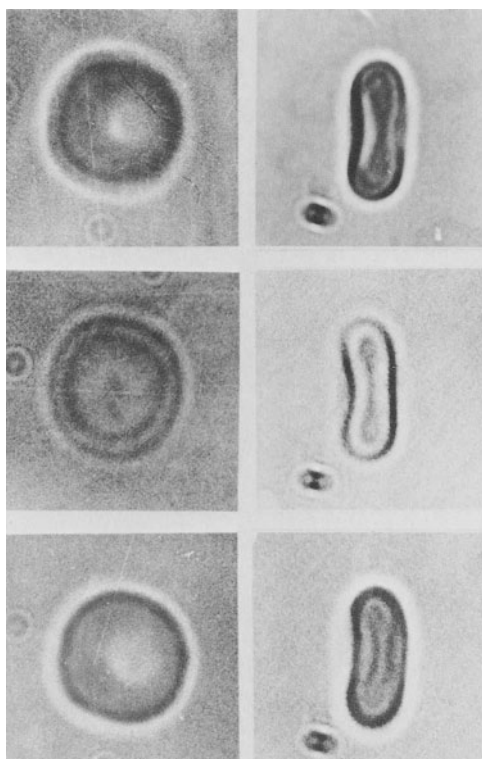


Figure 4.1:1 Two views of a normal human red blood cell suspended in isotonic solution as seen under a conventional optical microscope. Left: plane views. Right: side views. The three sets of images differ only in slight changes in focusing. These photographs illustrate the difficulty in accurately measuring the cell geometry with an optical microscope because of light diffraction. The isotonic Eagle-albumin solution is made up of 6.2 g NaCl, 0.36 g KCl, 0.13 g $\text{NaH}_2\text{PO}_4 \cdot \text{H}_2\text{O}$, 1.0 g NaHCO_3 , 0.18 g CaCl_2 , 0.15 g $\text{MgCl}_2 \cdot 6 \text{ H}_2\text{O}$, 0.45 g dextrose, and 1.25 g bovine serum albumin in 800 ml distilled water, buffered at pH 7.4. From Fung, Y.C. (1968) Microcirculation dynamics. *Biomed. Instrumentation* 4, 310–320.

In circulating blood, however, the red blood cells are severely deformed. Figure 4.1:2 shows photographs of blood flow in the capillary blood vessels in the mesentery of the rabbit and the dog. Note how different the cell shapes are compared with the isolated floating cells shown in Fig. 4.1:1! Some authors describe the red cells circulating in capillary blood vessels as parachute-shaped, others describe them as shaped like slippers or bullets.

The study of red blood cell geometry and deformability will throw light on the mechanical properties of cells and cell membranes, and thus is of basic importance to biology and rheology. It is also of value clinically, because change of shape and size and strength of red cells may be indicative of disease.

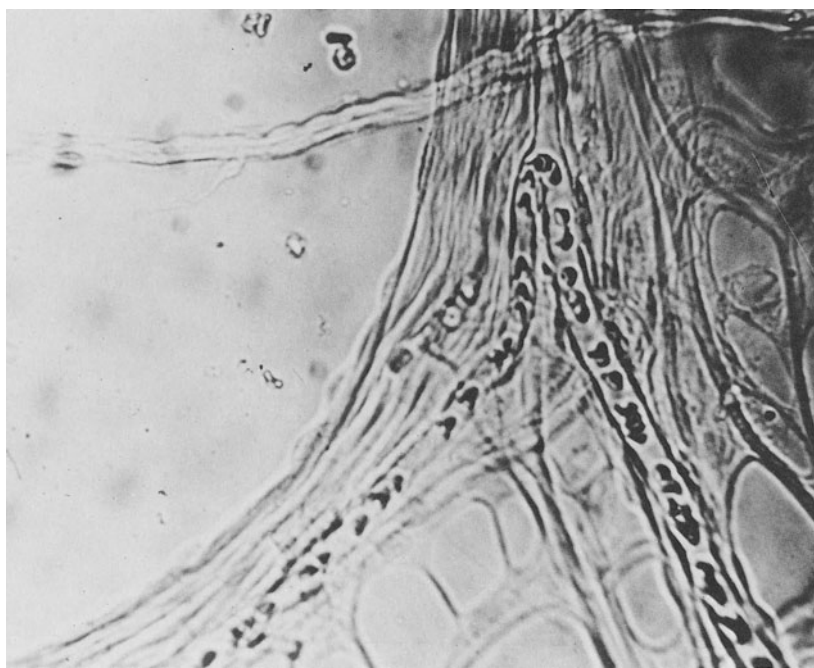
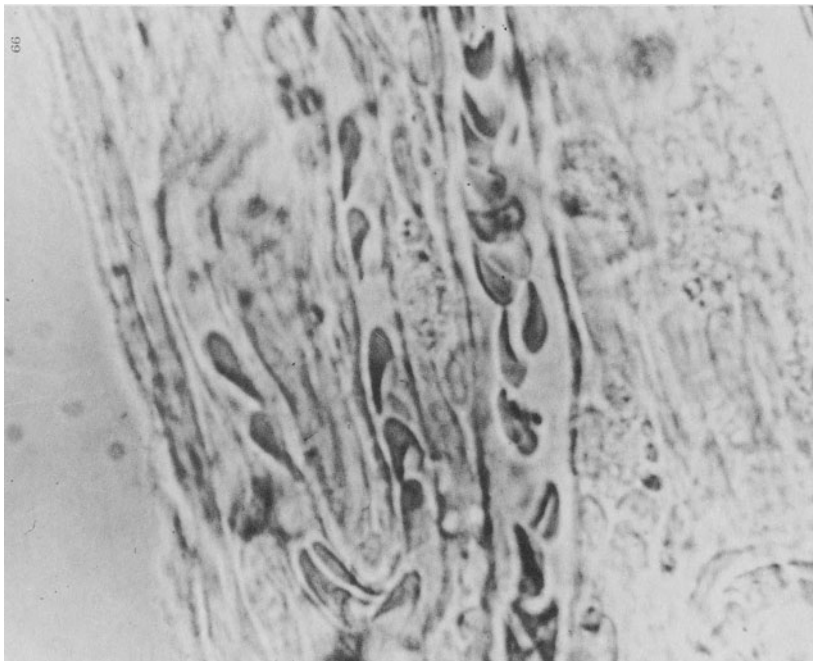


Figure 4.1.2 Photographs of red blood cells circulating in the capillary blood vessels in the mesentery of (left) a rabbit (courtesy of B.W. Zweifach); and of (right) a dog (courtesy of Ted Bond). From Fung, Y.C. (1969) Blood flow in the capillary bed. *J. Biomechanics* **2**, 353–372.

4.2 Human Red Cell Dimensions and Shape

All evidence shows that red blood cells are extremely deformable. They take on all kinds of odd shapes in flowing blood in response to hydrodynamic stresses acting on them. Yet when flow stops the red cells become biconcave disks. In isotonic Eagle-albumin solution the shape of the red cell is remarkably regular and uniform. We speak of red cell dimensions and shape in this static condition of equilibrium.

An accurate determination of red cell geometry is not easy. Photographs of a red blood cell in a microscope are shown in Fig. 4.1:1, from which one would like to determine the cell's diameter and thickness. The border of the cell appears as thick lines in the photographs. How can one determine where the real border of the cell is? In other words, how can we choose points in the thick image of the border in order to measure the diameter and thickness and other characteristics of red cell geometry?

The thickness of the cell border that appears in the photograph is not due to the cell being "out of focus" in the microscope. If we change the focus up and down slightly, the border moves, and a sequence of photographs as shown in Fig. 4.1:1 is obtained. Thus it is clear that the problem is more basic. It is related to the interaction of light waves with the red cells, because the thickness of the red cell is comparable with the wavelength of the visible light.

If we do not want to be arbitrary in making up a rule to read the photograph of images in a microscope for the determination of dimensions, we should have a rational procedure. Such a procedure must take into account the wave characteristics of light (physical optics). One approach is to describe the red cell geometry by an analytic expression with undetermined coefficients, calculate the image of such a body under a microscope according to the principles of physical optics, then compare the calculated image with the photographed image in order to determine the unknown coefficients. Such a program has been carried out by the author in collaboration with E. Evans (Evans and Fung, 1972). We used an interference microscope to obtain a photograph of the phase shift of light that passes through the red cell in a microscope. Figure 4.2:1 shows such a photograph. We assumed the following formula to describe the thickness distribution of the red blood cell:

$$D(r) = [1 - (R_0/r)^2]^{1/2} [C_0 + C_2(R_0/r)^2 + C_4(R_0/r)^4], \quad (1)$$

where R_0 is the cell radius, r is the distance from the axis of symmetry, and C_0 , C_2 , C_4 , and R_0 are numerical coefficients to be determined. The phase image corresponding to Eq. (1) is determined according to the principle of microscopic holography. The parameters C_0 , C_2 , C_4 , and R_0 are determined by a numerical process of minimization of errors between the calculated and photographed images. It was possible in this way to determine the geometric dimensions of the red cell to within $0.02 \mu\text{m}$. Hence a resolution of 0.5—1 % for the cell radius and 1 % for the cell thickness is achieved.

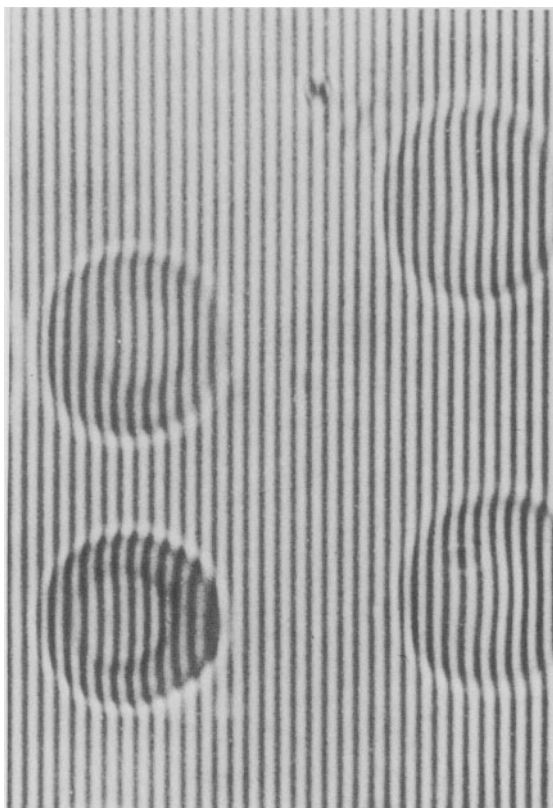


Figure 4.2:1 Picture of red blood cells taken with an interference microscope. Phase shift of light waves through the red cell leads to the deviations from the base lines.

The resolution of the cell surface area and cell volume are 2 and 3%, respectively.

Results obtained by Evans and Fung (1972) for the red cells of a man are shown in Tables 4.2:1 through 4.2:4. The cells were suspended in Eagle-albumin solution (see the legend of Fig. 4.1:1) at three different tonicities (osmolarity). At 300 mosmol the solution is considered isotonic. At 217 mosmol it is hypotonic. At 131 mosmol the red cells became spheres. In these tables the standard deviations of the samples are listed in order to show the spread of the statistical sample. The sample size was 50.

Figure 4.2:2 shows the cross-sectional shape and other geometric data of the average RBC from Evans and Fung (1972). It is seen that the thickness is most sensitive to environmental tonicity changes; the surface area is least sensitive. It is remarkable that the average surface area of the cell remained constant during the initial stages of swelling (300–217 mosmol).

The volume of the cell increases as the tonicity decreases. The χ^2 statistics data in Tables 4.2:1–4 show that the distribution of the maximum and minimum thickness and the volume are the closest to being normal for

TABLE 4.2:1 Statistics of 50 RBC in Solution at 300 mosmol at pH 7.4. From Evans and Fung (1972)

	Diameter	Minimum thickness	Maximum thickness	Surface area	Volume
Average	7.82 μm	0.81 μm	2.58 μm	135 μm^2	94 μm^3
Standard deviation σ	$\pm 0.62 \mu\text{m}$	$\pm 0.35 \mu\text{m}$	$\pm 0.27 \mu\text{m}$	$\pm 16 \mu\text{m}^2$	$\pm 14 \mu\text{m}^3$
2nd mom. M_2	3.77×10^{-1}	1.20×10^{-1}	7.13×10^{-2}	2.46×10^2	2.02×10^2
3rd mom. M_3	2.19×10^{-1}	-2.51×10^{-3}	3.26×10^{-4}	3.58×10^3	2.11×10^3
4th mom. M_4	4.81×10^{-1}	3.22×10^{-2}	1.73×10^{-2}	2.16×10^5	1.59×10^5
Skewness G_1	0.97	-0.063	0.018	0.96	0.76
Kurtosis G_2	0.57	-0.70	0.58	0.75	1.11
χ^2 for 10 groups	35.1	10.2	8.2	22.1	18.7

TABLE 4.2:2 Statistics of 55 RBC at 217 mosmol. From Evans and Fung (1972)

	Diameter	Minimum thickness	Maximum thickness	Surface area	Volume
Average	7.59 μm	2.10 μm	3.30 μm	135 μm^2	116 μm^3
Standard deviation σ	$\pm 0.52 \mu\text{m}$	$\pm 0.39 \mu\text{m}$	$\pm 0.39 \mu\text{m}$	$\pm 13 \mu\text{m}^2$	$\pm 16 \mu\text{m}^3$
2nd mom. M_2	2.66×10^{-1}	1.56×10^{-1}	1.50×10^{-1}	1.57×10^2	2.40×10^2
3rd mom. M_3	5.54×10^{-1}	1.02×10^{-2}	1.45×10^{-2}	-5.76×10^1	-1.25×10^3
4th mom. M_4	3.96×10^{-1}	8.82×10^{-2}	5.26×10^{-2}	1.21×10^5	2.07×10^5
Skewness G_1	0.41	0.17	0.26	-0.03	-0.35
Kurtosis G_2	2.98	0.80	-0.62	2.21	0.78
χ^2 for 10 groups	18.6	4.0	7.2	10.0	6.37

TABLE 4.2:3 Statistics of 50 RBC at 131 mosmol. From Evans and Fung (1972)

	Diameter	Surface area	Volume	Index of refraction difference
Average	6.78 μm	145 μm^2	164 μm^3	0.0447
Standard deviation σ	$\pm 0.32 \mu\text{m}$	$\pm 14 \mu\text{m}^2$	$\pm 23 \mu\text{m}^3$	± 0.0043
2nd mom. M_2	1.01×10^{-1}	1.84×10^2	5.34×10^2	1.82×10^{-5}
3rd mom. M_3	2.83×10^{-3}	4.42×10^2	3.29×10^3	8.83×10^{-9}
4th mom. M_4	2.31×10^{-2}	7.83×10^4	6.77×10^5	9.60×10^{-10}
Skewness G_1	0.09	0.18	0.28	0.12
Kurtosis G_2	-0.68	-0.63	-0.56	0.02
χ^2 for 10 groups	18.5	15.9	14.2	10.5

TABLE 4.2:4 Shape Coefficients for the Average RBC.
From Evans and Fung (1972)

Tonicity (mosmol)	R_0 (μm)	C_0 (μm)	C_2 (μm)	C_4 (μm)
300	3.91	0.81	7.83	-4.39
217	3.80	2.10	7.58	-5.59
131	3.39	6.78	0.0	0.0

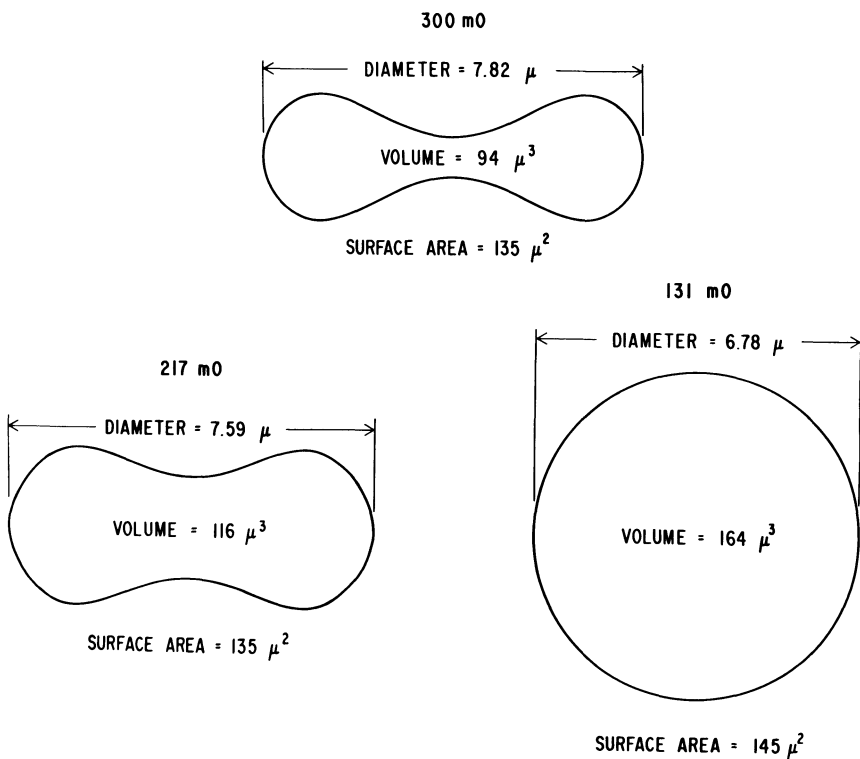


Figure 4.2:2 Scaled cross-sectional shape of the average RBC and other geometrical data of Evans. From Evans and Fung (1972).

each tonicity. Since these geometric properties are functionally related, it is not possible for all of them to have a normal distribution. For example, if the volume of a spherical cell is normally distributed, then the radius is not.

A more extensive collection of data based on the interferometric method named above was done by the author and W. C. O. Tsang (see Tsang, 1975). Table 4.2:5 shows the data from blood samples of 14 healthy men and women, with a total of 1581 cells. Figure 4.2:3 shows the average cell shape. Classification according to races, sexes, and ages showed no significant difference.

TABLE 4.2:5 The Geometric Parameters of Human Red Blood Cells. Statistics of Pooled Data from 14 Subjects; Sample Size $N = 1581$. 300 mosmol. From Tsang (1975).

	Diameter (μm)	Minimum thickness (μm)	Maximum thickness (μm)	Surface area (μm^2)	Volume (μm^3)	Sphericity index
<i>Mean</i>	7.65	1.44	2.84	129.95	97.91	0.792
<i>Std. error of mean</i>	± 0.02	± 0.01	± 0.01	± 0.40	± 0.41	± 0.001
<i>Std. dev., σ</i>	0.67	0.47	0.46	15.86	16.16	0.055
<i>Min. value</i>	5.77	0.01	1.49	86.32	47.82	0.505
<i>Max. value</i>	10.09	3.89	4.54	205.42	167.69	0.909
<i>Skewness G_1</i>	0.26	0.46	0.52	0.53	0.30	-1.13
<i>Kurtosis G_2</i>	1.95	1.26	0.24	0.90	0.30	3.27

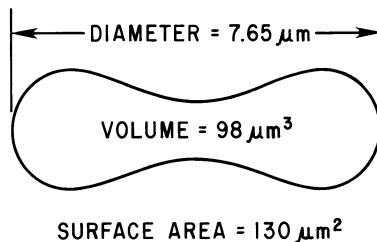


Figure 4.2:3 The average human red cell. From Tsang (1975); 14 subjects, $N = 1581$.

The red cell dimensions listed in Tables 4.2:1–5 may be compared with those published previously, but it must be realized that older data based on photographs through optical microscopes cannot discriminate any dimension to a sensitivity of $0.25 \mu\text{m}$ on account of the diffractive uncertainties mentioned in Sec. 4.1, and illustrated in Fig. 4.1:1. Data published before 1948 are summarized in Ponder (1948). Other important sources are those of Houchin, Munn, and Parnell (1958), Canham and Burton (1968), and Chien et al. (1971b).

The sphericity index in Tables 4.2:5 and 4.3:1 (p. 111) is equal to $4.84 (\text{cell volume})^{2/3} \cdot (\text{cell surface area})^{-1}$.

4.3 The Extreme-Value Distribution

How large is the largest red blood cell in a blood sample? The answer obviously depends on the size of the sample, but it cannot be obtained reliably by the ordinary procedure of adding a multiple of standard deviation to the mean. To assess the extreme value in a large sample, one has to use the statistical distribution of extreme values. The theory of statistics

of extremes is a well-developed subject. E. J. Gumbel (1958) has consolidated the theory in a book. He made many applications of the theory to such problems as the prediction of flood and drought, rain and snow, fatigue strength of metals, gust loading on aircraft, quality control in industry, oldest age in a population, etc. His method has been used by the author and P. Chen (Chen and Fung, 1973) to study red blood cells.

The method may be briefly described as follows. Take a random sample of blood consisting of, say, 100 red cells. By observation under a microscope, select and measure the diameter of the largest red cell in the sample. Throw away this sample; take another sample of 100 red cells, and repeat the process. In the end we obtain a set of data on the largest diameter in every 100. From this set of data we can predict the probable largest diameter in a large sample of, say, 10^9 cells.

It is fortunate that the asymptotic formula for the probability distribution of the largest among n independent observations turns out to be the same for a variety of initial distributions of the *exponential type*, which includes the exponential, Laplace, Poisson, normal, chi-square, logistic, and logarithmically transformed normal distributions. In these distributions the variates are unlimited toward the right, and the probability functions $F(x)$ converge with increasing x toward unity at least as quickly as an exponential function. The distribution of the diameter of red cells is most likely of the exponential type (past publications usually claim it to be approximately normal; see, for example, Ponder, 1948; Houchin, Munn, and Parnell, 1958; Canham and Burton, 1968), and hence we have great confidence in the validity of the extreme distribution. This was found to be the case by Chen and Fung (1973).

According to Gumbel (1954), the probability that the largest value in a sample of size n will be equal to or less than a certain value x is given by

$$F(x) = \exp[-\exp(-y)], \quad (1)$$

where

$$y = \alpha(x - u), \quad (2)$$

and α, u , are parameters depending on n . The parameter u is the *mode*, and is the most probable value of x . The inverse of the parameter α is a measure of dispersion, called the *Gumbel slope*. The parameters are determined by the following formulas:

$$\frac{1}{\alpha} = \frac{S\sqrt{6}}{\pi}, \quad u = \bar{x} - \frac{0.57722}{\alpha}, \quad (3)$$

where \bar{x} is the mean and S is the standard deviation of the extreme variate. The variable y is dimensionless and is called the *reduced largest value*. For a continuous variate there is a probability $1 - F(x)$ for an extreme value to be equal to or exceeded by x . Its reciprocal,

$$T(x) = \frac{1}{1 - F(x)}, \quad (4)$$

is called the *return period*, and is the number of observations required so that, on the average, there is one observation equalling or exceeding x .

Gumbel (1954, 1958) has reduced the procedure of testing the goodness of fit of the mathematical formula to any specific set of observed data, as well as the evaluation of parameters α and u , to a simple graphical method. He constructed a probability paper for extreme values in which the reduced largest value y , the cumulative probability $F(x)$, and the return period $T(x)$, are labeled on the abscissa, while the variate x is labeled linearly on the ordinate. This graph paper is given in King (1971). An example is given in Fig. 4.3:1. The entire set of n observed largest values is plotted onto this paper in the following manner. List all the data points in order of their magnitude, x_1 being the smallest, x_m the m th, and x_n the largest. Plot x_m against a cumulative probability

$$\bar{F}_m = \frac{m}{n+1}, \quad (5)$$

If the theoretical formula (1) applies, the data plotted should be dispersed about a straight line

$$x = u + \frac{y}{\alpha}, \quad (6)$$

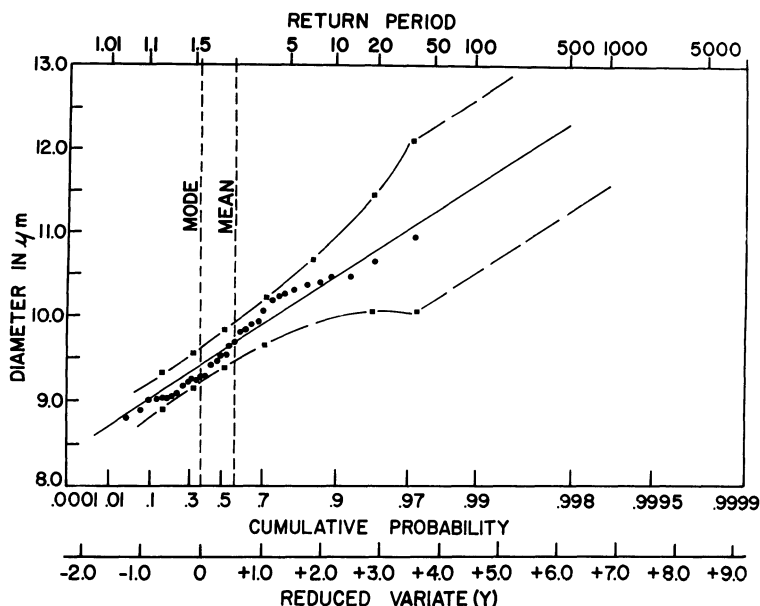


Figure 4.3:1 Extreme value distribution of red blood cells plotted on Gumbel's probability paper. The sample batch size is 100 cells. The set of data on the largest diameter in every 100 cells is plotted. The least-squares fit straight line is represented by $x = 9.386 + 0.4568y$. Circles represent experimental data. Squares are computed at 95% confidence limits. From Chen and Fung (1973).

The intercept and the slope of the fitted straight line give us the parameters u and α . Having this straight line, we can find the expected largest value corresponding to any desired large return period T from the reduced variate:

$$y = \log_e T(x). \quad (7)$$

Chen and Fung (1973) used the method of resolution of microscopic holography (Evans and Fung, 1972) discussed in Sec. 4.2, to obtain the dimensions of the red cells, and then used the Gumbel method to determine the extreme-value distribution.

The experimental results of four subjects in the age range 22–29 are summarized in Table 4.3:1. A typical extreme value plot for a subject is shown in Figure 4.3:1. Within the 95% confidence limit, it can be seen that the distribution of the largest diameter follows the theoretical asymptote for the exponential type of initial distribution. The Gumbel slope is relatively constant for all the subjects. When compared to the study of normal blood samples, the large cells have a larger surface area and volume, the minimum thickness is higher, the maximum thickness remains approximately the same, and the sphericity is lower. A correlation study shows that for the most probable largest cell in a sample of size n , the cell surface area and the minimum thickness are proportional to the cell diameter. The maximum thickness seems to be independent of the cell diameter. The sphericity index decreases with increasing cell diameter. There is no correlation between cell volume and cell diameter for the largest cell.

TABLE 4.3:1 Distribution of Diameter, Area, Volume, Maximum Thickness, Minimum Thickness, and Sphericity Index of Cells with the Largest Diameter in Samples of 100 Cells Each. 300 mosmol. From Chen and Fung (1973)

Subject	PC	JP	DV	MY
Sex	M	M	M	M
No. of Samples	55	36	35	37
Mode (μm) of largest diameter	9.083	9.372	9.386	9.168
Gumbel slope ($1/\alpha$) of largest diameter	0.5204	0.5255	0.4548	0.5314
Area	175.34	184.42	182.00	178.01
(μm^2) \pm SD	± 20.21	± 20.29	± 14.25	± 20.37
Volume	119.87	129.08	132.38	130.03
(μm^3) \pm SD	± 17.45	± 17.37	± 16.81	± 19.64
Maximum thickness	2.367	2.449	2.456	2.510
(μm) \pm SD	± 0.281	± 0.217	± 0.249	± 0.229
Minimum thickness	0.751	1.086	0.9716	1.0281
(μm) \pm SD	± 0.358	± 0.318	± 0.2815	± 0.314
Sphericity index	0.6711	0.6703	0.6907	0.6979

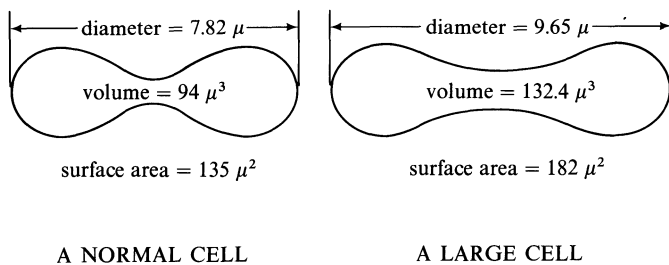


Figure 4.3:2 Comparison between a normal red blood cell from Evans and Fung (1972) and an extreme cell from Chen and Fung (1973).

Figure 4.3:2 shows a comparison between a mean cell from Evans and Fung (1972) and an extreme cell from Chen and Fung (1973). The difference in cell shape is quite evident. If we predict the size of the largest cell in a population of 10^8 cells, then for subject PC we obtain an impressive value of $15.66\text{--}17.06 \mu\text{m}$ for its diameter, as compared with the mean value of $7.82 \mu\text{m}$; i.e., the largest cell's diameter is more than twice that of the average.

The same technique can be used to study the smallest red cell in a given sample, but there seem to be no reason to do so. However, a study of the smallest cross-section of a blood vessel may have meaning. Sabin et al (1978) have used this method to determine the elasticity of pulmonary arterioles and venules. We can think of many biological variables whose extreme values are of interest. The method deserves to be widely known.

4.4 The Deformability of Red Blood Cells (RBC)

In flowing through capillary blood vessels, red cells are so highly deformed that they give an impression of great flexibility. An illustration of deformed red blood cells in flowing blood in the mesentery of a dog is shown in Fig. 4.1:2 in Sec. 4.1. The order of magnitude of the stresses that correspond to such a large deformation may be estimated as follows. Assume that a capillary blood vessel $500 \mu\text{m}$ long contains 25 RBC and has a pressure drop of $2 \text{ cm H}_2\text{O}$. Then the pressure drop is about 0.08 g/cm^2 per RBC. Imagine that the RBC is deformed into the shape of a cylindrical plug with an end area of $25 \mu\text{m}^2$ and a lateral area of $90 \mu\text{m}^2$. The axial thrust $0.08 \times 25 \times 10^{-8} \text{ g}$ is resisted by the shear force $\gamma \times 90 \times 10^{-8}$ acting on the lateral area. Then the shear stress γ is of the order of $0.08 \times \frac{25}{90} = 0.02 \text{ g/cm}^2$, or 20 dyn/cm^2 . Such a small stress field is sufficient to induce a deformation with a stretch ratio of the order of 200% in some places on the cell membrane! This stress level may be compared with the “critical shear stress” of about 420 dyn/cm^2 , which Fry (1968, 1969) has shown to cause changes in the endothelial cells of the arteries. It may also be compared with the “shearing” stress of about $50\text{--}1020 \text{ dyn/cm}^2$ acting at the interface between a leukocyte and an endothelium when

the leukocyte is adhering to or rolling on the endothelium of a venule (Schmid-Schoenbein, Fung, and Zweifach, 1975).

Red cell deformation can also be demonstrated in Couette flow and in Poiseuille flow (Schmid-Schonbein and Wells, 1969; Hochmuth, Marple, and Sutera, 1970). In fact, one of the successful calculations of the viscosity of the hemoglobin solution inside the RBC was made by Dintenfass (1968) under the assumption that the cell deforms like a liquid droplet in a Couette flow. Based on an analytical result on the motion of liquid droplets obtained earlier by G. I. Taylor, Dintenfass calculated the viscosity of the RBC contents to be about 6 cP. Experiments by Cokelet and Meiselman (1968) and Schmidt-Nielsen and Taylor (1968) on red cell contents, obtained by fracturing the cells by freezing and thawing and removing the cell membranes by centrifugation, showed that the hemoglobin solution in the red cell behaves like a viscous fluid with a coefficient of viscosity of about 6 cP. Thus one may infer that the red cell does behave mechanically like a liquid droplet wrapped in a membrane.

One would think that a liquid droplet without a membranous shell would be more flexible. Yet, compared with the red cell, such a droplet appears to be more rigid. In Fig. 3.4:3 in Sec. 3.4, we have shown a comparison of the viscosity of whole blood with that of various suspensions and emulsions of oil droplets. In such a fluid, the more flexible the particles are, the lower is the viscosity. Figure 3.4:3 shows that the whole blood often has a lower viscosity. The reason is the surface tension. The surface tension acting on the surface of the oil droplets is quite large (from 10's to 100's of dyn/cm), but the wall of the red blood cell appears to be unstressed in the static condition.

The question why red cells are so flexible is related to why they are biconcave. The second question refers to the equilibrium configuration of the cell under uniform external pressure, while the first refers to equilibrium when the cell is subjected to nonuniform normal and shear stresses. Neither of these questions has a full answer, although searching for the answers does lead to deeper understanding of the mechanical properties of cells.

The question why red blood cells are biconcave in shape has been debated for many years. Ponder (1948, p. 22) thinks that the biconcave disk shape is the optimum geometry for oxygen transfer. The analysis is correct but the reasoning is doubtful, because red cells assume a biconcave disk shape only when they are in static equilibrium: in a flowing condition they are deformed into the shape of a bullet or slipper in the capillary blood vessels, where oxygen transfer takes place. Canham (1970) thinks that the red cell membrane is flat if it is unstressed, that it behaves like a flat plate, and has a finite bending rigidity and negligible resistance to stretching. Then he shows that if such a flat bag is filled with fluid, the biconcave disk shape is the one that minimizes the potential energy. Such an analysis is interesting but somewhat futile. Perhaps it is more meaningful to accept the fact that the shape of the red cell at static equilibrium is biconcave and ask *what special consequences are implied by the biconcavity*. In fact, the answer to such a question can yield

information about the stresses in the cell membrane, the pressure in the interior of the cell, and the deformability and strength of the cell.

Biconcavity is a geometric property. A deduction made from geometry and the first principles of mechanics will be simple and general. Uncluttered by special chemical and biological hypotheses, the theory will be as transparent as a proposition in geometry. We shall present such a simple analysis in the following section.

4.5 Theoretical Considerations of the Elasticity of Red Cells*

We consider a red blood cell as a thin-walled shell containing a viscous incompressible liquid. We shall consider static equilibrium of such a shell, so that the liquid inside is not flowing, and the only stress it can have is a uniform pressure, which will be denoted as p_i . The thickness of the cell membrane is of the order of 7–10 nm. Since the cell diameter is about 8 μm , the radius-to-wall-thickness ratio is of the order 500. This qualifies the cell wall as “thin” in the sense of the theory of elastic shells. For such a thin shell, the bending stresses are small, and the stress resultants, the so-called “membrane” stresses, predominate.

For the purpose of mechanical analysis, there is no need to know the detailed structure of the cell membrane. An overall description of the membrane characteristics is sufficient. All we need to assume is that the cell membrane is elastic when the stresses in the wall are sufficiently small.

Stress Distribution in a Biconcave Shell of Revolution

Let us consider an axially symmetric biconcave shell of revolution in static equilibrium under internal pressure. Because of the axial symmetry, it is necessary only to consider a meridional cross-section as shown in Fig. 4.5:1. A point P on the shell can be identified by a pair of cylindrical polar coordinates (r, z) or by r and the angle ϕ between a normal to the shell and the axis of revolution. At each point on the shell, there are two principal radii of curvature: One is that of the meridional section, shown as r_1 in Fig. 4.5:1. The other is equal to r_2 , a distance measured on a normal to the meridian between its intersection with the axis of revolution and the middle surface of the shell. The lines of principal curvature, are the meridians and parallels of the shell.

The stresses in the shell may be described by stress resultants (membrane stresses) and bending moments. The stress resultants are the mean stress in

* The material in this section is taken from Fung (1966).

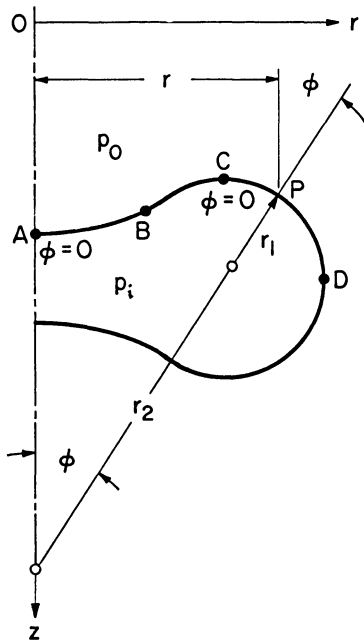


Figure 4.5:1 Meridional cross-section of the red blood cell. Angle ϕ , the radial distance r , or the arc length s may be chosen as the curvilinear coordinates for a point on the cell membrane. Note the principal radii of curvature r_1, r_2 at point P . Point B is a point of inflection.

the membrane multiplied by the thickness. The bending moments arise from the variation of the stresses within the thickness of the membrane. For very thin shells, the stress distribution in the shell is given accurately by the membrane theory (ignoring bending moments). The stress resultants acting on an element of the shell surface bounded between two meridional planes $\theta = \theta_0$, and $\theta = \theta_0 + d\theta$, and two parallel planes $\phi = \phi_0$ and $\phi = \phi_0 + d\phi$ are shown in Fig. 4.5:2. The symbol N_ϕ denotes the normal stress resultant (force per unit length, positive if in tension) acting on sections $\phi = \text{const}$, N_θ denotes the normal stress resultant (tension) per unit length acting on sections $\theta = \text{const}$. The symbol $N_{\theta\phi}$ is the shear resultant per unit length acting on sections $\theta = \text{const}$, and $N_{\phi\theta}$ is the shear acting on $\phi = \text{const}$. For axisymmetric loading, $N_{\theta\phi} = N_{\phi\theta} = 0$. The equations of equilibrium are (see Flügge, 1960, p. 23), for a shell subjected to a uniform internal pressure p_i and a uniform external pressure p_o :

$$\frac{d}{d\phi} (rN_\phi) - r_1 N_\theta \cos \phi = 0, \quad (1)$$

$$\frac{N_\phi}{r_1} + \frac{N_\theta}{r_2} = p_i - p_o. \quad (2)$$

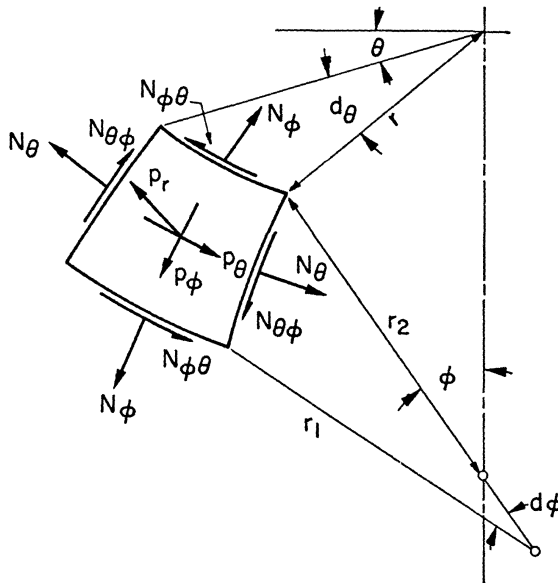


Figure 4.5:2 Notations. Vectors showing the stress resultants (force per unit length in the cell membrane) N_ϕ , N_θ , $N_{\phi\theta}$ and the external loads (force per unit area) p_r , p_θ , p_ϕ .

Solve Eq. (2) for N_θ , substitute into (1), and multiply by $\sin \phi$ to obtain

$$\frac{d}{d\phi} (r_2 N_\phi \sin^2 \phi) = r_1 r_2 (p_i - p_o) \cos \phi \sin \phi. \quad (3)$$

An integration gives the result

$$N_\phi = \frac{1}{r_2 \sin^2 \phi} \left[\int r_1 r_2 (p_i - p_o) \cos \phi \sin \phi \, d\phi + c \right] \quad (4)$$

where c is a constant. From Fig. 4.5:1, we can read off the geometric relations

$$r = r_2 \sin \phi, \quad \frac{dr}{d\phi} = r_1 \cos \phi, \quad \frac{dz}{d\phi} = r_1 \sin \phi. \quad (5)$$

Thus Eq. (4) can be reduced to the form

$$N_\phi = \frac{1}{r \sin \phi} \int_0^r (p_i - p_o) r \, dr. \quad (6a)$$

This solution yields the alarming result that at the top point C in Fig. 4.5:1 where $\phi = 0$ and r is finite, we must have $N_\phi \rightarrow \infty$ if $p_i - p_o \neq 0$. This result, that a finite pressure differential implies an infinitely large stress at the top (point C), is so significant that a special derivation may be desired. Consider the equilibrium of a circular membrane that consists of a portion of the shell near the axis, say, inside the point B in Fig. 4.5:1. The isolated circular membrane is shown in Fig. 4.5:3(a). The total vertical load acting on the

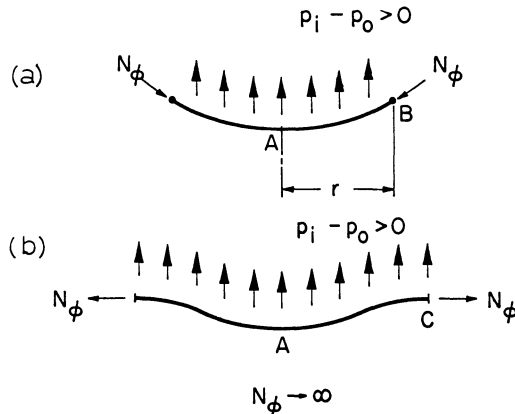


Figure 4.5:3 Equilibrium of a polar segment of the cell membrane. Pressure load is balanced by the membrane stress resultant N_ϕ . Transverse shear and bending stresses in the thin cell membrane are ignored. (a) At B the slope of the membrane $\neq 0$. (b) At C the slope = 0.

membrane is

$$(p_i - p_o)\pi r^2.$$

This load must be resisted by the vertical component of the stress resultant acting on the edges, namely, $N_\phi \sin \phi$, multiplied by the circumference $2\pi r$. Hence

$$2\pi r N_\phi \sin \phi = (p_i - p_o)\pi r^2,$$

or

$$N_\phi = \frac{p_i - p_o}{2} \frac{r}{\sin \phi}. \quad (6b)$$

At C , $r \neq 0$, $\phi = 0$, and N_ϕ must become infinitely large. Figure 4.5:3(b) shows this very clearly. Here the slope at C is horizontal. No matter how large N_ϕ is, the stress resultant on the edges cannot balance the vertical load. Hence $N_\phi \rightarrow \infty$.

Perhaps no biological membrane can develop such a large stress. Therefore, if we insist that $p_i - p_o \neq 0$, then we shall have a major difficulty. This difficulty is removed if we admit the natural conclusion that the pressure differential across the cell wall vanishes:

$$p_i - p_o = 0. \quad (7)$$

Then it follows that for a normal biconcave red cell, the membrane stresses N_ϕ , N_θ vanish throughout the shell:

$$N_\phi = N_\theta = 0. \quad (8)$$

Our conclusion is based on the biconcave geometry of the red cell. Nucleated cells and some pathological erythrocytes do not assume biconcave geometry; consequently, our conclusion does not apply. Sickle cells have a

crystalline hemoglobin structure inside the cell. Leukocytes have gelated pseudo pods. To them our analysis does not apply because in their interior the stress field cannot be described by pressure alone, and resistance to deformation is offered by viscoelasticity of the material.

How Is the Natural Shape of the Red Cell Maintained?

When the pressure differential is removed as a factor for maintaining the shape of the erythrocyte, it is clear that the cell membrane itself must be responsible for the natural shape. The cell takes up the biconcave shape whenever it is completely relaxed, for much the same reason as a rubber glove has a natural shape.

In the membrane stress analysis discussed above, the bending rigidity of the cell wall is ignored. In the following we shall briefly discuss the effects of bending and transverse shear. First, the difficulty of infinite tensile stress N_ϕ in the case shown in Fig. 4.5:3(b) at the point C can be removed by the introduction of transverse shear. But N_ϕ will remain large if the pressure differential $p_i - p_o$ is finite, so that our earlier conclusion remains valid. Second, consideration of bending is needed if the details of the shape changes in the process of swelling of the red cell in hypotonic solutions, (as illustrated by the three cases shown in Fig. 4.2:2) is to be explained (Zarda et al., 1977). But this does not alter the conclusion that the transmural pressure, $p_i - p_o$, remains small during the process.

As is well known in the theory of plates and shells, (see, e.g., Flügge, 1960), the bending rigidity of a thin isotropic plate or a thin shell is proportional to the cubic power of the wall thickness:

$$\text{bending rigidity } D = \frac{Eh^3}{12(1 - \nu^2)}, \quad (9)$$

where E is Young's modulus, h is the wall thickness, and ν is Poisson's ratio. In contrast, the extensional rigidity is Eh , proportional to the first power of the wall thickness. When the thickness h is very small, the bending rigidity is much smaller than the extensional rigidity.

It is intuitively clear that when an external load is applied to an elastic structure, the most rigid component will rise to resist the load and take up the greatest share of responsibility. Indeed this is true in the behavior of a thin shell. Because the extensional rigidity is much greater than that of bending, a thin shell will resist an external load essentially by membrane stresses (tension, compression, and shear). When equilibrium can be achieved by the action of membrane stresses alone, the shell is efficient and strong. However, when the curvature change is very large, the bending energy must be called into play. This is the case, for example, in the neighborhood of the point of application of a concentrated load, in the neighborhood of an edge, at a place with a sharp change of slope, or at a seam where a sudden change of thickness

or curvature occurs. In the absence of these large curvature changes, the membrane theory is accurate. This is why the conclusion reached in the previous section on stress distribution in a biconcave shell is a good approximation.

Summarizing, we may say that under the assumption that the red cell interior is a liquid, the natural biconcave shape can be maintained because the pressure differential across the cell membrane is small. As a consequence, the membrane stress in the cell wall is essentially zero when the cell is biconcave.

Isochoric Applicable Deformations

We shall now ignore bending stresses and consider possible change of shape of the red cells. We shall consider a cell as a deformable shell filled with an incompressible fluid. Let the shell be impermeable to the fluid. Any deformation of the shell must preserve the volume of the incompressible fluid. We call such a deformation *isochoric*. The deformation of an erythrocyte without mass transport across its membrane is isochoric.

In the theory of differential geometry (see, for example, Graustein, 1935, or Struik, 1950, a surface is said to be *applicable* to another surface if it can be deformed into the other by continuous bending without tearing and without stretching. A deformation of a surface into an applicable surface involves no change in the intrinsic metric tensor on the surface. No change in the membrane strain is involved in such a deformation. Accordingly, no change in membrane stresses will occur in such a deformation.

A deformation of a shell by continuous bending without tearing or stretching and with the enclosed volume kept constant is called an *isochoric applicable deformation*. From what has been said above, we conclude that an isochoric applicable deformation of an erythrocyte will induce no change in the membrane stresses in the cell wall.

Consider a spherical shell made of an elastic material. Let the shell be filled with an incompressible liquid and be placed in another fluid. Now suppose the external pressure is reduced. If the internal pressure does not change, the shell would expand. But such an expansion is impossible because the volume is fixed. Hence the internal pressure must be reduced to equal the reduced external pressure so that the stress in the shell will remain unchanged. Hence an elastic spherical shell transmits pressure changes perfectly, so that the changes in internal pressure are exactly equal to the changes in external pressure.

Next consider an arbitrary elastic shell containing an incompressible fluid. Although no longer so obvious, the same argument as above applies, and we conclude that neither a change in the membrane stress in the shell, nor a change in the pressure differential across the shell, can be achieved by

manipulating the external pressure alone, as long as the deformation is isochoric and applicable.

It is known in differential geometry that if two surfaces are applicable to each other, their Gaussian curvature (also called the total curvature, which is the product of the two principal curvatures) must be the same at corresponding points. Thus a developable surface (whose Gaussian curvature is zero) is applicable to another developable surface. A spherical surface is applicable to another spherical surface of the same radius. Some examples are shown in Fig. 4.5:4. In Figs. 4.5:4(a) and (b) it is seen that cylindrical and conical shells are applicable to each other and to flat sheets if they can be cut open. In Fig. 4.5:4(c) a diamond-patterned surface composed of flat triangles can be shown to be applicable to a cylinder. In Fig. 4.5:4(d) a dimple with reversed curvature on a sphere is applicable to the original sphere. Although deformations shown in Figs. 4.5:4(c) and (d) are not isochoric, they are important modes of buckling of cylindrical and spherical shells. In Fig. 4.5:4(e) a biconcave shell similar to an erythrocyte is shown. In this case an infinite variety of isochoric applicable surfaces exists.

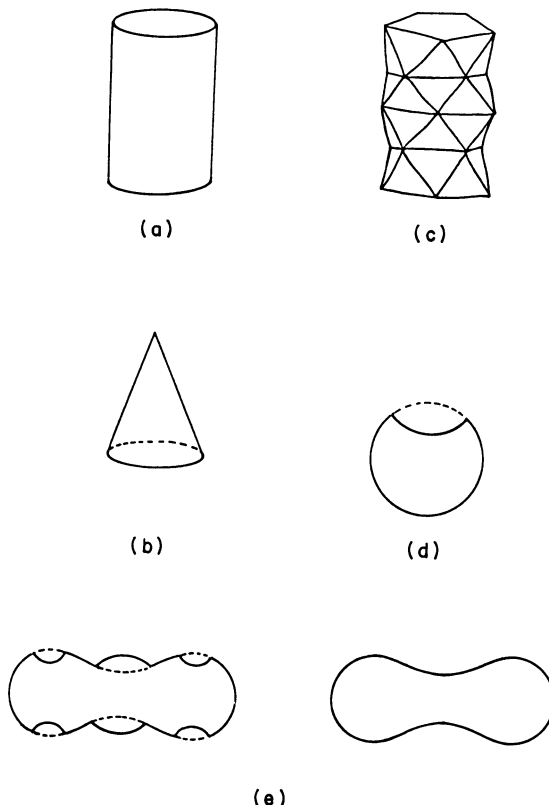


Figure 4.5:4 Examples of applicable surfaces. In e an isochoric applicable deformation of a red blood cell is shown.

The great liberty with which a biconcave erythrocyte can deform isochorically into an infinite variety of applicable surfaces must be the way nature has endowed a disarming simplicity to the mechanics of the erythrocyte. With this property, the erythrocyte can deform without inducing any membrane stresses in its cell membrane, and without any change in the pressure differential between the interior and the exterior.

Problems

- 4.1** Show that a circular cylindrical surface and a circular cone are both *applicable* to a plane, i.e., they can be deformed into a plane without stretching and tearing. The same is true for cylinders and cones of arbitrary cross-section. Note that the statement is true only in the sense of differential geometry; and not in a global sense. To deform a whole cylinder into a plane, a cut has to be made. The cut cylindrical surface can then be spread out into a plane. Verify that the deformations shown in Fig. 4.5:4 are applicable deformations.
- 4.2** According to Schmid-Schoenbein and Wells (1969), a red blood cell can be seen “tank-treading” in a shear flow; that is, under the microscope its wall seems to rotate about itself like the belt of a tank (Fig. P4.2). Different points on the belt take turns being at the front, bottom, rear, and on top. It follows that the material of the red cell membrane at the dimples and the equator is not fixed.

Show that, in accordance with the analysis given in Sec. 4.5, the biconcave disc is applicable to itself when it “tank-treads” (Fig. P4.2). Would the membrane stress in the cell membrane be changed in such a motion?

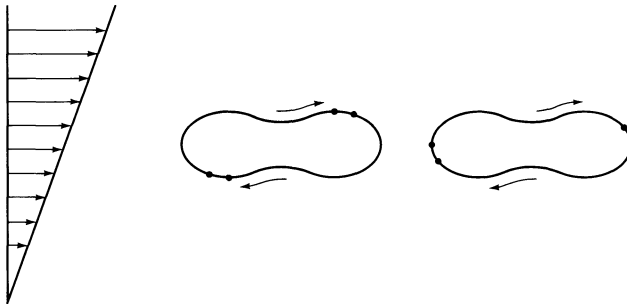


Figure P4.2 “Tank treading” of red blood cells in shear flow.

- 4.3** Imagine an arbitrary continuous curve in a three-dimensional space. A tangent line can be drawn at every point on the curve. As one moves continuously along the curve, the tangent lines of successive points form a continuum and sweep out a surface that is called a *tangent surface*. Show that a tangent surface generated by an arbitrary space curve is *developable*, i.e., it is *applicable* to a plane.
- 4.4** Prove that, for two surfaces to be applicable to each other, the total curvature (product of the principal curvatures) must remain the same at the corresponding points.

4.6 Cell Membrane Experiments

In the preceding section, we considered the consequences of the biconcave disc shape of the red blood cell and concluded that the geometry makes the cell flaccid so that it can deform into a great variety of shapes *without* inducing any membrane stresses (i.e., without stretching the membrane in any way), provided that the small bending stress (and rigidity) of the cell membrane is ignored. This great flexibility is, of course, a great asset to the red cell, which has to circulate all the time and to go through very narrow tubes in every cycle. If the cell can deform and squeeze through the narrow tubes without inducing any stress, then wear and tear is minimized.

It follows that in order to investigate the stress-strain relationship of the red cell membrane, one must induce “off design” deformations in the cell, deformations that are not obtainable by *isochoric* (without changing volume) and *applicable* (without stretching the cell membrane in any way) transformations. The following are several popular types of experiments:

1. Osmotic swelling in hypotonic solution (Figs. 4.2:2 and 4.6:1).
2. Compression between two flat plates [Fig. 4.6:2(b)].
3. Aspiration by a micropipet [Figs. 4.6:2(a) and 4.6:6].
4. Deflection of the surface by a rigid spherical particle [Fig. 4.6:2(c)].
5. Fluid shear on a cell tethered to a flat plate at one point (Fig. 4.6:5).
6. Transient recovery of deformed cell (Fig. 4.6:7).
7. Plastic flow and other details of tethers (Fig. 4.6:8).
8. Forced flow through polycarbonate sieves
9. Thermal effect of elastic response
10. Chemical manipulation of cell membrane

Grouped according to their objectives, these experiments can be classified as follows. *Strain types* are varied in the following experiments:

- a. Membrane surface area changes (Exps. 2, 3, 4, and the latter stages of Exp. 1)
- b. Area does not change, stretching different in different directions (earlier stages of Exps. 1 and parts of membrane in Exps. 2–8)
- c. Bending energy not negligible compared with stretching energy (earlier stages of Exp. 1)

With respect to variation in *time*, there are two kinds of experiments.

- a. Static equilibrium (Exps. 1–5)
- b. Dynamic process (Exps. 6 and 7)

With respect to *material properties*, there are three kinds:

- a. Elastic (Exps. 1–5)
- b. Viscoelastic (Exp. 6)
- c. Viscoplastic (Exp. 7.)

Through these experiments, information about the elasticity, viscoelasticity, and viscoplasticity of the red blood cell membrane is gathered. Some comments follow.

Osmotic Swelling

Osmotic swelling of a red cell is one of the most interesting experiments in biomechanics. When a red cell is placed in a hypotonic solution, it swells to the extent that the osmotic pressure is balanced by the elastic stress and surface tension in the cell membrane. Returning the cell to an isotonic solution recovers the geometry, so the transformation is reversible. Results of such experiments are given in Tables 4.2:1–4.2:4. Eagle-albumin solution at 300 mosmol is considered isotonic. In a hypotonic solution of 217 mosmol, the cell volume is increased 23%, but the surface area is unchanged. At 131 mosmol the volume is increased 74% but the surface area is increased only 7%. At 131 mosmol the red cell is spherical and it is on the verge of hemolysis. At a tonicity smaller than 131 mosmol the cells are hemolyzed. This shows that the red cell membrane area cannot be stretched very much before it breaks. On the other hand, a look at the red cells in other experiments, especially in tethering (Exp. 5) and aspiration (Exp. 3), convinces us that the red cell membrane is capable of very large deformation provided that its area does not have to change (locally as well as globally). A deformation called “pure shear,” stretching in one direction and shrinking in the perpendicular direction, is sustainable. Furthermore, it was found that the elastic modulus for cell membrane area change [tensile stress $\div (\Delta A/A)$, A being the membrane area] is three to four orders of magnitude larger than the shear modulus (shear stress \div shear strain). For these reasons, experiments are classified according to whether cell membrane area is changed or not.

In the initial stages of osmotic swelling (say, from 300 to 217 mosmol), the cell geometry is changed considerably without noticeable change in surface area. In this stage the bending rigidity of the cell membrane, though very small, is very important: without taking bending into account, the sequence of swelling configurations cannot be explained. Conversely, the swelling experiment provides information about cell membrane bending. See Zarda, et al. (1977).

A model experiment on a thin-walled rubber model of a red blood cell reveals some details which are quite instructive. Such a model with a diameter of about 4 cm and a wall thickness of about 40 μm (so that the radius-to-thickness ratio is about 500) is shown in Fig. 4.6:1. When this rubber cell was immersed in a water tank and its internal volume was controlled by water injection, the sequence of geometric changes was photographed and is shown in the figure. The top two pictures show the initial shape without pressure difference. The following pictures show the change in shape under

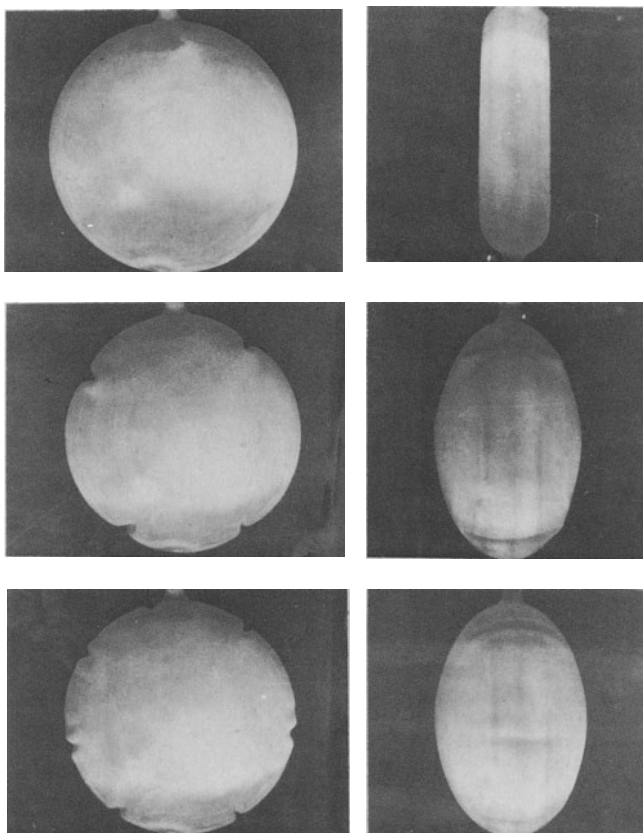


Figure 4.6:1 Thin-walled rubber model of red blood cell filled with water and immersed in a water tank. Figure shows the change of cell geometry with internal pressure. Top: natural shape. Second row: polar and equatorial regions buckled. Third row: the number of equatorial wrinkles increases with increasing pressure. From Fung (1966).

increasing internal pressure. In the initial stage, a sudden bulge of the dimples (i.e., buckling in the polar region of the cell) can be easily detected. The cell shown in the second row of Fig. 4.6:1 has already buckled. Note that the central, polar region bulges out. However, while the poles bulge, the equator of the cell contracts. In the successive pictures it is seen that the equator contracted so much that wrinkles parallel to the axis of symmetry were formed. The number of equatorial wrinkles increased with increasing internal pressure. At large internal pressure the cell swelled so much that the equator became smooth again.

This picture sequence is interesting in revealing a type of buckling in a thin-walled elastic shell when it is subjected to an increasing internal pressure. Engineers are familiar with elastic buckling of thin shell structures (e.g., spheres, cylinders, airplanes, submarines) subjected to external pressure. But here we have a type of the opposite kind. The principle is simple enough:

on increasing internal pressure and volume, the red cell swells into a more rounded shape. In doing so the perimeter at the equator is shortened, and buckling occurs.

The method of making the thin-walled rubber model of the RBC may be recorded here because it can be used to make other models of biomechanical interest. To make such a rubber shell model, a solid metal model of the RBC was machined according to the geometry shown in Fig. 4.2:1, with a diameter of about 4 cm. A female mold of plaster of Paris was then made from the solid metal model. From the female mold solid RBC models were cast with a material called "cerrolow" (Peck-Lewis Co., Long Beach, Calif.), which has a melting point of about 60°C. At room temperature this material appears metallic and can be machined and polished. A stem was left on each mold. Holding the stem, we dipped the mold into a cup of latex rubber in which a catalyst was added. Upon drying in air, a rubber membrane covered the mold. Each dip yielded a membrane of thickness of about 20 μm . In this way, a cell model with a wall thickness of 20–40 μm can be made satisfactorily. The solidified rubber model was then rinsed in hot water, in which the cerrolow melted and could be squeezed out, leaving a thin-walled red cell model.

Area Dilatation Experiments

The methods illustrated in Fig. 4.6:2 are aimed at changing the surface area of the cell. The *micropipet aspiration* method sucks a portion of the cell membrane into the pipet. The *compression* method flattens a cell. The *particle* method requires implantation of a magnetic particle into the cell, followed by observing the cell's distortion when it is placed in a magnetic field. See brief description in the legend of Fig. 4.6:2. These methods are best suited for spherical cells (e.g., spheroid red cells or sea urchin eggs). They can yield the modulus of elasticity with respect to area change of the membrane. But their analysis is by no means simple. See Evans and Skalak (1979) for detailed discussions of experimental results and their interpretations and analysis.

Experimenting on spheroid red blood cells, Evans and Hochmuth (1976) found that to aspire cell membrane into a pipet a pressure of the order of 10^5 dyn/cm^2 is needed. Assuming that that pressure is about equal to $p_i - p_o$, we can compute the membrane tension (stress resultant), N_ϕ , according to Laplace's formula given in Problem 1.4 in Sec 1.6 of Chapter 1. If N_ϕ is related to the area dilatation by the equation

$$N_\phi = K \frac{\Delta A}{A_0}, \quad (1)$$

where ΔA is the change of membrane area and A_0 is the initial area, and K is a constant of proportionality, which may be called the *elastic area*

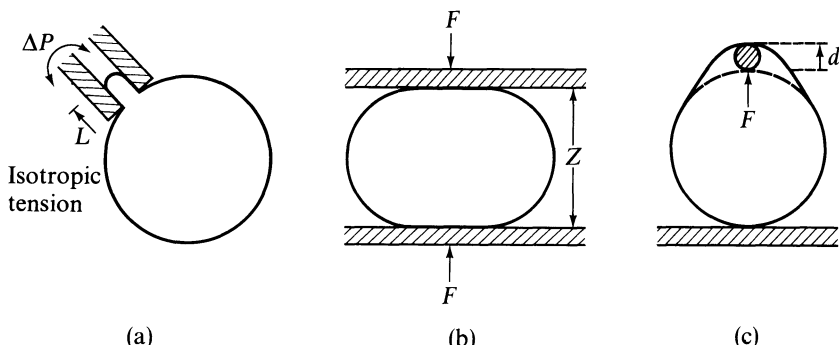


Figure 4.6:2 Three examples of mechanical experiments in which the dominant stress resultant in the surface is isotropic tension. If the membrane encapsulated system is spherical or nearly spherical, and the interior volume is fixed, then area dilation will be the primary deformation produced by mechanical experiments. The examples above schematically illustrate (a) micropipette aspiration, (b) compression between two flat surfaces, and (c) deflection of the surface by a rigid spherical particle. In (a), ΔP is the pressure difference between the pipette interior and the outside medium, and L is the length of the aspirated projection of the membrane. In (b), F is the force on each plate where the plates are separated from each other by a distance z . In (c), F is the force which displaces the magnetic particle and the surface by a distance d . From Evans and Skalak (1979), by permission.

compressibility modulus, Evans and Hochmuth found that K is about 450 dyn/cm at 25°C.

Membrane Shear Experiments

Distortion of a membrane without change of area is called *pure shear*. If a membrane is stretched in the x direction by a stretch ratio λ and shrunk in the perpendicular, y direction by a stretch ratio λ^{-1} , the deformation is pure shear; see Fig 4.6:3(a). In contrast, the deformation shown in Fig 4.6:3(b) is called *simple shear*. A general deformation of a membrane can be considered as composed of a pure shear plus an areal change. Since the

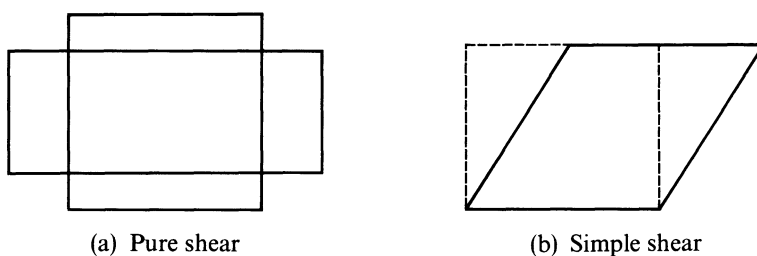


Figure 4.6:3 (a) Pure shear and (b) simple shear of a membrane.

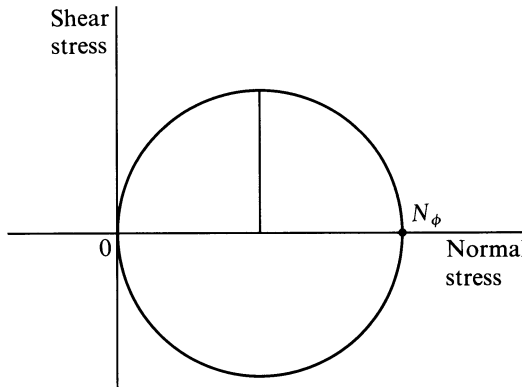


Figure 4.6:4 Mohr's circle of stress for the uniaxial stress state.

red cell membrane is so peculiar that it can sustain a large shear deformation but only a small area change (the cell membrane ruptures if the area is changed by more than a few percent), it is important to experiment on these two types of deformation separately.

Stresses acting on any small cross-sectional area in the membrane can be resolved into a normal stress and a shear stress. If a membrane is subjected to a tensile stress resultant N_ϕ in x direction and 0 in y direction, then on a cross-section inclined at 45° to the x axis, the shear and normal stress resultants are both $N_\phi/2$. This is called a *uniaxial stress state*: it is an effective way to impose pure shear. The Mohr's circle of stress resultants for this state is shown in Fig. 4.6:4.

The tethering experiment illustrated in Fig. 4.6:5 is designed to induce a uniaxial tension state of stress into the cell membrane. If red blood cells are suspended in an isotonic solution and the suspension is left in contact with a glass surface, some cells will become attached to the glass. Then if the solution is made to flow relative to the glass, the solution will sweep past the tethered red cell. This is analogous to the situation in which we hold a balloon tied to a string and stand in a strong wind. The wind will deform the balloon. In the case of the red cell the Reynolds number is very small and the viscous force dominates. Figure 4.6:5 shows the stress field in a membrane element of the red cell in this situation. By photographing the deformed red cell, one can approximately assess the modulus of elasticity of the cell membrane in a uniaxial state of stress. The shear modulus found by Hochmuth et al. (1973) by this method is of the order of 10^{-2} dyn/cm.

A different experiment for the same purpose is illustrated in Fig. 4.6:6. Suction is used to draw into a micropipette a portion of the cell membrane in the region of the poles of a flaccid red cell. Large deformation of the cell membrane occurs in the vicinity of the pipette mouth. If one assumes that the area of the membrane does not change, and that the suction is so localized that the cell remains flaccid and biconcave away from the pipette's mouth,

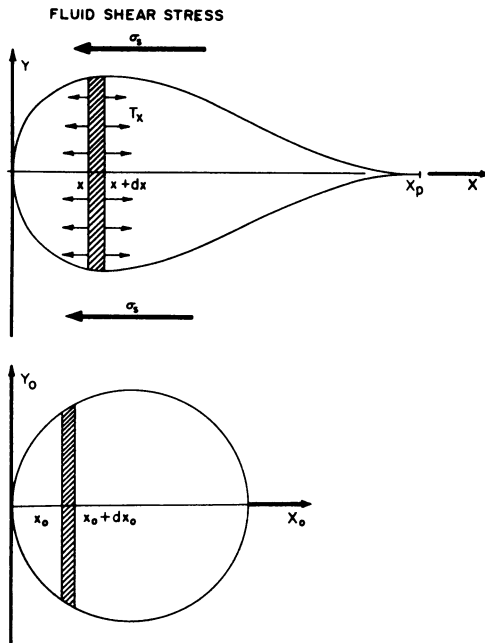


Figure 4.6:5 Schematic illustration of the uniaxial extension at constant area of a membrane element defined by $(x_0, x_0 + dx_0)$ into the element $(x, x + dx)$ under the action of a uniform fluid shear stress, σ_s . x_p is the location of the attachment point for the disk model. From Evans and Skalak (1979), by permission.

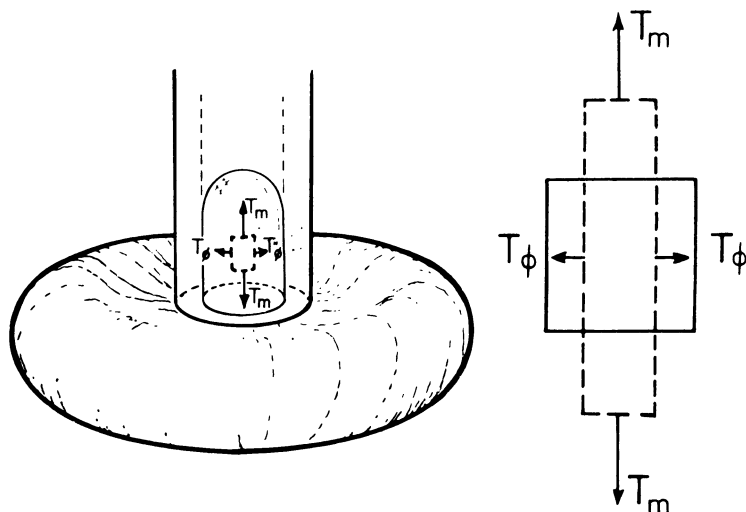


Figure 4.6:6 Illustration of membrane extension and deviation between force resultants produced by micropipette aspiration of a flaccid red blood cell. The principal force resultants (tensions) can be decomposed into isotropic and deviatoric (shear) contributions. From Evans and Skalak (1979), by permission.

then an approximate analysis of the membrane deformation can be made. The deformation is pure shear. With bending rigidity neglected, the equations of equilibrium can be set up. Combined with a constitutive equation (such as those proposed in Sec. 4.7), the deformation can be related to the sucking pressure in the pipette. Comparison of the experimental results with the calculated results will enable us to determine the elastic constants in the constitutive equation. If the membrane stress resultants are N_m , N_ϕ , as shown in Fig. 4.6:6, and the stretch ratio in the direction of N_m is λ_m , then the maximum shear stress resultant is

$$S_{\max} = \frac{N_m - N_\phi}{2}, \quad (2)$$

and the stress-strain relationship, Eq.(3) of Sec. 2.8, or Eq.(10) of Sec. 4.7, is reduced to the form

$$S_{\max} = 2\mu \cdot (\text{max. shear strain}). \quad (3)$$

Waugh (1977) found the value of the shear modulus μ to be 6.6×10^{-3} dyn/cm at 25°C , with an 18% standard deviation for 30 samples. This is more than four orders of magnitude smaller than the areal modulus.

Viscoelasticity of the Cell Membrane

The experiments considered above may be performed in a transient manner to measure response of the cell to step loading or step deformation, or to oscillatory loading and deformation, thus obtaining the viscoelastic characteristics of the cell membrane.

Hochmuth et al. (1979) experimented on the viscoelastic recovery of red cells by pulling a flaccid red cell disc at diametrically opposite locations on the rim of the cell: the cell is attached to glass on one side and pulled with a micropipet from the opposite side. The cell is then released and the recovery is observed with high speed photography. (See Fig. 4.6:7.)

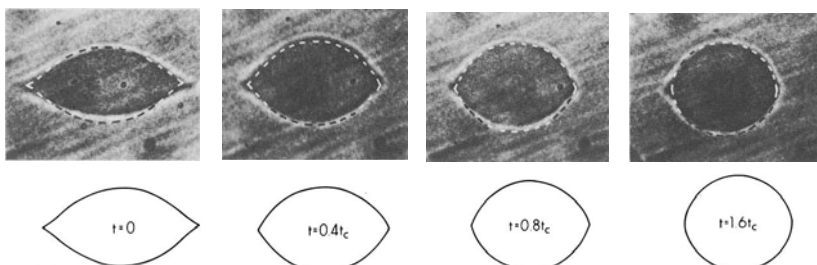


Figure 4.6:7 Comparison of the extensional recovery predicted for a viscoelastic disc model to that of a series of photographs taken of an actual red blood cell during recovery. The correlation provides a time constant, t_c , for the membrane recovery of 0.10 s in this case. The dashed lines are an overlay of the predicted model behavior onto the outline of the cell. From Evans and Skalak (1979), by permission.

A related case is suddenly stopping the flow in the experiment illustrated in Fig. 4.6:5 and observing the recovery of the red cell. Observation of cell response to suddenly applied pressure and release in micropipet aspiration [Fig. 4.6:2(a)] was done by Chien et al. (1978).

Viscoplastic Flow

When a flaccid red cell held with a micropipette for a certain length of time is suddenly expelled from the pipette, a residual “bump” remains in the membrane, which is interpreted as due to plastic deformation. At a given sucking pressure, the height of the bump was found to be proportional to the length of time the cell is held in the pipette.

Figure 4.6:8 illustrates another experiment by Evans and Hochmuth (1976). They observed that irrecoverable flow of material commences when the membrane shear resultant exceeds a threshold, or “yield” value. The membrane of a red cell tethered to a glass plate will flow plastically if the shear flow exceeds a certain limit. Analysis of the plastic flow yields the viscoplastic characteristics of the membrane.

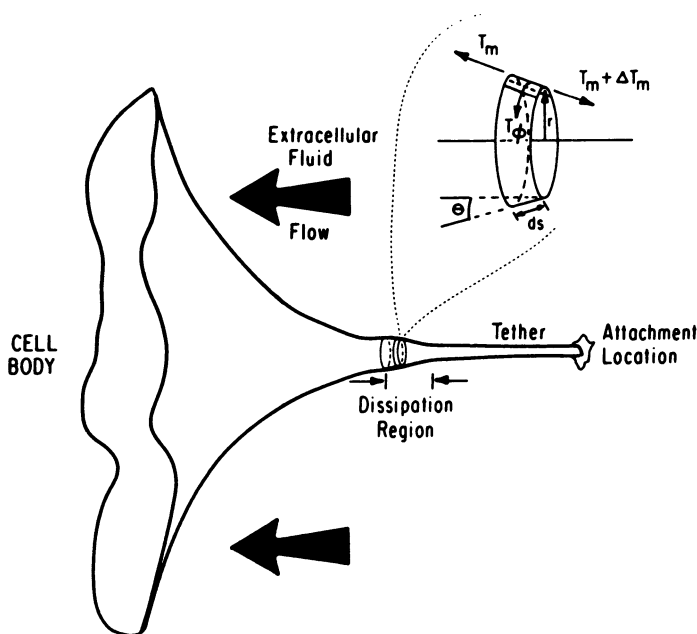


Figure 4.6:8 Schematic illustration of the microtether and the region of viscous dissipation in the “necking” region, where the plastic flow occurs. The geometry of a membrane flow element is shown in the enlarged view. From Evans and Hochmuth (1976), by permission.

Forced Flow of Red Cells through Polycarbonate Sieves

Gregersen et al.'s (1965) experiment on the flexibility of red cells remains a classic. They used a polycarbonate paper that has been bombarded by neutrons from a nuclear reactor (General Electric) and etched full of holes. These holes have the geometry of circular cylindrical tunnels. Their diameter can be controlled to within a relatively narrow limit. Gregersen et al. used this paper as a filter; supported it with a grid at the bottom of a small cup. Several ml of blood was put in the cup. A suction pressure was applied underneath the filter, and the period of time for the blood to be emptied was measured. During this time all the red cells in the cup flowed through the tunnels in the polycarbonate paper.

Many things were discovered by this experiment. For example, it was found that $2.3 \mu\text{m}$ diameter seems to be the lower limit of the tunnels through which human blood can be forced to flow through without hemolysis. Lingard (1974) showed that the white blood cells in the blood tend to plug off these tunnels and cause nonlinearity in the results. After removing the leukocytes with appropriate methods, the polycarbonate sieve offers a practical means to measure the flow properties of red cells.

Thermal and Chemical Experiments

The experiments mentioned above can be repeated at different temperatures to obtain the dependence of elastic and viscoelastic responses on temperature. The results provide some thermoelastic relations of the cell membrane. See Evans and Skalak (1979) and Waugh and Evans (1979).

Chemical manipulations to change spectrin or surface tension are associated with change of the shape of the red cell. See Steck (1974), Bennett and Branton (1977), and discussions in Sec. 4.8.

Problems

- 4.5** Draw Mohr's circles for the stress states in the cell membrane corresponding to uniaxial tension, biaxial tension, and various stages of osmotic swelling illustrated in Fig. 4.6:1. Draw Mohr's circles for the corresponding strain states; thus verify the discussions of experiments presented in Sec. 4.6.
- 4.6** Study an original paper in which one of the experiments discussed in Sec. 4.6 was first published (see Evans and Skalak, 1979, Chapter V, for detailed history and references). Discuss the analysis carefully from the point of view of continuum mechanics. Are the equations of equilibrium, the constitutive equation, the equation of continuity, and the boundary conditions satisfied rigorously? What are the approximations introduced? How good are these approximations? In which way can the approximations seriously affect the accuracy of the result?

4.7 Elasticity of the Red Cell Membrane

The outstanding feature of the red cell membrane is that it is capable of large deformation with little change in surface area. This fact has been observed for a long time and was elaborated by Ponder (1948). The data shown in Sec. 4.2 tell us that the red cell membrane is not unstretchable, but that even when the cell is spheroid in a hypotonic solution and on the verge of hemolysis the increase of surface area is only 7% of the normal.

A second remarkable feature is that the shape of the red cell at equilibrium in a hydrostatic field is extremely regular. The stress and strain history experienced by the red cell does not affect its regular shape in equilibrium. This suggests that the cell membrane may be considered elastic.

Based on these observations, several stress-strain relationships for the red cell membrane have been proposed. It was shown by Fung and Tong (1968) that for a two-dimensional generalized plane-stress field in an isotropic material, under the general assumption that the stress is an analytic function of the strain, the most general stress-strain relationship may be put in the form

$$\sigma_1 = \frac{E}{1 - \nu^2} (e_1 + \nu e_2), \quad \sigma_2 = \frac{E}{1 - \nu^2} (e_2 + \nu e_1), \quad (1a)$$

or

$$e_1 = \frac{1}{E} (\sigma_1 - \nu \sigma_2), \quad e_2 = \frac{1}{E} (\sigma_2 - \nu \sigma_1), \quad (1b)$$

where E and ν are elastic constants that are functions of the strain invariants,

$$e_1 + e_2, \quad e_1 e_2, \quad (2)$$

σ_1, σ_2 are the principal stresses referred to the principal axes x_1, x_2 , and e_1, e_2 are the principal strains. Although Eq. (1) has the appearance of Hooke's law, it is actually nonlinear if E and ν do not remain constant.

To apply Eq. (1) to the membrane, we may integrate the stresses through the thickness of the membrane and denote the stress resultants by N_i, N_2 ; then use Eq. (1) with σ_1, σ_2 replaced by N_1, N_2 . E is then the Young's modulus multiplied by the membrane thickness. The strains e_1, e_2 are measured in the plane of the membrane, and can be defined either in the sense of Green (Lagrangian) or in the sense of Almansi (Eulerian). If Green's strains are used, then the principal strains e_1, e_2 can be expressed in terms of the principal stretch ratios λ_1, λ_2 :

$$e_1 = \frac{1}{2}(\lambda_1^2 - 1), \quad e_2 = \frac{1}{2}(\lambda_2^2 - 1), \quad (3)$$

where λ_1 is the quotient of the changed length of an element in the principal direction (corresponding to the principal strain e_1) divided by the original length of that element in the unstressed state, and λ_2 is the stretch ratio corresponding to e_2 .

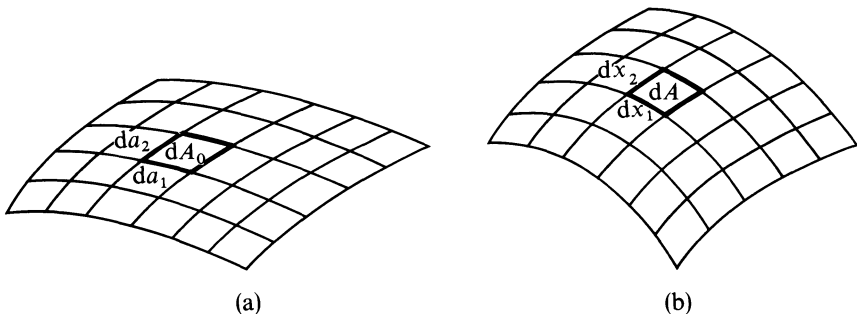


Figure 4.7:1 Deformation of a membrane. (a) Unstressed; (b) deformed.

If the area remains constant, then $\lambda_1\lambda_2 = 1$. If the membrane material is incompressible, then $\lambda_1\lambda_2\lambda_3 = 1$, where λ_3 denotes the stretch ratio in the direction perpendicular to the membrane. Hence if the area of an incompressible membrane remains constant, then the thickness of the membrane cannot change, ($\lambda_3 = 1$). The reverse is also true. Since the red cell membrane area remains almost constant, we conclude that its membrane thickness does not change much when the cell deforms.

The quasi-linear Eq. (1) does not account for the special feature that it is easy to distort the cell membrane, but hard to change its area. To account for this Skalak et al. (1973) and Evans and Skalak (1979) introduced the following strain measures:

$$(\lambda_1\lambda_2 - 1) \quad \text{for area and} \quad \frac{1}{2}(\lambda_1^2 - \lambda_2^2) \quad \text{for shear.} \quad (4)$$

The physical meaning of the quantity $(\lambda_1\lambda_2 - 1)$ is *the fractional change of the area of the membrane*. This can be seen by reference to Fig. 4.7:1, in which an element $da_1 \times da_2$ of area dA_0 in the unstressed membrane is deformed into an element $dx_1 \times dx_2$ of area dA ; and the ratio is

$$\frac{dA}{dA_0} - 1 = \frac{dx_1}{da_1} \frac{dx_2}{da_2} - 1 = \lambda_1\lambda_2 - 1. \quad (5)$$

On the other hand, according to Eq. (3)

$$e_1 - e_2 = \frac{1}{2}(\lambda_1^2 - \lambda_2^2). \quad (6)$$

By Mohr's circle, one-half of $|e_1 - e_2|$ is the maximum shear strain, γ_{\max} (Fig. 4.7:2). With these strain measures, Skalak et al. and Evans and Skalak wrote the following strain-stress resultant relationship:

$$N_1 = K(\lambda_1\lambda_2 - 1) + \mu \frac{\lambda_1^2 - \lambda_2^2}{2},$$

$$N_2 = K(\lambda_1\lambda_2 - 1) - \mu \frac{\lambda_1^2 - \lambda_2^2}{2}. \quad (7)$$

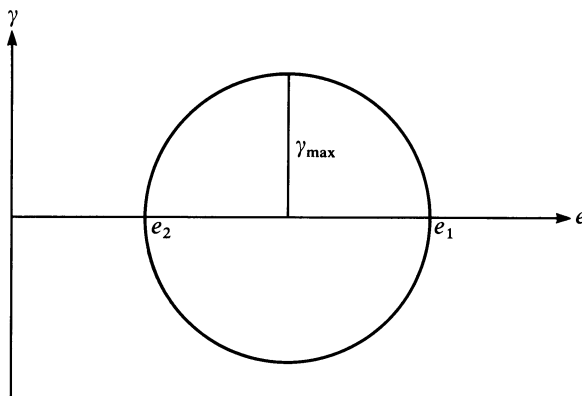


Figure 4.7:2 A Mohr's circle of strain. e is the normal strain; γ is the shear strain.

N_1, N_2 are the principal stress resultants. One-half of their sum is the mean stress resultant:

$$N_{\text{mean}} = \frac{1}{2}(N_1 + N_2) = K(\lambda_1 \lambda_2 - 1). \quad (8)$$

One-half of their difference is the maximum shear stress resultant:

$$S_{\text{max}} = \frac{1}{2}|N_1 - N_2| = \mu \frac{|\lambda_1^2 - \lambda_2^2|}{2} \quad (9)$$

Equation (8) shows that the mean stress resultant is proportional to the areal change. K is an *elastic modulus for area dilatation* in units of dyn/cm. If we divide K by the cell membrane thickness, then we obtain the elastic modulus with respect to areal dilatation in units of dyn/cm². On the other hand, Eq. (9) can be written as

$$S_{\text{max}} = 2\mu\gamma_{\text{max}}. \quad (10)$$

Equation (10) is of the same form as the Hooke's law, and the parameter μ can be called the *membrane shear modulus*. μ divided by the cell membrane thickness yields the usual shear modulus in units of dyn/cm².

The moduli K and μ are functions of the strain invariants. But as a first approximation they may be treated as constants. If the constant K is much larger than μ , then the resistance of the membrane to change of area is much greater than that for distortion without change of area.

The first estimate of the elastic modulus of the red cell membrane was given by Katchalsky et al. (1960) based on spherling experiments in a hypotonic solution. The estimated value of the elastic modulus during the spherical phase of the cell and just before hemolysis is 3.1×10^7 dyn/cm² (as corrected by Skalak et al. 1973). The general range of this estimate was confirmed by Rand and Burton (1964) based on experiments in which red cells were sucked into micropipettes whose diameter was of the order of 2 μm in diameter. Rand and Burton gave the range of the moduli as 7.3×10^6 to 3.0×10^8

dyn/cm^2 . Later, Hochmuth and Mohandas (1972) reported experiments in which red blood cells adhering to a glass surface were elongated due to shearing stress applied by the flow of the suspending fluid over the cells; they estimated that the modulus of elasticity is of the order of $10^4 \text{ dyn}/\text{cm}^2$. In another type of test in which the deformed cells were allowed to recover their natural shape, Hoeber and Hochmuth (1970) gave a value $7.2 \times 10^5 \text{ dyn}/\text{cm}^2$. Skalak et al. (1973) observed that the elongation in the spherling and pipette experiments that give the higher estimates is about 8%; that in the uniaxial tests giving the lower modulus is 40–60%. They therefore suggest that the lower values are appropriate for the constant μ , and the higher values are appropriate for the constant K . If the thickness of the cell membrane is assumed to be 50 Å, then $\mu = 10^4 \text{ dyn}/\text{cm}^2$ and $h = 50 \text{ \AA}$ gives a value $h\mu = 0.005 \text{ dyn}/\text{cm}$; whereas $K = 10^8 \text{ dyn}/\text{cm}^2$ and $h = 50 \text{ \AA}$ gives $hK = 50 \text{ dyn}/\text{cm}$.

4.8 The Red Cell Membrane Model

What kind of material makes up a membrane that has the elasticity, viscoelasticity, and viscoplasticity discussed above? The exact ultrastructure of the cell membrane of the blood cell is still unknown. A conceptual model advocated by Evans and Skalak (1979) is shown in Fig. 4.8:1. It shows the basic structure of a *unit membrane* consisting of two layers of phospholipid molecules (*bilayer*) with their hydrophilic heads facing outward and hydrophobic tails locking into each other in the interior by hydrophobic forces.

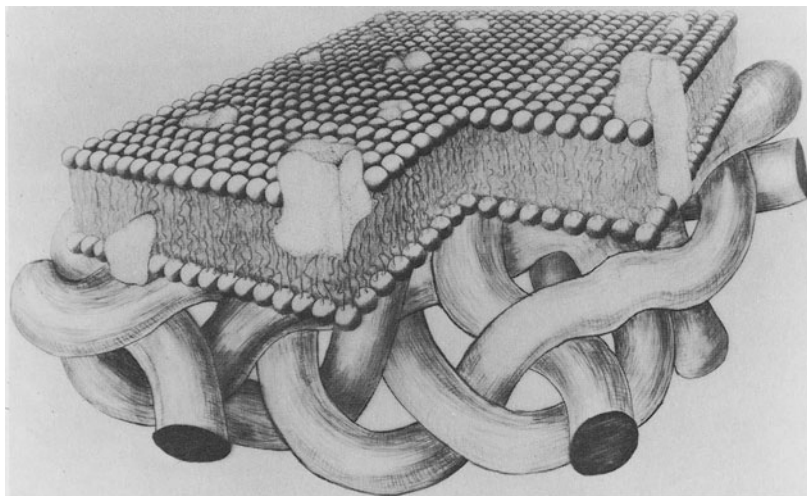


Figure 4.8:1 An idealized view of the red blood cell membrane composite. The underneath spectrin network provides structural rigidity and support for the fluid lipid-protein layer of the membrane. From Evans and Skalak (1979), by permission.

Globular proteins are partially embedded in the membrane, and partially protrude from it. The distribution of membrane protein is depicted as random at long range, although some aggregates may exist due to short range protein-protein interaction. A protein called *spectrin* lies on the cytoplasmic face of the red blood cell membrane. The spectrin is depicted as long chain molecules.

This model has evolved through many years of research by many scientists. The lipid bilayer was demonstrated by electron microscopy. The existence of globular protein in the membrane was demonstrated later (Seifriz, 1926; Norris, 1939). By studying the location of antibodies in the cell membrane through electron microscopic photographs, Singer and Nicolson (1972) concluded that the cell membrane behaves like a fluid; the globular protein (the antibody in their case) can move about in the lipid bilayer in a way similar to the way icebergs move about on the surface of the ocean. The lipid bilayer has a characteristic thickness that is invariable. The mobility of the protein and lipid molecules is restricted to the plane of the membrane. This model is therefore called the *fluid mosaic* model. Experiments also showed, however, that cell membranes exhibit properties of a solid, e.g., elasticity. Since the lipids are in a fluid state, the solid characteristics of the membrane must be attributed to connections of proteins and other molecules associated with the membrane. Marchesi et al. (1969, 1970) identified spectrin on the red cell membrane. Steck (1974) and Singer (1974) suggested that the spectrin supports the lipid bilayer, that it serves as a *cytoskeleton*, giving solid properties to the cell membrane. The spectrin and the lipid bilayer together can have elastic, viscoelastic, and viscoplastic properties.

If spectrin on the cytoplasmic side is responsible for red cell membrane elasticity, then association of spectrin to the outer face of the lipid layer can also provide solid characteristics; and since the membrane may be bent by associating spectrin to the outer face of the membrane, the red cell shape will change. Bennett and Branton (1977) and others have demonstrated these changes.

In cells that are more complex than the red blood cell, the cell membrane may have a more complex structure, including such elements as microtubules, microvilli, cytoplasmic elements, etc., which can also provide structural rigidity and even active deformation. Thus the mechanical properties have an ultrastructural basis. Conversely, the study of mechanical properties provides a powerful tool to probe the ultrastructure: it allows one to look into the dynamic relationship of the structural components, and obtain a deeper understanding of the ultrastructure.

References

- Bennett, V., and Branton, D. (1977) *J. Biol. Chem.* **252**, 2753–2763.
Canham, P. B. (1970) *J. Theoret. Biol.* **26**, 61–81.
Canham, P. B., and Burton, A. C. (1968) *Circulation Res.* **22**, 405–422.

- Chen, P., and Fung, Y. C. (1973) *Microvascular Res.* **6**, 32–43.
- Chien, S. (1972) In *Hemodilution: Theoretical Basis and Clinical Application*, Messmer, K., and Schmid-Schoenbein, H. (eds.). Karger, Basel.
- Chien, S., Usami, S., Dellenback, R. T., and Gregersen, M. I. (1967) *Science* **157**, 827–829.
- Chien, S., Luse, S. A., Jan, K. M., Usami, S., Miller, L. H., and Fremount, H. (1971a) *Proc. 6th European Conf. Microcirculation*. Karger, Basel, pp. 29–34.
- Chien, S., Usami, S., Dellenback, R. J., and Bryant, C. A. (1971b) *Biorheology* **8**, 35–57.
- Chien, S., Sung, K. L. P., Skalak, R., Usami, S., and Tozeren, A. (1978) *Biophys. J.* **24**, 463–487.
- Cokelet, G. R., and Meiselman, H. J. (1968) *Science* **162**, 275–277.
- Dintenfass, L. (1968) *Nature* **219**, 956–958.
- Evans, E., and Fung, Y. C. (1972) *Microvascular Res.* **4**, 335–347.
- Evans, E. A., and Hochmuth, R. M. (1976) *Biophys. J.* **16**, 13–26.
- Evans, E. A., Waugh, R., and Melnik, L. (1976) *Biophys. J.* **16**, 585–595.
- Evans, E. A., and Skalak, R. (1979) *Mechanics and Thermodynamics of Biomembranes*. CRC Critical Reviews in Bioengineering. Vol 3, issues 3 & 4. CRC Press, Boca Raton, Fla.
- Flügge, W. (1960) *Stresses in Shells*. Springer-Verlag, Berlin.
- Fry, D. L. (1968) *Circulation Res.* **22**, 165–197.
- Fry, D. L. (1969) *Circulation Res.* **24**, 93–108.
- Fung, Y. C. (1966) *Fed. Proc. Symposium on microcirculation*, **25**(6), Part I, 1761–1772.
- Fung, Y. C. (1968) *Biomed. Sci. Instrumentation* **4**, 310–320.
- Fung, Y. C., and Tong, P. (1968) *J. Biophysics* **8**(2), 175–198.
- Gregersen, M. I., Bryant, C. A., Hammerle, W. E., Usami, S., and Chien, S. (1967) *Science* **157**, 825–827.
- Graustein, W. C. (1935) *Differential Geometry*. Macmillan, New York.
- Gumbel, E. J. (1954) *Statistical Theory of Extreme Value and Some Practical Applications*. National Bureau of Standards, Applied Math Ser. 33. Superintendent of Documents, U.S. Government Printing Office, Washington, D.C., pp. 1–51.
- Gumbel, E. J. (1958) *Statistics of Extremes*. Columbia University Press, New York.
- Hochmuth, R. M., Marple, R. N., and Sutera, S. P. (1970) *Microvascular Res.* **2**, 409–419.
- Hochmuth, R. M., and Mohandas, N. (1972) *J. Biomechanics* **5**, 501–509.
- Hochmuth, R. M., Mohandas, N., and Blackshear, Jr., P. L. (1973) *Biophys. J.* **13**, 747–762.
- Hochmuth, R. M., Worthy, P. R., and Evans, E. A. (1979) *Biophys. J.* **26**, 101–114.
- Hoeber, T. W., and Hochmuth, R. M. (1970) *Trans. ASME Ser. D, J. Basic Eng.* **92**, 604.
- Houchin, D. W., Munn, J. I., and Parnell, B. L. (1958) *Blood* **13**, 1185–1191.
- Katchalsky, A., Kedem, D., Klibansky, C., and DeVries, A. (1960) In *Flow Properties of Blood and Other Biological Systems*, Copley, A. L., and Stainsby, G. (eds.). Pergamon, New York, pp. 155–171.

- King, J. R. (1971) *Probability Chart for Decision Making*. Industrial Press, New York.
- Lingard, P. S. (1974) *Microvascular Res.* **8**, 53–63, and 181–191.
- Lingard, P. S., and Whitmore, R. L. (1974) *J. Colloid Interface Sci.* **49**, 119–127.
- Marchesi, S. L., Steers, E., Marchesi, V. T., and Tillack, T. W. (1970) *Biochemistry* **9**, 50–57.
- Marchesi, V. T., Steers, E., Tillack, T. W., and Marchesi, S. L. (1969) In *Red Cell Membrane*, Jamieson, G. A. and Greenwalt, T. J. (eds.). Lippincott, Philadelphia, pp. 117.
- Norris, C. H. (1939) *J. Cell. Comp. Physiol.* **14**, 117–113.
- Ponder, E. (1948) *Hemolysis and Related Phenomena*. Grune & Stratton, New York.
- Rand, R. H., and Burton, A. C. (1964) *Biophys. J.* **4**, 115–135; 303–316.
- Schmid-Schoenbein, G., Fung, Y. C., and Zweifach, B. E. (1975) *Circulation Res.* **36**, 173–184.
- Schmid-Schoenbein, H., and Wells, R. E. (1969) *Science* **165**, 288–291.
- Schmidt-Nielsen, K., and Taylor, C. R. (1968) *Science* **162**, 274–275.
- Seifriz, W. (1927) *Protoplasma* **1**, 345–365.
- Singer, S. J. (1974) *Ann. Rev. Biochem.* **43**, 805–833.
- Singer, S. J., and Nicolson, G. L. (1972) *Science* **175**, 720–731.
- Skalak, R. (1973) *Biorheology* **10**, 229–238.
- Skalak, R., Tozeren, A., Zarda, R. P., and Chien, S. (1973) *Biophys. J.* **13**, 245–264.
- Sobin, S. S., Lindal, R. G., Fung, Y. C., and Tremer, H. M. (1978) *Microvascular Res.* **15**, 57–68.
- Steck, T. L. (1974) *J. Cell Biol.* **62**, 1–19.
- Struik, D. J. (1950) *Lectures on Classical Differential Geometry*. Addison-Wesley, Cambridge, Mass.
- Tsang, W. C. O. (1975) The size and shape of human red blood cells. M.S. Thesis. University of California, San Diego, Calif.
- Waugh, R. E. (1977) Temperature dependence of the elastic properties of red blood cell membrane. Ph.D. Thesis. Duke University, Durham, N.C.
- Waugh, R., and Evans, E. A. (1979) *Biophys. J.* **26**, 115–132.
- Zarda, P. R., Chien, S., and Skalak, R. (1977) *J. Biomechanics* **10**, 211–221.

CHAPTER 5

The Rheology of Blood in Microvessels

5.1 Introduction

The concept of viscosity has been discussed in Chapters 2 and 3. We have shown that the viscosity of whole blood is non-Newtonian. But the discussion so far has considered blood as a homogeneous fluid. We know, of course, that blood is not homogeneous: it is normally a concentrated mixture with almost half its volume occupied by suspended red blood cells. There are occasions when it is useful to consider blood as a homogeneous fluid, and there are other occasions when it is necessary to consider red blood cells as acting individually. For example, in studying the pulse waves in arteries whose diameters are many times larger than the red cell diameter, we can treat blood as a homogeneous fluid. On the other hand, in studying the flow of blood in capillary blood vessels whose diameters are about the same as the diameter of the red cells, we have to consider blood as a suspension.

In the following pages, we shall study the behavior of red cells in micro-blood vessels. The systematic study of blood circulation in microvessels in various organs, however, is deferred to *Biomechanics II*, the second volume of this series of books. In this chapter we focus on the general features of cell-vessel interaction, and their effect on the apparent viscosity of blood; thus providing a connection between the viscosity study discussed in Chapter 3 with the study of microcirculation.

5.2 Apparent Viscosity and Relative Viscosity

The need to consider cell-vessel interaction makes the rheology of blood in micro-blood vessels very different from ordinary macroscopic rheology. To link these topics together, let us consider two intermediate terms that are

useful in organizing experimental data, namely, the *apparent viscosity* and the *relative viscosity*. To explain their meaning, consider a flow through a circular cylindrical tube. If the fluid is Newtonian and the flow is laminar, we have the Hagen-Poiseuille formula [Eq. (8) of Sec. 3.3]:

$$\frac{\Delta p}{\Delta L} = \frac{8\mu}{\pi a^4} \dot{Q}, \quad (1)$$

where Δp is the pressure drop in length ΔL , μ is the coefficient of viscosity of the fluid, a is the radius of the tube, and \dot{Q} is the volume rate of flow. If the fluid is blood, this equation does not apply; but we can still measure $\Delta p/\Delta L$ and \dot{Q} , and use Eq. (1) to calculate a coefficient μ :

$$\mu = \frac{\pi a^4}{8} \frac{1}{\dot{Q}} \frac{\Delta p}{\Delta L}. \quad (2)$$

The μ so computed is defined as the *apparent coefficient of viscosity for the circular cylindrical tube*, and is denoted by μ_{app} . If μ_0 denotes the viscosity of plasma, which is Newtonian, then the ratio μ_{app}/μ_0 is defined as the *relative viscosity*, and is denoted by μ_r . Note that the unit of apparent viscosity is (force·time/area), or the poise (P), whereas the relative viscosity is dimensionless.

The concept of relative viscosity can be generalized to an organ system. To measure the relative viscosity of blood in such a system we perfuse it with a homogeneous fluid and measure the pressure drop Δp corresponding to a certain flow \dot{Q} . We then perfuse the same system with whole blood and again measure the pressure drop at the same flow. The ratio $\Delta p/\dot{Q}$ for whole blood divided by $\Delta p/\dot{Q}$ for the specific fluid is the relative viscosity, μ_r , of blood relative to that fluid.

The concept of apparent viscosity can be extended to any flow regime, including turbulent flow, as long as we can compute it from a formula that is known to work for a homogeneous Newtonian fluid. The concept of relative viscosity can be extended to any flow system, even if we do not know its structural geometry and elasticity, as long as flow and pressure can be measured. Neither μ_{app} nor μ_r needs to be constant. They are functions of all the dimensionless parameters defining the kinematic and dynamic similarities; and if the system is nonlinear, they are functions of pressure p and flow \dot{Q} .

Apparent and relative viscosities are not intrinsic properties of the blood; they are properties of the blood and blood vessel interaction, and depend on the data reduction procedure. There are as many definitions for apparent viscosities as there are good formulas for well-defined problems. Examples are: Stokes flow around a falling sphere, channel flow, flow through an orifice, and flow in a cylindrical tube. But if a vessel system has a geometry such that the theoretical problem for homogeneous fluid flow has not been solved, then we cannot derive an apparent viscosity for flow in such a system. But we can determine a relative viscosity if we can perform flow experiments in the system both blood and with a homogeneous fluid.

An Example

Let us consider the flow of blood in the capillary blood vessels of the lung. As an introduction, a few words about the anatomy of these vessels is necessary. The lung is an organ whose function is to oxygenate the blood. The venous blood of peripheral circulation is pumped by the right ventricle of the heart into the pulmonary artery. The artery divides and subdivides again and again into smaller and smaller blood vessels. The smallest blood vessels are the capillaries. Pulmonary capillaries have very thin walls (about $1 \mu\text{m}$ thick) across which gas exchange takes place. The oxygenated blood then flows into the veins and the heart. The pulmonary capillaries form a closely knit network in the interalveolar septa. Figure 5.2:1 shows a plan view of the network. Figure 5.2:2 shows a cross-sectional view of the network. It is clear that the network is two-dimensional. From a fluid dynamical point of

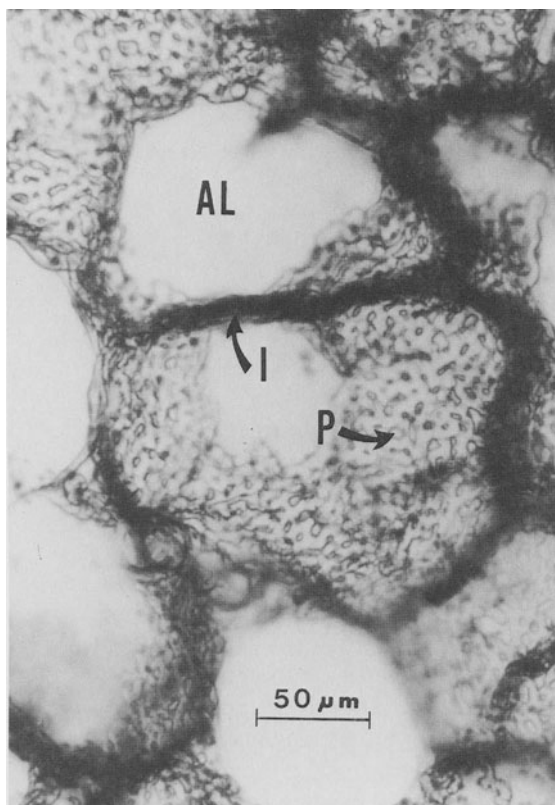


Figure 5.2:1 A view of the pulmonary capillary blood vessels of the cat photographed when the focal plane of the microscope is parallel to the plane of several interalveolar septa. The large white spaces are the alveolar air spaces (AL). The capillaries are the interconnected small channels seen on the septa. The islandlike spaces between the capillaries are called "posts," (P). "I" is an interalveolar septum perpendicular to the page. Courtesy of Dr. Sidney Sabin.

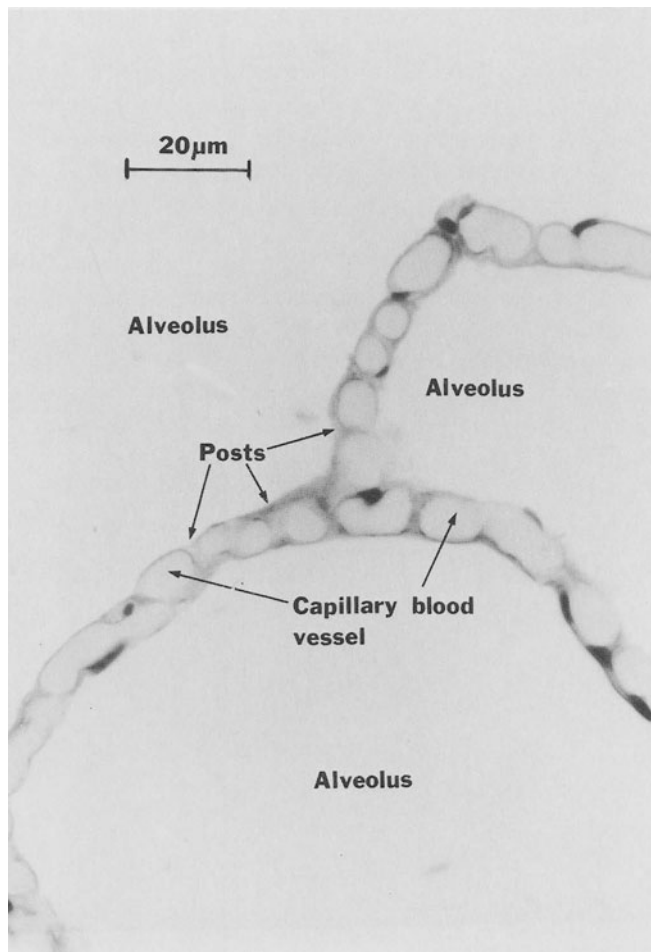


Figure 5.2:2 Another view of pulmonary capillary blood vessels of the cat photographed when the focal plane of the microscope cuts three interalveolar septa nearly perpendicularly. Courtesy of Dr. Sidney Sabin.

view, one may regard the vascular space as a thin sheet bounded by two membranes that are connected by an array of *posts*. The thickness of the sheet depends on the transmural pressure (blood minus alveolar gas pressure). If the transmural pressure is small and tending to zero, the sheet thickness tends to $4.3 \mu\text{m}$ in the cat, $2.5 \mu\text{m}$ in the dog, and $3.5 \mu\text{m}$ in man. In this condition the sheet thickness is smaller than one-half the diameter of the undeformed red blood cells of the respective species. Hence the red cells have to flow either sideways or become severely deformed. The sheet thickness increases almost linearly with increasing transmural pressure: at a rate of $0.219 \mu\text{m}$ per $\text{cm H}_2\text{O}$ in the cat, $0.122 \mu\text{m}/\text{cm H}_2\text{O}$ in the dog, and $0.127 \mu\text{m}/\text{cm H}_2\text{O}$ in man.

For blood flow through such a complicated system we would want to know how the resistance depends on the following factors: the hematocrit, the geometry of the network (sheet), the thickness of the sheet relative to the size of the red blood cells, the rigidity of the red cells, the Reynolds number, the size of the posts, the distance between posts, the pattern of the posts, the direction of flow relative to the pattern of the posts, and so on. If we know how the resistance depends on these factors, then we can make model experiments, discuss the effects of abnormalities, compare the lungs of different animal species, etc.

To deal with the problem, we first make a dimensional analysis. Let p be the pressure, μ be the apparent coefficient of viscosity, U be the mean velocity of flow, h be the sheet thickness, w be the width of the sheet, ε be the diameter of the post, a be the distance between the posts, and θ be the angle between the mean direction of flow relative to a reference line defining the postal pattern. The postal pattern is further described by the ratio of the volume occupied by the blood vessels divided by the total volume of the sheet, called the *vascular-space-tissue ratio* and denoted by S . Sabin et al. (1970, 1972, 1979) have experimentally measured S in the lungs of the cat, rabbit, and man. Let us consider first the flow of a homogeneous Newtonian viscous fluid in this system. We want to know the relationship between the pressure gradient (rate of change of pressure with distance, a vector with components $\delta p/\delta x$, $\delta p/\delta y$ and denoted by ∇p), and the velocity, U , the viscosity coefficient, μ , the sheet thickness, h , and the other factors, w , ε , a , θ , S , and ρ . The physical dimensions of these quantities are, with F denoting force, L denoting length, and T , the time:

$$\begin{aligned} \text{pressure: } & FL^{-2}, & \text{pressure gradient: } & FL^{-3}, \\ \text{velocity: } & LT^{-1}, & \text{sheet thickness: } & L, \\ \text{coefficient of viscosity = stress/shear rate: } & FL^{-2}T, \\ \text{density of fluid, } \rho = \text{mass/vol: } & FT^2L^{-4}. \\ h, w, \varepsilon, a: & L. & \theta, S: & \text{dimensionless} \end{aligned}$$

By simple trial we see that the following groups of parameters are dimensionless:

$$\frac{w}{h}, \quad S, \quad \frac{h}{\varepsilon}, \quad \frac{\varepsilon}{a}, \quad \theta, \\ \frac{h^2}{\mu U} \nabla p, \quad \frac{Uh\rho}{\mu} \equiv N_R \quad (\text{Reynold's number}). \quad (3)$$

These dimensionless parameters are independent of each other and they form a set from which any other dimensionless parameters that can be formed by these variables can be obtained by proper combinations of them.

Now, according to the principle of dimensional analysis, any relationship between the variables p , U , μ , h , etc. must be a relationship between these dimensionless parameters. In particular, the parameter we are most interested

in, that connecting the pressure gradient with flow velocity, may be written as

$$\frac{h^2}{\mu U} \nabla p = F\left(\frac{w}{h}, \frac{h}{\varepsilon}, \frac{\varepsilon}{a}, S, \theta, N_R\right), \quad (4)$$

where F is a certain function that must be determined either theoretically or experimentally. For a homogeneous Newtonian fluid flowing in a pulmonary interalveolar septum, in which the Reynolds number is much smaller than 1, the theoretical problem has been investigated by Lee and Fung (1969), Lee (1969), and Fung (1969). Yen and Fung (1973) then constructed a simulated model of the pulmonary alveolar sheet with lucite, and used a silicone fluid (which was homogeneous and Newtonian) to test the accuracy of the theoretically determined function $F(w/h, \dots)$ given by Lee and Fung; and it was found to be satisfactory.

We do have, then, a verified formula, Eq. (4), which is applicable to a homogeneous Newtonian viscous fluid. We can then use this formula for experimental determination of the apparent viscosity of blood flowing in pulmonary alveoli. From the experimental values of ∇p , U , h^2 , etc. we can compute the apparent viscosity μ_{app} from the following formula:

$$\nabla p = -\frac{U}{h^2} \mu_{app} F\left(\frac{w}{h}, \frac{h}{\varepsilon}, \dots\right) \quad (5)$$

The apparent viscosity is influenced by the plasma viscosity, the concentration of the red blood cells, the size of the red cells relative to the blood vessel, the elasticity of the red cells, etc. Let H be the hematocrit (the fraction of the red cell volume in whole blood), let D_c be the diameter of the red cell, and let μ_{plasma} be the viscosity of the plasma; then the apparent viscosity of blood in pulmonary alveoli must be a function of μ_{plasma} , H , D_c/h , etc. Hence, again on the basis of dimensional analysis, we can write

$$\mu_{pp} = \mu_{plasma} f\left(H, \frac{D_c}{h}, \dots\right), \quad (6)$$

where f is the function to be determined, and the dots indicate the cell elasticity and other parameters not explicitly shown.

Dimensional analysis is the basis for model experiments. For mechanical simulation the model must be geometrically and dynamically similar to the prototype. For geometric similarity the kinematic parameters listed in the first line of Eq. (3) must be the same for the model and prototype. For dynamic similarity the parameters in the second line of Eq. (3) must be the same for them. When these parameters are simulated, any relationship obtained from the model is applicable to the prototype. Yen and Fung (1973) experimented on a scale model of the pulmonary alveolar sheet, with the red blood cells simulated by soft gelatin pellets and with the plasma simulated by a silicone fluid. Their results show that the pressure-flow relationship is quite linear, and that for $h/\varepsilon < 4$, the relative viscosity of blood with respect to plasma depends on the hematocrit H in the following manner:

$$\mu_{\text{relative}} = 1 + aH + bH^2. \quad (7)$$

Thus, the apparent viscosity of blood in pulmonary capillaries is

$$\mu_{\text{app}} = \mu_{\text{plasma}}(1 + aH + bH^2). \quad (8)$$

Since Eq. (4) is verified for the plasma, Eq. (8) can be used in Eq. (6). These relations are illustrated in Fig. 5.2:3, where the values of the constants a and b are listed.

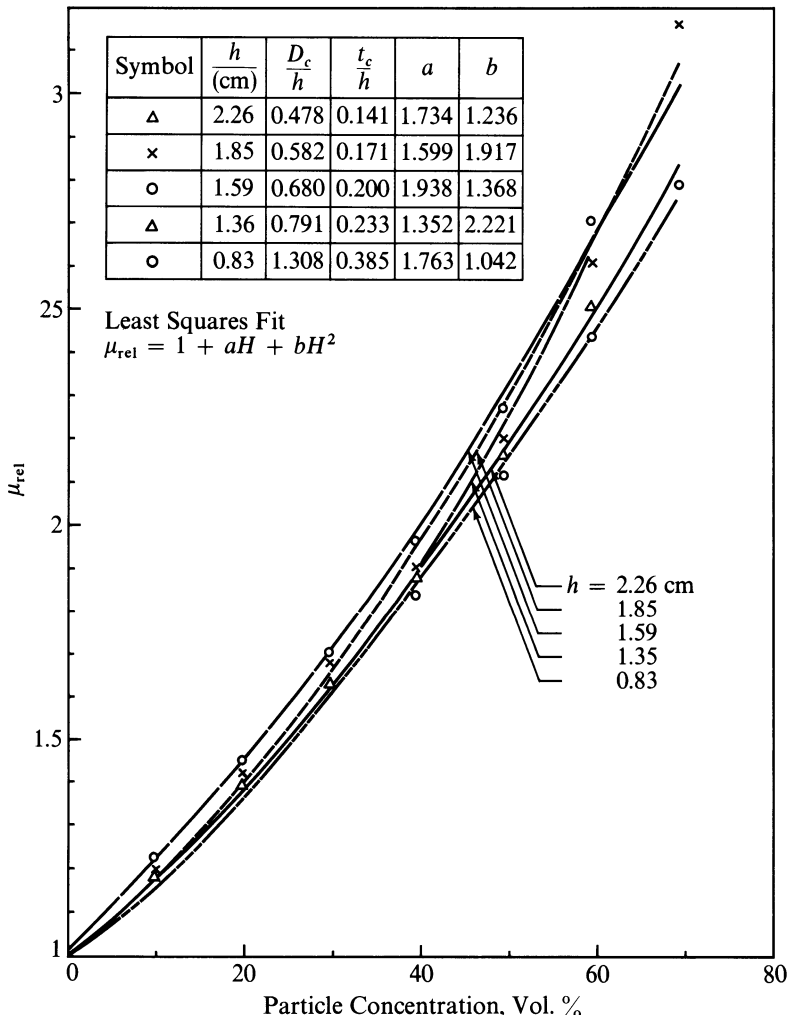


Figure 5.2:3 The relative viscosity of simulated whole blood (gelatin pellets in silicone oil) in a pulmonary alveolar model. Here D_c is the diameter of the red cell, h is the thickness of the alveolar sheet, t_c is the thickness of the red blood cell, and a, b are constants in Eq. (8). The model is so large that h is in centimeters, although in a real lung h is only a few microns. From Yen and Fung (1973).

This rather complex example is quoted here to show that (a) the definition of apparent viscosity is not unique, and (b) that it may not be simple. The selection of definition is guided only by its usefulness.

5.3 Effect of Size of the Blood Vessel on the Apparent Viscosity of Blood: The Fahraeus-Lindqvist Effect

For blood flow in cylindrical vessels, the apparent viscosity decreases with decreasing blood vessel diameter. This is shown in Fig. 5.3:1. This was first pointed out by Fahraeus and Lindqvist (1931), who tested blood flow in glass tubes connected to a feed reservoir in an arrangement illustrated in Fig. 5.3:2. They showed this trend in tubes of diameter in the range 500–

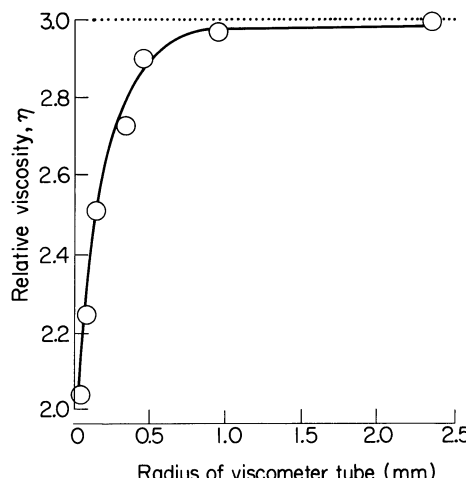


Figure 5.3:1 The change of relative viscosity of blood with the size of blood vessel. The data are Kümin's, analized by Haynes (*Am. J. Physiol.* **198**, 1193, 1960).

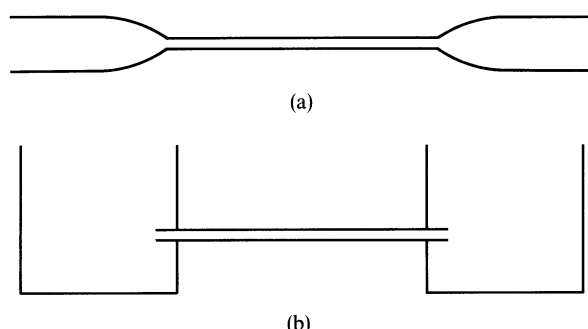


Figure 5.3:2 The capillary tubes used by (a) Fahraeus and Lindqvist (1931) and (b) by Barbee and Cokelet (1971) to measure the dependence of the apparent viscosity of blood on the diameter of circular cylindrical tubes.

$50\text{ }\mu\text{m}$. Barbee and Cokelet (1971) extended this experiment and showed that the trend continues at least to tubes of diameter $29\text{ }\mu\text{m}$. (Human blood was used. Remember that the average human red cell diameter is $7.6\text{ }\mu\text{m}$.) These experiments were done at rates of flow so high that the apparent viscosity does not vary significantly with the flow rate.

An explanation of the Fahraeus-Lindqvist effect was provided by Barbee and Cokelet (1971) and is based on an observation made by Fahraeus himself. Fahraeus (1929) found that when blood of a constant hematocrit is allowed to flow from a large feed reservoir into a small tube, the hematocrit in the tube decreases as the tube diameter decreases. This trend was shown by Barbee and Cokelet (1971) to continue down to a tube diameter of $29\text{ }\mu\text{m}$ (cf. Fig. 5.3:2). Barbee and Cokelet then showed that if one measures the apparent viscosity of blood in a large tube (say, of a diameter about 1 mm) as a function of the hematocrit, and use the data to compute the apparent viscosity of the same blood in the smaller tube at the actual hematocrit in that tube, a complete agreement with the experimental data can be obtained. This is an important finding, because it not only extends the usefulness of the apparent viscosity measurements, but also furnishes insight into the mechanism of flow resistance in microcirculation.

Verification of these statements is shown in Figs. 5.3:3 and 5.3:4. Figure 5.3:3 shows Barbee and Cokelet's result on how the average hematocrit of

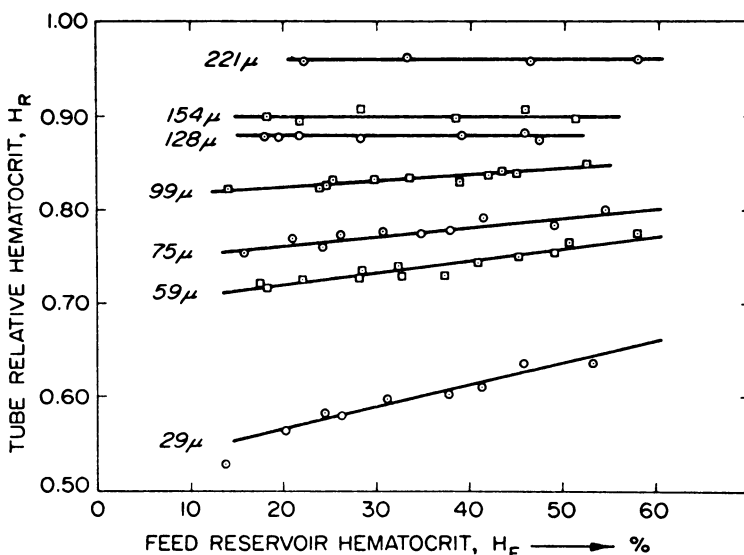


Figure 5.3:3 The Fahraeus effect: when blood flows from a reservoir into and through a small diameter tube, the average hematocrit in the tube is less than that in the reservoir. The tube relative hematocrit is defined as the average hematocrit of the blood flowing through a tube divided by the hematocrit of the blood in the reservoir feeding the tube. Numbers to the left of the lines are the tube diameters. From Barbee and Cokelet (1971), by permission.

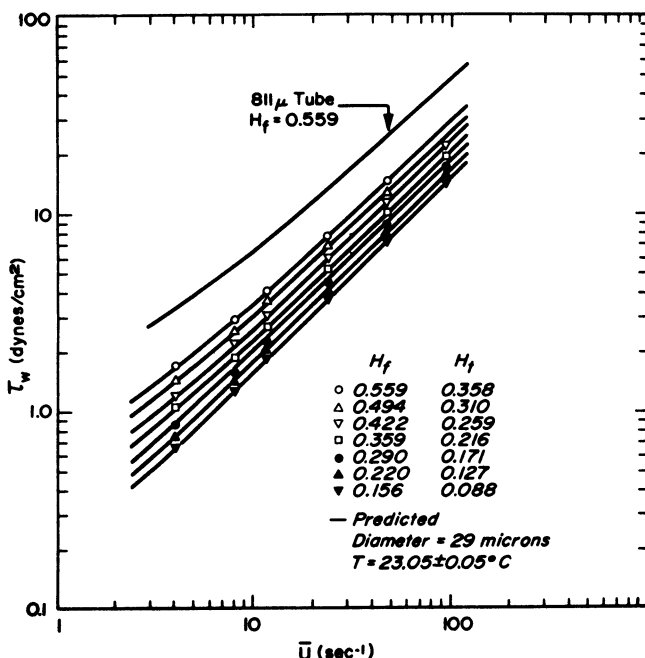


Figure 5.3:4 The flow behavior of blood in a $29\text{-}\mu$ diam. tube. The symbols are the actual flow data, recorded as the well shear stress τ_w and the bulk average velocity divided by the tube diameter, U . The solid curves through the points represent the behavior of the blood predicted from the data obtained in an $811\text{-}\mu$ diam. tube when the average tube hematocrit is the same as that experimentally found in the $29\text{-}\mu$ tube. In an $811\text{-}\mu$ tube, H_f , the feed reservoir hematocrit, and H_t , the average tube hematocrit, are equal. From Barbee and Cokelet (1971).

the blood in a tube (H_T) varies with the tube size and the feed reservoir blood hematocrit (H_F). The “relative hematocrit” H_R , plotted on the ordinate, is the ratio H_T/H_F . This figure demonstrates the Fahraeus effect. Figure 5.3:4 shows how the Fahraeus effect can be used to explain the Fahraeus-Lindqvist effect. The experimental data on the wall shear stress (τ_w) are plotted versus \bar{U} , the bulk average velocity of flow divided by the tube diameter. The data are plotted this way since it can be shown that for a fluid for which the rate of deformation is just a function of the shear stress, the same function applying at all points in the tube, the data should give one universal curve, even when the data are obtained with tubes of different diameters. The top curve in the figure represents data obtained with an $811\text{-}\mu\text{m}$ tube with $H_F = 0.559$. On the next curve, the circles represent experimental data obtained with a $29\text{-}\mu\text{m}$ tube with $H_F = 0.559$. These two sets of data should coincide if the shear stress-shear rate relationships are the same in these two tubes. But they do not agree, because the hematocrits in these two tubes are different. The true tube hematocrit is $H_T = 0.358$. If we obtain flow data in an $811\text{-}\mu\text{m}$ tube with $H_F = 0.358 (= H_T)$, we find that these data are represented by the solid curve, which happens to pass through the circles. Other data points corrected for

hematocrit show similar good agreement. Thus, in spite of the nonuniform distribution of red cells in the tubes, the Fahraeus-Lindqvist effect appears to be due entirely to the Fahraeus effect for tubes larger than $29 \mu\text{m}$.

Why does the hematocrit decrease in small blood vessels? One of the explanations is that a *cell-free layer* exists at the wall. See Chapter 3, Fig. 3.5:1. Another explanation is that the red cells are elongated and oriented in a shear flow. See Chapter 3, Fig. 3.4:5. The cell-free layer reduces the hematocrit. The smaller the vessel, the larger is the fraction of volume occupied by the cell-free layer, and the lower is the hematocrit. Furthermore, if a small side branch of a vessel draws blood from the vessel mainly from the cell-free layer, the hematocrit in the side branch will be smaller. This is usually referred to as *plasma skimming*.

The cell orientation effect reinforces the effect of plasma skimming. If a small side branch having a diameter about the same size as that of the red cell draws blood from a larger tube, (such as a capillary branching from an arteriole) the *entry condition* into the small branch is affected by the orientation of the red cells. If the entry section is aligned with the red cells it will be easier for the cells to enter. If the entry is perpendicular to the cells, some cells skim over the small branch and do not enter, and the hematocrit in the small branch will be decreased.

With a cell-free layer, the viscosity at the wall is that of the plasma and is smaller than that of whole blood. We have seen (Fig. 3.1:1) that the viscosity of blood increases with hematocrit. In a tube the hematocrit is higher at the core. Here the viscosity of blood in the blood vessel is higher at the core and lower at the wall. This affects the velocity profile. The apparent viscosity is a result of both of these factors.

5.4 The Distribution of Suspended Particles in Fairly Narrow Rigid Tubes

Mason and Goldsmith (1969) conducted an exhaustive series of experiments with suspensions of variously shaped particles, which may be rigid, deformable, or merely viscous immiscible droplets flowing through straight rigid pipes. Their results provide the best insight into the cell-free layer mentioned in the preceding section.

For a suspension of neutrally buoyant rigid spheres, the explanation of the cell-free layer is primarily geometrical, in that the center of the spheres must be at least a radius away from the wall. At a very low Reynolds number, whether there is any dynamical effect tending to force spheres away from the wall is still uncertain. Isolated rigid spheres in Poiseuille flow can be shown to experience no net radial force; they rotate, but continue to travel in straight lines; thus they cannot create a cell-free layer.

When inertia force is not negligible, rigid spheres in a Poiseuille flow do, in general, experience a radial force. They exhibit a *tubular pinch effect* demonstrated experimentally by Segre and Silberberg (1962), in which

particles near the wall move toward the axis, and particles near the axis move toward the wall. This effect is probably unimportant in arterioles or capillaries, where the Reynolds number is less than 1. Similar results are obtained for suspensions of rigid rods and discs. There is no overall radial motion unless inertial effect is important.

When the particles in suspension are deformable, Mason and Goldsmith found that they do experience a net radial hydrodynamic force even at very low Reynolds numbers, and tend to migrate towards the tube axis. The mechanism of this phenomenon is obscure, and a full theoretical analysis is not yet available.

5.5 The Motion of Red Cells in Tightly Fitting Tubes

Many capillary blood vessels in a number of organs have diameters smaller than the diameter of the resting red cell. It is extremely difficult to make *in vivo* measurements of velocity and pressure fields in these small blood vessels. To obtain some details, two alternative approaches may be taken: mathematical modeling and physical modeling. In the former the problem is described mathematically and solved to obtain the details of the flow field; but because of its heavy demand on mathematics we shall defer its discussion to the volume *Advanced Biomechanics* in this series. In this section we shall consider larger-scale physical model testing.

In Chapter 4, Sec. 4.6, we described how thin-walled rubber models of red blood cells can be made. These cells have a wall thickness to cell diameter ratio ranging from 1/100–1/150. Lee and Fung (1969) used these rubber models as simulated red cells in testing their interaction with tightly fitting tubes. An independent, similar testing was done by Sutera et al. (1970). Figure 5.5:1 shows a schematic diagram of the apparatus. The test section was made of interchangeable lucite tubes, 61 cm long, and with inner

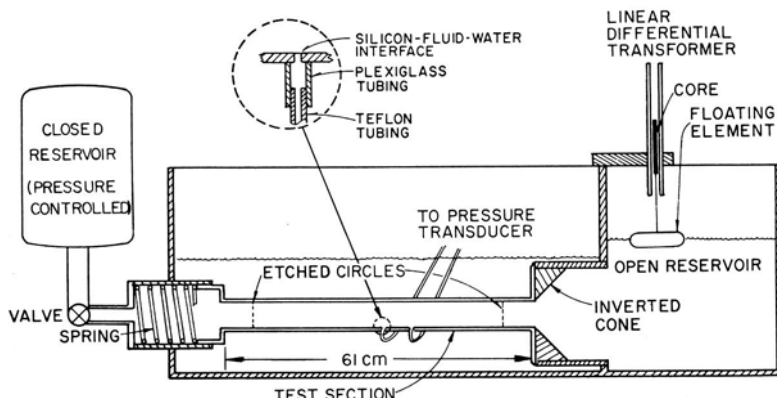


Figure 5.5:1 Schematic diagram of the testing apparatus. The flow is controlled by varying the pressure in the closed reservoir. From Lee and Fung, (1969).

diameters 2.54, 3.15, 3.81, 4.37, and 5.03 (± 0.03) cm. A conical section with a 60° inclination from the tube axis was used to guide the flow into the test section. The flow was controlled by a pressure reservoir. A constant mean velocity ranging from 0.03 to 3 cm/s could be maintained throughout each experiment. A silicone fluid with a viscosity 295 P at room temperature and a specific gravity 0.97 was used to simulate the plasma. The cell has a diameter of 4.29 ± 0.05 cm, a volume of 16.5 cm^3 , a wall thickness of 0.042 ± 0.01 cm in one model, and 0.03 in another, and is filled with the same silicone fluid. A nipple on the cell marks the pole location. The Reynolds number based on the cell diameter was in the range 0.0004–0.04.

If the tube diameter is larger than the cell diameter by more than 15%, the cell will flow in the stream without significant deformation. If the tube diameter is about equal to the resting cell diameter, then significant cell deformation occurs. Figure 5.5:2 shows such a case. Here V_M denotes the mean flow velocity, and V_c denotes the cell velocity. If the tube diameter is

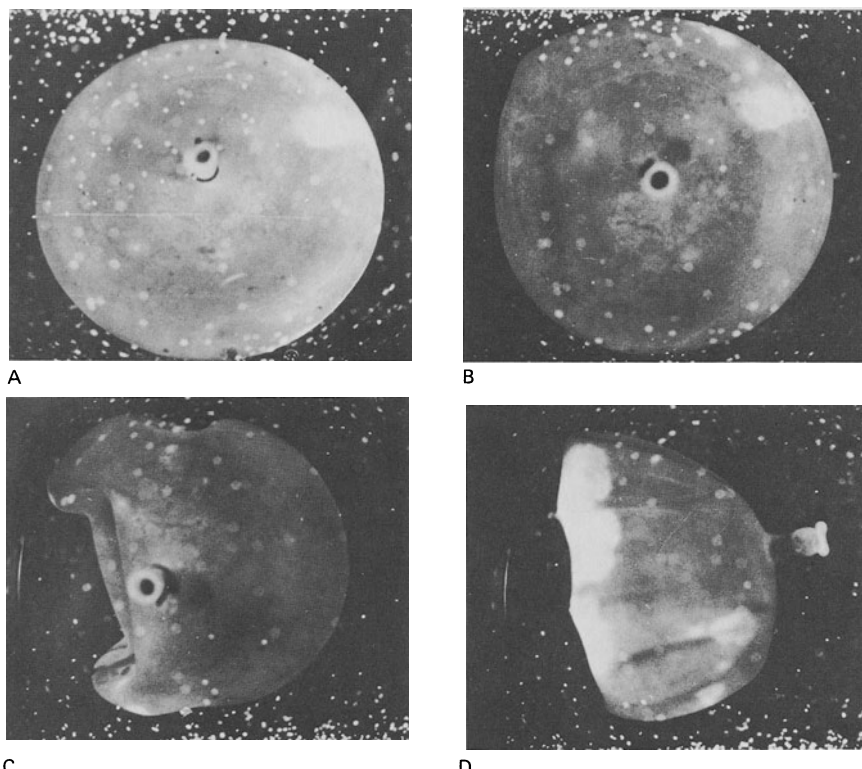


Figure 5.5:2 Change of shape of the 4.29-cm thin-walled cell in the 4.37-cm tube as the velocity increases: (A) cell velocity $V_c = 0.12$, mean flow velocity $V_m = 0.10$; (B) $V_c = 0.36$, $V_m = 0.28$; (C) $V_c = 2.49$, $V_m = 1.95$; (D) $V_c = 2.59$, $V_m = 2.16$. All velocities are in cm/s. Direction of flow: from left to right. From Lee and Fung (1969).

considerably smaller than the cell diameter, then large deformation of the cell occurs; there is severe buckling of the cell membrane; the leading edge of the cell bulges out, the trailing end caves in; and the natural tendency of the cell is to enter the tube sideways, or edge-on, (with its equatorial plane parallel to the cylinder axis). Forcing the cell to the other orientation (with the axis of the cell and the tube parallel) was not successful. In the case in which the tube diameter is equal to the resting cell diameter, the edge-on configuration is more stable. It is possible in this case for the cell to assume an axisymmetric configuration, as is shown in frame *D* in Fig. 5.5:2, but this seems to be an unstable situation and is rarely seen.

The Streamline Pattern and Cell Motion

The streamlines around the cell were determined in the 3.15-cm tube by photographing with short-duration exposure and are shown in the upper

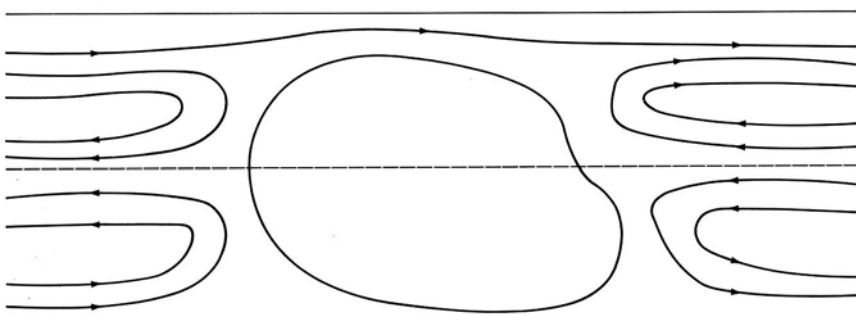
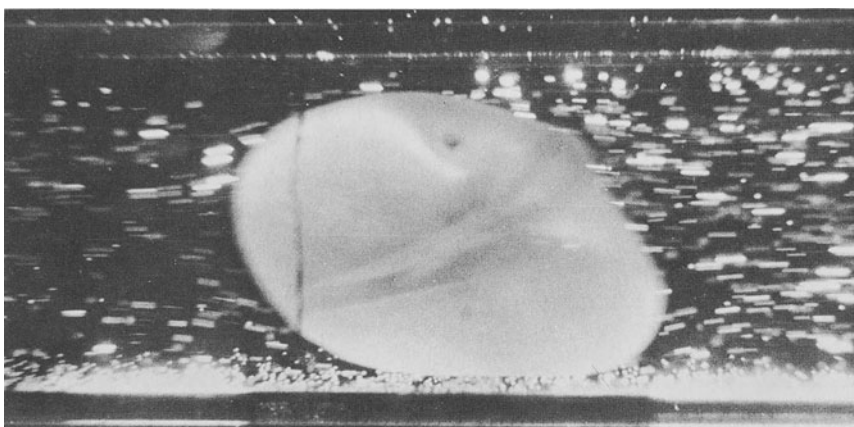


Figure 5.5:3 Short time exposures (0.5 sec) of tracer particles as a thin-walled cell of diameter 4.29 cm moves to the left in a 3.15-cm tube with a cell velocity $V_c = 0.93 \text{ cm/s}$. The lower figure shows the streamlines relative to the cell. In the upper panel the cell is moving to the left. In the lower panel the streamlines are drawn with the cell held stationary and the tube moves to the right. From Lee and Fung (1969).

panel of Fig. 5.5:3. When the streamlines are redrawn to coordinates moving with the cell, they appear as *bolus* flow as shown in the lower panel of Fig. 5.5:3.

The cell velocity is related to the mean flow velocity. The experimental data can be fitted by the equation

$$V_c = k(V_M - \alpha) \quad (1)$$

for V_M greater than α . The constants determined are:

Cell/tube diam. ratio	k	α (cm/s)
1.69	1.00	0.0
1.36	1.10	0.02
1.13	1.17	0.10
0.98	1.26	0.015

This is consistent with the observation that as the tube becomes larger, the cell will be more centrally located, where the velocity is higher than in the wall region.

Pressure Measurement

Figure 5.5:4 shows a typical record of pressure at a point midway in the 3.15-cm tube (cell diam. 4.29 cm). The pressure dropped at once as the fluid was sucked into the tube. When the cell approached the entrance, the pressure decreased further. After the cell passed the tap, the pressure returned approximately to the level in the tube before the entry of the cell. The difference between the pressure just upstream of the cell, p_u , and that just

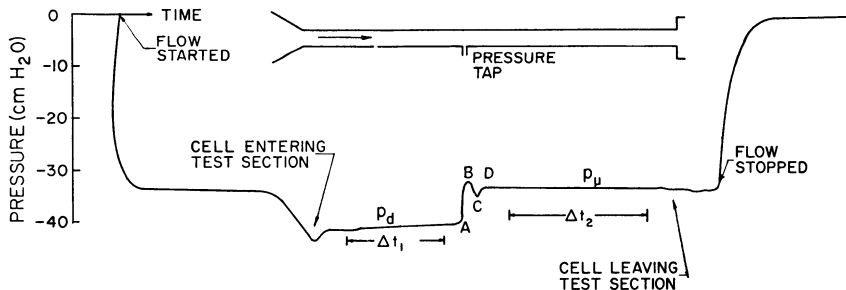


Figure 5.5:4 A typical record of the history of the pressure at the tap about midway in the test section and the change of fluid level in the open reservoir. The 4.29-cm cell moved at a velocity of 1.23 cm/sec in a 3.15-cm tube. The mean velocity was 1.18 cm/s. The position of the cell at any given instant of time can be found roughly by drawing a vertical line from the time scale to the tube sketched above the graph. Note the change of pressure at the cell's entering the test section, passing the pressure tap and leaving the test section. In the time intervals Δt_1 and Δt_2 , the cell was more than one cell diameter away from the ends of the test section and the pressure tap. The pressure in Δt_1 is the downstream pressure p_d , that in Δt_2 is the upstream pressure p_u . From Lee and Fung (1969).

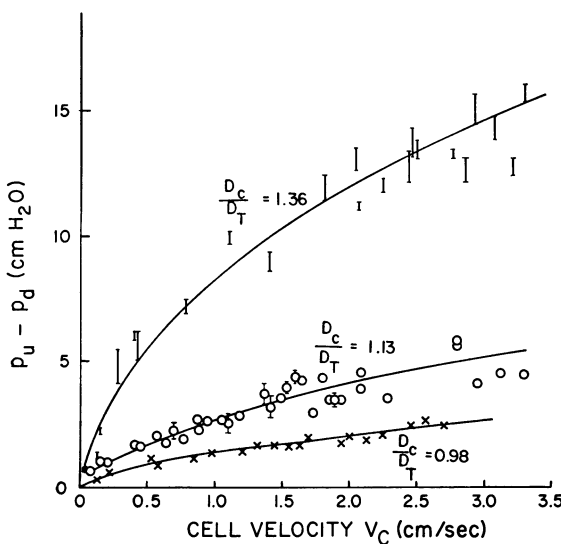


Figure 5.5:5 The resistance to red cell motion in 3.15-, 3.81-, and 4.37-cm tubes expressed in terms of the loss of pressure over and above that of the Poiseuille flow head, $p_u - p_d$, as a function of the cell velocity. The variation in the pressure difference was a result of minor shape changes of the red cell model and corresponds to the fluctuations of the downstream pressure. From Lee and Fung (1969).

downstream of the cell, p_d , is a measure of the resistance to the motion of the red cell. It is a function of the cell velocity and the ratio of the diameters of the cell and tube, as is shown in Fig. 5.5:5.

The details of the pressure change as the cell passes over the tap are very interesting. At the leading edge of the cell (point A in Fig. 5.5:4), the pressure rises rapidly. It reaches a peak at point B (on the front portion of the cell). Then comes a valley at point C (near the trailing edge of the cell), where the pressure is lower than that at the rear of the cell. This kind of pressure distribution is consistent with the predictions of lubrication layer theory (Sec. 5.8). The higher pressure at B than C will tend to push fluid into the gap between the cell and the wall toward the rear of the cell, thus reducing the velocity gradient at the wall, and decreasing the wall friction and apparent viscosity of the blood.

Critique of the Model

One unsatisfactory feature of the red cell model made of rubber is that the rubber elasticity is quite different from that of the red cell membrane. For the rubber membrane, the shear modulus and areal modulus are of the same order of magnitude. For the red cell membrane, the two moduli differ by a factor of 10^4 (see Chapter 4, Sec. 4.6). Hence the cell membrane elasticity

was not simulated. Furthermore, the bending rigidity of the red cell membrane is probably derived from electric charge or from fibrous protein attached to the membrane (see Chapter 4, Sec. 4.8), whereas that of the rubber membrane can be obtained only from the bending strain of the solid rubber. This failure to simulate the material properties could have effects which, however, are still unclear.

Observation of Red Cell Flow in Glass Capillaries

Figure 5.5:6 (from Hochmuth et al., 1970) shows data obtained from motion pictures of red cells traversing glass capillaries. The apparent plasma-layer thickness was calculated by taking the difference between the known capillary diameter and the maximum transverse dimension of the deformed cell. The plasma layer thickness seems to reach an asymptotic value at a velocity of about 2 mm/s. The scatter of the data is due in part to the random orientation of the cells relative to the plane of focus.

The increased clearance between cell and vessel wall reduces shear stress at the capillary wall due to the passing of the red cell. Hence according to

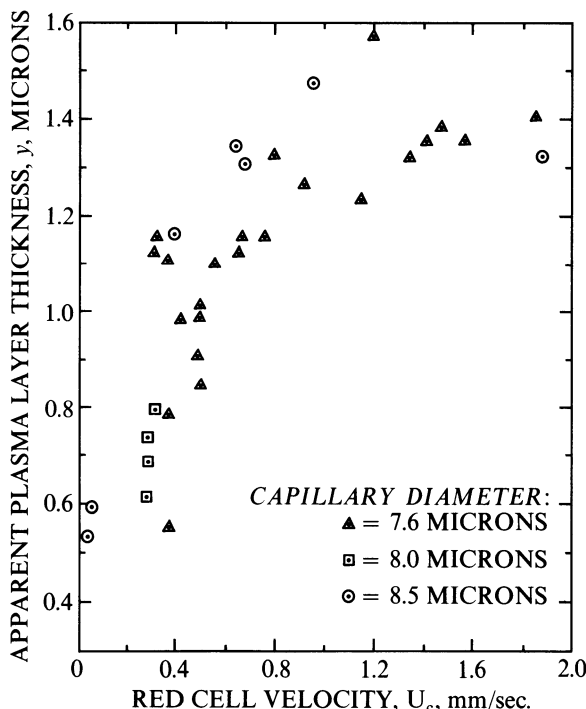


Figure 5.5:6 Variation of apparent plasma-layer thickness with red cell velocity in glass capillaries. Human red cells were used. From Hochmuth et al. (1970), by permission.

Fig. 5.5:6, the apparent viscosity of blood in the capillary should decrease as the velocity of flow increases; and by physical reasoning, the clearance will increase if the cell is more flexible, so the more flexible the cell is, the smaller is the additional pressure drop due to the red cell.

5.6 Inversion of the Fahraeus-Lindqvist Effect in Very Narrow Tubes

According to the result shown in Fig. 5.5:5 the additional pressure drop (i.e., the resistance) due to the motion of a single red blood cell increases greatly when the tube diameter becomes smaller than that of the resting red cell; and the smaller the tube, the higher is the resistance. Hence unless there is an extraordinary decrease in the number of red cells in the tube (which is not the case, as we shall show in Sec. 5.7), the resistance can be expected to increase with decreasing tube diameter when the tube is smaller than the red cell. This is the reverse of the Fahraeus-Lindqvist effect.

To calculate the resistance of red cells in a tightly fitting tube, we must know the interaction between the neighboring cells. Sutera et al. (1970) found that the additional pressure drop caused by a single cell is unaffected by a neighboring cell if the two are separated by a distance equal to or greater than one tube diameter. This short interaction distance is expected in low Reynolds number (N_R) flow. (In low Reynolds number tube flow the development length is of the order of one tube diameter, with a lower limit of 0.65 D_T in the limit $N_R \rightarrow 0$; see Lew and Fung (1969b, 1970).) Therefore, when the cells are separated by a space equal to or greater than one tube diameter, we can calculate the total pressure drop in the tube by adding the additional pressure drop due to individual cells to the Poiseuillean value. Since the pressure gradient in a Poiseuille flow is $-32\mu_0 V_M / D_T^2$ (using notations of the previous section, with V_M denoting the mean flow velocity, and D_T the tube diameter), we can write the total pressure drop per unit length of the tube as

$$-\frac{\partial p}{\partial x} = \frac{32\mu_0 V_M}{D_T^2} + n\Delta p^*, \quad (1)$$

where n is the number of cells per unit length, and Δp^* is the additional pressure drop per single cell. μ_0 is the coefficient of viscosity of the suspending fluid (plasma). If H_T is the hematocrit in the capillary tube, then n is equal to the volume of the tube per unit length divided by the volume of one red blood cell:

$$n = \frac{H_T \pi D_T^2}{4(\text{RBC vol.})}. \quad (2)$$

Δp^* , as presented in Fig. 5.5:6, can be made dimensionless with respect to the characteristic shear stress $\mu_0 V_M / D_T$. It is a function of D_c , D_T , V_M , μ_0 ,

and the elasticity of the cell. Let the elastic modulus of the cell membrane for pure shear be denoted by E_c (see Chapter 4, Sec. 4.7); then a dimensionless parameter is $\mu_0 V_M / (E_c D_T)$. This parameter is the ratio of a typical shear stress $\mu_0 V_M / D_T$ to the membrane elasticity modulus, and thus can be called a *characteristic membrane strain*.

Figure 5.6:1 shows the normalized additional pressure drop of a single cell given by Sutera et al. (1970). We can then combine Eqs. (1) and (2) as

$$-\frac{\partial p}{\partial x} = \frac{32\mu_0 V_M}{D_T^2} + \frac{\pi H_T D_T^2}{4(\text{RBC vol.})} \left(\frac{\Delta p^*}{\mu_0 V_M / D_T} \right) \frac{\mu_0 V_M}{D_T}. \quad (3)$$

But if we invoke the concept of *apparent viscosity*, we can also write

$$-\frac{\partial p}{\partial x} = \frac{32\mu_{\text{app}} V_M}{D_T^2}. \quad (4)$$

Comparing Eqs. (4) and (5), we obtain the *relative apparent viscosity* μ_r :

$$\mu_r = \frac{\mu_{\text{app}}}{\mu_0} = 1 + \frac{\pi H_T}{128} \left(\frac{D_T^3}{\text{RBC vol.}} \right) \left(\frac{\Delta p^*}{\mu_0 V_M / D_T} \right). \quad (5)$$

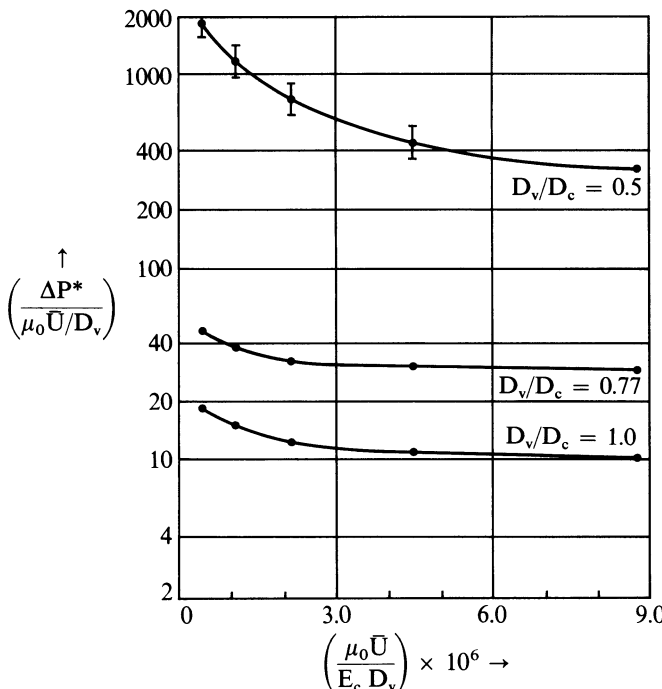


Figure 5.6:1 Additional pressure drop due to a single cell as a function of strain parameter, from large-scale model. In this figure, D_v is used in place of D_T , the vessel or tube diameter, and \bar{U} is used in place of V_M the mean flow velocity. From Sutera et al. (1970), by permission.

If the data of Fig. 5.6:1 are examined in the light of this equation, it will be found that μ_r increases with decreasing D_T/D_c when $D_T/D_c < 1$, for any fixed values of H_T . This is opposite to the Fahraeus-Lindqvist effect. If a simplified expression relating the hematocrit in the tube, H_T , to that in the reservoir, H_F , as given in Eqs. (1) and (2) of Sec. 5.7, is used in Eq. (5) above, then the results shown in Fig. 5.6:2 are obtained at a reservoir hematocrit of 40%.

Equations (1)–(5) are derived under the assumption that the red cells are sufficiently apart from each other in the tube. If the cells are more closely packed, the situation is more complex. Sutera (1978), citing his model experiments (1970), believes that these equations are applicable irrespective of the spacing between the red cells, so that the resistance is linearly proportional to the hematocrit without limitation on the hematocrit value. A similar conclusion is reached by Lighthill's (1968, 1969) lubrication layer theory, because the interaction between the red cell and the endothelium of the capillary blood vessel is localized. Experiments by Jay et al. (1972), however, showed that the relative viscosity of blood tends to be independent of the

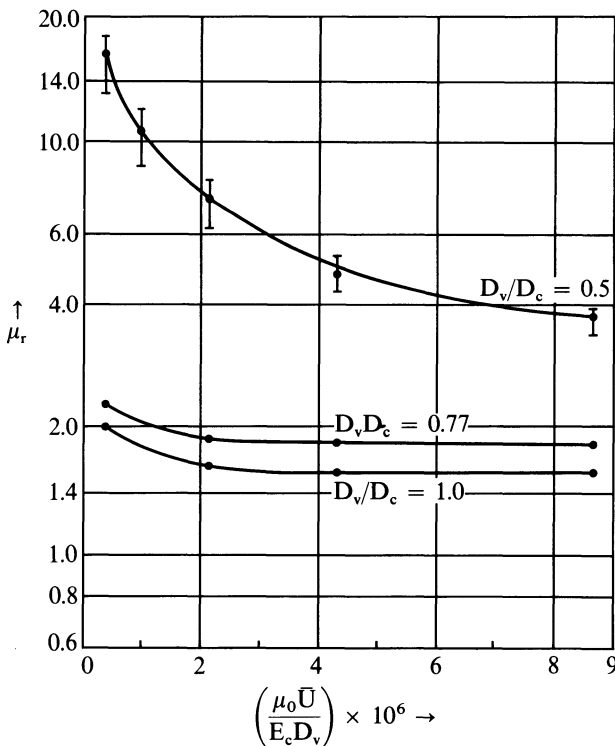


Figure 5.6:2 Apparent relative viscosity of blood in capillaries according to model experiment results of Sutera et al. (1970) and calculated for the “reservoir” or “feed” hematocrit $H_F = 40\%$. From Sutera (1978), by permission.

hematocrit for human blood flowing in glass tubes of 4 to 15 μm in diameter. Earlier, such a phenomenon was also described by Prothero and Burton (1961, 1962). Jay et al. believed that this is a direct contradiction to the Lighthill–Fitz-Gerald theory. Chien (1972) points out, however, that the theoretical analysis by Skalak et al. (1972) showed that when the spacing between the red cells is small, the plasma trapped between the cells moves with the cell. Hence when the hematocrit is sufficiently high, the cell-plasma core moves almost like a rigid body, and the apparent viscosity will be independent of the hematocrit. Furthermore, the size of the core depends on the deformation of the red cell. One can estimate the size of the red cell core from the experimental results shown in Fig. 5.5:6. It is seen that even in very narrow capillaries there is a sizable gap between the cell and endothelium if the blood flows at a speed close to the *in vivo* value. The gap becomes very small only if the flow velocity becomes very small, i.e., in a near stasis condition.

Summarizing, we conclude that the relative viscosity of single-file flow of red cells in very narrow capillaries is proportional to the tube hematocrit if the spacing between the red cells is of the order of a tube diameter or larger. If the spacing is smaller, and the flow velocity approaches 1 mm/s or larger, then the cell-plasma core moves like a rigid body, and the relative viscosity will tend to be independent of the tube hematocrit. If the spacing between red cells is smaller than the tube diameter and the flow velocity is smaller than, say 0.4 mm/s, then the gap between the cell and endothelium decreases, the resistance of each cell increases, and the relative viscosity will be proportional to the number of red cells per unit length of the vessel.

5.7 Hematocrit in Very Narrow Tubes

Since the apparent viscosity of blood depends on hematocrit [see, for example, Eq. (8) of Sec. 5.2], we should know the way hematocrit changes from one blood vessel to another in a microvascular bed. When one examines microcirculation in a living preparation under a microscope, one is impressed by the extreme nonuniformity in hematocrit distribution among the capillary blood vessels, and by the unsteadiness of the flow. The red blood cells are not uniformly distributed. In a sheet of mesentery or omentum, or a sheet of muscle, sometimes we see a long segment of the capillary without any red cells; at another instant we see cells tightly packed together. In any given vessel, the velocity of flow fluctuates in a random manner (Bond and Guest, 1967; Johnson and Wayland, 1967). Similarly, in the capillaries of the pulmonary alveoli, the velocity of flow fluctuates (Kot, 1971). The distribution of red cells appears “patchy” at any given instant of time (Warrell et al., 1972), i.e., the distribution is nonuniform in the alveolar sheet: capillaries in certain areas have a high density of red cells, while neighboring areas have few red cells.

These dynamic features have many causes. Figure 5.7:1 shows some examples. Consider a balanced circuit connecting a vessel at pressure p_1 to another at pressure p_0 (Fig. 5.7:1). Let us assume that all branches, A, B, C, D, E, are of equal length and diameter. Let us also assume that at the beginning all the red cells are identical and are uniformly distributed in all vessels. Then it is clear that there will be uniform flow in the branches A, B, C, D, but no flow in E. Now suppose that branch B receives one red cell more than A. The balance is then upset. The pressure drop in B will be increased, and a flow is created in the branch E. The same will happen if branch B, instead of getting an extra cell, gets a red cell that is larger than those in A, or a leukocyte. The flow in E, thus created, will continue unless the resistance is balanced again. Thus, because of the statistical spread of the red cell sizes, and the existence of leukocytes, continued fluctuation in branch E is expected. Finally, active control due to sphincter action of vascular smooth muscle will have the same effect, as is shown in the lower right panel in Fig. 5.7:1.

Another cause of flow fluctuation is the basic particulate nature of the blood. To clarify the idea, consider the situation shown in Fig. 5.7:2, in which rigid spherical particles flow down a tube which divides into two equal branches. Let the tube diameter be almost equal to the diameter of the spheres. Consider a sphere that has just reached the point of bifurcation. We

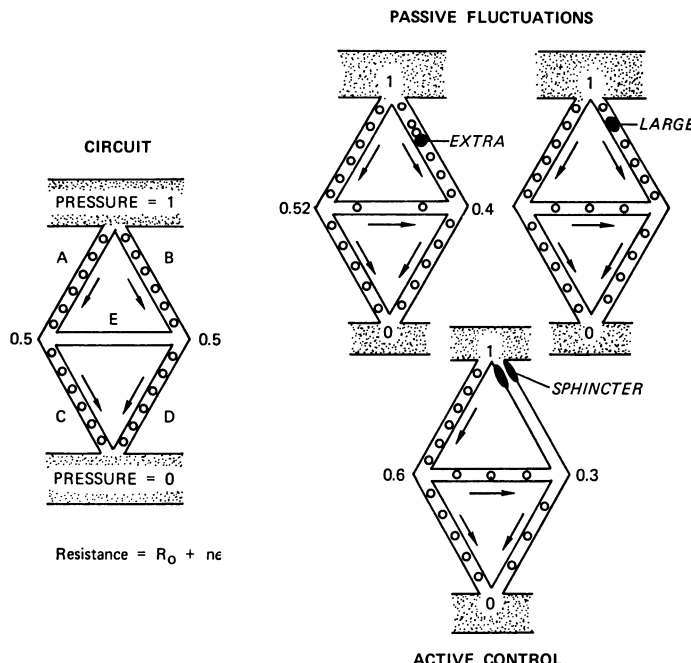


Figure 5.7:1 An idealized capillary blood flow circuit. (Left), balanced. (Right), balance upset by (a), an extra cell in branch B, (b) an extremely large cell in branch B, and (c) a sphincter contraction. From Fung (1973).

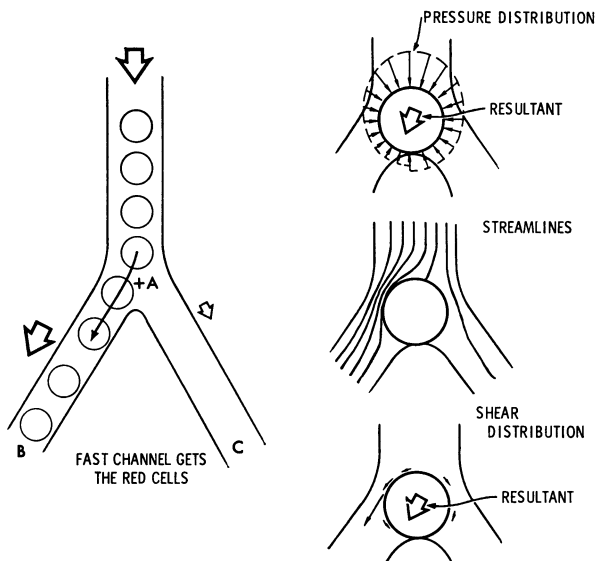


Figure 5.7:2 At a branch point of a capillary blood vessel, the branch with the faster stream gets the red blood cells. (Left), spherical balls flow in a cylindrical tube which bifurcates into two equal branches. (Right), the forces acting on the sphere at the moment when it is located at the point of bifurcation of the vessel. The resultants of the pressure forces (top) and shear stress (bottom) both point to the faster stream. From Fung (1973).

shall see that the ball has a tendency to move into the branch in which the flow is faster. Let us assume that the flow in the branch to the left, AB, is faster than that in the branch to the right, AC (see the left-hand drawing in Fig. 5.7:2). The reason for the flow in AB to be faster must be that the pressure gradient is larger in AB than in AC. Now consider all the forces acting on the ball, which is situated centrally at the junction as shown in the right-hand side of Fig. 5.7:2. These are pressure forces and shear forces. The pressure on the top side of the ball is nearly symmetric with respect to right and left. The pressure on the underside is lower on the left as we have just explained. Therefore, the net pressure force will pull the ball into the left branch. Next consider the shear stress. Assume that the ball comes down the vertical tube without rotation. At the junction, the ball is temporarily stopped at the fork. The fluid will tend to stream past the ball at this position. This streaming is more rapid on the left side, because we have assumed that the branch at the left has a faster flow. Therefore, the shear strain rate and the shear stress are larger on the left. The net shear force is a vector pointing into the left channel. Therefore, in this configuration both the pressure force and the shear force tend to pull the ball into the faster stream.

When the next ball reaches the junction the same situation prevails. Therefore, under the assumption made above the more rapid stream will get all the balls. If the velocity in AB is twice that in AC, the theoretical ratio of the density of red cells in AB to that in AC is not 2 to 1, but infinity.

In capillary blood flow, each blood cell would have to make the same decision when it reaches a crossroad: which branch should it go into? The decision making is influenced by the size of the blood cell relative to the blood vessel, the flexibility of the blood cell, and the ratio of the velocities in the branches. A detailed investigation of these factors has been made by the author and R. T. Yen (Yen and Fung, 1978). We showed that when a capillary blood vessel bifurcates into two daughter vessels of equal diameter, the red cells will be distributed nonuniformly to the two daughter branches if the velocities in the two branches are unequal. The faster side gets more cells. If the cell-to-tube diameter ratio D_c/D_t is of the order of 1 or larger, and the velocity ratio of the flow in the two branches is less than a certain critical value, then the hematocrit ratio in the two branches is proportional to the velocity ratio. If the velocity ratio exceeds a critical value, then the faster branch gets virtually *all* the red cells. In that case the hematocrit in the slower branch is zero. The critical velocity ratio is of the order of 2.5, with the exact value depending on the cell-to-tube diameter ratio D_c/D_t and the elasticity of the red cell.

A way to produce a large velocity ratio in capillary branches is to occlude the downstream end of a vessel. Svanes and Zweifach (1968), using a micro-occlusion technique, have shown that it is possible to clear any capillary vessels of its red cells.

Our discussion so far has stressed the importance of the entry condition of flow into branches of equal diameter on the hematocrit distribution. How about flow into branches of unequal diameter? Or flow from a reservoir into a small tube (as in Fahraeus' experiment, Fig. 5.3:2)? Or from a larger tube into a smaller side branch as in the case of a capillary blood vessel issuing from an arteriole (Fig. 5.7:3)? In these cases the hematocrit in the smaller branch may be reduced for three reasons:

1. Due to the entry condition into the capillary (affected by the geometry of the entry section of the tube, and the flow just outside of the entrance section)
2. Due to a decrease of hematocrit at the wall of the larger tube, where the capillary siphons off the blood (The *plasma skimming* effect discussed in Chapter 3, Sec. 3.5, and Chapter 5, Sec. 5.3)

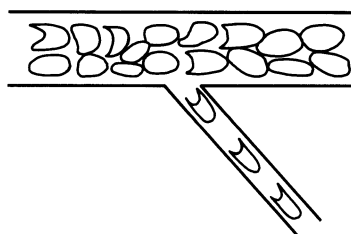


Figure 5.7:3 A small vessel branching out from a larger one.

3. Due to the fact that the red cell moves faster than the plasma in the capillary blood vessel

If the effects (1) and (2) are ignored, then we can calculate the effect of (3) as follows. Let the mean velocity of blood in a capillary be V_m , and that of the red cell be V_c . In a unit interval of time the capillary draws a volume of blood equal to $V_m A$ from the reservoir, where A is the cross-sectional area of the capillary. If the hematocrit of the reservoir is H_F , the volume of red cells flowing in is $V_m A H_F$. At the same time, the volume occupied by the red cells (which are arranged in single file in very narrow capillaries) is $V_c A H_T$, where H_T denotes the hematocrit in the capillary. Thus, obviously,

$$V_m A H_F = V_c A H_T,$$

or

$$H_T = H_F \frac{V_m}{V_c}. \quad (1)$$

This is a statement of the conservation of red cell volume. Since $V_m/V_c < 1$ (see Sec. 5.5), we have $H_T < H_F$, the Fahraeus effect.

The effect of the two factors (1) and (2) ignored above, however, may render Eq. (1) nonvalid. The actual hematocrit of the blood drawn in by the capillary from the arteriole (or reservoir) may not be equal to H_F , the average hematocrit in the larger vessel. The hematocrit in the reservoir in the neighborhood of the entry section can be smaller or larger than H_F by a factor F . Thus

$$H_T = F H_F \frac{V_m}{V_c}. \quad (2)$$

To clarify the entry effect and determine F , Yen and Fung (1977) made a model experiment in which gelatin particles (circular discs) were suspended in a silicone fluid to simulate the blood. When the diameter of the undeformed cell was equal to or greater than the tube diameter, the volume fraction of the cells in the tube was found to increase to a value equal to or greater than that in the reservoir. This is the reverse of the Fahraeus effect.

Additional experiments showed that the hematocrit in the tube could be greatly influenced by the flow condition outside the entrance to the tube. If the tube was nearly perpendicular to the main direction of flow in the reservoir (as is the case in most arteriole-capillary junctions), it was found that the velocity of flow in the reservoir just outside the entrance to the tube could affect the hematocrit in the tube. Some details are given in the following.

Two models were tested. See Fig. 5.7:4. The first model employs a tube with a smooth entry section opening into a still reservoir. For this model an "entry cone" is inserted in front of the tube, similar to the configuration tested by Fahraeus and Lindqvist [Fig. 5.3:2(a)]. The second model uses a tube with an abrupt entry section opening perpendicularly into a stream, which has a definite shear gradient. The end of the tube is cut squarely and sharply, similar to the configuration tested by Barbee and Cokelet

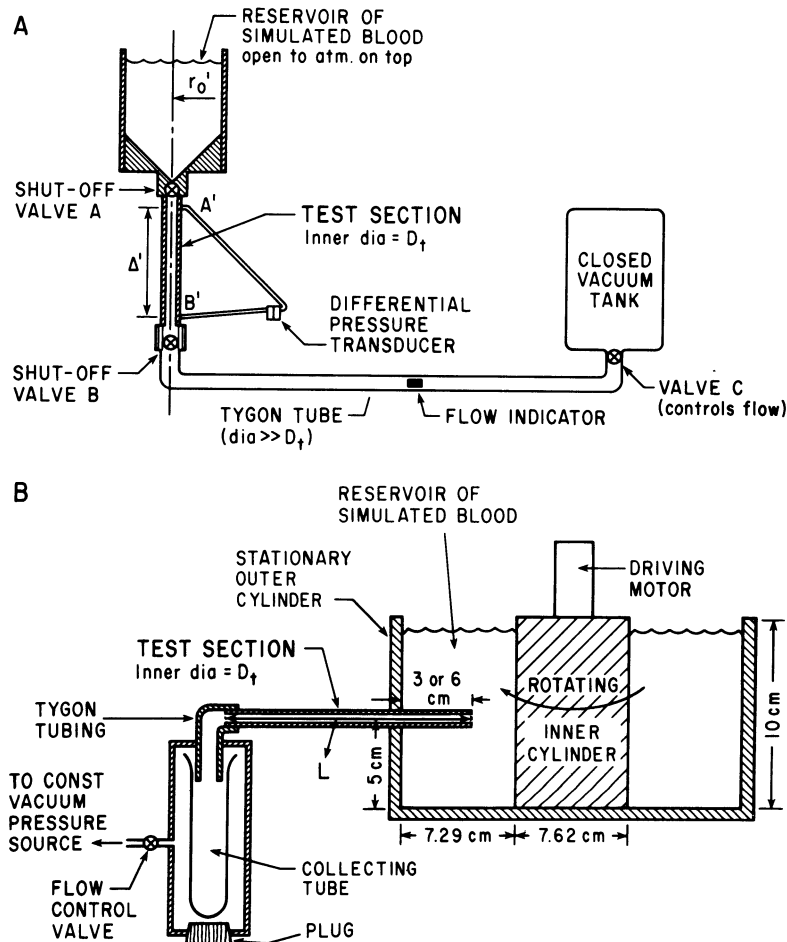


Figure 5.7:4 Schematic diagram of test models: (A) Model I, (B) Model II. For Model II, the length of the tygon tubing attached to the outflow end of the test tubes was 6.4 cm. The inner diameter of the tygon tubing was equal to the outer diameter of the test tube. The three test tubes have inner diameters $D_t = 0.67, 0.45$, and 0.32 cm ; whereas the simulated red cells (gelatin pellets) have a diameter of 0.32 cm and a thickness of 0.1 cm . From Yen and Fung (1977).

[Fig. 5.3:2(b)]. The reservoir of the second model is a cylindrical tank containing a rotating inner core which imparts a steady shear flow to the fluid. This is considered to be the mainstream flow. The tube is placed perpendicular to the direction of main flow in the reservoir in order to simulate the flow condition at an arteriole-capillary blood vessel junction.

A suspension of gelatin pellets in a silicone fluid was used to simulate blood. The pellets were circular cylindrical discs, with a diameter of 1.08 cm and a thickness of 0.32 cm in the first model, and a diameter of 0.32 cm and a thickness of 0.1 cm in the second model. The buoyancy of the pellets was

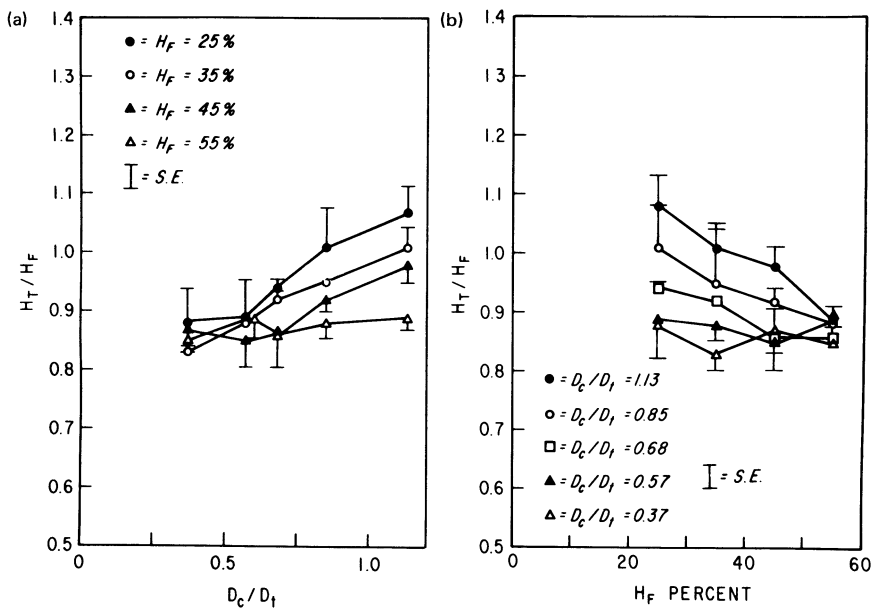


Figure 5.7:5 Experimental results from Model I, showing mean and standard errors of the mean (a) Plot of ratio of tube hematocrit (H_T) to feed hematocrit (H_F) as a function of ratio of cell diameter (D_c) to tube diameter (D_t). (b) Tube hematocrit to feed hematocrit ratio (H_T/H_F) as a function of feed hematocrit (H_F). From Yen and Fung (1977).

controlled by mixing a suitable amount of alcohol with water in making them. The viscosity of the fluid was 100 P, and the Reynolds number based on the tube diameter was 10^{-2} to 10^{-4} , similar to *in vivo* values in capillaries. In each experiment, the pellets were carefully mixed with the silicone fluid; the mixture was stirred until uniform and then poured into the reservoir. To determine the particle concentration at any flow condition, the flow was suddenly stopped, the number of particles present in the tube was counted, and their volume computed.

Figure 5.7:5(a) shows the ratio of hematocrit in the "capillary" tube to that in the reservoir of Model I, plotted against the ratio of particle to tube diameters. The H_T/H_F ratio increases with increasing ratios of D_c/D_t . Thus for a given cell diameter, the tube hematocrit increases when the tube diameter decreases (reverse Fahraeus effect). This is more evident at lower reservoir concentrations.

Figure 5.7:5(b) shows the variation of the hematocrit ratio H_T/H_F as a function reservoir hematocrit H_F for fixed values of D_c/D_t . It shows a tendency toward increased relative hematocrit in the capillary tube at a lower reservoir hematocrits.

Typical results from Model II are shown in Fig. 5.7:6. H_D is the "discharge" hematocrit of the outflow from the tube. H_F is the reservoir hematocrit.

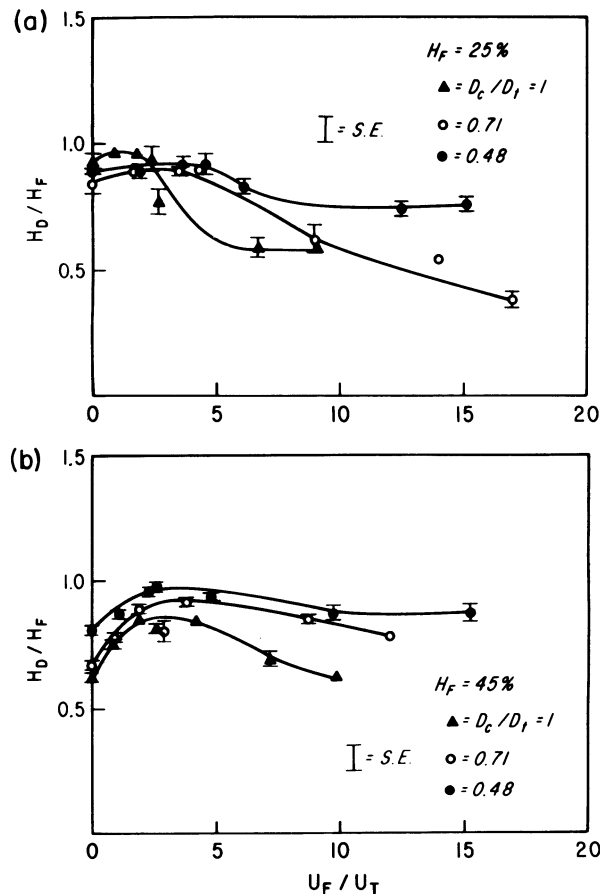


Figure 5.7:6 Experimental results from Model II, showing mean and standard errors of the mean. (a) Relative *discharge hematocrit* as a function of the ratio of tangential velocity in the reservoir at tube entrance and mean tube flow velocity for feed hematocrit $H_F = 25\%$. (b) The same for feed hematocrit $H_F = 45\%$. From Yen and Fung (1977).

The ratio H_D / H_F is the factor F of Eq. (2), because by the principle of conservation of matter (red cell volume), we obtain, by reasoning identical to the derivation of Eq. (1),

$$\frac{H_D}{H_T} = \frac{\text{Discharge hematocrit}}{\text{Tube hematocrit}} = \frac{\text{mean speed of pellets}}{\text{mean speed of tube flow}} = \frac{V_c}{V_m} \quad (3)$$

Substituting Eq. (3) into Eq. (2), we obtain

$$F = \frac{H_D}{H_F} \quad (4)$$

Figure 5.7:6 shows that H_D / H_F , hence the factor F , varies with the ratio of the mainstream velocity at the entrance section of the tube, U_F , to the

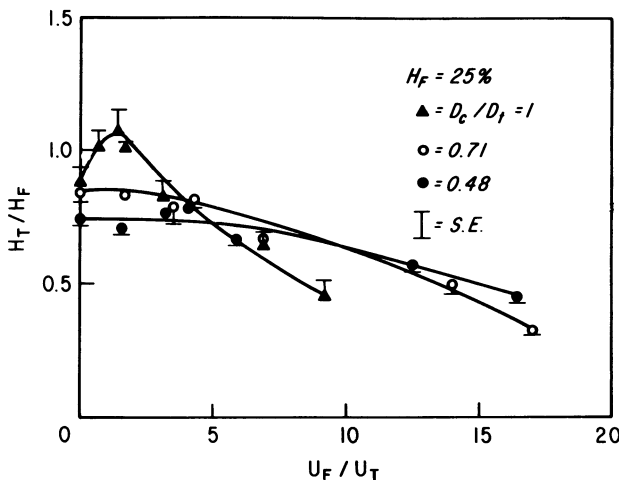


Figure 5.7:7 Relative tube hematocrit in Model II as a function of the ratio of tangential velocity in the reservoir at tube entrance to mean tube flow velocity for feed hematocrit $H_F = 25\%$. From Yen and Fung (1978).

mean velocity of flow in the tube, U_T . The curves are seen to be bell-shaped. From a certain initial value of H_D/H_F , the discharge hematocrit rises to a peak value at a ratio of U_F/U_T in the range 1 to 4. For higher velocity ratios (U_F/U_T from 4 to 17), the discharge hematocrit declines.

In Fig. 5.7:7 the ratio of the hematocrit in the “capillary” tube to that in the reservoir is plotted against the ratio of the mainstream velocity in the reservoir at the tube entrance to the mean velocity of flow in the tube, for a reservoir hematocrit of 25% in Model II. A comparison of Figs. 5.7:7 and 5.7:6(a) shows that the capillary tube hematocrit and the discharge hematocrit are not equal. Both H_T and H_D vary with the mainstream velocity and are influenced by the entrance condition.

Motion pictures of the flow in tubes with D_c/D_t equal to 1 or larger show that most of the pellets (discs) enter the tube “edge-on.” Thus the force of interaction between a pellet and the entry section of the tube is concentrated on two areas at the edge of the cell. In general, buckling of the cell membrane occurs at these points.

It is clear that the seemingly simple motion of suspended flexible particles from a reservoir into a small tube is a complicated phenomenon to analyze.

5.8 Theoretical Investigations

Even in very narrow capillary blood vessels, moving red cells never come to solid-to-solid contact with the endothelium of the blood vessel. There is a thin fluid layer in between. The thicker the fluid layer, the smaller would be the shear strain rate, and the smaller the viscous stress. On the other hand,

for any given thickness of the fluid layer, the shear stress depends on the velocity profile in the gap. Is there any way the shear stress on the vessel wall (endothelium) can be reduced, and thereby reducing the resistance of the blood? The answer is “yes”: by forcing the fluid into the gap in such a way as to reduce the slope of the velocity profile on the vessel wall. This is the hydrodynamic lubrication used in engineering, in journal bearings. Lighthill (1968, 1969) pointed out that such an effect can be expected from a red cell squeezing through a very narrow capillary vessel. The effect is due to a “leak-back” in the gap between the cell and the vessel wall.

The physical picture is illustrated in Fig. 5.8:1, from Caro et al. (1978). In the figure the velocity vectors are drawn with respect to an “observer” moving with the red cell. The cell then appears to be at rest, and the capillary wall moving backward with speed U . In Fig. 5.8:1(a) the velocity profile is assumed to be linear. Under this hypothesis the rate of fluid (volume) flow in the gap, which is equal to the area of the velocity profile multiplied by the length (in the direction perpendicular to the paper), will be nonuniform: smaller at the point x in the figure than that at y . This is impossible in an incompressible fluid; hence the hypothesis is untenable. It follows that the velocity profile cannot be linear everywhere.

In Fig. 5.8:1(b), a nonlinear velocity profile is shown at x . This profile has a zero velocity on the cell wall and U on the capillary, as the boundary conditions demand. In the gap the profile bulges to the left so that the area under the profile at x , where the gap is thinner, is equal to the area of the

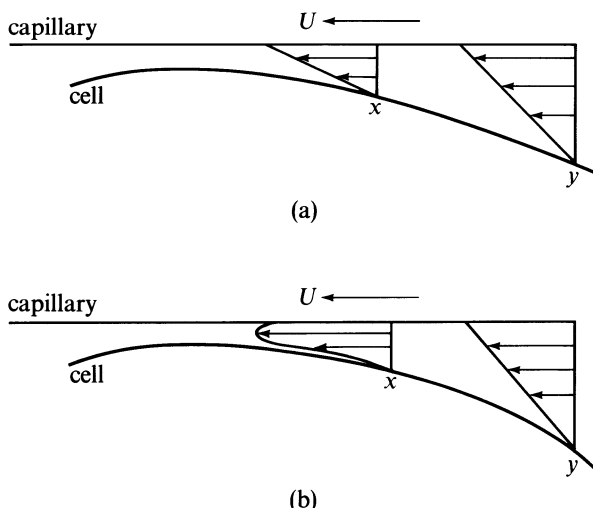


Figure 5.8:1 Diagram showing the need for leak-back past a red cell in a capillary (cell taken to be at rest, capillary wall moving). (a) Linear profile everywhere leads to nonuniform flow rate, which is not permitted. (b) Continuity upheld by the superposition of a parabolic component, requiring a pressure gradient. From Caro et al. (1978), p. 404, by permission.

triangle at y . Then the principle of conservation of mass is satisfied. The slope of the nonlinear velocity profile at the capillary wall at point x is smaller than that at y . The shear stress, which is proportional to the slope, is therefore smaller at x than at y . In the special case sketched in Fig. 5.8:1(b), this slope is negative, so the shear stress acts in a direction to propel the blood!

In general, the more the velocity profile deviates from the linear profile, the more reduction of shear stress on the capillary wall is obtained. Correspondingly, the negative pressure gradient in the layer is reduced. Let Q be the volume flow rate associated with this departure from the linear profile (proportional to the area under the velocity profile minus $\frac{1}{2}Uh$, the area of a hypothetical linear profile). Let x be the distance along the capillary wall measured from left to right, and let h be the thickness of the layer. Then, according to a detailed analysis of force balance, Lighthill shows that the pressure gradient (dp/dx) is the sum of two terms, one positive and proportional to Q/h^3 , and the other negative and proportional to $-U/h^2$. Thus

$$\frac{dp}{dx} = \frac{12\mu Q}{h^3} - \frac{6\mu U}{h^2}, \quad (1)$$

where μ is the viscosity of the plasma, and Q is the leak-back. The lubrication quality is derived from Q .

So far the analysis is indisputable. To complete it, we must compute the thickness h as a function of x . This cannot be done without specifying the elasticity of the red cell and the endothelium. Lighthill (1968) and Fitz-Gerald (1969a,b) assumed both of these to behave like an elastic foundation, with local deflection directly proportional to local pressure. This assumption is questionable, especially with regard to the red cell which, according to what is described in Chapter 4, should behave more like a very thin-walled shell with a very small internal pressure. For this reason the many interesting predictions made by these authors remain to be evaluated.

The concept of a lubrication layer is pertinent to red cells moving in capillary blood vessels so narrow that severe deformation of the cells is necessary for their passage. In larger capillaries whose diameters are larger than that of the red cells, the deformation of the red cells is minor, and the mathematical analysis can be based on Stoke's equation for the plasma, which is a Newtonian fluid. Skalak and his students (see reviews in Skalak, 1972, and Goldsmith and Skalak, 1975) have carried out a sequence of investigations of flows of this type: the flow of a string of equally spaced rigid spheres in a circular cylindrical tube, the flow of oblate and prolate spheroids in the tube, the flow of spherical and deformable liquid droplets in the tube, and finally the flow of red blood cells with membrane properties specified by Eq. (7) of Sec. 4.7 in the tube. In the last case they also included very narrow tubes, which call for large deformation of the cells under the assumption that the radius of the cell at any point is linearly dependent on the pressure at that point. Among other things, they showed that, in the case

of the flow of rigid spheres down the center of a tube, the pressure drop required for a given volume flow rate increases when the ratio of the diameters of the sphere, b , and of the tube, a , increases. But even when $b/a = 0.9$, and the spheres are touching, the pressure drop is only about 2.0 times that required by the same flow with plasma only, without spheres. But the apparent viscosity of whole blood is at least 2.5 times that of plasma, so the lubrication layer effect is operating even when b/a is as small as 0.9.

Problems

- 5.1** Show that, theoretically, in man the average circulation time for red blood cells is different from the average circulation time of blood plasma. Do you feel uneasy about this concept?

Note. A flowing river carries sand in its current; the average speed of the water does not have to be equal to that of the sand.

- 5.2** Discuss the hematocrit variation in the large and small arteries and veins, arterioles, venules, and capillaries.

- 5.3** Discuss the ways in which an entry section can influence the hematocrit distribution.

- 5.4** Since red blood cells and albumin or other plasma proteins can be selectively labeled with radioactive substances, one should be able to measure the circulation time of red blood cells and plasma by the indicator dilution technique. Look into the literature on indicator dilution for evidence of the different circulation time of red cells and plasma.

- 5.5** Formulate a mathematical theory of flow of a fluid in a pipe containing particles (spherical or otherwise) whose diameters are comparable to that of the pipe. Write down all the field equations and boundary conditions. Show that the problem is mathematically well defined (theoretically solvable and has a unique solution). Outline a procedure to determine the apparent viscosity of the fluid and particle mixture as a function of the size and shape of the particles and the vessel.

- 5.6** Consider the flow of water in a circular cylindrical pipe. As the flow velocity increases, the flow becomes turbulent. How does the apparent viscosity change with velocity of flow?

- 5.7** Blood flow in arteries with severe stenosis often give out bruit (vibrational noise of the arterial wall) due to flow separation [Fig. P5.7]. Flow separation can also

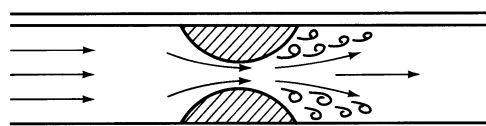


Figure P5.7 Flow separation in divergent flow. Divergence can be seen from the pattern of the streamlines.

occur at arterial bifurcation points if the velocities in the two daughter branches are very different. Describe the change of apparent viscosity of flow in these vessels due to flow separation as a function of the flow velocities.

- 5.8** A small capillary vessel leaves a larger vessel at a right angle (Fig. P5.8). The fluid contains particles whose diameter is comparable to that of the small branch. Consider first spherical particles. Analyze the tendency for the sphere to enter the small branch as a function of the ratio of the average velocity in the larger vessel to that in the small branch. Then consider red cells. In shear flow the red cells tend to be elongated and lined up with the flow. What is the chance for a red cell to be sucked into the capillary branch? Use the result to discuss the expected hematocrit ratio in the two branches.

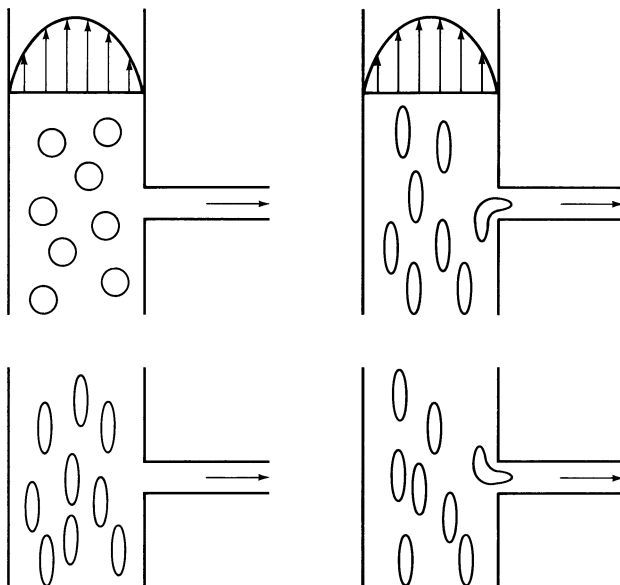


Figure P5.8 Flow into a small branch from a larger vessel. The tendency of a particle to enter the branch depends on the resultant force acting on the particle when it is in the neighborhood of the entry section.

- 5.9** Consider the bifurcating circular cylindrical tube shown in Fig. 5.7:2. Let the spheres shown in the figure be replaced by flexible discs (such as red blood cells in small capillaries). Analyze the new situation and determine the direction of motion of the pellets.

Use this result to analyze single-file flow of red cells in a bifurcating capillary blood vessel and derive a relationship between the hematocrits in the two daughter branches and the velocity ratio v_1/v_2 . (cf. Yen and Fung, 1978).

- 5.10** Consider turbulent flow in a blood vessel. Turbulences consist of eddies of various sizes. The statistical features of these eddies can be stated in the form of velocity correlation functions in space and time. From these correlation functions, scales of turbulence can be defined. Now let the fluid be blood, and consider two related

questions: (a) the effect of red cells on turbulence, especially on the transition from laminar to turbulent flow, and (b) the effect of turbulence on the stresses induced in the membranes of red cells and platelets. These interactions obviously depend on the ratio of the red cell diameter to the scale of turbulence, or the spatial correlation of the velocity field. Present a rational discussion of these questions.

- 5.11** The question (a) of the preceding problem is relevant to the shear stress imparted by the fluid on the blood vessel wall, and hence may be significant with respect to the genesis of atherosclerosis. The question (b) is relevant to hemolysis and thrombosis. Discuss the significance of the solutions of Problem 5.10 with regard to the situations described in Problem 5.7.

References

- Barbee, J. H., and Cokelet, G. R. (1971) *Microvascular Res.* **3**, 6–21.
- Benis, A. M., Chien, S., Usami, S., and Jan, K. M. (1973) *J. Appl. Physiol.* **34**, 383–389.
- Braasch, D. (1967) *Pflügers Archiv. ges. Physiol.* **296**, 143–147.
- Braasch, D. and Jennett, W. (1968) *Pflügers Archiv. ges. Physiol.* **302**, 245–254.
- Caro, C. G., Pedley, T. J., Schroter, R. C., and Seed, W. A. (1978) *The Mechanics of circulation*. Oxford Univ. Press, New York.
- Chien, S. (1972) In *Hemodilution: Theoretical Basis and Clinical Application*, Messmer, K., and Schmid-Schoenbein, H. (eds.). Karger, Basel, pp. 1–45.
- Fahraeus, R. (1929) *Physiol. Rev.* **9**, 241–274.
- Fahraeus, R., and Lindqvist, T. (1931) *Am. J. Physiol.* **96**, 562–568.
- Fitz-Gerald, J. M. (1969a) *Proc. Roy. Soc. London, B*, **174**, 193–227.
- Fitz-Gerald, J. M. (1969b) *J. Appl. Physiol.* **27**, 912–918.
- Fitz-Gerald, J. M. (1972) In *Cardiovascular Fluid Dynamics*, Bergel, D. H. (ed.). Academic, New York, Vol. 2, Chap. 16, pp. 205–241.
- Fung, Y. C. (1969a) *J. Biomechanics* **2**, 353–373.
- Fung, Y. C. (1969b) *Proc. Canad. Congr. Appl. Mechanics*, May, 1969. University of Waterloo, Canada, pp. 433–454.
- Fung, Y. C. (1973) *Microvascular Res.* **5**, 34–48.
- Goldsmith, H. L. (1971) *Biorheology* **7**, 235–242.
- Goldsmith, H. L. and Skalak, R. (1975) *Ann. Rev. Fluid Mech.* **7**, 213–247.
- Gross, J. F., and Aroesty, J. (1972) *Biorheology* **9**, 255–264.
- Haynes, R. H. (1960) *Am. J. Physiol.* **198**, 1193–1200.
- Hochmuth, R. M., Maple, R. N., and Sutera, S. P. (1970) *Microvascular Res.* **2**, 409–419.
- Jay, A. W. C., Rowlands, S. and Skibo, L. (1972) *Canad. J. Physiol. Pharmacol.* **5**, 1007–1013.
- Johnson, P. C., and Wayland, H. (1967) *Am. J. Physiol.* **212**, 1405–1415.
- Kot, P. (1971) Motion picture shown at the Annual Meeting of the Microcirculatory Society, Atlantic City, N.J., April, 1971.
- Lee, J. S. (1969) *J. Biomechanics* **2**, 187–198.

- Lee, J. S., and Fung, Y. C. (1969) *Microvascular Res.* **1**, 221–243.
- Lew, H. S., and Fung, Y. C. (1969a) *Biorheology* **6**, 109–119.
- Lew, H. S., and Fung, Y. C. (1969b) *J. Biomechanics* **2**, 105–119.
- Lew, H. S., and Fung, Y. C. (1970a) *J. Biomechanics* **3**, 23–38.
- Lew, H. S., and Fung, Y. C. (1970b) *Biophys. J.* **10**, 80–99.
- Lighthill, M. J. (1968) *J. Fluid Mech.* **34**, 113–143.
- Lighthill, M. J. (1972) *J. Fluid Mech.* **52**, 475–497.
- Mason, S. G., and Goldsmith, H. L. (1969) In *Circulatory and Respiratory Mass Transport*. A ciba Foundation Symposium, Wolstenholme, G. E. W. and Knight, J. (eds.) Churchill, London, p. 105.
- Prothero, J., and Burton, A. C. (1961) *Biophysical J.* **1**, 565–579; **2**, 199–212; **2**, 213, 222. 1962.
- Segre, G., and Silberberg, A. (1962) *J. Fluid Mech.* **14**, 136–157.
- Seshadri, V., Hochmuth, R. M., Croce, P. A., and Sutera, S. P. (1970) *Microvascular Res.* **2**, 424–434.
- Skalak, R. (1972) In *Biomechanics: Its Foundations and Objectives*, Fung, Y. C., Perrone, N., and Anliker, M. (eds.). Prentice-Hall, Englewood Cliffs, N.J., pp. 457–500.
- Skalak, R., Chen, P. H., and Chien, S. (1972) *Biorheology* **9**, 67–82.
- Skalak, R. (1973) *Bioreology* **10**, 229–238.
- Sobin, S. S., Tremer, H. M., and Fung, Y. C. (1970) *Circulation Res.* **26**, 397–414.
- Sobin, S. S., Fung, Y. C., Tremer, H. M., and Rosenquist, T. H. (1972) *Circulation Res.* **30**, 440–450.
- Sobin, S. S., Fung, Y. C., Tremer, H. M., and Lindal, R. G. (1979). *Microvascular Res.* **17**, (3, part 2, Abstract), p. S 87.
- Sutera, S. P. (1978) *J. Biomech. Eng. Trans. ASME* **100**(3), 139–148.
- Sutera, S. P., and Hochmuth, R. M. (1968) *Biorheology* **5**, 45–73.
- Sutera, S. P., Seshadri, V., Croce, P. A., and Hochmuth, R. M. (1970) *Microvascular Res.* **2**, 420–442.
- Svanes, K., and Zweifach, B. W. (1968) *Microvascular Res.* **1**, 210–220.
- Warrell, D. A., Evans, J. W., Clarke, R. O., Kingaby, G. P., and West, J. B. (1972) *J. Appl. Physiol.* **32**, 346–356.
- Yen, R. T., and Fung, Y. C. (1973) *J. Appl. Physiol.* **35**, 510–517.
- Yen, R. T., and Fung, Y. C. (1977) *J. Appl. Physiol.* **42**(4), 578–586.
- Yen, R. T., and Fung, Y. C. (1978) *Am. J. of Physiol.* **235**(2): H251–H257.

CHAPTER 6

Bio-viscoelastic Fluids

6.1 Introduction

Most biofluids are viscoelastic. Our saliva, for example, behaves more like an elastic body than like water. Mucus, sputum, and synovial fluids are well known for their elastic behavior. Viscoelasticity is an important property of mucus. In the respiratory tract mucus is moved by cilia lining the walls of the trachea and bronchi. If the mucus were a Newtonian fluid, the ciliary motion will be less effective in moving it. Similar ciliary motion is responsible for the movement of the ovum from ovary to uterus through the fallopian tube.

Clinical observers have noted that in many obstructive pulmonary diseases such as chronic bronchitis and cystic fibrosis, there is an increase in the “viscosity” of the mucous secretion. Many treatment modalities have been adopted in an attempt to reduce the viscosity and hence increase the clearance rate of secretions. Thus measurement of viscoelasticity is a useful tool for clinical investigation, and artificial control of viscoelasticity of mucous secretion is an objective of drug research. The social importance of such studies becomes evident when one thinks of the working days lost in the nation due to broncho-pulmonary disease.

There are many ways viscoelasticity of a fluid can be revealed. For example, if one swirls a synovial fluid in a flask and stops the movement suddenly, the elastic recoil sets it rotating for a moment in the opposite direction. Another striking demonstration was given by Ogston and Stainier (1953). A drop of fluid was placed on an optically flat surface and a convex lens was set on top (see Fig. 6.1:1). The lens was pressed down and the interference patterns known as Newton's rings were used to measure the distance between the lens and the optical flat (cf. Problem 6.1 at the end of this section).

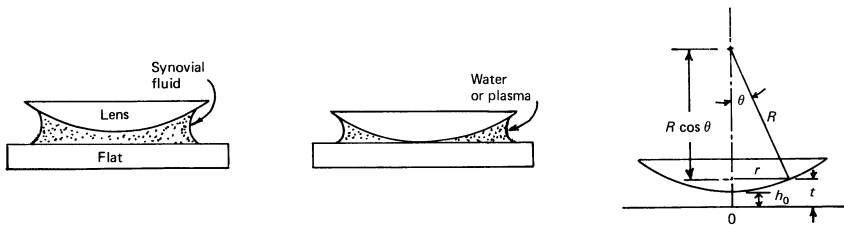


Figure 6.1:1 Ogston and Stainer's (1953) demonstration of the elasticity of synovial fluid by Newton's ring.

When the experiment was done with water, the lens was easily pressed into contact with the optical flat. The same happened with blood plasma diluted to have the same protein composition as synovial fluid. With glycerol, the lens moved very slowly down toward the flat. With synovial fluid, the lens stopped moving while it was still some distance above the optical flat. The distance depended on the load pressing it down. Moreover, when the load was removed, the lens moved slightly up again due to elastic recoil. This property of synovial fluid suggests that it may be impossible to squeeze it out entirely between the articulating surfaces in joints, just as it cannot be squeezed from between a lens and an optical flat. This would obviously be a valuable property for a lubricant.

Accurate quantitative measures of viscoelasticity can be obtained with a rheogoniometer (see Chapter 2, Sec. 2.14). But there are occasions in which it is difficult to collect a sufficient amount of test samples, or the samples may be quite inhomogeneous, or it may be suspected that testing in a rheometer would disturb the structure of the fluid too much from the *in vivo* condition for the results to be meaningful. In these situations special methods are used. A typical example is the study of protoplasm, which, like blood, tends to coagulate when removed from the cell, or when the cell is injured. Hence methods must be found to measure viscosity within the cell itself.

The properties of protoplasm, mucus, etc., tend to be very complex, and the literature is replete with various qualifying words which are supposed to describe the properties of these materials. Some knowledge of these terms is useful. In the first place, the term *rheology* is defined as the science of the deformation and flow of matter. It is a term coined by E. C. Bingham. The term *biorheology*, the rheology of biological material, was introduced by A. L. Copley. The meanings of terms like *hemorheology*, the study of blood rheology, are obvious; but terms like *thixotropy*, *rheopexy*, *dilatancy*, *spinability*, etc., are sometimes confusing. The word *thixotropy* was introduced by H. Freundlich to describe sol-gel transformation of colloidal solutions. Many suspensions and emulsions (solid and liquid particles, respectively, dispersed in a liquid medium) and colloids (liquid mixture with very fine suspended particles that are too small to be visible under an ordinary

light microscope) show a fall in viscosity as the shear stress is increased, and the fall in viscosity (or “consistency”) is recovered slowly on standing. This recovery is called thixotropy. A typical example of a thixotropic material is kitchen jello, which in a gel form can be liquified if violently shaken, but returns to gel form when left standing for some time. Thixotropy is generally associated with a change from liquid state into a gel. Some rheologists, however, use the term *thixotropy* to describe all recoverable losses in consistency produced by shearing.

If the consistency or viscosity falls when shearing increases, the material is said to show *shear thinning*. The reverse effect, an increase in viscosity with increasing shear rate, is called *shear thickening*. If the material consistency is increased when sheared but “softens” when left to stand, it is said to show *reverse thixotropy* or *negative thixotropy*. Shear thinning is often explained by breaking up of the structure by shearing, as in the example of whole blood (see Chapter 3, Sec. 3.1). One of the possible reasons for shear thickening is the crowding of particles, as sand on a beach: the closely packed particles have to move apart into open packing before they can pass one another. This is called *dilatancy*.

The term *rheopexy* was used by some authors to describe certain thixotropic systems that reset more quickly if the vessel containing them is rotated slowly. But other authors use the term for negative thixotropy. Thus the meaning of the word is not unique.

Of course, the precise description of a rheological property is the constitutive equation. If a mathematical description is known, all looseness is gone.

Problem

- 6.1 Newton's Rings.** If the convex surface of a lens is placed in contact with a plane glass plate with a drop of fluid between them, as in Fig. 6.1:1, a thin film of fluid is formed between the two surfaces. The thickness of the film is very small at the center. Such a film is found to exhibit interference colors, produced in the same way as colors in a thin soap film. The interference bands are circular and concentric with the point of contact. When viewed by reflected light, the center of the pattern is black, as it is in a thin soap film. When viewed by transmitted light, the center of the pattern is bright.

If light travels through the film vertically, destructive interference will occur whenever the thickness of the fluid is equal to integral multiples of half-wavelength, i.e., $\frac{1}{2}\lambda_0, \lambda_0$, etc. Hence by measuring the radius of a bright or dark ring, the thickness of the film can be found. With reference to Fig. 6.1:1, show that the thickness of the fluid film, t , is given by

$$t = h_0 + (R - R \cos \theta) \doteq h_0 + \frac{r^2}{2R}.$$

Hence, show that in monochromatic light in normal incidence, the radii of dark fringes are

$$r = \sqrt{mR\lambda - 2Rh_0}, \quad m = 0, 1, 2, \dots$$

See M. Born and E. Wolf, *Principles of Optics*, 3rd Edition, Pergamon Press, New York, 1965, p. 289, for details.

6.2 Methods of Testing and Data Presentation

The most prevalent viscoelastic biofluid is protoplasm, the contents of all living cells. It is also the most complex and difficult to test. It is rheologically complex because in its various forms it shows almost all the modes of behavior that have been found in other fields. It is difficult to test because it coagulates when it is taken out of the cell, or when the cell membrane is injured. To test the mechanical properties of the protoplasm one should test it inside the living cell. The methods are therefore specialized and limited. We shall discuss some of them in Sec. 6.3.

Most other biofluids can be collected and tested in laboratory instruments. Generally speaking, there are two kinds of tests: (a) small perturbations from an equilibrium condition, and (b) measurements in a steady flow. In the first case we think of the material as a solid. We speak of strain. We measure the relationship between stress and strain history. Deviations from static equilibrium are kept small in the hope that the material behavior will be linear, that is, the stress will be linearly related to strain history. In the second case we think of the material as a fluid. We speak of flow and velocity gradient. We focus attention not only on viscosity, but also on normal stresses.

Many interesting features of rheological properties of biofluids are revealed in experiments not belonging to these two classes. Some call for large deformation from equilibrium. Others call for accelerated or decelerated flow, or transition from rest to steady motion. Pertinent experiments of this last category will be mentioned later when occasion arises. In the present section we shall consider the two main categories of experiments.

Small Deformation Experiments

The most common tests are creep, relaxation, and oscillations. The instruments mentioned in Chapter 2, Sec. 2.14, namely, the concentric cylinder viscometer, the cone-and-plate viscometer, and the rheogoniometer, can be used for this purpose.

For testing very small samples, say 0.1 ml or less, the oscillating magnetic microrheometer may be used. We shall discuss a model used by Lutz et al. (1973) in some detail to illustrate the principle of this instrument and the method of data analysis and presentation. A sketch of the instrument is

shown in Fig. 6.2:1. In this instrument, the fluid is stressed by moving a microscopic sphere of iron (with a diameter of the order of $200 \mu\text{m}$) through the fluid under the influence of a magnetic force. The motion of the sphere is transduced into an electric signal by an instrument called an “optron.” The fluid is held in a cavity hollowed out in a copper block so that with circulating water good temperature control can be obtained.

An analysis of the instrument is as follows. The force that acts on the particle, F_m , in a magnetic field generated by an electromagnet, is proportional to the square of the current, I , passing through the coils; thus

$$F_m = cI^2, \quad (1)$$

where c is a constant. In the instrument shown in Fig. 6.2:1, two magnets were used, and the circuit is hooked up in such a way that the force is given by

$$F_m = c(I_1^2 - I_2^2), \quad (2)$$

where I_1, I_2 are the currents in the two magnets:

$$I_1 = I_0 + I_A \sin \omega t, \quad I_2 = I_0 - I_A \sin \omega t, \quad (3)$$

so that

$$F_m = 4cI_0I_A \sin \omega t. \quad (4)$$

I_0 and I_A are, respectively, the d.c. and a.c. amplitudes of the currents from a signal generator; ω is the frequency. The constant c can be determined by calibration of the instrument in a Newtonian fluid.

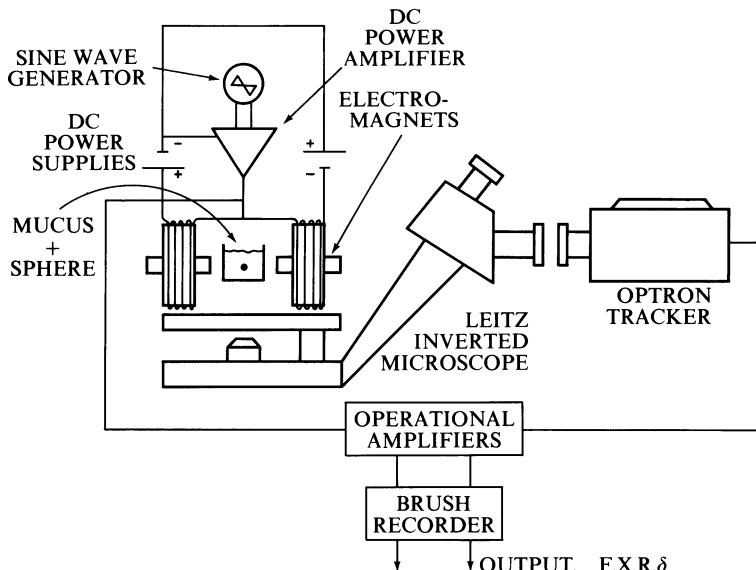


Figure 6.2:1 Schematic diagram of an oscillating magnetic microrheometer. From Lutz, Litt, and Chakrin (1973), by permission.

Since the driving force $F_m(t)$ is sinusoidal, the movement of the sphere, $x(t)$, tracked by the optron, must be sinusoidal also, as long as the amplitude of oscillation is small, so that the system remains linear. Hence we can use the complex representation of a harmonic oscillation (Chapter 2, Sec. 2.12) to write

$$F_m(t) = F_0 e^{i\omega t}, \quad x(t) = x_0 e^{-i\delta} e^{i\omega t}, \quad (5)$$

where F_0 , x_0 , and δ are real numbers. δ is the phase lag of the displacement x from the force $F_m(t)$. Recall that the physical interpretation of $F_m(t)$ is either the real part of $F_0 e^{i\omega t}$, namely, $F_0 \cos \omega t$, or the imaginary part, $F_0 \sin \omega t$. Similarly, $x_0 e^{-i\delta} e^{i\omega t}$ means

$$x(t) = x_0 \cos(\omega t - \delta) \quad \text{or} \quad x_0 \sin(\omega t - \delta). \quad (5a)$$

The force $F_m(t)$ is balanced by the viscoelastic drag and inertia. To calculate the drag force acting on the sphere, we need the stress-strain relationship of the fluid. Let τ and γ be the shear stress and shear strain, both represented by complex numbers. We shall write the stress-strain relationship in the form

$$\tau = G(i\omega)\gamma, \quad (6)$$

where $G(i\omega)$ is the *complex modulus of elasticity* (see Chapter 2, Sec. 2.12). If we write

$$G(i\omega) = G'(\omega) + iG''(\omega), \quad (7)$$

then $G'(\omega)$ is called the *storage modulus*, whereas $G''(\omega)$ is the *loss modulus*. These names are associated with the fact that if the material obeys Hooke's law, G'' is zero, and the strain energy stored in the material is proportional to G' . On the other hand, if the material behaves like a Newtonian viscous fluid, $G' = 0$, and the energy dissipated is proportional to G'' .

Equation (6) is also written frequently as

$$\tau = \mu\dot{\gamma} = i\omega\mu\gamma, \quad (8)$$

where

$$\mu(\omega) = \mu' + i\mu'' = \frac{1}{i\omega} G(i\omega). \quad (9)$$

Hence

$$G' = -\omega\mu'', \quad G'' = \omega\mu'. \quad (10)$$

The advantage of the form given by Eq. (8) is that it is identical with the Newtonian viscosity law. Using it in the basic equations of motion and continuity, it can be shown (Problem 6.3) that if the amplitude of the motion is very small (so that the square of velocity is negligible), the fluid drag acting on the sphere is given by Stokes' formula:

$$F_D = 6\pi\mu(\omega)rv, \quad (11)$$

where r is the radius of the sphere, and v is the velocity of the sphere. The difference of F_m and F_D is equal to the mass of the sphere times acceleration.

Hence

$$\frac{4}{3} \pi r^3 \rho_s \frac{d^2 x}{dt^2} = F_m - 6\pi\mu r \frac{dx}{dt}. \quad (12)$$

Here ρ_s is the density of the iron sphere. Substituting Eq.(5) into Eq.(12), we obtain

$$-\frac{4}{3} \pi r^3 \rho_s \omega^2 x_0 e^{-i\delta} = F_0 - 6\pi\mu r(i\omega)x_0 e^{-i\delta}. \quad (13)$$

Solving for μ , we have

$$\mu = \frac{-i}{6\pi r \omega} \left(\frac{F_0}{x_0} e^{i\delta} + \frac{4}{3} \pi r^3 \rho_s \omega^2 \right) \quad (14)$$

and, by Eq (9),

$$G(i\omega) = \frac{F_0}{6\pi r x_0} e^{i\delta} + \frac{2}{9} \rho_s r^2 \omega^2. \quad (15)$$

Note that if r is very small, so that the last term is negligible, then Eq. (15) yields

$$G' = \frac{F_0}{6\pi r x_0} \cos \delta, \quad G'' = \frac{F_0}{6\pi r x_0} \sin \delta. \quad (16)$$

Experimental results for G' and G'' are often plotted against the frequency ω on a logarithmic scale. Typical examples will be shown in the following sections. The curves of G' , G'' are often interpreted in terms of Maxwell and Voigt models and their combinations, as discussed in Chapter 2, Sec. 2.13.

Complementing the oscillation tests, there are relaxation and creep tests. These can be done with a rheogoniometer or similar instrument. Theoretically, information on creep, relaxation, and small oscillations are equivalent: from one the others can be computed.

Flow Experiments

Flow tests on viscoelastic fluids can be done by the same means as for ordinary viscous fluids considered in Chapter 2, Sec. 2.14. Attention is called, however, to the tensile stresses associated with shear flow. An elegant theory of viscoelastic fluids leads to the definition of a “simple fluid.” Consequently, it is tempting to check the experimental data of a biofluid to see if it fits the definition of a “simple fluid.” The theory of a simple fluid is presented in detail in Chapter 1, Sec. 1.5, of *Advanced Biomechanics*. Physical reasons why such normal stresses should arise, as well as various phenomena that may follow, are discussed in Chapter 1, Secs. 1.6 and 1.7, of *Advanced Biomechanics*.

We should remark here, however, that the coefficient of viscosity of a biofluid measured in a steady viscometric flow should not be expected to

agree with the complex viscosity coefficient measured by oscillations of small amplitude. In a steady flow, the strain rate is constant; the strain therefore increases indefinitely. The molecular structure of the fluid will not be the same as that in the equilibrium condition. Hence the coefficient of viscosity will be different in these two cases.

6.3 Protoplasm

Protoplasm is the sum of all the contents of the living cell, not including the cell membrane that surrounds the cell. It is therefore the most abundant of all biological materials. It consists of a continuous liquid phase, the cytoplasm, with various types of particles, granules, membranous structures, etc., suspended in it.

Since protoplasm tends to coagulate when removed from the cell, it is desirable to measure its rheological properties within the cell itself. One way to do this is to measure the rate of movement of granules existing within the cell, or by introducing particles into the cell artificially and then to measure their rate of movement. In the latter case one has to show that the rheological behavior of the protoplasm is not unduly disturbed. A centrifuge can be used to drive the particles. However, if iron or nickel particles are inserted, a magnetic field can be used. The viscosity of the protoplasm can be computed from the force and the rate of movement of the particles. The Stokes formula (see Problem 6.2 at the end of this chapter) needs corrections for a particle of nonspherical shape, influence of the finite container (cell membrane), and the influence of neighboring particles. The last correction is especially important because small granules are present in large quantities in protoplasm. The specific gravity of the granules can be determined by floating them (if this can be done) in sugar solutions of different concentrations and finding the specific gravity of the solution in which they neither rise nor fall.

Another way for assessing the viscosity of protoplasm is based on Brownian motion of the granules. The usual technique is to centrifuge the granules to one side of the cell and measure their return. According to Albert Einstein (1905) the displacement D_x of a particle in Brownian motion is related to the time interval t , by the formula

$$D_x^2 = 14.7 \times 10^{-18} \frac{Tt}{\eta a}, \quad (1)$$

where T is the absolute temperature, a is the diameter of the particle, and η is the coefficient of viscosity. This formula was later improved by von Smoluchowski by multiplying the right-hand side by a factor of about 1.2. Many simplifying assumptions are involved, and the value for the viscosity obtained can be only approximate. For this and other formulas based on Brownian motion, see the review article by E. N. Harvey (1938).

By means of these methods, L. V. Heilbrunn (1958) and others have shown that protoplasm has a complex rheological behavior. Heilbrunn suggests that the granule-free cytoplasm of plant cells has a viscosity of about 5 cP (i.e., about five times the viscosity of water), and that the entire protoplasm, including granules, has a viscosity several times as great. For protozoa, amoeba and paramecium have been studied extensively. Paramecium protoplasm shows shear thickening. Slime moulds show even more complex features, shear thickening, shear thinning, thixotropy, self-excited oscillations, viscoelasticity, and complex inhomogeneity.

Marine eggs of sea urchins, starfish, worms, and clams are spherical in shape and have become standard objects of study. Heilbrunn (1926) determined the viscosity of the protoplasm of the egg of *Arbacia punctata* (Lamarck) to be 1.8 cP, using the colorless granules that constitute a majority of the inclusions. These granules of various sizes interfere with one another, and the value for the viscosity of the entire protoplasm is given as 6.9 cP. The alternative Brownian movement method yielded a viscosity value of 5 cP.

There are more reasons why we want to study the rheological properties of protoplasm than obtaining a few approximate values of centipoise. The most compelling reason is trying to understand the interaction of various parts (vesicles, granules, vacuoles, etc.) of the cell, to learn something beyond the morphological picture provided by electron microscopists, and the chemical species determined by biochemists from macerated cells. The rheological properties provide some clues to the interaction between these parts.

6.4 Mucus from the Respiratory Tract

The viscoelasticity of mucus is strongly influenced by bacterial DNA, and questions arise whether certain properties of sputum are basic to certain diseases or are due to the concomitant infection. Because of its very high molecular weight, DNA is elastic even at quite a low weight concentration. Hence it is very important to collect samples that can be called normal. For dogs this can be done by the tracheal pouch method (Wardell et al., 1970). In this preparation, a 5–6-cm segment of cervical trachea is separated, gently moved laterally, and formed *in situ* into a subcutaneously buried pouch. The respiratory tract is anastomosed to reestablish a patent airway. After the operation, the pouch retains its autonomic innervation and circulation, as it is histologically and histochemically normal reflection of the intact airway. Milliliter quantities of tracheal secretions that accumulate within the pouch may be collected periodically by aspiration through the skin.

With this method of collection, Lutz et al. (1973) showed that normal mucus of the respiratory tract is heterogeneous, and shows considerable variation in dry weight/volume and pH from sample to sample from the same animal from day to day, as well as from animal to animal. A typical example is shown in Fig. 6.4:1, which shows the storage modulus G' and loss

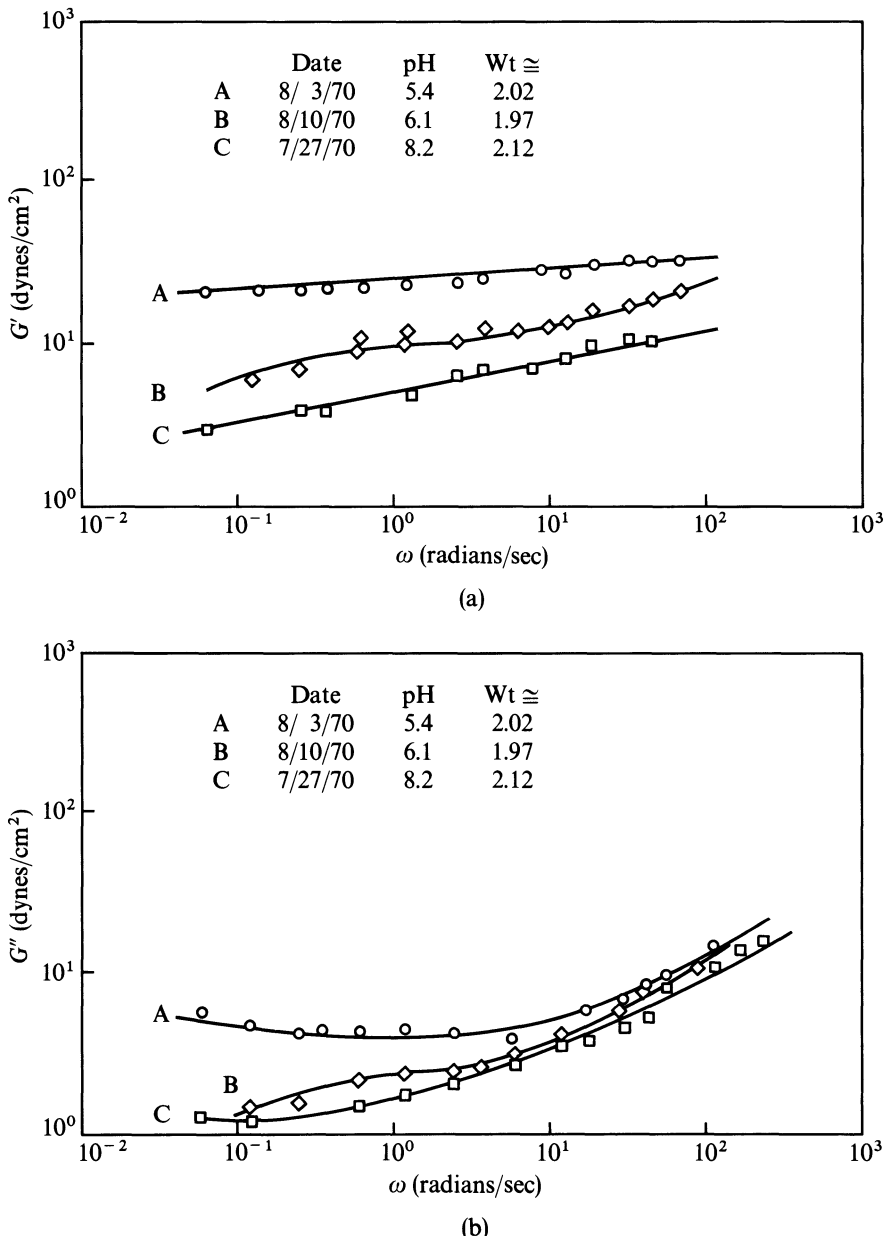


Figure 6.4:1 Viscoelasticity of normal mucus of the respiratory tract of the dog. (a) Storage modulus versus frequency; (b) loss modulus. From Lutz, Litt, and Chakrin (1973), by permission.

modulus G'' as a function of frequency for whole secretions over a period of time. The variations of pH and weight concentration are also shown in the figure. At the lowest pH, the G' curve is almost flat, showing little indication of dropping off even at low frequency, and thus suggesting an entangled or cross-linked system. At higher pH the moduli are smaller. Samples from other dogs show that considerable variation exists also in concentration. At a weight concentration of 5–6%, the values of G' at 1 rad/s are on the order of 100 dyn/cm².

To clarify the physical and chemical factors influencing mucus rheology, Lutz et al. collected mucus from dogs with similar blood type over a period of many weeks, and immediately freeze dried and stored the samples. After a sufficient amount of material had been collected, it was pooled, dialyzed against distilled water to remove electrolytes, and lyophilized, to obtain the dried polymer. The material was then reconstituted in 0.1M tris buffer at the desired weight concentration, pH, and sodium chloride concentration. Testing of such reconstituted mucus makes it possible to study the individual chemical factors. Data show that lowering of the pH not only gives elevated values of G' and G'' , but also that the curves do not fall off sharply with decreasing frequency. The effect of pH on G'' is smaller, implying that pH affects elastic components of the dynamic modulus, but does not as significantly change the viscous components. Ionic strength changes can also bring about significant changes of G' and G'' . Interpretation of these changes in terms of the molecular configuration of the mucin glycoprotein is discussed by Lutz et al.

These examples show that the viscoelasticity of normal mucus varies over a quite wide range. Hence in clinical applications one must be careful on interpreting rheological changes.

Testing mucus by creep under a constant shear stress is one of the simplest methods for examining its viscoelastic behavior. An example of such a test result is shown in Fig. 6.4:2, from Davis (1973). A cone-and-plate rheogoniometer was used. A step load is applied at time zero. The load is removed suddenly at a time corresponding to the point D. The curve ABCD gives the creep function.

Mathematically, the creep function and the complex moduli $G'(\omega)$ and $G''(\omega)$ can be converted into each other through Fourier transformation. In practice, creep testing furnishes more accurate information on $G'(\omega)$, $G''(\omega)$ at low frequency (say, at $\omega < 10^{-2}$ rad/s), than the direct oscillation test. On the other hand, the complex modulus computed from the creep function at high frequency (say, at $\omega > 10^{-1}$ rad/s), is usually not so accurate. A combination of these two methods would yield better results over a wider range of frequencies, with $G'(\omega)$, $G''(\omega)$ computed from the creep function at lower frequencies, and measured directly from oscillation tests at higher frequencies.

Mucus from the respiratory tract is so elastic that it is rarely tested in the steady flow condition, because one fears that the structure of the mucus would

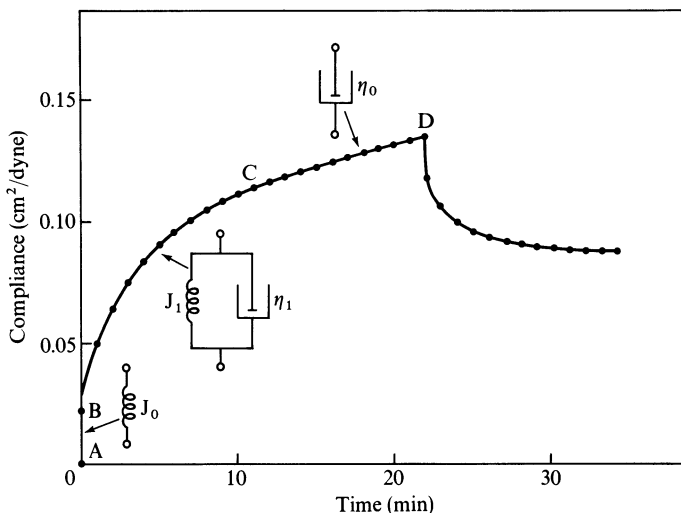


Figure 6.4:2 Creep characteristics for sputum at 25°C. The different segments of the curve are: A–B, elastic region; B–C, Voigt viscoelastic region; C–D, viscous region. From Davis (1973), by permission.

be very different in steady flow as compared with that *in vivo*. But the response of mucus to a varying shear strain that goes beyond the infinitesimal range is of interest, because it reveals certain features not obtainable from small perturbation tests. Figure 6.4:3 shows a record for sputum that was tested in a cone-and-plate viscometer, the control unit of which gave uniform acceleration of the cone to a preset maximum speed and then a uniform deceleration. The stress history shows a large hysteresis loop. There exists a *yield point* on the loading curve at which the mucus structure apparently breaks down. Beyond the yield point, the stress response moves up and down very much like steels tested in the plastic range beyond their yield point. On the

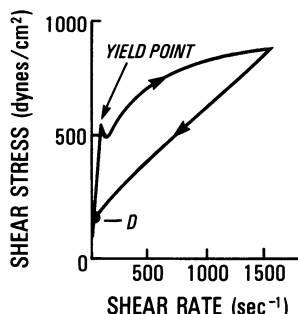


Figure 6.4:3 A typical rheogram for sputum subjected to varying shear strain at 25°C. Data from Davis (1973).

return stroke the curve is linear over a considerable part of its length, but does not pass through the origin. It cuts the stress axis at another point, D, which is a residual stress left in the specimen after the completion of a strain cycle.

It is not easy to explain the yield point in detail. Other investigators, using different instruments and different testing procedures, have obtained yield stresses that are much smaller than that of Davis. The usefulness of the information is not yet clear.

6.5 Saliva

It is interesting to learn that saliva is elastic. A typical test result on a sample of saliva of man tested in a rheogoniometer is shown in Fig. 6.5:1, from Davis (1973). The value of the real part of the complex viscosity coefficient, $\mu' [= G''/\omega]$; see Eq. (10) of Sec. 6.2] is seen to be very dependent on frequency, having a value in excess of 100 P at low frequency, falling to less than 0.5 P at high frequency. The storage modulus G' gradually increases with frequency and has a value between 10 and 50 dyn/cm². Also shown in Fig. 6.5:1 are typical curves of the sputum obtained by the same author. The variations in G' and μ' with frequency are similar for both sputum and saliva, except

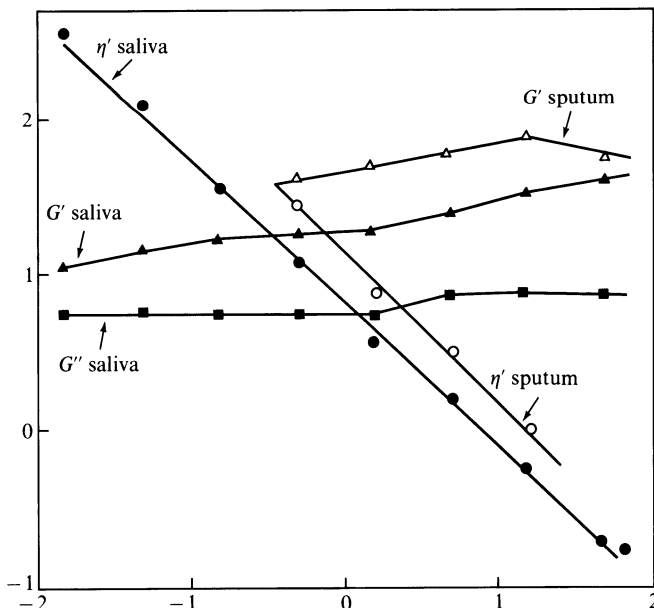


Figure 6.5:1 Viscoelasticity data for saliva and sputum (25°C) subjected to a small oscillation test in a Weissenberg rheogoniometer. Abscissa: log frequency (rad/s). Ordinate: log dynamic viscosity μ' (P), log storage and loss moduli (G' , G'') (dyn/cm²). Solid symbols: saliva. Open symbols: sputum. From Davis (1973), by permission.

that the latter is approximately half as elastic and half as viscous at any given frequency.

Since it is easy to collect saliva samples, it has been proposed to use it to test mucolytic drugs.

6.6 Cervical Mucus and Semen

Sex glands produce viscoelastic fluids. The mucus produced in glands in the uterine cervix is viscoelastic. Research on the viscoelasticity of cervical mucus has a long history, mainly because it was found that the consistency of the mucus changes cyclically in close relationship with various phases of ovarian activity. Gynecologists suggested that measurements of consistency may yield an efficient way to determine pregnancy. Veterinarians suggested that changes in cervical mucus viscoelasticity may indicate the presence of "heat" in cows and other animals. In extreme climatic conditions of low or high temperature, the physical symptoms of "in heat" may become obscure, and a mechanical test can be very helpful. For a farmer, being able to tell when a cow is in heat is to eliminate a waste of time if reproduction is desired.

A detailed account of the history of this topic is given by Scott Blair (1974). Figure 6.6:1, from Clift et al. (1950), shows the type of results to be expected

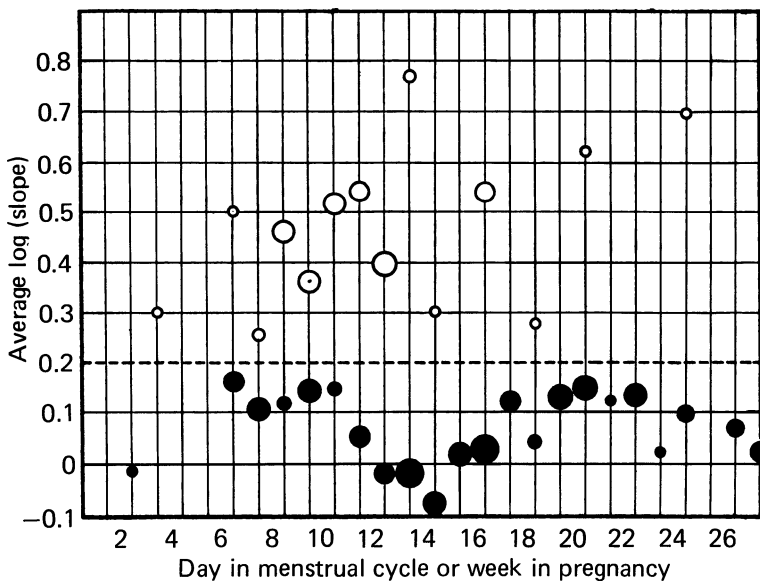


Figure 6.6:1 Average log (slope) of cervical secretions at different stages of menstrual cycle or of pregnancy in 86 nonpregnant women (solid circles) and 35 pregnant women (open circles). Areas of circles are proportional to the number of cases included in the average, the smallest circle representing one case. From Clift et al. (1950), by permission.

in man. Samples were taken with great care from the os of the cervix. Clift et al. measured the varying pressure required to extrude the mucus from a capillary tube at a constant rate of extrusion. As an "index" of consistency, they took the logarithm of the slope of pressure vs flow curve (i.e., dp/dQ , where Q is the flow rate). The time scale in Fig. 6.6:1 is in days (of menstrual cycle) for nonpregnant women, and in weeks for pregnant women. The data show a marked minimum of the index of consistency at the time of ovulation (as confirmed by endometrial biopsy and temperature), and a less marked minimum before menstruation. Some patients showing relatively low consistency in early pregnancy later aborted.

What is the meaning of the variation of viscoelasticity of the cervical mucus? Chemically, the changing viscoelasticity reflects the effect of hormones on the mucus composition. Physically, what purpose does the changing consistency serve? Many people have looked for an answer through a study of the swimming of spermatozoa in semen and in cervical mucus. Von Khreningen-Guggenberger (1933) showed that sperm cannot move vertically upward in a salt solution, but they do so in vaginal mucus. Lamar et al. (1940) placed little "blobs" of cervical mucus and semen in a capillary tube, separated by air bubbles. The sperm thus had to pass along the very thin, moist layer on the wall of the tube. It was found that the penetration by the sperm was maximal for cervical mucus collected at about the 14th day of the cycle.

The swimming of spermatozoa is a problem of great interest to mechanics. G. I. Taylor (1951, 1952) first showed that sperm will save energy to reach a greater distance if they swim in shoals with their bodies nearly parallel to each other in executing wave motion. Following Taylor, much work has been done on the mechanics of swimming of microbes in general, and sperm in particular (see Wu et al., 1974).

6.7 Synovial Fluid

Our elbow and knee joints are marvelous mechanisms. They have a very low coefficient of friction if used dynamically. If you stand still for a long time, the static load may make your joints stiff, but they loosen up as soon as you exercise. The friction coefficient in our joints is much smaller than that in most man-made machines. It is much smaller than the friction between an automobile tire and the ground, or that between the piston and cylinder in an engine, or that between the shaft and journal bearing in a generator. What makes our joints so efficient? For one thing, the cartilage on the surfaces of the joints is an amazing material. Cartilage against cartilage has a coefficient of friction much lower than teflon against teflon. For another, there is the synovial fluid, whose rheological properties seem to be particularly suited for joint lubrication.

Synovial fluid fills the cavities of the synovial joints of mammals. It is similar in constitution to blood plasma, but it contains less protein. It contains some hyaluronic acid, which is a polysaccharide with long molecules apparently combined with protein. Synovial fluid is much more viscous than blood, and this seems to be due to the hyaluronic acid. A synovial fluid that contains less hyaluronic acid than normal has a lower viscosity. An enzyme that destroys the hyaluronic acid greatly reduces the viscosity.

Ogston (1970) explains the nature of the synovial fluid containing hyaluronic acid this way: A single molecule of hyaluronic acid, with a molecular weight of 10 million, occupies a sphere of diameter about $1\text{ }\mu\text{m}$, or a volume of about 5 liter/g. It follows that, at a concentration of only 0.2 mg/ml, the hyaluronic acid molecules would, without overlap, occupy the whole volume of the solution. At 1 mg/ml there has to be, on the average, an 80% overlap or entanglement; at 5 mg/ml, a 96% overlap. The structure of solutions of these polysaccharides, at the concentrations in which they occur *in vivo*, is therefore typically a continuous network or felt of entangled molecular chains. The nature of this structure will depend little upon whether the molecules are linear or branched, on the molecular size (provided that it is large), or upon the occurrence or absence of more specific cross-linking between parts of the molecules.

This picture is very suggestive. It suggests that the viscoelastic property of the synovial fluid depends strongly on the concentration of the hyaluronic acid. It suggests that in a steady shear flow, which tends to straighten out the long chain molecules and line them up, the viscosity will decrease if the shear rate is increased.

The anticipated elasticity was confirmed by Ogston and Stanier's (1953) experiment on Newton's ring and the elastic recoil mentioned in Sec. 6.1. Balazs (1966) showed further that hyaluronic acid solutions above a certain minimum concentration and salt content exhibit extremely elastic properties at pH 2.5, and form a viscoelastic paste.

The viscoelasticity of hyaluronic acid solution can be measured by the two types of experiments discussed in Sec. 6.2: small perturbations from equilibrium and steady flow. A typical result of a test of the first kind is shown in Fig. 6.7:1, from Balazs and Gibbs (1970), who used an oscillating Couette rheometer. The real and imaginary part of the complex dynamic shear modulus $G^*(i\omega)$, i.e., the storage modulus G' and the loss modulus G'' , are plotted against the angular frequency. It is seen that as the frequency of oscillation is increased, the modulus of rigidity of the fluid, the vector sum of G' and G'' , increases. More importantly, the curves representing the loss and storage moduli cross each other. Thus hyaluronic acid solutions are predominantly viscous at low frequencies, and predominantly elastic at high frequencies. This means that at low frequencies configurational adjustments of the polysaccharide chain, through Brownian motion, are rapid enough to allow the chains to maintain the random configurations under the imposed strain and to slip by each other, resulting in viscous flow. At high frequencies the chains

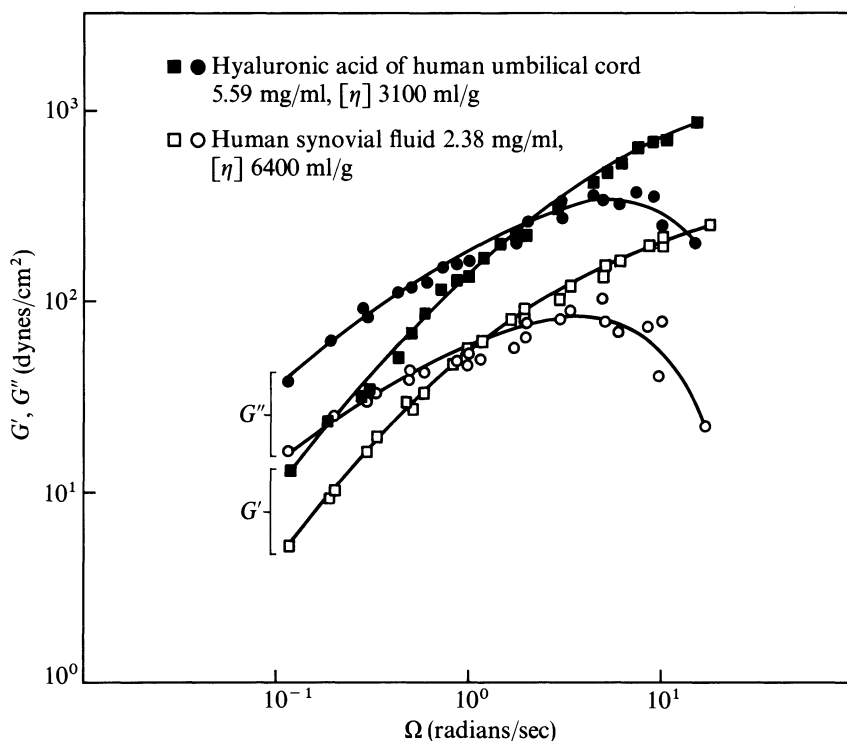


Figure 6.7:1 Dynamic storage moduli G' (open and solid squares) and dynamic loss of moduli G'' (open and solid circles) of a hyaluronic acid solution and synovial fluid from normal young male knee joints plotted against frequency, after reduction of data at various temperatures to 37°C. The concentration of hyaluronic acid and its limiting viscosity number, $[\eta]$, are given for each sample. From Balazs and Gibbs (1970), by permission.

cannot adjust as rapidly as the oscillating strain and thus are deformed sinusoidally.

The magnitude of the moduli were found to increase with increasing concentration of hyaluronic acid. The frequency at which the crossover of G' and G'' occurs depends strongly on the concentration of hyaluronic acid, the pH, and the concentration of NaCl in the solution.

In a similar way, the viscoelasticity of synovial fluids from old and osteoarthrotic persons were tested by Balazs and his associates. Their results are shown in Fig. 6.7:2. The synovial fluids of the normal knee joints of young (27–39 years) and older (52–78 years) human donors did not show significant differences in concentrations of hyaluronic acid, proteins, and sialic acid. The moduli curves in both groups exhibited rapid transition from viscous to elastic behavior. However, the curves for young and older persons were significantly different at higher frequencies, at which the loss modulus G'' of the synovial fluid from young persons was found to be much smaller than that of

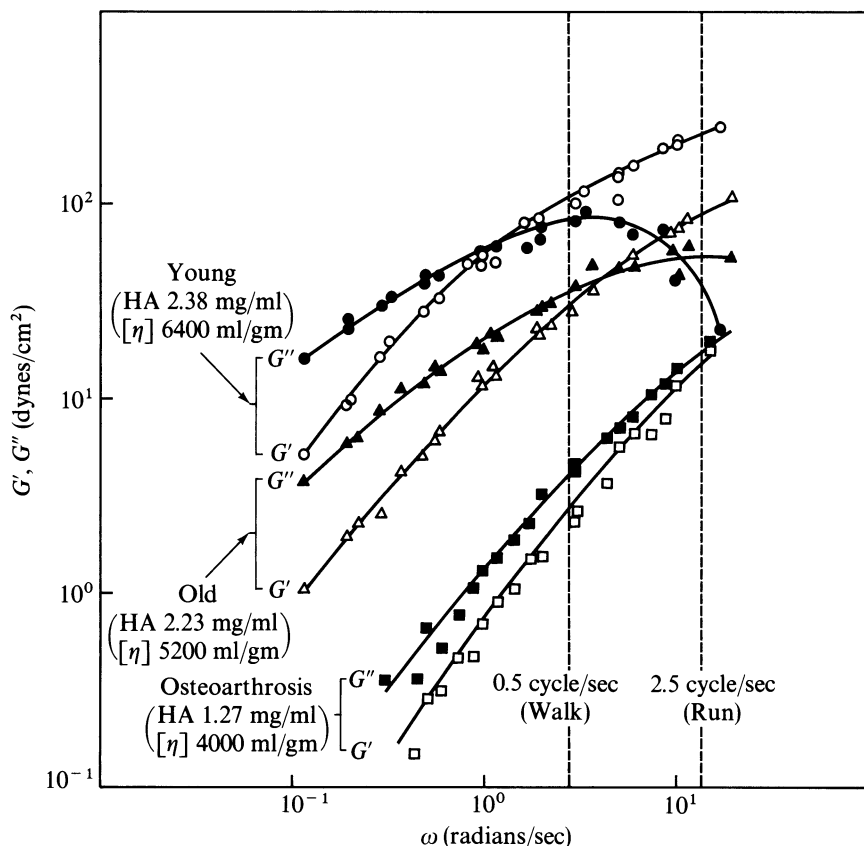


Figure 6.7:2 Dynamic storage moduli G' (open symbols) and dynamic loss moduli G'' (solid symbols) of three human synovial fluid samples plotted against frequency, after reduction of data from various temperatures to 37°C . Broken vertical lines indicate the frequencies that correspond approximately to the movement of the knee joint in walking and in running. The concentration of hyaluronic acid and its limiting viscosity number, $[\eta]$, in each sample are given in parentheses. Reproduced from Balazs (1968), by permission.

fluid from older persons. Thus the ratio of energy stored to energy dissipated at high frequencies decreases with aging.

Balazs found that G' and G'' depend strongly on the concentration and size of the hyaluronic molecule. The logarithm of $|G^*(i\omega)|$ was shown to be linearly proportional to the logarithm of the product of the hyaluronic acid concentration and molecular weight. A 10-fold change of the latter product results in approximately a 100-fold change in $|G^*(i\omega)|$.

Figure 6.7:2 also shows the moduli of synovial fluids from osteoarthritic patients. Chemically, these fluids have lower hyaluronic acid and higher protein concentrations than normal persons. Rheologically, the lower hyaluronic acid concentration resulted in a significantly lower shear modulus,

and caused the crossover from viscous to elastic behavior to occur at a much higher frequency.

Tests of synovial fluids obtained from patients with gout, chondrocalcinosis, traumatic synovitis, and arthritis also exhibited a lower $G^*(i\omega)$ than normal fluids. In patients treated with corticosteroids, it was shown that the rheological properties are rapidly restored.

The viscoelastic properties of synovial fluid and hyaluronic acid solutions led Balazs to hypothesize that the biological function of synovial fluid is to serve as a shock absorber. It also led him to propose the use of hyaluronic acid as a viscoelastic paste to be injected into the joint when the normal function is impaired. Trials of such injections into race horses and human patients have claimed a certain measure of success.

Let us turn to the other type of test of synovial fluid as a liquid in steady flow. King (1966) tested synovial fluids of bullocks in a cone-and-plate rheogoniometer in the rotation mode. His results are illustrated in Fig. 6.7:3. It is seen that synovial fluid is strongly shear-thinning. Its viscosity is high at low shear rate, but decreases rapidly as the shear rate increases.

As suggested by the theory of "simple fluids," one expects the normal stress to develop in a viscometer flow. In a cone-and-plate experiment, the measurable normal stress is the difference between that normal to the plate, P_{11} , and the radial stress, P_{22} . King's results are shown in Fig. 6.7:4. It is seen that considerable normal stress develops in a pure shear flow. This very interesting phenomenon is seen in other polymer solutions. The theoretical formulation

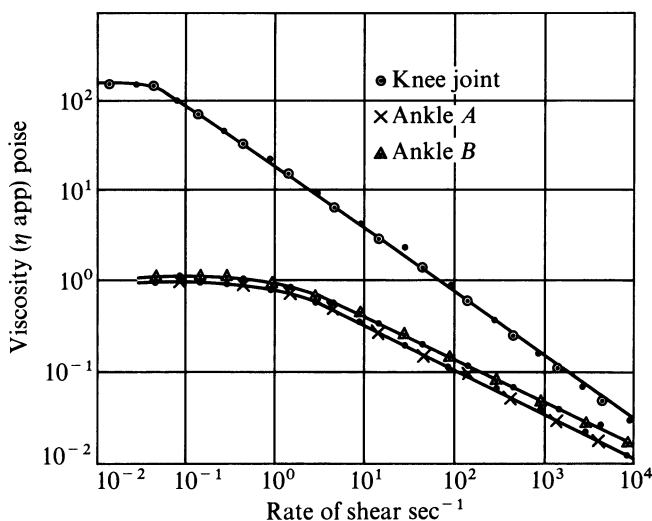


Figure 6.7:3 Bullock's ankle and knee joint fluids tested in a Weissenberg rheogoniometer in the rotation mode. At low shear rates the coefficients of apparent viscosity are constant and the fluids exhibit Newtonian characteristics. At higher shear rates they are shear thinning. Note that the knee joint fluid has a much higher apparent viscosity. From King (1966), by permission.

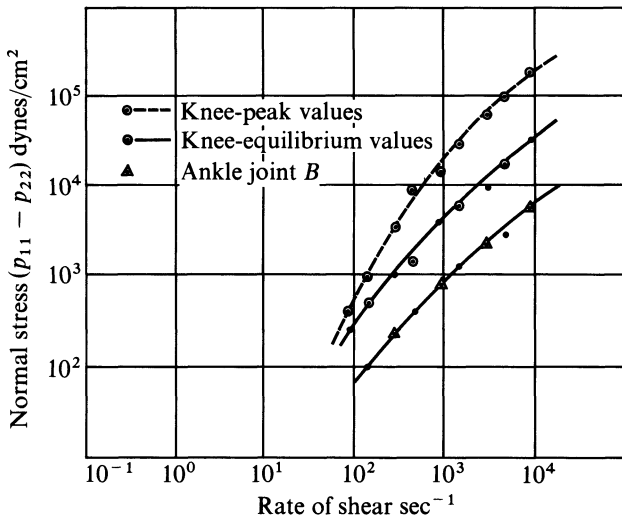


Figure 6.7:4 The normal stress associated with shear stress in the rotation mode. Fluids from bullock's ankle and knee joints. The peak values of the normal stress are the ones that developed within a few seconds after the clutch was suddenly turned on. The normal stress then fell immediately after the peak, and reached an equilibrium value some time later (around 50 s). For the knee joint fluid the difference between the peak and equilibrium values is large. For the ankle joint, the peak value was only 30% above the equilibrium value on average, and only the equilibrium values are plotted. From King (1966), by permission.

and physical basis are discussed in *Advanced Biomechanics*. The mathematical formulation of the constitutive equations of the synovial fluid is also relegated to *Advanced Biomechanics*. Lai, Kuei, and Mow (1978) presented an excellent review.

Problems

- 6.2** Consider a sphere moving in an incompressible (Newtonian) viscous fluid at such a small velocity that the Reynolds number based on the radius of the sphere and velocity of the center is much smaller than 1. Write down the governing differential equations and boundary conditions. Derive Stokes' result (1850) that the total force of resistance, F , imparted on the sphere by the fluid is

$$F = 6\pi\mu aU,$$

where μ is the coefficient of viscosity, a is the radius of the sphere, and U is the velocity of the sphere.

This result applies only to a single sphere in an infinite expanse of homogeneous fluid. If the fluid container is finite in size or if there are other spheres in the neighborhood, or if the Reynolds number approaches 1 or larger, then the equation above needs "corrections." For Stokes' solution, see C. S. Yih (1977) *Fluid Mechanics*,

pp. 362–365. For the correction for inertial forces in slow motion, see “Oseen’s approximation” in the same book, pp. 367–372. Dynamic effects due to sphere oscillation, sudden release from rest, or variable speed are also discussed in Yih’s book. For the correction for neighboring spheres, see E. Cunningham (1910) *Proc. Roy. Soc. A* **83**, 357.

- 6.3** Prove that Stokes’ formula, Eq. (11) of Sec. 6.2, is valid for a sphere oscillating at an infinitesimal amplitude in a linear viscoelastic fluid obeying the stress-strain relationship, Eq. (8) of Sec. 6.2.

Hint. Write down the equations of motion, continuity, and the stress-strain relationship. Show that the basic equations are the same as those of Problem 6.2, except that μ is now a complex number.

- 6.4** Consider the magnetic microrheometer discussed in Sec. 6.2. The force F_0 in Eq. (16) of Sec. 6.2 cannot be measured directly, but can be calibrated by testing the sphere in a Newtonian viscous fluid. Work out details.

References

- Balazs, E. A. (1968) *Univ. Michigan Med. Center J., Special Issue*, **34**, 225.
- Balazs, E. A., (1966) *Fed. Proc.* **25**, 1817–1822.
- Balazs, E. A., and Gibbs, D. A. (1970) In *Chemistry and Molecular Biology of the Intercellular Matrix*, (Balazs, E. A.) (ed.). Academic Press, New York, Vol. 3, pp. 1241–1253. For details see Gibbs et al (1968) *Biopolymers*, **6**, 777–791.
- Clift, A. F., Glover, F. A. and Scott Blair, G. W. (1950) *Lancet*, **258**, 1154–1155.
- Davis, S. (1973) In *Rheology of Biological Systems*, Gabelnick, H. L., and Litt, M. (eds.). Charles C. Thomas, Springfield, Ill., pp. 158–194.
- Frey-Wyssling, A. (ed.) (1952) *Deformation and Flow in Biological Systems*. North-Holland, Amsterdam.
- Gabelnick, H. L. and Litt, M. (eds.) (1973) *Rheology of Biological Systems*. Charles C Thomas, Springfield, Ill.
- Harvey, E. N. (1938) *J. Appl. Phys.* **9**, 68–80.
- Heilbrunn, L. V. (1926) *J. Exp. Zool.* **43**, 313–320.
- Heilbrunn, L. V. (1958) *The Viscosity of Protoplasm. Plasmatologia* **2**(1) (monograph). Springer-Verlag, Wien, 109 p.
- King, R. G. (1966) *Rheol. Acta* **5**, 41–44.
- Lai, W. M., Kuei, S. C., and Mow, V. C. (1978) Rheological equations for synovial fluids. *J. Biomech. Eng. Trans. ASME* **100**, 169–186.
- Lamar, J. K., Shettles, L. B., and Delfs, E. (1940) *Am. J. Physiol.* **129**, 234–241.
- Lutz, R. J., Litt, M., and Chakrin, L. W. (1973) In *Rheology of Biological Systems*, Gabelnick, H. L., and Litt, M. (eds.). Charles C Thomas, Springfield, Ill., pp. 119–157.
- Ogston, A. G. (1970) In *Chemistry and Molecular Biology of the Intercellular Matrix*, Balazs, E. A. (ed.). Academic Press, New York, pp. 1231–1240.
- Ogston, A. G., and Stanier, J. E. (1953) *J. Physiol. (London)* **119**, 224, and 253. See also, *Biochemical J.* (1952), **52**, 149–156.
- Scott Blair, G. W. (1974) *An Introduction to Biorheology*. Elsevier, New York, 1974.

- Taylor, G. I. (1951) *Proc. Roy. Soc. A* (London) **209**, 447–461.
- Taylor, G. I. (1952) *Proc. Roy. Soc. A* (London) **211**, 225–239.
- von Krennen-Guggenberger, J. (1933) *Arch. für Gynäk.* **153**, 64–66.
- Wardell, J. R., Jr., Chakrin, L. W., and Payne, B. J. (1970) *Am. Rev. Resp. Dis.* **101**, 741–754.
- Wu, T. Y., Brokaw, C. J., and Brennen, C. (eds.) (1974) *Swimming and Flying in Nature*, 2 vols. Plenum Press, New York.
- Yih, C. S. (1977) *Fluid Mechanics, a Concise Introduction to the theory*. Corrected edition. West River Press, Ann Arbor, Michigan.

CHAPTER 7

Bio-viscoelastic Solids

7.1 Introduction

Solids provide “body” to living organisms and are proper provinces of biomechanics. Some biosolids are more “elastic,” others are more “viscous”; altogether they are viscoelastic.

The attention of this chapter is focused on soft tissues. We shall first consider some of the most elastic materials in the animal kingdom: abductin, resilin, elastin, and collagen. Collagen will be discussed in greater detail because of its extreme importance to human physiology. Then we shall consider the thermodynamics of elastic deformation, and make clear that there are two sources of elasticity: one associated with change of internal energy, and another associated with change of entropy. Following this, we shall consider the constitutive equations of soft tissues. Results of uniaxial tension experiments will be considered first, leading to the concept of quasi-linear viscoelasticity. Then we will discuss biaxial loading experiments on soft tissues, methods for describing three-dimensional stresses and strains in large deformation, and the meaning of the pseudo strain energy function.

In Sec. 7.10 we give an example: the constitutive equation of the skin. In Sec. 7.11 we present equations describing generalized viscoelastic relations. The chapter is concluded with a discussion of the method for computing strains from known stresses if the stress-strain relationship is given in the other way: stresses expressed as functions of strains.

In the chapters to follow, we consider in detail the blood vessels, skeletal muscle, heart muscle, and smooth muscles. Muscles are the materials that make biomechanics really different from any other mechanics. Finally, in Chapter 12, we discuss bone and cartilage.

7.2 Some Elastic Materials

Elastin is the most “linearly” elastic biosolid materials known. If a cylindrical specimen of elastin is prepared and subjected to uniaxial load in a tensile testing machine, a tension-elongation curve as shown in Fig. 7.2:1 is obtained. [by the initial (unloaded) length of the specimen]. The ordinate is the stress. Note that the loading curve is almost a straight line. Loading and unloading do lead to two different curves, showing the existence of an energy dissipation mechanism in the material; but the difference is small. Such elastic characteristics remain at least up to $\lambda = 1.6$.

Elastin is a protein found in vertebrates. It is present as thin strands in areolar connective tissue. It forms quite a large proportion of the material

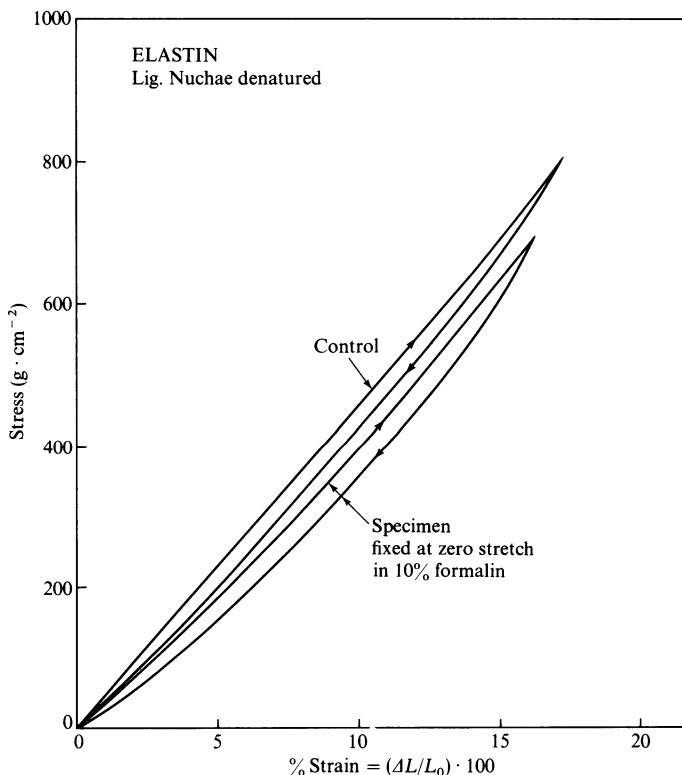


Figure 7.2:1 The stress-strain curve of elastin. The material is the ligamentum nuchae of cattle, which contains a small amount of collagen that was denatured by heating at 100°C for an hour. Such heating does not change the mechanical properties of elastin. The specimen is cylindrical with rectangular cross-section. Loading is uniaxial. The curve labeled “control” refers to native elastin. The curve labeled “10% formalin” refers to a specimen fixed in formalin solution for a week without initial strain. From the author’s laboratory in collaboration with Dr. Sabin.

in the walls of arteries, especially near the heart. It is a prominent component of the lung tissue. The ligamentum nuchae, which runs along the top of the neck of horses and cattle, is almost pure elastin. Specimens for laboratory testing can be prepared from the ligamentum nuchae of ungulates, (but cat, dog, and man have very small ligamentum nuchae). These ligaments also contain a small amount of collagen, which can be denatured by heating to 66°C or above. Heating to this degree and cooling again does not change the mechanical properties of elastin.

The function of the ligamentum nuchae in the horse is clear: it holds up the heavy head and permits its movement without having to pay energy cost. If the horse depended entirely on muscles to hold its head up, energy for maintaining tension in the muscle would be needed.

The function of elastin in the arteries and lung parenchyma is to provide elasticity of these tissues, especially at lower stress levels. The collagen fibers in these tissues are loosely arranged and are wavy so they do not become tight until the artery or the parenchyma is distended.

One particular property of elastin has probably had a profound influence on our knowledge of anatomy and histology. In the microscopic examination of a tissue, the tissue is usually fixed by formalin, formaldehyde, or glutaraldehyde; then embedded, sectioned, and stained. Elastin cannot be fixed: when elastin is soaked in these fixation agents for a long period of

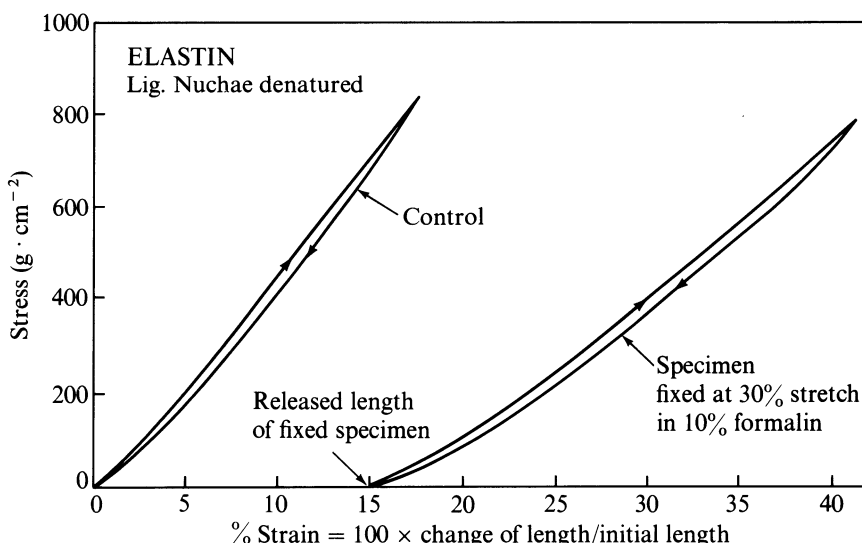


Figure 7.2:2 The stress-strain curve of a specimen of elastin that was first stretched 30% and then soaked in 10% formalin for two weeks. On releasing the stretch, the specimen shortened, but 15% of stretch remained. Subsequent loading produced the stress-strain curves shown on the right-hand side. These curves may be compared with the "control." The arrows on the curves show the direction of loading (increasing strain) or unloading (decreasing strain). From the author's laboratory.

time, (hours, days, or weeks), it retains its elasticity. If an elastin specimen is stretched under tension and then soaked in these agents, upon release the specimen does not return to its unstretched length entirely, but it can recover 40–70% of its stretch (depending on the degree of stretch), and then still behave elastically. An example is shown in Fig. 7.2:2, which refers to a specimen that was stretched to a length 1.3 times its unstressed length, soaked in formalin for two weeks, and released and tested for its stress-strain relationship. It is seen that the “fixed” specimen behaves elastically, although its Young's modulus is somewhat smaller.

If the strain (stretch ratio minus one) at which a specimen is stretched while soaked in the fixative agent is plotted against the retained strain after the “fixed” specimen is released (stress-free), we obtain Fig. 7.2:3. In this figure the abscissa shows the initial stretch during fixation, and the ordinate shows the retained stretch upon release. It is seen that elastic recovery occurs in elastin at all stretch ratios. In other words, what is commonly believed to be “fixed” is not fixed at all.

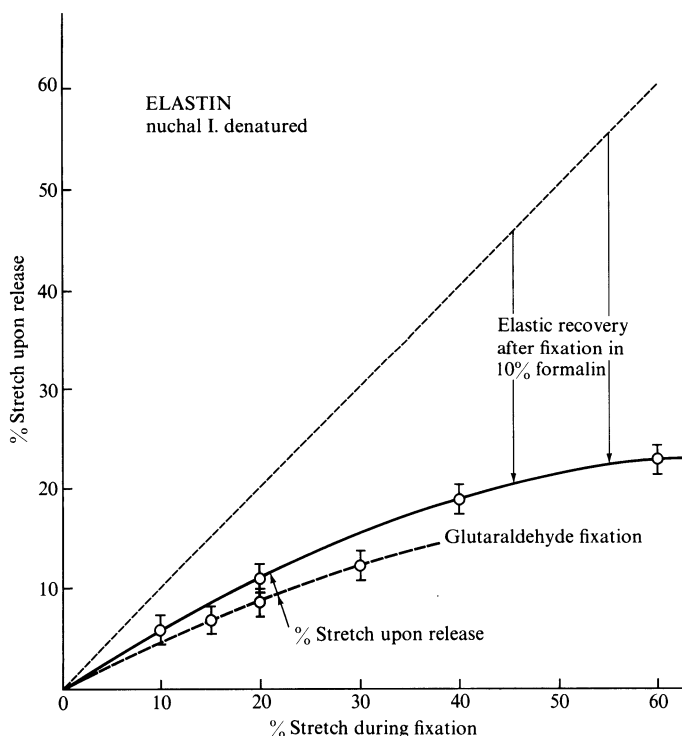
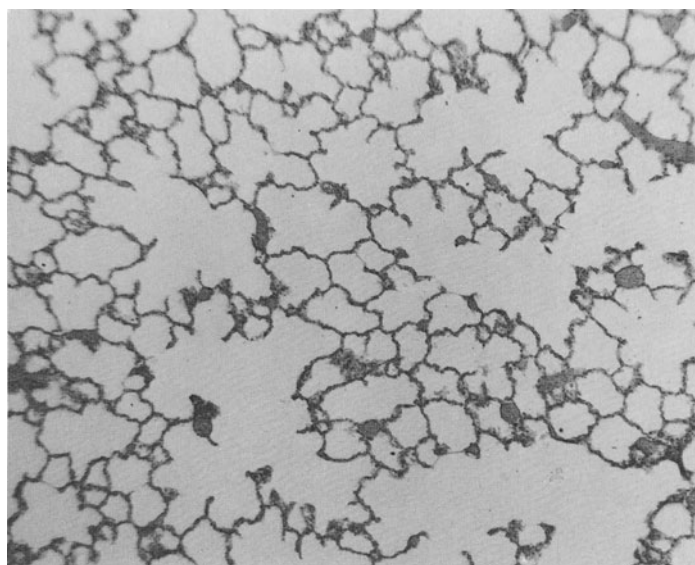
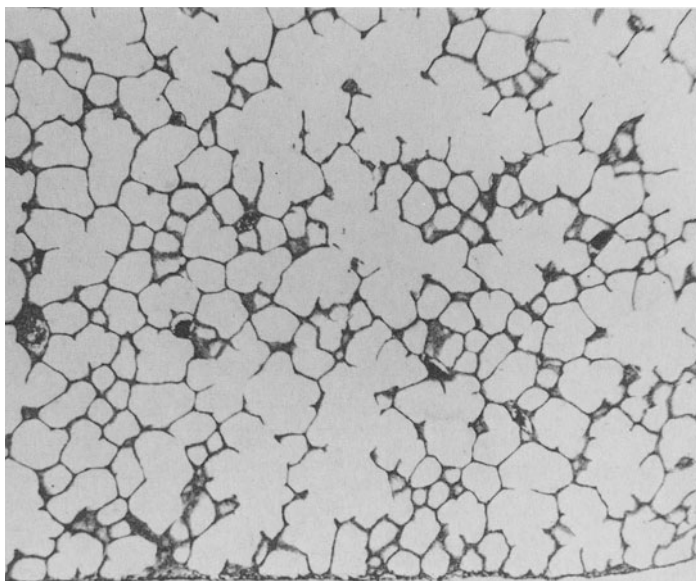


Figure 7.2:3 Elastic recovery of elastin after fixation in formalin and glutaraldehyde solutions. Specimens of elastin were stretched and then fixed in the solution. Upon release from the stretch, the retained elongation of the specimen was measured. The retained stretch is plotted against the initial stretch. The distance between the 45° line and the curves is the amount of strain recovered elastically. From the author's laboratory.



(a)



(b)

Figure 7.2:4 Photomicrographs of the lung tissue of a spider monkey. The lung was fixed in the chest by inspiration of glutaraldehyde solution into the airway. The two photomicrographs here were taken from histological slides prepared in two different ways. The photomicrograph shown in (a) was taken from a slide for which at one stage of its preparation the tissue was allowed to shrink in a stress-free state. The photomicrograph in (b) was taken from a tissue that was not allowed to shrink after it is “fixed” *in situ*. Courtesy of Dr Sidney Sabin.

Now if a tissue is fixed in one of these fixing agents in a state of stress, e.g., an inflated lung, or a distended artery (as these organs are usually fixed by perfusion), and then sectioned under no load, the elastin fibers will shrink, and the *in vivo* structure will be deformed. This is illustrated in Figures 7.2:4(a) and (b). In Fig. 7.2:4(a) is shown the lung parenchyma of a spider monkey, which was fixed in glutaraldehyde and embedded in wax. In Fig. 7.2:4(b) is shown parts of the same lung, which was embedded in celloidin, a hard plastic. The wax-embedded specimen was allowed to shrink when the wax melted at one time, whereas the celloidin-embedded specimen was never allowed to shrink. The difference in the appearance of the pulmonary alveoli in these two photographs is evident. Thus we may say that the wrinkled appearance of most published photomicrographs of the lung tissue is an artefact caused by the unsuspected elastic recovery of the elastin fibers in the tissue. The elastin fibers are stretched in the living condition. If the tension in the fibers is allowed to become zero during the preparation of the histological specimen, the fibers will contract and change the appearance of the tissue.

A biosolid similar to elastin in mechanical behavior but quite different in chemical composition is *resilin*. Resilin is a protein found in arthropods. It is hard when it is dry, but in the natural state it contains 50 to 60% water and is soft and rubbery. Dried resilin can be made rubbery again by soaking it in water. It can be stretched to three times its initial length. In the range of stretch ratio $\lambda = 1-2$, the Young's modulus is about 1.8×10^7 dyn/cm². The shear modulus G is 6×10^6 dyn/cm². Insects use resilin as elastic joints for their wings, which vibrate as an elastic system. Fleas and locusts use resilin at the base of their hind legs as catapults in their jumping.

An elastic protein found in scallops' hinges is *abductin*. Scallops use it to open the valves (the adductor muscle is used to close the valves). See Fig. 7.2:5. The elastic moduli of *abductin* and elastin are about the same.

These materials, like rubber, are constituted of long flexible molecules that are joined together here and there by cross-linking to form three-dimensional network. The molecules are convoluted and thermal energy

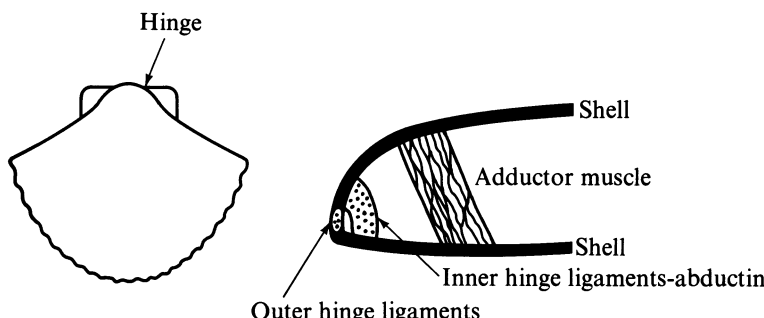


Figure 7.2:5 A plane view of a scallop (*Pecten*) and a sketch of the hinge and the adductor muscle.

keeps them in constant thermal motion. The molecular configurations, hence the entropy, change with the strain. From entropy change elastic stress appears (see Sec. 7.4). With this interpretation, Treloar (1958) showed that the shear modulus, G , is related to the density of the material, ρ , the average value of the weight of the piece of molecule between one cross-link and the next, M , and the absolute temperature, T , according to the formula

$$G = \frac{\rho RT}{M}, \quad (1)$$

where R = gas constant = 8.3×10^7 erg/deg mol. The Young's modulus is related to the shear modulus G by the formula

$$E = 2(1 + v)G, \quad (2)$$

where v is the Poisson's ratio. If the material is volumetrically incompressible so that $v = \frac{1}{2}$, then $E = 3G$.

In using the formula above for rubbery protein, ρ should be the concentration of the protein in g/cm³ of material. Water contributes to density, but not to shear modulus, hence its weight should be excluded from ρ . This formula is probably correct for those proteins which are already diluted with water at the time they were cross-linked. There is a different rule for materials that were not diluted until after they had been cross-linked. In the latter case, the dilution then stretches out the molecules so that they are no longer randomly convoluted. Rubber swollen with paraffin is such an example.

Crystalline materials derive their elastic stress from changes in internal energy. Their elastic moduli are related to the strain of their crystal lattices (see Y. C. Fung, *First Course in Continuum Mechanics*, p. 222). Equation (1) does not apply to crystalline materials, neither does it apply to fibers whose elasticity comes partly from internal energy changes and partly from entropy changes.

Most materials that can sustain finite strain have rubbery elasticity. But not all. For example, hair can be stretched to 1.7 times its initial length,

TABLE 7.2:1 Mechanical Properties of Some Common Materials

Material	Young's modulus (dyn/cm ²)	Tensile strength (dyn/cm ²)
Resilin	1.8×10^7	3×10^7
Abduction	$1-4 \times 10^7$	
Elastin	6×10^6	
Collagen (along fiber)	1×10^{10}	$5-10 \times 10^8$
Bone (along osteones)	1×10^{11}	1×10^9
Lightly vulcanized rubber	1.4×10^7	
Oak	1×10^{11}	1×10^9
Mild steel	2×10^{12}	5×10^9

and will spring back, but this is because the protein keratin, of which it is made, can exist in two crystalline forms—one with tight α helices, and one with looser, β helices (Ciferri, 1963; Feughelman, 1963). When hair is stretched, some of the α helices are changed into β helices. Table 7.2:1 gives the average values of the Young's modulus and tensile strength for several common materials.

Fibers

Fibers form a distinctive class of polymeric materials. X-ray diffraction shows that fibers contain both crystalline regions, where the molecules are arranged in orderly patterns, and amorphous regions, where they are arranged randomly (see Hearle, 1958, 1963; and Hearle and Peters, 1963). A typical example is collagen. Plant fibers and synthetic textile fibers belong to this class. Elastin "fibers" do not: they are merely thin strands of a rubbery material.

Crystallization Due to Strain

Raw (unvulcanized) rubber can be stretched to several times its length and held extended. Stress relaxation is almost complete. On release it does not recoil to its original length. But this is not a viscous flow, because it can be made to recoil by heating. The stress relaxation of rubber is due to crystallization. Stretching extends the molecules so that they tend to run parallel to each other and crystallize. Heating disrupts the crystalline structure. Based on the same principle, crystallization of a polymer solution can be induced in other ways. A high polymer solution may be made to enter a tube in the liquid state, crystallize under a high shear strain rate, and emerge as a fiber. A biological example is silk, which contains two proteins: fibroin and sericin. Sericin is a gummy material which dissolves in warm water and is removed in the manufacturing of silk thread. Silkworm (*Bombyx*) has a pair of glands which spin two fibroin fibers enveloped in sericin. Fibroin taken directly from the silk glands is soluble in water and non-crystalline. It becomes a fiber when it passes through the fine nozzle of a spinneret. The Young's modulus of silk is about 10^{11} dyn/cm². It breaks at a stretch ratio of about 1.2. Spider's web is similar to silk.

7.3 Collagen

Collagen is a basic structural element for soft and hard tissues in animals. It gives mechanical integrity and strength to our bodies. It is present in a variety of structural forms in different tissues and organs. Its importance to man may

be compared to the importance of steel to our civilization: steel is what most of our vehicles, utensils, buildings, bridges, and instruments are made of. Collagen is the main load carrying element in blood vessels, skin, tendons, cornea, sclera, bone, fascia, dura mater, the uterian cervix, etc.

The mechanical properties of collagen are therefore very important to biomechanics. But, again in analogy with steel, we must study not only the properties of all kinds of steels, but also the properties of steel *structures*; here we must study not only collagen molecules, but also how the molecules wind themselves together into fibrils, how the fibrils are organized into fibers, and fibers into various tissues. In each stage of structural organization, new features of mechanical properties are acquired. Since in physiology and biomechanics, our major attention is focused on the organ and tissue level, we must study the relationship between function and morphology of collagen in different organs.

Collagen Molecules, Fibrils, and Fibers

Collagen is a fibrous protein. The primary building unit of collageneous tissue is the tropocollagen molecule, which is composed of polypeptide chains. In each tropocollagen molecule there are three amino acid chains coiled into a

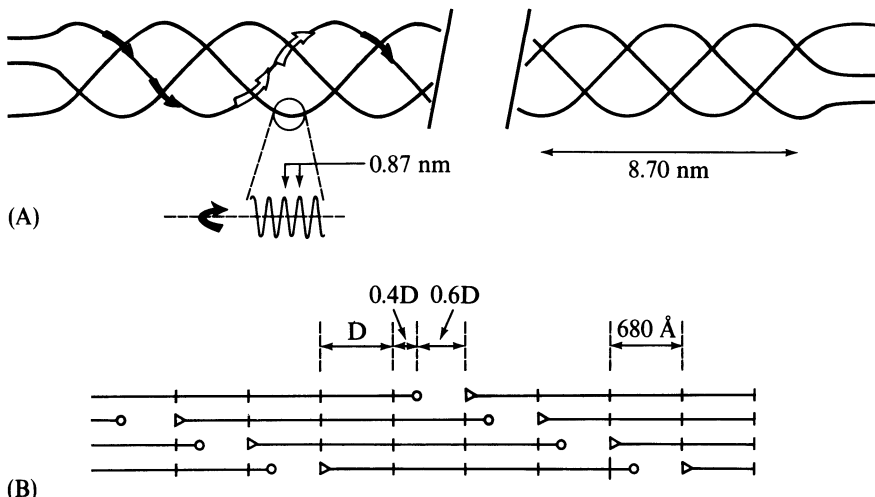


Figure 7.3:1 Current concept of the collagen molecule and protofibril. (A) Sketch showing three chains of amino acid residues constituting left-handed helices with a pitch of 0.87 nm wound together into a right-handed superhelix with a pitch of 8.70 nm. (B) The concept of quarter-stagger of the molecules combined with overlaps and gaps. The length of the molecule is 4.4 times that of a period (D). From Viidik (1973), and Viidik (1977), by permission.

left-handed helix, the composition being the same in two of them and slightly different in the third. The molecule itself is constituted as a right-handed superhelix formed by these three chains. This concept is shown in Fig. 7.3:1(a).

A collection of tropocollagen molecules forms a collagen fibril. In an electron microscope, the collagen fibrils appear to be cross-striated, as is illustrated in the cases of tendon and skin in Fig. 7.3:2. The periodic length of the striation is 640 Å in native fibrils and 680 Å in moistened fibrils. The exact organization of collagen fibrils is much debated. The model shown in Fig. 7.3:1(b) represents a current view. The length of the molecule is 4.4 times that of the period of the native fibril. Hence each molecule consists of five segments, four of which have a length D , whereas the fifth is shorter, of length $0.4D$. In a parallel arrangement of these molecules, a gap of $0.6D$ is left between the ends of successive molecules. The alignment of the molecules is shown in Fig. 7.3:1(b) as perfectly straight and parallel; but another current view is that they are not so perfect, but are bent somewhat and have varying spacing between neighboring molecules, with the degree of bending varying with the attachment of water molecules.

The diameter of the fibrils varies within a range of 200 to 400 Å, depending on the animal species and the tissue.

Bundles of fibrils form fibers, which have diameters ranging from 0.2 to 12 µm. Two examples are shown in Fig. 7.3:2. In the light microscope they are colorless; they are birefringent in polarized light. In tendons, they are

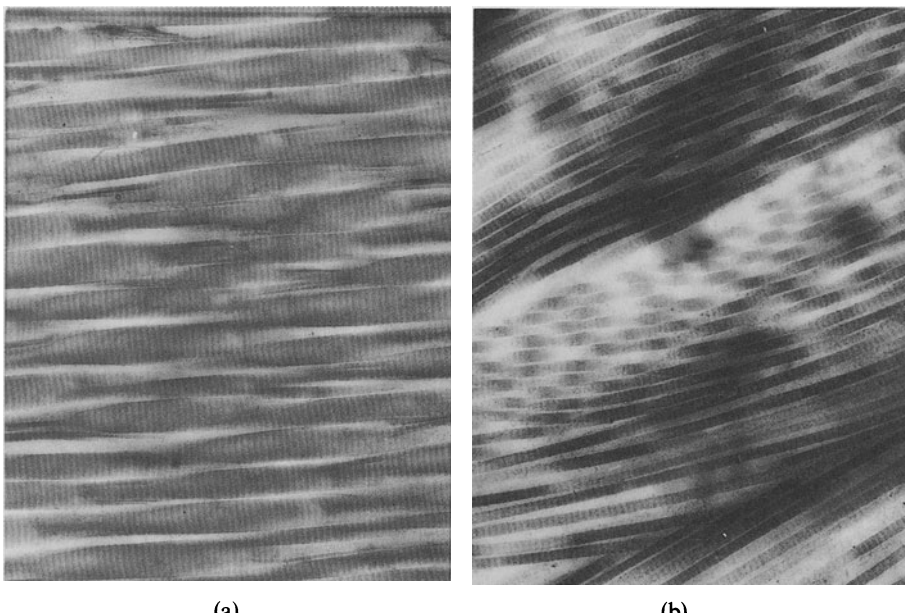


Figure 7.3:2 Electron micrographs of (a) parallel collagen fibrils in a tendon, and (b) mesh work of fibrils in skin ($\times 24\,000$). From Viidik (1973), by permission.

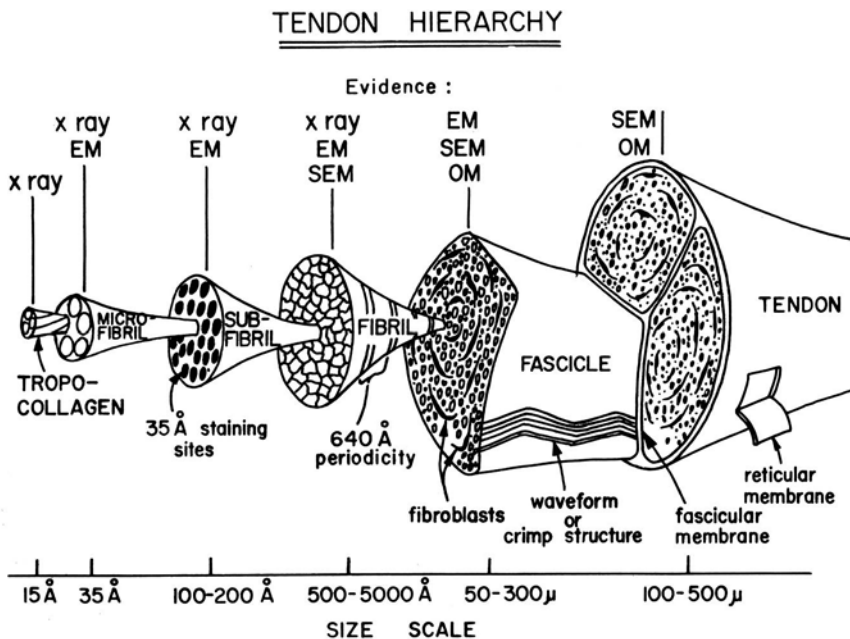


Figure 7.3:3 Hierarchy of structure of a tendon according to Kastelic et al. (1978). Reproduced by permission. Evidences are gathered from X ray, electron microscopy (EM), scanning electron microscopy (SEM), and optical microscopy (OM).

probably as long as the tendon itself. In connective tissues their length probably varies considerably; there is no definite information on this point.

Packaging of collagen fibers has many hierarchies, depending on the tissue. In parallel-fibered structures such as tendon, the fibers are assembled into primary bundles, or fascicles, and then several fascicles are enclosed in a sheath of reticular membrane to form a tendon. Figure 7.3:3 shows the hierarchy of the rat's tail tendon according to Kastelic et al. (1978). The fibers frequently anastomose with each other at acute angles, in contrast to the fibrils, which are considered not to branch at all in the native state.

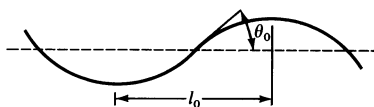
The Wavy Course of the Fibers

Diamont, Baer, and their associates (1972) examined rat's tail tendon in the polarized light microscope and found a light and dark pattern with a periodicity of the order of 100 μm , which they interpreted as the waviness of the collagen fiber in the *fascicle* shown in Fig. 7.3:3. When the tendon is stretched, the amplitude of the waviness of the crimped fibers decreases. By rotating the tendon specimen between crossed polaroids, Diamont et al. (1972) and Dale et al. (1972) showed that the wave shape of the crimps is planar. When

TABLE 7.3:1 Typical Wave Parameters from Various Tendons at Zero Strain (Unstretched Condition). From Dale et al. (1972)

Source and age	l_0 (μm)	θ_0 (deg)
Rat tail (14 months)	100	12
Human diaphragm (51 years)	60	12
Kangaroo tail (11.7 years)	75	8–9
Human achilles (46 years)	20–50	6–8

Definition of wave parameters:



the tendon was teased down to fine bundles, it was observed that the physical outlines of these subbundles followed the waveform that was deduced from the polarizing optics of the intact tendon bundle. The typical waveform parameters are given in Table 7.3:1. As the fiber is stretched, the “bending angle,” θ_0 , decreases and tends to zero when the fiber is straight. The fiber diameter is age dependent (see Torp et al., 1974). For example, the rat’s tail tendon fiber diameter increases from 1000 to 5000 Å as the rat ages. The scatter of data for the wavelength l_0 and angle θ_0 can be considerable.

Thus the basic mechanical units of a tendon are seen to be bent collagen fibers. The question arises whether the fibers are intrinsically bent because of some fine structural features of the fibrils. Gathercole et al. (1974), using SEM to resolve the individual collagen fibrils about 100 nm in diameter as they follow the waveform in rat’s tail tendon, failed to find any specific changes in morphology and fine structure along the length of the waveform. It is then suggested that the curvature of the fibers might be caused by the shrinking of the noncollagen components or “ground substance” of the tendon, i.e., that the curvature is caused by the buckling of the fibers. This suggestion is consistent with the experience that the integrity of the ground substance is of great importance to the mechanical integrity of the tendon. Enzymatic digestion directed at the noncollagen components can greatly change the mechanical properties of the tendon. The buckling model was investigated by Dale and Baer (1974), and it was suggested that hyaluronic acid, which is a major space filling material and which has a fairly high metabolic turnover rate, maybe responsible for the buckling of the collagen fibers.

In other connective tissues, it has been suggested that elastin and collagen together form a major unit of composite material. In connective tissues, the

elastin fibers are usually seen to be straight. These straight elastic fibers attached to the bent collagen fibers can then have the mechanical properties exhibited by the composite material.

Ground Substance

Collagen fibers are integrated with cells and intercellular substance in a tissue. In dense connective tissue, the cells are mostly fibrocytes; the intercellular substance consists of fibers of collagen, elastin, reticulin, and a hydrophilic gel called *ground substance*. Dense connective tissues contain a very small amount of ground substance; loose connective tissues contain a lot. The composition of the ground substance varies with the tissue, but it contains mucopolysaccharides (or glycosaminoglycans), and tissue fluid. The mobility of water in the ground substance is a problem of profound interest in biomechanics, but it is an extremely complex one. The hydration of collagen, i.e., the binding of water to the collagen molecules, fibrils, and fibers, is also an important problem in biomechanics with respect to the problem of movement of fluid in the tissues, as well as to the mechanical properties of the tissue.

Structure of Collagenous Tissues

Depending on how the fibers, cells, and ground substance are organized into a structure, the mechanical properties of the tissue vary. The simplest structure, from the point of view of collagen fibers, is parallel fibered, as in tendon and ligaments. The two- and three-dimensional networks of the skin are more complex, whereas the most complex are the structures of blood vessels, intestinal mucosa, and the female genital tracts. Let us consider these briefly.

The most rigorously parallel-fibered structure of collagen is found in each lamina of the cornea. In adjacent laminae of the cornea, the fiber orientation is varied. The transparency of the cornea depends on the strict parallelism of collagen fibers in each lamina.

Tissues whose function is mainly to transmit tension can be expected to adopt the parallel-fibered structure. Tendon functions this way, and is quite regularly parallel fibered, as is shown in Figs. 7.3:2(a) and 7.3:3. The fiber bundles appear somewhat wavy in the relaxed condition, but become more straight under tension.

A joint ligament has a similar structure, but is less regular, with collagen fibers sometimes curved and often laid out at an angle oblique to the direction of motion. Different collagen fibers in the ligament are likely to be stressed differently in different modes of function of the ligament. Most ligaments are

purely collagenous, the only elastin fibers being those that accompany the blood vessels. But the ligamenta flava of the spine and ligamentum muchae of some mammals are mostly elastin.

A ligament has both ends inserted into bones, whereas a tendon has only one insertion. The transition from a ligament into bone is gradual; the rows of fibrocytes are transformed into groups of osteocytes, first arranged in rows and then gradually dispersed into the pattern of the bone, by way of an intermediate stage, in which the cells resemble chondrocytes. The collagen fibers are continuous and can be followed into the calcified tissue. The transition from a tendon into a bone is usually not so distinct; the tendon inserts broadly into the main fibrous layer of the periosteum.

The other end of a tendon is joined to muscle. Generally the tendon bundles are invaginated into the ends of the muscle fibers in the many terminal indentations of the outer sarcolemmal layer. Recent investigation suggests that collagenous fibrils, which are bound to the plasma membranes as well as to the collagen fibers, provide the junction.

Parallel fibers that are spread out in sheet form are found in those fasciae into which muscle inserts, or in those expanded tendons called *aponeuroses*, which are membranous sheets serving as a means of attachment for flat muscles to the bone. The tendinous center of the diaphragm is similarly structured. These sheets appear white and shiny because of their tight structure. Other membranes that contain collagen but the fibers of which are not so regularly structured are opaque. To this group belong the periosteum, perichondrium, membrana fibrosa of joint capsules, dura mater, sclera, some fasciae, and some organ capsules. The cells in these membranes are irregular both in shape and in arrangement.

The structure of collagen fibers in the skin is more complex, and must be considered as a three-dimensional network of fibrils [see Fig. 7.3:2(b)], although the predominant fiber direction is parallel to the surface. These fibers are woven into a more or less rhombic parallelogram pattern, which allows considerable deformation without requiring elongation of the individual fibers. In the dermis, collagen constitutes 75% of skin dry weight, elastin about 4%.

The collagen fiber structure in blood vessels is three-dimensional and is intimately integrated with elastin fibers and smooth muscles. A more detailed picture is presented in Chapter 8, Sec. 8.2.

The female genital tract is a muscular organ, with smooth muscle cells arranged in circular and spiral patterns. Actually, in the human uterus only 30–40% of its wall volume is muscle, and in the cervix only 10%; the rest is connective tissue. In the connective tissue of the genital tract the ground substance dominates, as the ratio of ground substance to fiber elements is 1.5:1 in the nonpregnant corpus and 5:1 in the cervix near full term. During pregnancy, the ground substance grows at the rate of the overall growth, while collagen increases more slowly, and elastin and reticulin almost not at all. Hence the composition of the connective tissue changes.

This brief sketch shows that collagen fibers are organized into many different kinds of structures, the mechanical properties of which are different.

The Stress-Strain Relationship

A typical load-elongation curve for a tendon tested in simple elongation at a constant strain rate is shown in Fig. 7.3:4. It is seen that the curve may be divided into three parts. In the first part, from O to A, the load increases exponentially with increasing elongation. In the second part, from A to B, the relationship is fairly linear. In the third part, from B to C, the relationship is nonlinear and ends with rupture. The "toe" region, from O to A, is usually the physiological range in which the tissue normally functions. The other

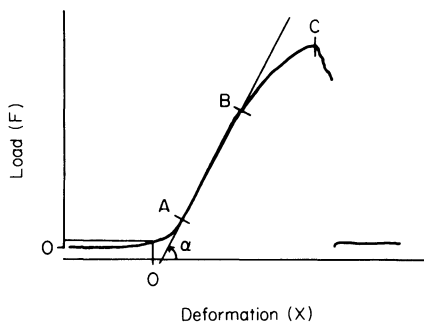


Figure 7.3:4 A typical load-elongation curve for a rabbit limb tendon brought to failure with a constant rate of elongation. The "toe" part is from O to A. The part A-B is almost linear. At point C the maximum load is reached. α is the angle between the linear part of the curve and the deformation axis. The slope, $\tan \alpha$, is taken as the "elastic stiffness," from which the Young's modulus listed in Table 7.2:1 is computed. From Viidik (1973), by permission.

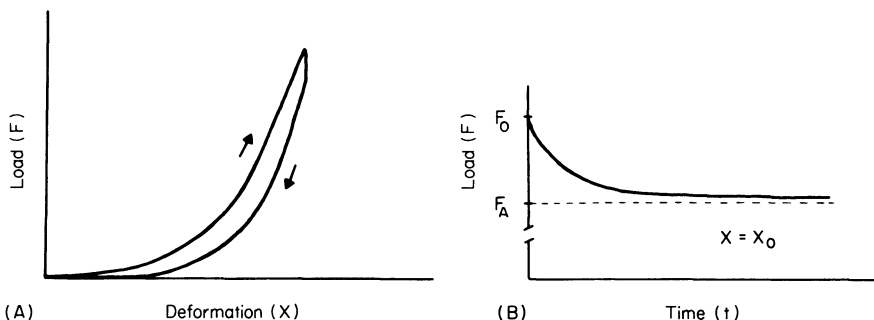


Figure 7.3:5 The load-elongation and relaxation curves of an anterior cruciate ligament specimen. In (A), the specimen was loaded to about one-third of its failure load and then unloaded at the same constant speed. In (B), the specimen was stretched at constant speed until the load reached F_0 ; then the stretching was stopped and the length was held constant. The load then relaxed. From Viidik (1973), by permission.

regions, AB and BC, correspond to reserve strength of the tendon. The ultimate stress of human tendon at C lies in the range 50–1000 N/mm². The maximum elongation at rupture is usually about 10–15%.

If the tissue is loaded at a finite strain rate and then its length is held constant, it exhibits the phenomenon of stress relaxation. An example is shown in Fig. 7.3:5, for an anterior cruciate ligament. The figure on the left-hand side (A) corresponds to case in which the ligament was loaded to about one-third of its failure load and then unloaded immediately at a constant speed. The figure on the right-hand side (B) corresponds to the case in which the ligament was loaded to the same load F_0 , and then the length was held constant. The load then relaxes asymptotically to a limiting value F_A .

A third feature should be noted. If a tissue is taken from an animal, put in a testing machine, tested for a load-elongation curve by a cycle of loading and unloading at a constant rate of elongation, left alone at the unstressed condition for a resting period of 10 min or so until it has recovered its relaxed length, and then tested a second time following the same procedure, the load-elongation curve will be found to be shifted. Figure 7.3:6 shows an example. In the first three consecutive tests, the stress-strain curves are seen to shift to the right, with an increased region of the "toe." The first three relaxation curves (shown in the right side panel), however, are seen to shift upward. If the test is repeated indefinitely, the difference between successive cycles is decreased, and eventually disappears. Then the specimen is said to have been *preconditioned*.

The reason that preconditioning occurs in a specimen is that the internal structure of the tissue changes with the cycling. By repeated cycling, eventually a steady state is reached at which no further change will occur unless the cycling routine is changed. Changing the upper and lower limits of the cycling will change the internal structure again, and the specimen must be preconditioned anew.

These features: a nonlinear stress-strain relationship, a hysteresis loop in cyclic loading and unloading, stress relaxation at constant strain, and preconditioning in repeated cycles, are common to other connective tissues such

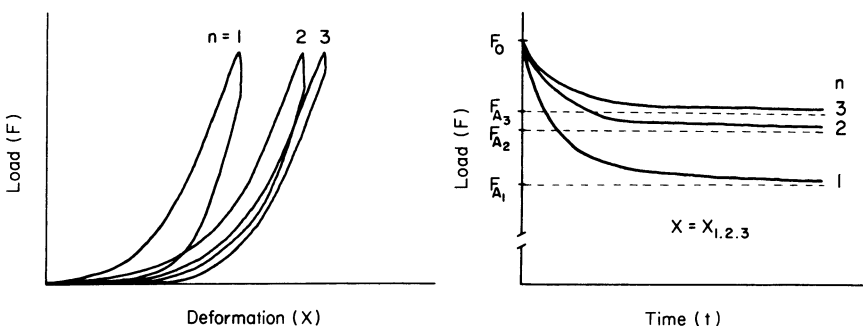


Figure 7.3:6 Preconditioning of an anterior cruciate ligament. The load-elongation and relaxation curves of the first three cycles are shown. From Viidik (1973), by permission.

as the skin and the mesentery. They are seen also in blood vessels and muscles; but the degrees are different for different tissues. The hysteresis loop is quite small for elastin and collagen, but is large for muscle. The relaxation is very small for elastin, larger for collagen, and very large for smooth muscle. Pre-conditioning can be achieved in blood vessels very quickly (in two or three cycles) if blood flow into the blood vessel wall (*vasa vasorum*) is maintained, but it may take many cycles if flow in the *vasa vasorum* is cut. We shall encounter these features again and again in the study of bioviscoelastic solids.

Change of Fiber Configuration with Strain

By the electron microscopy method, it can be shown that if a tendon is stretched 10%, the spacing of the characteristic light and dark pattern increases 9%. Thus 1% of the stretching is due to straightening of the fiber (Cowan et al., 1955). It is believed that in the basic 680A unit of the collagen structure, the fifth segment [see Fig. 7.3:1(b)] in which the amino acids are more or less randomly placed, contributes most of the stretch when a specimen is stressed.

Critical Temperatures

At 65°C, mammalian collagen shrinks to about one-third of its initial length. This is the basis of the technique of making shrunken human heads (Harkness, 1966). The shrinkage is due to breakdown of the crystalline structure. Shrunken collagen gives no x-ray diffraction pattern (Flory and Garrett, 1958). It is rubbery, with a Young's modulus of about 10^7 dyn/cm².

Change with Life Cycle

As the function of an organ changes in life, the mechanical properties of its tissue change also. Perhaps no example is more impressive in this regard than the event of childbirth. M. L. R. and R. D. Harkness (1959a) investigated the uterine cervix of the rat during pregnancy and after birth. In nonpregnant rat the uterine cervix contains 5–10% of collagen by weight. The rat cervix enters the vagina via two canals (horns of uterus). In a transversal section through the cervix of a rat uterus the canals appear as flattened ellipses with fibers arranged roughly concentric around each canal. The Harknesses used cervixes cut from rats at various stages of pregnancy. They slipped a rod through each of the canals, fixed one rod and applied a force to the other. They recorded the extension of the cervix under a constant load. Their results are shown in Fig. 7.3:7. Cervixes from rats that were not pregnant, or had been

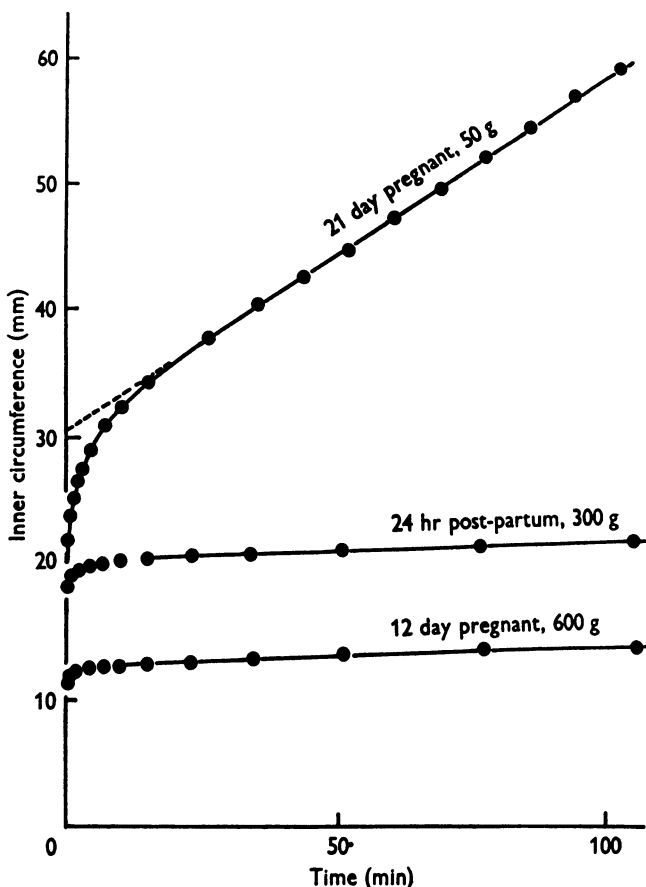


Figure 7.3:7 The creep curves of the cervixes of rats in various stages of pregnancy, stretched by the loads indicated. From Harkness and Harkness (1959), by permission.

pregnant up to 12 days, were relatively inextensible and showed little creep. Later in pregnancy the cervix enlarges and becomes much more extensible, and creeps more under a constant load. At 21 days the cervix that is stretched by a sufficiently large constant load creeps at a constant rate. It seems that the stretching is not resisted by elastic restoring force, but instead by viscosity. Within a day after the young have been born the cervix reverts to its original properties, although it is still larger than it was before pregnancy.

The restoration of mechanical properties of the cervix was studied in greater detail by Viidik and Rundgren (See Viidik, 1973). Figure 7.3:8 shows both the load-length relationship and the "stress"-strain relationship. The change of length at zero load with days post partum shows the rapid change of size of the cervix. The distensibility increases but the strength decreases with days post partum. If "stress" is calculated by excluding ground substance and including only the estimated collagen fibers' cross-sectional

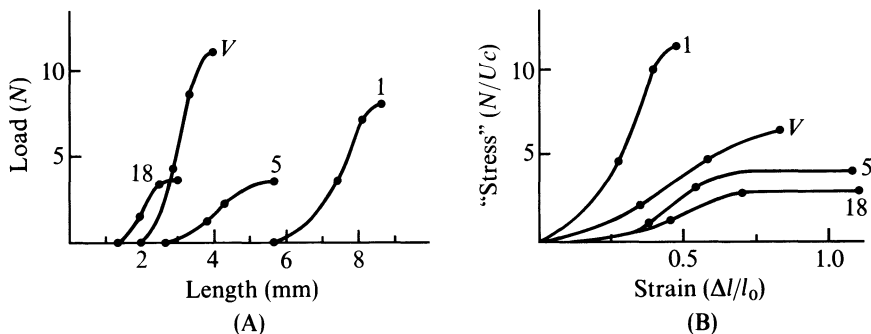


Figure 7.3:8 The mechanical behavior of the uterine cervix of the rat, virginal (V), and 1,5, and 18 days post partum. Figure on the left (A) shows load versus length, with specimens relaxed at zero load and then loaded until failure. Figure on the right (B) shows “stress-strain” curves for the same experiment. From Viidik (1973), who attributed the data to Dr. A. Rundgren. Reproduced by permission.

area, then Fig. 7.3:8(b) shows that the collagen framework *per se* is actually stronger at one day post partum than in the virgin state. Then the strength decreases during the resorative and restorative phase to well below the values for the virginal animal.

It was suggested by the Harknesses (1959b) that the creep characteristics of the near-term uterine cervix are due to changes in the ground substance. They treated the cervix with the enzyme trypsin, which does not attack collagen, and found that the creep rate was greatly increased. They also found that the uterus of the nonpregnant rat undergoes cyclic changes in water content but not in dry weight, whereas the maximum tensile strength decreases when the tissue is swollen. Thus a swollen cervix with increased water content and changed ground substance properties may be the reason for the dramatic distensibility of uterine cervix in the process of giving birth.

7.4 Thermodynamics of Elastic Deformation

In the preceding sections we considered a number of elastic solids. It would be interesting to consider the relationship between the elasticity and the internal constitution of the material: whether it is crystalline or amorphous. Without going into the details of molecular structure and material constitution, we can clarify the essence of the problem from thermodynamic considerations.

There are two sources of elastic response to deformation: change of internal energy, and change of entropy. To see this, let us consider the laws of thermodynamics connecting the specific internal energy \mathcal{E} (internal energy per unit mass), specific entropy S (entropy per unit mass), absolute

temperature T , pressure p , specific volume V , density ρ , stress σ_{ij} , strain e_{ij} , and stress and strain deviations σ'_{ij} , e'_{ij} . The first law of thermodynamics (law of conservation of energy) states that in a given body of material of unit volume an infinitesimal change of internal energy is equal to the sum of heat transferred to the body, dQ , and work done on the body, which is equal to the product of the stress σ_{ij} and the change of strain de_{ij} , i.e., $\sigma_{ij} de_{ij}$. Expressing all quantities in unit mass (mass in unit volume is ρ), we obtain

$$d\mathcal{E} = dQ + \frac{1}{\rho} \sigma_{ij} de_{ij}. \quad (1)$$

Note that the summation convention for indexes is used here: a repetition of the index i or j means summation over the range 1, 2, and 3.

The second law of thermodynamics states that the heat input dQ is equal to the product of the absolute temperature T and the change of entropy dS :

$$dQ = T dS. \quad (2)$$

Combining these expressions, we have

$$d\mathcal{E} = T dS + \frac{1}{\rho} \sigma_{ij} de_{ij}. \quad (3)$$

(See Y. C. Fung, *Foundations of Solid Mechanics*, p. 348 et seq. for details.) In mechanics it is useful to separate out the pressure (negative of the mean stress) from the stress and write

$$\sigma_{ij} = -p \delta_{ij} + \sigma'_{ij}. \quad (4)$$

where σ'_{ij} represents the *stress deviations*. Correspondingly, the strain is separated into a volumetric change and a distortion part:

$$e_{ij} = \frac{1}{3} e_{\alpha\alpha} \delta_{ij} + e'_{ij}, \quad (5)$$

where $e_{\alpha\alpha}$ is the change of volume dV , and e'_{ij} represents the *strain deviations*. Using Eqs. (4) and (5), we can write Eq. (3) as

$$d\mathcal{E} = T dS - p dV + \frac{1}{\rho} \sigma'_{ij} de'_{ij}. \quad (6)$$

If \mathcal{E} and S are considered as functions of the strain e_{ij} and temperature T , then we obtain from Eq. (3):

$$\sigma_{ij} = \rho \left(\frac{\partial \mathcal{E}}{\partial e_{ij}} - T \frac{\partial S}{\partial e_{ij}} \right)_T. \quad (7)$$

This equation shows that the stress σ_{ij} arises from two causes: the increase of specific internal energy with respect to strain, $\partial \mathcal{E} / \partial e_{ij}$, and the decrease of the specific entropy with respect to strain, $-\partial S / \partial e_{ij}$, both converted to values per unit volume of the material through multiplication by the density

ρ . Alternatively, we may use the change of specific volume (vol. per unit mass), $dV = e_{\alpha\alpha}/\rho$ and the strain deviations to describe the deformation; then the use of Eq. (6) yields

$$\sigma'_{ij} = \rho \left(\frac{\partial \mathcal{E}}{\partial e'_{ij}} - T \frac{\partial S}{\partial e'_{ij}} \right)_T, \quad (8)$$

$$-p = \left(\frac{\partial \mathcal{E}}{\partial V} - T \frac{\partial S}{\partial V} \right)_T. \quad (9)$$

From Eq. (7) we see that if the entropy does not change (isentropic process), then

$$\sigma_{ij} = \rho \left. \frac{\partial \mathcal{E}}{\partial e_{ij}} \right|_{S,T}. \quad (10)$$

But if the internal energy does not change, then the stresses arise from the entropy,

$$\sigma_{ij} = -\rho T \left. \frac{dS}{de_{ij}} \right|_{\mathcal{E},T}. \quad (11)$$

According to statistical mechanics, entropy is proportional to the logarithm of the number of possible configurations that can be assumed by the atoms in a body. The more the atoms are randomly dispersed or in random motion, the higher is the entropy. If order is imposed, the entropy decreases. The entropy source of stress arises from the increased order or decreased disorder of the atoms in a material when strain is increased.

There are two ways with which the entropy of a body can be changed: by conduction of heat through the boundary, and by internal entropy production through internal irreversible processes such as viscous friction, thermal currents between crystals, polymer chain changes, and structural configuration changes. In laboratory experiments isentropic condition is not easy to achieve. If the internal entropy production does not vanish, then to maintain a constant entropy in the specimen a certain exact amount of heat must be conducted away from the surface. Hence in practice, the use of Eq. (10) is limited.

On the other hand, an isothermal (constant temperature) condition is easier to maintain. If temperature and strain are considered as the independent variables, we can transform Eq. (3) by introducing a new dependent variable

$$F = \mathcal{E} - TS, \quad (12)$$

which is called the *specific free energy* (i.e., free energy per unit mass). Differentiating Eq. (12) and using Eq. (3), we obtain

$$\begin{aligned} dF &= d\mathcal{E} - T dS - S dT \\ &= \frac{1}{\rho} \sigma_{ij} de_{ij} - S dT. \end{aligned} \quad (13)$$

In analogy with Eq. (7), we obtain

$$\sigma_{ij} = \rho \left(\frac{\partial F}{\partial e_{ij}} + S \frac{\partial T}{\partial e_{ij}} \right)_S, \quad (14)$$

which is another way of stating the sources of stress: through change of free energy and temperature. In the particular case of an isothermal process, $T = \text{const.}$, we obtain

$$\sigma_{ij} = \rho \frac{\partial F}{\partial e_{ij}} \Big|_T \quad (15)$$

Equations (10), (11) and (15) can also be derived by observing that for any function F of T and e_{ij} , we must have

$$dF = \frac{\partial F}{\partial T} \Big|_e dT + \frac{\partial F}{\partial e_{ij}} \Big|_T de_{ij}, \quad (16)$$

which, when compared with Eq. (13), yields

$$\frac{1}{\rho} \sigma_{ij} = \frac{\partial F}{\partial e_{ij}} \Big|_T, \quad (17)$$

$$-S = \frac{\partial F}{\partial T} \Big|_e. \quad (18)$$

Differentiating Eq. (15) with respect to T and Eq. (18) with respect to e_{ij} , we see that they are both equal to $\partial^2 F / \partial T \partial e_{ij}$. Hence

$$\frac{\partial}{\partial T} \left(\frac{\sigma_{ij}}{\rho} \right) = - \frac{\partial S}{\partial e_{ij}}. \quad (19)$$

Substituting back into Eq. (7), we have

$$\sigma_{ij} = \rho \frac{\partial \mathcal{E}}{\partial e_{ij}} \Big|_T - T \frac{\partial}{\partial T} (\sigma_{ij}) \Big|_{e_{ij}} \quad (20)$$

The factor ρ in the last term can be canceled because ρ does not change when e_{ij} is held constant.

Equation (20) is a transformation of Eq. (7) into a form more convenient for laboratory experimentation. We see from Eqs. (20) and (19) that the contribution to stress due to entropy change can be measured by measuring the change of stress σ_{ij} with respect to temperature under the condition of constant strain. Let a piece of material be held stretched at constant strain while the temperature T is altered. The equilibrium stress σ_{ij} is measured, which gives σ_{ij} as a function of T . We can then compute $T(\partial \sigma_{ij} / \partial T)$, which gives us the contribution of entropy change to stress response to changing strain. Note that $T(\partial \sigma_{ij} / \partial T)$ is equal to $(\partial \sigma_{ij} / \partial \ln T)$; hence if σ_{ij} at constant strain is plotted against $\log_e T$, then the slope of the curve of σ_{ij} versus $\log_e T$ is equal to the stress due to entropy, the second term of Eq. (20).

Experiments of this sort have been done on rubber, and it has led to the conclusion that rubber elasticity is derived mainly from entropy change. Similar experiments can be done on biological materials, except that the range of temperature at which a living tissue can remain viable is usually very limited, and the range of $\log T$ could be too small to be useful. If the material changes with changing temperature, then again the method cannot be applied. For example, it does not work for table jelly, whose cross-links break as the temperature rises. It does not work for elastin, which takes up water from the surroundings as the temperature changes.

Engineers are familiar with the concept of *strain energy function*. If a material is elastic and has a strain energy function W , which is a function of the strain components $e_{11}, e_{22}, e_{33}, e_{12}, e_{23}, e_{31}$, then the stress can be obtained from the strain energy function by differentiation:

$$\sigma_{ij} = \frac{\partial W}{\partial e_{ij}}. \quad (21)$$

This equation appears very similar to Eqs. (10) and (17). Hence the strain energy function can be identified with the internal energy per unit volume in an isentropic process, or the free energy per unit volume in an isothermal process. In a more general situation, entropy and internal energy both change, or free energy and temperature both change; then Eq. (21) would have to be identified with Eqs. (7) or (14). Thus the strain energy function depends on the thermodynamic process. The identification of Eq. (21) with the thermodynamic equations (7), (10), (11), (14), and (15) is considered to be a justification of the assumption of the existence of the strain energy function.

Finally, note that all the discussion above presupposes that the state variables are T , S , and e_{ij} , that is, the internal energy and the free energy are functions of the strain e_{ij} , and not of the history of strain, or strain rate, or any other factors such as pH, electric charges, chemical reaction, etc. If these other variables are also significant, then the stress will depend not only on strain, but also on the other variables. In other words, the discussion above is applicable only to elastic bodies and elastic stress. The concept of strain energy function embodied in Eq. (21) is applicable only to elastic bodies.

Problem

- 7.1** Take a tube of gas or a piece of steel and give it a quick stretch while there is no heat added. The material will cool down. Take a rubber band or a strip of muscle and give it a quick stretch. It will heat up. (A very easy demonstration is to take a rubber band, touch it with your forehead to feel its temperature. Then quickly stretch the rubber band and touch the skin on the forehead again. It will be found that it has heated up.)

Explain these phenomena on the basis that gas and steel mainly derive their stress from internal energy whereas rubber and muscle mainly derive their stress from entropy changes.

7.5 Behavior of Tissues Under Uniaxial Loading*

So far we have discussed some more or less “pure” biological materials. From here on we shall consider tissues that are composed of these materials and ground substances.

From the point of view of biomechanics, the properties of a tissue are known if its constitutive equation is known. The constitutive equation of a material can only be determined by experiments. Therefore biorheology is basically an experimental science.

The simplest experiment that can be done on a biosolid is the uniaxial tension test. For this purpose a specimen of cylindrical shape is prepared and stretched in a testing machine. The load and elongation are recorded for prescribed loading or stretching histories. From these records we can deduce the stress-strain relationship of the material under uniaxial loading.

That the stress-strain relationship of animal tissues deviates from Hooke’s law was known to Wertheim (1847), who showed that the stress increases much faster with increasing strain than Hooke’s law predicts. It is also known that tissues in the physiological state are usually not unstressed. If an artery is cut, it will shrink away from the cut. A broken tendon retracts away; the lung tissue is in tension at all times.

If a segment of an artery is excised and tested in a tensile testing machine by imposing a cyclically varying strain, the stress response will show a hysteresis loop with each cycle, but the loop decreases with succeeding cycles, rapidly at first, then tending to a steady state after a number of cycles (see Fig. 7.5:1). The existence of such an initial period of adjustment after a large disturbance seems common to all tissues. From the point of view of mechanical testing, the process is called *preconditioning*. Generally, only mechanical data of preconditioned specimens are presented.

The hysteresis curves of a rabbit papillary muscle (unstimulated) are shown in Fig. 7.5:2. Simple tension was imposed by loading and unloading at the rates indicated in the figure. It is seen that the hysteresis loops did not depend very much on the rate of strain. In general, this insensitivity with respect to the strain rate holds within at least a 10^3 - fold change in strain rate.

Figure 7.5:3 shows a stress-relaxation curve for the mesentery of the rabbit. The specimen was strained at a constant rate until a tension T_1 was

* The following material up to p. 235 is taken from the author’s paper “Stress-Strain-History Relations of Soft Tissues in Simple Elongation,” in *Biomechanics: Its Foundations and Objectives*, Fung, Y. C., Perrone, N., and Anliker, M. (eds.), Prentice-Hall, 1972.

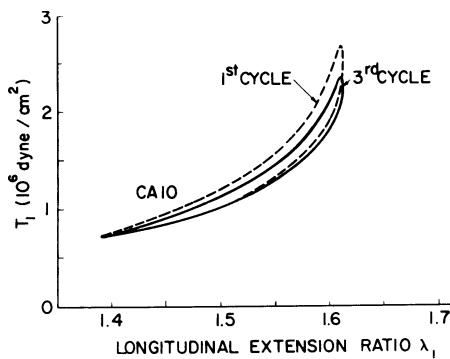


Figure 7.5:1 Preconditioning. Cyclic stress response of a dog's carotid artery, which was maintained in cylindrical configuration (by appropriate inflation or deflation) when stretched longitudinally. λ_1 is the stretch ratio referred to the relaxed length of the segment; 37° , 0.21 cycles/min. Physiological length $L_p = 4.22$ cm. $L_p/L_0 = 1.67$. Diameter at physiological condition = 0.32 cm. $A_0 = 0.056$ cm 2 . Dog wt., 18 kg. From Lee, Frasher and Fung (1967).

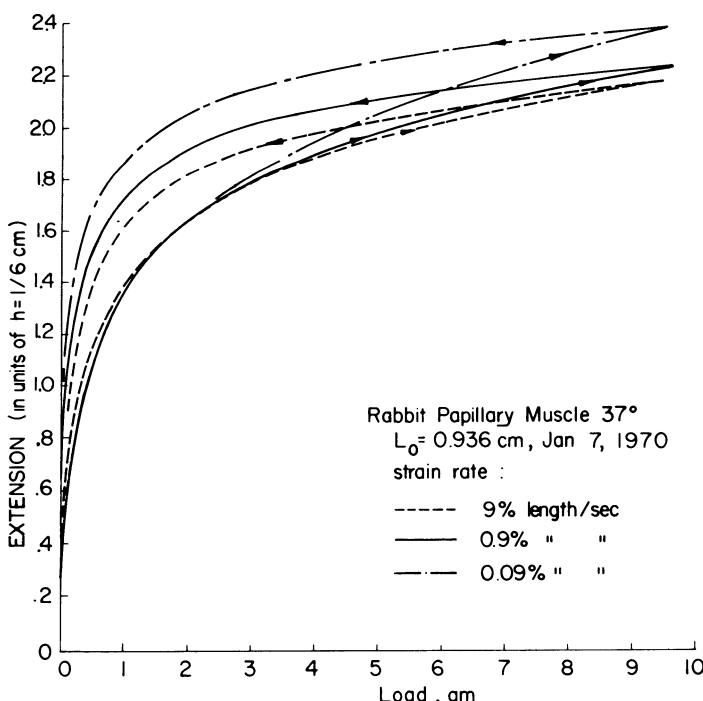


Figure 7.5:2 The length-tension curve of a resting papillary muscle from the right ventricle of the rabbit. (a) Hysteresis curves at strain rates 0.09% length/s; 0.9% length/s; and 9% length/s. Length at 9 mg = 0.936 cm. 37°C . From Fung (1972), by courtesy of Dr. John Pinto.

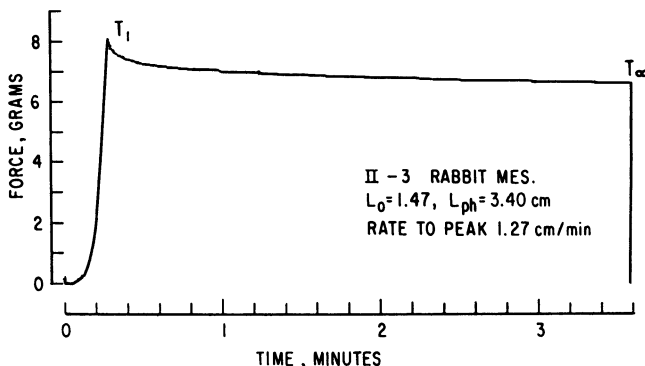


Figure 7.5:3 Relaxation curve of a rabbit mesentery. The specimen was stressed at a strain rate of 1.27 cm/min to the peak. Then the moving head of the testing machine was suddenly stopped so that the strain remained constant. The subsequent relaxation of stress is shown. From Fung (1967).

obtained. The length of the specimen was then held fixed and the change of tension with time was plotted. In a linear scale of time only the initial portion of the relaxation curve is seen. Relaxation in a long period of time is shown in Fig. 7.5:4, in which the abscissa is $\log t$. It is seen that in 17 hours a large

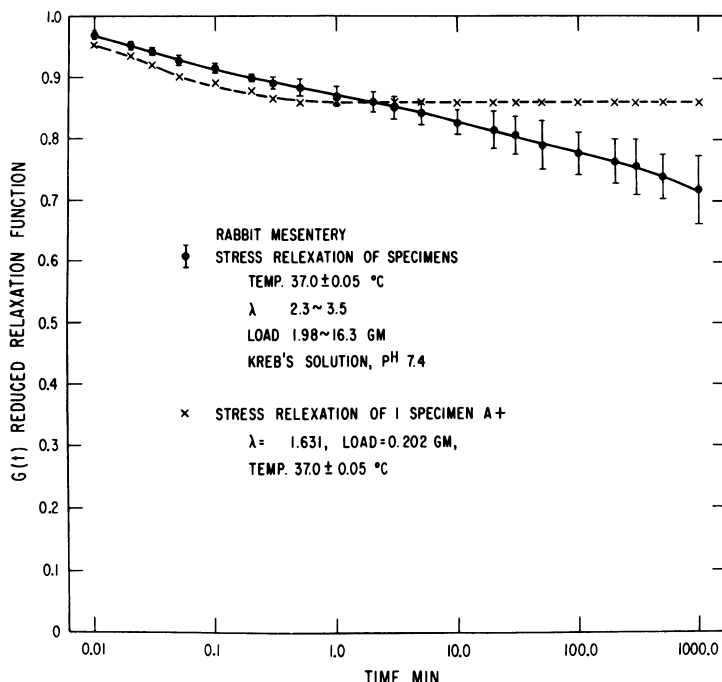


Figure 7.5:4 Long-term relaxation of rabbit mesentery. Solid curve shows the mean reduced relaxation function for 16 different initial stress values. The dashed curve refers to one test at a much lower stress level. By H. Chen; reproduced from Fung (1972).

portion of the initial stress was relaxed. If the initial stress is sufficiently high, the relaxation curve does not level off even at $t = 10^5$ s (see the solid curve in Fig. 7.5:4). If, however, the initial stress is lower than a certain value, the stress levels off at the elapse of a long time, as shown by the dashed curve in Fig. 7.5:4. Apparently, at the higher stress levels, the relaxation has not stopped even at 10^5 s. The reduced relaxation function $G(t)$ shown here is defined by Eq. (1) on p. 226.

Figure 7.5:5 illustrates the creep characteristics of the papillary muscles of the rabbit loaded in the resting state under a constant weight. The change of length was recorded and replotted on a logarithmic scale of time. The creep characteristics depend very much on the temperature and the load.

These features of hysteresis, relaxation, and creep at lower stress ranges ("physiological") are seen on all materials tested in our laboratory: the mesentery of the rabbit and dog, the femoral and carotid arteries and the veins of the dog, cat, and rabbit, the ureter of several species of animals, including human, and the papillary muscles at the resting state. The major differences among these tissues are the degree of distensibility. In the physiological range, the mesentery can be extended 100–200% from the relaxed (unstressed) length, the ureter can be stretched about 60%, the resting heart muscle about 15%, the arteries and veins about 60%, the skin about 40%, and the tendons 2–5%. Beyond these ranges the tissues usually have a large reserve strength before they rupture and fail.

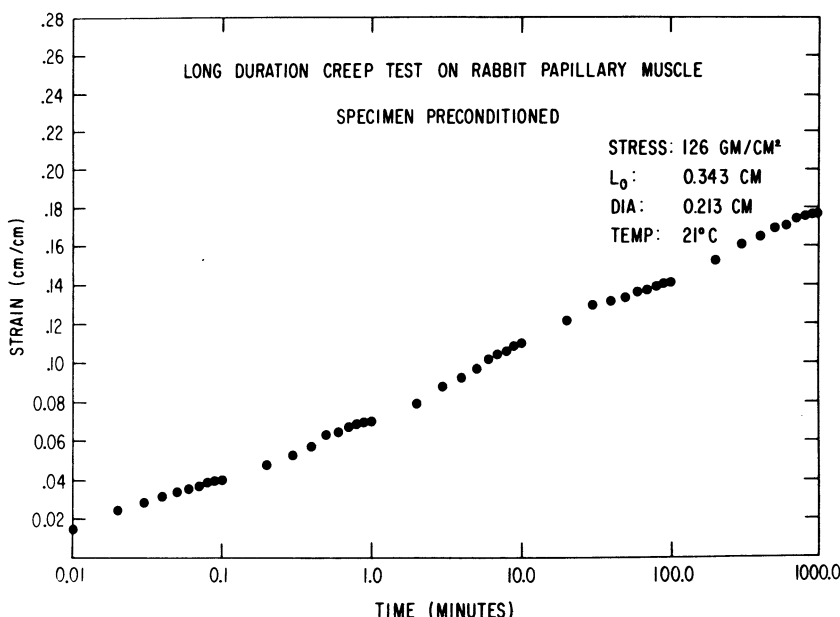


Figure 7.5:5 Creep characteristics of the papillary muscle of the rabbit. By J. Pinto; reproduced from Fung (1972).

Stress Response in Loading and Unloading

In the following we speak of stress and strain in the Lagrangian sense. For a one-dimensional specimen loaded in tension, the tensile stress T is the load divided by the “reference” area; the “stretch ratio” λ is the ratio of the length to the “reference” length; the tensile strain ε is defined as $(\lambda^2 - 1)/2$. The “reference” state can be arbitrarily chosen, subject to the requirement that it be physiological and definitive. In engineering mechanics, we always choose the “natural” state as the reference state, that is, one that represents the relaxed, unstressed material. In biological specimens it turns out that one of the most difficult practical problems is to determine the dimensions of the test specimen at the natural state. The reason is that at this state the material is usually very soft, and it is difficult to handle when measuring the cross-sectional area and length. As a result, the “natural” length is usually not a reliable number, often the most inaccurate of the experimental data. For this reason, experimental results on biological tissues are better presented with respect to a well-defined reference state. The natural state—still very useful in any analysis—should be determined by extrapolation; but the question of accuracy should always be remembered.

For an incompressible material, the cross-sectional area of a cylindrical specimen is reduced by a factor $1/\lambda$ when the length of the specimen is increased by a factor λ . Hence the Eulerian stress σ (which is referred to the cross-section of the deformed specimen and is sometimes called the “true” stress) is λ times T :

$$\sigma = \frac{P}{A} = \frac{P}{A_{\text{ref}}} \lambda = T\lambda. \quad (1)$$

Consider first the relationship between load and deflection in the *loading* process. If the slope of the T versus λ curve as shown in Fig. 7.5:2 is plotted against T , the result as shown in Fig. 7.5:6 is obtained. As a first approximation, we may fit the experimental curve by a straight line in the range of T exhibited and by the equation

$$\frac{dT}{d\lambda} = \alpha(T + \beta). \quad (2)$$

Then, an integration gives

$$T + \beta = ce^{\alpha\lambda}. \quad (3)$$

The integration constant can be determined by finding one point on the curve, say $T = T^*$ when $\lambda = \lambda^*$. Then

$$T = (T^* + \beta)e^{\alpha(\lambda - \lambda^*)} - \beta. \quad (4)$$

Note that if λ is referred to the natural state, we must have, by definition, $T = 0$ when $\lambda = 1$; this is possible only if

$$\beta = \frac{T^* e^{-\alpha(\lambda^* - 1)}}{1 - e^{-\alpha(\lambda^* - 1)}} \quad (5)$$

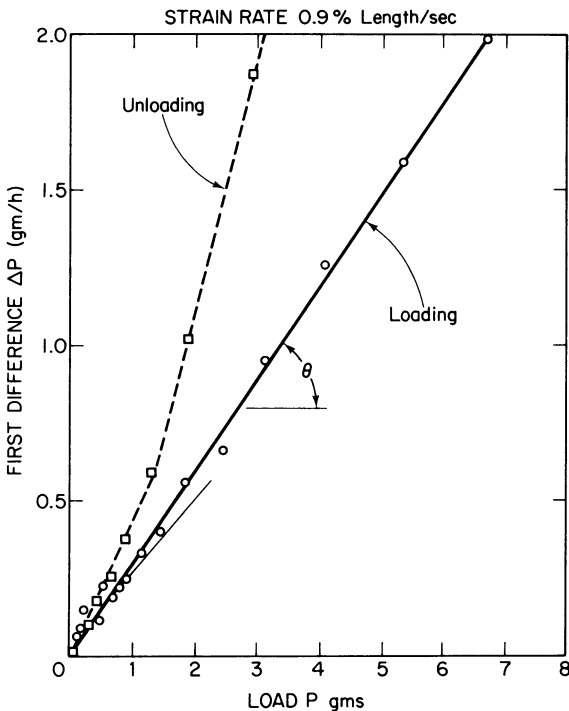


Figure 7.5:6 The variation of the Young's modulus with load at strain rate 0.9% length/s, illustrating the method of determining the constants $\hat{\alpha}_1$, $\hat{\beta}_1$. Near the origin, a different straight line segment is required to fit the experimental data. In this figure, the Young's modulus, $dT/d\lambda$, is replaced by the difference $\Delta T/\Delta\lambda$, to which $dT/d\lambda$ is proportional because of Eq. (3); and T is written as P . For the ordinate, we used $\Delta\lambda = h = 1/6$ cm, and $\Delta T/\Delta\lambda$ is expressed as ΔP per unit of h . From Fung (1972).

Equation (2) includes Hookean materials, for which

$$\frac{dT}{d\lambda} = \text{const.} \quad (6)$$

A more refined representation of the experimental data shown in Fig. 7.5:6 can be made by several straightline segments. The reason for such a choice is a practical one: in the analysis of the function of the organs (such as the contraction of the heart or the peristalsis of the ureter), the function $dT/d\lambda$ appears frequently, and it is desirable to have it represented by as simple a form as possible (in the linear elasticity theory $dT/d\lambda$ is a constant). The form given in Eq. (2) is about as simple as can be, although in the case represented in Figure 7.5:6 it is necessary to specify two straight line segments:

$$\begin{aligned} \frac{dT}{d\lambda} &= \alpha_1(T + \beta_1) && \text{for } 0 \leq T \leq T_1, \\ \frac{dT}{d\lambda} &= \alpha_2(T + \beta_2) && \text{for } T_1 \leq T \leq T_2. \end{aligned} \quad (7)$$

In this case, the integrated curve must be represented by two expressions in the form of Eq. (4), matched at the juncture $T = T_1$.

Unloading at the same strain rate results in similar straight lines with much larger slopes, as shown by the dotted curve in Fig. 7.5:6.

Other Expressions in the Literature

One of the best known approaches to the elasticity of bodies capable of finite deformation is to postulate the form of an elastic potential, or strain energy function, W . For example, if a body is elastically isotropic, the strain energy function must be a function of the strain invariants. Well-known examples of strain-energy functions are those of Mooney (1940), Rivlin (1947), Rivlin and Saunders (1951). See the treatise of Green and Adkins (1960), where references are given.

Valanis and Landel (1967) presented a very useful strain-energy function,

$$W = \sum_{i=1}^3 f(\ln \lambda_i). \quad (8)$$

where $\lambda_1, \lambda_2, \lambda_3$ are the principal stretch ratios and f is certain function. Specific application of Valanis's form to soft tissues was made by Blatz et al. (1969), who proposed the following:

$$f(\ln \lambda_i) = C(\lambda_i^\alpha - 1). \quad (9)$$

When applied to the rabbit's mesentery, Blatz et al. (1969) found $\alpha = 18$. For skeletal muscle in the resting state, they found $\alpha = 8$; for latex rubber, $\alpha = 1.5$.

Blatz et al (1969) proposed also the following

$$f(\ln \lambda_i) = C[e^{\alpha(\lambda_i^2 - 1)} - 1], \quad (10)$$

for which the uniaxial tension case of an incompressible material gives

$$\sigma = \left(\frac{G}{\alpha + 1} \right) \left\{ \lambda e^{\alpha(\lambda^2 - 1)} - \frac{1}{\lambda^2} e^{\alpha((1/\lambda)^2 - 1)} \right\}. \quad (11)$$

Veronda and Westmann (1970) proposed the following form for the strain potential of an isotropic material expressed in terms of the strain invariants I_1, I_2, I_3 :

$$I_1 = \lambda_1^2 + \lambda_2^2 + \lambda_3^2, \quad I_2 = \lambda_1^2 \lambda_2^2 + \lambda_2^2 \lambda_3^2 + \lambda_3^2 \lambda_1^2, \quad I_3 = \lambda_1 \lambda_2 \lambda_3. \\ W = C_1 [e^{\beta(I_1 - 3)} - 1] + C_2(I_2 - 3) + g(I_3), \quad (12)$$

where C_1, C_2, β , are constants and g is a function which becomes zero if the material is incompressible, $g(1) = 0$. For cat's skin, they suggested the following constants:

$$C_1 = 0.00394, \quad \beta = 5.03, \quad C_2 = -0.01985.$$

These expressions presuppose isotropy. However, it is almost axiomatic that biological tissues are not isotropic.

Other expressions proposed, but not reduced to the form of strain energy, and not pretending to be generally valid for three-dimensional stress states, are the following:

Wertheim (1847)	$\varepsilon^2 = a\sigma^2 + b\sigma,$
Morgan (1960)	$\varepsilon = a\sigma^n,$
Kenedi et al. (1964)	$\sigma = k\varepsilon^d,$ $\sigma = B[e^{m\varepsilon} - 1],$
Ridge and Wright (1964)	$\varepsilon = C + k\sigma^b,$ $\varepsilon = x + y \log \sigma.$

(13)

7.6 Quasi-linear Viscoelasticity of Soft Tissues

The experimental results illustrated in Figs. 7.5:1 through 7.5:6 show that biological tissues are not elastic. The history of strain affects the stress. In particular, there is a considerable difference in stress response to loading and unloading.

Most authors discuss their experimental results in the framework of the linear theory of viscoelasticity relating stress and strain, generally on the basis of the Voigt, Maxwell, and Kelvin models. Buchthal and Kaiser (1951) formulated a continuous relaxation spectrum that corresponds to a combination of an infinite number of Voigt and Maxwell elements. A nonlinear theory of the Kelvin type was proposed by Viidik (1966) on the basis of a sequence of springs of different natural length, with the number of participating springs increasing with increasing strain.

It is reasonable to expect that for oscillations of small amplitude about an equilibrium state, the theory of linear viscoelasticity should apply. For finite deformations, however, the nonlinear stress-strain characteristics of the living tissues must be accounted for.

Instead of developing a constitutive equation by gradual specialization of a general formulation, I shall go at once to a special hypothesis. Let us consider a cylindrical specimen subjected to tensile load. If a step increase in elongation (from $\lambda = 1$ to λ) is imposed on the specimen, the stress developed will be a function of time as well as of the stretch λ . The history of the stress response, called the *relaxation function*, and denoted by $K(\lambda, t)$, is assumed to be of the form

$$K(\lambda, t) = G(t)T^{(e)}(\lambda), \quad G(0) = 1, \quad (1)$$

in which $G(t)$, a normalized function of time, is called the *reduced relaxation function*, and $T^{(e)}(\lambda)$, a function of λ alone, is called the *elastic response*. We then assume that the stress response to an infinitesimal change in stretch,

$\delta\lambda(\tau)$, superposed on a specimen in a state of stretch λ at an instant of time τ , is, for $t > \tau$:

$$G(t - \tau) \frac{\partial T^{(e)}[\lambda(\tau)]}{\partial \lambda} \delta\lambda(\tau). \quad (2)$$

Finally, we assume that the superposition principle applies, so that

$$T(t) = \int_{-\infty}^t G(t - \tau) \frac{\partial T^{(e)}[\lambda(\tau)]}{\partial \lambda} \frac{\partial \lambda(\tau)}{\partial \tau} d\tau, \quad (3)$$

that is, the tensile stress at time t is the sum of contributions of all the past changes, each governed by the same reduced relaxation function.

Rewriting Eq. (3) in the form

$$T(t) = \int_{-\infty}^t G(t - \tau) \dot{T}^{(e)}(\tau) d\tau, \quad (4)$$

where a dot denotes the rate of change with time, we see that the stress response is described by a linear law relating the stress T with the elastic response $T^{(e)}$. The function $T^{(e)}(\lambda)$ plays the role assumed by the strain ε in the conventional theory of viscoelasticity. Therefore, the machinery of the well-known theory of linear viscoelasticity (see Chapter 2, pp. 41–56, and the author's *Foundations of Solid Mechanics*, Chapter 15) can be applied to this hypothetical material.

The inverse of Eq. (4) may be written as

$$T^{(e)}[\lambda(t)] = \int_{-\infty}^t J(t - \tau) \dot{T}(\tau) d\tau, \quad (5)$$

which defines the *reduced creep function* $J(t)$. Let $T^{(e)}(\lambda) = F(\lambda)$ and $\lambda = F^{-1}(T^{(e)})$ be the inverse of $F(\lambda)$, i.e., the stretch ratio corresponding to the tensile stress $T^{(e)}$. Then for a unit step change of the tensile stress T at $t = 0$, the time history of the stretch ratio is

$$\lambda(t) = F^{-1}[J(t)]. \quad (6)$$

The lower limits of integration in Eqs. (3), (4), and (5) are written as $-\infty$ to mean that the integration is to be taken before the very beginning of the motion. If the motion starts at time $t = 0$, and $\sigma_{ij} = e_{ij} = 0$ for $t < 0$, Eq. (3) reduces to

$$T(t) = T^{(e)}(0+)G(t) + \int_0^t G(t - \tau) \frac{\partial T^{(e)}[\lambda(\tau)]}{\partial \tau} d\tau. \quad (7)$$

If $\partial T^{(e)}/\partial t$, $\partial G/\partial t$ are continuous in $0 \leq t < \infty$, the equation above is equivalent to

$$T(t) = G(0)T^{(e)}(t) + \int_0^t T^{(e)}(t - \tau) \frac{\partial G(\tau)}{\partial \tau} d\tau \quad (8a)$$

$$= \frac{\partial}{\partial t} \int_0^t T^{(e)}(t - \tau)G(\tau) d\tau. \quad (8b)$$

Equation (8a) is suitable for a simple interpretation. Since, by definition, $G(0) = 1$, we have

$$T(t) = T^{(e)}[\lambda(t)] + \int_0^t T^{(e)}[\lambda(t - \tau)] \frac{\partial G(\tau)}{\partial \tau} d\tau. \quad (9)$$

Thus the tensile stress at any time t is equal to the instantaneous stress response $T^{(e)}[\lambda(t)]$ decreased by an amount depending on the past history, because $\partial G(\tau)/\partial \tau$ is generally of negative value. The question of experimental determination of $T^{(e)}(\lambda)$ and $G(t)$ will be discussed in the following sections.

The Elastic Response $T^{(e)}(\lambda)$

By definition, $T^{(e)}(\lambda)$ is the tensile stress instantaneously generated in the tissue when a step function of stretching λ is imposed on the specimen. Strict laboratory measurement of $T^{(e)}(\lambda)$ according to this definition is difficult, because at a sudden application of loading, transient stress waves will be induced in the specimen and a recording of the stress response will be confused by these elastic waves. However, if we assume that the relaxation function $G(t)$ is a continuous function, then $T^{(e)}(\lambda)$ may be approximated by the tensile stress response in a loading experiment with a sufficiently high rate of loading. In other words, we may take the $T(\lambda)$ obtained in Sec. 7.5 as $T^{(e)}$.

A justification of this procedure is the following. The relaxation function $G(t)$ is a continuously varying decreasing function as shown in Fig. 7.5:4 (normalized to 1 at $t = 0$). Now, if by some monotonic process λ is increased from 0 to λ in a time interval ε , then at the time $t = \varepsilon$ we have, according to Eq. (9),

$$T(\varepsilon) = T^{(e)}(\lambda) + \int_0^\varepsilon T^{(e)}[\lambda(\varepsilon - \tau)] \frac{\partial G(\tau)}{\partial \tau} d\tau. \quad (10)$$

But, as τ increases from 0 to ε , the integrand never changes sign, hence

$$T(\varepsilon) = T^{(e)}(\lambda) \left[1 - \varepsilon \frac{\partial G}{\partial \tau}(c) \right], \quad (11)$$

where $0 \leq c \leq \varepsilon$. Since $\partial G/\partial \tau$ is finite, the second term tends to 0 with ε . Therefore, if ε is so small that $\varepsilon |\partial G/\partial \tau| \ll 1$, then

$$T^{(e)}(\lambda) \doteq T(\varepsilon). \quad (12)$$

The Reduced Relaxation Function $G(t)$

It is customary to analyze the relaxation function into the sum of exponential functions and identify each exponent with the rate constant of a relaxation

mechanism; thus

$$G(t) = \frac{\sum C_i e^{-v_i t}}{\sum C_i}. \quad (13)$$

Two important points are often missed:

1. If an experiment is cut off prematurely, one may mistakenly arrive at an erroneous limiting value $G(\infty)$, which corresponds to $v_0 = 0$ in Eq. (13).
2. The exponents v_i should not be interpreted literally without realizing that the representation of empirical data by a sum of exponentials is a nonunique process in practice.

As an example of the first point, the relaxation curves of Buchthal and Kaiser (1951) terminate at 100 ms. However, the data in Fig. 7.5:4 show that relaxation goes on beyond 1000 min! Examples of the second kind lead to the observation that a measured characteristic time of a relaxation experiment often turns out to be the length of the experiment. Lanczos (1956, p.276) gives an example in which a certain set of 24 decay observations was analyzed and found that it could be fit equally well by three different expressions for x between 0 and 1:

$$\begin{aligned} f(x) &= 2.202e^{-4.45x} + 0.305e^{-1.58x}, \\ f(x) &= 0.0951e^{-x} + 0.8607e^{-3x} + 1.5576e^{-5x}, \\ f(x) &= 0.041e^{-0.5x} + 0.79e^{-2.73x} + 1.68e^{-4.96x}. \end{aligned} \quad (14)$$

Lanczos comments, "It would be idle to hope that some other modified mathematical procedure could give better results, since the difficulty lies not with the manner of evaluation but with the extraordinary sensitivity of the exponents and amplitudes to very small changes of the data, which no amount of least-square or other form of statistics could remedy."

Realizing these difficulties, we conclude first that for a living tissue, a viscoelasticity law based on the fully relaxed elastic response, $G(t)$ as $t \rightarrow \infty$, is unreliable. In fact, a formulation based on $G(\infty)$ may run into a true difficulty because often it seems that $G(t) \rightarrow 0$ when $t \rightarrow \infty$. Secondly, one should look into other experiments, such as creep, hysteresis, and oscillation, in order to determine the relaxation function.

In this regard the salient feature of the hysteresis curve comes to mind: the hysteresis loop is almost independent of the strain rate within several decades of the rate variation. This insensitivity is incompatible with any viscoelastic model that consists of a finite number of springs and dashpots. Such a model will have discrete relaxation rate constants. If the specimen is strained at a variable rate, the hysteresis loop will reach a maximum at a rate corresponding to a relaxation constant. A discrete model, therefore, corresponds to a discrete hysteresis spectrum, in opposition to the feature of living tissues that we have just described. This suggests at once that one should

consider a continuous distribution of the exponents v_i : thus passing from a discrete spectrum α_i associated with v_i to a continuous spectrum $\alpha(v)$ associated with a continuous variable v between 0 and ∞ .

To make these remarks clear, let us consider a *standard linear solid* (Kelvin model), for which the governing differential equation is [see Chapter 2, Sec. 2.11, Eq. (2.11:7)]

$$T + \tau_e \dot{T} = E_R [T^{(e)} + \tau_\sigma \dot{T}^{(e)}], \quad (15)$$

where τ_e , τ_σ , E_R are constants. Equation (15) is subjected to the initial condition

$$\tau_e T(0) = E_R \tau_\sigma T^{(e)}(0). \quad (16)$$

However, our special definition of the reduced relaxation function requires that

$$T^{(e)}(0) = T(0), \quad G(0) = 1, \quad (17)$$

hence

$$E_R = \frac{\tau_e}{\tau_\sigma}. \quad (18)$$

By integrating Eq. (15) with the initial condition specified above, we obtain the response $T^{(e)}$ to a unit step increase in stress $T(t) = \mathbf{1}(t)$: the creep function

$$J(t) = \frac{1}{E_R} \left[1 - \left(1 - \frac{\tau_e}{\tau_\sigma} \right) e^{-t/\tau_\sigma} \right] \mathbf{1}(t). \quad (19)$$

Conversely, the relaxation function is obtained by integrating the differential equation for stress T for a unit step increase in the elastic response:

$$G(t) = E_R \left[1 + \left(\frac{\tau_\sigma}{\tau_e} - 1 \right) e^{-t/\tau_e} \right] \mathbf{1}(t). \quad (20)$$

With these expressions the meaning of the constants τ_σ , τ_e , E_R are clear. τ_σ is the time constant for creep at constant stress, τ_e is the time constant for relaxation at constant strain, and E_R is the “residual,” the fraction of the elastic response that is left in the specimen after a long relaxation, $t \rightarrow \infty$. These physical constants are related through Eq. (18).

If a sinusoidal oscillation is considered, so that

$$T(t) = T_0 e^{i\omega t}, \quad T^{(e)}(t) = T_0^{(e)} e^{i\omega t}, \quad (21)$$

then

$$T_0/T_0^{(e)} = i\omega \int_{-\infty}^{\infty} G(t) e^{-i\omega t} dt = \mathcal{M} = |\mathcal{M}| e^{-i\delta}, \quad (22)$$

where \mathcal{M} is the complex modulus. By using Eq. (20), or, more simply, Eq. (15), we obtain

$$\mathcal{M} = \frac{1 + i\omega \tau_\sigma}{1 + i\omega \tau_e} E_R, \quad |\mathcal{M}| = \left(\frac{1 + \omega^2 \tau_\sigma^2}{1 + \omega^2 \tau_e^2} \right)^{1/2} E_R. \quad (23)$$

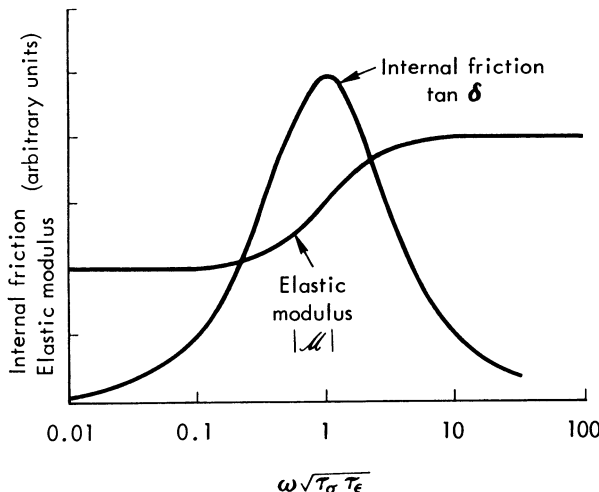


Figure 7.6:1 The dynamic modulus of elasticity $|M|$ and the internal damping $\tan \delta$ plotted as a function of logarithm of frequency ω , for a standard linear solid. From Fung (1972).

δ is the phase shift, and $\tan \delta$ is a measure of “internal damping”:

$$\tan \delta = \frac{\omega(\tau_\sigma - \tau_\epsilon)}{1 + \omega^2(\tau_\sigma \tau_\epsilon)}. \quad (24)$$

When the modulus $|M|$ and the internal damping $\tan \delta$ are plotted against the logarithm of ω , curves as shown in Fig. 7.6:1 are obtained. The damping reaches a peak when the frequency ω is equal to $1/\sqrt{\tau_\sigma \tau_\epsilon}$. Correspondingly, the elastic modulus $|M|$ has the fastest rise for frequencies in the neighborhood of $1/\sqrt{\tau_\sigma \tau_\epsilon}$. If the internal friction (hysteresis loop) is insensitive to frequency ω , we must spread out the peak. This can be done by superposing a larger number of Kelvin models. This is the basic reason for introducing a continuous spectrum of relaxation time into our problem.

To implement this idea, let us first rewrite the relaxation function in a different notation. Let

$$S = \frac{\tau_\sigma}{\tau_\epsilon} - 1, \quad E_R = \frac{1}{1 + S}. \quad (25)$$

Then substituting into Eqs. (20) and (23), we obtain

$$G(t) = \frac{1}{1 + S} [1 + S e^{-t/\tau_\epsilon}], \quad (26)$$

$$M = \frac{1}{1 + S} \left(1 + S \frac{\omega \tau_\epsilon}{\omega \tau_\epsilon + \frac{1}{\omega \tau_\epsilon}} + i S \frac{1}{\omega \tau_\epsilon + \frac{1}{\omega \tau_\epsilon}} \right). \quad (27)$$

Now, let τ_e be replaced by a continuous variable τ , and Let $S(\tau)$ be a function of τ . For a system with a continuous spectrum, we replace S by $S(\tau) d\tau$ in Eqs. (26), (27), and (19) and integrate with respect to τ to obtain the following generalized reduced relaxation function and complex modulus:

$$G(t) = \left[1 + \int_0^\infty S(\tau) e^{-t/\tau} d\tau \right] \left[1 + \int_0^\infty S(\tau) d\tau \right]^{-1} \quad (28)$$

$$\mathcal{M}(\omega) = \left[1 + \int_0^\infty S(\tau) \frac{\omega\tau d\tau}{\omega\tau + \frac{1}{\omega\tau}} + \int_0^\infty iS(\tau) \frac{d\tau}{\omega\tau + \frac{1}{\omega\tau}} \right] \left[1 + \int_0^\infty S(\tau) d\tau \right]^{-1} \quad (29)$$

A normalization factor is added to each of these formulas to meet the definition that $G(t) \rightarrow 1$, $J(t) \rightarrow 1$ when $t \rightarrow 0$.

Our task is to find the function $S(\tau)$ that will make $G(t)$, $J(t)$, and $\mathcal{M}(\omega)$ match the experimental results. In particular, we want $\mathcal{M}(\omega)$ to be nearly constant for a wide range of frequency.

A specific proposal is to consider

$$S(\tau) = \frac{c}{\tau} \quad \text{for } \tau_1 \leq \tau \leq \tau_2, \quad (30)$$

$$= 0 \quad \text{for } \tau < \tau_1, \tau > \tau_2, \quad (31)$$

where c is a constant. Then

$$\begin{aligned} \mathcal{M}(\omega) &= \left\{ 1 + \int_{\tau_1}^{\tau_2} \left[c \frac{\omega\tau}{1 + (\omega\tau)^2} + \frac{ic}{1 + (\omega\tau)^2} \right] d(\omega\tau) \right\} \left\{ 1 + \int_{\tau_1}^{\tau_2} \frac{c}{\tau} d\tau \right\}^{-1} \\ &= \left\{ 1 + \frac{c}{2} [\ln(1 + \omega^2\tau_2^2) - \ln(1 + \omega^2\tau_1^2)] \right. \\ &\quad \left. + ic[\tan^{-1}(\omega\tau_2) - \tan^{-1}(\omega\tau_1)] \right\} \left\{ 1 + c \ln \frac{\tau_2}{\tau_1} \right\}^{-1} \end{aligned} \quad (32)$$

This results in a rather constant damping for $\tau_1 \leq 1/\omega \leq \tau_2$, as can be seen from Fig. 7.6:2 for an example in which $\tau_1 = 10^{-2}$, $\tau_2 = 10^2$. The variable part of the stiffness [the real part of $\mathcal{M}(\omega)$] is also plotted in Fig. 7.6:2. The maximum damping occurs when the frequency is $\omega_n = 1/\sqrt{(\tau_1\tau_2)}$. The stiffness rises the fastest in the neighborhood of ω_n . At ω_n , the maximum damping is proportional to

$$\tan^{-1} \left[\frac{1}{2} \left(\sqrt{\frac{\tau_2}{\tau_1}} - \sqrt{\frac{\tau_1}{\tau_2}} \right) \right], \quad (33)$$

which varies rather slowly with τ_2/τ_1 ratio, as can be seen from Fig. 7.6:3, in which the above quantity divided by $\ln(\tau_2/\tau_1)$ is plotted.

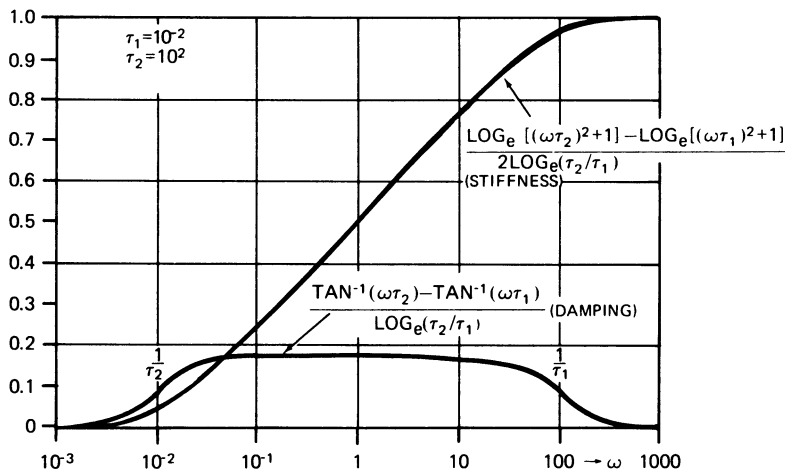


Figure 7.6.2 The stiffness (real part of the complex modulus M) and the damping plotted as functions of the logarithm of the frequency ω ; corresponding to a continuous relaxation spectrum $S(\tau) = c/\tau$ for $\tau_1 \leq \tau \leq \tau_2$ and zero elsewhere. $\tau_1 = 10^{-2}$, $\tau_2 = 10^2$. From Neubert (1963).

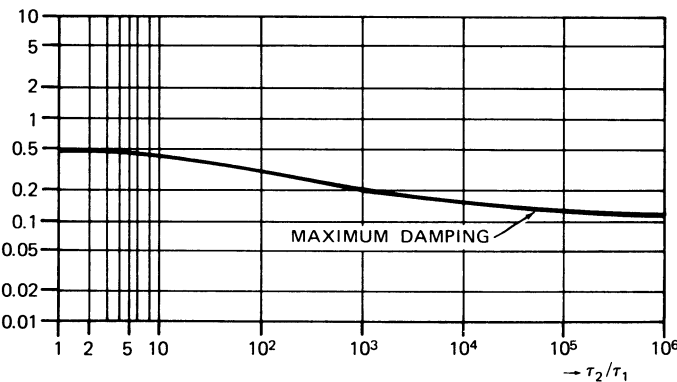


Figure 7.6.3 The maximum damping as a function of the ratio τ_2/τ_1 for a solid corresponding to a continuous relaxation spectrum. $S(\tau) = c/\tau$ for $\tau_1 \leq \tau \leq \tau_2$, and zero elsewhere. From Neubert (1963).

The corresponding reduced relaxation function can be evaluated in terms of the exponential integral function which is tabulated. Figure 7.6.4 shows an example in which the fraction of the relaxation to the residual stress is plotted as a function of time. The portion in the middle, $\tau_1 \ll t \ll \tau_2$, is nearly a straight line; therefore the stresses decreases with $\ln t$ in that segment. This specific spectrum, therefore, gives us the features desired. We are left with three parameters, c , τ_1 , τ_2 , to adjust with respect to the experimental data.

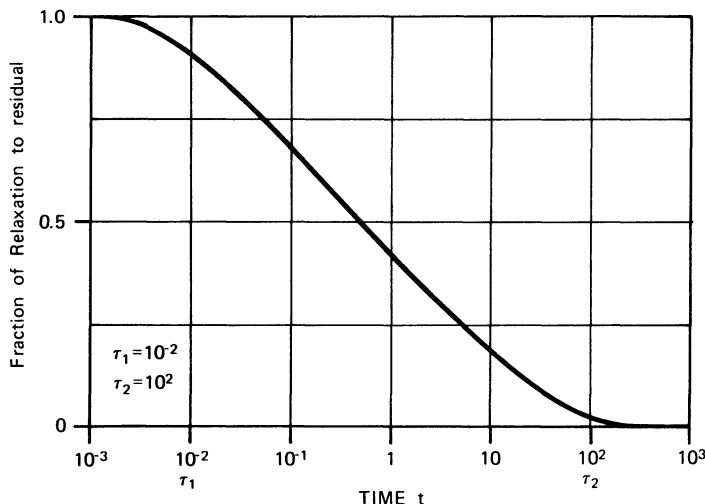


Figure 7.6:4 The reduced relaxation function $G(t)$ of a solid with a continuous relaxation spectrum $S(\tau) = c/\tau$ for $\tau_1 \leq \tau \leq \tau_2$, and zero elsewhere. From Neubert (1963).

By proposing the specific spectrum, Eq. (30), we do not mean to exclude other possibilities. Any fairly flat and broad continuous spectrum will serve to render hysteresis less dependent on frequency.

Although we found Eq. (30) for biological tissues according to the reasoning presented above (Fung, 1972), we found later that this spectrum has had a long history. Hysteresis insensitive to frequency was described by Becker and Föppl (1928) in their study of electromagnetism in metals [see Becker and Döring (1939)]. Wagner (1913) described it in dielectricity. Theodorsen and Garrick (1940) introduced it into the theory of airplane flutter; it is now called "structural" damping by engineers, Knopoff (1965) showed that the earth's crust has an internal friction which is independent of the frequency. Routbart and Sack (1966) showed that the internal friction for nonmagnetic materials is either constant or decreases slightly with frequency in the range 1–40 kHz. Mason (1969) attributed the reason for this to the existence of a kind of "kink" in the dislocation line and the associated kink energy barrier. Bodner (1968) formulated a special plasticity theory to account for the phenomena.

The concept of a continuous relaxation spectrum was considered by Wagner and Becker. Wagner (1913) investigated the function

$$S(\tau) d\tau = \frac{kb}{\sqrt{\pi}} e^{-b^2 z^2} dz, \quad (34)$$

where

$$z = \log\left(\frac{\tau}{t_0}\right), \quad (35)$$

and k, b, t_0 are constants. Becker and Foppl (1928) introduced the spectrum given in Eq. (30). Neubert (1963) developed the Becker theory thoroughly. Guth et al. (1946) have shown that the viscoelasticity of rubber follows Eq. (30) also.

It is important to note that although a linear viscoelasticity law is posed in Eq. (24) to relate the stress T with the elastic response $T^{(e)}$, the relation between $T^{(e)}$ and λ is nonlinear.

In developing the theory of a continuous spectrum considered above, the elastic response $T^{(e)}$ is assumed to oscillate harmonically. The corresponding oscillation of the extension is anharmonic. Figure 7.6:5(a) shows the time course of $T^{(e)}$ and λ when $T^{(e)}$ oscillates harmonically. If λ oscillates sinusoidally, then $T^{(e)}$ oscillates anharmonically as shown in Fig. 7.6:5(b). If the amplitude of oscillation is small, an approximate linear relationship holds, and both stress and strain will oscillate harmonically. Patel et al. (1970) show that linear viscoelasticity applies to arteries as long as the superimposed sinusoidal strain remains below 4% (on top of $\lambda = 1.6$), and that their data were reproducible up to 16 h following removal of tissue. Many other workers reached similar conclusions.

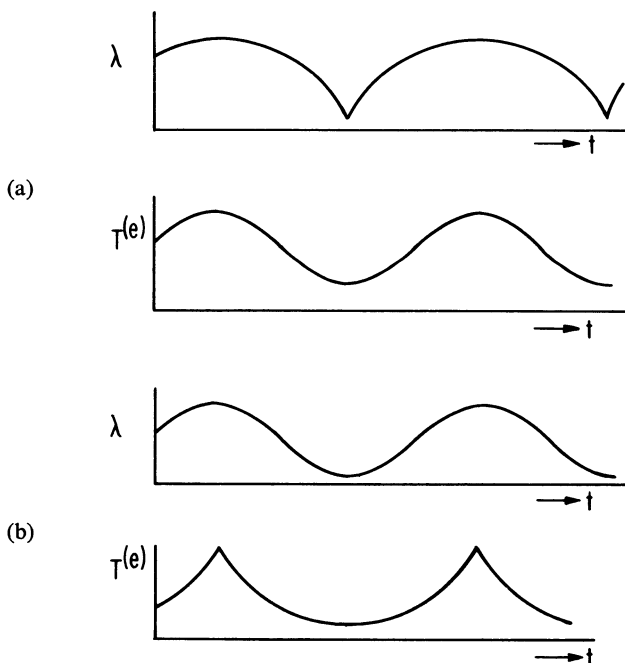


Figure 7.6:5 The quasi-linear stress-strain-history relationship proposed in Eq. (9). (a) The time course of the extension λ when the elastic response $T^{(e)}$ oscillates sinusoidally. (b) The time course of the elastic response $T^{(e)}$ when the extension λ varies sinusoidally. From Fung (1972).

Example: Rabbit Mesentery. Chen and Fung (1973) showed that the rabbit mesentery data can be fitted by Eq. (30), which leads to the following generalized reduced relaxation function, $G(t)$, and reduced creep function, $J(t)$:

$$G(t) = \left\{ 1 + c \left[E_1 \left(\frac{t}{\tau_2} \right) - E_1 \left(\frac{t}{\tau_1} \right) \right] \right\} \left[1 + c \ln \left(\frac{\tau_2}{\tau_1} \right) \right]^{-1}, \quad (36)$$

$$J(t) = \left\{ 1 - c \left[E_1 \left(\frac{t}{c + \tau_2} \right) - E_1 \left(\frac{t}{c + \tau_1} \right) \right] \right\} \left[1 - c \ln \left(\frac{c + \tau_2}{c + \tau_1} \right) \right]^{-1}, \quad (37)$$

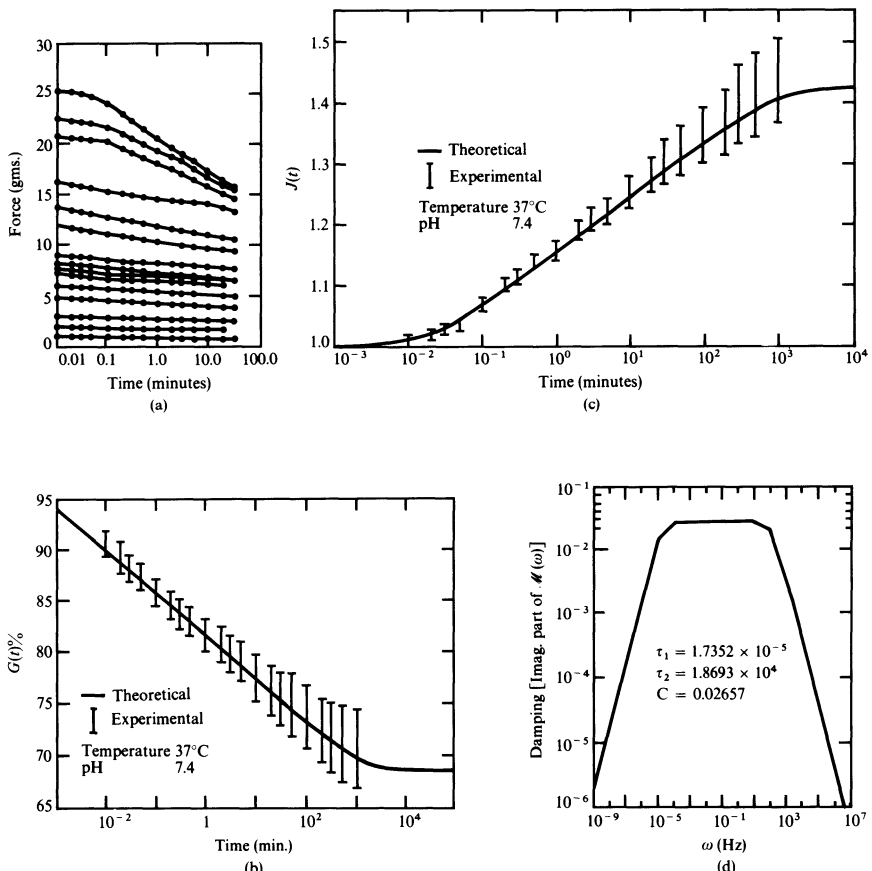


Figure 7.6:6 Fitting of the quasi-linear viscoelasticity formula with a continuous relaxation spectrum [Eqs. (28) and (31)] to the experimental data for rabbit mesentery. (a) shows experimental relaxation data. (b) shows normalized experimental data in mean \pm S.D. The mathematical representation with the constants named in (d) is shown by a solid line. (c) gives the corresponding creep data. (d) presents the theoretical damping. From Chen and Fung (1973).

where $E_1(z)$ is the exponential integral function defined by the equation

$$E_1(z) = \int_z^\infty \frac{e^{-t}}{t} dt \quad (|\arg z| < \pi) \quad (38)$$

and tabulated in Abramowitz and Stegun (1964). For $t \rightarrow \infty$, $E_1(t/\tau_2)$ and $E_1(t/\tau_1) \rightarrow 0$, and

$$G(\infty) = \left[1 + c \ln\left(\frac{\tau_2}{\tau_1}\right) \right]^{-1}. \quad (39)$$

For values of t of the order of 1s,

$$G(t) = [1 - c\gamma - c \ln(t/\tau_2)][1 + c \ln(\tau_2/\tau_1)]^{-1} \quad (40)$$

where γ is the Euler's constant. In an interval within (τ_1, τ_2) , the slopes of the relaxation and creep curves versus the logarithm of time are

$$\frac{dG}{d(\ln t)} = \frac{c}{1 + c \ln(\tau_2/\tau_1)}, \quad (41)$$

$$\frac{dJ}{d(\ln t)} = \frac{c}{1 - c \ln[(\tau_2 + c)/(\tau_1 + c)]}. \quad (42)$$

From the experimental data, Chen and Fung plotted $G(t)$ and $J(t)$ against the logarithm of time, and evaluated the slope at a typical point $[G(t_0), t_0]$ in the middle portion of the curve. Then τ_1 , τ_2 , and c can be solved from Eqs. (39)–(42). Figure 7.6:6 shows the comparison of the experimental results with the formulas named above, with $\tau_1 = 1.735 \times 10^{-5}$ s, $\tau_2 = 1.869 \times 10^4$ s, and $c = 0.02657$. In Fig. 7.6:6(a), the relaxation data obtained at 37°C for various maximum loads is shown. In Fig. 7.6:6(b) the normalized form of the same data shows that the reduced relaxation function $G(t)$ is essentially independent of the stretch. Data in Fig. 7.6:6(c) show that the reduced creep function is essentially a linear function of log time in the middle portion of the curve. The load seems to have little effect on the creep of the mesentery. Figure 7.6:6(d) shows the damping of the system, i.e., the imaginary part of $\mathcal{M}(\omega)$, computed according to Eq. (32). The damping is rather constant over a range of eight decades, which indicates the frequency-indifferent behavior of the hysteresis loops.

Problem

7.2 A well-known result of Hardung (1952), Bergel (1961) and others is illustrated in Fig. P7.2. It shows a rather small change in phase angle over a range of frequencies from 1 to 10 Hz, and a gentle stiffening of the dynamic modulus. Could this be explained by a Maxwell model of viscoelasticity? If not, then what kind of model would be consistent with the experimental findings?

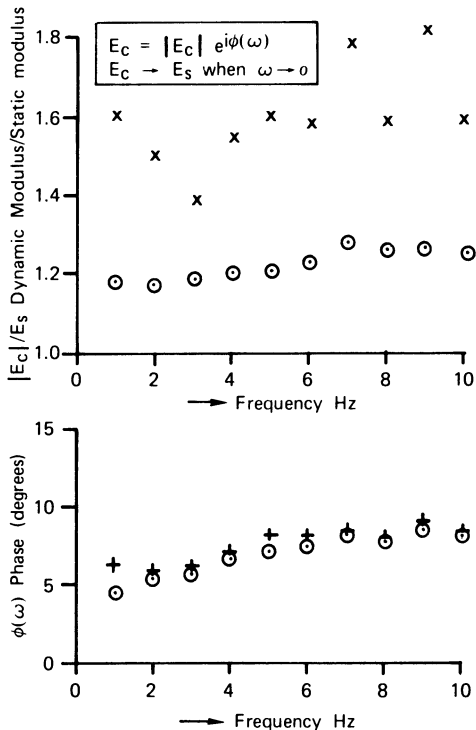


Figure P7.2 The dynamic modulus and damping phase angle ϕ [angle δ in Eq. (22)] of arteries from the data of Hardung (1952) and Bergel (1961). Circles: aorta. Crosses: other arteries. From Westerhof and Noordergraaf (1970).

7.7 Incremental Laws. The Concept of Pseudo-elasticity

We have shown that the mechanical properties of soft tissues such as arteries, muscle, skin, lung, ureter, mesentery, etc., are qualitatively similar. They are inelastic. They do not meet the definition of an elastic body, which requires that there be a single-valued relationship between stress and strain. These tissues show hysteresis when they are subjected to cyclic loading and unloading. When held at a constant strain, they show stress relaxation. When held at a constant stress, they show creep. They are anisotropic. Their stress-strain-history relationships are nonlinear. Arterial properties vary with the sites along the arterial tree, aging, short or long-term effects of drugs, hypertension, and innervation or denervation. When all these factors are coupled, the problem of how to describe the mechanical properties of tissues in a simple and accurate mathematical form becomes quite acute.

A popular approach to nonlinear elasticity uses the incremental law: a linearized relationship between the incremental stresses and strains obtained by subjecting a material to a small perturbation about a condition

of equilibrium. This approach was applied to the arteries in the 1950s. But the elastic constants so determined are meaningful only if the initial state from which the perturbations are applied is known, and are applicable only to that state. It turns out that these incremental moduli are strongly dependent on the initial state of stress, (and, for some tissues, on strain history). Usually the incremental law is derived for a selected meaningful equilibrium state, such as the state of uniform expansion in all directions, or a well defined physiological state.

An example is shown in Fig. 7.7:1, in which the little loops inside the large loops are stress-strain relations obtained when a dog's mesentery was subjected to small cyclic variations of strain.

An important feature of the incremental stress-strain relationship is revealed in Fig. 7.7:1. The small loops are not parallel to each other. Neither are they tangent to the loading or unloading curves of the large loop. Thus the incremental law does vary with the level of stress, and is *not equal* to the tangent of the loading or unloading curve of finite strain. This important observation must be borne in mind when one considers the relationship between the incremental law and the stress-strain relation in finite deformation. There are many authors who derive a relationship between stress and strain in finite strain (usually in a loading process) and carelessly identify its derivative with the modulus of the incremental law. One should expect

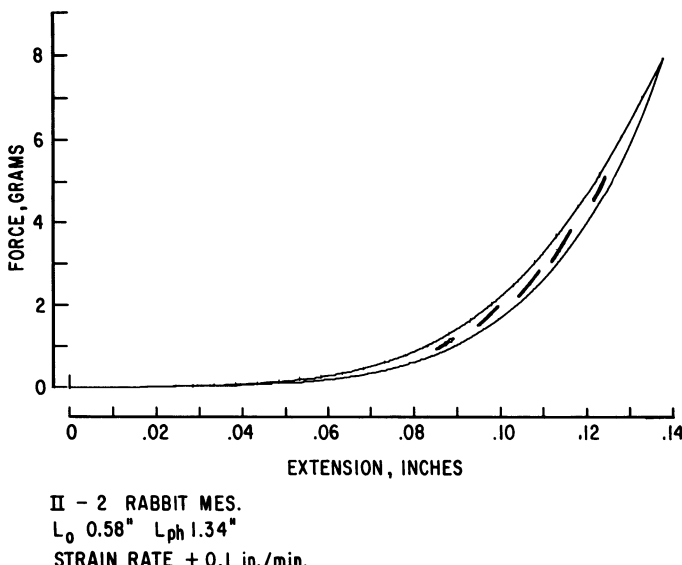


Figure 7.7:1 Typical loading-unloading curves of the rabbit mesentery tested in uniaxial tension at 25°. The large loops were obtained when the specimen was stretched and unloaded between $\lambda = 1$ and $\lambda = 1.24$. The small loops were obtained by first stretching the specimen to the desired strain, then performing loading and unloading loops of small amplitude. Preconditioning was done in every case. From Fung (1967).

that in general they would not agree. The incremental moduli should be determined by incremental experiments.

Since the relationship between the incremental stresses and the infinitesimal incremental strains is linear, the methods of the classical linearized theory of elasticity is applicable. For finite deformation, Biot (1965) has shown how the incremental law can be used step by step to deal with finite deformation. Biot's research is especially important in dealing with those cases in which the strains are small but the rotations are large. The coefficients in the incremental law of biological tissues are more sensitive to the state of stress than the examples considered by Biot, but the method of the finite element can take care of the complications.

Successful incremental laws have been developed by Wilson (1972) and Lai-Fook et al. (1976, 1977) for lung tissue in small perturbation from a state of uniform expansion, and by Bergel (1961), Patel and Vaishnav (1972), and others for large blood vessels.

For most problems in finite deformation of tissues in organ physiology, it is more convenient to use constitutive equations relating stresses to finite strains. For the purpose of comparing changes of mechanical properties of a tissue due to the states of health and disease, or to drugs and other factors, it may also be more convenient to compare material constants involved in the constitutive equation for finite deformation.

One's ability to identify the constitutive equation of a tissue is based on the tissue's being able to be *preconditioned*. To test a tissue in any specific procedure of loading and unloading, it is necessary to perform the loading cycle a number of times before the stress-strain relationship is repeatable. This process is called *preconditioning*. Confining our attention to preconditioned tissues subjected to cyclic loading and unloading at constant strain rates, we see that by the definition of preconditioning, the stress-strain relationship is well defined, repeatable, and predictable. For the *loading branch* and the *unloading branch* separately, the stress-strain relationship is unique.

Since stress and strain are uniquely related in each branch of a specific cyclic process, we can treat the material as one elastic material in loading, and another elastic material in unloading. Thus we can borrow the method of the theory of elasticity to handle an inelastic material. To remind us that we are really dealing with an inelastic material, we call it *pseudo-elasticity*.

Pseudo-elasticity is, therefore, not an intrinsic property of the material. It is a convenient description of the stress-strain relationship in specific cyclic loading. By its use the very complex property of the tissue is more simply described. Fortunately, the usefulness of the concept of pseudo-elasticity is greatly enhanced by the fact that it is rather insensitive to the strain rate. By virtue of rate insensitivity, pseudo-elasticity acquires a certain measure of independence.

The strain-rate insensitivity has been demonstrated in Sec. 7.5; e.g., in Fig. 7.5:2. A large amount of data exists on various soft tissues which shows

that for a 1000-fold change in strain rate that can be easily achieved in most laboratories, the change in stress for a given strain usually does not exceed a factor of 1 or 2. The extreme situation is encountered in ultrasound experiments. It is known that with few exceptions the energy dissipation does not change more than a factor of two or three when the frequency changes from 1000 Hz to 10^7 Hz. Dunn et al. (1969) reviewed the subject critically, and showed that for most tissues the attenuation per cycle is virtually independent of frequency (see their curves of α/f versus f , where f is the frequency, α is the attenuation per unit distance, and α/f is the attenuation per wave). Although stress fluctuation is very small in the ultrasound experiments, as compared with the stress variation in the arterial wall due to pulsatile blood flow, yet it is interesting to observe this uniform behavior in a frequency range from nearly 0 to millions of Hz. Translated into the language of the relaxation spectrum presented in Eq. (30) of Sec. 7.6, the ultrasound experiments suggest that the lower limit of relaxation time, τ_1 , is very small for most living tissues; perhaps in the range of 10^{-8} s.

The use of pseduo-elasticity for soft tissues is very convenient, but, of course, it is only an approximation. A detailed account of the frequency effect is not simple. All who have looked for the effect of strain-rate on the stress-strain relationship of living tissues found it. McElhaney (1966), in his study of the dynamic response of muscles, shows that there is a 2.5-fold increase in stress at any given strain when the strain rate is increased from 0.001 to 1000 per second, an increase of 10^6 -fold. Van Brocklin and Ellis (1965) state that in tendons there is no strain-rate effect when the rate is small, but the effect becomes significant when the rate is high. Collins and Hu (1972), using explosive methods (as in a shock tube) to impose a high strain rate ($\dot{\varepsilon}$) onto human aortic tissue (a study relevant to the safety against automobile crash problem), obtained the result

$$\sigma = (0.28 + 0.18\dot{\varepsilon})(e^{12\dot{\varepsilon}} - 1) \quad \text{for } \dot{\varepsilon} < 3.5 \text{ s}^{-1}. \quad (1)$$

Bauer and Pasch (1971), working with rat tail artery, found that the dynamic Young's modulus is independent of frequency from 0.01 to 10 Hz, but the loss coefficient does vary with frequency. All these do not give a uniform picture, but our suggestion of pseudo-elasticity representation does offer a great simplification.

The mathematical formulation presented in Sec. 7.6 is consistent with the concept of pseudo-elasticity. We introduced the concept of "elastic response" $T^{(e)}$ and formulated a quasi-linear viscoelasticity law. By the introduction of a broad continuous spectrum of relaxation time into the viscoelasticity law we made the hysteresis nearly constant over a wide range of frequencies. In this way we unified the phenomena of the nonlinear stress-strain relationship, relaxation, creep, hysteresis, and pseudo-elasticity into a consistent theory. The utility of the pseudo-elasticity concept, however, lies in the possibility to describe the stress-strain relationship in loading

or unloading by a law of elasticity, instead of viscoelasticity. Further simplification is obtained if one assume that a strain energy function exists. We shall discuss this in the following section.

7.8 Biaxial Loading Experiments on Soft Tissues

The uniaxial loading experiments discussed so far cannot provide the full relationship between all stress and strain components. To obtain the tensorial relationship, it is necessary to perform biaxial and triaxial loading tests.

Figure 7.8:1 shows a possible way of testing a rectangular specimen of uniform thickness in biaxial loading. Figure 7.8:2 shows the schematic view of the equipment developed in the author's laboratory. The specimen floats in physiological saline solution contained in an open-to-atmosphere upper compartment of a double compartment tray. The lower compartment is a part of a thermoregulation system. Water of specified temperature is supplied by a temperature regulator. The solution is slowly circulated, compensated for evaporation from time to time, and maintained at pH 7.4 by bicarbonate buffer.

The specimen is hooked along its four edges by means of small staples. Each hook is connected by means of a silk thread to a screw on one of the four force-distributing platforms (see Fig. 7.8:1). This setup allows individual adjustment of the tension of each thread. The force-distributing platforms

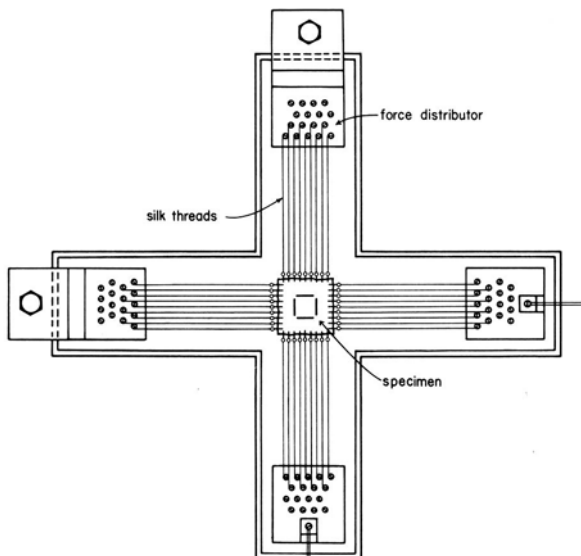


Figure 7.8:1 Setup of specimen hooking and force distribution. From Lanir and Fung (1974a).

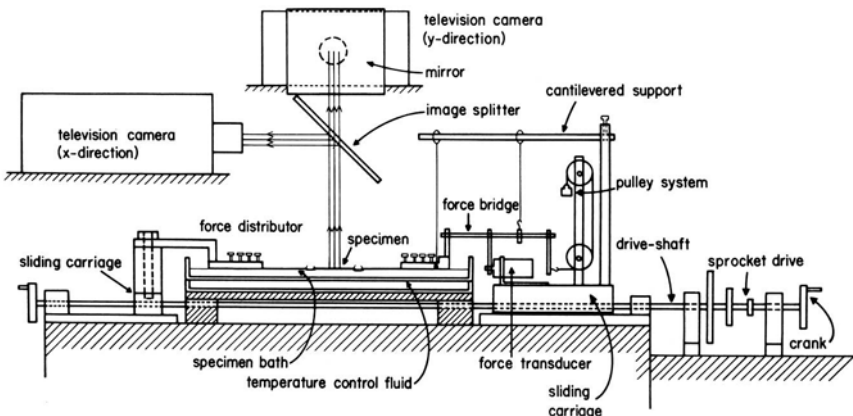


Figure 7.8:2 Schematic view of stretching mechanism in one direction and optical system. From Lanir and Fung (1974a).

are bridged over the edges of the saline tray in an identical manner for both directions (Fig. 7.8:2). One platform is rigidly mounted to the carriage of a sliding mechanism, the opposite platform is horizontally attached to a force transducer. Both the support and transducer are rigidly connected to the carriage of another sliding unit. A pulley system on this carriage allows the force distributor to be pulled by a constant weight on top of the force exerted by the transducer. The carriages of the opposite sliding units are displaced by means of an interconnected threaded drive-shaft. The threads of the left and right sliding units are pulled by the drive shaft at an equal rate in opposite directions, so that the specimen can be stretched or contracted without changing its location.

The loading strings are approximately parallel when the equipment is in operation. For a specimen varying in size from 3×3 to 6×6 cm the maximum deviation of the loading strings from the centerline is less than 0.05 rad. Thus at the very corners of the rectangular specimen a shear stress of the order of $\frac{1}{20}$ th of the normal stress may exist at the maximum stretch. However, the distance between the "bench marks" (the black rectangular marks) whose dimensional changes are measured is approximately half of the overall dimensions; therefore the maximum shear stress acting at the corners of the bench marks is expected to be no more than 2 or 3% of the normal stress. These strings are "tuned" (in the manner of piano tuning by turning a set of screws) at the beginning (during the preconditioning process) in such a way that the rectangular bench marks made on a relaxed specimen remain rectangular upon loading, without visible distortion.

The dimensions of the specimen are continuously measured and monitored by a video dimension analyzer (VDA). This system consists of a television camera, a video processor, and a television monitor. The video processor provides an analog signal proportional to the horizontal distance

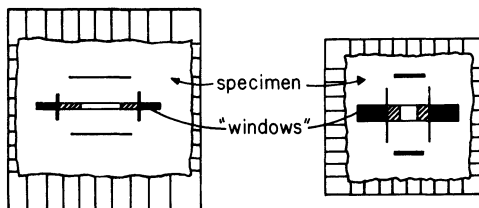


Figure 7.8:3 Typical display of the specimen on the two VDA monitors. From Lanir and Fung (1974a).

between independently selectable levels of optical density, in two independent areas (windows) in the televised scene. (Fig. 7.8:3). The video processor operates directly with the composite video signal from the camera. It utilizes the vertical and horizontal synchronization pulses to define the $X-Y$ coordinates of the windows as well as their height and width. When video signal is within the window it is continuously compared with a preselected voltage which corresponds to the shade of grey of the edge being measured. When the raster voltage exceeds this reference, a counting circuit is started. The circuit is stopped by a similar process in the second window, and the count thus becomes a measure of the distance between the desired shades of grey. Each raster line within the windows is processed in the same fashion. The final count is averaged exactly and then presented to a sample and hold circuit that is updated in the next frame, when the whole procedure is repeated.

The strain in the specimen can be measured in two perpendicular directions. Two pairs of parallel black lines are painted on the specimen. The distance between each pair of these lines is analyzed by an independent VDA.

The stretching mechanism can stretch the tissue in two directions either independently or coordinated according to a prescribed program. The control unit, feedback system, and the performance characteristics are described in Lanir and Fung (1974a). Applications to the testing of skin are presented in Lanir and Fung (1974b). Applications to the testing of lung tissue, with an additional method for thickness measurement, are presented in Vawter, Fung and West (1978). A more recent model uses a digital computer to control the stretching in the two directions, and record and analyze the data. Similar equipment used to perform biaxial loading tests on arteries is described by Fronek et al. (1976), a sketch of which is given in Fig. 2.14:5.

The biaxial-loading testing equipment has to be much more elaborate than the uniaxial one because of the need to control boundary conditions. The edges must be allowed to expand freely. In the target region, the stress and strain states should be uniform so that data analysis can be done simply. The method described above is aimed at this objective. The target region is small and away from the outer edges in order to avoid the disturbing influence of the loading device. Strain is measured optically to avoid mechanical disturbance.

Triaxial loading experiments on cuboidal specimens of lung tissue using hooks and strings for loading have been done by Hoppin et al. (1975). But there is no way to observe a smaller region inside the cuboidal specimen.

Whole Organ Experiments

An alternative to testing excised tissues of simple geometry is to test whole organs. For the lung, one observes a whole lobe *in vivo* or *in vitro*. For the artery, one measures its deformation when internal or external pressures are changed, or when longitudinal tension is imposed. In whole organ experiments, the tissues are not subjected to traumatic excision, and one can measure their mechanical properties in conditions closer to *in vivo* conditions. But usually there are difficulties in analyzing whole organ data, either because of difficulties in knowing the stress and strain distributions, or because some needed pieces of data cannot be measured. On the other hand, no experiment on an excised tissue can be considered complete without an evaluation of the effect of the trauma of dissection. Therefore, whole organ experiments and excised tissue experiments complement each other.

7.9 Description of Three-Dimensional Stress and Strain States

To avoid getting into overly complicated situations, let us consider a rectangular plate of uniform thickness and of orthotropic material as shown in Fig. 7.9:1. Two pairs of forces F_{11} , F_{22} , act on the edges of the plate. No shear stress acts on these edges; hence we say that the coordinate axes x , y are the *principal axes*. Let the original (unstressed) size of the rectangle be L_{10} , L_{20} . After the imposition of the forces the plate becomes bigger, and the edge lengths become L_1 , L_2 . Let the thickness of the original and the

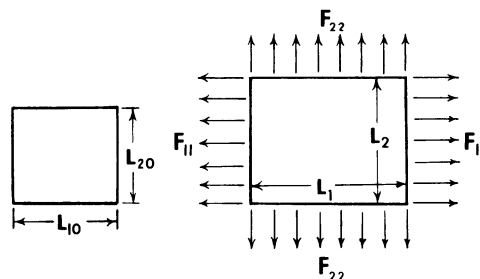


Figure 7.9:1 Deformation of a rectangular membrane. The membrane is subjected to tensile forces in the x and y directions. There is no shear force acting on the edges. The directions x , y are, therefore, the principal directions. From the forces and the deformation, various stresses and strains are defined in Eqs. (1) through (5).

deformed plate be h_0 and h , respectively. Then we define the stresses

$$\begin{aligned}\sigma_{11} &= \frac{F_{11}}{L_2 h}, & \sigma_{22} &= \frac{F_{22}}{L_1 h}, & T_{11} &= \frac{F_{11}}{L_{20} h_0}, & T_{22} &= \frac{F_{22}}{L_{10} h_0}, \\ S_{11} &= \frac{1}{\lambda_1} T_{11} = \frac{\rho_0}{\rho} \frac{1}{\lambda_1^2} \sigma_{11}, & S_{22} &= \frac{1}{\lambda_2} T_{22} = \frac{\rho_0}{\rho} \frac{1}{\lambda_2^2} \sigma_{22},\end{aligned}\quad (1)$$

where σ_{11} , σ_{22} are stresses defined in the sense of Cauchy and Euler. T_{11} , T_{22} are stresses defined in the sense of Lagrange and Piola, and S_{11} , S_{22} are stresses defined in the sense of Kirchhoff. ρ_0 and ρ are the densities of the material in the initial and deformed states, respectively. Clearly these three stresses are convertible to each other. All three are used frequently. Lagrangian stresses are the most convenient for the reduction of laboratory experimental data. Kirchhoff stresses are directly related to the strain energy function. Eulerian or Cauchy stresses are used in equations of equilibrium or motion. Thus in practice the little effort of remembering all three definitions can be well repaid.

For the description of deformation, the ratios

$$\lambda_1 = \frac{L_1}{L_{10}}, \quad \lambda_2 = \frac{L_2}{L_{20}} \quad (2)$$

are defined as the principal stretch ratios. The strains

$$E_1 = \frac{1}{2}(\lambda_1^2 - 1), \quad E_2 = \frac{1}{2}(\lambda_2^2 - 1) \quad (3)$$

are defined and used according to the method of Green and St. Venant, whereas

$$e_1 = \frac{1}{2} \left(1 - \frac{1}{\lambda_1^2} \right), \quad e_2 = \frac{1}{2} \left(1 - \frac{1}{\lambda_2^2} \right) \quad (4)$$

are defined and used according to Almansi and Hamel. See Chapter 2, Sec. 2.3. The strain measures

$$\varepsilon_1 = \frac{L_1 - L_{10}}{L_{10}} = \lambda_1 - 1, \quad \varepsilon_2 = \frac{L_2 - L_{20}}{L_{20}} = \lambda_2 - 1 \quad (5)$$

are called infinitesimal strains. Again, use of any one of these strain measures is sufficient. But the literature is strewn with all of them, and it pays to know their differences. They are different numerically. For example, if $L_1 = 2$ and $L_{10} = 1$, then $E_1 = \frac{3}{2}$, $e_1 = \frac{3}{8}$, and $\varepsilon_1 = 1$. But if the deformation is small, then E , e , and ε are approximately the same. For example, if $L_1 = 1.01$, $L_{10} = 1.00$, then $E_1 \doteq e_1 \doteq \varepsilon \doteq 0.01$. Green's strain and Almansi's strain both reduce to the infinitesimal strain when the deformation is infinitesimal.

In the description of a large deformation, it turns out that the most convenient quantity to consider is the square of the distance between any two points, because to the square of distances Pythagoras' rule applies. This is

why the Green and Almansi strains are introduced. Some authors call $\log \lambda$ the “true” strain, which is also a useful strain measure.

Theoretical analysis of bodies subjected to finite deformation is quite complex. A brief description suitable for biomechanics is given in the author’s *Foundations of Solid Mechanics*, Chapter 16. One of the most important results proved there is the use of the *strain potential*, or synonymously, the *strain-energy function*. Let W be the strain energy per unit mass of the tissue, and ρ_0 be the density (mass per unit volume) in the initial, unloaded, relaxed state, then $\rho_0 W$ is the strain energy per unit volume of the tissue in the initial state. Let W be expressed in terms of the nine strain components $E_{11}, E_{22}, E_{33}, E_{12}, E_{21}, E_{23}, E_{32}, E_{31}, E_{13}$, and be written in a form that is symmetric in the symmetric components E_{12} and E_{21} , E_{23} and E_{32} , and E_{31} and E_{13} . The nine strain components are treated as independent variables when partial derivatives of $\rho_0 W$ are formed. Then when such a strain-energy function exists, the stress components S_{ij} can be obtained as derivatives of $\rho_0 W$:

$$S_{ij} = \frac{\partial(\rho_0 W)}{\partial E_{ij}}. \quad (6)$$

More explicitly, for the rectangular element shown in Fig. 7.9:1, we have

$$S_{11} = \frac{\partial(\rho_0 W)}{\partial E_{11}}, \quad S_{22} = \frac{\partial(\rho_0 W)}{\partial E_{22}}, \quad S_{33} = \frac{\partial(\rho_0 W)}{\partial E_{33}}. \quad (7)$$

Not all elastic materials have a strain energy function. Those that do are called *hyperelastic* materials. (For definitions of elasticity, hyperelasticity, and hypoelasticity, see *Foundations of Solid Mechanics*, p. 445).

It can be shown that these formulas are equivalent to the following. Let W be expressed not in terms of E_{ij} but in the nine components of the *deformation gradient tensor* $\partial x_i / \partial a_j$, where (a_1, a_2, a_3) denote the coordinates of a material particle in the initial state of the body, and (x_1, x_2, x_3) are the coordinates of the same particle in the deformed state of the body, both referred to a rectangular cartesian frame of reference. Then the Lagrangian stresses are

$$T_{ij} = \frac{\partial(\rho_0 W)}{\partial(\partial x_i / \partial a_j)}. \quad (8)$$

Note that since $\partial x_i / \partial a_j$ is, in general, not equal to $\partial x_j / \partial a_i$, the tensor component T_{ij} is in general not equal to T_{ji} , i.e., T_{ij} is not symmetric. Referring to the rectangular element shown in Fig. 7.9:1, we have

$$T_{11} = \frac{\partial(\rho_0 W)}{\partial \lambda_1}, \quad T_{22} = \frac{\partial(\rho_0 W)}{\partial \lambda_2}, \quad T_{33} = \frac{\partial(\rho_0 W)}{\partial \lambda_3}, \quad (9)$$

where

$$\lambda_1 = \frac{\partial x_1}{\partial a_1}, \quad \lambda_2 = \frac{\partial x_2}{\partial a_2}, \quad \lambda_3 = \frac{\partial x_3}{\partial a_3} \quad (10)$$

are called the stretch ratios. It is useful also to record the general relationship between the Cauchy, Lagrange, and Kirchhoff stresses (see Fung, *Foundations of Solid Mechanics*, p. 439):

$$T_{ij} = S_{ip} \frac{\partial x_j}{\partial a_p}, \quad S_{ij} = \frac{\partial a_i}{\partial x_\alpha} T_{j\alpha}, \quad (11a)$$

$$\sigma_{ji} = \frac{\rho}{\rho_0} \frac{\partial x_i}{\partial a_p} T_{pi} = \frac{\rho}{\rho_0} \frac{\partial x_i}{\partial a_\alpha} \frac{\partial x_j}{\partial a_\beta} S_{\beta\alpha}, \quad (11b)$$

$$T_{ji} = \frac{\rho_0}{\rho} \frac{\partial a_j}{\partial x_m} \sigma_{mi}, \quad S_{ji} = \frac{\rho_0}{\rho} \frac{\partial a_i}{\partial x_\alpha} \frac{\partial a_j}{\partial x_m} \sigma_{mi} \quad (11c)$$

The question arises whether a strain energy function exists for a given material. If the material is perfectly elastic, then the existence of a strain energy function can often be justified on the basis of thermodynamics (see Sec. 7.4). But living tissues are not perfectly elastic. Therefore, they cannot have a strain-energy function in the thermodynamic sense. We take advantage, however, of the fact mentioned in Sec. 7.7, that in cyclic loading and unloading the stress-strain relationship after preconditioning does not vary very much with the strain rate. If the strain-rate effect is ignored altogether; then the loading curve and the unloading curve (they are unequal) can be separately treated as a uniquely defined stress-strain relationship, which is associated with a strain energy function. We shall call each of these curves a *pseudoelasticity* curve, and the corresponding strain energy function the *pseudo strain energy function*. The existence of a pseudo strain energy is an assumption that must be justified by experiments consistent with the accepted degree of approximation.

The formulas (6) and (8) need modification if the material is incompressible, i.e., if its volume does not change with stresses. For an incompressible material the *pressure* in the material is not related to the strain in the material. It is an indeterminate quantity as far as the stress-strain relationship is concerned. The pressure in a body of incompressible material can be determined only by solving the equations of motion or equilibrium and the boundary conditions. The general relationship in this case is

$$S_{ij} = \frac{\partial(\rho_0 W)}{\partial E_{ij}} - p \frac{\partial a_i}{\partial x_r} \frac{\partial a_j}{\partial x_r}, \quad (12)$$

where p is the pressure (see Fung, *Foundations of Solid Mechanics*, p. 450).

7.10 The Constitutive Equation of Skin

Although biaxial experiments alone are not sufficient to derive a three-dimensional stress-strain relationship, for membranous material they are sufficient to yield a two-dimensional constitutive equation for plane states

of stress. Such an equation connects the three components of stresses in the plane of the membrane with the three components of strains in the membrane.

Biaxial experiments on rabbit skin have been reported by Lanir and Fung (1974a,b) from whose data Tong and Fung (1976) gleaned the pseudo strain energy function for a loading process (increasing strain). The skin specimens were taken from the rabbit abdomen. It was first verified that the mechanical property was orthotropic, and that in cyclic loading and unloading at constant strain rates the stress-strain relationship is essentially independent of the strain rate. Hence the argument discussed in Sec. 7.7 applies and a pseudo strain energy function can be defined for either loading or unloading. Let the x_1 axis refer to direction along the length of the body, from head to tail, and the x_2 axis the direction of the width. Let $E_1 (= E_{11})$, $E_2 (= E_{22})$ be the strains defined in the sense of Green [see Eq. (3) of Sec. 7.9]. Tong and Fung (1976) chose the following form for the pseudo strain energy function for skin (the reason for this choice will be explained later (following Eq. (3) in this section):

$$\begin{aligned}\rho_0 W^{(2)} = & \frac{1}{2}(\alpha_1 E_1^2 + \alpha_2 E_2^2 + \alpha_3 E_{12}^2 + \alpha_3 E_{21}^2 + 2\alpha_4 E_1 E_2) \\ & + \frac{1}{2}c \exp(a_1 E_1^2 + a_2 E_2^2 + a_3 E_{12}^2 + a_3 E_{21}^2 + 2a_4 E_1 E_2) \quad (1) \\ & + \gamma_1 E_1^3 + \gamma_2 E_2^3 + \gamma_4 E_1^2 E_2 + \gamma_5 E_1 E_2^2),\end{aligned}$$

where the α 's, a 's, γ 's, and c are constants, and E_{12} is the shear strain [see Eq. (15) of Sec. 2.3] which is included in Eq. (1), but was kept at zero in the experiments. This is a two-dimensional analog of the strain energy function discussed in Sec. 7.9. If, for a membrane, we are concerned only with the plane state of stress caused by stretching in the plane of the membrane, then we may use such a two-dimensional strain energy function in the manner of Eq. (6) of Sec. 7.9 (with the index i, j limited to 1 and 2). Thus, from Eq. (1) above and Eqs. (6) or (7) of Sec. 7.9 we obtain the Kirchhoff stresses:

$$\begin{aligned}S_{11} &= \frac{\partial(\rho_0 W^{(2)})}{\partial E_1} = \alpha_1 E_1 + \alpha_4 E_2 + c A_1 X, \\ S_{22} &= \frac{\partial(\rho_0 W^{(2)})}{\partial E_2} = \alpha_2 E_1 + \alpha_2 E_2 + c A_2 X, \quad (2) \\ S_{12} &= \frac{\partial(\rho_0 W^{(2)})}{\partial E_{12}} = \alpha_3 E_{12} + c a_3 E_{12} X\end{aligned}$$

where

$$\begin{aligned}A_1 &= a_1 E_1 + a_4 E_2 + \frac{3}{2} \gamma_1 E_1^2 + \gamma_4 E_1 E_1 + \frac{1}{2} \gamma_5 E_2^2, \\ A_2 &= a_4 E_1 + a_2 E_2 + \frac{3}{2} \gamma_2 E_2^2 + \frac{1}{2} \gamma_4 E_1^2 + \gamma_5 E_1 E_2, \quad (3) \\ X &= \exp(a_1 E_1^2 + a_2 E_2^2 + a_3 E_{12}^2 + a_3 E_{21}^2 + 2a_4 E_1 E_2, \\ &+ \gamma_1 E_1^3 + \gamma_2 E_2^3 + \gamma_4 E_1^2 E_2 + \gamma_5 E_1 E_2^2).\end{aligned}$$

The first term in Eq. (1) was introduced because the data appear to be "biphasic." We use the second term to express the behavior of the material

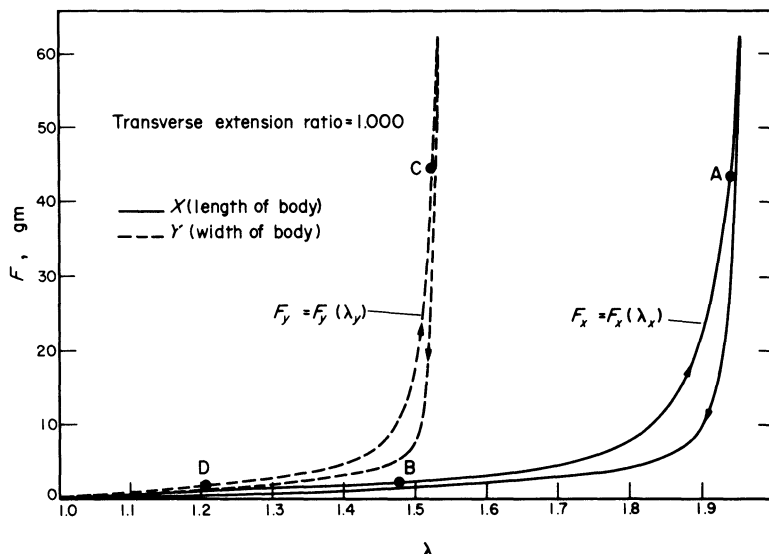


Figure 7.10:1 Force vs stretch ratio curves in the x experiments (λ_y was fixed while λ_x varied; solid curves) and in the y experiments (λ_x fixed; dotted). The choice of the points A, B, C, D is illustrated. In this example, $\lambda_y = 1$ in the x experiment, and $\lambda_x = 1$ in the y experiment. The difference of the curves is due to anisotropy. Rabbit abdominal skin: The x or x_1 -axis points in the direction from the head to the tail. From Tong and Fung (1976), by permission. Experimental results are from Lanir and Fung (1974b).

at a high stress level, and use the first term to remedy the situation at a lower stress level.

From Eqs. (2) we can compute the derivatives $\partial S_1 / \partial E_1$, $\partial S_2 / \partial E_2$, and $\partial S_1 / \partial E_2 = \partial S_2 / \partial E_1$. We then determine the constants denoted by the α 's, a 's, and c by requiring that S_{11} , S_{22} and their derivatives measured experimentally are fit exactly by the equations named above at some selected points. The choice of these points is illustrated in Fig. 7.10:1, in which the stress-strain relationships with E_2 fixed are shown in the solid curves, and those with E_1 fixed are shown by the dashed curves. A pair of points A and C are located on the curves in a region where stresses change rapidly, whereas the points B and D are located in a region in which the strains are relatively small. The constants α_1 , α_2 , α_4 are determined essentially by experimental data at B and D, whereas a_1 , a_2 , a_4 and c are determined essentially by the data at A and C. The exact locations of the points A, B, C and D are not very important. The values of the constants change very little by choosing different (reasonable) points on any two sets of data curves.

A typical comparison between the experimental data and the mathematical expression is shown in Fig. 7.10:2. In Fig. 7.10:2(a) the longitudinal force F_x is plotted against the longitudinal stretch ratio λ_x , while the transverse direction is kept at the natural length so that $\lambda_y = 1$, whereas in the other direction, F_y is plotted against λ_y , while λ_x is kept at 1. The experimental

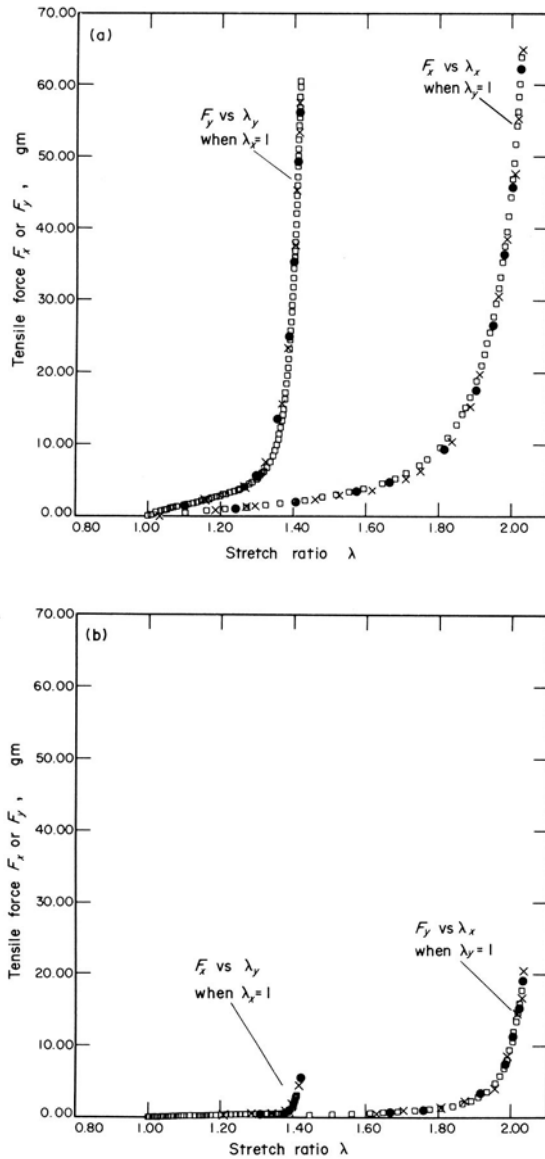


Figure 7.10:2 Comparison between experimental data and mathematical expression. The tensile forces F_x , F_y are given in g. Lagrange stress T_x is equal to F_x divided by A_x , the cross-sectional area perpendicular to the x axis. Squares: experimental data. Circles: from Eqs. (1) and (2) with $\alpha_1 = \alpha_2$, all γ 's = 0. $a_1 = 3.79$, $a_2 = 12.7$, $a_4 = 0.587$, $c = 0.00794$, $\alpha_1 = \alpha_2 = 10.4$, and $a_4 = 2.59$. Crosses: From Eq. (2) with $\alpha_1 = \alpha_2$, $\gamma_1 = \gamma_2 = 0$, $\gamma_4 = \gamma_5 \neq 0$. $a_1 = 3.79$, $a_2 = 18.4$, $a_4 = 0.587$, $c = 0.00794$, $\alpha_1 = \alpha_2 = 10.4$, and $a_4 = 2.59$. $\gamma_4 = \gamma_5 = 15.6$. From Tong and Fung (1976), by permission. Experimental data are from Lanir and Fung (1974b).

data points are shown as squares. Data computed from our theoretical formulas (1)–(7) are plotted as circles for case A (all γ 's = 0), and as crosses for case B ($\gamma_4 = \gamma_5$). The fit is good for the entire curve. In Fig. 7.10:2(b) the stress in the transverse direction is plotted against the longitudinal stretch ratio, while the transverse strain is kept at zero, and vice versa. Again the fit between the mathematical formula and the experimental data is good. Although these good fittings are not surprising because the constants α_1 , α_2 , etc., are determined from these two sets of experimental data, the ability of the mathematical formulas to fit the entire set of data when data at only four points on the curves are used is nontrivial. Considering the tremendous nonlinearity of these curves, one might say that the fitting is remarkably good.

One may conclude that the pseudo strain energy function, Eq. (1), is suitable for rabbit skin for stresses and strains in the physiological range. For all practical purposes, the third-order terms in the exponential function [the last line of Eq. (1)] involving the constants γ are unimportant; and there is no significant loss of accuracy if we set all γ 's equal to zero. Hence we may simplify Eq. (1) to the form

$$\rho_0 W^{(2)} = f(\alpha, e) + c \exp[F(a, e)], \quad (4)$$

where

$$f(\alpha, e) = \alpha_1 E_{11}^2 + \alpha_2 E_{22}^2 + \alpha_3 E_{12}^2 + \alpha_3 E_{21}^2 + 2\alpha_4 E_{11} E_{22}, \quad (5)$$

$$F(a, e) = a_1 E_{11}^2 + a_2 E_{22}^2 + a_3 E_{12}^2 + a_3 E_{21}^2 + 2a_4 E_{11} E_{22}. \quad (6)$$

Finally, if one is concerned mainly with higher stresses and strains in the physiological range, and does not care for great accuracy at very small stress levels, then the first term in Eq. (4) can be omitted, and we have simply

$$\rho_0 W^{(2)} = c \exp[F(a, e)]. \quad (7)$$

Other Examples

The pseudo strain energy function for arterial walls presented in Chapter 8, Sec. 8.6, is also of the form of Eq. (7). That for lung tissue is given by Fung (1975), Fung et al. (1978), and Vawter et al. (1979) and is also of the form of Eq. (7).

The genesis of Eqs. (1) and (7) lies in a general feature of soft tissues in simple elongation, described in Sec. 7.6. As shown in Eq. (2) of Sec. 7.6, the slope of the stress-strain curve is proportional to the tensile stress. As a consequence [Eq. (3) of Sec. 7.6], the stress is an exponential function of the strain. Generalizing this, Fung (1973) proposed a pseudo strain energy function in the form

$$W = \frac{1}{2} \alpha_{ijkl} E_{ij} E_{kl} + (\beta_0 + \beta_{mnpq} E_{mn} E_{pq}) \exp(\gamma_{ij} E_{ij} + \kappa_{ijkl} E_{ij} E_{kl} + \dots), \quad (8)$$

where α_{ijkl} , β_0 , β_{mnpq} , γ_{ij} , and κ_{ijkl} are constants to be determined empirically, and the indices $i, j, k \dots$, range over 1, 2, 3. The summation convention is used (Chapter 2, Sec. 2.2). Equations (1) and (7) are simplified versions of Eq. (8). It is amusing to note that it took several years before we realized that a better fit with experimental data can be obtained by dropping the first-order terms ($\gamma_{ij}E_{ij}$) in the exponential function in Eq. (8).

7.11 Generalized Viscoelastic Relations

Since we regard biosolids as viscoelastic bodies, it seems appropriate to conclude our discussion with a proposal for their constitutive equations. We have discussed the quasi-linear viscoelasticity of tissues in uniaxial state of stress in Sec. 7.6. It is logical to generalize the results to two or three dimensions by changing Eq. (7) of Sec. 7.6 into a tensor equation:

$$S_{ij}(t) = S_{kl}^{(e)}(0+)G_{ijkl}(t) + \int_0^t G_{ijkl}(t-\tau) \frac{\partial S_{kl}^{(e)}[\mathbf{E}(\tau)]}{\partial \tau} d\tau.$$

This generalization is analogous to the classical relation, Eq. (24) of Sec. 2.11. Here S_{ij} is the Kirchhoff stress tensor; \mathbf{E} , with components E_{ij} , is the Green's strain tensor; and G_{ijkl} is the reduced relaxation function tensor, the word "reduced" referring to the condition $G_{ijkl} = 1$ when $t = 0$. $S_{ij}^{(e)}$ is the "elastic" stress tensor corresponding to the strain tensor \mathbf{E} . It is a function of the strain components E_1, E_{22}, E_{12} , etc. $S_{ij}^{(e)}$ is the stress that is reached instantaneously when the strains are suddenly increased from 0 to E_{11}, E_{22} , etc. Following the arguments of Sec. 7.6, we assume that the "elastic" responses $S_{ij}^{(e)}$ can be approximated by the pseudoelastic stresses. The range of the indexes is 1, 2 if the material is a membrane subjected to a plane state of stress, and is 1, 2, 3 if it is a three-dimensional body.

Although G_{ijkl} is a tensor or rank 4, it will have only two independent components if the material is isotropic. If the material is anisotropic, a careful consideration of the material symmetry as presented in Green and Adkin's *Large Elastic Deformation* will be helpful. It is likely that G_{ijkl} will have a relaxation spectrum of the same kind as discussed in Sec. 7.6.

7.12 The Complementary Energy Function: Inversion of the Stress-Strain Relationship

If stresses are known analytic functions of strains, one should be able to express strains as analytic functions of stresses. In linear elasticity Hooke's law can be expressed both ways. In nonlinear elasticity, however, it is not always simple to invert a stress-strain law. For example, if the stress s is a cubic function of the strain ε

$$s = a\varepsilon + b\varepsilon^2 + c\varepsilon^3.$$

We know that ϵ cannot be expressed as a rational function of s, a, b , and c . If we think of ϵ, s, a, b, c as tensors, then an inversion is more difficult; in fact, unknown.

However, the exponential strain energy function given in Eq. (7) of Sec. 7.10 can be easily inverted. Such an inversion is useful whenever one wishes to calculate strains from known stresses; or when one wishes to use the complementary energy theorem in numerical analysis. Inversion is needed also if one wishes to use the method of stress functions, which is still applicable in finite deformation, because the equations of equilibrium remain linear when expressed in terms of Cauchy stresses.

The general theory is presented by Fung (1979). We express stresses in terms of strains in a constitutive equation

$$S_{ij} = \frac{\partial \rho_0 W}{\partial E_{ij}}, \quad (1)$$

where S_{ij} and E_{ij} are the Kirchhoff stress tensor and Green's strain tensor, respectively, W is the strain energy function (expressed in terms of strain) per unit mass, and ρ_0 is the density of the material in the initial, unstressed condition, so that $\rho_0 W$ is the strain energy per unit volume. Then according to the theory of continuum mechanics (see, for example, the author's *Foundations of Solid Mechanics*, p. 454), it is known that if the constitutive equation (1) can be inverted, there exists a complementary energy function $W_c(S_{11}, S_{12}, \dots)$ of the stress components, such that

$$\rho_0 W_c = S_{ij} E_{ij} - \rho_0 W, \quad (2)$$

in which the summation convention over repeated indexes is used, and

$$E_{ij} = \frac{\partial \rho_0 W_c}{\partial S_{ij}}. \quad (3)$$

On the other hand, if a complementary energy function can be found, then Eq. (3) at once gives the inversion of the stress-strain relation. The problem of inversion consists of finding $\rho_0 W_c$ from $\rho_0 W$ through the contact transformation given in Eqs. (2) and (3).

Let us relabel the six independent components of E_{ij} as E_1, E_2, \dots, E_6 , and the six independent components of stresses S_{ij} as S_1, S_2, \dots, S_6 . Let a square matrix $[a_{ij}]$ be symmetric and nonsingular. We define a quadratic form

$$Q = \sum_{i=1}^6 \sum_{j=1}^6 a_{ij} E_i E_j. \quad (4)$$

We shall show that if the strain energy function $\rho_0 W$ is an analytic function of Q ,

$$\rho_0 W = f(Q), \quad (5)$$

then it can be inverted. We proceed as follows. Since

$$S_i = \frac{\partial \rho_0 W}{\partial E_i} = \frac{df}{dQ} \frac{\partial Q}{\partial E_i} = 2 \frac{df}{dQ} \sum_{j=1}^6 a_{ij} E_j \quad (6)$$

is a linear equation for E_i , we can solve for E_i . Let us use matrix notations, with $\{ \}$ denoting a column matrix, $[]$ denoting a square matrix, T denoting transpose, and -1 power denoting inverse. Then we have

$$\{E_i\} = \left(2 \frac{df}{dQ}\right)^{-1} [a_{ij}]^{-1} \{S_j\}. \quad (7)$$

A substitution into Eq. (4) gives

$$Q = \left(2 \frac{df}{dQ}\right)^{-2} \{S_i\}^T [a_{ij}]^{-1} \{S_j\}. \quad (8)$$

If we define a polynomial P of stresses by

$$P = \frac{1}{4} \{S_i\}^T [a_{ij}]^{-1} \{S_j\}, \quad (9)$$

then Eq. (8) becomes

$$P = Q \left(\frac{df}{dQ}\right)^2. \quad (10)$$

When $f(Q)$ is given, Eq. (10) can be solved for Q as a function of P . Now according to Eqs. (2), (1), and (5),

$$\rho_0 W_c = \sum_{i=1}^6 \frac{df}{dQ} \frac{\partial Q}{\partial E_i} E_i - \rho_0 W. \quad (11)$$

Since Q is a homogeneous function of E_i of degree 2, we know by Euler's theorem for a homogeneous function that $E_i (\partial Q / \partial E_i) = 2Q$. Hence

$$\rho_0 W_c = 2Q \frac{df(Q)}{dQ} - f(Q). \quad (12)$$

When the solution of Eq. (10) is substituted into the right-hand side of Eq. (12), it becomes a function of P , i.e., of stresses. The inversion is thus accomplished.

Example

Although the derivation given above refers to three-dimensional cases, it applies equally well to two dimensions if appropriate changes are made in the range of the indexes. As an example, consider the strain energy function

given in Eq. (3) of Sec. 8.5, for arteries, for which

$$Q = a_1 E_1^2 + a_2 E_2^2 + 2a_4 E_1 E_2, \quad (13)$$

$$\rho_0 W = f(Q) = \frac{c}{2} e^Q. \quad (14)$$

Then Eq. (8) is reduced to

$$Q = c^{-2} (a_1 a_2 - a_4^2)^{-1} e^{-2Q} (a_2 S_1^2 + a_1 S_2^2 - 2a_4 S_1 S_2). \quad (15)$$

If we define in this case

$$P = c^{-2} (a_1 a_2 - a_4^2)^{-1} (a_2 S_1^2 + a_1 S_2^2 - 2a_4 S_1 S_2), \quad (16)$$

then P and Q are related by the equation

$$Q e^{2Q} = P, \quad (17)$$

which is independent of the material constants. Reading Q as a function P through Eq. (17) renders Eq. (12) a function of P . Q.E.D.

The Universal Function $Q(P)$

Note that Eq. (17) does not contain material constants, and it defines a universal relationship between P and Q for an exponential strain energy function. Taking the logarithm of both sides, we obtain

$$\ln Q + 2Q = \ln P. \quad (18)$$

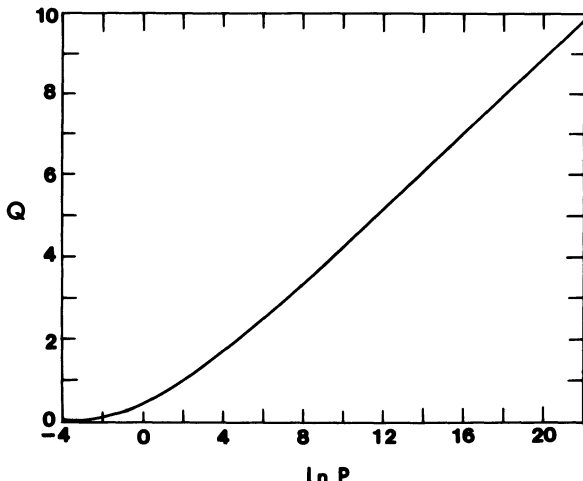


Figure 7.12:1 The universal function $Q(P)$ for inverting a nonlinear stress-strain relationship of the exponential type with the pseudo strain energy function given in Eqs. (13) and (14). From Fung (1979).

The function $Q(P)$ is best exhibited in terms of $\ln P$, as is given in Fig. 7.12:1.

Problems

- 7.3** The exponential integral $E(z)$ is defined by Eq. (38) of Sec. 7.6. It enters naturally into the relaxation function of a material with a continuous relaxation spectrum specified in Eq. (30) of Sec. 7.6. How does $E(z)$ behave when z is either very large or very small? Derive asymptotic formulas for this function when $z \rightarrow 0$ and $z \rightarrow \infty$.
- 7.4** Is there a two-dimensional strain energy function that corresponds to the stress-strain relation for the red blood cell membrane proposed in Eq. (7) of Sec. 4.7 in Chapter 4?
- 7.5** The following question is concerned with the practical process of data reduction. Experimental data on stress are usually tabulated at specified values of stretch ratio. Let the stretch ratios be uniformly spaced at $\lambda_0 + \Delta\lambda, \lambda_0 + 2\Delta\lambda, \dots$ and the corresponding stresses be T_1, T_2, \dots . From this we can compute the finite differences $\Delta T_n = T_n - T_{n-1}$, and evaluate the ratio $\Delta T / \Delta\lambda$ at $\lambda = \lambda_n$ as $\Delta T_n / \Delta\lambda$. Assume that a differential equation as given by Eq. (2) of Sec. 7.5 is valid. What is the corresponding difference equation (i.e. one expressed in terms of $\Delta T_n / \Delta\lambda$ and T_n)? In practice we examine the difference equation and then infer whether the differential equation is valid. The material constants α and β can be determined directly from the finite differences without going through the process of numerical differentiation.

- 7.6** Let the relaxation function be

$$G(t) = e^{-vt}$$

and the elastic response be given by Eq. (4) of Sec. 7.5:

$$T^{(e)}(\lambda) = (T^* + \beta)e^{\alpha(\lambda - \lambda^*)} - \beta$$

Find the tension history $T(t)$ for the following cases according to Eq. (4) of Sec. 7.6:

- (a) λ is a unit step function $1(t)$,
- (b) λ is a ramp function, $\lambda = 1 + ct$,
- (c) λ is oscillating, $\lambda = \lambda_0 + ce^{i\omega t}$

- 7.7** If the relaxation function $G(t)$ is given by Eqs. (28) and (30) of Sec. 7.6, and $T^{(e)}(\lambda)$ is given by Eq. (4) of Sec. 7.5, determine the tension history $T(t)$ according to Eq. (4) of Sec. 7.6 for the three cases named in Problem 7.6. For the case (c), work out the answer only for an oscillation of small amplitude, $c \ll 1$, so that the dependence on c can be linearized.

References

- Abramowitz, M., and Stegun, A. (1964) *Handbook of Mathematical Functions*. National Bureau of Standards, Applied Math. Ser. 55, U.S. Government Printing Office, Washington, D.C.
- Alexander, R. M. (1968) *Animal Mechanics*. University of Washington Press, Seattle.

- Bauer, R. D., and Pasch, Th. (1971) *Pflügers Arch.* **330**, 335–345.
- Becker, E., and Föppl, O. (1928) *Forschung aus dem Gebiete des Ingenieurwesens*. V.D.I., No. 304.
- Becker, E., and Döring, W. (1939) *Ferronmagnetismus*. Springer, Berlin, Chap. 19.
- Bergel, D. H. (1961) *J. Physiol.* **156**, 445–457(a); 458–469 (b).
- Biot, M. A. (1965) *Mechanics of Incremental Deformations*. Wiley, New York.
- Blatz, P. J., Chu, B. M., and Wayland, H. (1969) *Trans. Soc. Rheol.* **13**, 83–102.
- Bodner, S. R. (1968) In *Mechanical Behavior of Materials under Dynamic Loads*, Lindholm, U.S. (ed.). Springer, New York, pp. 176–190.
- Buchthal, F., and Kaiser, E. (1951) *The Rheology of the Cross Striated Muscle Fibre with Particular Reference to Isotonic Conditions*. Det Kongelige Danske Videnskabernes Selskab, Copenhagen, Dan. Biol. Medd. 21, No. 7, pp. 318.
- Chen, H. Y. L., and Fung, Y. C. (1973) In *1973 Biomechanics Symposium*. ASME Publ. No. AMD-2, American Society of Mechanical Engineers, New York, pp. 9–10.
- CifERRI, A. (1963) *Trans. Faraday Soc.* **59**, 562–569.
- Collins, R., and Hu, W. C. (1972) *J. Biomech.* **5**, 333–337.
- Cowan, P. M., North, A. C. T., and Randall, J. T. (1955) *Symp. Soc. Exp. Biol.* **9**, 115–126.
- Dale, W. C., and Baer, E. (1974) *J. Mater. Sci.* **9**, 369–382.
- Dale, W. C., Baer, E., Keller, A., and Kohn, R. R. (1972) *Experientia* **28**, 1293–1295.
- Diamant, J., Keller, A., Baer, E., Litt, M., and Arridge, R. G. C. (1972) *Proc. Roy. Soc. London B* **180**, 293–315.
- Dunn, F., Edmonds, P. D., and Fry, W. J. (1969) Ultrasound. In *Biological Engineering*, Schwan, H. P. (ed.) McGraw-Hill, New York, p. 205.
- Feughelman, M. (1963) *Nature* **200**, 127–129.
- Flory, P. J., and Garrett, R. R. (1958) *J. Am. Chem. Soc.* **80**, 4836–4845.
- Fronek, K., Schmid-Schoenbein, G., and Fung, Y.C. (1976) *J. Appl. Physiol.* **40**(4), 634–637.
- Fung, Y. C. (1965) *Foundations of Solid Mechanics*. Prentice-Hall, Englewood Cliffs, N. J.
- Fung, Y. C. (1967) *Am. J. Physiol.* **213**, 1532–1544.
- Fung, Y. C. (1968) *Appl. Mech. Rev.* **21**, 1–20.
- Fung, Y. C. (1972) In *Biomechanics: Its Foundations and Objectives*, Fung, Y. C., Perrone, N., and Anliker, M. (eds.) Prentice-Hall, Englewood Cliffs, N.J.
- Fung, Y. C. (1973) *Biorheology* **10**, 139–155.
- Fung, Y. C. (1975) *Circulation Res.* **37**, 481–496.
- Fung, Y. C. (1977) *A First Course in Continuum Mechanics*. Prentice-Hall, Englewood Cliffs, N.J.
- Fung, Y. C. (1979) *J. Biomech. Eng. Trans. ASME* **101**, 23–27.
- Fung, Y. C., Tong, P., and Patitucci, P. (1978) *J. Eng. Mech. ASCE* **104**(EMI), 201–224.
- Gathercole, L. J., Keller, A., and Shah, J. S. (1974) *J. Microscopy* **102**, 95–105.
- Green, A. E., and Adkins, J. E. (1960) *Large Elastic Deformations*. Oxford University Press, New York.

- Guth, E., Wack., P. E., and Anthony, R. L. (1946) *J. Appl. Phys.* **17**, 347–351.
- Hardung, V. (1952) *Helv. Physiol. Pharm. Acta* **10**, 482–498.
- Harkness, R. D. (1966) *Collagen. Sci. Progr.* **54**, 257–274.
- Harkness, M. L. R., and Harkness, R. D. (1959a) *J. Physiol.* **148**, 524–547.
- Harkness, M. L. R., and Harkness, R. D. (1959b) *Nature* **183**(1), 821–822.
- Hearle, J. W. S. (1958) *J. Polymer Sci.* **28**, 432–435.
- Hearle, J. W. S. (1963) *J. Appl. Polymer Sci.* **7**(1), 172–192; 207–223.
- Hearle, J. W. S.: and Peters, R. H. (eds.) (1963) *Fiber Structure*. The Textile Institute and Butterworths, London.
- Hiltner, A., Nomura, S., and Baer, E. (1974) In *Peptides, Polypeptides, and Proteins*, Blout, Bovey, Goodman, and Lotan, (eds.). Wiley, New York.
- Hoppin, F. G., Lee, J. C., and Dawson, S. V. (1975) *J. Appl. Physiol.* **39**, 742–751.
- Kastelic, J., Galeski, A., and Baer, E. (1978) *J. Connective Tissue Res.*, **6**, 11–23.
- Kenedi, R. M., Gibson, T., and Daly, C. H. (1964) In *Structure and Function of Connective and Skeletal Tissue*, Jackson, S. F., Harkness, S. M., and Tristram, G. R. (eds.). Scientific Committee, St. Andrews, Scotland, pp. 388–395.
- Knopoff, L. (1965) In *Physical Acoustics*, Mason, W. P. (ed.). Academic Press, Inc, New York. Vol. IIIB, Chapter 7.
- Lai-Fook, S. J. (1977) *J. Biomechanics*, **10**, 357–365.
- Lai-Fook, S. J., Wilson, T. A., Hyatt, R. E., and Rodarte, J. R. (1976) *J. Appl. Physiol.* **40**, 508–513.
- Lanczos, C. (1956) *Applied Analysis*. Prentice-Hall, Englewood Cliffs, N.J.
- Lanir, Y., and Fung, Y. C. (1974) *J. Biomech.* **7**, 29–34(a); 171–182(b).
- Lee, J. S., Frasher, W. G., and Fung, Y. C. (1967) *Two-dimensional finite-deformation on experiments on dog's arteries and veins*. Tech. Rept. No. AFOSR 67–1980, University of California, San Diego, Calif.
- Lee, J. S., Frasher, W. G., and Fung, Y. C. (1968) *J. Appl. Physiol.* **25**, 799–801.
- McElhaney, J. H. (1966) *J. Appl. Physiol.* **21**, 1231–1236.
- Mason, W. P. (1969) *A source of dissipation that produces an internal friction independent of the frequency*. Rept. No. 61, contract NONR 266(91), Dept. of Civil Eng. & Eng. Mech., Columbia University, New York.
- Moooney, M. (1940) *J. Appl. Phys.* **11**, 582–592.
- Morgan, F. R. (1960) *J. Soc. Leather Trades Chem.* **44**, 171–182.
- Neubert, H. K. P. (1963) *Aeronaut. Quart.* **14**, 187–197.
- Patel, D. J., Tucker, W. K., and Janicki, J. S. (1970) *J. Appl. Physiol.* **28**, 578–582.
- Patel, D. J. and Vaishnav, R. N. (1972) In *Cardiovascular Fluid Dynamics*, Bergel, D. H. (ed.). Academic, New York, Vol. 2, pp. 1–64.
- Pinto, J., and Fung, Y. C. (1973) *J. Biomech.* **6**, 597–616; 617–630.
- Ridge, M. D., and Wright, V. (1964) *Biorheology* **2**, 67–74.
- Rivlin, R. S. (1947) *J. Appl. Phys.* **18**, 444–449.
- Rivlin, R. S., and Saunders, D. W. (1951) *Phil. Trans. A.* **243**, 251–288.
- Routbart, J. L., and Sack, H. S. (1966) *J. Appl. Phys.* **37**, 4803–4805.
- Theodorsen, T., and Garrick, E. (1940) *Mechanism of flutter*. Rept. 685, U.S. Nat. Adv. Comm. Aeronaut.

- Tong, P., and Fung, Y. C. (1976) *J. Biomech.* **9**, 649–657.
- Torp, S., Arridge, R. G. C., Armeniades, C. D., and Baer, E. (1974) In *Proc. 1974 Colston Conf.*, Dept. of Physics, University of Bristol, U.K., pp. 197–222.
- Torp, S., Baer, E., and Friedman, B. (1974) *Proc. 1974 Colston Conf.*, pp. 223–250.
- Treloar, L. R. G. (1967) *The Physics of Rubber Elasticity*, 2nd ed. Oxford University Press, New York.
- Valanis, K. C., and Landel, R. I. (1967) *J. Appl. Phys.* **38**, 2997–3002.
- Van Brocklin, J. D., and Ellis, D. (1965) *Arch. Phys. Med. Rehab.* **46**, 369–375.
- Vawter, D., Fung, Y. C., and West, J. B. (1978) *J. Appl. Physiol.* **45**(2), 261–269.
- Vawter, D., Fung, Y. C., and West, J. B. (1979) *J. Biomech. Eng., Trans. ASME* **101**, 38–45.
- Veronda, D. R., and Westmann, R. A. (1970) *J. Biomech.* **3**, 111–124.
- Viidik, A. (1966) In *Studies on the Anatomy and Function of Bone and Joints*, Evans, F. G. (ed.), Springer, New York, pp. 17–39.
- Viidik, A. (1973) *Int. Rev. Connective Tissue Res.* Academic, New York, Vol. 6.
- Viidik, A. (1977) *Proc. Anatomisches Gessellschaft*, 72. Versammlung in Aachen.
- Wagner, K. W. (1913) *Ann. Physik* **40**, 817–855.
- Wertheim, M. G. (1847) *Ann. Chimie Physique, Paris*, Ser. 3, Vol. 21, pp. 385–414.
- Westerhof, N., and Noordergraaf, A. (1970) *J. Biomech.* **3**, 357–379.
- Wilson, T. A. (1972) *J. of Appl. Physiol.* **33**, 472–478.

CHAPTER 8

Mechanical Properties of Blood Vessels

8.1 Introduction

Blood vessels belong to the class of soft tissues discussed in Chapter 7. They do not obey Hooke's law. Figure 7.5:1 in Chapter 7, Sec. 7.5 demonstrates the nonlinearity of the stress-strain relationship and the existence of hysteresis. They also creep under constant stress and relax under constant strain. These mechanical properties must have a structural basis. In Sec. 8.2 we shall consider the structure of the blood vessel wall and its correlation with the mechanical properties. From Sec. 8.3 on, however, our attention will be concentrated on the mathematical description of the mechanical properties. In Secs. 8.3–8.5 we formulate a quasi-linear viscoelastic theory for blood vessels, using the pseudo-elasticity concept introduced in Chapter 7. In Sec. 8.6 we discuss the use of arterial pulse waves as a means to determine the mechanical properties of arteries. In Secs. 8.7–8.9 we consider the mechanical properties of arterioles, capillary blood vessels, venules, and veins. Finally, in Sec. 8.10, we discuss the long-term response of blood vessels to stresses: their reaction to hypertension, growth, regeneration, and resorption.

Blood vessel wall is a composite material that derives most of its elasticity through entropy changes (see Chapter 7, Sec. 7.4). It has no "natural" state, i.e., a unique state to which the material always returns when all the external stresses are removed. But in the living condition, blood vessels do experience homeostasis, at which the tissue reaches a mechanical and biochemical dynamic equilibrium in which causes and effects are uniquely related. Homeostasis is defined for each living condition, and any large change in living condition changes the homeostatic set point. In mechanical terms we say that the "natural" state changes.

When laboratory experiments on blood vessels are performed, new "natural" states can be established by repeated application of the same loading and unloading procedure. This process is called *preconditioning*. After preconditioning, the stress and strain relationship is uniquely established for each cyclic process. The results to be discussed below refer to preconditioned specimens.

8.2 Correlation of the Mechanical Properties of a Vessel with the Content and Structure of Its Material Composition

The arterial wall consists of three layers: the intima, media, and adventitia, as is illustrated in Fig. 8.2:1. The intima consists of the endothelial cells, the basement membrane, and a layer composed of a diffuse aggregation of delicate collagen, elastin, and reticular fibers, as well as smooth muscle and other cells. The transition to media is marked by an internal elastic membrane. The media is muscular, divided into concentric layers by elastic lamellae which, however, have fenestrations through which collagen and elastin fibers pass to tie the structure together three-dimensionally. Whereas the smooth muscle cells are frequently attached to elastic fibers (Fig. 8.2:2), the collagen fibers seem to run independently. In "relaxed", or rather, contracted blood vessels, the fibers seem to be randomly distributed in the

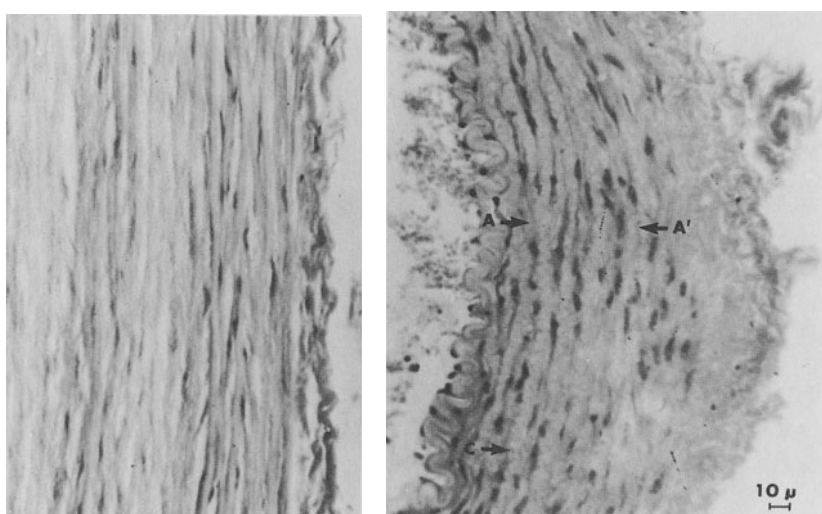


Figure 8.2:1 Photomicrograph of wall of the aorta (left) and femoral artery (right) at identical magnification. Internal diameter of aorta, 4 mm; that of femoral artery, 1 mm. The part between A and A' is the muscular media of the femoral artery; it is not present in the aorta. C is the serpiginous collagen bundle. From W. G. Frasher (1966), by permission.

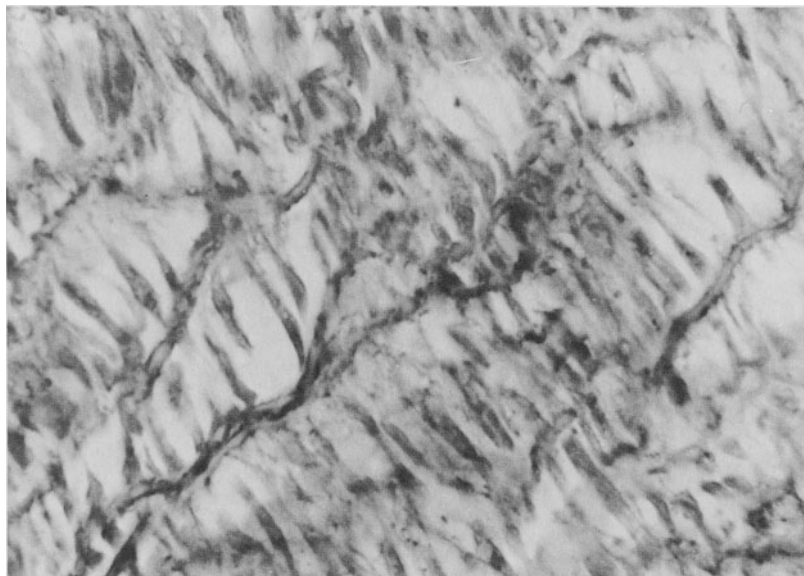


Figure 8.2:2 Photomicrograph of a portion of the aortic wall of a cat. The black, spindle-shaped structures are smooth muscle cells. Note that this “tension muscle” attaches independently to elastic fibrils at each end. From W. G. Frasher (1966), by permission.

lamellae. In the stretched state of the vessel, the helical pattern of the collagen fibers in the media becomes more evident. The adventitia outside the external elastic membrane is a loosely organized connective tissue.

The blood vessel walls themselves are supplied with blood flow (except the smallest blood vessels, whose cells are within a short distance, say $25\text{ }\mu\text{m}$, from blood). The blood vessels perfusing larger blood vessel walls are called *vasa vasorum*. An illustration for a pulmonary artery is given in Fig. 8.2:3. Arteries seem to be somewhat less dependent on the vascular supply for their integrity. Veins, however, rapidly degenerate when the vascular supply is interrupted.

The mechanical properties of a material depend not only on its composition, but also on its structure and ultrastructure. The properties of an artery depend not only on how much collagen it has, but also on how the collagen fibers are laid down in the tissue. Histological study of the contents is relatively easy, but a quantitative study of the structure is very difficult. For arteries, current knowledge about the structure remains at the level of qualitative description.

The structure of blood vessels varies along the arterial tree. Harkness et al. (1957) showed that there is a sharp distinction between the intrathoracic aorta and all other arteries, including the pulmonary artery, in terms of chemically determined elastin/collagen ratios. For the thoracic aorta the



Figure 8.2:3 Photograph of the pulmonary artery of a rabbit, showing the vasa vasorum in the wall. The wall substance has been rendered transparent by glycerin immersion. The microvessels have been injected with silicone elastomer. The white background is an injected mass filling the cavity of the artery. From W. G. Frasher (1966), by permission.

ratio of elastin/collagen is 2, and elsewhere it is $\frac{1}{2}$. The laminar structure of the media of the blood vessel changes along the arterial tree. In large arteries the number of lamellar layers increases with wall thickness, which itself is a constant proportion of the vessel diameter. In smaller arteries, such as femoral or carotid, the relative wall thickness is slightly increased, the elastin is less prominent in the media, and with increasing distance from the aorta, eventually only the inner and outer elastic laminae can be clearly seen. The muscle fibers increase in amount, arranged in quasi-concentric layers with prominent muscle-muscle attachment, and in a helical pattern that has finer pitch in the more peripheral vessels. As one passes more peripherally still, the muscularity increases, but in the capillaries only the endothelium remains.

The basic structure of the veins is similar to that of the arteries. The relative wall thickness is generally lower than in the arteries, and the media contains very little elastic tissue. The intimal surface of most larger veins is thrown into fine folds, which form crescentic semilunar valves, generally arranged in pairs and associated with a distinct sinus or local widening of the vessel. The adventitia of veins is relatively thick and contains much collagen. In the abdominal vena cava and its main tributaries, and in the

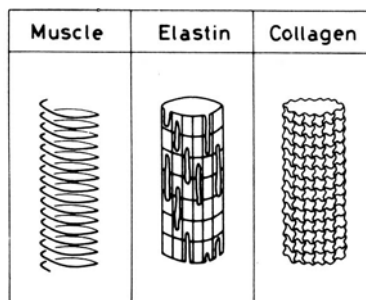


Figure 8.2:4 A sketch of the structure of the vein. From Azuma and Hasegawa (1973), reproduced by permission.

mesenteric veins, there are prominent longitudinal muscle fibers. Veins contain a relatively high amount of collagen; the collagen-elastin ratio is about 3:1.

Roach and Burton (1957) studied vessel elasticity before and after digestion with formic acid or trypsin to remove elastin and collagen, respectively. They showed that the slopes of the distensibility curves of the trypsin treated specimens were similar to those of the untreated specimens in the low stress region, whereas in the high stress region, whether the elastin was depleted or not did not seem to matter. Many other authors followed this line of attack to correlate the overall mechanical properties of a vessel with the content and structure of the material components.

Figure 8.2:4 shows a simplified and stylized drawing of the structure of veins by Azuma and Hasegawa (1973). They propose that the smooth muscle fibers are arranged in helices with very short pitch, that the elastin fibers form a network which has several longitudinal cracks, and that the collagen fibers from another network which is in a crimped state when the stress is low, and becomes increasingly stretched out as tensile strain increases. From such a structure it is easy to speculate on the possible stress-strain relationships of the vein. But this drawing is oversimplified. Real vessel wall structure is much more complex. See Bohr et al (1980), pp. 1–31, for greater details.

One notes, as shown in Figs. 8.2:5 and 8.2:6, the differences in the mechanical properties of elastin, collagen, and smooth muscle. Here ligament nuchae, with collagen denatured by heating at 76°C, represents elastin. It has a low elastic modulus, a very small hysteresis loop, and a very little stress relaxation. Tendon represents collagen; it has a moderate stress relaxation characteristic, a moderate hysteresis loop in cyclic loading and unloading, and a high stress response at smaller elongation. The smooth muscle characteristics are represented by that of the intestine. It has lower stress response and larger deformation, a tremendous hysteresis loop in cyclic loading, and a relaxation characteristic that tends to almost zero at large time. When a composite material is made up of components having such diverse properties, one expects the resultant to depend not only on the

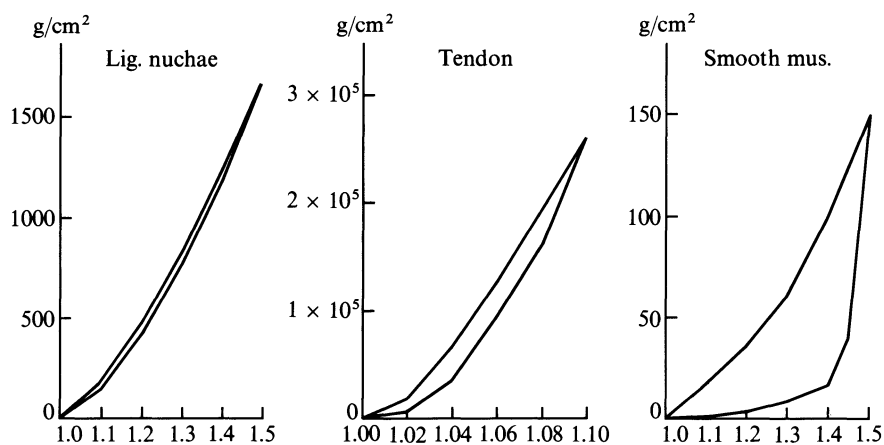


Figure 8.2:5 Patterns of hysteresis loop in non-vascular tissues: the ligamentum nuchae, tendon, and intestinal smooth muscle. The abscissas show the stretch ratio; the ordinates, stress. From Azuma and Hasegawa (1973), by permission.

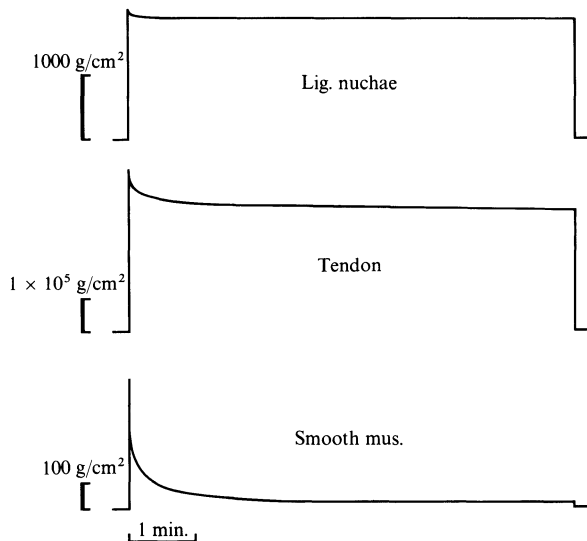


Figure 8.2:6 Patterns of stress relaxation in nonvascular tissues, i.e., the ligamentum nuchae, tendon, and intestinal smooth muscle. From Azuma and Hasegawa (1973), by permission.

composition, but also on the structure. One has to consider which element is brought into action at what strain level. The Azuma-Hasegawa proposal is consistent with the experimental finding that at a low strain level the elastin and smooth muscle contribute much to the elastic response, whereas at higher strain levels the collagen predominates. But these suggestions remain quali-

tative. To put these histological observations on a quantitative basis would be a rewarding effort for the future.

8.3 The Behavior of Arteries Under Uniaxial Loading

The simplest experiment that can be done on a blood vessel is the uniaxial loading test. Take a vessel, or a strip of the wall, pull it lengthwise, and record the force-elongation relationship. The lateral sides are left free.

Let the initial length of the specimen at the no-load condition be L_0 . Let the specimen be cylindrical in the initial condition, with a rectangular cross-section with width w_0 and thickness h_0 . L_0 , w_0 , h_0 are determined after preconditioning. The question arises whether L_0 , w_0 , h_0 so determined are unique, i.e., if they remain constant after various experiments. The answer depends on the type of stretching cycles imposed on the specimen. If a biaxial stretching is imposed on the specimen in such a way that the specimen is never shortened in x and y directions, then experience shows that the initial dimensions L_0 , w_0 , h_0 are preserved. On the other hand, if the lateral edges are permitted to shrink, as in uniaxial tests, the lateral dimensions are not controlled, and the uniqueness of L_0 may be lost. In other words, in uniaxial tests the lateral dimensions may gradually take on arbitrary changes that are irreversible. Thus a second measurement of L_0 after a course of uniaxial tests may yield a value that is different from the initial one; whereas in biaxial tests the value of L_0 will be preserved, provided that the stretch ratios λ_x , λ_y are never less than 1. Therefore, in reporting uniaxial tests, only the initial values of L_0 , w_0 , h_0 are used. This sets uniaxial tests apart from biaxial tests. Although the former is theoretically a special case of the latter, in reality it is a separate class.

Blood vessel specimens are often subjected to three types of tests: cyclic loading, creep, and relaxation. In a relaxation test a specimen is subjected to a sudden stretch and maintained at its new length for a period of time. The tension is recorded as a function of time. In a creep test, a constant force is suddenly applied to the specimen, and the continuous elongation of the specimen is recorded.

The ratio of the current length of the specimen, L , to the initial length L_0 , is the *stretch ratio*, λ . The load divided by the initial cross-sectional area A_0 yields the tensile stress T :

$$T = \frac{\text{load}}{A_0}. \quad (1)$$

An example of the stress-strain relationship, $T(\lambda)$, for a specimen of dog's aorta which was loaded at a constant rate until a maximum tension was reached and then immediately unloaded at the same constant rate (triangular strain history), is shown in Fig. 7.5:1.

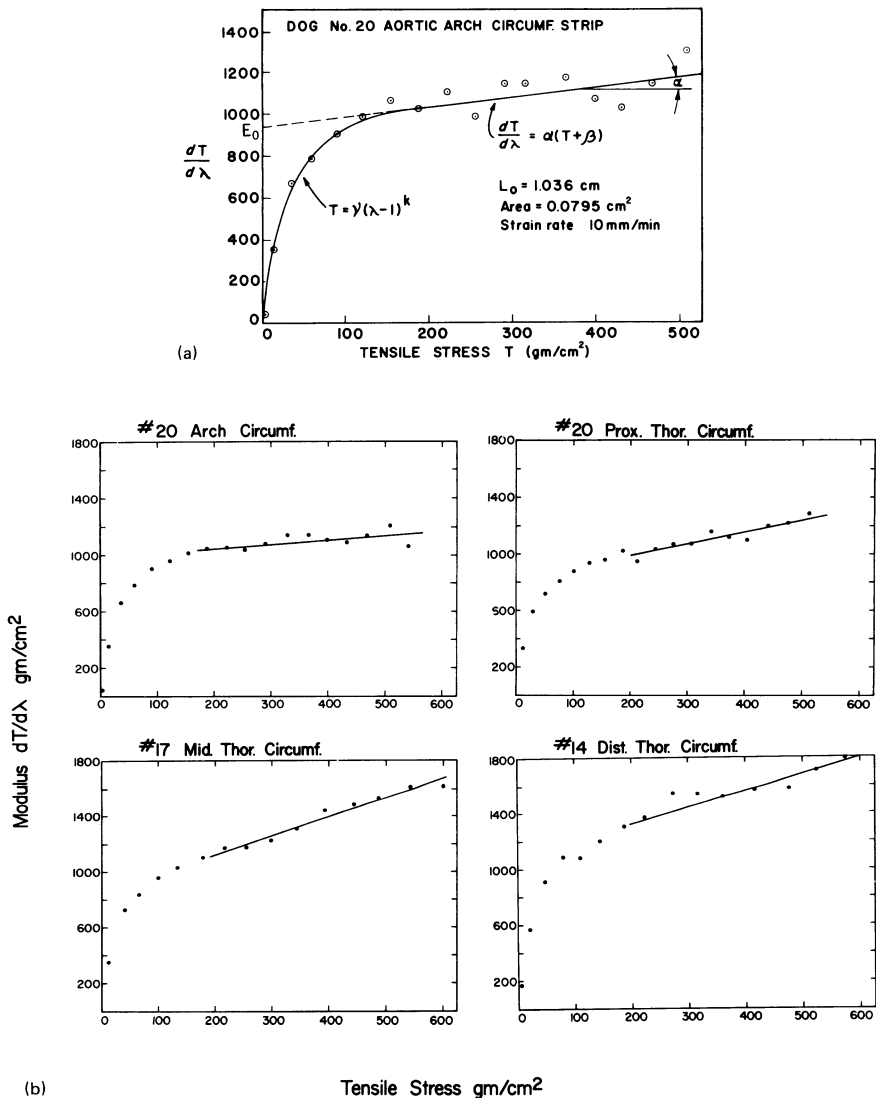


Figure 8.3:1 Plot of the Young's modulus (tangent modulus, $dT/d\lambda$) versus the tensile stress (T) in a specimen of thoracic aorta of the dog in a loading process. Part (a) shows a law for small T and an approximate straight line for T greater than 200 g/cm^2 . Part (b) shows the straight-line representation for various segments of the aorta. The straight line represents Eq. (5). From Tanaka and Fung (1974), by permission.

After a sufficient number of repeated cycling the stress-strain loop is stabilized and does not change any further. Then the stress can be related to the strain in the form

$$T = f_1(\lambda) \quad \text{when } \frac{d\lambda}{dt} > 0, \quad (2)$$

$$T = f_2(\lambda) \quad \text{when } \frac{d\lambda}{dt} < 0, \quad (3)$$

where f_1, f_2 are two functions. If $f_1(\lambda) = f_2(\lambda)$, then the material is *elastic*. If $f_1(\lambda) \neq f_2(\lambda)$, then the material is *inelastic*. Figure 7.5:1 shows that arteries are inelastic.

As it is discussed in Chapter 7, Sec. 7.6, the hysteresis loop of arteries is rather insensitive to strain rate. Mathematically this is equivalent to saying that $f_1(\lambda), f_2(\lambda)$ depend on the instantaneous values of λ and that their dependence on the rate of change of λ may be ignored in many cases.

A convenient way to examine the functions $f_1(\lambda)$ and $f_2(\lambda)$ is to plot the slope $dT/d\lambda$ against T . An example is shown in Fig. 8.3:1 [from Tanaka and Fung (1974)]. If a material obeys Hooke's law, such a plot will show a horizontal straight line. The example shows that the artery does not obey Hooke's law. For tensile stress T greater than 200 g/cm² and less than about 600 g/cm² (a physiological range, but much below the breaking strength of the aorta) the curves in Fig. 8.3:1 can be represented by straight lines, and the following approximation is valid:

$$dT/d\lambda = \alpha(T + \beta) = \alpha T + E_0, \quad (4)$$

where α, β , and $E_0 = \alpha\beta$ are constants. This implies an exponential stress-strain relationship (Fung, 1967)

$$T = (T^* + \beta)e^{\alpha(\lambda - \lambda^*)} - \beta \quad (5)$$

for $200 < T < 600$ g/cm², where (λ^*, T^*) represents one point on the stress-strain curve in the region of validity of Eq. (4).

The mean values of the physiological constants α and E_0 , defined for tensile stress in the range 200–600 g/cm², are presented in Fig. 8.3:2 for aortic specimens obtained by cutting strips in the longitudinal and circumferential directions along the aortic tree of the dog. The parameter α represents the rate of increase of the Young's modulus with respect to increasing tension (corresponding to the slope of the curves in Fig. 8.3:1 at stress T greater than 200 g/cm²). Figure 8.3:2 shows that for circumferential segments of arteries, α increases toward the periphery, i.e., arteries become more highly nonlinear further away from the heart. The corresponding data on α for the longitudinal segments show a less regular variation along the aortic tree. The parameter E_0 is the intercept of the straight line segment extended to $T = 0$. Figure 8.3:2 shows that E_0 varies greatly along the aortic tree; and its value for longitudinal segments can be very

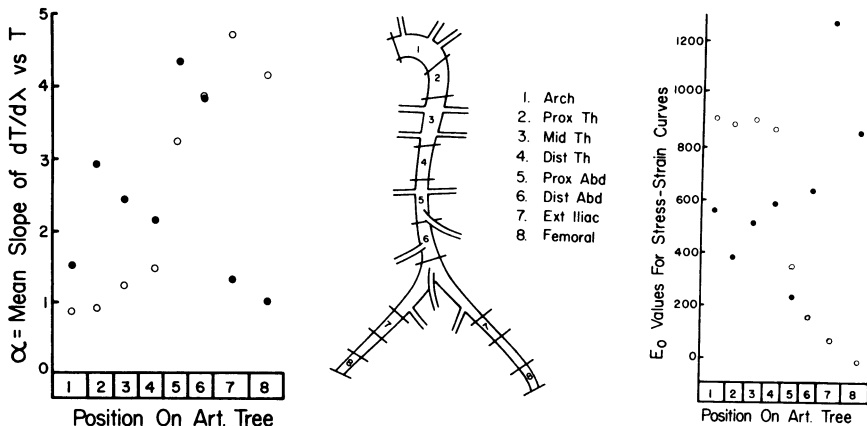


Figure 8.3:2 Middle panel: Sketch of arterial segments. Left panel: variation of α along the aortic tree. Open circles, circumferential segments. Filled circles, longitudinal segments. Right panel: variation of the constant E_0 of Eq. (4) describing the stress-strain curve in an exponential form. Open circles: circumferential segments. Filled circles: longitudinal segments. Numbering of segments: see middle panel. From Tanaka and Fung (1974), by permission.

different from that of the circumferential segments; the more so toward the periphery, further away from the heart. These differences undoubtedly reflect the structural changes in the arterial wall, with regard to the composition and configuration of collagen, elastin, and smooth muscle fibers, as well as ground substances.

Frank (1920) was the first to study the relationship between Young's modulus ($dT/d\lambda$) and stress (T). The linear relationship given in Eq. (4) is not inconsistent with the curves published by Frank [see Kenner, (1967) and Wetterer and Kenner (1968)]. Laszt (1968), Hardung (1953), and Bauer and Pasch (1971) presented similar data. Tanaka and Fung (1974) pointed out that such a relationship is valid only if the stress is sufficiently large; for low stress levels they showed that a power law fits the experimental data. A power law was used by Wylie (1966) in a theoretical analysis of arterial waves. The variation of the mechanical properties of blood vessels along the arterial tree has been studied by McDonald (1968), Anliker (1972), and others by means of arterial pulse waves, and by Azuma, Hasegawa, and Matsuda (1970) and Azuma and Hasegawa (1971) by *in vitro* experiments.

Stress Relaxation at a Constant Strain

As is the case with other tissues, the relaxation function of the aorta depends on the stress level. In the physiological range with stress $T > 200 \text{ g/cm}^2$, the relaxation function is normalizable; i.e., it is possible to express the

stress history in response to a *step change in strain* in the form

$$T(t, \lambda) = G(t) * T^{(e)}(\lambda) \quad G(0) = 1, \quad (6)$$

where $G(t)$ is a function of time, and $T^{(e)}(\lambda)$ is a function of strain, the $*$ symbol being a multiplication sign. If the strain history were continuously variable, it may be regarded as consisting of a superposition of many step functions, and the resulting stress history would still be given by Eq. (6), but the symbol $*$ has to be interpreted as a convolution integration. The function $G(t)$ is the *normalized relaxation function*. The function $T^{(e)}(\lambda)$ is the *pseudo-elastic stress* corresponding to the instantaneous stress ratio λ .

The mean normalized relaxation function $G(t)$ of the dog's aorta is shown in Fig. 8.3:3 (from Tanaka and Fung, 1974), in which the horizontal axis indicates the time elapsed after the step load, plotted on a logarithmic scale, whereas the vertical axis is the ratio of the tensile stress at t to that at the end of step strain. Figure 8.3:3 refers to circumferential segments of the arteries. Longitudinal segments are similar. The relaxation function varies from specimen to specimen. Figure 8.3:3 shows the mean and standard deviation at each instant of time following the step load. The variability, indicated by the standard deviation, is the least for the aortic arch, and increases toward the periphery. Since the standard deviation is caused by differences in age, sex, etc., the results shown in Fig. 8.3:3 suggest that the effect of these factors on the mechanical properties of arteries is bigger in the smaller arteries.

The value of the normalized relaxation function $G(t)$ at a given value of t is smaller for smaller arteries. This means that the smaller arteries relax faster and more fully. Stress relaxation is very fast at the beginning; then it slows down logarithmically. When $t = 1$ s, 9% of the tension in an aortic arch is relaxed, whereas in a femoral artery 20% of the tension is relaxed. At $t = 300$, most of the relaxation has taken place. In the literature it is often postulated that the normalized relaxation function $G(t)$ decreases with time like a logarithm of t . Thus

$$G(t) = \mathcal{R} \log t + d. \quad (7)$$

From Fig. 8.3:3, it is seen that this representation is not very good for the arteries. Nevertheless, it is a useful approximation for relatively small values of t , say for $1 < t < 100$ s.

The variation of the viscoelastic property of the artery along the arterial tree can be examined by comparing certain characteristic constants of the curves of relaxation. One of the characteristic numbers is the slope of the relaxation curve versus $\log t$ at a specific value of t . This is the constant \mathcal{R} of Eq. (7). With \mathcal{R} evaluated at $t = 1$ s, the results are shown in the right-hand panel of Fig. 8.3:4. It is seen that \mathcal{R} is negative, and for circumferential segments, the absolute value of \mathcal{R} increases toward the periphery away from the heart. For the longitudinal segments the absolute value of \mathcal{R} decreases at first until the level of abdominal aorta, then increases toward smaller

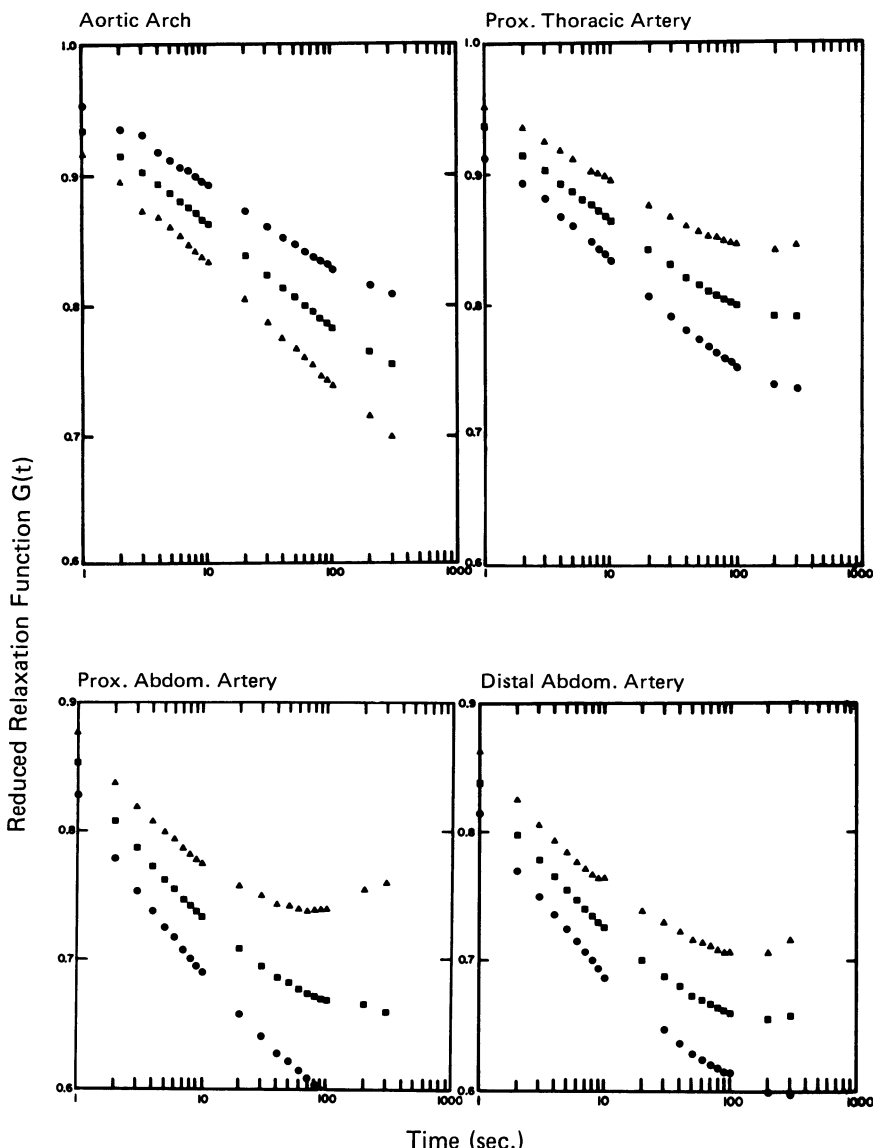


Figure 8.3.3 Normalized relaxation function $G(t)$ for circumferential segments of arteries. Mean \pm SD ($n = 10$). Note that the vertical coordinates range over 0.6 to 1.0 in the upper panels; but they are from 0.6 to 0.9 in the lower panels. $G(t)$ is dimensionless. From Tanaka and Fung (1974), by permission.

Note: By definition, $G(0)$ is 1. At each value of the time t , the middle data point (square) represents the mean value of $G(t)$ in ten experiments, whereas the circle and triangle symbols represent the mean \pm one standard deviation. Note the very large standard deviations in abdominal arteries at large t . The mean value of $G(t)$, (as well as each individual relaxation curve,) never increases with increasing time. Do not read $G(t) \pm S.D.$ as $G(t)$.

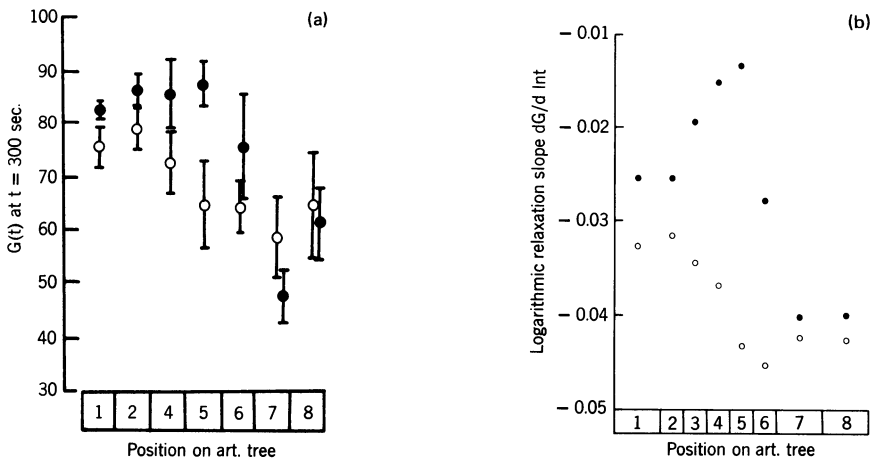


Figure 8.3:4 (a) Variation of the value of the normalized relaxation function $G(t)$ at $t = 300$ s along the aortic tree. Open circles: circumferential segments. Filled circles: longitudinal segments. Numbering of segments: see Fig. 8.3:2. (b) Variation of the slope of the curve of normalized relaxation function $G(t)$ vs $\log t$ evaluated at $t = 1$ s. Open circles: circumferential segments. Filled circles: longitudinal segments. Numbering of segments: see Fig. 8.3:2. From Tanaka and Fung (1974), by permission.

arteries. Another characteristic parameter is the value of $G(t)$ at a larger value of t . For $G(t)$ at 300 s, the results are shown in the left panel of Fig. 8.3:4. Here we see that smaller arteries relax more.

The variation of arterial elasticity and viscoelasticity along the arterial tree can be explained qualitatively by the composition and structure of the arterial wall. Elastin is soft, elastic, and relaxes very little, while collagen is also elastic, but has a much larger Young's modulus than elastin, and relaxes more than elastin. Smooth muscle has a low modulus of elasticity, but a tremendous relaxation. In terms of the parameter discussed above, smooth muscle has a large negative \mathcal{R} , and a very small $G(t)$ at $t = 300$ s. The results shown in Fig. 8.3:4 reflect the change in composition of the arterial wall along the arterial tree. Azuma and his associates (1970, 1971, 1973) have explained qualitative correlation between mechanical properties and arterial wall composition. Moritake et al. (1973) and Hayashi et al. (1971, 1974) have examined the mechanical properties and degenerative process of brain arteries in post-mortem specimens of brain aneurysm. They showed that aging and aneurysm are associated with an increase of collagen and a decrease of smooth muscle in these vessels, while the percentage of elastin remained almost constant.

We have based the discussion above on Eq. (6), which is a useful approximation. For greater accuracy the relaxation function $G(t)$ depends somewhat on the stretch ratio λ . See Sharma (1974), and Wetterer, Bauer, and Busse (1978). Such a dependence exists because the structure of the arterial wall changes with the stress level.

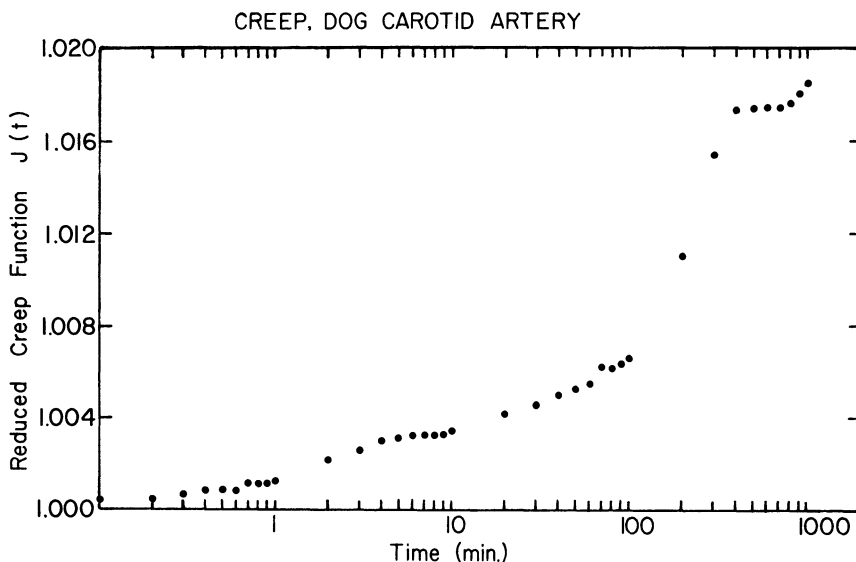


Figure 8.3:5 A typical creep curve, plotted as a reduced creep function $J(t) = [\lambda(t) - 1]/[\lambda(0) - 1]$. Dog carotid artery. From Tanaka and Fung (1974), by permission.

Creep Under a Constant Load

A typical curve showing creep under a constant load is shown in Fig. 8.3:5, in which the abscissa indicates time on a logarithmic scale, and the vertical axis is the change of strain after the imposition of a step loading. It is seen that the creep of the dog's artery is remarkably small. In the *in vitro* tests, the creep process was irreversible; after a long period of creep, the specimen could not return to its original length after the load was removed.

Unification of Hysteresis, Relaxation, and Creep

Since relaxation, hysteresis, and the difference between static and dynamic elasticity are revelations of the same phenomenon, there should exist a unified relation among them. As is discussed in Chapter 7, Sec. 7.6, a method proposed by Fung (1972) consists of interpreting the multiplication sign * in Eq. (6) as a convolution operator, so that the right-hand side of Eq. (6) represents a convolution integral between $G(t)$ and $T^{(e)}[\lambda(t)]$. The factor $T^{(e)}[\lambda]$ is nonlinear. The convolution operator is linear. The equation is therefore quasi-linear.

It is intuitively clear that we have no right to expect the quasi-linear relationship to be valid for the full range of the inelastic phenomenon in a large deformation. In the analogous case of metals, rubber, and other high polymers, it is known that the viscoelastic law [Eq.(6)] works for small strains, but not for creep to failure. We expect the same to be true with biological tissues.

Fung (1972) reasoned that since the stress-strain relationship of arteries is found to be insensitive to strain rate over a wide range of the rates, the relaxation spectrum must be broad. If the relaxation function is written in the form

$$G(t) = \frac{1}{A} \left[1 + \int_0^\infty S(\tau) e^{-t/\tau} d\tau \right], \quad (8)$$

where

$$A = \left[1 + \int_0^\infty S(\tau) d\tau \right]$$

is a normalization factor, then the spectrum $S(\tau)$ is expected to be a continuous function of the relaxation time τ . A special form of $S(\tau)$ is proposed:

$$\begin{aligned} S(\tau) &= c/\tau && \text{for } \tau_1 \leq \tau \leq \tau_2 \\ &= 0 && \text{for } \tau < \tau_1, \tau > \tau_2. \end{aligned} \quad (9)$$

The theoretical relaxation and creep functions corresponding to Eq. (9) are given in Sec. 7.6. The theoretical slope of the relaxation curve versus $\log t$ [Eq. (7)] is

$$\mathcal{R} = -c \left[1 + c \ln \left(\frac{\tau_2}{\tau_1} \right) \right]^{-1} \quad \text{for } \tau_1 < \tau < \tau_2. \quad (10)$$

TABLE 8.3:1 The Constants c , τ_1 , τ_2 , Defining the Relaxation Spectrum of the Aorta in Eq. (9). From Tanaka and Fung (1974)

	c	$\tau_1(\text{sec})$	$\tau_2(\text{sec})$
<i>Circumferential</i>			
Arch	0.0424	434	0.367
Prox Th	0.0399	192	0.260
Mid Th	0.0459	286	0.211
Dist Th	0.0512	230	0.118
Prox Abd	0.0655	162	0.059
Dist Abd	0.0687	98.6	0.051
Ext Iliac	0.0726	282	0.015
Femoral	0.0646	119	0.040
<i>Longitudinal</i>			
Arch	0.0311	451	0.431
Prox Th	0.0297	93.9	0.137
Mid Th	0.0230	245	0.101
Dist Th	0.0178	757	0.051
Prox Abd	0.0153	428	0.064
Dist Abd	0.0373	452	0.0599
Ext Iliac	0.0832	2480	0.0065
Femoral	0.0638	107.5	0.0096

When this procedure is applied to the aorta, the results listed in Table 8.3:1 are obtained. The comparison between the theoretical relaxation function and the experimental one is good. We must say, however, that the virtue of Eq. (9) does not lie only in the fact that it fits a specific relaxation curve, but that, in addition, it makes the stress-strain relationship insensitive to the strain rate over a very broad range (between a strain rate of 0.001 to 1.0 length/s in these examples).

8.4 Stresses in Arteries Under Biaxial Loading

A normal artery is a circular cylindrical tube subjected to an internal pressure and a longitudinal stretch. The wall thickness is not very thin, but is thin enough to justify some simplifying assumptions with regard to stress distribution. The simplifications we wish to make are that the normal stress in the radial direction, σ_{rr} , is negligible compared with the normal stress in the circumferential direction, $\sigma_{\theta\theta}$; and that the stresses $\sigma_{\theta\theta}$ and σ_{zz} are approximately uniform throughout the wall thickness. Here we use r , θ , and z for radial, circumferential, and axial coordinates, respectively, in a cylindrical polar frame of reference with the axis located at the center of the tube.

We shall accept the simplifying assumption of uniform $\sigma_{\theta\theta}$ and σ_{zz} and zero σ_{rr} . Then the problem is reduced to a *two-dimensional* one, and we have

$$\begin{aligned} S_{\theta\theta} &= \frac{\sigma_{\theta\theta}}{\lambda_\theta^2} = \frac{\partial(\rho_0 W^{(2)})}{\partial E_{\theta\theta}}, \\ S_{zz} &= \frac{\sigma_{zz}}{\lambda_z^2} = \frac{\partial(\rho_0 W^{(2)})}{\partial E_{zz}}. \end{aligned} \quad (1)$$

Here λ_θ and λ_z are the stretch ratios of the middle surface of the blood vessel wall in the circumferential and axial directions, respectively, and

$$E_{\theta\theta} = \frac{1}{2}(\lambda_\theta^2 - 1), \quad E_{zz} = \frac{1}{2}(\lambda_z^2 - 1). \quad (2)$$

Note that the blood vessel wall, regarded as a two-dimensional body, is not “incompressible” (i.e., its area can change). Hence there is no indeterminacy in the mean stress.

Let subscripts i and o denote the inner and outer surfaces, respectively. Then, the equilibrium condition yields

$$\begin{aligned} \text{average value of } \sigma_{\theta\theta} &= \frac{p_i r_i - p_o r_o}{h}, \\ \text{average value of } \sigma_{zz} &= \frac{F + p_i \pi r_i^2 - p_o \pi r_o^2}{\pi(r_o^2 - r_i^2)}, \end{aligned} \quad (3)$$

where F is the force applied at the ends of the vessel. See Problem 1.4 in chapter 1.

8.5 Mathematical Representation of the Pseudoelastic Stress-Strain Relationship

Although many authors have proposed a large variety of mathematical expressions to describe stress-strain relationship in uniaxial tests, (see Chapter 7, Sec. 7.5), for biaxial and triaxial tests there are essentially only two schools: one uses polynomials (Patel and Vaishnav, 1972; Vaishnav et al., 1972; Wesley et al., 1975), while the other uses exponential functions (Ayorinde et al., 1975; Brankov et al., 1974, 1976; Demiray, 1972; Fung, 1973, 1975; Fung et al., 1979; Gou, 1970; Hayashi et al., 1974; Kasyanov, 1974; Snyder, 1972; Tanaka and Fung, 1974). Both schools utilize strain energy functions to simplify the mathematical analysis. Strain functions are discussed in Chapter 7, Sec. 7.9. In the two-dimensional case the strain energy function $\rho_0 W^{(2)}$ is a function of the strains $E_{\theta\theta}$ and E_{zz} . A form of $\rho_0 W^{(2)}$ advocated by the polynomial school is, according to Patel and Vaishnav (1972),

$$\rho_0 W^{(2)} = Aa^2 + Bab + Cb^2 + Da^3 + Ea^2b + Fab^2 + Gb^3, \quad (1)$$

where $a = E_{\theta\theta}$, $b = E_{zz}$, and A, B, \dots, G are material constants. If all coefficients except A, B, C vanish, then we obtain Hooke's law of the linear theory. The seven-constants form shown in Eq. (1) is the simplest polynomial to be devised for the nonlinear theory. If the fourth degree terms are included the number of constants increases to 12. Patel and Vaishnav (1972) have shown that the accuracy of the function is not much improved by the inclusion of the fourth degree terms.

Most other authors use exponential functions. The form we prefer is the following (Fung, 1973; Fung, Fronek, Patitucci, 1979):

$$\rho_0 W^{(2)} = \frac{C}{2} \exp[a_1(E_{\theta\theta}^2 - E_{\theta\theta}^{*2}) + a_2(E_{zz}^2 - E_{zz}^{*2}) + 2a_4(E_{\theta\theta}E_{zz} - E_{\theta\theta}^*E_{zz}^*)], \quad (2)$$

where C (with the unit of stress, N/m²) and a_1, a_2, a_4 (dimensionless) are material constants, and $E_{\theta\theta}^*, E_{zz}^*$ are strains corresponding to an arbitrarily selected pair of stresses $S_{\theta\theta}^*, S_{zz}^*$ (usually chosen in the physiological range.) In principle it is unnecessary to specify the asterisk quantities, because they can be absorbed into the constant C to yield a form

$$\rho_0 W^{(2)} = \frac{C'}{2} \exp[a_1 E_{\theta\theta}^2 + a_2 E_{zz}^2 + 2a_4 E_{\theta\theta} E_{zz}]. \quad (3)$$

But in practice it is very helpful to introduce $E_{\theta\theta}^*, E_{zz}^*$. Not only are the values of $E_{\theta\theta}^*, E_{zz}^*$ corresponding to $S_{\theta\theta}^*, S_{zz}^*$ very important information, but also their use makes the identification of the constants C, a_1, a_2, a_4 from experimental data much easier for each set of test specimens.

The efficacy of the mathematical representation can be tested on two grounds: (a) its ability to fit the experimental data over the full range of strains of interest, and (b) the usefulness of the parameters in distinguishing the

TABLE 8.5.1 Material Constants for Four Arteries of the Rabbit. The Protocol “p” Refers to Inflation with Increasing Internal Pressure. From Fung et al. (1979).

(a)	Mean values for all tests with protocol “p”: exponential strain energy function							
	C 10 kPa	a_1	a_2 (nondimensional)	a_4	$E_{\theta\theta}^*$ (nondimensional)	E_{zz}^*	$S_{\theta\theta}^*$ (10^5 dyn/cm 2)	S_{zz}^*
Carotid	2.9307	2.5084	0.4615	0.1764	0.5191	0.9939	3.4000	1.3000
Left iliac	2.1575	8.1674	1.2173	1.0546	0.2418	0.8834	4.5000	1.9000
Lower aorta	2.1744	9.5660	3.0913	0.8805	0.2743	0.6495	4.9000	3.0000
Upper aorta	3.3836	2.8173	0.5239	0.5790	0.4061	0.9566	5.2000	1.9000

(b)	Mean values for all tests with protocol “p”: polynomial strain energy function						
	A	B	C	D (10 kPa)	E	F	G
Carotid	-7.1889	3.1255	0.1911	1.3711	10.2775	-3.3677	0.0787
Left iliac	-16.3871	-0.3854	2.9122	16.0463	29.6790	1.1872	-2.2552
Lower aorta	-14.7220	-4.1606	4.4821	16.5753	29.9390	6.2093	-1.8999
Upper aorta	-12.0062	5.1405	-1.5936	-2.1292	23.5706	-7.3431	2.2069

members of a family of stress-strain curves. To obtain the needed data for evaluation, Fung et al. (1979) tested selected rabbit arteries. The results of two series of tests are analyzed. In one series, each artery was first stretched longitudinally to an approximate *in vivo* length (λ_z equal to 1.6 for the carotid artery, 1.5 for the iliac and lower abdominal aorta, 1.4 for upper abdominal aorta); then it was inflated with internal pressure, and the pressure, diameter, gauge length, and axial force were recorded. In another series, the internal pressure was kept at zero, (i.e., same as the external pressure) and the vessel was stretched while the diameter, gauge length, and axial force were recorded. These experimental data are then matched with the theoretical stress-strain relationship derived from Eqs. (1) and (2).

For the exponential strain energy function, the constants C, a_1, a_2, a_4 are determined by a modified Marquart's (1963) nonlinear least squares algorithm—by minimizing the sum of the squares of the differences between the experimental and theoretical data. For the polynomial, the ordinary least squares procedure suffices. Some results for the exponential strain energy function are given in Table 8.5:1. $S_{\theta\theta}^*, S_{zz}^*$ correspond to about 100 mm Hg internal pressure and $\lambda_z = 1.6$. The overall fit is quite good; the average correlation coefficients are 0.988 for $S_{\theta\theta}$ and 0.861 for S_{zz} for the carotid artery.

The results of matching experimental data with the polynomial Eq. (1) are given in Table 8.5:1. The standard deviations of the material constants A, B, \dots are sometimes very large compared with the mean. Some of the coefficients change sign in different runs of the same specimen. The average correlation coefficients are 0.971 for $S_{\theta\theta}$ and 0.878 for S_{zz} for the same carotid artery.

In Table 8.5:1 we present the material constants for four arteries of the rabbit to illustrate the systematic variation of these constants along the arterial tree. The entries are mean values for all tests with protocol "P". The change of sign of the polynomial coefficients from one artery to another is an unpleasant feature of the polynomial approach. These changes are caused by the sensitivity of the coefficients to relatively small changes in the shape of the stress-strain curves. The overall smaller coefficients of variation (ratio of standard deviation to the mean) indicate that the exponential form of the strain energy function is preferred.

The Question of Parameter Identification

The question discussed above is the question of parameter identification—determination of physical parameters from a given set of experimental data. It should be noted that although the experimental data can be fitted accurately, the parameters themselves may not have much meaning. For example, in one experiment [rabbit carotid artery, Exp. 71, protocol P + L

in Fung et al (1979)], we obtained the pseudo strain energy function

$$\rho_0 W^{(2)} = -2.4385a^2 - 0.3589ab - 0.1982b^2 + 4.6334a^3 + 3.2321a^2b + 0.3743ab^2 + 0.3266b^3,$$

which correlates with a set of experimental data with correlation coefficients 0.971 for $S_{\theta\theta}$, and 0.878 for S_{zz} . Here $a = E_{\theta\theta}$, $b = E_{zz}$, and $\rho_0 W^{(2)}$ is in units of 10 kPa. For the same arterial test specimen but in another test (Exp 71.1, protocol P), the pseudo strain energy function obtained was

$$\rho_0 W^{(2)} = -8.1954a^2 + 2.5373ab + 0.2633b^2 + 2.7949a^3 + 11.1749a^2b - 3.0092ab^2 - 0.1166b^3,$$

which has the correlation coefficients 0.958 for $S_{\theta\theta}$ and 0.794 for S_{zz} . It is amazing that two polynomials so disparate can represent the same artery. Although the coefficients A, B, \dots are very different, the stress-strain curves are quite similar in the experimental range. In other words, the coefficients are very sensitive to small changes in the data on stress-strain relationship. Workers in viscoelasticity and other branches of physics are familiar with this situation. (See another example in Chapter 7, p. 229.)

The Meaning of the Material Constants in the Exponential Pseudo-strain Energy Function

The question is often asked: What is the “physical” meaning of the material constants C , a_1 , a_2 , and a_4 in Eq. (2) or (4). We can interpret the question in two ways: (1) How do the stresses change when these constants are changed? (2) What meaning can be attributed to these constants from the point of view of the structure and materials of the arteries?

The first question can be answered quite easily. We have chosen to require the stress-strain curves to pass through two states: the resting state (where $S_{ij} = E_{ij} = 0$) and the state characterized by S_{ij}^* and E_{ij}^* . Between these two states the stress-strain curve is more curved if a_1 , a_2 is larger. If E_{zz} is zero, then for a larger a_1 , the curve of $S_{\theta\theta}$ versus $E_{\theta\theta}$ will leave the origin closer to the strain axis, and then rise more rapidly to the point $(S_{\theta\theta}^*, E_{\theta\theta}^*)$. This is illustrated in Fig. 8.5:1. Similarly, a_2 would affect the curve for S_{zz} vs E_{zz} . The constant a_4 specifies the crosstalk between the circumferential and longitudinal directions. The constant C fixes the scale on the stress axis. The larger the values of a_1 , a_2 , and a_4 , the smaller would be C .

The second question cannot be answered definitively. The artery is composed of collagen and elastin networks, smooth muscles, and ground substances. The fibers of collagen gradually take up more and more stresses as they become straightened and stretched. Without going into details, we may roughly characterize the normal stress acting on a surface of unit area

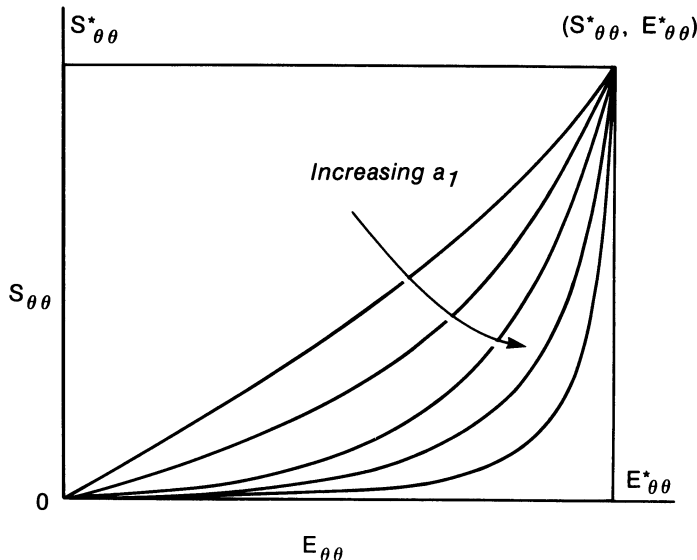


Figure 8.5:1 The effect of the material constants a_1, a_2 , on the shape of the stress-strain curves. The scales of the coordinates are so chosen that all curves pass through the point S^*, E^* . The curves pass through the origin if $E_{zz} = 0$; otherwise they do not.

(1 cm^2) as equal to the number of fibers in that area, N , which are stretched and carrying a force, f . Thus $S = Nf$. Now let the artery be stretched a little more, so that the strain $E_{\theta\theta}$ is increased by an amount $dE_{\theta\theta}$. In response to this increase in strain, the number of the stretched molecules, N , and the tensile force in them, f , will be increased. Let the increase be $d(Nf)$. The ratio $d(Nf)/dE_{\theta\theta}$ depends on the structure of the material. If the ratio

$$\frac{d(Nf)}{dE_{\theta\theta}} = \text{constant}, \quad (8a)$$

then the material is said to obey Hooke's law. Arteries do not obey Hooke's law. They are better approximated by the relation

$$\frac{d(Nf)}{dE_{\theta\theta}} = a_1(Nf) + \text{const.} \quad (8b)$$

In other words, if we assume that the rate of increase of the number of stretched molecules and the force in them with respect to an increase of strain is proportional to the number of stretched molecules itself, and the force in them, then the constant a_1 represents the constant of proportionality. Equation (8b) refers to the circumferential direction. The constant a_2 is approximately related to the rate of increase of Nf in the longitudinal direction with respect to an increase in longitudinal strain. The constant a_4 refers to crosstalk between the longitudinal and circumferential directions. The constants a_1, a_2, a_4 , and C depend on the strain process: one set of

values for loading, another for unloading, and a third for incremental experiments.

We have to say “approximately” above. We can say “exactly” if we express our idea in terms of the quadratic function of strain, Q :

$$Q = a_1 E_{\theta\theta}^2 + a_2 E_{zz}^2 + 2a_4 E_{\theta\theta} E_{zz}. \quad (9)$$

If we say that *the strain energy depends on Q, and that as Q changes, the rate of change of strain energy is equal to the current value of the strain energy*, then

$$\frac{d\rho_0 W^{(2)}}{dQ} = \rho_0 W^{(2)}, \quad (9a)$$

and an integration gives

$$\rho_0 W^{(2)} = \frac{c'}{2} e^Q, \quad (9b)$$

exactly as in Eq.(2). Here c' is a constant of integration. This is perhaps the most definitive statement that can be made about the pseudo strain energy function proposed in this chapter.

8.6 Dynamic Testing: Wave Propagation

Seismologists deduce the structure of the earth and the elastic constants of various parts inside the earth by examining the propagation of seismic waves around the globe. By analogy, a physiologist should be able to deduce the properties of a blood vessel by watching the propagation of waves in the blood and in blood vessels. The basic principle for this method is that wave motion in an elastic body is the result of a balance between elastic force and inertia force. Hence if we know the density (inertia) of the material, we should be able to deduce the elasticity from the wave motion.

If we consider progressive waves of radial motion of long wavelength and infinitesimal amplitude propagating in an infinitely long circular cylindrical vessel filled with an inviscid fluid and having a linearly elastic wall, then the speed c of the wave is governed by the Moens-Korteweg equation

$$c^2 = \frac{Eh}{2\rho_f a}. \quad (1)$$

Here ρ_f is the density of the fluid, E is the Young's modulus of the vessel wall in the circumferential direction, h is the wall thickness of the vessel, and a is its radius. The long string of qualifying words preceding Eq. (1) is necessary for the validity of this equation. Thus blood viscosity and compressibility and the vessel wall mass and initial stresses are ignored. Furthermore, the wavelength must be very long, and the wave amplitude must be very small compared with the vessel radius; otherwise the bending rigidity of the vessel wall and the nonlinear convective fluid inertia would have to be accounted for.

The many restrictions imposed on the Moens-Korteweg formula suggest that the formula is of limited use. The most serious limitation is that the waves must be progressive. For vessels of finite length, waves will be reflected at the ends and what one can observe are not harmonic progressive waves. In the human body, with the wave motion generated by the heart, the distance between the heart and the capillary blood vessels at the periphery is approximately a quarter wavelength. In this distance the vessel diameter is reduced rapidly toward the periphery, and many generations of branching exist. These factors make it necessary to abandon this beautifully simple formula, and to resort to a much more complex mathematical analysis of the arterial waves.

Many other types of wave motion are possible in a blood vessel. For example, axial waves and torsion waves in the vessel wall have been predicted and confirmed. Nonaxisymmetric waves are found to be strongly dispersive.

In unstressed vessels that are firmly tethered in the axial direction, that is, in vessels whose walls cannot move in the axial direction, the speed of axisymmetric pressure waves with frequencies approaching zero is

$$c^2 = \frac{Eh}{2(1 - v^2)\rho_f a}, \quad (2)$$

where v is the Poisson's ratio of the vessel wall. In deriving this equation, it is assumed that the ratio $\rho_w h / \rho_f a \ll 1$, where ρ_w is the density of the wall tissue. On the other hand for an untethered cylindrical vessel, i.e., one whose wall motion in the axial direction is not externally restrained, we also have the speed c for axial waves when their frequencies approach zero,

$$c^2 = \frac{E}{\rho_w(1 - v^2)}, \quad (3)$$

and that for torsion waves,

$$c^2 = \frac{G}{\rho_w}, \quad (4)$$

where G is the shear modulus of elasticity of the wall material.

Anliker et al. (1968, 1969) and Anliker (1972) have studied the wave motion in arteries by superimposing, on the naturally occurring pressure fluctuations, artificially induced transient signals in the form of finite trains of high frequency sine waves. In particular, this method is used to study the attenuation of the wave amplitude along the path of propagation, thus deducing the viscoelastic properties of the blood vessel. Using pressure waves in the 20–200-Hz range in a dog's aorta, the wave train may be considered as progressive waves. They find that the amplitude attenuates exponentially:

$$A = A_0 e^{-k(\Delta x/\lambda)} \quad (5)$$

where A_0 is the amplitude at the proximal transducer, A is the amplitude at the distal one, k is the logarithmic decrement, Δx is the distance between the

transducers, and λ is the wavelength. For pressure waves propagating downstream (away from the heart), k is of the order of 0.7 to 1.0. The logarithmic decrement k for the torsion and axial waves are higher, in the range 3.5–4.5. In all cases the logarithmic decrements are essentially independent of frequency between 40 and 200 Hz. Wave speed increases with increasing blood pressure.

8.7 Arterioles

Arterioles regulate peripheral blood flow. The mechanical properties of arterioles are of the utmost physiological significance; but direct mechanical testing of the type discussed in the preceding sections is difficult.

By measuring the inner and outer radii of the blood vessels simultaneously with pressure in the isolated, autoperfused mesentery of 14 cats during changes in systemic blood pressure, Gore (1974) was able to obtain the relationship between the mean diameter and the wall stress in several groups of vessels. Figure 8.7:1 shows Gore's results. Here the wall stress was computed from the formula

$$\langle \sigma_\theta \rangle = p \frac{r_i}{h}$$

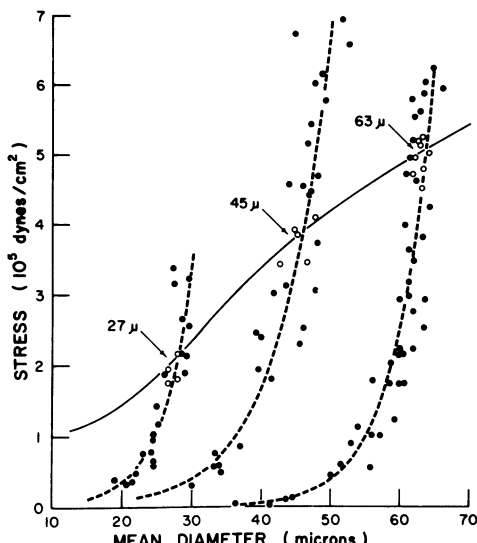


Figure 8.7:1 Stress-diameter curves (broken lines) identify three types of arterioles in the cat mesentery: 63- μ large arterioles, 45- μ arterioles, and 27- μ terminal arterioles. Open circles show stress states existing in these vessel segments when the mean systemic blood pressure was 100 ± 10 (SD) mm Hg. Solid line is the control stress distribution curve for vessels between a mean diameter of 12 to 70 μ . From Gore (1974), by permission.

where p is the functional mean pressure, r_i is the inner radius of the vessel, and h is the wall thickness. $\langle \sigma_\theta \rangle$ is the average circumferential stress in the wall only under the assumption that the pressure acting on the outside of the vessel is zero, because the full formula is

$$\langle \sigma_\theta \rangle = \frac{p_i r_i - p_o r_o}{h},$$

where the subscripts i and o refer to inside and outside of the vessel, respectively. The mean diameter was computed as the sum of inner and outer diameters divided by 2. Figure 8.7:1 shows that the stress-diameter relationship of arterioles (shown by the broken lines) is similar to that of the larger arteries.

The solid line in Fig. 8.7:1 shows the mean circumferential stress in precapillary microvessels when the mean systemic blood pressure was 100 ± 10 (SD) mm Hg. It is seen that the stress level decreases with decreasing vessel diameter. In an earlier paper, Gore (1972) showed that the response of frog microvessels to norepinephrine depends on the mean wall stress $\langle \sigma_\theta \rangle$ in the vessel. During iontophoretic application of constant, supramaximal doses of norepinephrine, maximum constriction of the frog mesenteric vessels occurred when $\langle \sigma_\theta \rangle$ was in an optimum range S_t^* of $1-1.5 \times 10^5$ dyn/cm². The magnitude of constriction was less in arterioles and arteries with $\langle \sigma_\theta \rangle$ greater or less than S_t^* . Gore suggested that $\langle \sigma_\theta \rangle$ in arterioles is normally equal to S_t^* , so they develop maximum force to overcome distending pressure; whereas $\langle \sigma_\theta \rangle$ in terminal arteries and arteries is normally greater than S_t^* , so these larger vessels cannot develop their full constrictive potential.

The response of the smooth muscles in the arterioles to changes in stretch, stress (or blood pressure), oxygen, norepinephrine, or other factors is the key to the regulation of blood flow. The response to blood pressure can be illustrated by a result by Baez et al. (1960) who isolated and perfused the rat mesoappendix and measured the diameters of the small vessels as the static perfusion pressure was varied. Figure 8.7:2 shows their results on a nerve-intact preparation. Note that there is a region of pressure in which the metarteriole (middle curve) does not change its diameter with pressure. For a small precapillary vessel (lower curve) this flat region is even larger. The existence of such a flat region, which is opposed to passive elasticity, implies the existence of an active response from the vascular smooth muscle. As the internal pressure is reduced below a certain limit, the muscle contraction closes the vessel. Since automatic closing is not possible without an active contraction, the closing phenomenon again reflects smooth muscle action.

The results shown in Fig. 8.7:2 were obtained in static condition. The vessels were perfused, but the arterial and venous pressures were equalized so that there was no flow. Related *in vivo* data with normal blood flow were given by Johnson (1968), who studied the change of arteriole diameter with respect to large-artery pressure in the cat mesentery. In experiments on

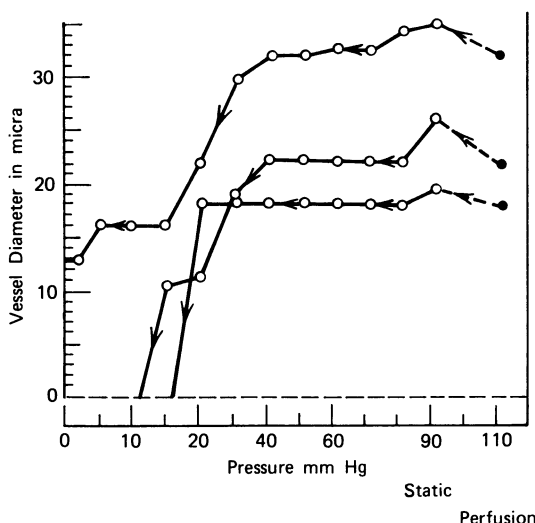


Figure 8.7:2 The change of vessel diameter with blood pressure measured by Baez et al. in the meso-appendix of the rat. Nerve-intact preparation. The phenomenon of unchanging diameter in certain ranges of pressure is exhibited. From Baez et al. (1960), by permission.

34 arterioles, 10 vessels showed a simple decrease in diameter as pressure was reduced; 24 showed a biphasic response. In the latter group, the vessel narrowed for the first 5–15 s, but then the vessel dilated. In 12 of these the diameter became larger in hypotension than it had been at normal arterial pressure. When pressure was suddenly restored, the vessel dilated at first but returned to the control size later. These results show how complex arteriolar behavior can be. For greater details, see Johnson's critical reviews (1978, 1980).

8.8 Capillary Blood Vessels

In vivo observation of elasticity of capillary blood vessels in mesentery and muscles in isolated preparations can be made under varying perfusion pressure in a no-flow condition. There are, however, few published data on capillary compliance, mainly because the change of diameter is so small that it cannot be accurately measured. Burton (1966), in summarizing W. Jerrad's unpublished data, stated that the frog mesenteric capillaries were certainly less distensible than 0.2% per mm Hg, and probably less than 0.08% per mm Hg. Similarly, during the occlusion of single capillaries in the mesentery of the rat and rabbit by micromanipulation, Zweifach and Intaglietta (1968) stated that there were no measurable changes in the diameter of the capillary vessels. In other words, the capillary behaves like a rigid tube. Fung (1966a) suggested that capillaries in the mesentery behave like a tunnel in a gel and that capillary behavior cannot be tested independently of this surrounding gel. Then

Fung, Zweifach and Intaglietta (1966) measured the stress-strain relation of the mesentery, and Fung (1966b) used the result to compute the contribution of the surrounding tissue to the rigidity of the capillary blood vessels contained therein. He showed that when the mesentery was stretched to the extent used in most physiological experiments, the surrounding media contributed over 99% of the rigidity to the capillary blood vessels in the mesentery, with less than 1% contributed by the endothelium and basement membrane if the elastic modulus of the basement membrane is similar to that of the small artery or arteriole. It follows that the compliance of the capillaries depends on the amount of surrounding tissue that is integrated with the blood vessel, and to the degree the surrounding tissue is stressed. If the surrounding tissue is large compared with the capillary, and is stressed to the degree used in Zweifach and Intaglietta's (1968) observations, then the rigidity of the capillary would be derived mostly from the surrounding tissue. If the surrounding tissue is small compared with the capillary, and the tissue is much more relaxed, then the capillary will be more distensible.

An alternative hypothesis that can explain the observed rigidity of the capillary is that the basement membrane is thicker than previously assumed and has an elastic modulus as large as that of a taut tendon (like a collagen bundle under high tension, *not* like the collagen network in large arteries, which has a low modulus of elasticity unless the artery is stretched to a tension higher than the normal physiological range). This hypothesis remains to be verified. Although collagen-like molecules have been identified in the basement membrane, the typical cross-striation structure of collagen fibers has not been seen in basement membrane.

The tunnel-in-gel concept was further examined from the point of view of water movement between the capillary blood vessel and the surrounding media when the pressure in the capillary changes during micromanipulations. Intaglietta and Plomb (1973) showed that the concept is consistent with the observed fluid movement data.

One important corollary to the tunnel-in-gel concept of the capillary is the capillary blood vessel will not collapse under a uniform external compression. A capillary in a compressed tissue can remain open for the same reason that an underground tunnel can remain open under tremendous earth pressure.

On the other hand, there are small blood vessels that do not receive much support from the surrounding tissue. A typical example is the capillary blood vessels of the pulmonary alveoli, which are separated from the air by a wall less than $1\mu\text{m}$ thick. These vessels are found to be distensible.

Networks of pulmonary capillaries are organized in sheet form in the interalveolar septa. These are shown in Figs. 5.2:1 and 5.2:2 and again in Fig. 8.8:1. In the plane view [Fig. 8.8:1(a)], the vessels are crowded against each other; the "post" space between the vessels is filled with connective tissue. Hence in the plane view, there is no space to expand if the blood pressure changes; indeed, the blood vessels appear rigid with respect to blood pressure changes. However, in cross-section [Fig. 8.8:1(b)], the interalveolar

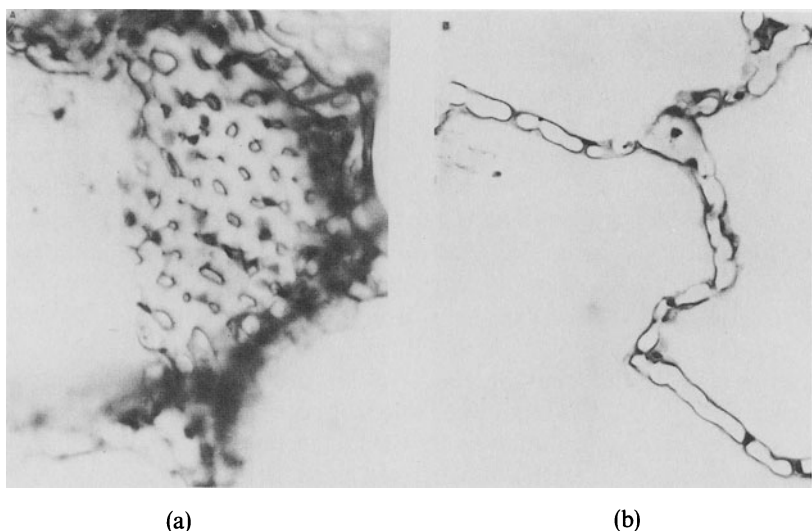


Figure 8.8:1 Two views of the interalveolar septa of the cat's lung. Left: A plane view. Right: A cross-sectional view. The vascular space was perfused with catalyzed silicone elastomer, so that no red cells can be seen. From Fung and Sobin (1972), by permission.

septa (capillary sheets) are thin-walled structures. Under increased blood pressure, the membranes will bulge out and the average thickness of the sheet will increase. This is illustrated in Fig. 8.8:2 [Sobin et al. (1972)]. Experimental results on the variation of the thickness of the alveolar septa of the cat's lung with respect to the transmural pressure (Δp = local pressure of the

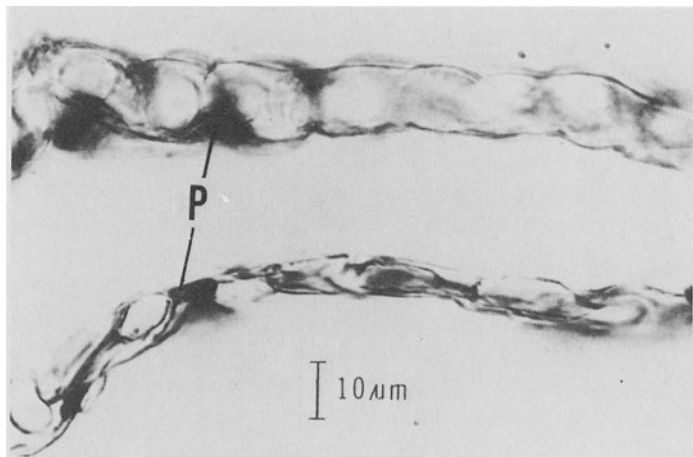


Figure 8.8:2 Photomicrograph of cat lung interalveolar septa cut in cross-section and aligned parallel to optical axis. Stained basement membrane can be clearly seen. P = post; 20-m thick section. Top: sheet thickness = 10.5 μm at $\Delta p = 27.4 \text{ cm H}_2\text{O}$. Bottom: 6.0 μm at $\Delta p = 6.3 \text{ cm H}_2\text{O}$. From Sobin et al. (1972), by permission.

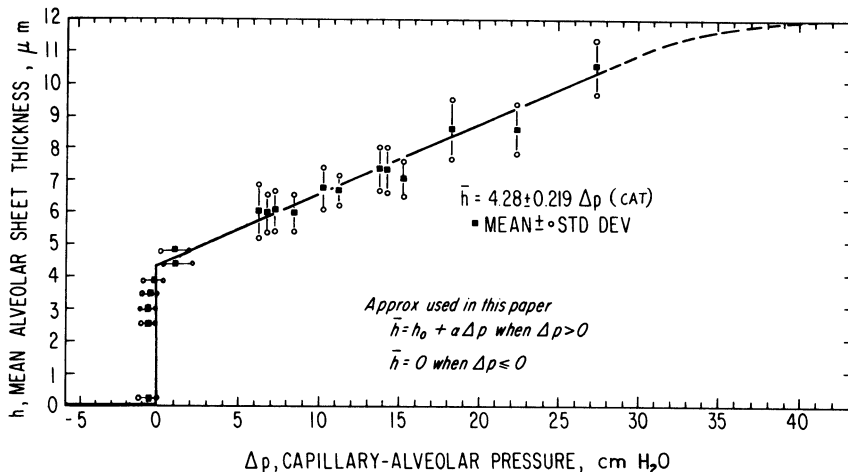


Figure 8.8:3 The sheet thickness (the average vascular space thickness in the interalveolar septa) of the cat's lung, plotted as a function of the transmural pressure p (the blood pressure minus the alveolar air pressure). The alveolar air pressure was maintained at 10 cm H₂O above the intrapleural pressure, which was atmospheric (taken as 0). A composite plot with data from Sobin et al. (1972) and Fung and Sobin (1972).

blood minus the alveolar gas pressure) are shown in Fig. 8.8:3. These results may be summarized as follows: when the transmural pressure is positive, the thickness, h , increases linearly with increasing pressure according to the formula

$$h = h_0 + \alpha \Delta p, \quad (1)$$

where h_0 and α are constants. When the transmural pressure is negative, it is a good approximation to take the thickness h as zero. When the transmural pressure exceeds an upper limit, Eq. (1) ceases to be valid. As Δp increases beyond that limit, h tends asymptotically to be a constant.

This example shows that the pulmonary capillaries should not be considered as tubes. It is more apt to call them *sheets*. Based on the measured sheet elasticity of the pulmonary alveolar septa (Fig. 8.8:3), detailed examinations have been made on the unique pressure-flow relationship of the lung, the transit time of red cells in the lung, the blood volume in the pulmonary microvascular bed, the fluid exchange, the input impedance, the parenchyma elasticity, and the conditions of edema and atelectasis of the lung. A consistent agreement was obtained between theoretical predictions and experimental results. References to this literature can be found in Fung and Sobin (1977).

Thus the distensibility of capillary blood vessels with respect to blood pressure depends on the relationship of these vessels to the surrounding media. The mesentery and the lung provide two extreme examples. Larger blood vessels, such as the arterioles, venules, arteries, and veins, have the same problem; their compliances are also influenced by the surrounding tissue to varying degrees. Capillary blood vessels in different organs have different

topologies and special structures and as a consequence have special mechanical properties.

In 1979, Bouskela and Wiederhielm found that the capillaries in the bat's wing are very distensible. The bat's wing is thin and unstretched so that the surrounding tissue is relaxed. The capillaries apparently do not receive much support from the surrounding tissue. (Remember that the Young's modulus of a soft tissue is nearly proportional to the stress in the tissue.) This points out the importance of controlling the tension in the tissue in physiological experiments involving capillaries.

8.9 Veins

The structure of veins is not very different from that of arteries. The constitutive equation is expected to be similar. Indeed, the stress-strain curves of veins, as shown in Fig. 8.9:1, from Azuma and Hasegawa (1973), are quite similar

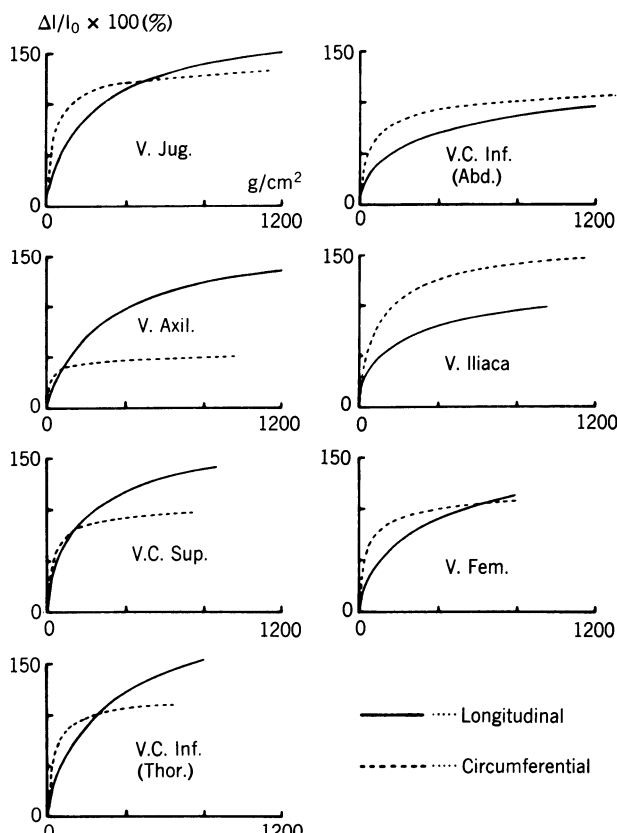


Figure 8.9:1 The stress-strain curves for the veins of the dog. Abscissas: stress. Ordinates: percent strain. From Azuma and Hasegawa (1973), by permission.

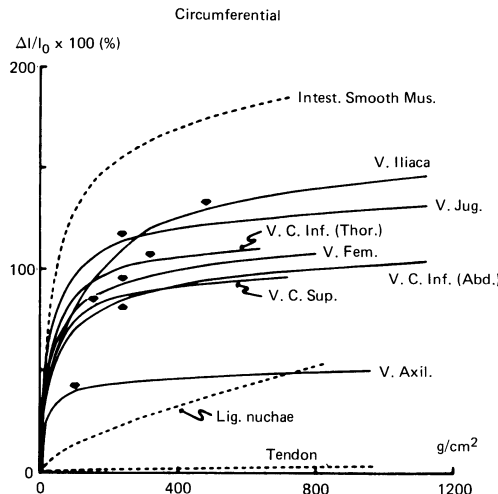


Figure 8.9:2 A comparison of the stress-strain relationships of various veins of the dog with that of the ligament nuchae, tendon, and intestinal smooth muscle. Abscissas: tensile stress. Ordinates: strain. From Azuma and Hasegawa (1973), by permission.

to those of arteries. Figure 8.9:2 shows a comparison of the stress-strain curves of seven veins with several nonvascular tissues.

To determine the constitutive equation, the same kind of test procedure and precautions as discussed in Secs. 8.1 and 8.3 must be followed. To obtain a steady-state response in cyclic loading and unloading, preconditioning is necessary. The stress-strain curve corresponding to an *increasing stretch* is called a *loading* curve. That corresponding to a *decreasing stretch* is called an *unloading* curve. For preconditioned specimens, the loading and unloading curves are stabilized, and are essentially independent of the *strain rate* (i.e., the speed) at which the cycling is done. Hence the concept of *pseudoelasticity*, as discussed in Chapter 7, Sec. 7.7, is applicable to veins.

Data presented in Figs. 8.9:1 and 8.9:2 refer to uniaxial tests on strips of tissue in which only one component of stress does not vanish. If $\rho_0 W$ represents a three-dimensional strain energy function, it can be reduced to the uniaxial condition through the conditions $S_{11} = S, S_{22} = S_{33} = S_{12} = S_{23} = S_{31} = 0$. As an alternative, one may derive a one-dimensional strain energy function $\rho_0 W^{(1)}$, as a function of the uniaxial strain E , whose derivative with respect to E yields the uniaxial stress (Kirchhoff stress S , Lagrangian stress T , and Cauchy stress σ):

$$S = \frac{\partial(\rho_0 W^{(1)})}{\partial E}, \quad T = \lambda S, \quad \sigma = \lambda^2 S, \quad (1)$$

where

$$E = \frac{1}{2}(\lambda^2 - 1),$$

and λ is the uniaxial stretch ratio, i.e., the ratio of the changed length of the specimen divided by the reference length of the specimen. Following the same reasoning as in Sec. 8.5, we prefer the following form for $\rho_0 W^{(1)}$:

$$\rho_0 W^{(1)} = \frac{1}{2} C \exp[\alpha(E^2 - E^{*2})], \quad (2)$$

where C and α are material constants, and E^* is the strain that corresponds to a selected value of stress S^* . The Lagrangian stress T corresponding to Eq. (2) is

$$T = \alpha E C \lambda \exp[\alpha(E^2 - E^{*2})], \quad (3)$$

$$T^* = \alpha C E^* \lambda^*. \quad (4)$$

It is easy to see that α determines how curved the stress-strain curve is. The more nonlinear the stress-strain relationship is, the larger is the constant α . The product of the constants αC is similar to the familiar Young's modulus,

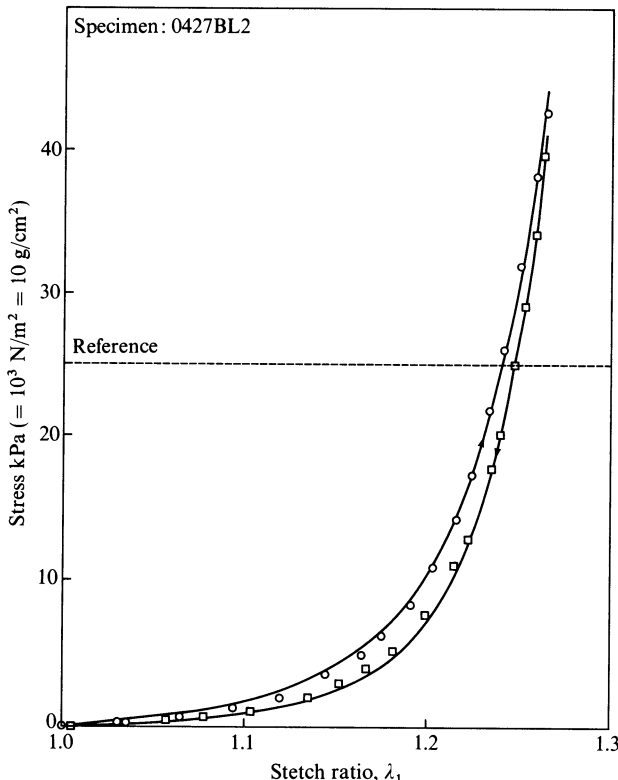


Figure 8.9:3 The stress-stretch ratio relationship of a post mortem human vena cava specimen tested in a uniaxial tensile loading condition. λ_1 is the axial stretch ratio. Circles: experimental data on loading (increasing strain). Squares: unloading. Solid curves are calculated from Eq. (3). Material constants for the loading curve: $C = 11.3 \text{ g/cm}^2$, $\alpha = 180.4$, $\lambda^* = 1.24$, $T^* = 250 \text{ g/cm}^2$. From P. Sabin (1977).

provided that the modulus is defined as the ratio of the Kirchhoff stress to Lagrangian strain, S^*/E^* , where $S^* = T^*/\lambda^*$.

A typical stress-strain curve for cyclic loading and unloading at a constant strain rate is shown in Fig. 8.9:3. This figure refers to data obtained by P. Sabin (1977) in the author's laboratory on human vena cava from autopsy material. The dots represent the experimental values; the solid curves are those of Eq. (3). The reference length is defined as that length at which the stress is returned to zero in the cyclic loading process. Table 8.9:1 presents the numerical values of the constants for human inferior vena cava at a reference stress of $T^* = 250\text{g/cm}^2$, for the loading process only. It is seen that the venous mechanical property (as reflected by these parameters) varies a

TABLE 8.9:1 Material Constants Based on Fitting Eq. (3) to Experimental Data Obtained from Post Mortem Human Vena Cava Specimens Subjected to Uniaxial Tension. From Sabin (1977)

A. Circumferential						
Specimen	Sex	Age (yrs.)	C (g/cm ²)	α	λ^*	Corr. coeff.
0427BC1	M	65	10.193	153.034	1.16	0.999
0427BC2	M	65	11.345	180.401	1.12	0.998
0511LC1	F	11	6.326	365.308	1.11	0.999
0511LC2	F	11	14.658	45.127	1.37	0.999
0511BC1	F	11	12.135	43.715	1.425	0.997
0523BC1	M	20	15.746	157.891	1.115	0.998
0523BC2	M	20	17.612	130.712	1.13	0.999
0523CL1	M	20	11.890	85.197	1.25	0.998
0523CL2	M	20	12.861	74.177	1.26	0.999
0523BC1	M	20	17.003	43.593		0.998
0525LC1	M	49	16.194	44.542		1.000
0525LC2	M	49	11.908	87.114		1.000

B. Longitudinal						
Specimen	Sex	Age (yrs.)	C (g/cm ²)	α	λ^*	Corr. coeff.
0427BL1	M	65	17.403	61.561	1.225	1.000
0427BL2	M	65	31.383	30.939	1.24	1.000
0511LL2	F	11	17.877	134.399	1.104	0.997
0523BL1	M	20	29.182	37.964	1.21	0.998
0523BL2	M	20	44.030	14.202	1.36	0.998
0523LL1	M	20	72.931	8.310	1.345	0.999
0523LL2	M	20	137.952	3.136	1.450	0.998
0525BL1	M	49	59.273	7.287		0.991
0525BL2	M	49	50.269	9.419		0.990
0525LL2	M	49	76.114	3.124		0.994

great deal from one individual to another, and for the same individual from one location to another.

Test results on veins subjected to a biaxial stress field are reported by Wesley et al. (1975). A comparison of the incremental elastic moduli between a segment of human saphenous vein and a canine carotid artery is presented in Table 8.9:2. This comparison is of interest because in certain surgical operations a vein is used to substitute for an artery. Normally, of course, the internal pressure of vein is smaller than that in the artery.

Wave propagation in veins has been studied by Anliker et al. (1969). General features were the same as those in arteries, except that local changes of wave speeds were found to be significant, indicating the existence of local variation in geometry, mechanical properties of the vessel wall, and tethering. Wave speed increases with increasing transmural pressure (e.g., in the vena

TABLE 8.9:2 The Properties of Veins and Carotid Artery of the Dog. From Wesley et al. (1975)

Pressure (cm H ₂ O)	Extension ratio		Incremental venous elastic modulus		Carotid artery incremental modulus ^a	
	λ_θ	λ_z	E_θ (dyn/ cm ² × 10 ⁶)	E_z (dyn/ cm ² × 10 ⁶)	E_θ (dyn/ cm ² × 10 ⁶)	E_z (dyn/ cm ² × 10 ⁶)
Canine jugular vein						
10	1.457	1.481	15 ± 3 ^b	1.2 ± 0.18 ^c	7.62	5.16
25	1.463	1.530	47 ± 6 ^c	4.4 ± 0.3 ^c	8.39	7.15
50	1.472	1.597	88 ± 7 ^c	11.8 ± 2.1	9.51	10.69
75	1.478	1.646	98 ± 7 ^c	46 ± 13 ^b	10.37	13.97
100	1.482	1.675	117 ± 10 ^c	67 ± 25	10.92	16.24
125	1.484	1.686	134 ± 24 ^c	39 ± 32	11.16	17.17
150	1.484	1.686	171 ± 9 ^c	113 ± 1 ^c	11.16	17.17
Human saphenous vein						
10	1.357	1.169	0.27 ± 0.12 ^c	1.61 ± 0.32 ^b	5.30	0.017
25	1.417	1.206	0.65 ± 0.13 ^c	2.03 ± 0.39 ^b	5.82	0.328
50	1.500	1.266	1.89 ± 0.41 ^c	2.75 ± 0.78	6.00	0.735
75	1.561	1.325	9.85 ± 1.6	3.18 ± 0.76	9.66	1.80
100	1.602	1.381	15.0 ± 2.6	3.56 ± 0.58	12.77	3.15
125	1.621	1.430	20.4 ± 1.6 ^b	3.98 ± 0.96	14.79	4.59
150	1.621	1.470	25.1 ± 7.5	4.75 ± 1.2	15.51	5.93

^a The incremental modulus of the carotid artery is computed at the same extension ratios ($\lambda_\theta, \lambda_z$) as experienced by the veins at the pressure listed. Carotid moduli are quoted as a function of vessel strain, not as a function of pressure.

^b $P < 0.05$ for the comparison between the venous and carotid moduli.

^c $P < 0.01$ for the comparison between the venous and carotid moduli.

cava during inspiration). The logarithmic decrement lies in the range 0.6–3.3 per wavelength, again essentially independent of frequency between 40 and 200 Hz.

Compared with arteries, veins work in a much lower pressure regime, in which the Young's modulus is highly dependent on the tensile stress and has low values. The low elastic modulus (i.e., high compliance) is the main reason why the capacity of the veins is so sensitive to postural changes and neural and pharmacological controls.

Veins are rich in smooth muscle, which responds to neural, humoral, pharmacological, and mechanical stimuli. The functional response of the veins to these stimuli is very important in physiology, because the veins contain 75% or more of the total blood volume. Any change in pressure or muscle tension or contraction will change the blood volume in the veins and hence the cardiac output. The panorama of neural, humoral, and pharmacological control of veins is summarized in the magnificent book of Shepherd and Vanhoutte (1975).

Because veins are thin-walled, they are easily collapsible when they are subjected to external compressions. Many interesting phenomena occur in venous blood flow because of this.

A notable paper by Gaehtgens and Uekermann (1971) reports the distensibility of mesenteric venous microvessels, which contain some 25% of the total blood volume of the body. Working with the dog's mesentery, they measured the diameters of venous vessels of 22–148 μm internal diameter in response to arterial and venous pressure changes. Over a range of arterial pressure between 0 and 170 mm Hg (while venous outflow pressure was 0) venular diameter changed by $31.8 \pm 8.8\%$ and venular length by $6.3 \pm 4.4\%$. With a venous pressure elevation from 0 to 30 mm Hg (while arterial pressure = 0) an increase of the volume of the venous microvessels of about 360% was measured. Thus the venous microvessel appear to be one of the most distensible elements of the vascular system.

8.10 Long Term Response to Stress

Over a long period of time, tissue responds to stresses by growth or resorption. Ronald Crystal (1974) experimented on the growth of lung tissue under stress. Working with young rabbits, he tied off one-half of their lungs. The other half then expanded to fill the entire chest cavity. He then measured the collagen content of that lung. He found a rapid growth following the expansion of the lung, at a rate approaching the same as the neonatal rabbit. In two weeks the growth rate slowed down, and in four weeks it returned to normal. Bevan et al. (1975) studied the effect of acute hypertension on the arterial wall of the dog. They partially ligated the renal artery to create hypertension and then excised the auricular artery and examined the cell

division activity with the fluorescence technique. Normally there is no observable cell division. But mitosis activity started when the vessel became hypertensive. The course of the activity change was roughly the same as that in the lung: in a couple of weeks the activity reached a peak; then it slowed down.

Fry (1968, 1969) studied the changes in the endothelium of the aorta when the shear stress due to blood flow artificially increased. He found that when the shear stress exceeded a certain critical value, histological and biochemical changes occurred in the endothelium: its response to staining chemicals changed. Based on certain histological criteria, Fry (1968) found that the "acute critical yield stress" for endothelial cells of the thoracic aorta of the dog is 379 ± 85 (SD) dyn/cm^2 . Later, in a study of the chemical response of endothelium to shear stresses (Fry, 1969), he found that the stress corresponding to the greatest rate of change of normal to abnormal cell forms is, on the average, $< 420 \text{ dyn/cm}^2$. It is suspected that these endothelial cell changes due to shear stresses are related to the genesis of atherosclerosis. Fry created high shear stress in the aorta by inserting into the vessel a cylindrical plug that contained a groove on the surface. The blood was forced to flow into the groove, and its velocity was increased by the reduction in cross-sectional area.

In normal blood vessels, the shear stress is much smaller than those created by Fry. Only one source of such high shear stress is known; and that is the interaction of white blood cells with the endothelium. White blood cells are often seen sticking to the endothelial wall or rolling slowly on it, while the plasma and red cells flow around them. By high-speed motion picture photography of the flow around a white cell sticking to the endothelium of a venule, the flow field can be determined. Then the force of interaction of the white cell and the endothelium can be calculated either theoretically or according to model experiment data. With this method Schmid-Schoenbein, Fung and Zweifach (1975) found that the interacting shear stress between the white cell and the endothelium of the venule of the rabbit omentum varies in the range $50\text{--}1060 \text{ dyn/cm}^2$. (The variation is so large mainly because of large changes of local hematocrit.) This stress range is greater than Fry's critical stress on the upper end. The interacting area, of course, is very small, randomly distributed, and transient. Whether this random pecking of the white cells on the endothelium, persisting over a lifetime, has the same effect as Fry's acute shear stress is yet unknown.

Problems

- 8.1** Consider the equilibrium of a vertical column of liquid of density ρ , height h , in a gravitational field with gravitational acceleration g . Let the cross-sectional area of the column be A . Then the weight of the column is ρghA . Let the pressures at the top and bottom of the column be p_0 and p_1 , respectively. Consider the balance of forces

and show that

$$p_1 - p_0 = \rho gh.$$

- 8.2** Derive the equation in Problem 8.1 by integrating the equation of equilibrium [see Eq. (4) of Chapter 2, Sec. 2.2] for the special case in which

$$\sigma_{11} = \sigma_{22} = \sigma_{33} = -p, \quad \sigma_{12} = \sigma_{23} = \sigma_{31} = 0$$

and

$$X_1 = 0, \quad X_2 = 0, \quad X_3 = -g.$$

Here $\sigma_{11}, \sigma_{12} \dots$ are the components of the stress tensor.

- 8.3** Apply the results of preceding problems to calculate the hydrostatic pressure in the arteries and veins of man. In physiology, pressure is *actually measured* most frequently with a mercury manometer, and is stated in terms of mm Hg. Show that the mean pressure distribution in the blood vessels of a standing man as shown in Fig. P8.3 is roughly correct. The atmospheric pressure is taken as zero.

Note. The density of blood is approximately 1 g cm^{-3} . The density of mercury is $\rho = 13.6 \text{ g cm}^{-3}$. $g = 980 \text{ cm s}^{-2}$. $1 \text{ mm Hg pressure} = 133 \text{ N/m}^2 = 1330 \text{ dyn/cm}^2$.

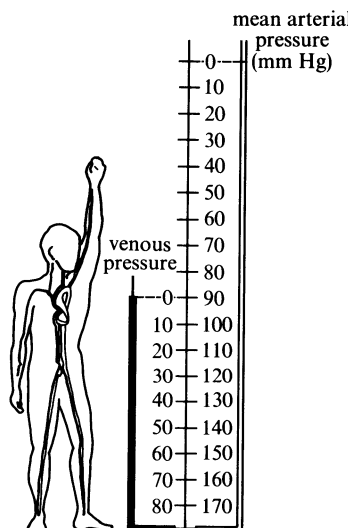


Figure P8.3 Mean arterial and venous pressures in human circulation, relative to atmospheric pressure. After Rushmer (1970), by permission.

- 8.4** Using the distensibility data of veins shown in Fig. 8.9:3, estimate the ratio of the volume of segments of veins in the leg of man when he/she is standing to that when he/she is lying down. The pressure external to the veins may be assumed to be atmospheric (taken as zero). The venous blood pressure at the level of the heart may be assumed zero in both postures.

Note. This may explain *fainting* that occurs sometimes when a person stands up from a reclining position or suddenly straightens up from stooping. The abnormal increase of the blood volume in the leg veins will decrease the venous filling pressure

of the heart. This leads to a fall in cardiac output and thus of blood supply to the brain.

One of the reasons why everyone does not faint on standing is that reflex constriction of the smooth muscles in veins in the legs normally occurs so that their ability to act as a reservoir is greatly reduced. Another reason is that the smooth muscles in the arterioles also contract upon sudden increase of tension in the arteriole wall, so that the resistance to blood flow is increased and the arterial blood flow to the legs does fall. If smooth muscle action is impaired (e.g., by certain drugs or diseases), fainting or dizziness on standing become common.

If the veins are maximally dilated as in hot climates or after a hot bath, the smooth muscles are relaxed and fainting is more common. On the other hand, a pilot executing a “high-*g*” turn will accentuate the problem by increasing the values of *g*, and black-out sometimes occurs. In this connection, how would you design an “anti-*g*” suit for pilots?

8.5 The average tensile stress in a blood vessel wall is given by the “law of Laplace” (see Chapter 1, Problem 1.4).

$$\langle \sigma_\theta \rangle = \frac{p_i r_i - p_o r_o}{h},$$

where r_i and r_o are the inner and outer vessel radii, p_i and p_o are the internal and external pressures, respectively, and h is the vessel wall thickness. With the elasticity of the artery presented in Secs. 8.3 and 8.4, derive a formula for the arterial radius as a function of the pressures p_i and p_o .

Discuss the variation of p_i and p_o for the blood vessels in the body. In addition to the hydrostatic pressure distribution considered in Problems 8.1–8.4, consider the pulsatile pressure due to the heart, and the variation of pleural pressure in the thorax due to breathing.

References

- Anliker, M., Histand, M. B., and Ogden, E. (1968) *Circulation Res.* **23**, 539–551.
- Anliker, M., Wells, M. K., and Ogden, E. (1969) *IEEE Trans. Biomed. Eng.* **BME-16**, 262–273.
- Anliker, M. (1972) In *Biomechanics: Its Foundations and Objectives*, Fung, Y. C., Perrone, N., and Anliker, M. (eds.). Prentice-Hall, Englewood Cliffs, N.J., 1972, pp. 337–380.
- Ayorinde, O. A., Kobayashi, A. S., and Merati, J. K. (1975) In *1975 Biomechanics Symposium*. ASME, New York, p. 79.
- Azuma, T., Hasegawa, M., and Matsuda, T. (1970) In *Proceedings of the 5th International Congress on Rheology*, Onogi, S. (ed.) University of Tokyo Press, Tokyo and University Park Press, Baltimore, pp. 129–141.
- Azuma, T., and Hasegawa, M. (1971) *Japan J. Physiol.* **21**, 37–47.
- Azuma, T., and Hasegawa, M. (1973) *Biorheology* **10**, 469–479.
- Baez, S., Lamport, H., and Baez, A. (1960)*In *Flow Properties of Blood and Other Biological Systems*, Copley, A. L., and Stainsby, G. (eds.). Pergamon Press, Oxford, pp. 122–136.

- Bauer, R. D., and Pasch, T. (1971) *Pflügers Arch.* **330**, 335–346.
- Bergel, D. H. (1972) In *Biomechanics: Its Foundations and Objectives*, Fung, Y. C., Perrone, N., and Anliker, M. (eds.). Prentice-Hall, Englewood Cliffs, N.J. Chap. 5, pp. 105–140.
- Bevan, J. A., Bevan, R. D., Chang, P. C., Pegram, B. L., Purdy, R. E., and Su, C. (1975) *Circulation Res.* **37**, 183–190.
- Bevan, R. D. (1976) *Blood Vessels* **13**, 100–124.
- Bohr, D. F., Somlyo, A. P., and Sparks, H. V., Jr. (eds.) (1980) *Handbook of Physiology*. Sec. 2. *The Cardiovascular System*. Vol. 2: *Vascular Smooth Muscle*. American Physiological Society, Bethesda, Md.
- Bouskela, E. and Wiederhielm, C. (1979) *Microvascular Res.* **17**, No. 3, Part 2, p. S1, (abstract).
- Burton, A. C. (1966) *Fed. Proc.* **25**, 1753–1760.
- Brankov, G., Rachev, A., and Stoychev, S. (1974) *Biomechanica* (Bulgarian Academy of Sciences, Sofia) **1**, 27–35.
- Brankov, G., Rachev, A., and Stoychev, S. (1976) *Biomechanica* (Bulgarian Academy of Sciences, Sofia) **3**, 3–11.
- Carew, T. E., Vaishnav, R. N., and Patel, D. J. (1968) *Circulation Res.* **23**, 61–68.
- Caro, C. G., Pedley, T. J., Schroter, R. C., and Seed, W. A. (1978) *The Mechanics of the Circulation* Oxford University Press, Oxford, 1978.
- Cox, R. H. (1976–1978) *Am. J. Physiol.* **230**, 462–470, 1976; **231**, 420–425, 1976; **233**, H243–H255, 1977; **234**, H280–288, 1978.
- Crystal, R. G. (1974) *Fed. Proc.* **33**, 2248–2255.
- Demiray, H. J. (1972) *J. Biomechanics* **5**, 309–311.
- Doyle, J. M., and Dobrin, P. B. (1971) *Microvascular Res.* **3**, 400–415.
- Doyle, J. M., and Dobrin, P. B. (1973) *J. Biomechanics* **6**, 631–639, 1973.
- Fisher, G. M., and Llaurado, J. G. (1967) *Arch. Pathol.* **84**, 95–98.
- Frank, O. (1920) *J. Biol.* **71**, 255–272.
- Frasher, W. G. (1966) In *Biomechanics, Proc. Symp.*, Fung, Y. C. (eds.). ASME, New York, 1966.
- Fry, D. L. (1968) *Circulation Res.* **22**, 165–197.
- Fry, D. L. (1969) *Circulation Res.* **24**, 93–108.
- Fung, Y. C. (1966a) In *Biomechanics, Proc. of a Symp.* Fung, Y. C. (ed.). ASME, New York, pp. 151–166.
- Fung, Y. C. (1966b) *Fed. Proc.* **25**, 1761–1772.
- Fung, Y. C. (1967) *Am. J. Physiol.* **28**, 1532–1544.
- Fung, Y. C. (1972) In *Biomechanics: Its Foundations and Objectives*, Fung, Y. C., Perrone, N., and Anliker, M. (eds.). Prentice-Hall, Englewood Cliffs, N.J., pp. 181–208.
- Fung, Y. C. (1973) *Biorheology* **10**, 139–155.
- Fung, Y. C. (1975) *Mechanika Polymerov LSSR*, **10**, 850–867.
- Fung, Y. C. (1975) *Circulation Res.* **37**, 481–496.
- Fung, Y. C., and Sabin, S. S. (1969) *J. Appl. Physiol.* **26**, 472–488.
- Fung, Y. C., and Sabin S. S. (1972) *Circulation Res.* **30**, 451–469; 470–490.

- Fung, Y. C., and Sabin, S. S. (1977) In *Bioengineering Aspects of Lung Biology*, West, J. B. (ed.). Marcel Dekker, New York, Chapter 4, pp. 267–358.
- Fung, Y. C., Zweifach, B. W., and Intaglietta, M. (1966) *Circulation Res.* **19**, 441–461, 1966.
- Fung, Y. C., Fronek, K., and Patitucci, P. (1979) *Am. J. Physiol.* **237**(5): H620–H631. or *Am. J. Physiol.: Heart and Circulation*, **6**(5): H620–H631.
- Gaehtgens, P., and Uekermann, U. (1971) *Pflügers Arch.* **330**, 206–216.
- Gore, R. W. (1972) *Am. J. Physiol.* **222**(1), 82–91.
- Gore, R. W. (1974) *Circulation Res.* **34**, 581–591.
- Gou, P. E. (1970) *J. Biomechanics* **3**, 547–550.
- Hardung, V. (1953) *Helv. Physiol. Pharmacol. Acta* **11**, 194–211.
- Harkness, M. L. R., Harkness, R. D., McDonald, D. A. (1957) *Proc. Roy. Soc. B* **146**, 541–51.
- Hayashi, K., Handa, H., Mori, K., and Moritake, K. (1971) *J. Soc. Material Sci. (Japan)* **20**, 1001–1011.
- Hayashi, J., Sato, M., Handa, H., and Moritake, K. (1974) *Exper. Mech.* **14**, 440–444.
- Intaglietta, M., and Plumb, E. P. (1973) *Microvascular Res.* **7**, 153–168.
- Johnson, P. C. (1968) *Circulation Res.* **22**, 199–212.
- Johnson, P. C. (ed.) (1978) *Peripheral Circulation*. Wiley, New York.
- Johnson, P. C. (1980). *The myogenic response*. In Bohr et al. (1980) *loc. cit.*, pp. 409–442.
- Kasyanov, V. (1974) *Mechanika Polymerov LSSR*, 874–884.
- Kasyanov, V., and Knets, I. (1974) *Mechanika Polymerov. LSSR*, 122–128.
- Kenner, T. (1967) *Arch. Kreislaufforschung* **54**, 68–139.
- Laszt, L. (1968) *Angiologica* **5**, 14–27.
- Lee, J. S., Frasher, W. G., and Fung, Y. C. (1967) *Two-dimensional finite deformation experiments on dog's arteries and veins*. Rept. No. AFOSR 67–198, Dept. of Applied Mechanics and Engineering Science—Bioengineering, University of California, San Diego, Calif.
- Marquart, D. W. (1963) *J. Soc. Indust. Appl. Math.* **2**, 431–441.
- McDonald, D. A. (1968) *J. Appl. Physiol.* **24**, 73–78.
- Moritake, K., Handa, H., Hayashi, K., and Sato, M. (1973) *Japan J. Brain Surg.* **1**(2), 115–123.
- Patel, D. J., and Vaishnav, R. N. (1972) In *Cardiovascular Fluid Dynamics*, Bergel, D. H. (ed.) Academic Press, New York, Vol. 2, Chapter 11, pp. 2–65.
- Roach, M. R., and Burton, A. C. (1957) *Canad. J. Biochem. Physiol.* **35**, 681–690.
- Rushmer, R. F. (1970) *Cardiovascular Dynamics*, 3rd edn. W. B. Saunders, Philadelphia, p. 196.
- Schmid-Schoenbein, G. W., Fung, Y. C., and Zweifach, B. W. (1975) *Circulation Res.* **36**, 173–184.
- Sharma, M. G. (1974) *Biorheology* **11**, 279–291.
- Shepherd, J. T., and Vanhoutte, P. M. (1975) *Veins and Their Control*. W. B. Saunders, Philadelphia.
- Snyder, R. W. (1972) *J. Biomechanics* **5**, 601–606.
- Sabin, P. (1977) *Mechanical Properties of Human Veins*. M. S. Thesis, University of California, San Diego, Calif.

- Sobin, S., Fung, Y. C., Tremer, H. M., and Rosenquist, T. H. (1972) *Circulation Res.* **30**, 440–450.
- Tanaka, T. T., and Fung, Y. C. (1974) *J. Biomechanics*. **7**, 357–370.
- Vaishnav, R. N., Young, J. T., Janicki, J. S., and Patel, D. J. (1972) *Biophysical J.* **12**, 1008–1027.
- Wesley, R. L. R., Vaishnav, R. N., Fuchs, J. C. A., Patel, D. J., and Greenfield, J. C., Jr. (1975) *Circulation Res.* **37**, 509–520.
- Wetterer, E., and Kenner, T. (1968) *Grundlagen der Dynamik des arterienpulses*. Springer-Verlag, Berlin.
- Wetterer, E., Bauer, R. D., and Busse, R. (1978) In *The Arterial System*, Bauer, R. D. and Busse, R. (eds.) Springer-Verlag, New York.
- Wylie, E. B. (1966) in *Biomechanics, Proc. ASME Symp.*, Fung, Y. C. (ed.). American Society of Mechanical Engineers, New York. pp. 82–95.
- Zweifach, B. W., and Intaglietta, M. (1968) *Microvascular Res.* **1**, 83–101.

CHAPTER 9

Skeletal Muscle

9.1 Introduction

So far we have dealt with the passive properties of tissues. Now we shall consider tissues capable of active contraction. These are, of course, the muscles. There are three kinds of muscles: skeletal, heart, and smooth muscles. Skeletal muscle makes up a major part of the animal body. It is the prime mover of animal locomotion. It is controlled by voluntary nerves. It has the feature that if it is stimulated at a sufficiently high frequency, it can generate a maximal tension, which remains constant in time. It is then said to be *tetanized*. The activity of the contracting mechanism is then thought to be maximal.

Since a resting skeletal muscle is a viscoelastic material with quite ordinary properties, the really interesting part of the properties of skeletal muscle is the contraction. Hence skeletal muscle is often studied in the tetanized condition. For the frog sartorius muscle at an optimal length, the maximum stress of contraction is about 2×10^6 dyn/cm² (i.e., about 2 kg/cm²), which is much larger than the stress in the same muscle at the same length when unstimulated. Hence the resting stress does not play an important role in skeletal muscle mechanics, except in setting the resting length of the muscle.

Heart muscle is also striated like skeletal muscle, but in its normal function it is never tetanized. Heart muscle functions in single twitches. Each electric stimulation evokes one twitch, which has to run a definite course. Until a certain refractory period is passed, another electric stimulation will not evoke a response. In this way heart muscle is very different from skeletal muscle. Another difference is that the resting heart muscle is stiffer than the resting skeletal muscle. The resting stress in heart muscle is not negligible.

compared with the stress in the contractile element. Hence the study of heart muscle needs greater attention to the resting state.

Smooth muscles are not striated, and are not controlled by voluntary nerves. There are many kinds of smooth muscles, with widely different mechanical properties.

These three classes of muscles will be discussed in this Chapter and Chapters 10 and 11.

9.2 The Functional Arrangement of Muscles

The strategic deployment of muscles to control the mechanisms of animal locomotion is itself a subject of great beauty and importance. Nature has developed many ingenious devices for this purpose. As an introduction to muscle mechanisms, let us consider some patterns of arrangements of muscle fibers when severe geometric constraints are imposed. Consider the claws of a crab. The crab uses muscles in its legs to move its claws. The leg has a rigid shell which is almost completely filled with muscle. It is necessary therefore to arrange the muscle fibers in a pinnate arrangement [see Fig. 9.2:1(a)], so that when contraction occurs, no lateral expansion will occur. If the muscle fibers were arranged parallelly, as shown in Fig. 9.2:2(a), then a contraction in muscle length would induce an increase of its lateral dimension, because the muscle has to preserve its volume. Since the rigid shell prevents any increase of lateral dimension, a bundle of parallel fibers will not be able to contract at all. Thus the pinnate arrangement of the leg muscle is a necessity for the crab.

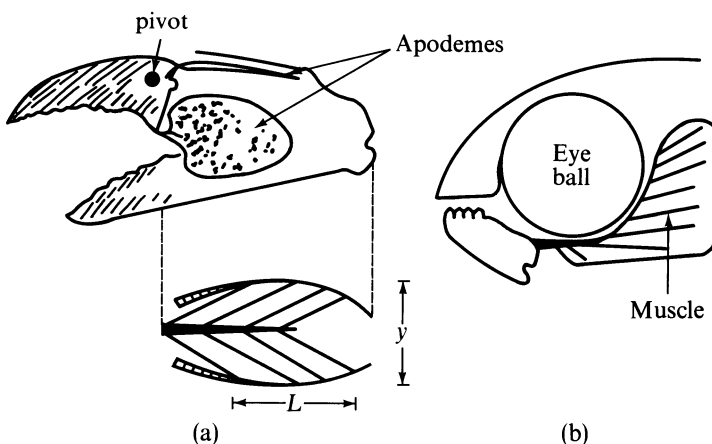


Figure 9.2:1 (a) The skeleton of a crab chela, opened to show the apodemes, and (below) a diagrammatic horizontal section showing the pinnate arrangement of the muscle that closes the chela. (b) A diagram showing the pinnate arrangement of the main jaw muscle of a characroid fish. From Alexander (1968), by permission.

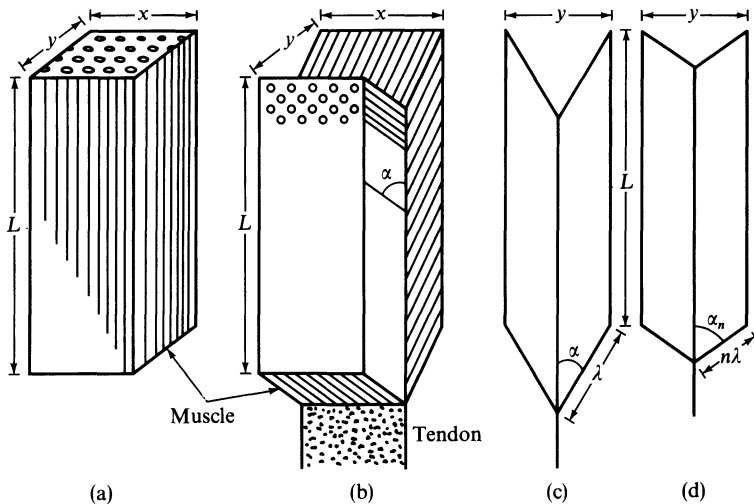


Figure 9.2:2 Diagram illustrating (a) parallel-fibered and (b) pinnate muscles. (c) and (d) illustrate pinnate muscle contraction. From Alexander (1968), by permission.

Figure 9.2:1(b) shows another interesting arrangement of the muscle in the jaw of a characinoid fish. This fish has a large eyeball. The muscles are arranged in such a manner that when they contract, a component of the tension pulls the muscle away from the eyeball to leave it free from undue stresses. Such beautiful mechanisms are everywhere in nature. Think of our own body. How marvelously our muscles are arranged so that we can do all the things we want to do!

Problem

- 9.1** Compare the force transmission in parallel and in pinnate arrangements of muscle fibers, and show the possible mechanical advantage of the pinnate arrangement.

Solution. Refer to Fig. 9.2:2. Let both muscles have the same relaxed dimensions x , y , and L . Let each muscle fiber have a relaxed cross-sectional area A . Then in the *parallel* arrangement [Fig. 9.2:2(a)], the number of muscle fibers in the cross-sectional area xy is xy/A . Let the muscle contract by a *contraction ratio* n (= shortened length/initial length) and generate a force F_n in each fiber. Then

$$\text{Total force} = xyF_n/A.$$

For a *pinnate* arrangement, let α be the angle between the muscle and the tendon, and λ be the relaxed length of each fiber. Then we have [Fig. 9.2:2(c)]

$$\lambda \sin \alpha = y/2.$$

When the fibers contract by a contraction ratio n to a new length $n\lambda$, α is changed to α_n . Since $n\lambda \sin \alpha_n = y/2$, we have $\sin \alpha_n = (\sin \alpha)/n$, and $\cos \alpha_n = (n^2 - \sin^2 \alpha)^{1/2}/n$. If the force in each fiber is F_n , the vertical component transmitted to the tendon is

$F_n \cos \alpha_n$. The number of fibers being $xL/(A/\sin \alpha)$, the total vertical force from both sides of the pinnate muscles is $2xL \cdot \sin \alpha \cdot F_n \cdot \cos \alpha_n/A$. Hence the ratio

$$\frac{\text{Total vertical force lifted by the pinnate muscle}}{\text{Total vertical force lifted by the parallel muscle}} = \frac{2xL \sin \alpha F_n \cos \alpha_n}{A(xyF_n/A)} = ny/2L \sin \alpha (n^2 - \sin^2 \alpha)^{1/2}.$$

This ratio can be either greater than 1 or less than 1 depending on the geometric parameters.

Example. Crab (Carcinus) chela [Fig. 9.2:1(a)]. $\alpha = 30^\circ$, $L/y \doteq 2$. Then at rest ($n = 1$), the ratio above is $2 \times 2 \times \frac{1}{2}(1 - \frac{1}{4})^{1/2} \doteq \sqrt{3} \doteq 1.73$. At contraction, $n = 0.7$, the ratio becomes 1.39.

9.3 The Structure of Skeletal Muscle

In the previous section we considered the structure of muscle on a scale visible to the naked eye. At a finer scale we may examine muscle with an optical microscope, with which we can see things down to about $0.2 \mu\text{m}$. And we can turn to the electron microscope, which has a theoretical resolution of 0.002 nm, but in practice about 0.2 nm.

What can be seen at various levels of magnification is shown in Fig. 9.3:1. It is seen that the units of skeletal muscle are the muscle fibers, each of which is a single cell provided with many hundreds of nuclei. These fibers are arranged in bundles or *fasciculi* of various sizes within the muscle. Connective tissue fills the spaces between the muscle fibers within a bundle. Each bundle is surrounded by a stronger connective tissue sheath; and the whole muscle is again surrounded by an even stronger sheath.

A skeletal muscle fiber is elongated, having a diameter of $10\text{--}60 \mu\text{m}$, and a length usually of several millimeters to several centimeters; but sometimes the length can reach 30 cm in long muscles. The fibers may stretch from one end of muscle to another, but often extend only part of the length of the muscle, ending in tendinous or other connective tissue intersections.

The flattened nuclei of muscle fibers lie immediately beneath the cell membrane. The cytoplasm is divided into longitudinal threads or *myofibrils*, each about $1 \mu\text{m}$ in diameter. These myofibrils are striated when they are stained by dyes and when they are examined optically. Some zones stain lightly with basic dyes such as hematoxylin, rotate the plane of polarization of light weakly, and are called *isotropic* or *I bands*. Others, alternating with the former, stain deeply with hematoxylin and strongly rotate the plane of polarization of light to indicate a highly ordered substructure. They are called *anisotropic* or *A bands*. The I bands are bisected transversely by a thin line also stainable with basic dyes: this line is called the *zwischenscheibe* or *Z band*. The A bands are also bisected by a paler line called the *H band*.

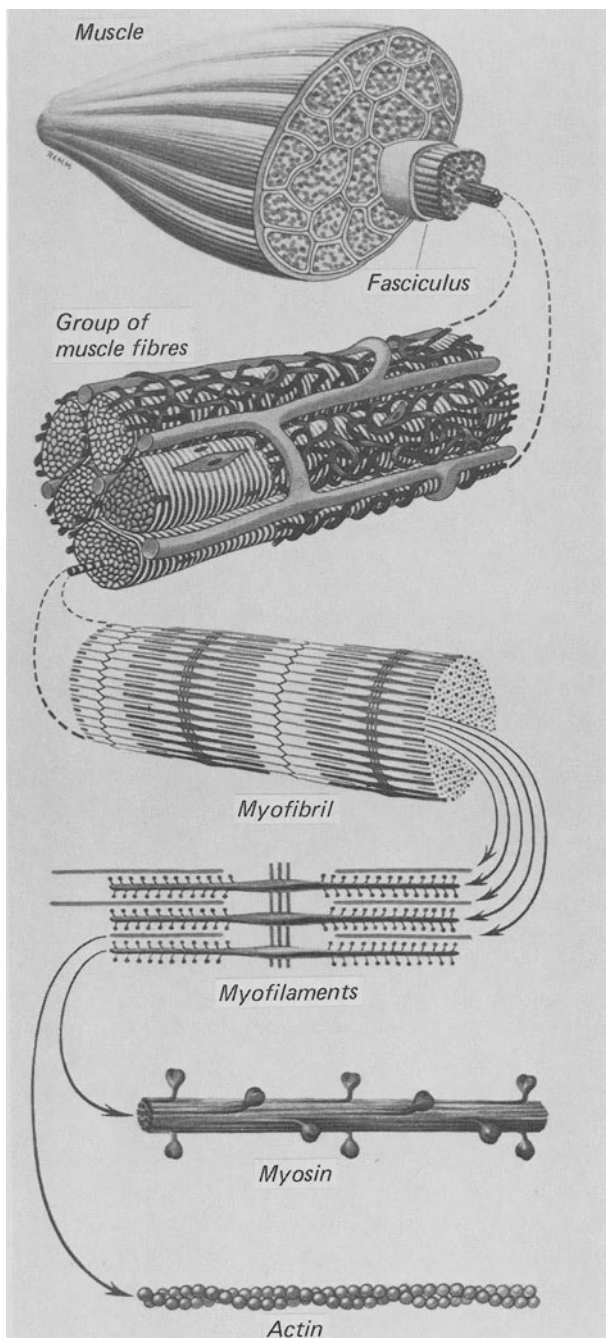


Figure 9.3:1 The organizational hierarchy of skeletal muscle. From *Gray's Anatomy*, 35th British edn. (1973), edited by Warwick and Williams, by permission.

These bands are illustrated in Fig. 9.3:2. If the muscle contracts greatly, the I and H bands may narrow to extinction, but the A bands remain unaltered. The lower part of Fig. 9.3:1 shows what is known about the fine structure of the myofibrils. Each myofibril is composed of arrays of *myofilaments*. These are divided transversely by the Z bands into serially repeating regions termed *sarcomeres*, each about 2.5 μm long, with the exact length dependent on the force acting in the muscle and the state of excitation. Two types of myofilament are distinguishable in each sarcomere, fine ones about 5 nm in diameter and thicker ones about 12 nm across. The fine ones are *actin* molecules. The thick ones are *myosin* molecules. The actin filaments are each attached at one end to a Z band and are free at the other to interdigitate with the myosin filaments. The spatial arrangements of these fibers are shown in Figs. 9.3:2. It is seen that the A band is the band of myosin filaments, and the I band is the band of the parts of the actin filaments that do not overlap with the myosin. The H bands are the middle region of the A band into which the actin filaments have not penetrated. Another line, the *M band*, lies transversely across the middle of the H bands, and close examination shows this to consist of fine strands interconnecting adjacent myosin filaments. The hexagonal pattern of arrangement of these filaments is shown in Fig. 9.3:2. The last two sketches of Fig. 9.3:1 show the structure of actin and myosin filaments in the muscle.

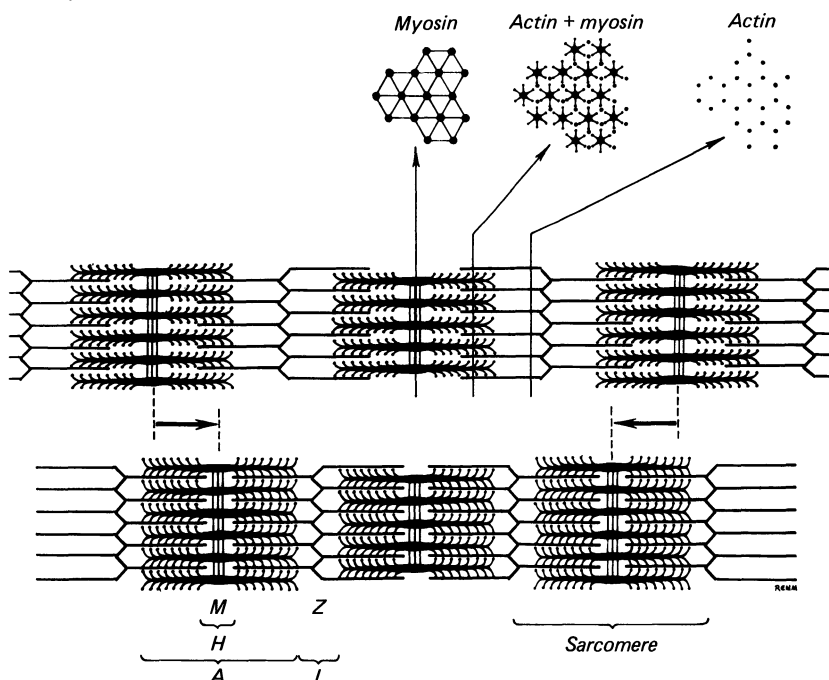


Figure 9.3:2 The structure of a myofibril, showing the spatial arrangement of the actin and myosin molecules. From *Gray's Anatomy*, 35th British edn. (1973), edited by Warwick and Williams, by permission.

9.4 The Sliding Element Theory of Muscle Action

To explain how the actin and myosin filaments move relative to each other has been the great theme of muscle mechanics research since the 1950s. There is little doubt that during muscle contraction, the two kinds of filaments slide against each other with relatively small change in their own lengths. But how do these filaments interact? What chemical events take place?

Chemical and electron microscopic studies have revealed the fine structure of the myosin filaments. It is shown that each myosin filament consists of about 180 myosin molecules. Each molecule has a molecular weight of about 500 000 and consists of a long tail piece and a “head,” which on close examination is seen to be a double structure. On further treatment the molecule can be broken into two moieties: *light meromyosin*, consisting of most of the tail, and *heavy meromyosin* representing the head with part of the tail. The myofilament is formed by the tails of the molecules which lie parallel in a bundle, with their free ends directed toward the midpoint of the long axis. The heads project laterally from the filament in pairs, at 180° to each other and at 14.3 nm intervals. Each pair is rotated by 120° with respect to its neighbors to form a spiral pattern along the filament. These heads seem to be able to nod: they lie close to their parent filament in relaxation, but stick out to actin filaments when excited. They are called *cross-bridges*. How do they work is the subject of several theories.

The mechanics of cross-bridges belongs rightfully to the theory of biomechanics. But to summarize the contending theories will require a volume to itself. Furthermore, fascinating as they are, none of the theories has reached the level of being able to precisely predict the constitutive equation of the muscle, including its behavior when it is unstimulated and stimulated at different frequencies. Since the objective of this book is to treat the biomechanics of organs, we shall rely on experimental constitutive equation, and leave the cross-bridge theory for the future. Fortunately, just as the study of oceanography may start with an empirical constitutive equation of the water and not necessarily with the structure of the water molecule, an analysis of the heart may start with a constitutive equation of the heart muscle. The details of chemical and physical reactions between the actin and myosin molecules may be relegated to the background. The accuracy of the functional analysis of the organ depends solely on the accuracy of the constitutive equation and the rigor of the mathematical analysis.

9.5 Single Twitch and Wave Summation

Skeletal muscle responds to stimulation by nerve, electric, or chemical impulses. Each adequate stimulation elicits a single twitch lasting for a fraction of a second.

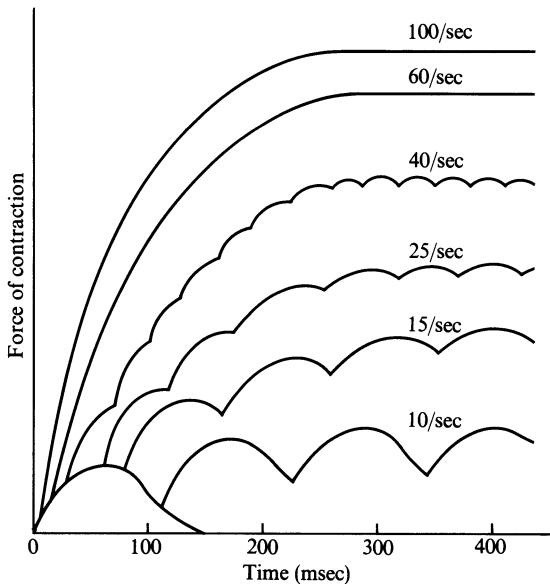


Figure 9.5:1 Wave summation and tetanization.

Successive twitches may add up to produce a stronger action. Figure 9.5:1 illustrates the phenomenon. A single isometric twitch is shown in the lower left-hand corner. It is followed by successive twitches at varying frequencies. When the frequency of twitch is 10 per second, the first muscle twitch is not completely over when the second one begins. This results in a stronger contraction. The third, fourth, and additional twitches add still more strength. This tendency for summation is stronger if the twitches come at a higher frequency. Finally, a *critical frequency* is reached at which the successive contractions fuse together and cannot be distinguished one from the other. This is then the *tetanized state*. For frequencies higher than the critical frequency further increase in the force of contraction is slight. This kind of reinforcement by successive twitches is called *wave summation*.

9.6 Contraction of Skeletal Muscle Bundles

So far we have considered only the behavior of a single muscle fiber. A muscle has many fibers. They are stimulated by motor neurons. Each motor neuron may innervate many muscle fibers. Not all the muscle fibers are excited at the same time. The total force of contraction of a muscle depends on how many muscle fibers are stimulated. Thus there is an interesting problem of correlating the numbers of excited neurons and muscle fibers with the intensity of contraction of a muscle.

Organizing many muscle fibers into a large muscle is like organizing individual people into a society. The society acquires certain features that are not simply a magnification of individual behavior. One of the features is the precision of response of a muscle to stimuli, and this has to do with the size of the *motor unit*, defined as all the muscle fibers innervated by a single motor nerve fiber. In general, small muscles that react rapidly and whose control is exact have small motor units (as few as two to three fibers in some of the laryngeal muscles), and have a large number of nerve fibers going into each muscle. Large muscles that do not require a fine degree of control, such as the gastrocnemius muscle, may have as many as 1000 muscle fibers in each motor unit. The fibers in adjacent motor units usually overlap, with small bundles of 10 to 15 fibers from one motor unit lying among similar bundles of the second motor unit. This interdigitation allows the separate motor units to acquire a certain harmony in action.

The size of motor units in a given muscle may vary tremendously. One motor unit may be many times stronger than another. The smaller units are more easily excited than the larger ones because they are innervated by smaller nerve fibers whose cell bodies in the spinal cord have a naturally higher level of excitability. This effect causes the gradations of muscle strength during weak muscle contraction to occur in very small steps, while the steps become progressively greater as the intensity of contraction increases. Further smoothing of muscle action is obtained by firing the different motor units asynchronously. Thus while one is contracting, another is relaxing; then another fires, followed by still another, and so on.

Feedback from muscle cells to the spinal cord is done by the *muscle spindles* located in the muscle itself. Muscle spindles are sensory receptors that exist throughout essentially all skeletal muscles to detect the degree of muscle contraction. They transmit impulses continually into the spinal cord, where they excite the anterior motor neurons, which in turn provide the necessary nerve stimuli for *muscle tone*, a residual degree of contraction in a skeletal muscle at rest causing it to be taut.

It is easy to see that the total system of nerves and motor units furnishes biomechanics with many interesting problems; but in this chapter we shall concentrate on the mechanics of a single muscle fiber, or often, to a single sarcomere. The mechanics of the sarcomere is the foundation on which mechanics of muscle bundles can be built by the addition of other constituents.

9.7 Hill's Equation for Tetanized Muscle

Hill's equation (due to Archibald Vivian Hill, 1938) is the most famous equation in muscle mechanics. This equation is

$$(v + b)(P + a) = b(P_0 + a), \quad (1)$$

in which P represents tension in a muscle, v represents the velocity of contraction, and a , b , P_0 are constants. It looks very much like a gas law (van der Waal's equation). Roughly, if we ignore the constants a and b on the left-hand side of the equation, then Eq. (1) says that the rate of work done, and hence the rate of energy conversion from chemical reaction, is a constant. This seems reasonable in the tetanized condition, for which the equation is derived.

Hill's equation refers to the ability of a tetanized skeletal muscle to contract. It is an empirical equation based on experimental data on frog sartorius muscle. A muscle bundle is held fixed in length L_0 (*isometric*: iso, equal; metric, measure) by having its ends clamped. It is stimulated electrically at a sufficiently high voltage and frequency so that the maximum tension P_0 (a function of the muscle length L_0) is developed in the muscle. At this tetanized condition the muscle is released suddenly (by releasing an end clamp) to a tensile force P smaller than P_0 . The muscle begins to contract immediately, and the velocity of contraction, v , is measured. The relationship between P and v is plotted on a graph, such as the one shown in Fig. 9.7:1. An empirical equation is then derived to fit the experimental data. The fitting of Eq. (1) with the experimental data is shown in Fig. 9.7:1.

Hill's equation shows a hyperbolic relation between P and v . The higher the load, the slower is the contraction velocity. The higher the velocity, the lower is the tension. This is in direct contrast to the viscoelastic behavior of a passive material, for which higher velocity of deformation calls for

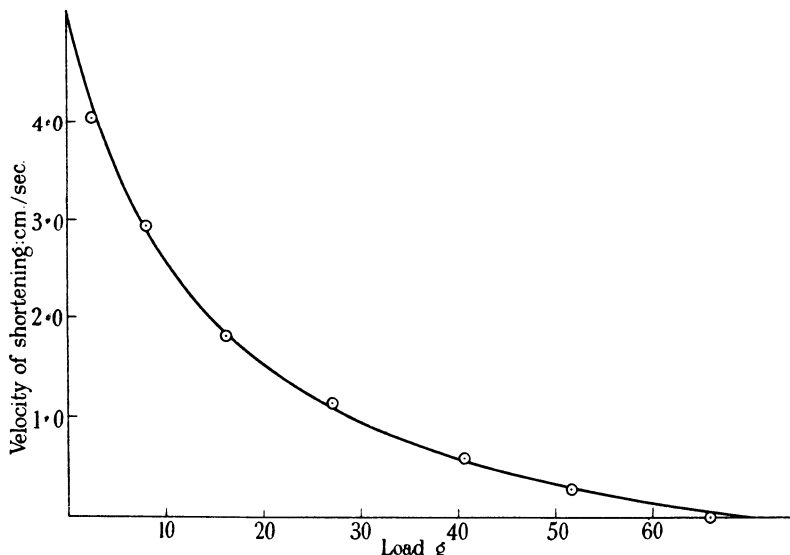


Figure 9.7:1 The experimental data (circles) on force (P , gram weight) and velocity of isotonic shortening (v , cm s^{-1}) from quick release of frog skeletal muscle in the tetanized condition, as compared with Eq. (1) (solid curve). From Hill (1938), by permission.

higher forces that cause the deformation. Therefore, the active contraction of a muscle has no resemblance to the viscoelasticity of a passive material.

The original derivation of this equation is as follows. One writes, first of all, the equation of balance of energy:

$$E = A + S + W, \quad (2)$$

where

- E is the rate of energy release,
 - A is the activation or maintenance heat per unit of time,
 - W is the rate of work done, equal to Pv ,
- (3)

and

S is the shortening heat.

If the muscle is not allowed to shorten, i.e., it is in an isometric condition, then Eq. (2) is reduced to

$$E = A,$$

i.e., the rate of energy release is equal to the activation energy. When the muscle contracts, an additional chemical reaction takes place, and it releases an amount of "extra energy" equal to the sum of the shortening heat and the work done, $S + W$, in Eq. (2). By measuring E and A , Hill identified the term $S + W$, the rate of "extra energy," and showed that it is represented by the empirical equation

$$S + W = b(P_0 - P), \quad (4)$$

where P_0 is the (maximal) isometric tension. He asserts further that empirically,

$$S = av. \quad (5)$$

Combining Eqs. (3), (4), and (5), we obtain

$$S + W = b(P_0 - P) = av + Pv. \quad (6)$$

Rearranging terms, we have

$$(a + P)v = b(P_0 - P) = b(-P - a) + bP_0 + ab.$$

Hence

$$(a + P)(v + b) = b(P_0 + a),$$

which is Eq. (1).

Hill's major contribution lies in his ingenious methods for accurately measuring the heats E , A , W , and S . His method of derivation of Eq. (1) endows a thermomechanical meaning to the constants a and b . Later, by employing a technique of rapid freezing and phosphate analysis, Carlson, Siger (1960), Mommaerts (1954), and Mommaerts et al. (1962) measured E in terms of phosphocreatine split, thus opening the way to biochemical studies of muscle contraction.

Three years earlier than Hill (1938), Fenn and Marsh (1935) presented a relationship between v and P , which is of the form

$$P = Ae^{-v/B} + C, \quad (7)$$

where A , B , and C are constants. Although it differs from Eq. (1) considerably in form, it behaves numerically very much the same in the range $0 < P < P_0$, $0 < v < v_0$. On the other hand, Polissar (1952) proposed another form:

$$v = \text{const}(k_L e^{-C_L P} - k_s e^{C_s P}), \quad (8)$$

where k_L , C_L , k_s , and C_s are constants. However, Hill's equation remains the most popular. Many years later, Hill (1970) admitted that it is better to think of Eq. (1) directly as a force-velocity relationship, and not as a thermo-mechanical expression, because improved experiments do not always support Eqs. (4) and (5). In 1966 Hill changed the constant a in Eq. (1) to α , in order to dissociate it from its former meaning.

Hence, from the point of view of biomechanics, we shall regard Hill's equation as an empirical equation describing the force-velocity relationship of a tetanized skeletal muscle upon immediate release from an isometric condition.

The Dimensionless Form of Hill's Equation

Let us recapitulate: Hill's equation refers to a property of skeletal muscle in the tetanized condition. A muscle bundle is fixed at a certain length, L_0 . It is then stimulated electrically at a frequency that is sufficiently high to tetanize the muscle to the maximum tension T_0 (henceforth we shall use T for tension in place of P). In this tentanized condition the muscle is released to a new length L , which is smaller than L_0 , or a new tension T which is smaller than T_0 . Immediately after release, the velocity of contraction $v = -dL/dt$ and the tension T are measured. Then an empirical relationship between T and v is Hill's equation:

$$(T + a)(v + b) = b(T_0 + a).$$

This can be rewritten as

$$v = b \frac{T_0 - T}{T + a}, \quad (9)$$

or

$$T = \frac{bT_0 - av}{v + b} = a \frac{v_0 - v}{v + b}. \quad (10)$$

When $T = 0$, the velocity v reaches the maximum

$$v_0 = \frac{bT_0}{a}, \quad (11)$$

which is used in Eq. (10). We can write Eqs. (9) and (10) in the nondimensional form

$$\frac{v}{v_0} = \frac{1 - (T/T_0)}{1 + c(T/T_0)} \quad (12)$$

or

$$\frac{T}{T_0} = \frac{1 - (v/v_0)}{1 + c(v/v_0)}, \quad (13)$$

where

$$c = \frac{T_0}{a}. \quad (14)$$

It is customary to call v_0 the maximum velocity and designate it by v_{\max} . But if a small compressive stress is imposed (as it can be in cardiac muscle; see Sec. 10.5), the velocity of contraction can exceed v_0 ; so v_0 is not the maximum velocity achievable. Similarly, if a muscle tetanized at length L_0 is stretched a little greater than L_0 , the tension can exceed T_0 , and T_0 is not the maximum tension achievable.

Behavior of the Constants a , b , T_0 , v_0 , and c in Hill's Equation

Hill's equation contains three independent constants. Writing it in the form of Eq. (1), the constants are a , b , T_0 . Writing it in the form of Eqs. (12) and (13), the constants are T_0 , v_0 and $c = T_0/a$. These constants are functions of the initial muscle length L_0 , the temperature and composition of the bath, ionic concentration of calcium, drugs, etc.

The maximum isometric tension T_0 depends strongly on L_0 . If L_0 is too small or too large, T_0 drops to zero. There is an optimum length L_0 at which T_0 is the maximum. Figure 9.7:2 shows the relationship between T_0 and L_0 (expressed as sarcomere length) for a single fiber of frog's skeletal muscle. This figure is reproduced from Gordon et al. (1966), who tested single skeletal fibers with two gold leaf markers attached to the surface of the muscle to interrupt the focused light spots from a dual beam oscilloscope, so as to control the amount of light falling on two photocells. By linking the photocell output to the deflection of the spots, the markers can be followed and a signal obtained that is proportional to marker separation. This allows a strain measurement of the middle portion of the fiber, thus avoiding the end effects due to clamping. In this way data of high quality can be obtained.

Figure 9.7:2 shows the result for a frog muscle cell, whose slack sarcomere length is $2.1 \mu\text{m}$ (the sarcomere length to which the resting muscle returns when unloaded). It is seen that when the sarcomere length is in the range $2.0\text{--}2.2 \mu\text{m}$, the maximum developed active tension does not depend on the muscle length. When the muscle fiber is maintained at a length outside this

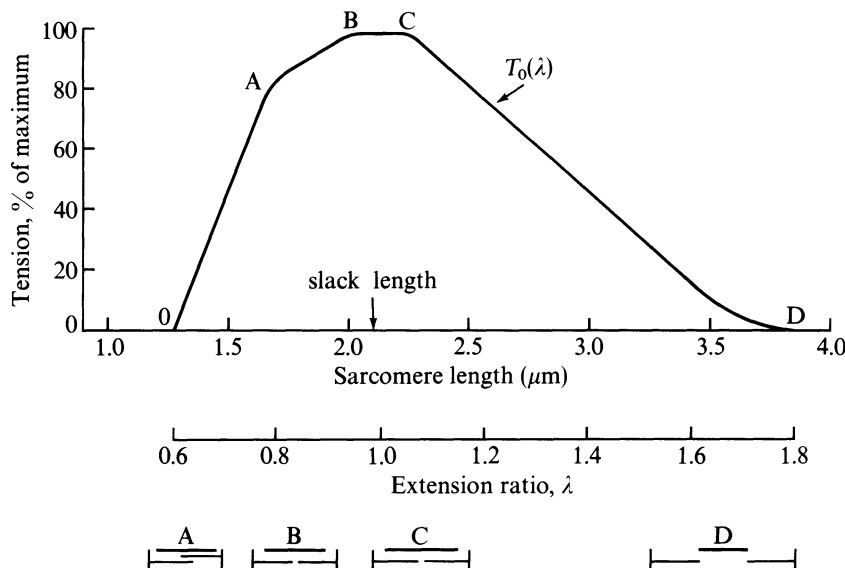


Figure 9.7.2 The steady-state or isometric tension-length curve as found by Gordon et al. (1966) for intact frog skeletal muscle fibers. The slack length ($2.1 \mu\text{m}$) is the sarcomere length to which the muscle will return when unloaded. It defines the reference point for the extension ratios shown below. The left-hand part of the curve (OA, AB) is commonly referred to as the ascending limb, the central flat portion (BC) is the plateau region, and the right-hand part (CD) is the descending limb. The relative positions of the actin and myosin filaments at different sarcomere lengths from A to D are shown at the bottom. From Gordon et al. (1966), by permission.

range, the maximum developed active tension is smaller. This feature is often explained in terms of the variation of the number of cross-bridges between myosin and actin fibers. If the muscle length is too long, the actin and myosin filaments are pulled too far apart, the cross-bridge number decreases, and the tension drops. If the muscle is too short, the actin filaments interfere with each other; they may shield each other and hinder the function of cross-bridges.

The maximum velocity v_0 does not depend as much on the muscle length L_0 . In fact, whether v_0 is independent of L_0 or not was a long controversy in cardiology. For a time it was believed that v_0 is independent of L_0 , and hence it was used as an index of “contractility,” related to the state of health of the muscle, and its change with drug intervention was used to indicate the effectiveness of drugs. Today it is generally agreed that v_0 does depend on L_0 in some complex but minor way.

The constant c seems to be almost independent of L_0 . It follows that the constant a is almost proportional to T_0 . The constant b is equal to v_0/c . The value of c for skeletal muscle is in the range of 1.2 to 4.

Other Equivalent Forms

A dimensionless form corresponding to Eq. (7) by Fenn and Marsh is

$$\frac{T}{T_0} = \frac{e^{-\beta(v/v_0)} - e^{-\beta}}{1 - e^{-\beta}}, \quad (15)$$

where β is a constant. An analogous equation is

$$\frac{v}{v_0} = \frac{e^{-\gamma(T/T_0)} - e^{-\gamma}}{1 - e^{-\gamma}}, \quad (16)$$

where γ is a constant.

9.8 Hill's Three-Element Model

Hill's equation was derived from quick-release experiments on frog sartorius muscle in tetanized condition. It reveals only one aspect of the muscle behavior. It cannot describe a single twitch, nor a wave summation. It cannot even describe the force-velocity relationship when a tetanized muscle is subjected to a slow release, nor to a strain that varies with time. It cannot describe the mechanical behavior of an unstimulated muscle. To remedy these shortcomings a more comprehensive approach is needed. Several methods have been proposed. Of these the best known is the Hill's three-element model.

For 40 years, since 1938, Hill's model of muscle contraction has dominated the field. It is, therefore, useful to know this model and to understand its strength and weakness. In the 40 year period many ideas have been added to the model in order to accommodate newly discovered facts. Originally quite simple, gradually the "series elastic" element became a very complex entity. To explain the single twitch, an "active state" function was introduced, the exact meaning of which turned out to be elusive. The arrangement of the three elements in the model is not unique. These difficulties gradually contributed to the decline of Hill's method.

To make the presentation as brief and definitive as possible, we present a version (Fung, 1970) that uses the language of sliding-element theory, and we base the discussion on a single sarcomere. A muscle is regarded as an accumulation of sarcomeres, although the assumption that all sarcomeres are identical is one of the dubious assumptions.

The Model and the Related Basic Equations

Hill's model (Fig. 9.8:1) represents an active muscle as composed of three elements. Two elements are arranged in series: (a) a contractile element, which at rest is freely extensible (i.e., it has zero tension), but when activated

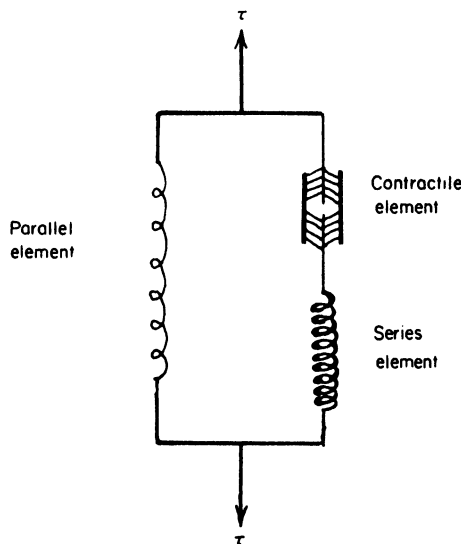


Figure 9.8:1 Hill's functional model of the muscle.

is capable of shortening; and (b) an elastic element arranged in series with the contractile element. To account for the elasticity of the muscle at rest, a “parallel elastic element” is added. This parallel element was ignored in Section 9.7. We now include it for the general case.

Most authors would identify the contractile element with the sliding actin-myosin molecules, and the generation of active tension with the number of active cross-bridges between them. Many suggestions have been made about the structural and ultrastructural basis of the parallel and series elastic elements; but none is definitive. The series elasticity may be due to the intrinsic elasticity of the actin and myosin molecules and cross-bridges, and of the Z band and connective tissues. It may arise also from the nonuniformity of the sarcomeres and nonuniform activation of the myofibril filaments. The parallel elasticity may be due to connective tissues, cell membranes, mitochondria and collagenous sheaths; but the most unsettling question is whether the actin-myosin complex is truly free in the resting state of the muscle. Some of the complex behavior of the parallel element, its dependence on the contraction history of the muscle, drugs, and temperature, may be due to the residual coupling of actin-myosin complex.

Assuming that the contractile element contributes no tension in a resting muscle, then the stress-strain-history relationship of a resting muscle determines the constitutive equation of the parallel element. The difference between the mechanical properties of the whole muscle and those of the parallel element then characterizes the contractile and series elastic elements in combination. Unfortunately, since these elements are connected in series, the division of the total strain between these two elements is not unique unless some additional assumptions are added.

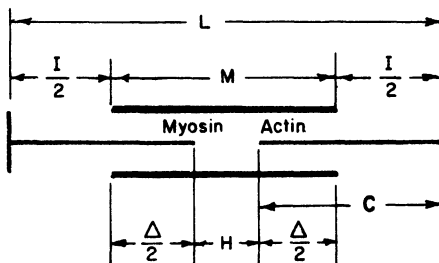


Figure 9.8:2 Geometric nomenclature of various elements of a muscle sarcomere unit.

Let us make the usual assumptions that the contractile element is tension-free when the muscle is in the resting state (a corollary is that the resting state is unique), and that the series elastic element is truly elastic (not viscoelastic). Let us express the geometric change of a muscle sarcomere in terms of the actin and myosin fibers as shown in Fig. 9.8:2, where

M = myosin filament length

C = actin filament length

Δ = insertion of actin filaments, i.e., the overlap between actin and myosin filaments

H = H-band width

I = I-band width

L = total length of sarcomere

L_0 = length of sarcomere at zero stress*

η = extension of the series elastic element in a sarcomere

We define the insertion Δ by the equation

$$\Delta = M - H = 2C - I \quad (1)$$

and the length L by

$$L = M + I = M + 2C - \Delta \quad (\text{without elastic extension}) \quad (2)$$

and

$$L = M + I + \eta = M + 2C - \Delta + \eta \quad (\text{with elastic extension}). \quad (3)$$

On differentiating Eq. (3) with respect to time, we obtain the basic kinematic relation

$$\frac{dL}{dt} = -\frac{d\Delta}{dt} + \frac{d\eta}{dt}. \quad (4)$$

Now consider the stress. The strain in the parallel elastic element can be defined as $(L - L_0)/L_0$; but since L_0 is a constant we can write simply[†]

$$\tau^{(P)} = P(L) \quad (5)$$

* Note the specific meaning of L_0 here. It is different from the L_0 in Sec. 9.7.

[†] For simplicity we assume that the parallel element is elastic. But it is very easy to generalize this analysis to the case in which the parallel element is viscoelastic (See Prob. 9.8.)

for the stress contributed by the parallel elastic element. Similarly, we write the stress contributed by the activated actin-myosin filaments:

$$\tau^{(s)} = S(\eta, \Delta). \quad (6)$$

$S(\eta, \Delta)$ is identically zero when the muscle is at rest; so that

$$S(\eta, \Delta) \geq 0 \quad \text{when } \eta \geq 0$$

and

$$S(\eta, \Delta) = 0 \quad \text{when } \eta = 0. \quad (7)$$

The total tensile stress is the sum of the contributions from the series and parallel elements:

$$\tau = \tau^{(p)} + \tau^{(s)} = P(L) + S(\eta, \Delta). \quad (8)$$

If the stress varies with time, we have

$$\frac{d\tau}{dt} = \frac{dP}{dL} \frac{dL}{dt} + \left. \frac{\partial S}{\partial \eta} \right|_{\Delta} \frac{d\eta}{dt} + \left. \frac{\partial S}{\partial \Delta} \right|_{\eta} \frac{d\Delta}{dt}. \quad (9)$$

On substituting Eq. (4) into Eq. (9) we obtain the basic dynamic equation

$$\begin{aligned} \frac{d\tau}{dt} &= \frac{dP}{dL} \frac{dL}{dt} + \left. \frac{\partial S}{\partial \eta} \right|_{\Delta} \left(\frac{dL}{dt} + \frac{d\Delta}{dt} \right) + \left. \frac{\partial S}{\partial \Delta} \right|_{\eta} \frac{d\Delta}{dt} \\ &= \left(\frac{dP}{dL} + \left. \frac{\partial S}{\partial \eta} \right|_{\Delta} \right) \frac{dL}{dt} + \left(\left. \frac{\partial S}{\partial \eta} \right|_{\Delta} + \left. \frac{\partial S}{\partial \Delta} \right|_{\eta} \right) \frac{d\Delta}{dt}. \end{aligned} \quad (10)$$

Two special cases of great interest are:

Isometric contraction: $L = \text{const.}$ and $dL/dt = 0$,

$$\frac{d\tau}{dt} = \left(\left. \frac{\partial S}{\partial \eta} \right|_{\Delta} + \left. \frac{\partial S}{\partial \Delta} \right|_{\eta} \right) \frac{d\Delta}{dt}; \quad (11)$$

Isotonic contraction: $\tau = \text{const.}$ and $d\tau/dt = 0$,

$$\left(\frac{dP}{dL} + \left. \frac{\partial S}{\partial \eta} \right|_{\Delta} \right) \frac{dL}{dt} + \left(\left. \frac{\partial S}{\partial \eta} \right|_{\Delta} + \left. \frac{\partial S}{\partial \Delta} \right|_{\eta} \right) \frac{d\Delta}{dt} = 0. \quad (12)$$

Let us illustrate the application of these equations by considering the methods for determining the characteristics of the series elastic element.

The Quick Release Experiment

This experiment consists of three steps:

1. Preload the muscle in an unstimulated state to a length L_1 .
2. Stimulate isometrically until the tensile stress develops to a specific value τ_1 .
3. Suddenly change the tensile stress from τ_1 to τ_2 .

Let us denote the length corresponding to τ_2 by L_2 , the actin-myosin insertion at τ_1 by Δ_1 , and the elastic extension of the series element corresponding to τ_1 and τ_2 by η_1 and η_2 , respectively. The hypothesis is made that the process in step 3 takes place so fast that Δ does not change when the stress drops from τ_1 to τ_2 . Then

$$\Delta_2 = \Delta_1, \quad (13a)$$

$$\tau_1 = P(L_1) + S(\eta_1, \Delta_1), \quad (13b)$$

$$\tau_2 = P(L_2) + S(\eta_2, \Delta_1). \quad (13c)$$

Substracting, we obtain

$$\tau_1 - \tau_2 = P(L_1) - P(L_2) + S(\eta_1, \Delta_1) - S(\eta_2, \Delta_1). \quad (13d)$$

Applying Eqs. (3) and (13a) to the conditions at τ_1 and τ_2 , and noting that M , C , and Δ are unchanged, we have

$$L_1 - L_2 = \eta_1 - \eta_2. \quad (13e)$$

Equations (13d) and (13e) give us $S(\eta_1, \Delta_1) - S(\eta_2, \Delta_1)$ as a function of $\eta_1 - \eta_2$ when τ_1 , τ_2 , L_1 , L_2 , $P(L_1)$, and $P(L_2)$ are measured. To determine $S(\eta_1, \Delta_1)$ as a function of η_1 , we need to find a certain muscle length L_2 at which η_2 and $S(\eta_2, \Delta_1)$ are zero. This can be found by trial and error. Suppose we find a special value of $\tau_2 = \tau_2^*$ that corresponds to a length $L_2 = L_2^*$, at which

$$\tau_2^* = P(L_2^*), \quad (13f)$$

then by Eq. (8) we must have

$$S(\eta_2^*, \Delta_2) = 0, \quad (13g)$$

and hence, by Eq. (7),

$$\eta_2^* = 0. \quad (13h)$$

Combining these results with Eqs. (13d) and (13e), we have

$$\eta_1 = L_1 - L_2^*, \quad (13i)$$

$$S(\eta_1, \Delta_1) = \tau_1 - P(L_1). \quad (13j)$$

Thus the tensile stress S in the series elastic element can be plotted as a function of the extension η_1 .

The Isometric-Isotonic Change-Over Method

This method consists of three steps:

1. Preload at stress τ_p , leading to length L_p .
2. Stimulate isometrically at length L_p until a preassigned afterload τ_{aft} is reached.
3. Isotonic contraction follows with tensile stress remaining at τ_{aft} .

According to Eq. (11) and with obvious notation, we obtain at the end of step 2:

$$\frac{d\tau}{dt} \Big|_{\text{isometric}, \tau_{\text{aft}}} = \left\{ \frac{\partial S}{\partial \eta} \Big|_{\Delta} (\eta_{\text{aft}}, \Delta_{\text{aft}}) + \frac{\partial S}{\partial \Delta} \Big|_{\eta} (\eta_{\text{aft}}, \Delta_{\text{aft}}) \right\} \times \frac{d\Delta}{dt} \Big|_{\text{isometric}}, \quad (14a)$$

whereas at the beginning of step 3, according to Eq. (12),

$$\frac{d\Delta}{dt} \Big|_{\text{isotonic}} = - \left[\frac{dP}{dL} + \frac{\partial S}{\partial \eta} \Big|_{\Delta} \right] \left[\frac{\partial S}{\partial \eta} \Big|_{\Delta} + \frac{\partial S}{\partial \Delta} \Big|_{\eta} \right]^{-1} \frac{dL}{dt} \Big|_{\text{isotonic}} \quad (14b)$$

Under the basic assumption that for an activated muscle $d\Delta/dt$ is a function of the stress S , the insertion Δ , the length L , and the time interval after stimulation t , but nothing else, the rates $d\Delta/dt$ in Eqs. (14a) and (14b) can be equated and we obtain, at the instant of change over,

$$\begin{aligned} \frac{d\Delta}{dt} \Big|_{\text{isometric}} &= \frac{(d\tau/dt)|_{\text{isometric}, \tau_{\text{aft}}}}{(\partial S/\partial \eta)|_{\Delta} + (\partial S/\partial \Delta)|_{\eta}} = \frac{d\Delta}{dt} \Big|_{\text{isotonic}} \\ &= - \left[\frac{dP}{dL} + \frac{\partial S}{\partial \eta} \Big|_{\Delta} \right] \left[\frac{\partial S}{\partial \eta} \Big|_{\Delta} + \frac{\partial S}{\partial \Delta} \Big|_{\eta} \right]^{-1} \cdot \frac{dL}{dt} \Big|_{\text{isotonic}}, \end{aligned}$$

that is,

$$\frac{\partial S}{\partial \eta} \Big|_{\Delta} + \frac{dP}{dL} \Big|_{\tau_{\text{aft}}} = - \frac{(d\tau/dt)|_{\text{isometric}, \tau_{\text{aft}}}}{(dL/dt)|_{\text{isotonic}, \tau_{\text{aft}}}}. \quad (14c)$$

Since dP/dL is known $\partial S/\partial \eta$ can be computed and plotted as a function of τ_{aft} .

Experimental Results on the Series Element

Extensive work by many authors has shown that when $\partial S/\partial \eta$ is plotted against $\tau_{\text{aft}} = S + P$, it turns out to be a straight line. For a given preload, P is a constant; hence a curve of $\partial S/\partial \eta$ vs S is also a straight line.

To express this result together with the requirement that S must be zero when η vanishes, we write

$$\frac{\partial S}{\partial \eta} = \alpha(S + \beta), \quad (15)$$

which integrates to

$$S = (S^* + \beta)e^{\alpha(\eta - \eta^*)} - \beta. \quad (16)$$

Here α, β are constants and S^*, η^* are a pair of corresponding experimental values, $S = S^*$ when $\eta = \eta^*$. The condition $S = 0$ when $\eta = 0$ requires that

$$\beta = \frac{S^* e^{-\alpha \eta^*}}{1 - e^{-\alpha \eta^*}}. \quad (17)$$

It is sometimes necessary to adjust the experimental values of β, S^* , and η^* so that Eq. (17) is satisfied. Parmley and Sonnenblick (1967) showed that

for a cat's papillary muscle

$$\begin{aligned}\alpha &= 0.4 \text{ per } 1\% \text{ muscle length,} \\ \alpha\beta &= 0.8 \text{ per } 1\% \text{ muscle length.}\end{aligned}$$

Velocity of Contraction

As soon as the length of the muscle is broken down into two components in series, we have to speak of three velocities: the rate of change of the muscle length, that of the contractile element, and that of the series elastic element. They are related by Eq. (4).

In Sec. 9.7 we speak of the velocity-tension relationship. In the three-element model we have two tensions, P and S , and three velocities. Which is related to which? Or more precisely, Hill's equation represents a relationship between which tension and which velocity? In Hill's own experiments the initial length of the muscle was so small that the force in the parallel element, P , was negligible. If P is finite, it is expected not to be related to the velocity as in Hill's equation. Hence it is logical to assume that Hill's equation describes S , the tension in the contractile element. How about velocity? To answer the question, let us consider the redevelopment of tension after a step change in length. If S were related to dL/dt , then since $dL/dt = 0$ after the step change, there can be no change in S , and the phenomenon of tension redevelopment cannot be dealt with. Hence S must be related to dA/dt or $d\eta/dt$, which in this case are equal and opposite. With these considerations, we write Hill's equation [see Eq. (12) of Sec. 9.7] as

$$\frac{1}{v_0} \frac{dA}{dt} = \frac{1 - (S/S_0)}{1 + c(S/S_0)}, \quad (18)$$

where c is a constant, S_0 is the tension in the series element in a tetanized isometric contraction, and v_0 is the velocity of dA/dt when $S = 0$. This equation is expected to be valid for, and only for, a tetanized muscle.

To describe a single twitch or wave summation or other dynamic events in a muscle, Eq. (18) must be modified to include a time factor—a function of time after stimulation. An example of such a modification is given in Chapter 10, Sec. 10.4, for the heart muscle which normally functions in successive single twitches. See Eq. (5), Sec. 10.4. The function $f(t)$ in Eq. (10.4:5) has to be determined by experiments; that given in Eq. (6) of Sec. 10.4 is gleaned from Edman and Nilsson's work. But we shall defer further discussions to Chapter 10.

Tension Redevelopment After a Step Change in Length

To illustrate the application of the preceding equations, consider the redevelopment of tension after a step shortening in length of an isometric tetanized muscle. Let the new length be L and the tension be S_1 at time

$t = 0$ immediately after the step change. Let L be sufficiently small so that P is negligible compared with S . Assume that $\partial S/\partial \eta$ is given by Eq. (15) and that $\partial S/\partial A = 0$. Equations (11) and (18) apply. Hence by substitution, Eq. (11) becomes

$$\frac{d\sigma}{dt} = \alpha\gamma v_0 \frac{(1 - \sigma)(\sigma + k)}{\sigma + \gamma}, \quad (19)$$

where

$$\sigma = \frac{S}{S_0}, \quad k = \frac{\beta}{S_0}, \quad \sigma_1 = \frac{S_1}{S_0}, \quad \gamma = \frac{1}{c}. \quad (20)$$

An integration of Eq. (19) yields the time for stress to change from σ_1 to σ :

$$t = \frac{1}{\alpha\gamma v_0} \int_{\sigma_1}^{\sigma} \frac{x + \gamma}{(x + k)(1 - x)} dx. \quad (21)$$

The time required for the tension to reach the maximum isometric tension S_0 corresponding to L is

$$t|_{\sigma=1} = \frac{1}{\alpha\gamma v_0} \int_{\sigma_1}^1 \frac{x + y}{(x + k)(1 - x)} dx. \quad (22)$$

Note that the integral is divergent at the upper limit, so that its value is infinite. When $\sigma < 1$ but tends to 1, the time $t(\sigma)$ tends to $-\log(1 - \sigma)$, i.e., it tends to infinity logarithmically.

Since a peak tension is always observed at finite time under isometric conditions, the inaccessibility of maximum isometric tension is an undesirable theoretical difficulty that comes with Hill's model combined with Hill's equation. By modifying the Hill's equation [see, e.g., Eq. (9) of Sec. 10.4], however, this difficulty can be avoided [by using $n < 1$ in Eq. (9) of Sec. 10.4].

Critique of Hill's Model

Hill's model is simple if the contractile element is entirely stress free and freely distensible in the resting state, and is described exactly by Hill's equation when the muscle is activated, if the series and parallel elements are elastic, and if the whole muscle is a simple combination of identical sarcomeres in series and in parallel. Unfortunately, none of these is true.

Modifications have been proposed. In some, the series and parallel elements are made viscoelastic. In another, these elements are arranged differently, with one element parallel with the contractile, and another in series with the combination. But in all models it is necessary to modify Hill's equation for the contractile element if the muscle is not tetanized. To describe a single twitch, it is necessary to acknowledge the time-dependent character of the contractile element with respect to stimulation.

The basic difficulty with Hill's model and all its modifications is that the division of forces between the parallel and contractile elements and the division of extensions between the contractile and the series elements are

arbitrary. These divisions cannot be made without introducing auxiliary hypotheses. Consequently, experimental evaluation of the properties of the elements (contractile, series, and parallel) depends on the arbitrary hypotheses. The experimentally determined properties of these elements are not intrinsic properties of the muscle, but only the reflection of muscle property through a model that cannot be uniquely defined. Further discussion of these points is given in Sec. 10.5.

9.9 Other Approaches

There are other approaches to muscle mechanics. In the realm of phenomenological and empirical approach, a promising method is based on the concept of fading memory, analogous to the viscoelasticity theory presented in Chapter 7, Sec. 7.6. In a viscoelastic material the stress at a given time is not only related to the deformation or rate of deformation at that instant of time, but also to the history of shape changes. Now, the stress in a tetanized muscle, suddenly released from an isometric condition, is related to the velocity of contraction and muscle length. Then, if this tetanized muscle is subjected to a general deformation history, would it not be logical to assume a fading memory so that the stress at the time t is more closely related to the velocity of contraction that occurred immediately before t than what occurred a long time ago?

The simplest memory is the linear memory, for which all the past experience is assumed to be linearly superposable. Let $x(t)$ represent the history of the “cause,” and $y(t)$, the “effect.” If $x(t)$ is a step function that is zero for time $t < 0$, suddenly jumps to a value $x(0)$ at $t = 0$, and remains constant afterward, let the effect $y(t)$ be proportional to $x(0)$:

$$y(t) = \phi(t)x(0). \quad (1)$$

By the principle of linear memory, any step increase in x at any time will cause an effect by this expression after that time. Now, if $x(t)$ is a continuous function of time, t , we can build up $x(t)$ by a sequence of infinitesimal steps, and according to the remarks above we can compute the effect $y(t)$ by a superposition of a sequence of infinitesimal responses. Thus, if in a time interval from τ to $\tau + d\tau$ the value of x is increased by the amount $[dx(\tau)/d\tau]d\tau$, the value of the response $y(t)$ will be increased by the amount

$$dy(t - \tau) = \phi(t - \tau) \frac{dx(\tau)}{d\tau} d\tau.$$

Here t is replaced by $t - \tau$ because the response dy is evaluated at t for an excitation that took place in the time interval from τ to $\tau + d\tau$. By the assumed principle of linear superposition, we have

$$y(t) = \int dy = \phi(t)x(0) + \int_0^t \phi(t - \tau) \frac{dx(\tau)}{d\tau} d\tau \quad (2)$$

or

$$y(t) = \phi(t)x(0) + \int_0^t \phi(\tau) \frac{dx(t-\tau)}{d(t-\tau)} d\tau, \quad (2a)$$

which embodies the *principle of linear memory*. That Eq. (2a) follows Eq. (2) can be seen by transforming the variable $t - \tau$ to τ' in Eq. (2), and then dropping the prime.

Apply this to the tetanized skeletal muscle. What shall we take for x ? And what for y ? To decide this, consider the special case of quick release. Immediately after a quick release we have

$$y(0) = \phi(0)x(0), \quad (3)$$

because the integral in Eq. (2) vanishes as $t \rightarrow 0$. But this should be the Hill's equation. Hence by comparing Eq. (3) with Eqs. (12) and (13) of Sec. 9.7, we see that we may take $\phi(0) = 1$ and

$$x \text{ or } y = \frac{v}{v_0}, \quad y \text{ or } x = \frac{1 - (T/T_0)}{1 + c(T/T_0)}; \quad (4)$$

or

$$x \text{ or } y = \frac{T}{T_0}, \quad y \text{ or } x = \frac{1 - (v/v_0)}{1 + c(v/v_0)}. \quad (5)$$

On the other hand, if we use the alternative Eqs. (15) and (16) of Sec. 9.7; we may take

$$x \text{ or } y = \frac{v}{v_0}, \quad y \text{ or } x = \frac{1}{1 - e^{-\gamma}} (e^{-\gamma T/T_0} - e^{-\gamma}); \quad (6)$$

$$x \text{ or } y = \frac{T}{T_0}, \quad y \text{ or } x = \frac{1}{1 - e^{-\beta}} (e^{-\beta v/v_0} - e^{-\beta}). \quad (7)$$

Which choice is the best would have to be decided by comparison with experimental data.

The function $\phi(t)$ is the *relaxation function* and may assume the form

$$\phi(t) = \sum_{i=1}^N A_i e^{-\alpha_i t}, \quad (8)$$

where $\alpha_i \geq 0$ and $\phi(0) = 1$. The constants $1/\alpha_i$ are *characteristic times* and A_i as a function of α_i is the *spectrum* of the relaxation function.

Bergel and Hunter (1979) first proposed this method by choosing x to be v/v_0 or $[d\lambda(t)/dt]/v_0$ and $y = [(1 - (T/T_0))/[1 + c(T/T_0)]]$. They examined the dynamics of a tetanized skeletal muscle fiber. In step release in length, they showed that the use of Eqs. (2) and (8) can fit the experimental data of Huxley (1974) and Ford, Huxley and Simmons (1977) quite well. In transient length response to step release in tension, their results compare well with experimental data of Podolsky and Nolan (1971), and Julian and Sollins

(1975). In frequency response to sinusoidal variation in length, the formula again fits quite well with the data of Julian and Sollins (1975).

The next step to be taken is to extend the fading memory theory to single twitch and other dynamic phenomena. The best test ground is the heart muscle. For this extension several alternative choices has to be made. Beside choosing x and y , we must decide what to do with T_0 and v_0 which are now functions of time after stimulation. This is a topic of current research.

So far we have discussed the phenomenological approach. A more basic approach was made by A. F. Huxley (1957, 1974). His model took account of the known structures of the muscle, as well as the mechanical and thermodynamic observations. The main features are that cross bridges act cyclically, attaching and detaching according to rate constants, which are functions of their position. The original theory is gradually modified to accept new results. See discussions by Simmons and Jewell (1974) and White and Thorson (1973).

Another basic theory was proposed by Iwazumi (1970) who sought a formulation in terms of the electromagnetic field generated by electrons attached to the fixed charge sites on the actin and myosin molecules and their changes during stimulation. This theory is discussed by Noble and Pollack (1977).

On the other hand, thermodynamicists have tried to formulate a theory on the basis of mechanochemistry. This includes Hill's own approach, and several new approaches based on the thermodynamics of irreversible processes and chemical dynamics.

Finally, a theory by Caplan (1966) derives Hill's equation on the basis of the principles of optimum design.

All these theories are very ingenious. They focus on the contractile element. None of them provide a full constitutive equation because they ignore such details as the cellular structure, mitochondria, membranes, collagen fibers, capillary blood vessels, etc. They pay no attention to the details of the transmission of forces from one cell to another in a muscle bundle, or the effect of deformation of one part of muscle on another. To account for these is difficult and tedious in a theoretical construction, but without such an account the accuracy of the constitutive equation will be poor. This speaks for the phenomenological approach presented earlier, in which the constitutive equation is based on experimental results: it can be highly accurate, although it furnishes no explanation.

Problems

9.2 Use Eqs. (2) and (8) of Sec. 9.9, and introduce the stretch ratio λ as a basic variable.

Write

$$v(t) = -\frac{d\lambda(t)}{dt}, \quad \frac{d\phi(t)}{dt} = \psi(t)$$

Choose x and y as Bergel and Hunter (1979) did. Derive an equation relating $T(t)$ and $\lambda(t)$.

- 9.3** Apply the result of Problem 9.2 to study the redevelopment of tension after a tetanized muscle is subjected to a small step release in length (say, a shortening of the order of 1% in length). Derive an equation for the tension history.
- 9.4** Apply the result of Problem 9.2 to study the transient change in muscle length following a sudden step release in tension.
- 9.5** Reconsider Problem 9.3 or 9.4 if the step change is accomplished by a ramp function in a finite interval of time Δt ; for example, by a length change specified by $\dot{\lambda} = 0$ when $t < 0$ and $t > \Delta t$, whereas $\dot{\lambda} = \Delta\lambda/\Delta t$ when $0 < t < \Delta t$.
- 9.6** Let a tetanized muscle be subjected to a small sinusoidal change in length. Using the result of Problem 9.2, determine the amplitude and phase of the force response.
- 9.7** Describe an alternative solution to Problem 9.6 on the basis of Hill's three-element model.
- 9.8** If the parallel element in Hill's model analyzed in Sec. 9.8 is viscoelastic, we replace Eq. (5) of Sec. 9.8 by

$$\tau^{(P)} = G * P(L),$$

where $G(t)$ is the normalized relaxation function (so normalized that $G(0) = 1$) and the symbol $*$ represents a convolution integral operation, i.e.,

$$\tau^{(P)}(t) = P[L(t)] + \int_0^t P[L(t - \tau)] \frac{\partial G(t)}{\partial \tau} d\tau.$$

$P(L)$ then represents the “elastic” response of the resting muscle. See Sec. 7.6, Eqs. (7.6:8) et seq. With this replacement, present a generalization of the analysis given in Sec. 9.8.

References

- Alexander, R. M. (1968) *Animal Mechanics*. Univ. of Washington Press, Seattle.
- Bergel, D. H., and Hunter, P. J. (1979) *The Mechanics of the Heart*. In *Quantitative Cardiovascular Studies* (Hwang, N. H. C., Gross, D. R., and Patel, D. J., eds.). University Park Press, Baltimore. Ch. 4, 151–213.
- Caplan, S. R. (1966) *J. Theor. Biol.* **11**, 63–86.
- Carlson, F. D., and Siger, A. (1960) *J. Gen. Physiol.* **43**, 33–60.
- Fenn, W. P., and Marsh, B. S. (1935) *J. Physiol.* **85**, 277.
- Ford, L. E., Huxley, A. F., and Simmons, R. M. (1977) *J. Physiol.* **269**, 441–515.
- Fung, Y. C. (1970) *J. Biomech.* **3**, 381–404.
- Gordon, A. M., Huxley, A. F., and Julian, F. J. (1966) *J. Physiol.* **184**, 170–192.
- Hill, A. V. (1938) *Proc. Roy. Soc., London, Ser. B* **126**, 136–195.
- Hill, A. V. (1970) *First and Last Experiments in Muscle Mechanics*. Cambridge University Press, Cambridge, U.K.
- Huxley, A. F. (1957) *Prog. Biophys. Biophys. Chem.* **7**, 255–318.
- Huxley, A. F. (1974) *J. Physiol.* **243**, 1–43.
- Huxley, A. F., and Simmons, R. M. (1971) *Nature* **233**, 533–538.

- Huxley, H. E. (1957) *J. Biophys. Biochem. Cytol.* **3**, 631–643.
- Huxley, H. E. (1969) *Science* **164**, 1356–1366.
- Iwazumi, T. (1970) *A new field theory of muscle contraction*. Ph.D. thesis. Univ. of Pennsylvania. Philadelphia.
- Julian, F. J., and Sollins, M. R. (1975) *Circulation Res.* **37**, 299–308.
- Kreuger, J. W., and Pollack, G. H. (1975) *J. Physiol.* **251**, 627–643.
- Mommaerts, W. F. H. M. (1954) *Nature* **174**, 1083–1084.
- Mommaerts, W. F. H. M., Olmsted, M., Seraydarian, K., and Wallner, A. (1962) *Biochim. Biophys. Acta* **63**, 82–92, 75–81.
- Noble, M. I. M., and Pollack, G. H. (1977) *Circulation Res.* **40**, 333–342.
- Parmley, W. W., and Sonnenblick, E. H. (1967) *Circulation Res.* **20**, 112–123.
- Podolsky, R. J. and Nolan, A. C. (1971). In *Contractility of Muscle Cells and Related Processes*. Podolsky R. J. (ed.), pp. 247–260. Prentice-Hall, Englewood Cliffs, N.J.
- Polissar, M. J. (1952) *Am. J. Physiol.* **168**, 766–781.
- Simmons, R. M., and Jewell, B. R. (1974) In *Recent Advances in Physiology*. Linden, R. J. (ed.) **9**, 87–147. Churchill, London.
- Warwick, R., and Williams, P. L. (eds.) (1973) *Gray's Anatomy*, 35th British edn. W. B. Saunders, Philadelphia.
- White, D. C. S., and Thorson, J. (1973). *Prog. Biophys. Mol. Biol.* **27**, 173–255.

CHAPTER 10

Heart Muscle

10.1 Introduction: The Difference Between Myocardial and Skeletal Muscle Cells

Both myocardial and skeletal muscle cells are striated. Their ultrastructures are similar. Each cell is made up of sarcomeres (from Z line to Z line), containing interdigitating thick myosin threads and thin actin threads. The basic mechanism of contraction must be similar in both; but important differences exist.

The most important difference between skeletal and cardiac muscle is the semblance of a *syncytium* in cardiac muscle with branching interconnecting fibers. See Fig. 10.1:1 and compare it with Fig. 9.3:1. The myocardium is not a true anatomical syncytium. Laterally, each myocardial cell is separated from adjacent cells by their respective sarcolemmas (cell membranes). At the ends, each myocardial cell is separated from its neighbor by dense structures, *intercalated discs*, which are continuous with the sarcolemma. Nevertheless, cardiac muscle functions as a syncytium, since a wave of depolarization is followed by contraction of the entire myocardium when a suprathreshold stimulus is applied to any one focus in the atrium. Graded contraction, as seen in skeletal muscle by activation of different numbers of cells, does not occur in heart muscle. All the heart's cells act as a whole (all-or-none response).

The second difference is the abundance of mitochondria (*sarcosomes*) in cardiac muscle as compared with their relative sparsity in skeletal muscle. See Fig. 10.1:2 and compare it with Fig. 9.3:1. Mitochondria extract energy from the nutrients and oxygen and in turn provide most of the energy needed by the muscle cell. On the membranes in the mitochondria are attached the

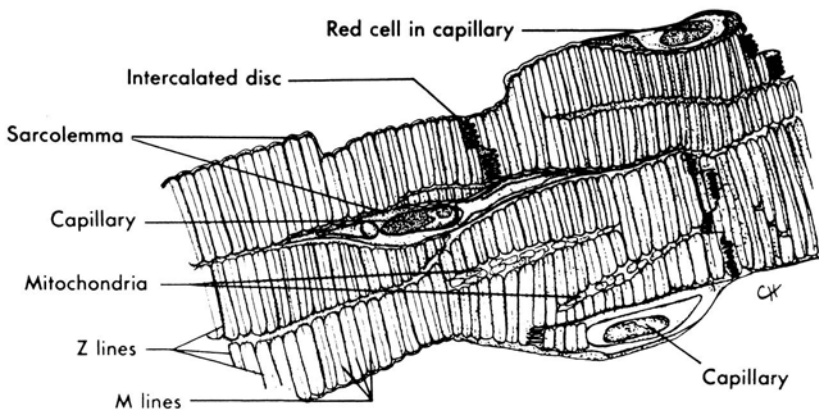


Figure 10.1:1 Diagram of cardiac muscle fibers illustrating the characteristic branching, the cell boundaries (sarcolemmas and intercalated discs), the striations, and the rich capillary supply (approxi. $\times 3000$). From Berne and Levy (1972), by permission.

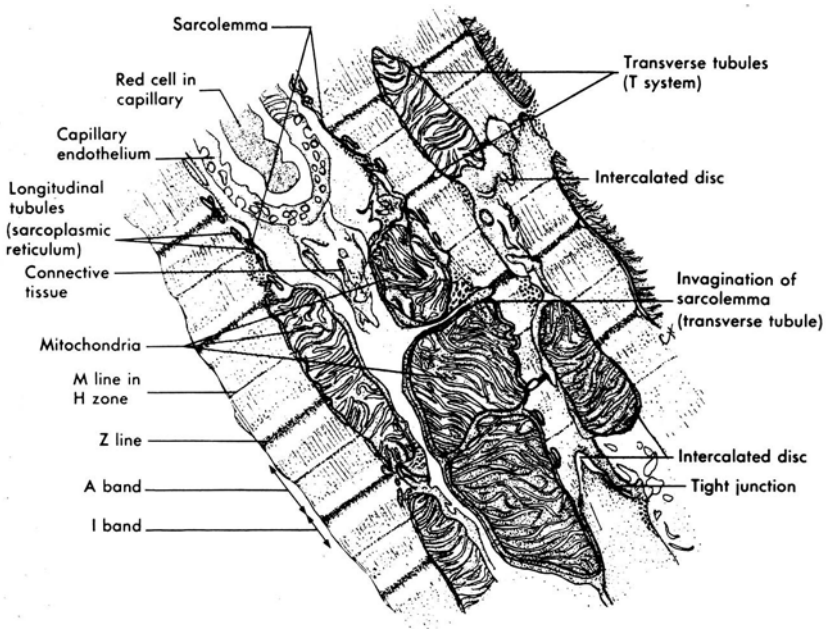


Figure 10.1:2 Diagram of an electron micrograph of cardiac muscle showing large numbers of mitochondria, the intercalated discs with tight junctions (nexi), the transverse tubules and the longitudinal tubules (approx. $\times 24\,000$). From Berne and Levy (1972), by permission.

oxidative phosphorylation enzymes. In the cavities between the membranes are dissolved enzymes. These enzymes oxidize the nutrients, thereby forming carbon dioxide and water. The liberated energy is used to synthesize a high energy substance called adenosine triphosphate (ATP). ATP is then transported out of the mitochondrion and diffuses into the myosin-actin matrix to permit the sliding elements to perform contraction and relaxation. The heart muscle relies on the large number of mitochondria to keep pace with its energy needs. The skeletal muscle, which is called on for relatively short periods of repetitive or sustained contraction, relies only partly on the immediate supply of energy by mitochondria. When a skeletal muscle contracts, the remaining energy needed is supplied by anaerobic metabolism, which builds up a substantial oxygen debt. This debt is repaid slowly by the mitochondria after the muscle relaxes. In contrast, the cardiac muscle has to contract repetitively for a lifetime, and is incapable of developing a significant oxygen debt. Hence the skeletal muscle can live with fewer mitochondria than the cardiac muscle must have.

A third difference is the abundance of capillary blood vessels in the myocardium (about one capillary per fiber) as compared with their relatively sparse distribution in the skeletal muscle (see Figs. 10.1:1 and 10.1:2). This is again consistent with the greater need of the myocardium for an immediate supply of oxygen and substrate for its metabolic machinery. With the close spacing of capillaries, the diffusion distances are short, and oxygen, carbon dioxide, substrates, and waste material can move rapidly between myocardial cell and capillary.

The exchange of substances between the capillary blood and the myocardial cells is helped further by a system of longitudinal and transverse tubules; see Figs. 10.1:2 and 10.1:3. These tubules are revealed by electron micrographs. The transverse tubules (T tubules) are deep invaginations of the sarcolemma into the interior of the fiber. The lumina of these T tubules are continuous with the bulk interstitial fluid; hence these tubules facilitate diffusion between interstitial and intracellular compartments. The transverse tubules may also play a part in excitation-contraction coupling. They are thought to provide a pathway for the rapid transmission of the electric signal from the surface sarcolemma to the inside of the fibers, thus enabling nearly simultaneous activation of all myofibrils, including those deep within the interior of the fiber. In mammalian ventricles the transverse tubules are connected with each other by longitudinal branches, forming a rectangular network. In the atria of many mammals the T system is absent or poorly developed.

Mechanically, the most important difference between cardiac and skeletal muscles lies in the importance of the resting tension in the normal function of the heart. The stroke volume of the heart depends on the end-diastolic volume. The end-diastolic volume depends on the stress-strain relationship of the heart muscle in the diastolic condition. Figure 10.1:4 shows the

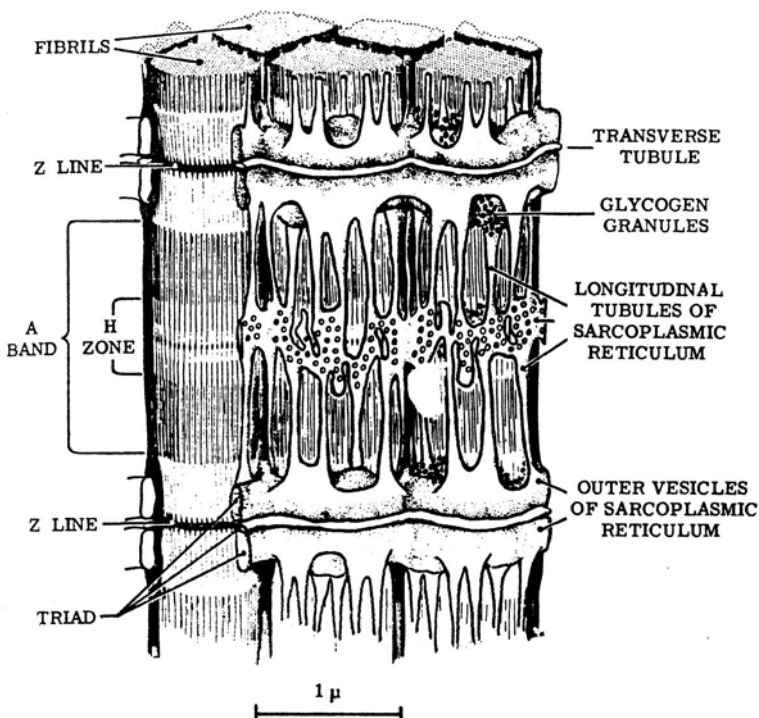


Figure 10.1:3 The internal membrane system of skeletal muscle. Contraction is initiated by a release of stored calcium ions from the longitudinal tubules. This "trigger" calcium has only a short distance to diffuse in order to reach the myofilaments in the *A* band. From Peachey (1965).

relationship between the end-diastolic muscle fiber length and the end-diastolic and peak systolic pressure in the left ventricle of a dog. If the tension in the muscle is computed from the pressure and is plotted against the length of muscle fibers, a diagram similar to Fig. 10.1:4 will be obtained with the ordinate reading muscle tension and the abscissa reading the muscle length. When such a diagram is compared with Fig. 9.7:2 for the skeletal muscle, two observations can be made. (a) In the normal (physiological) range of muscle length, the resting tension is entirely negligible in the skeletal muscle, but is significant in the heart muscle. (b) Because of the resting tension the operational range of the length of the heart muscle is quite limited, whereas that of the skeletal muscle can be larger. For example, at a filling pressure of 12 mm Hg a normal intact heart will reach its largest developed tension while the sarcomere length is 2.2 μm . If the filling pressure is raised to 50 mm Hg, the sarcomere length of the heart muscle will become 2.6 μm . Further increase in filling pressure will not greatly increase the sarcomere length. On the other hand, for the skeletal muscle the optimum sarcomere length for maximum developed tension is also 2.2 μm ; but with stretching a sar-

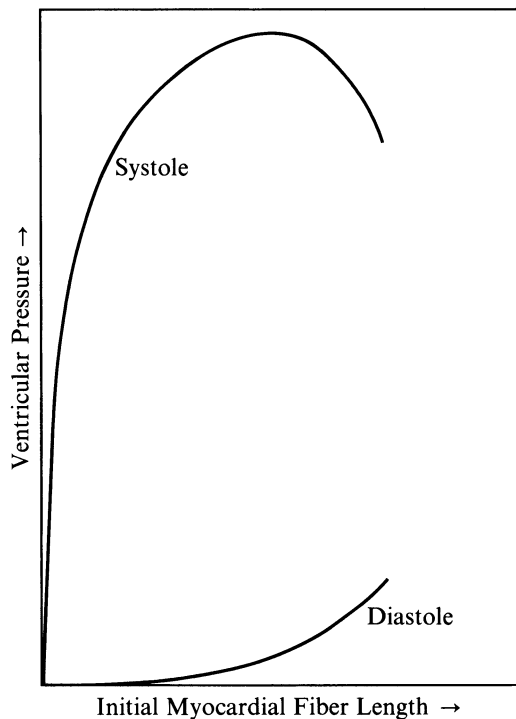


Figure 10.1:4 Relationship of left ventricular end-diastolic volume to end-diastolic and peak systolic ventricular pressure in intact dog heart. From Berne and Levy (1972), by permission. Figure redrawn from Patterson et al. (1914).

comere length of $3.65 \mu\text{m}$ can be obtained quite easily. From these observations we see that while the resting tension can be ignored in normal skeletal muscle mechanics, it cannot be ignored in cardiac mechanics.

10.2 Properties of Unstimulated Heart Muscle

As pointed out in the preceding section, the resting tension in a heart muscle is a significant determinant of the function of the heart, because it determines the end-diastolic volume and hence the stroke volume of the heart. Hence in this section we consider the mechanics of unstimulated heart muscle, with some details of test procedures and results.

A normal heart has a pacemaker, which initiates an electrical potential that causes the muscle to contract. Hence an isolated whole heart can beat by itself. An isolated papillary or trabecula muscle of the ventricles, however, does not have a strong pacemaker and can be tested in the unstimulated state.

From the mechanical point of view, a heart muscle in the resting state is an inhomogeneous, anisotropic, and incompressible material. Its properties

change with temperature and other environmental conditions. It exhibits stress relaxation under maintained stretch, and creep under maintained stress. It dissipates energy and has a hysteresis loop in cyclic loading and unloading. Thus, heart muscle in the resting state is viscoelastic.

A papillary or trabecula muscle test specimen is often obtained from the rabbit or cat. The specimen is put in a modified Kreb-Ringer solution bubbled with a 95% O₂ and 5% CO₂ mixture of gases. A specimen with diameter smaller than 1 mm can be kept alive in such a bath for at least 36 h without any diminishing of its force of contraction. Larger specimens cannot maintain their viability by diffusion alone without blood circulation, and are not used in *in vitro* experiments.

As in the testing of other biosolids, the specimen must be preconditioned in order to obtain repeatable mechanical responses to stress or strain. After preconditioning, measurement of a reference length (L_{ref}) and reference diameter (d_{ref}) can be made. A reference state is a standard condition, which for convenience is defined as a slightly loaded state of the specimen. In Pinto and Fung (1973), the load is caused by a 12-mg hook hanging from the lower end of the specimen which is suspended freely in a bath containing Kreb-Ringer solution. Thus the reference state referred to here is not a stress-free state, but an arbitrarily defined state convenient for laboratory work. For a very flexible nonlinear material, the specimen has no well-defined geometry in the stress-free state, and an accurate measure of length and cross-section is impossible. The reference state, however, while arbitrary, has the virtue of being definitely measurable. Extrapolation to the stress-free state can be done mathematically afterwards.

Relaxation Test Results

Relaxation test results Pinto and Fung (1973) are illustrated in Fig. 10.2:1. The specimen was subjected to a step stretch. The force history was recorded and normalized by the force reached immediately after the step. Figure 10.2:1 shows the data obtained at 15°C for five different stretch ratios ($\lambda = 1.05 - 1.30$) performed on a specimen. The ordinate $G(t)$ represents a normalized function of time known as the *reduced relaxation function*, which is defined as

$$G(t) = \frac{T(t)}{T_r}, \quad (1)$$

where $T(t)$ is the Lagrangian stress (total load divided by the cross-sectional area in the reference state) in the specimen at time t , and T_r is the Lagrangian stress in the specimen reached immediately after the step.

From Fig. 10.2:1 it is seen that $G(t)$ is essentially independent of the stretch λ . This independence is also observed at other temperatures. Figure 10.2:2 shows a plot of $G(t)$ vs time at $\lambda = 1.30$ for seven temperatures. The trend is

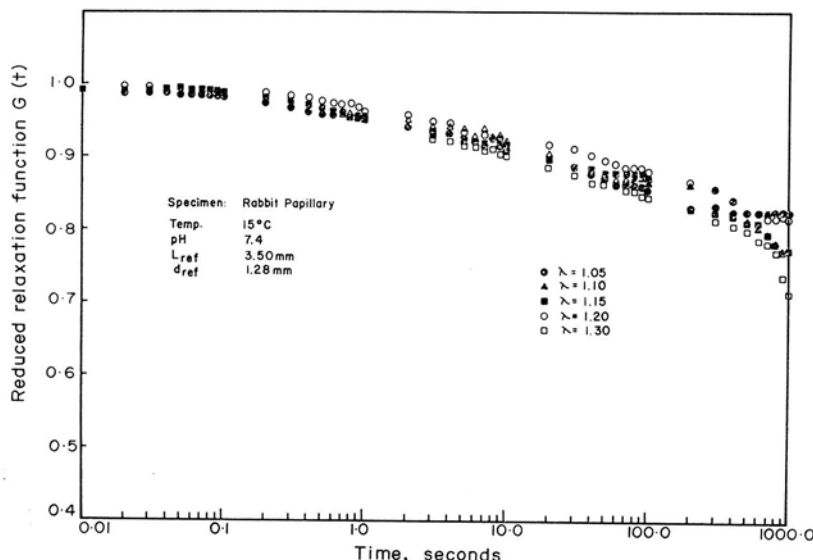


Figure 10.2:1 Reduced relaxation function of rabbit papillary muscle, showing the effect of the stretch ratio λ on $G(t)$. From Pinto and Fung (1973), by permission.

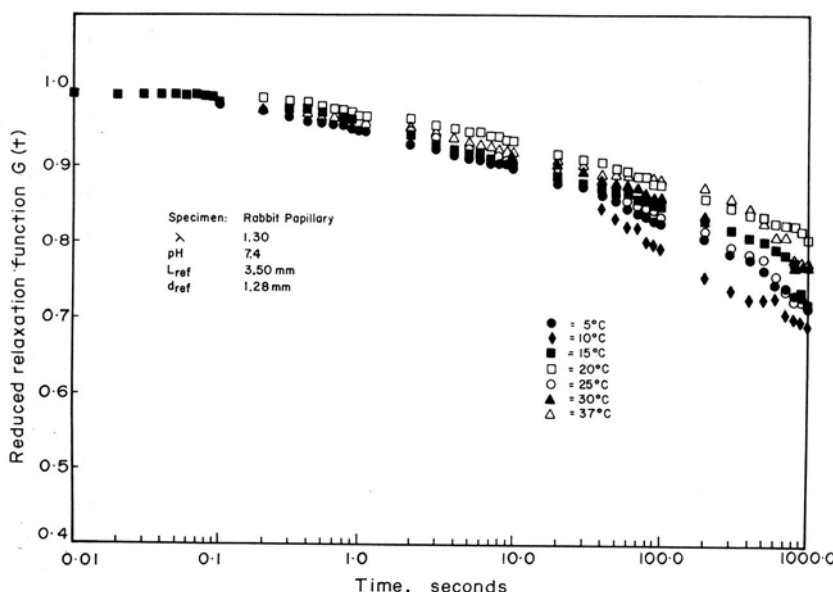


Figure 10.2:2 The effect of temperature on the reduced relaxation function of rabbit papillary muscle. From Pinto and Fung (1973), by permission.

not grossly temperature dependent, particularly in periods of time less than 1 s.

The response of a specimen to a step function in strain is called the relaxation function. For a heart muscle the relaxation function $T(t)$ is in general a function of many variables, such as the time, t , the stretch ratio λ , the temperature θ , the pH, and the chemical composition of the fluid environment, signified by the mole number of the i th chemical species, N_i :

$$T(t) = T(\lambda, \theta, \text{pH}, N_i \dots t). \quad (2)$$

If only λ and θ are varied while pH and the osmolarity of the chemical environment are maintained constant, then $T(t)$ can be written as

$$T(t) = T(\lambda, \theta, t). \quad (3)$$

The experimental results shown in Figs. 10.2:1 and 10.2:2 suggest that T can be written in the form

$$T(\lambda, \theta, t) = G(t)T^{(e)}(\lambda, \theta), \quad (4)$$

where $G(t)$ is a normalized function of time alone and is so defined that $G(0) \equiv 1$. In Eq. (4), $T^{(e)}(\lambda, \theta)$ is the so-called *elastic response* (Fung, 1972), a stress that is a function of stretch λ and temperature θ . We have seen that Eq. (4) is approximately valid for the artery (Chapter 8) and other tissues (Chapter 7). For those tissues for which Eq. (4) is valid, the stress $T(t)$ at any time t is linearly related to the elastic response $T^{(e)}[\lambda(t), \theta]$ for an arbitrary loading history $\lambda(t)$ by a convolution integral as follows:

$$T(t) = G(t)*T^{(e)}[\lambda(t), \theta], \quad (5)$$

where the $*$ denotes the convolution operator. See Chapter 7, Sec. 7.6.

The Elastic Response $T^{(e)}(\lambda, \theta)$

By definition $T^{(e)}(\lambda, \theta)$ is the tensile stress generated instantly in the tissue when a step stretch λ is imposed on the specimen at temperature θ . Measurement of $T^{(e)}(\lambda, \theta)$ strictly according to the definition is not possible, not only because a true step change in strain is impossible to obtain in the laboratory, but also because in rapid loading, the inertia of the matter will cause stress waves to travel in the specimen so that uniform strain throughout the specimen cannot be obtained. For this reason $T^{(e)}$ is a hypothetical quantity. A rational way to deduce $T^{(e)}$ from a stress-strain experiment is to apply Eq. (5) to a loading-unloading experiment at constant rate, then mathematically invert the operator to compute $T^{(e)}$, i.e., experimentally determine $T(t)$ and compute $T^{(e)}$ and $G(t)$.

To see what can be obtained by attempting a step loading anyway, without regard to its true meaning, a series of “high speed” stretches and releases of varying magnitude were imposed on the papillary muscle. Each quick stretch

was followed by a quick release of the same magnitude so that the muscle was unloaded to its reference dimensions (L_{ref} and d_{ref}). The muscle relaxed for about 10 s following the stretch before it was released. Rise time for these stretches varied from under 1 to 10 ms, depending upon the magnitude of stretch. Results of such a “quick stretch, quick release” test are shown in Fig. 10.2:3. The force-extension curve obtained at the same temperature (20°C) and at a uniform rate of loading and unloading is also shown for comparison.

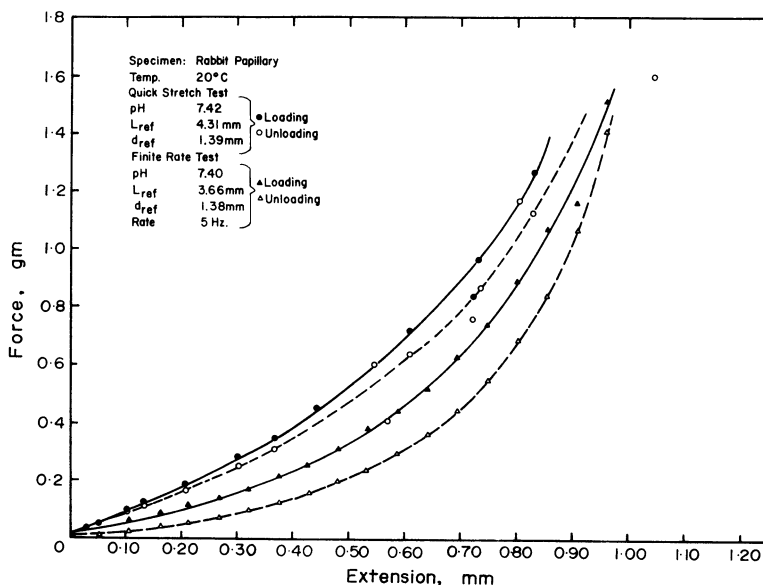


Figure 10.2:3 The elastic response $T^{(e)}(\lambda, \theta)$ of a rabbit papillary muscle. The circular dots refer to results of quick stretch tests. The triangular dots refer to results of loading and unloading at a finite constant rate. From Pinto and Fung (1973).

Figure 10.2:3 shows that the difference between the two sets of curves is considerable. The difference can be considered as the effect of strain rate. Since the relaxation function $G(t)$ is a monotonically decreasing function, stress response to straining at a finite rate is expected to be lower than the quick “elastic” response.

That the stress response in loading and unloading is different even under slow and uniform rates of stretch and release is a feature common to all living tissues (see Chapters 7 and 8). Test results for the rabbit papillary muscle stretched at various rates of loading and unloading are shown in Fig. 10.2:4, which demonstrates that the stress-strain relationship does not change very much as the strain rate is changed over a factor of 100. Other tests show that the changes remain small in the strain rate range of 10 000. This insensitivity is again in common with other tissues (see Chapters 7 and 8).

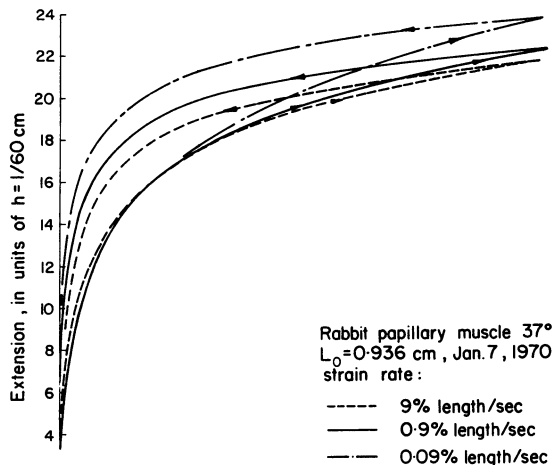


Figure 10.2:4 The stress-strain curves (loading and unloading loops) of a rabbit papillary muscle at different strain rates. From Pinto and Fung (1973).

To reduce the curves in Fig. 10.2:4 to a mathematical expression, the method of Sec. 7.5 can be used. One observes that if the slope of the stress-strain curve, $d\sigma/d\lambda$, is plotted against the stress σ (Fig. 10.2:5), a straight line is obtained for each loading and unloading branch. Denoting the slope of the regression line by α (a dimensionless number), and the intercept on the vertical

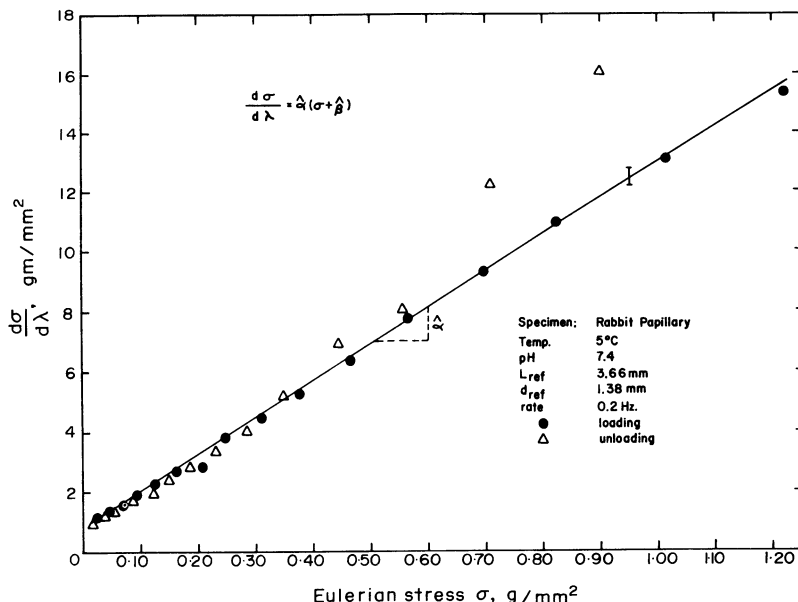


Figure 10.2:5 The exponential law of the stress-strain relationship for the rabbit papillary muscle. From Pinto and Fung (1973).

axis by $\alpha\beta$ (units, g/mm²), we can write the stress-strain relationship in uniaxial loading as

$$\frac{d\sigma}{d\lambda} = \alpha(\sigma + \beta). \quad (6)$$

An integration gives

$$\sigma + \beta = ce^{\alpha\lambda}, \quad (7)$$

where c is a constant of integration. To determine c , let a point be chosen on the curve: $\sigma = \sigma^*$ when $\lambda = \lambda^*$. Then

$$\sigma = (\sigma^* + \beta)e^{\alpha(\lambda - \lambda^*)} - \beta. \quad (8)$$

This procedure is valid only in the range in which Eq. (6) can be trusted. Usually Eq. (6), and hence Eq. (8), do not apply in the region $\sigma \rightarrow 0$, $\lambda \rightarrow 1$. For this reason the point (σ^*, λ^*) is usually chosen at the upper end of the curve (a large stress in the physiological range).

The need to exclude the origin is an unsatisfactory feature of Eq. (8). Use of a uniaxial strain energy function, which is an exponential function of the square of the strain (see Sec. 8.9) will remedy this situation. Table 10.2:1 lists some typical values of α and β . An extensive listing given in Pinto and Fung (1973) shows that for the papillary muscle α and β are rather insensitive to strain rates and temperature within the range of $1 < \lambda < 1.3$ and 5.37°C.

TABLE 10.2:1 Values of α and β from Eq. (6) for Rabbit Papillary Muscle. From Pinto and Fung (1973)^a

Rate (Hz)	Loading			Unloading		
	$\alpha \pm$ S.E.	β	σ^* (g/mm ²)	$\alpha \pm$ S.E.	β	σ^* (g/mm ²)
0.01	11.46 ± 0.11	0.58	0.74	17.08 ± 0.45	0.01	0.66
0.02	12.33 ± 0.22	0.50	0.77	17.47 ± 0.62	0.06	0.69
0.05	12.56 ± 0.14	0.54	0.81	16.95 ± 0.44	0.13	0.74
0.08	12.70 ± 0.20	0.60	0.83	17.27 ± 0.49	0.18	0.77
0.10	12.73 ± 0.13	0.52	0.84	17.08 ± 0.39	0.25	0.78
0.20	13.37 ± 0.14	0.44	0.87	17.84 ± 0.38	0.24	0.84
0.50	12.18 ± 0.37	0.55	0.66	16.00 ± 0.57	0.34	0.54
0.80	12.94 ± 0.14	0.49	0.66	17.47 ± 0.39	0.31	0.56
1.00	13.12 ± 0.16	0.24	0.66	16.99 ± 0.36	0.29	0.55
2.00	13.72 ± 0.17	0.43	0.70	18.43 ± 0.53	0.12	0.61
5.00	14.00 ± 0.30	0.20	0.75	17.34 ± 0.45	0.02	0.63
10.00	13.52 ± 0.14	0.17		16.98 ± 0.33	0.05	

^a L_{ref} , 3.66 mm; d_{ref} , 1.38 mm; max. stretch, 30%; $\lambda^* = 1.25$; pH, 7.4; temp., 37°C.

Oscillations of Small Amplitude

Figure 10.2:6 shows the frequency response of a papillary muscle subjected to a sinusoidal strain of an amplitude equal to 4.06% of the reference length superposed on a steady stretch with a stretch ratio of 1.22. The ordinate shows the dynamic stiffness, which has been normalized with respect to the stiffness at 0.01 Hz. It is seen that in a frequency range that varied 10 000-fold, the dynamic stiffness increased by less than a factor of 2. This modest frequency dependence is again in accord with the general behavior of other biosolids (see Secs. 7.6 and 7.7).

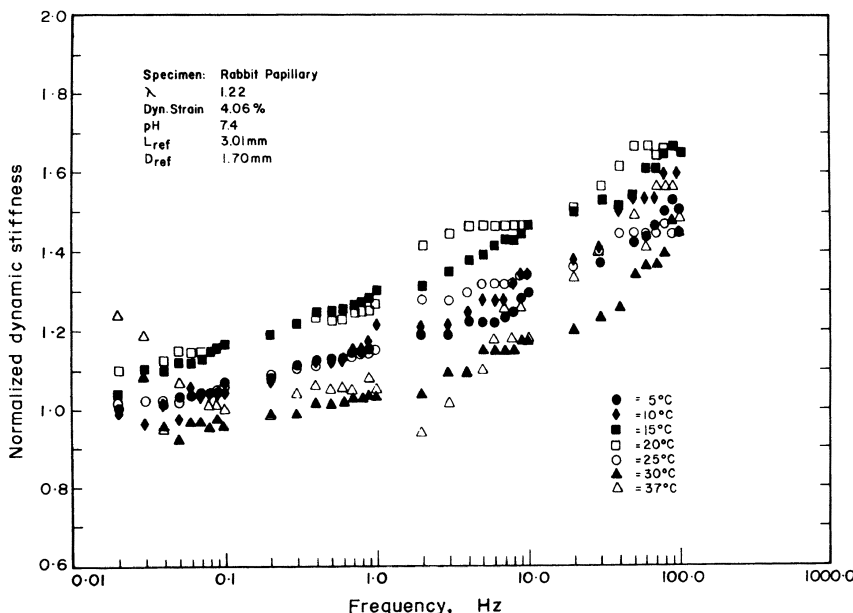


Figure 10.2:6 The frequency response of a rabbit papillary muscle to sinusoidal oscillations of small amplitude. From Pinto and Fung (1973).

Creep Tests

Creep (deformation with time under constant load) of the cardiac muscle over short durations of time has relevance to intact heart behavior and is of particular importance to hypertrophied heart. Figure 10.2:7 shows the creep characteristics of four rabbit papillary muscles. The ordinate is the strain expressed as a percentage of the reference length. It is seen that for a given stress and temperature, creep is essentially a linear function of $\log t$ for the first 10 min. Beyond 10 min it increases more rapidly with $\log t$.

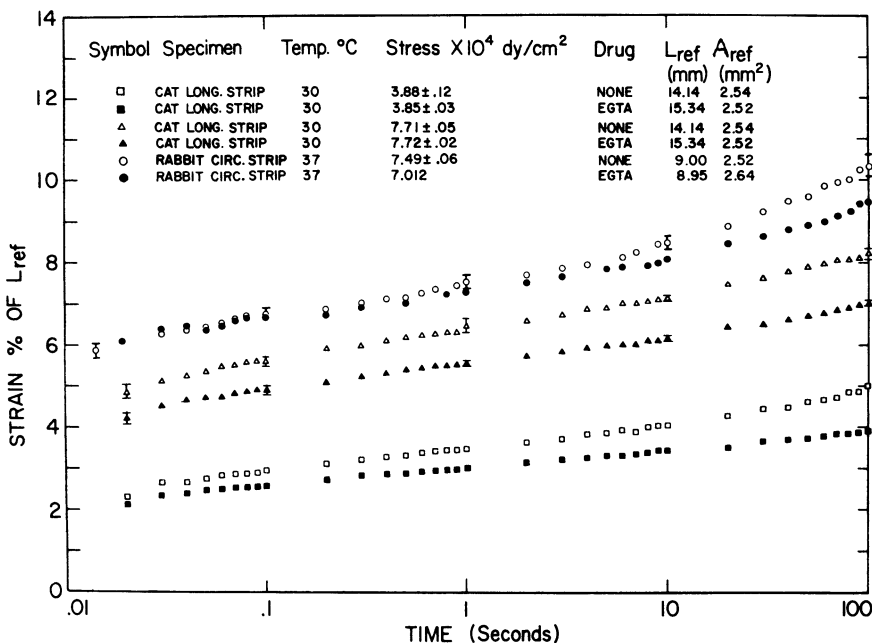


Figure 10.2:7 The creep characteristics of the papillary muscle of the cat and rabbit at different levels of stress and different temperatures, with and without EGTA. The application of $2\mu M$ EGTA to the bath (0.76 g/liter) abolishes spontaneous contractile activity of the muscle. Chelating calcium by EGTA reduces creep strain over a given time. From Pinto and Patitucci (1977), by permission.

Summary

In summary, it is seen that in the resting state, the mechanical behavior of heart muscle is quite similar to that of other living tissues. For relaxation under constant strain, the reduced relaxation function $G(t)$ is independent of the stretch ratio for strains up to 30% of muscle length. For time periods comparable with the heartbeat (1 s), the function $G(t)$ is independent of temperature in the range 5–37°C. This permits the application of the theory of quasi-linear viscoelasticity (Sec. 7.6) to the heart in the end-diastolic condition.

When a heart muscle is subjected to a cyclic loading and unloading at a constant strain rate, the stress-strain curve stabilizes into a unique hysteresis loop, which is independent of temperature (in the range 5–37°C) and is affected by the strain rate only in a minor way. Thus the pseudoelasticity concept (Sec. 7.7) is applicable. For the loading curve, the stress varies approximately as an exponential function of the strain. Unloading follows a similar curve with different characteristic constants.

In harmonic oscillations of small amplitude, the dynamic stiffness increases slowly with increasing frequency, by a factor of 2 when the frequency is increased from 0.01 to 100 Hz. In creep tests the heart muscle shows considerable creep strain under a constant load.

The relative insensitivity of stresses to strain rate in the cyclic process of stretching and release, and the small effect of frequency on dynamic stiffness and damping, can be explained by a continuous relaxation spectrum as presented in Sec. 7.6.

10.3 The Behavior of Active Myocardium

For the purpose of analyzing the dynamics of the heart, we need to know the constitutive equation of the myocardium in systole and diastole and the states in between. The constitutive equation describes the force-velocity-length-and-time relationship for the muscle. It contains certain material constants. The change of these constants in health and disease, and with the muscle's environmental conditions (e.g., ionic composition, presence of inotropic agents, and temperature) and neural and humoral controls, will supply the information desired for clinical applications.

At the present time the constitutive equation of an active myocardium is still unknown. For a while it was thought that Hill's three-element model (Sec. 9.8), together with a description of the contractile element by Hill's equation, would be sufficient to provide a constitutive equation for the heart muscle. Almost all cardiological investigations of the past four decades have been guided by this thought. Roughly speaking, this idea is confirmed. The only modification that is needed is to introduce a factor of an "active state" to relate the "maximum" force T_0 and "maximum" velocity v_0 that occur in Hill's equation with the time after stimulation. The confirmation is generally quite good if the muscle is tested at a length so small that the resting tension in the parallel element (see Sec. 9.8) is negligible compared with the active tension (setting $P = 0$ in the equations of Sec. 9.8).

Trouble appeared, however, when experiments were done on muscles at such a length that the resting tension is not negligible. To account for the rest tension, there are two different but equivalent ways. One is to use the model discussed in Sec. 9.8, and shown in Fig. 10.3:1(B). The other is shown in Fig. 10.3:1(C). These two models are called the "parallel resting tension" and the "series resting tension" models, respectively. By identifying the experimental results with these models, one can evaluate the properties of the contractile element. It was then found that the contractile element property is model-dependent, the Hill's equation does not apply, the force-velocity relationship is complex, and the active state is hard to define. Thus the handling of the parallel element has not been successful. This leads one to question the Hill's three-element model and to search for an alternative method of approach. These will be discussed in the next two sections.

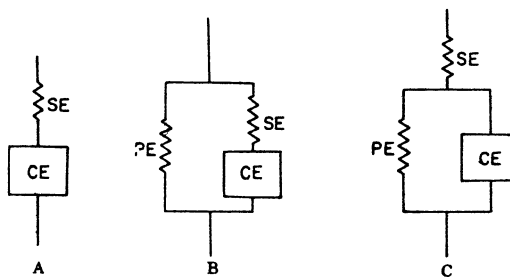


Figure 10.3:1 Mechanical analogues of mammalian papillary muscle. (A) Simple model with only a contractile element (CE) and a series elastic element (SE). (B) Parallel resting tension model in which a parallel elastic element (PE) bears resting tension. (C) Series resting tension model in which a series elastic element (SE) also bears resting tension.

10.4 Active Muscle at Shorter Length with Negligible Resting Tension

The relative magnitudes of resting tension and active tension in a heart muscle are shown in Fig. 10.1:5. If the muscle length is sufficiently small, the resting tension is negligible. Then Hill's model is reduced to the two-element model of Fig. 10.3:1(A). In this case, if the series element is assumed elastic, then its elastic characteristics can be determined by the methods described in Sec. 9.8, namely, either by the quick-release or by the isometric-isotonic-change-over method. With the series elastic element's property determined, the contractile element behavior can be identified with the experimental data in a simple and unambiguous manner.

In the following discussion, we shall summarize the experimental results using the mathematical analysis presented in Sec. 9.8. The symbol S denotes tension in the series element. P denotes tension in the parallel element, which is assumed to be zero in the present section. The total tension $\tau = S + P$ is therefore equal to S . The length of the muscle is denoted by L . The elastic extension of the series element is η . The “insertion” or summation of the overlap between actin and myosin fibers is Δ .

The Series Element

Extensive work on the series element was reported by Sonnenblick (1964), Parmley and Sonnenblick (1967), Edman and Nilsson (1968), and others. Their results may be summarized by the equation

$$\frac{dS}{d\eta} = \alpha(S + \beta), \quad (1)$$

where α and β are constants. Thus the stiffness $ds/d\eta$ is linearly related to the

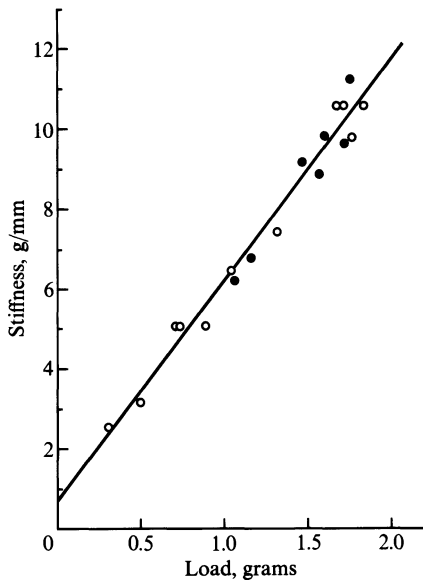


Figure 10.4.1 The straight-line relationship between the elastic modulus and tension in the series element. Rabbit papillary muscle. Open symbols: Measurements carried out during the rising phase of the isometric twitch. Filled symbols: those measured during the decay phase. Contraction frequency, 36 per min. Temp., 31°C. From Edman and Nilsson (1972), by permission.

tension S . See Fig. 10.4.1. For the cat's papillary muscle with a cross-sectional area $A_0 = 0.98 \text{ mm}^2$, subjected to a preload of 0.5 g and an elastic extension of 4–5% of the initial muscle length at a developed tension of 10 g, corresponding to a stress of approximately 1 kg/cm^2 , or 1 atm, or 100 kPa, the value of α is 0.4 for η measured in % muscle length, and $\beta = 2 \text{ g}$.

Equation (1) integrates to

$$S = (S^* + \beta)e^{\alpha(\eta - \eta^*)} - \beta, \quad (2)$$

where $S = S^*$ when $\eta = \eta^*$. The condition $S = 0$ when $\eta = 0$ implies

$$\beta = \frac{S^* e^{-\alpha\eta^*}}{1 - e^{-\alpha\eta^*}}, \quad (3)$$

which requires that the point (S^*, η^*) be related to β in a specific way. Equations (1) and (2) also apply to many connective tissues (see Secs. 7.5 and 8.3), as well as to the unstimulated papillary muscle (Sec. 10.2).

The Contractile Element

Edman and Nilsson (1968, 1972) showed that if the force-velocity relationship of a papillary muscle is measured at any specific length of the contractile

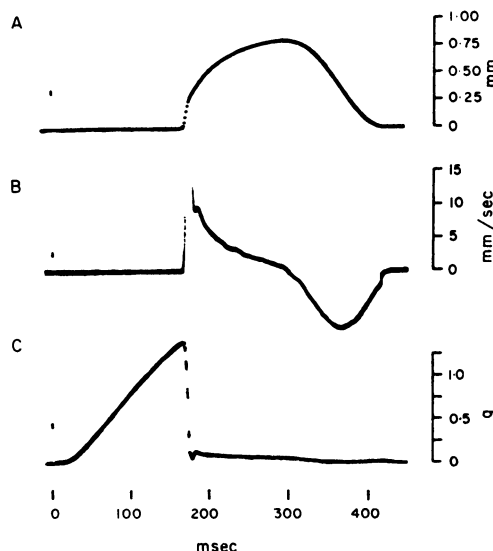


Figure 10.4:2 Oscilloscope records of release experiment. (A) Shortening. (B) Velocity of shortening (electrical differentiation). (C) Tension. Stimulation signal at zero time. Temp., 29.5°C. Contraction frequency, 30 per min. From Edman and Nilsson (1968), by permission.

element, reached at a given time after stimulus, then it can be fitted by Hill's equation. Their experimental procedure is illustrated in Fig. 10.4:2. They used a small preload of 100 dyn on rabbit papillary muscles with diameters in the range 0.5–1.0 mm and length in the range 3.8–7.0 mm. Each specimen was stimulated at a frequency of 30–48 per min and allowed to contract isometrically. At a selected instant of time after stimulation, the load is suddenly released to a lower value [Fig. 10.4:2.(C)], and the isotonic contraction of the muscle is recorded [Fig. 10.4:2.(A)]. The velocity of contraction is obtained by differentiating the displacement signal electronically [Fig. 10.4:2.(B)]. The velocity of shortening at a fixed sarcomere length (occurring at a fixed time interval after stimulation) is plotted against the load in Fig. 10.4:3, to which Hill's equation is fitted by the least squares method. The correlation is better than 0.99. Figure 10.4:3 shows the force-velocity relation at several instants of time. It is seen that the hyperbolic relations at different instants of time are parallel to each other, indicating that the muscle's ability to shorten and ability to generate tension vary with time in the same way. The constants a and b in Hill's equation Eq.(1) of Sec. 9.7 are listed in the figure.

In a later paper, Edman and Nilsson (1972) demonstrated the importance of "critical damping" in the recording instrument on the shape of the force-velocity curve. They installed a dash pot containing silicone oil to damp out the oscillation of the lever. A 1-mm wide by 14-mm long duralumin

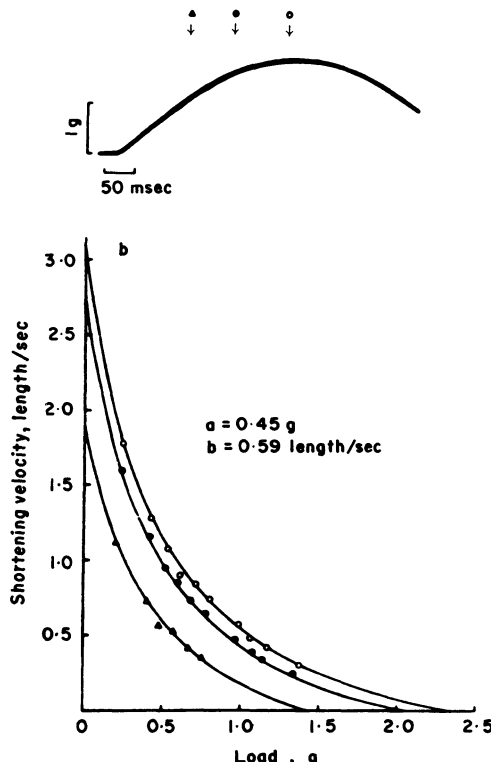


Figure 10.4:3 Force-velocity curves (lower diagram) defined at different times indicated by arrows in the isometric myogram (upper diagram). Curves drawn according to Hill's equation for values of a and b listed. The velocity values at a given load refer to the same length of the contractile unit (with variations <0.5% of resting muscle length) in all curves of the same experiment. Contraction frequency, 45 per min. Temp., 27.5°C. From Edman and Nilsson (1968), by permission.

rod extended from the lever to the damping fluid. A thin disc of aluminum (diam. 3.7 mm, thickness 0.4 mm) was attached perpendicular to the end of the rod. The degree of damping was varied by using silicone oils of different viscosity. With 60-stoke silicone fluid, the damping is considered "critical." Figure 10.4:4 shows the effect of damping on the force-velocity curve. The critically damped curve can be fitted with Hill's equation; the substantially underdamped ones cannot. The reason for this is not entirely clear.

We can condense Edman and Nilsson's results by modifying Hill's equation.

$$v = \frac{b(S_0 - S)}{a + S} \quad (4)$$

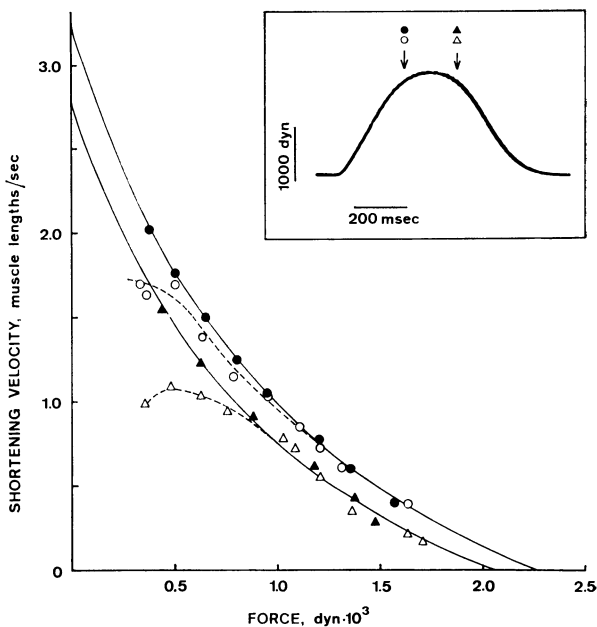


Figure 10.4:4 Force-velocity curves derived from quick release recordings carried out during the rising and falling phases of the isometric twitch. Arrows on top of inserted isometric myogram indicate times for collection of experimental data. Filled symbols: lever movements were critically damped. Open symbols: lever movements were under-damped. Solid lines (referring to filled symbols) have been fitted according to Hill's equation, using the following values of the constants a and b : ●, $a = 1.17 \times 10^3$ dyn, $b = 1.68$ lengths/s; ▲, $a = 1.17 \times 10^3$ dyn, $b = 1.57$ lengths/s. Correlation coefficient between experimental points and data predicted from the hyperbolic curve: ●, 0.999; ▲, 0.998. Dashed lines have been fitted by eye to data obtained from underdamped releases. From Edman and Nilsson (1968), by permission.

to the form (Fung, 1970)

$$v = \frac{b[S_0 f(t) - S]}{a + S}, \quad (5)$$

where $f(t)$ is a function of time after stimulation. We shall call $f(t)$ the *characteristic time* function. Edman and Nilsson's results suggest that $f(t)$ can be represented by a half-sine wave which is normalized to a unit amplitude:

$$f(t) = \sin \left[\frac{\pi}{2} \left(\frac{t + t_0}{t_{ip} + t_0} \right) \right] \quad (6)$$

In Eqs. (5) and (6) the constants a and b are functions of muscle length L at the time of stimulation, S_0 is the peak tensile stress arrived at in an isometric contraction at length L , t is the time after stimulus, t_0 is a phase shift related

to the initiation of the active state at stimulation, and t_{ip} is the time to reach the peak isometric tension after the instant of stimulation. The velocity v is the velocity of the contractile element, dA/dt . The constant $a(L)$ is known empirically to be proportional to S_0 , and can be written as

$$a(L) = \gamma S_0(L). \quad (7)$$

The numerical parameter γ is of the order of 0.45.

Brady's Test of the Validity of Hill's Equation

Brady (1965) plotted the ratio $(S_0 - S)/v$ against S . For Hill's equation we have

$$\frac{S_0 - S}{v} = \frac{a + S}{b}, \quad (8)$$

and Brady's plot should be a straight line. But the experimental data plotted in Fig. 10.4:5 do not fall on such a straight line.

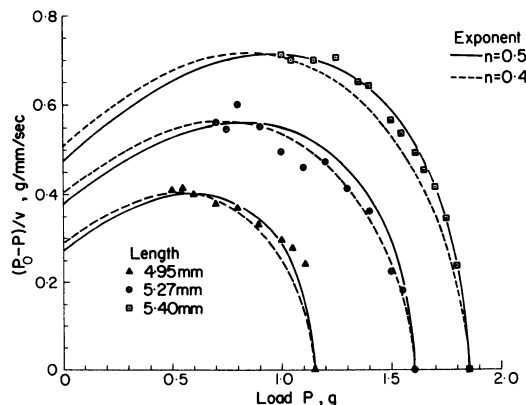


Figure 10.4:5 Comparison of Brady's data (1965) on rabbit papillary with the theoretical curve given by Eq. (9). Ordinate, g/mm per s. Abscissa, g. $\gamma = 0.45$. From Fung (1970). In this figure, S is written as P .

The deviation is principally caused by the nonhyperbolic relationship in the high tension, low velocity region. Such deviations are seen in many other publications. For example, Fig. 10.4:6 shows the data of Ross et al. (1966) on the dog's heart. The data near the toe ($S/S_0 \sim 1$) show a sigmoid relationship.

Fung (1970) showed that Edman and Nilsson's curves (Figs. 10.4:2 and 10.4:3) as well as those of Brady and Ross et al. can be represented by a modified Hill's equation:

$$v = \frac{B[S_0 f(t) - S]^n}{a + S}, \quad (9)$$

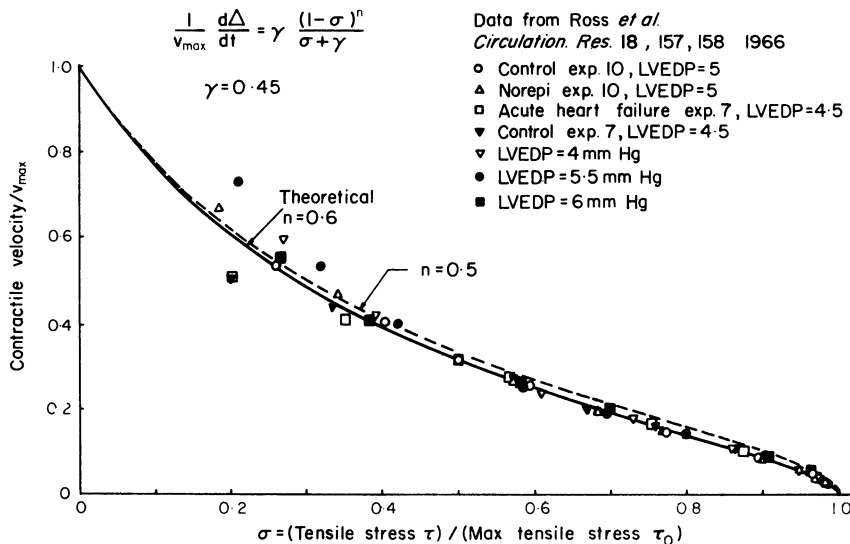


Figure 10.4:6 Comparison of the force-velocity data of dog's left ventricle obtained by Ross et al. (1966) with theoretical curves given by Eq. (9). $\gamma = 0.45$, $n = 0.6, 0.5$. From Fung (1970).

where v is the contractile element velocity, $f(t)$ is the characteristic time function given in Eq. (6), and n is a numerical factor. B is, of course, different from b both in numerical value and in units. Figures 10.4:5 and 10.4:6 show the fitting of Eq. (8) to the data of Brady and Ross et al. In Fig. 10.4:6, Eq. (9) is presented in a dimensionless form:

$$v = \gamma v_{\max} \frac{(1 - \sigma)^n}{\gamma + \sigma}, \quad (10)$$

where

$$v_{\max} = \frac{BS_0^{n-1}}{\gamma}, \quad \sigma = \frac{S}{S_0}, \quad (11)$$

$$a = \gamma S_0, \quad \text{and} \quad v \rightarrow v_{\max} \quad \text{when} \quad \sigma \rightarrow 0. \quad (12)$$

Here v represents $d\Delta/dt$. In Eq. (10), as well as in Figs. 10.4:5 and 10.4:6, we have set the characteristic time function $f(t)$ of Eq. (9) to unity, $f(t) = 1$, because the experiments were done at a time near the peak isometric tension, i.e., $t \rightarrow t_{ip}$ in Eq. (6). Further, with Eqs. (9) and (10) the right-hand side becomes a complex number if $S > S_0 f(t)$ or $S > S_0$ and $n \neq 1$. In that case, we define the right-hand side of Eqs. (9) and (10) as the real part of the complex number. With these equations, good fitting of curves in Figs. 10.4:2 and 10.4:3 is demonstrated in Fung (1970). Incidentally, the introduction of the exponent n with a value less than 1 removes the difficulty mentioned in Sec. 9.8, namely, that the time required for the redevelopment of tension after a step shortening in length of an isometric tetanized muscle to reach a

peak is infinity if Hill's equation holds strictly. See Eq. (22) of Sec. 9.8. The exponent n was originally introduced for the purpose to remove this difficulty.

All the formulas of this section apply only to papillary muscles of shorter lengths in which resting tension is negligible.

10.5 Stimulated Papillary Muscle at Lengths at Which Resting Tension Is Significant

For cardiac muscle at such a length that the resting tension must be taken into account, the analysis of the experimental data according to the three-element model becomes more complex (and nonunique) and the behavior of the contractile element appears very complex. Many authors have looked into this problem, and varying results are reported.

Brady (1965) found no hyperbolic relation between force and the velocity of contraction. Hefner and Bowen (1967) and Noble et al. (1969) found bell-shaped force-velocity curves and concluded that the maximum velocity of shortening occurs for loads appreciably larger than zero. They found near-hyperbolic behavior, however, for large resting tensions. Pollack et al. (1972) observed that the stiffness of the series elastic element depends on the time after stimulation.

When the same experimental data were analyzed by two different but equivalent three-element models as shown in Fig. 10.3:1(B) and (C), the derived contractile element force-velocity relations were found to be different for the two models. Thus the results are model-dependent and are not unique. Therefore, it does not represent an intrinsic property of the material.

There are other complications. When quick stretch experiments were done (Brady, 1965), it was found that the modulus of elasticity of the series elastic element in quick stretch is different from that in quick release. Thus the series spring must be interpreted as viscoelastic or viscoplastic.

It is disappointing that the behavior of the three elements of Hill's model have all turned out to be so complicated. Some years ago, the author thought that the problem might lie in instrumentation. After spending several years constructing test equipment which he thought was superior, he and Pinto (see Pinto and Fung, 1973) found in their experiments on rabbit papillary muscle that a simple picture did not emerge. They obtained a diagram showing that $\partial S/\partial \eta$, the elastic modulus of the series element, is not linearly proportional to the tension S . They found that the velocity of contraction $\partial A/\partial t$ cannot be correlated with the tension S by Hill's equation, nor can it be correlated by the modified equations (5) or (9) of Sec. 10.4. Furthermore, their results show that both the series elastic element stiffness $\partial S/\partial \eta$ and the velocity of contraction $\partial A/\partial t$ depend very much on the actin-myosin fiber insertion A , that is, $\partial S/\partial \eta$ and $\partial A/\partial t$ vary a great deal with the interval of time between the instant of stimulation and the instant of quick release.

Since all these complications are associated with attempts to take the parallel element into account, we must conclude that the present method of analyzing the parallel element by identifying it with the unstimulated resting muscle has been unsuccessful. Technically, much of the difficulty stems from the viscoelastic (inelastic and strain-history-dependent) behavior of the unstimulated resting muscle. But the full reason probably goes deeper. Since separation of tension into parallel and contractile components depends on the assumptions concerning the contractile element, we wonder if those assumptions are valid. In particular, are the contractile elements stress free when the muscle is unstimulated? In smooth muscles a resting state cannot be defined uniquely (See Secs. 11.4, 11.5 in Chapter 11); hence the contractile mechanism is not "free" between twitches. It follows that the three-element model is inappropriate for smooth muscles. Perhaps it is also inappropriate for the heart muscle for the same reason.

Furthermore, the separation of displacements between the series and contractile elements depends on the assumption of perfect elasticity of the series element. This amounts to a definition, and cannot be tested uniquely by experiment.

With these difficulties, we have to agree with Brady (1979) that Hill's model is severely limited in empirical value. An alternative method of approach must be sought. In my opinion, the fading memory theory mentioned in Section 9.9 is the most hopeful. Its mathematical form is suitable for the analysis of the heart, and its generality enables it to fit any experimental results.

10.6 Heart Muscle Mechanics and Whole Heart Behavior

So far we have considered the heart papillary muscle in the hope that its behavior is the same as every other bundle of muscle in the heart. If the constitutive equation of every muscle fiber is known, then by synthesizing the fibers into a structure we can deduce the mechanical behavior of the whole heart. An orderly process of studying the heart can then be laid out: First, study the anatomy. Find the muscle fiber geometry, especially the fiber direction in every part of the heart. Next, study the electric events. Determine the time sequence in which muscle fibers in different parts of the heart are stimulated. Then, with the constitutive equation of the muscle, the method of continuum mechanics should be able to yield the details of blood flow, the pressure distribution in the blood, the stress and strain distribution in the myocardium, etc., for any specified boundary conditions. The boundary conditions include the condition at the valves, the external load and/or constraints acting on the pericardium, and the tension and curvature of the pericardium. Often the most exciting problem of research is the coupling of the heart to the lung and to the peripheral circulation through the valves.

In this methodology, the constitutive equation of the heart muscle occupies a central position.

But testing the heart papillary muscle has many difficulties, the most severe of which is the question of damage to the cells in the isolated specimen due to mechanical clamping and due to loss of blood circulation. Kreuger and Pollack (1975) have dramatically called attention to the important effects of end conditions on papillary muscle test results. In addition to possible cell damage, the nonuniform local strain distribution at the ends caused by clamping and by tapering must also contribute significantly to the uncertainties of the experimental results.

An alternative procedure is to study the mechanical properties of the whole heart. Then the problems of cell damage and end conditions are minimized, but it would be very difficult to use the experimental results to identify the constitutive equation for muscle. The problem is too complex and too many factors are involved.

There is a very large literature on whole-heart experiments and analysis. Much of it will be discussed in a subsequent volume. The following idealized problems are given to develop some ideas.

Problems

- 10.1** Let the left ventricle be approximated by a thick-walled hemispherical shell of uniform thickness. The valves and valve ring will be assumed to be infinitely compliant. In diastolic condition the left ventricle is subjected to an internal pressure p_i and an external pressure p_0 . p_i is a function of time. Ignoring inertia effects, what is the average stress in the wall?
- 10.2** Let the inner radius of the hemisphere be a_0 and the wall thickness be h_0 at the no-load condition, $p_i = p_0 = 0$. Assume that the average strain is related to the average stress in the same way as stress is related to strain in the uniaxial case [see Eq. (8) in Sec. 10.2]. Under the assumptions of Problem 10.1, what will the radius $a(t)$ and the wall thickness $h(t)$ be as functions of time t in response to $p_i(t)$ and p_0 ? Assume the wall material to be incompressible. See Fig. P10.2.

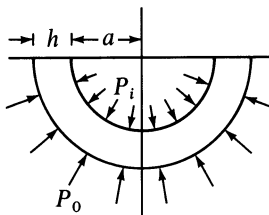


Figure P10.2 A ventricle subjected to internal and external pressures.

- 10.3** At time $t = 0$, the valves are closed and every muscle fiber in the shell begins to contract. Assume that the plane of the valves remain plane and the volume enclosed

by the hemispherical shell remains constant. Compute the course of pressure change $p_i(t)$ under the assumption that the equations of Sec. 10.4 are applicable.

- 10.4** Under the same assumptions of Problems 10.1–10.3, but considering an electric event different from that of Problem 10.3, let the wave of depolarization begin at the axis of symmetry $\theta = 0$ (see Fig. P10.4) and spread with a constant angular velocity in the circumferential direction, $d\theta/dt = c$, a constant. As the muscle fibers shorten, the shell will be distorted. It is necessary to consider bending of the shell wall in this case. Develop an approximate theory for the change of shape of the shell as a function of time, assuming that the equation of Secs. 10.2 and 10.4 are applicable. Make a reasonable assumption about the compliance of the valves.

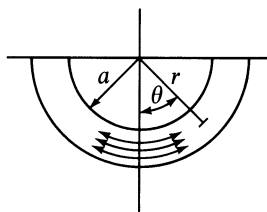


Figure P10.4 A wave of depolarization propagating circumferentially.

- 10.5** Consider another electric event: the wave of depolarization beginning at the inner wall and propagating radially at a constant velocity V . As in Problem 10.4, determine the history of the shape change of the shell. In the real left ventricle the wave of depolarization is determined by conduction pathways [see Scher, A. M. and Spach, M. S. (1979), Cardiac depolarization and repolarization and the electrocardiogram, in *Handbook of Physiology*, Sec. 2., *The Cardiovascular System*, Vol. 1, *The Heart*, Berne, R. M., Sperelakis, N., and Geiger, S. R. (eds.) American Physiol. Soc., Bethesda, Md., pp 357–392]. See Fig. P10.5.

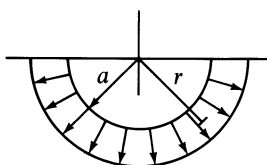


Figure P10.5 A wave of depolarization propagating radially.

- 10.6** Discuss the improvements that are necessary in order to bring the idealized analyses of preceding problems closer to reality.

References

- Abbott, B. C., and Mommaerts, W. F. H. M. (1959) *J. Gen. Physiol.* **42**, 533–551.
 Berne, R. M., and Levy, M. N. (1972) *Cardiovascular Physiology*, 2nd edn. C. V. Mosby, St. Louis, 1972.

- Brady, A. J. (1965) *Fed. Proc.* **24**, 1410–1420.
- Brady, A. (1979) In *Handbook of Physiology*, Sec. 2, *The Cardiovascular System*. Vol. 1: *The Heart*. American Physiological Society, Bethesda, Md., Chap. 12, pp. 461–474.
- Brutsaert, D. I., and Sonnenblick, E. H. (1969) *Circulation Res.* **24**, 137–149.
- Edman, K. A. P., and Nilsson, E. (1968) *Acta Physiol. Scand.* **72**, 205–219.
- Edman, K. A. P., and Nilsson, E. (1972) *Acta Physiol. Scand.* **85**, 488–500.
- Fung, Y. C. (1970) *J. Biomech.* **3**, 381–404.
- Fung, Y. C. (1971a) *J. Biomech.* **4**, 289–295.
- Fung, Y. C. (1971b) Muscle controlled flow. In *Proc. 12th Midwest Mechanics Conf.* University of Notre Dame Press, Notre Dame Ind., pp. 33–62.
- Fung, Y. C. (1972) In *Biomechanics, Its Foundations and Objectives*, Fung, Y. C., Perrone, N., and Anliker, M. (eds.). Prentice-Hall, Englewood Cliffs, N.J., pp. 191–208.
- Fung, Y. C. (1973) *Microvascular Res.* **5**, 34–48.
- Gordon, A. M., Huxley, A. F., and Julian, F. J. (1966) *J. Physiol.* **184**, 170–192.
- Hefner, L. L., and Bowen, T. E., Jr. (1967) *Am. J. Physiol.* **212**, 1221–1227.
- Noble, M. I. M., Bowen, T. E., and Hefner, L. L. (1969) *Circulation Res.* **24**, 821–834.
- Patterson, S. W., Piper, H., and Starling, E. H. (1914) *J. Physiol.* **48**, 465–513.
- Parmely, W. W., and Sonnenblick, E. H. (1967) *Circulation Res.* **20**, 112–123.
- Peachey, L. D. (1965) *J. Cell Biol.* **25**, 209–231.
- Pinto, J. G., and Fung, Y. C. (1973) *J. Biomech.* **6**, 597–616, 617–630.
- Pinto, J. G., and Patitucci, P. (1977) *Am. J. Physiol.* **232**(6), H 553–H 563.
- Pollack, G. H., Huntsman, L. L., and Verdugo, P. (1972) *Circulation Res.* **31**, 569–579.
- Ross, Jr., J., Covell, J. W., Sonnenblick, E. H., and Braunwald, E. (1966) *Circulation Res.* **18**, 149–163.
- Sommer, J. R., and Johnson, E. A. (1979) In *Handbook of Physiology*, Sec. 2, *The Cardiovascular System*. Vol. 1: *The Heart*. American Physiological Society, Bethesda, Md., Chap. 5, pp. 113–186.
- Sonnenblick, E. H. (1964) *Am. J. Physiol.* **207**, 1330–1338.

CHAPTER 11

Smooth Muscles

11.1 Types of Smooth Muscles

Muscles in which striations cannot be seen are called smooth muscles. Smooth muscles of the blood vessels are called vascular smooth muscles. That of the intestine is intestinal smooth muscle. Different organs have different smooth muscles: there are sufficient differences among these muscles anatomically, functionally, mechanically, and in their responses to drugs to justify studying them one by one. But there are also common features. All muscles, skeletal, heart, and the various smooth muscles, contain actin and myosin. All rely on ATP for energy. Change in the cell membrane induces Na^+ and K^+ ion fluxes and action potential. The Ca^{++} flux furnishes the excitation-contraction coupling. A strongly coupled reaction in the cell membrane makes it behave as an active ion pump. These properties are similar in all muscles. Yet with all the similarities there are differences in their mechanical behavior. A biomechanicist should know these differences, just as a structural engineer should know the differences in the mechanical properties of lead, aluminum, and steel, while the general public may simply refer to them as metals.

In analyzing the function of internal organs, we need the constitutive equations of the smooth muscles. The constitutive equations are unknown at this time, and research to fill this gap is most urgently needed. In anticipation of rapid progress in this area, we outline in this chapter some of the basic features that are known, and on which constitutive equations will be built.

Cell Dimensions

Smooth muscle cells are generally much smaller than skeletal and heart muscle cells. Table 11.1:1 gives some typical dimensions obtained by electron microscopy (see Burnstock, 1970, for original references).

TABLE 11.1:1 Size of Smooth Muscle Cells

Tissue	Animal	Length (μm)	Diameter in nuclear region (μm)
Intestine	Mouse	400	
Taenia coli	Guinea pig	200 (relaxed)	2–4
Nictitating membrane	Cat	350–400	
Vas deferens	Guinea pig	450	
Vascular smooth muscle			
Small arteries	Mouse	60	1.5–2.5
Arterioles	Rabbit	30–40	5

Arrangement of Muscle Cells Within Bundles

There are a variety of patterns of smooth muscle packing. In guinea pig vas deferens, the thick middle portion of the cell that contains the nucleus lies adjacent to the long tapering ends of surrounding cells. In many blood vessels, the muscle cells meet in end-to-end fashion. In the uterus of the pregnant female, interdigititation between cells is common. The pattern in guinea pig vas deferens and taenia coli is such that in any one plane cross-section, each muscle cell is surrounded by 6 others, but there is an irregular longitudinal splicing of neighboring cells, so that each muscle cell is surrounded by about 12 others over its length. The cells are not straight, but are bent and interwoven with each other. The separation of neighboring muscle cells is generally between 500 and 800 Å in most organs. Basement membrane material and sometimes scattered collagen filaments fill the narrow spaces between muscle cells within bundles.

In the extracellular space, a variety of materials, including collagen, blood vessels, nerves and Schwann cells, macrophages, fibroblasts, mucopolysaccharides, and elastic tissue may be seen. Abundant “micropinocytotic” or “plasmalemmal” vesicles are seen in the extracellular space, some of which appear to be connected with an intracellular endoplasmic tubular system. These fine structures are probably very important in facilitating ion exchange across the cell membrane during depolarization, and in creating excitation-contraction coupling.

The size of extracellular space from various measurements is shown in Table 11.1:2 Again see Burnstock (1970) for references to original papers.

TABLE 11.1:2 Extracellular Space in Smooth Muscles

Tissue	Extracellular space (% of total) measured by	
	Electron microscope	Uptake of solutes (inulin)
Visceral smooth muscle		
Guinea pig taenia coli	12	30–39
Cat intestine	9	
Mouse vas deferens	12 (adult) 50 (neonatal)	
Cat uterus		31–40
Vascular smooth muscle		
Pig carotid artery	39	
Mouse femoral artery	30	
Rat aorta		35
Rabbit aorta		62
Dog carotid artery	25	

Note the difference in extracellular space between the visceral and the vascular smooth muscles of large arteries. The latter are often called *multi-unit smooth muscles*, each fiber of which operates entirely independently of the others and is often innervated by a single nerve ending, as in the case of skeletal muscle fibers. See sketch in Fig. 11.1:1. Their control is exerted almost entirely by nerve signals, and very little by other stimuli such as local tissue factors. They do not exhibit spontaneous contractions. Smooth muscle fibers of the ciliary muscle of the eye, the iris of the eye, and the piloerector muscles that cause erection of the hairs when stimulated by the sympathetic nervous system, are also multiunit smooth muscles.

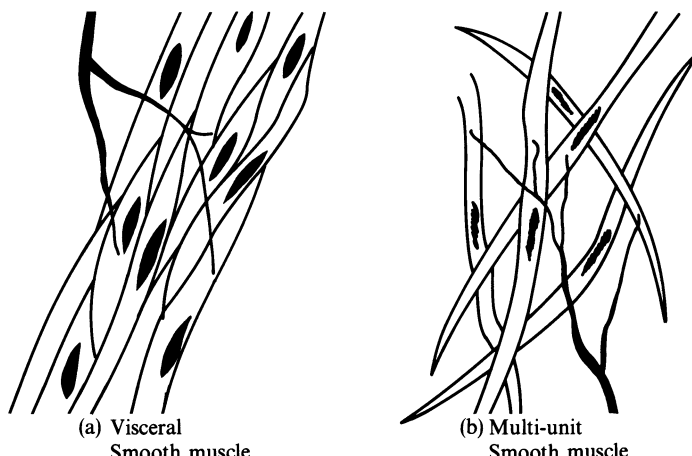


Figure 11.1:1 Sketch of (a) a single-unit and (b) a multi-unit smooth vessel.

In contrast, the visceral smooth muscle cells are crowded together, and behave somewhat like those of the heart muscle. They are usually stimulated and act as a unit. Conduction is from muscle fiber to muscle fiber. They are usually spontaneously active. A sketch is given in Fig. 11.1:1.

11.2 The Contractile Machinery

The contractile machinery of smooth muscle is presumably the same as that for the striated muscle. It has been known for a long time that smooth muscles have the same contractile proteins: actin and myosin. But myosin filaments and cross-bridges were seen on electron micrographs only recently. Actin filaments were identified earlier. Figures 11.2:1 and 11.2:2 show the electron micrographs of a vascular smooth muscle cell of a rabbit vein.

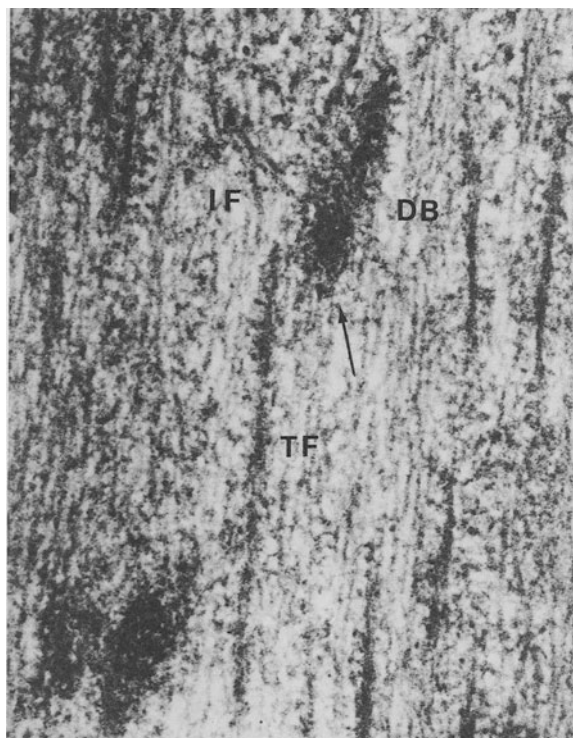


Figure 11.2:1 An electron micrograph of a vascular smooth muscle cell from the rabbit portal-anterior mesenteric vein. Longitudinal section. Two dense bodies (DB) are included in the section. The arrow near the center of the figure points to thin filaments attaching to one of the dense bodies. Many cross-bridges are evident on the thick filament (TF), traversing the center of the section. Intermediate size filaments (IF) may be seen arranged obliquely to the left of the upper dense body. From Ashton, Somlyo, and Somlyo (1975), reproduced by permission.

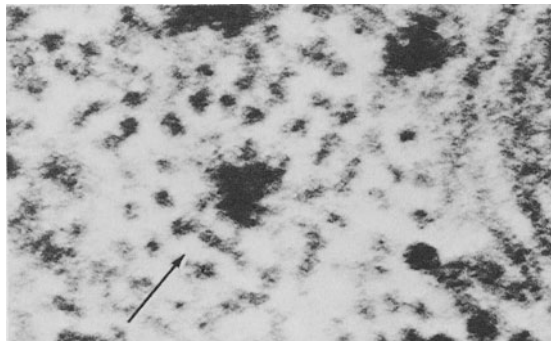


Figure 11.2.2 Transverse section of vascular smooth muscle cell from rabbit portal-anterior mesenteric vein. The thick filament in the center of the figure is surrounded by an array of thin filaments. The arrow points to an area where cross-bridges may be seen linking the thick to thin filaments. From Ashton, Somlyo and Somlyo (1975), reproduced by permission.

The thick filament shown in Fig. 11.2:1, comprised of myosin molecules, has a transverse dimension of 14.5 nm. Cross-bridges extending from the thick filament are evident in these figures. X-ray diffraction suggests that the repeat distance for the cross-bridge is 14.4 nm, identical to that of striated muscle. The length of the thick filament in vascular smooth muscle is 2.2 μm , which is larger than the 1.6 μm length of striated muscle by a factor of $2.2/1.6 = 1.4$. The significance of the longer myosin filaments is that, under the assumption that the cross-bridge of smooth muscle is the same as that in striated muscle, the tension generated per filament in smooth muscle is larger than that in striated muscle by about 40%. This is because the cross-bridges are arranged in parallel and at equal spacing; hence the sum of forces is proportional to the myosin fiber length.

The thick filaments of vascular smooth muscle appear to be arranged in groups of three to five adjacent filaments that terminate in the same transverse serial section. The thin filaments are attached to *dense bodies* throughout the sarcoplasm and are also attached to the plasma membrane in numerous areas (dark areas). These are suggestive of a rudimentary sarcomere arrangement. The lack of periodic sarcomere structure is probably responsible for the slow action of the smooth muscle, because in each cycle of the cross-bridge attachment-movement-detachment movement, all cross-bridges associated with one actin filament move a definite small unit step. Summation of the steps from all sarcomeres results in the change of length, which is equal to the product of unit step length and the number of sarcomeres. Hence the shorter the sarcomere the faster is the velocity of contraction. The longer the actin filament, the longer is the sarcomere, and the slower is the contraction.

In vascular smooth muscle, thin filaments, composed of actin and tropomyosin, are far more numerous than thick filaments, giving a thin-to-thick

ratio of 15:1. The thin filaments in vascular smooth muscle have an average diameter of 6.4 mm.

The contractile proteins are thus quite similar to those of striated muscle. However, the excitation mechanism, the excitation-contraction coupling, the metabolism of ATP and Ca^{++} , and the chemomechanical transducing by actomyosin to produce contraction, have many details special to each smooth muscle. The electrophysiology and biochemistry of muscle contraction is too extensive a subject to be summarized here, and the reader is referred to the books of Guyton (1976), Davson (1964), Bohr (1978), Bohr et al. (1980), and Burnstock (1970). These works, however, do not treat the mechanics of contraction in sufficient depth to the point of obtaining the constitutive equation. Hence in the following sections we appeal directly to laboratory experiments to learn something about the quantitative aspects of muscle contraction. Fortunately, the mechanics of smooth muscle contraction can be studied with only a minor reference to electrophysiology and biochemistry.

11.3 Rhythmic Contraction of Smooth Muscle

Spontaneous contraction is a phenomenon common to many muscular organs. Thus an analysis of peristaltic transport, lymphatic pumping, and autoregulation of blood flow requires knowledge of the mechanical properties of self-excited smooth muscle cells.

Little is known about the mechanical properties of smooth muscle during spontaneous contractions. Most *in vitro* work on smooth muscles has attempted to follow the work of Hill (1939) on skeletal muscle. It is usually claimed that Hill's equation (see Sec. 9.7) works for smooth muscles; but concrete evidence is meager. *In vivo* observations have a long history. Engelmann (1869), Bayliss and Starling (1899) determined that the contractions of the ureter and intestine are myogenic. More recent studies have shown that the tension response of visceral smooth muscle is correlated with the electrical events of the cell membrane. Although these electrical events occur in the absence of stretch, Burnstock and Prosser (1960) have shown that step stretch can alter the cell membrane potential (excitability).

The length-tension relationship for spontaneous contraction of *taenia coli* was studied by Bülbürg and Kuriyama (1963) and Mashima and Yoshida (1965). Their results do not agree with respect to the role of minimum tension (or passive tension) during a spontaneous contraction. Golenhofen (1964) studied sinusoidal length oscillations and found two resonance frequencies for maximum tension amplitude. He concluded that a mechanical coupling between muscle units may play a role in synchronization. Golenhofen (1970) also studied the influence of various environmental factors such as temperature, pH, glucose concentration, and CO_2 tension on spontaneous contraction. Since the time duration of a single isometric spontaneous contraction is on the order of 1 min, Golenhofen has used the term *minute rhythm* to describe these contractions.

Wave Form of Contraction in Taenia Coli

Details of the contraction process of the taenia coli muscle from the cecum of guinea pigs are presented by Price, Patitucci and Fung (1977). To avoid the effect of drugs, the animals were sacrificed by a sharp blow to the head which fractured the spinal cord. The *in vivo* length, L_{ph} , (read the subscript "ph" as "physiological"), of 10 mm or more was marked on the specimen before dissection. Immediately after dissection the specimen was mounted in a test chamber at a length of approximately L_{ph} and 37°C. In a few minutes the muscle began to contract spontaneously and rhythmically. Testing could begin after letting the muscle contract for an hour or more. The solution in the bath, environment control, test equipment, and test procedure are similar to those used for heart muscle (Sec. 10.2); details are reported in the original paper.

When taenia coli is tested isometrically at various lengths, the tension history as shown in Figs. 11.3:1 and 11.3:2 is obtained. Each dot on the

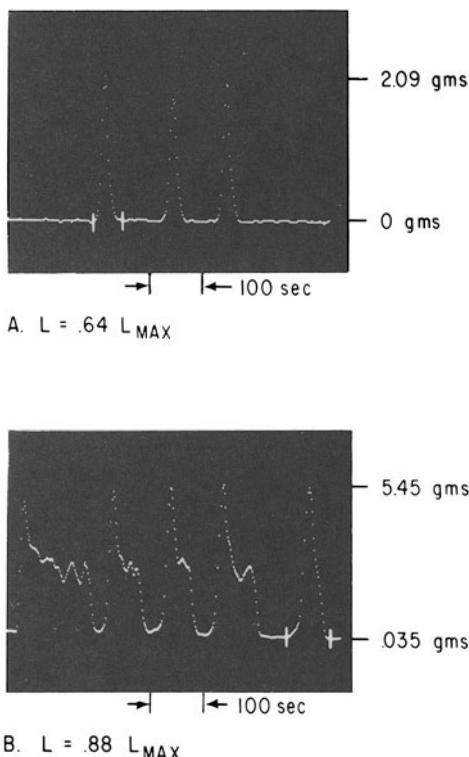


Figure 11.3:1 Computer display of spontaneous contractions in real time for $L < L_{max}$. Time increases from left to right. Each point represents a reading of force on muscle. Time between points is 2 s. (A) Contractions for $L = 0.64 L_{max}$. (B) Contractions for $L = 0.88 L_{max}$. Reference dimensions for specimen are: $L_{max} = 13 \text{ mm}$, $A_{max} = 0.36 \text{ mm}^2$, $L_{ph} = 10 \text{ mm}$. From Price, Patitucci, and Fung (1977), by permission.

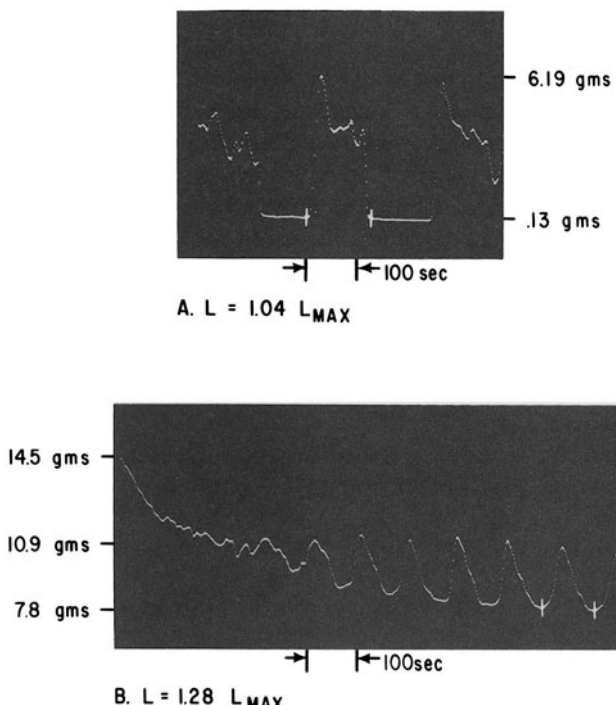


Figure 11.3:2 Computer display of spontaneous contractions in real time for $L \geq L_{max}$. Same specimen as Fig. 11.3:1. (A) Contractions for $L = 1.04 L_{max}$. (B) Contractions for $L = 1.28 L_{max}$. From Price, Patitucci and Fung (1977), by permission.

photographs represents the level of force that is sampled every 2 s. Figure 11.3:1 shows the muscle response when the length is shorter than the length for maximum activity. Figure 11.3:2 shows the muscle response at the length for maximum activity (upper) and the response at extremely stretched lengths (lower). The maximum tension (10.9 g) for a long time after stretch is also marked for Fig. 11.3:2. The transient nature of these records arose because the muscle needed time to readjust to a change of length. To obtain the traces of these figures the muscle length change was accomplished in 100 s. Then the new length was held constant for 1000 s; and the force history was recorded, part of which is shown in these figures. The lower trace of Fig. 11.3:2 shows a record that began immediately after the length change.

These figures tell us that the wave form of the tension in taenia coli in the isometric condition varies with the muscle length. The values of the tension (especially the maximum and minimum) depend on the muscle length, as can be seen from the numbers marked on these curves.

Response to Step Change in Length or Tension

The stress response of taenia coli to a step stretch in length is shown in Fig. 11.3:3. The ordinate, $G(t)$, is the ratio of the tension in the muscle at time t divided by the tension σ_{ss} immediately following the stretch, which ends at time t_{ss} (read the subscript "ss" as "step stretch"). The abscissa is time on a log scale. The response can be divided into two phases, the latent period for $t < 1$ s and the minute rhythm for $t > 1$ s. During the latent phase, the stress decreases monotonically to less than 40% of the peak stress (σ_{ss}) that occurred at t_{ss} . At 1 s after stretch, the minute rhythm begins. The minute rhythm is capable of decreasing the tension to a negligibly small value for $t > 100$ s. Gradually the minute rhythm tends to a steady state. In Fig. 11.3:3 there are eight cycles of contraction from 100 to 1000 s, with approximately 112 s per cycle.

On the other hand, if a taenia coli muscle is tested isotonically at a constant tension, it does not generate a large amplitude length oscillation.

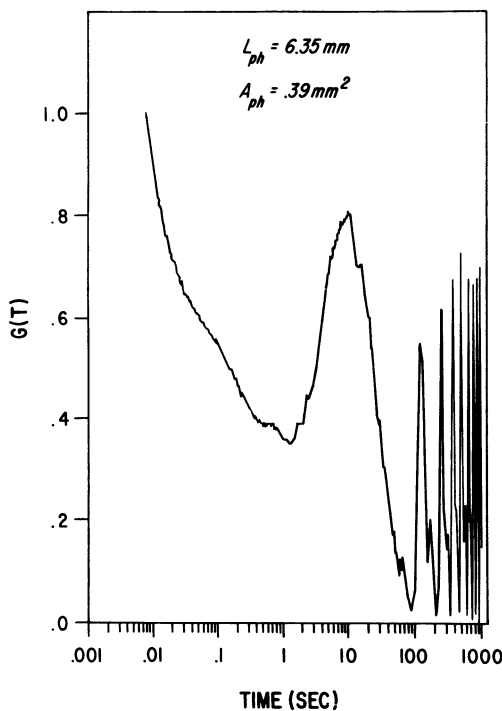


Figure 11.3:3 Stress response to a 10% of L_{ph} step change in length. Response, $G(t)$, is stress, $\sigma(t)$, normalized to stress in the specimen, σ_{ss} , at the end of ramp (10 ms after beginning of stretch). Time is displayed on a logarithmic scale. $\sigma_{ss} = 133 \times 10^4 \text{ dyn/cm}^2$. From Price, Patitucci and Fung (1977), by permission.

Instead, the length change appears as small amplitude irregular oscillations with periods much less than 1 min. Thus, in the isotonic state, the minute rhythm is lost and the contractions are weaker and faster.

Active Tension

For a muscle at length L , let the maximum stress in a cycle of spontaneous contraction be denoted by $\sigma(L)_{\max}$ and the minimum stress by $\sigma(L)_{\min}$. The stress, σ , is the sum of two parts: the active tension produced by the contractile elements of the smooth muscle cells and the passive stress due to stretching of the connective tissue in the muscle. Although it is difficult to evaluate these two parts exactly, an indication can be obtained. Following Fung (1970), we define the “active” stress $S(L, t)$ as the difference between $\sigma(L, t)$ and $\sigma(L)_{\min}$; $\sigma(L, t)$ being the stress at length L and time t . Then the maximum active stress is given by $S(L)_{\max} = \sigma(L)_{\max} - \sigma(L)_{\min}$.

If the values of $S(L)_{\max}$ are plotted as a function of length, then an upper bound, S_{ub} , is reached at a certain length, L_{\max} . This length is used as the reference length because it is characteristic of the contractile element, and it is easily measured. The corresponding reference area, A_{\max} , is used to compute the stress on the specimen in the Lagrangian sense. The results of a typical experiment are shown in Fig. 11.3:4. This figure shows the functional dependence of $S(L)_{\max}$, $\sigma(L)_{\max}$, and $\sigma(L)_{\min}$ on muscle length. In addition

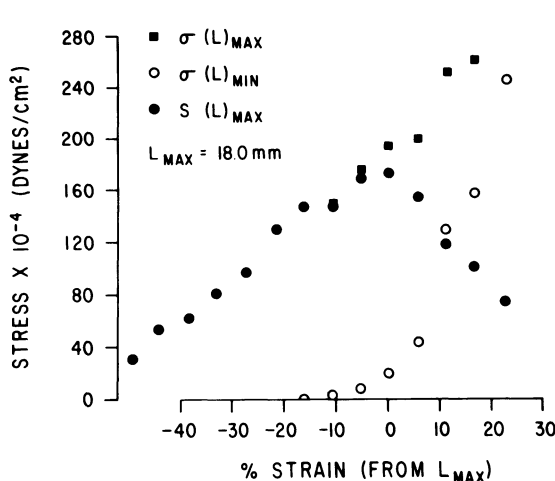


Figure 11.3:4 Dependence of $\sigma(L)_{\max}$, $\sigma(L)_{\min}$, and $S(L)_{\max}$ on muscle length. Parameters from each phase plane curve are plotted as a function of length from L_{\max} . L_{\max} is defined as the length at which $S(L)_{\max}$ is maximum. Specimen dimensions are $L_{\max} = 18$ mm, $A_{\max} = 0.32$ mm², and $L_{ph} = 10$ mm. From Price, Patitucci, and Fung (1977), by permission.

to the existence of an optimum length, L_{\max} , for tension development, it shows an almost symmetrical decrease in active tension as the length varies in either direction from L_{\max} . As the length increased from L_{\max} , the values of $\sigma(L)_{\min}$ increase from a relatively small value in a nonlinear fashion. For muscle lengths above approximately 110% of L_{\max} , $\sigma(L)_{\min}$ and $\sigma(L)_{\max}$ increase very rapidly. If the length is decreased to about 20% below L_{\max} , the value of $\sigma(L)_{\min}$ falls to zero. The length range for active tension production is on the order of $\pm 50\%$ from L_{\max} . Some statistical data for the five specimens tested over the entire range of muscle length are as follows. The mean value of $S(L)_{\max}$ at L_{\max} is $160.1 \times 10^4 \pm 8.38 \times 10^4$ (SE) dyn/cm². The mean value of $\sigma(L)_{\min}$ at L_{\max} is $9.3 \times 10^4 \pm 3.36 \times 10^4$ (SE) dyn/cm².

Summary

Spontaneous contraction occurs in taenia coli in the isometric condition when the environment is favorable. A step stretch in length produces a period of relaxation in which the muscle behaves as a resting tissue before the spontaneous contractions begin. The minute rhythm is abolished if the load becomes isotonic, which induces small amplitude oscillations with frequencies in the order of 10–20 per min. Other experiments have shown that a quick succession of stretches will reduce the tension in minute rhythm, and vibrations of appropriate frequency and amplitude will inhibit contraction tension.

The spontaneous maximum active tension in each cycle, $S(L)_{\max}$, depends on the muscle length, L . There exists an optimal length, L_{\max} , at which the tension $S(L)_{\max}$ has an absolute maximum (upper bound). This feature is reminiscent of Figs 9.7:2 and 10.1:4 for the striated muscles.

11.4 The Property of a Resting Smooth Muscle: Ureter

One of the basic differences between smooth muscles and striated muscles is the lack of spontaneous contraction or the ease of arresting them in the latter. Hence, it is usually assumed that in the striated muscle, the contractile element offers no resistance to elongation or shortening when the muscle is in the resting state. This is the basic reason for separating the muscle force into “passive” and “active” components, or, in the terminology of Hill’s three-element model discussed in Chapters 9 and 10, the “parallel” and “series” elements and the “contractile” element. Usually implied in this definition is the uniqueness of the passive elements, that they have constitutive equations independent of the active state of the contractile element. This assumption might be acceptable for skeletal muscle, but is sometimes questioned for the heart (see Sec. 10.5). For smooth muscles it seems to be entirely doubtful. For example, in the taenia coli smooth muscle, spontaneous contractions

can be arrested by several methods, but different methods lead to somewhat different mechanical behavior of the muscle. Therefore the contractile element cannot be assumed to be freed up completely when the spontaneous contraction is arrested. Thus not all the concepts of the mechanics of striated muscles can be borrowed to deal with smooth muscles.

The lack of a unique resting state of a smooth muscle means that the constitutive equation may not be considered as the sum of two components: passive and active. One would have to experiment on the active muscle and deduce its constitutive equation directly. Nevertheless, it is still interesting to study the properties of smooth muscle in the resting states, not only because they are physiological, but also because they furnish a base upon which the active state can be better understood.

The Relative Magnitude of Active and Resting Stresses in Ureter

The relative importance of the resting and active forces in a smooth muscle may be illustrated by Fig. 11.4:1, from data obtained on the dog's ureter. The test specimen was stimulated electrically in an isometric condition at

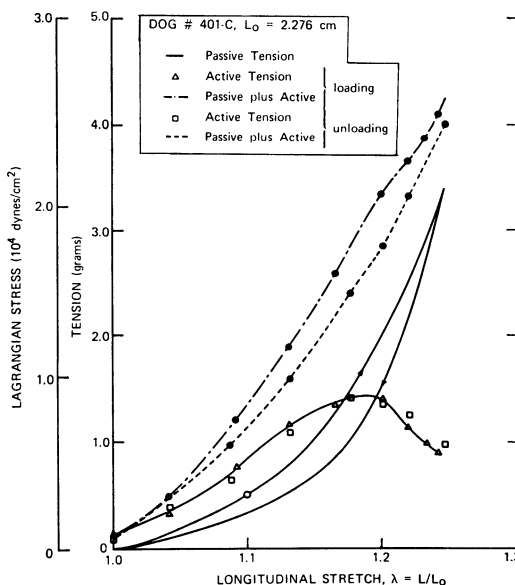


Figure 11.4:1 Graph showing typical relationships between total tension, resting tension, and active tension in the dog's ureter for both loading and unloading. Optimal stimulus: square-wave dc pulse, 9 V, 500 ms, 1 pulse/twitch. Temp.: 37°C. Stretching rate, 2% of L_0 min⁻¹. Releasing rate, same. For each twitch, time from stimulation to peak tension: 1.195 ± 0.097 s, time of 90% relaxation from peak tension to 10% of peak: about 1.35 s. Delay time between stimulation and onset of mechanical contraction 297 ± 105 ms. From Yin and Fung (1971).

various levels of stretch. When unstimulated and quiescent the ureter does not contract spontaneously, and hence is resting. A resting ureteral muscle is viscoelastic, hence it is necessary to distinguish loading (increasing stretch) and unloading (decreasing stretch) processes. It was found that each twitch requires one stimulus for most animals, except for the rabbit, for which two consecutive pulses are required to elicit the maximal response. The maximum tension or Lagrangian stress developed in a twitch at specific lengths of the ureter is plotted as the ordinate in Fig. 11.4: 1. Solid lines refer to the resting state and broken lines refer to the stimulated state, whereas the triangular and square symbols represent the active tension (total tension minus resting tension). The open circle represents the *in situ* value of stretch. It is seen that the ureter develops the maximum active tension at such a muscle length that there is a considerable amount of resting tension. The magnitude of the maximum active tension is about equal to the resting tension at such a muscle length. This is in sharp contrast with skeletal muscle (see Sec. 9.1) and heart muscle (see Fig. 10.1:4), in which the resting stress is either insignificant or relatively minor compared with the maximum active tension in normal physiological condition.

Cyclically Stretched Ureteral Smooth Muscle

The ureter is a thick-walled cylindrical tube. In the normal relaxed condition it contracts to such an extent that its lumen becomes practically zero. In the animal the lumen is increased with the passage of urine, and the stretching of the ureteral wall induces active response in the form of peristalsis. Electric events accompany the ureteral contraction, which in turn can be elicited by electric stimulation. In the pelvis of the kidney and in the ureter, there are pacemakers; but specimens that are segments taken from the ureter apparently do not have pacemakers strong enough to make them spontaneously contracting. Ureteral segment specimens remain resting until stimulated.

The mechanical properties of ureter in the longitudinal direction can be determined by using isolated segments of intact ureters subjected to simple elongation. Properties in the circumferential direction can be determined by using slit ring segments subjected to simple elongation. The test equipment, specimen preparation, preconditioning, experimental procedure, and bath composition are similar to those described in Sec. 10.2.

For simple elongation tests the specimen is first loaded at a given strain rate to some final stress level and then unloaded at the same rate. Figure 11.4:2 shows some typical results. The stress-strain curves are quite similar to those discussed in Chapters 7–10 for other soft tissues. If the rate of change of stress with respect to stretch is plotted against the stress, we obtain the results shown in Fig. 11.4:3. Over a range of stretch ratios this appears to be representable as a straight line, so that as in Sec. 7.5, we can write the relationship between the Lagrangian stress T (tension divided by the initial

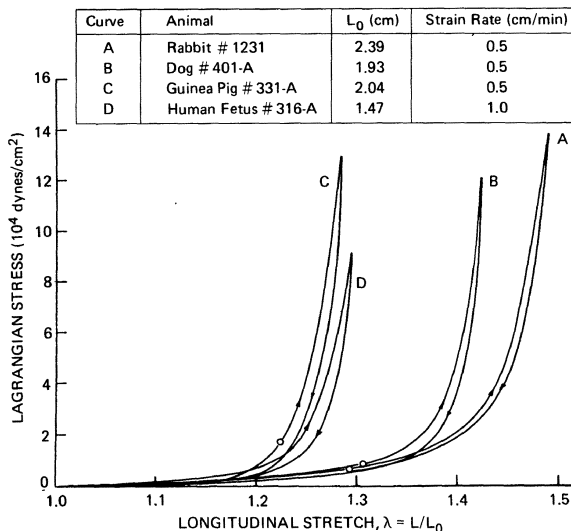


Figure 11.4:2 Typical stress-strain curves in loading and unloading for species studied. Open circles denote the *in situ* stretch value. Temp.: 22°C. From Yin and Fung (1971), by permission.

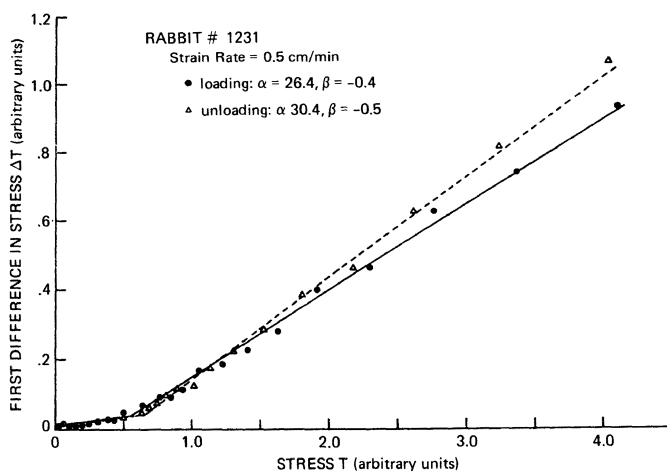


Figure 11.4:3 Sketch of typical results obtained from curve A of Fig. 11.4:2. Solid and dotted lines are least-squares fit to the data on the loading and unloading processes, respectively. Two different straight line segments are used to fit the data in the lower (1.0–1.37) and higher (1.37–1.5) ranges of λ in each case. From Yin and Fung (1971), by permission.

cross-sectional area), and the stretch ratio, λ , by the equation

$$T = (T^* + \beta)e^{\alpha(\lambda - \lambda^*)} - \beta \quad (\lambda_1 \leq \lambda \leq \lambda_2), \quad (1)$$

where α , β , T^* , and λ^* are experimentally determined constants. T^* and λ^* are a pair of specified stress and strain constants, and α and β are the elasticity parameters in the range of λ tested. α represents the slope of the curve of $dT/d\lambda$ vs T ; β represents (approximately) the intercept on the T axis, α is dimensionless, and β has the units of stress. In Fig. 11.4:3 the finite difference ΔT , instead of $dT/d\lambda$, is plotted against T . According to Eq. (1),

$$\Delta T_i = T_{i+1} - T_i = (e^{\alpha \Delta \lambda} - 1)(T_i + \beta), \quad (2)$$

where T_i represents the i th tabular value of T listed at equal intervals of λ , and $\Delta \lambda$ is the size of the λ interval chosen. It can be easily proved that the slope of the curve, ΔT_i vs T_i , or $\tan \theta$, is given by

$$\tan \theta = e^{\alpha \Delta \lambda} - 1, \quad (3)$$

from which α can be easily calculated.

Tabulated results for α and β for the ureters of the dog, rabbit, guinea pig, and man are given in Yin and Fung (1971). It is shown for the rabbit ureter that the *in situ* value of λ falls into the range in which the data can be fitted by an exponential curve of the form of Eq. (1). The hysteresis, as revealed by the difference in the values of α for loading and unloading, is small. Paired statistical analysis of the results in the higher ranges of λ obtained by using the student t test ($P = 0.05$) showed the following: (a) the distal segments have a significantly higher value of α than the proximal segments; (b) varying the strain rate from 0.03 to 3 muscle lengths per min produces no significant differences in the elasticity parameters during either loading or unloading in dog's ureter; and (c) an obstructed-dilated ureteral segment has a significantly lower value of α than a normal segment.

The strain rate effect on α , however, depends on the animal. In the range of λ and $d\lambda/dt$ tested, α of the guinea pig ureter depends on the strain rate, but α of the dog ureter does not.

Stress-Relaxation in Ureter

The relaxation test is done by stretching a specimen to a desired strain level, then holding the strain constant and measuring the change of force with time. Typical relaxation curves for circumferential segments of the dog's ureter are shown in Fig. 11.4:4, where the abscissa represents the time elapsed from the end of stretch, and the ordinate represents the ratio of the stress at time t to that at 0.1 s after the end of stretch. Note how fast and thoroughly the tissue relaxed! At 10 s, 50 to 65% of initial stress is lost; at 1000 s (not shown in this figure) 70 to 80% of the stress is gone. Such thorough relaxation is not seen in other connective tissues such as the skin and mesentery.

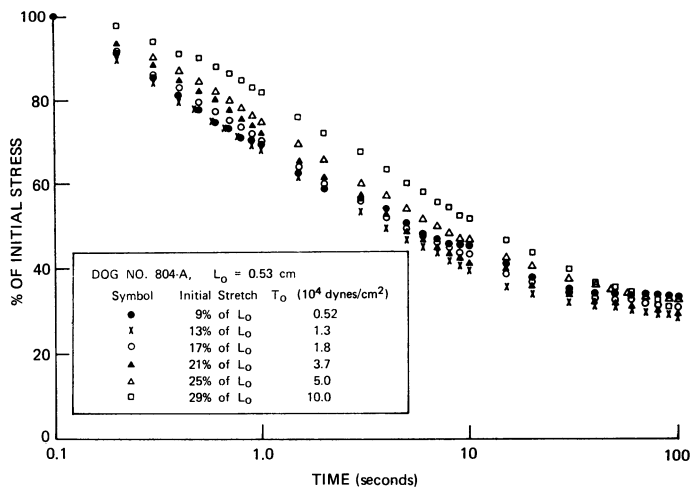


Figure 11.4:4 Stress relaxation of circumferential segments of a dog's ureter, showing dependence on amount of initial stretch. Temp.: 37°C. Initial strain rate 20 L_0 /min. From Yin and Fung (1971), by permission.

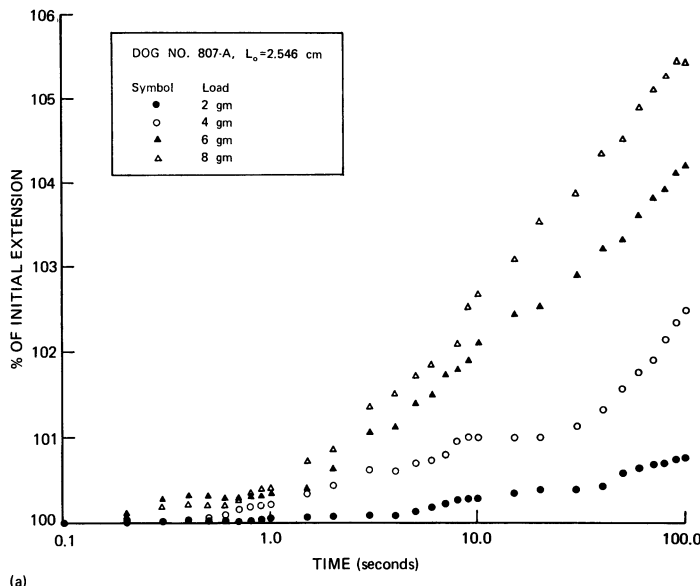


Figure 11.4:5 (a) Short-term creep results from a dog ureter specimen showing load dependence. Temp.: 37°C. From Yin and Fung (1971). (b) Long-term creep data from rabbit specimens. Temp.: 37°C. From Yin and Fung (1971), by permission.

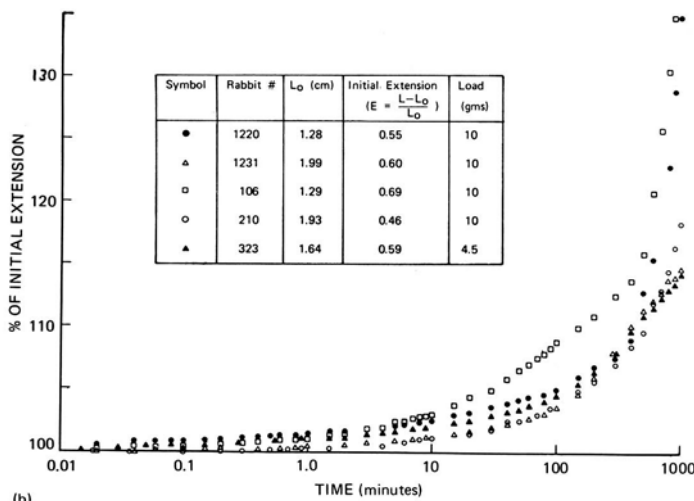


Figure 11.4:5 (Continued)

Creep of Ureter

The counterpart of relaxation is creep, the continued elongation under a fixed load. Typical creep characteristics of the ureter are illustrated in Fig. 11.4:5. The creep rate depends clearly on the stress level.

11.5 Resting Smooth Muscle: Taenia Coli

Taenia coli muscle of the intestine differs from the ureter in that normally it contracts spontaneously. To test taenia coli in a resting state it is necessary to suppress its spontaneous activity. The suppressed state depends on the method of suppression, and is not unique.

Three convenient methods can be used to suppress the spontaneous activity in taenia coli: (a) the use of calcium-free EGTA solution, (b) the use of epinephrine, and (c) the lowering of the temperature to less than 20°C. The first two methods consist of a change in the bathing fluid for the muscle. In normal experiments, the specimen is bathed in a physiological solution that has the following composition (mM): NaCl, 122; KCl, 4.7; CaCl₂, 2.5; MgCl₂, 1.2; KH₂PO₄, 1.2; NaHCO₃, 15.5; and glucose, 11.5; the solution is constantly bubbled with O₂ (95%) and CO₂ (5%). The calcium-free EGTA solution is obtained by replacing CaCl₂ with 2 mM EGTA (disodium ethylene glycol-bis-(β-aminoethyl ether)-N, N'-tetraacetic acid). The epinephrine treated solution is obtained by injecting adrenalin chloride solution directly into the bath to obtain an initial concentration of 0.1 mg/ml.

These methods probably have different ways of acting on the actin-myosin coupling. Removal of calcium ion can depolarize the cell membrane, and this action is temperature dependent. Bülbring and Kuriyama (1963) have shown that 20°C is a critical temperature for spontaneous electric activity in *taenia coli*. They also showed that inactivation of *taenia coli* by epinephrine is associated with an increased membrane potential and a block of action potential; epinephrine increases the amount of creatine phosphate and ATP, and the utilization of these substances in hyperpolarization of the cell membrane.

Relaxation After a Step Stretch

Using the same testing equipment mentioned in Secs. 10.2 and 11.3, Price et al. (1978) tested guinea pig *taenia coli* by procedures similar to those described in Sec. 11.3. The tissue was stretched at a constant strain rate from time $t = 0$ to time $t_{ss} = 10$ ms (the subscript "ss" stands for the time to "step stretch"), and the length was maintained constant thereafter. The stress at t_{ss} is denoted as σ_{ss} . The stress $\sigma(t)$ at time $t > t_{ss}$ divided by σ_{ss} is defined as the *normalized relaxation function*, $G(t)$.

On a spontaneously contracting specimen, step-stretch test begins at the end of a contraction cycle when the tension was zero. $G(t)$ for various degrees

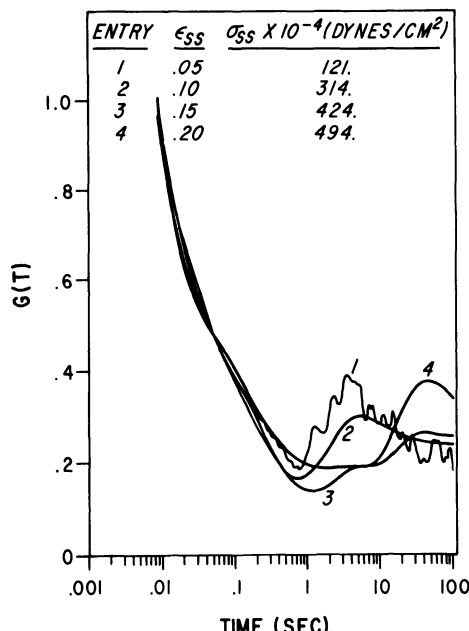


Figure 11.5:1 Step-stretch response of spontaneous *taenia coli* for various amounts of stretch. Reference dimensions: $L_0 = 6.17$ mm and $A_0 = 0.198$ mm². From Price, Patitucci, and Fung (1979), by permission.

of stretch of a spontaneously contracting specimen is shown in Fig. 11.5:1. A latent period occurs immediately following stretch, in which the response is a monotonically decreasing function of time. During the latent period the membrane action potential is absent. The latent period ends approximately 1 s after the initiation of stretch due to the resumption of membrane electric activity and the onset of contraction. Although the contractile response varies with the amount of stretch, $G(t)$ in the latent period appears to be independent of stretch. The delay time, or the time to the onset of contraction, increases with increasing stretch. The strain ϵ_{ss} in Fig. 11.5:1 is defined as the change of length divided by L_0 , the longest length of the specimen under a preload of 100 mg, while the muscle contracted spontaneously.

When the bath was replaced by the calcium-free EGTA solution, the normalized relaxation functions became those shown in Fig. 11.5:2. The step size for all the curves in this figure was 10% of the initial Length L_0

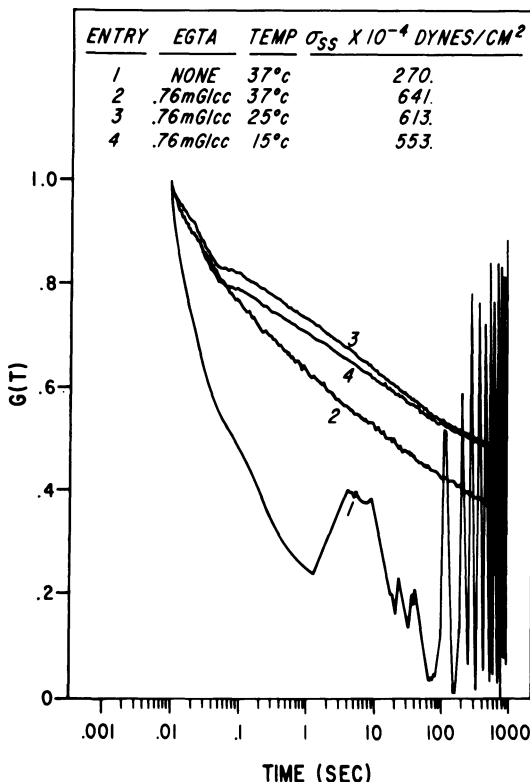


Figure 11.5:2 Step-stretch response before and after calcium removal. Each response is for a stretch of 10% L_0 . Entries 3 and 4 show effect of lower temperature after calcium removal. Reference dimensions for entry 1, $L_0 = 7.35$ mm and $A_0 = 0.34$ mm²; for entry 2, $L_0 = 8.10$ mm and $A_0 = 0.31$ mm²; for entry 3, $L_0 = 9.19$ mm and $A_0 = 0.27$ mm²; and for entry 4, $L_0 = 9.25$ mm and $A_0 = 0.27$ mm². From Price, Patitucci, and Fung (1979), by permission.

arbitrarily defined as the length of the tissue in the bath under a load of 100 mg). The relaxation function $G(t)$ is now seen to be monotonically decreasing, with no resumption of spontaneous contraction. The effect of decreasing temperature after calcium removal is shown by the curves 3 and 4 in the figure. It is seen that removal of calcium ions suppresses spontaneous activity, increases the stiffness of the taenia coli (as reflected in the higher values of σ_{ss}), and decreases the rate of relaxation.

When the temperature is lowered from 37°C, the stiffness and the relaxation rate both decrease. If temperature is lowered while the specimen is bathed in normal physiological saline, then σ_{ss} decreases. For $\varepsilon_{ss} = 0.10$ (a 10% stretch), σ_{ss} at 37, 25, and 15°C is 1.33, 1.36, and 0.59×10^6 dyn/cm², respectively. Spontaneous contractions remain at 25°C, but are abolished at 15°C.

The response before and after injection of epinephrine into the bath is shown in Fig. 11.5:3. Curve No. 5 refers to a spontaneously contracting specimen subjected to a step stretch of 10% of L_0 in a bath without epinephrine injection. Entries 1 through 4 refer to specimens in a bath after the injection of epinephrine. At the same strain step ε_{ss} , the values of σ_{ss} are lower after epinephrine injection, whereas the relaxation function $G(t)$ continues

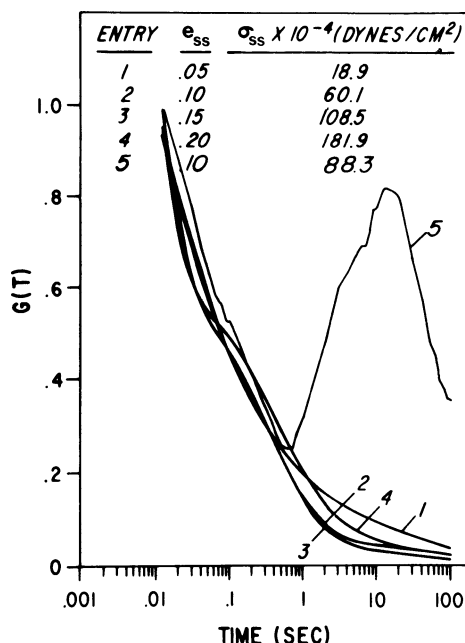


Figure 11.5:3 Step-stretch response before and after treatment with epinephrine. Entry 5 is the response to a stretch of 10% L_0 with no epinephrine. Entries 1–4 are responses to step stretch in 0.1 mg/ml epinephrine. Reference dimensions for entry 5, $L_0 = 4.75$ mm and $A_0 = 0.338$ mm²; for entries 1–4, $L_0 = 5.65$ mm and $A_0 = 0.283$ mm². From Price, Patitucci, and Fung (1979), by permission.

to be monotonically decreasing. Note that in this case $G(t)$ becomes less than 5% at 100 s. It seems that at large time the stress will be relaxed to almost zero. Such a behavior is seen in ureteral smooth muscle (see Fig. 11.4:4), but is not seen in other tissues such as the arteries, veins, skin, mesentery, and striated muscles.

Response of a tissue to a step change in length may be represented by the simplified formula

$$K(\varepsilon, t) = G(t)T^{(e)}(\varepsilon), \quad (1)$$

as discussed in Secs. 7.6, 8.3, and 10.2. Here $G(t)$ is the normalized relaxation function, which is assumed to be a function of time, and is independent of the strain. $T^{(e)}(\varepsilon)$ is a function of strain alone. This assumption is supported by the experimental data shown in Fig. 11.5:3. Resting taenia coli seems to obey such a relation. The mathematical form for $G(t)$ has been discussed in Sec. 7.6. Although curves as shown in Fig. 11.5:3 can be represented by a sum of a few exponential functions, the simultaneous requirement of the rate-insensitivity feature shown in Fig. 11.5:4 for cyclic loading suggests the use of a continuous spectrum. The form proposed by the author (Fung, 1972) is

$$G(t) = \frac{1}{A} \left[1 + c \int_{\tau_1}^{\tau_2} \frac{1}{\tau} e^{-(t/\tau)} d\tau \right], \quad (2)$$

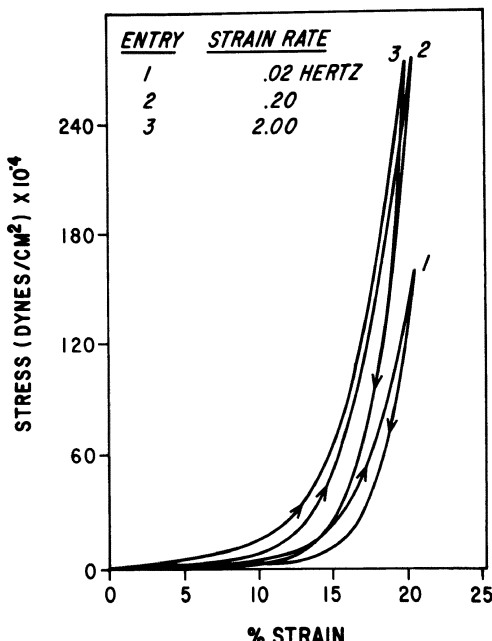


Figure 11.5:4 Stress-strain relationship of taenia coli in epinephrine solution at various strain rates. Peak strain is 0.205 for each test. Reference dimension are $L_{\max} = 12.15$ mm and $A_{\max} = 0.493$ mm². From Price, Patitucci, and Fung (1979), by permission.

where c , τ_1 and τ_2 are constants and A is the value of the quantity in the brackets at $t = 0$:

$$A = 1 + c \int_{\tau_1}^{\tau_2} \frac{1}{\tau} d\tau = 1 + c \log_e \left(\frac{\tau_2}{\tau_1} \right) \quad (2a)$$

A comparison of the values of $G(t)$ predicted by Eq. (2) with those by experiments is shown in Fig. 11.5:5, and is seen to be satisfactory.

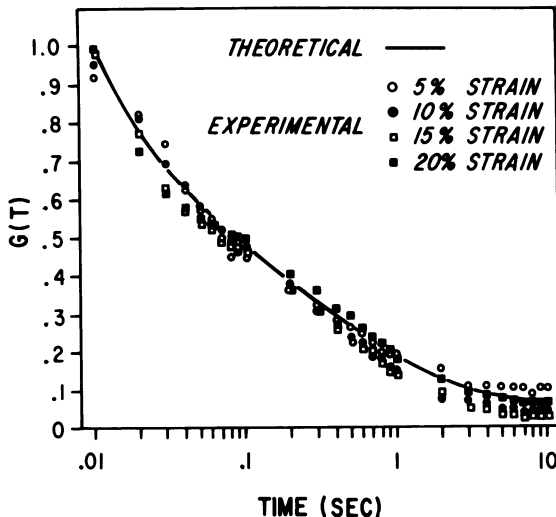


Figure 11.5:5 Comparison of theoretical and experimental values of $G(t)$ of taenia coli smooth muscle in epinephrine treated solution. Specimen is the same as in Fig. 11.5:3. Parameters defining theoretical $G(t)$ are $c = 2.25$, $\tau_1 = 0.003$ s, and $\tau_2 = 3.38$ s. From Price, Patitucci and Fung (1979), by permission.

Cyclic Loading and Unloading Tests

The specimen is stretched at a constant rate (dL/dt) to a specified length and immediately reversed at the same strain rate, resulting in a cyclic triangular strain history. The resulting stress-strain relationship of taenia coli in epinephrine treated solution is illustrated in Fig. 11.5:4. Here the stress is Lagrangian (force divided by initial cross-sectional area), and the strain is $\Delta L/L_0$, L_0 being the length of muscle in epinephrine at 100 mg preload. The features shown in Fig. 11.5:4 are similar to those of other soft tissues discussed in Chapter 7. The stress is a nonlinear function of strain and depends on the strain rate. The relationship is different in loading from that in the unloading process. At higher strain rates (above 0.2 Hz), the loops are almost independent of the frequency. This last mentioned property is decisive in selecting the relaxation spectrum presented in Eq. (2).

Information on the “elastic response” $T^{(e)}(\varepsilon)$ can be extracted from experimental results as shown in Fig. 11.5:4. Assuming that at sufficiently high

rates of stretching the stress-strain relationship is essentially independent of the strain rate, then the stress corresponding to the strain on the loading curve (increasing strain) can be considered to approximate $T^{(e)}(\varepsilon)$. Under such an assumption our problem is to find a mathematical expression for $T^{(e)}(\varepsilon)$. A replot of the loading curves shown in Fig. 11.5:4 on a log-log scale yields the results shown in Fig. 11.5:6. Each curve in Fig. 11.5:6 can be represented by two straight line segments. Because a straight line on a log-log plot represents a power law, we see that the data in Fig. 11.5:6 can be expressed by the equations

$$T = \beta \varepsilon^\alpha \quad \text{for } 0 < \varepsilon < \varepsilon^*, \quad (3)$$

and

$$T = \beta' \varepsilon^{\alpha'} \quad \text{for } \varepsilon > \varepsilon^*, \quad (4)$$

where α and α' are the respective slopes of the log-log plot, and β and β' are constants determined by a known point on the curve. Let the intersection of the two straight lines be the point $T = T^*$, $\varepsilon = \varepsilon^*$, then

$$\beta = T^*/(\varepsilon^*)^\alpha, \quad \beta' = T^*/(\varepsilon^*)^{\alpha'}. \quad (5)$$

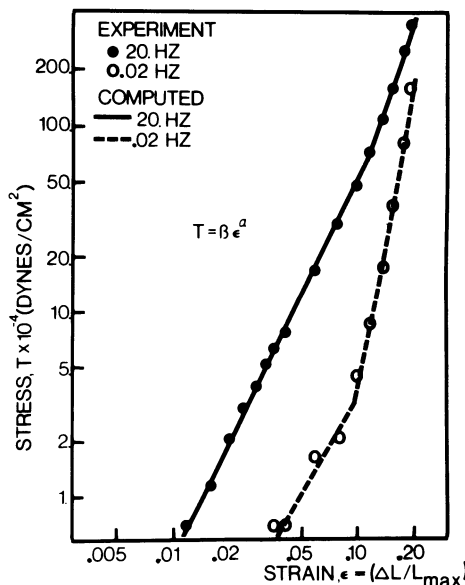


Figure 11.5:6 Log-log graph of stress vs increasing strain for epinephrine treated taenia coli specimens from guinea pigs. Experimental points are shown for the same specimen as in Fig. 11.5:5. The computed curves are based on Eqs. (3) and (4) with the following constants and standard errors: At 0.02 Hz, $\alpha = 1.77 \pm 0.213$, $\beta = 0.193 \pm 0.043$, $\alpha' = 5.21 \pm 0.29$, $\beta' = 534.0 \pm 28.0$, $\varepsilon^* = 0.1006$, $T^* = 0.0033$. At 20 Hz, $\alpha = 2.04 \pm 0.041$, $\beta = 5.31 \pm 0.389$, $\alpha' = 2.80 \pm 0.108$, $\beta' = 27.50 \pm 0.53$, $\varepsilon^* = 0.117$, $T^* = 0.065$. The units of β , β' , and T^* are 10^7 dyn/cm² or MPa. From Price, Patitucci and Fung (1979), by permission.

Experimental values of α for guinea pig taenia coli range from 1.77 to 5.21, which is similar to the values of α found for the aorta, i.e., 1.23–3.05 (Tanaka and Fung, 1974).

Relative Magnitude of Active and Passive Stresses in Taenia Coli

If the tension in an epinephrine treated resting taenia coli at various lengths is compared with the minimum tension of spontaneously contracting muscle at the same lengths, it is found that they are approximately equal. This is shown in Fig. 11.5:7. If the resting tension is compared with the active tension shown in Fig. 11.3:4, it is seen that the resting tension is not large at L_{\max} , the length at which the maximum active tension is generated. Unlike the ureter, taenia coli operates normally in a range of length in which the resting tension is negligible compared with the active tension.

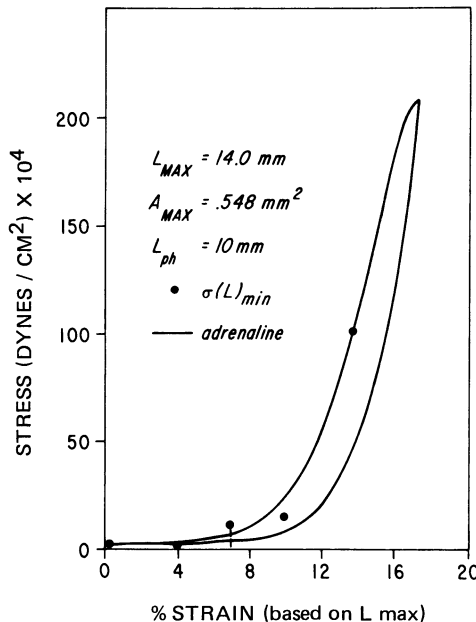


Figure 11.5:7 Comparison of stress in epinephrine relaxed muscle and $\sigma(L)_{\min}$. Length changes are shown as percent strain from L_{\max} . A length-tension test was performed first on a spontaneous specimen; then a stress-strain test (0.01 Hz) was done after the addition of epinephrine (0.1 mg/ml). From Price, Patitucci and Fung (1979), by permission.

Summary

The main lesson we have learned from the study of resting smooth muscles is that the passive state may depend on the method by which the spontaneous activity is suppressed. This implies that the contractile mechanism is not

entirely freed up when the electric activity is arrested. This is the case with taenia coli, but not with ureter. The point is, however, that the conventional concept of separating the mechanical action of a muscle to “parallel”, “series”, and “contractile” elements (see Sec. 9.8) may fail with smooth muscles, because the parallel element is inseparable from the contractile element in the resting condition.

Of the properties of resting smooth muscles, the most remarkable is the thorough stress relaxation under a constant strain. After a long time following a step change in length, the stress may relax to almost zero. This implies that the geometry of an internal organ whose structure is dominated by smooth muscles could be quite plastic in its behavior, and moldable by environmental forces and constraints.

Although the constitutive equation that mathematically describes the contraction process of smooth muscles is still unknown, a vast amount of information has been accumulated with respect to the fine structure of the muscles, as well as their electrical activity, metabolic characteristics, pharmacological responses, innervation, growth, and proliferation. The reader may be referred to the books by Huddart (1975), Huddart and Hunt (1975), Wolf and Werthessen (1973), and Aidley (1971), as well as those mentioned in Secs. 11.1 and 11.2. The recent volume of *Handbook of Physiology*, Sec. 2, Vol. 2, *Vascular Smooth Muscle* (ed. by Bohr et al., 1980) contains a wealth of material and should be consulted.

Problem

- 11.1** Consider an approximate theory of ureteral peristalsis. The urine is a Newtonian fluid and the Reynolds number of flow is much less than one. The ureteral wall is incompressible; its mechanical properties in the resting state have been described in Sec. 11.4. By a wave of contraction of the ureteral muscle the urine is sent through the ureter from the kidney to bladder. Under normal conditions urine is moved one bolus at a time; the muscle contraction is strong enough to completely close the lumen of the ureter at the ends of the bolus. In the diseased condition of hydrourerter, the ureter is dilated, and the force of contraction is not enough to close the lumen.

Interaction of fluid pressure and muscle tension must be considered. The course of contraction is quite similar to a single twitch of the heart papillary muscle, hence, as an approximation we may use the equations presented in Sec. 10.4 to describe the active ureteral muscle contraction. Assume that the fluid bolus is axisymmetric and is so slender that its diameter is much smaller than its length. Let the geometry of the fluid bolus and the ureter be as shown in Fig. P11.1. Use polar coordinates (r, θ, x) with the x -axis coinciding with the axis of the ureter, write down the equation of equilibrium of the tube wall (the Laplace equation given in Problem 1.4 in Chapter 1), the equation of motion of the fluid, the equation of continuity for the conservation of mass, and the appropriate boundary conditions. Solve the equations to obtain the velocity profile, and the radial velocity at the wall. Let $U(x, t)$ be the axial velocity on the centerline and r_i be the radius of the

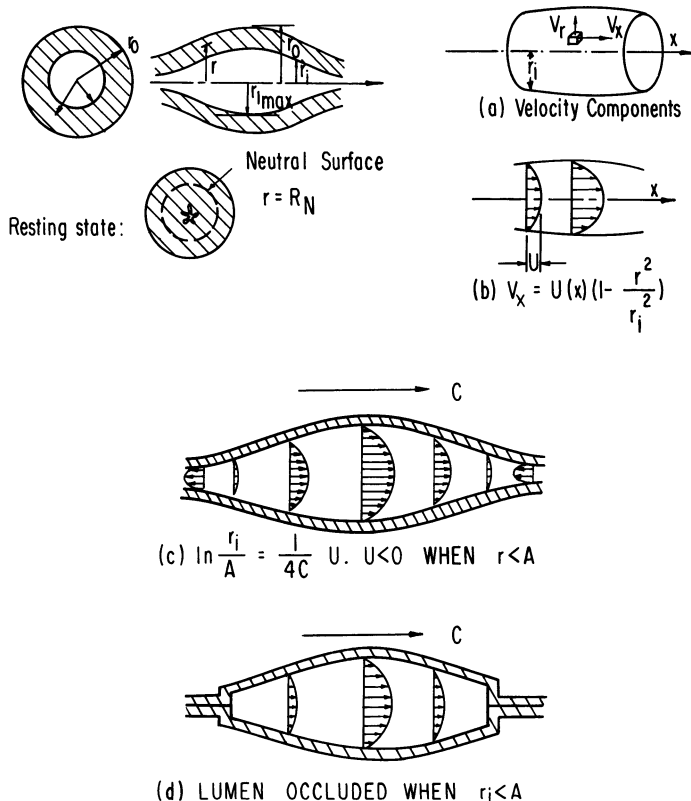


Figure P11.1(a) and (b): Notations and coordinates for the analysis of ureteral peristalsis. (c) and (d): Fluid velocity distribution as demanded by the equation of continuity.

inner wall. The velocity components are shown in Fig. P11.1 (a), (b). Show that

$$\frac{\partial r_i(x, t)}{\partial t} = -\frac{r_i}{4} \frac{\partial U(x, t)}{\partial x}. \quad (1)$$

In a steady peristaltic motion for which the whole pattern moves in the x direction at a constant velocity, c , r_i and U are functions of the single variable $x - ct = \zeta$, and Eq. (1) can be integrated to

$$\log \frac{r_i(\zeta)}{A} = \frac{1}{4C} U(\zeta) \quad (2)$$

with an integration constant A . Thus the velocity U is positive (agreeing with the direction of propagation of the peristaltic wave) when $r_i > A$; it is negative when $r_i < A$. Backward flow (U negative) occurs if the tube is open with a radius less than A ; it does not occur if the ureter is closed both at the front and rear as shown in Fig. P11.1(c), (d).

To determine the shape of the bolus we must consider the action of the muscle. Formulate the mathematical problem and work out the details (cf. Fung, Y. C., 1971a and 1971b, and Jaffrin and Shapiro, 1971).

References

- Abbott, B. C., and Lowy, J. (1957) *Proc. Roy Soc. London Ser. B* **146**, 280–288.
- Aberg, A. K. G., and Axelsson, J. (1965) *Acta Physiol. Scand.* **64**, 15–27.
- Aidley, D. J. (1971) *The Physiology of Excitable Cells*. Cambridge University Press, Cambridge, U.K.
- Ashton, F. T., Somlyo, A. V., and Somlyo, A. P. (1975) *J. Mol. Biol.* **98**, 17–29.
- Axelsson, J. (1970) In *Smooth muscle*, Bülbring, E. et al. (eds.). Arnold, London, pp. 289–316.
- Axelsson, J., and Bülbring, E. (1961) *J. Physiol. (London)* **156**, 344–356.
- Bayliss, W. M., and Starling, E. H. (1899) *J. Physiol. (London)* **24**, 99–143.
- Bohr, D. (1978) In *Peripheral Circulation*, Johnson, P. (ed.). Wiley, New York, Chap. 1.
- Bohr, D. F., Somlyo, A. P., and Sparks, H. V., Jr. (1980) *Handbook of Physiology*, Sec. 2, *Cardiovascular System*, Vol. 2., *Vascular Smooth Muscle*. American Physiological Society, Bethesda, Maryland.
- Bozler, E. (1936) *Cold Spring Harbor Symp. Quant. Biol.*, Vol. 4, pp. 260–266.
- Bülbring, E. (1955) *J. Physiol. (London)* **128**, 200–221.
- Bülbring, E., and Kuriyama, H. (1963) *J. Physiol. (London)* **166**, 24–58; **169**, 198–212.
- Bülbring, E., Brading, A. F., Jones, A. W., and Tomita, T. (eds.) (1970) *Smooth Muscle*. Arnold, London.
- Bülbring, E., and Tomita, T. (1970) *J. Physiol. (London)* **210**, 217–232.
- Burnstock, G. (1970) In *Smooth Muscle*, Bülbring, E. et al. (eds.). Arnold, London, Chap. 1, pp. 1–69.
- Burnstock, G., and Prosser, C. L. (1960) *Am. J. Physiol.* **198**, 921–925.
- Cox, R. H. (1975–1978) *Am. J. Physiol.* **229**, 807–812 (1975); **230**, 462–470 (1976); **231**, 420–425 (1976); **233**, H248–H255 (1977); **234**, H280–H288 (1978).
- Davson, H. (1964) *A Textbook of General Physiology*. Little, Brown, Boston.
- Dobrin, P. B. (1973) *Am. J. Physiol.* **225**, 664–670.
- Engelmann, T. W. (1869) *Pflüger's Archiv*, **2**, 243–293.
- Fung, Y. C. (1970) *J. Biomech.* **3**, 381–404.
- Fung, Y. C. (1971a) In *Developments in Mechanics*, *Proc. 12th Midwest Mechanics*. **6**, 33–62. Univ. of Notre Dame Press, South Bend, Ind.
- Fung, Y. C. (1971b) In *Urodynamic* (Boyarsky, S. et al, eds.) Academic Press, New York, pp. 177–198.
- Fung, Y. C. (1972) In *Biomechanics: Its Foundations and Objectives*, (Fung, Y. C., Perrone, N., and Anliker, M., eds) Prentice-Hall, Englewood Cliffs, N.J. pp. 181–208.
- Golenhofen, K. (1964) *J. Physiol. (London)* **173**, 13–15.
- Golenhofen, K. (1970) In *Smooth Muscle*, Bülbring, E. et al. (eds.). Arnold, London, pp. 316–342.
- Gordon, A. R., and Siegman, M. H. (1971) *Am. J. Physiol.* **221**, 1243–1254.
- Guyton, A. C. (1976) *Textbook of Medical Physiology*. W. B. Saunders, Philadelphia.
- Hill, A. V. (1939) *Proc. Roy. Soc. London Ser. B* **126**, 136–195.
- Hill, A. V. (1950) *Proc. Roy. Soc. London Ser. B* **137**, 273–280.

- Huddart, H. (1975) *The Comparative Structure and Function of Muscle*. Pergamon, New York.
- Huddart, H., and Hunt, S. (1975) *Visceral Muscle. Its Structure and Function*. Blackie, Glasgow.
- Jaffrin, M. Y., and Shapiro, A. H. (1971) *Annual Review of Fluid Mechanics* **3**, 13–36.
- Johnson, P. C. (ed.) (1978) *Peripheral Circulation*. Wiley, New York.
- Kurihara, S., Huriyama, H., and Magaribuchi, T. (1974) *J. Physiol. London* **238**, 413–426.
- Lowy, J., and Mulvany, M. J. (1973) *Acta Physiol. Scand.* **88**, 123–136.
- Mashima, H., and Yoshida, T. (1965) *Jpn. J. Physiol.* **15**, 463–477.
- Merrillees, N. C. R., Burnstock, G., and Holman, M. E. (1963) *J. Cell Biol.* **19**, 529–550.
- Needham, D. M., and Shoenberg, C. F. (1964) *Proc. Roy. Soc. London Ser. B* **160**, 517–522.
- Price, J. M., Patitucci, P., and Fung, Y. C. (1977) *Am. J. Physiol.* **233**(1), C47–C55.
Am. J. Physiol.: Cell Physiol. **2**(1), C47–C55.
- Price, J. M., Patitucci, P., and Fung, Y. C. (1979) *Am. J. Physiol.* **236**(5), C211–C220.
Am. J. Physiol.: Cell Physiol. **5**(3), C211–C220.
- Siegman, M. J., Butler, T. M., Moores, S. U., and Davies, R. E. (1976) *Am. J. Physiol.* **231**, 1501–1508.
- Tanaka, T. T. and Fung, Y. C. (1974) *J. Biomech.* **7**, 357–370.
- Uvelius, B. (1976) *Acta Physiol. Scand.* **97**, 1–12.
- Wolf, S., and Werthessen, N. T. (1973) *The Smooth Muscle of the Artery*. Plenum, New York.
- Yin, F. C. P., and Fung, Y. C. (1971) *Am. J. Physiol.* **221**, 1484–1493.

CHAPTER 12

Bone and Cartilage

12.1 Mechanical Properties of Bone

Bone is hard and has a stress-strain relationship similar to many engineering materials. Hence stress analysis in bone can be made in a way similar to the usual engineering structural analysis. Figure 12.1:1 shows the stress-strain relationship of a human femur subjected to uniaxial tension. It is seen that dry bone is brittle and fails at a strain of 0.4%; but wet bone is less so, and fails at a strain of 1.2%. Since the range of strain is so small, it suffices to use the infinitesimal strain measure (the strain defined in the sense of Cauchy):

$$\varepsilon_{ij} = \frac{1}{2} \left(\frac{\partial u_i}{\partial x_j} + \frac{\partial u_j}{\partial x_i} \right),$$

where x_1, x_2, x_3 are rectangular cartesian coordinates, u_1, u_2, u_3 are displacements referred to x_1, x_2, x_3 , and ε_{ij} represents the strain components. Figure 12.1:1 suggests that Hooke's law is applicable for a limited range of strains. For uniaxial loading below the proportional limit, the stress σ is related to the strain ε by

$$\sigma = E\varepsilon,$$

where E is the Young's modulus.

Table 12.1:1 gives the mechanical properties of wet compact bones of some animals and man. It is seen that the ultimate strength and ultimate strain in compression are larger than the corresponding values in tension for all the bones, whereas the modulus of elasticity in tension is larger than that in compression. The difference in the mechanical properties in tension and compression is caused by the nonhomogeneous anisotropic composite

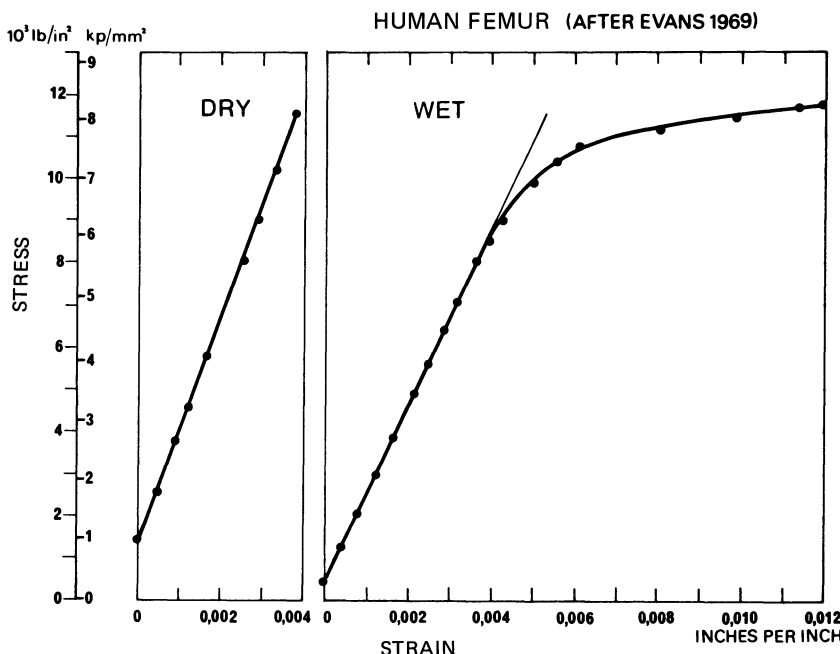


Figure 12.1:1 Stress-strain curves of human femoral bone. Adapted from Evans (1969).

structure of bone, which also causes different ultimate strength values when a bone is tested in other loading conditions. Thus, for adult human femoral compact bone, the ultimate bending strength is 160 MPa (16 kg/mm^2), and the ultimate shear strength in torsion is $54.1 \pm 0.6 \text{ MPa}$, whereas the modulus of elasticity in torsion is 3.2 GPa (326 kg/mm^2).

It is well known also that the strength of bone varies with the age and sex of the animal, the location of the bone, the orientation of the load, the strain rate, and the test condition (whether it is dry or wet). The strain rate effect may be especially significant, with higher ultimate strength being obtained at higher strain rate (see Schmitt, 1968). Yamada (1970), Evans (1973), Crowningshield and Pope (1974), and Reilly and Burstein (1974) have presented extensive collections of data from the literature.

The strength and modulus of elasticity of spongy bone are much smaller than those of compact bone. Again, see Yamada (1970) for extensive data on human vertebrae.

The Anatomy of a Long Bone

In the above, we have spoken of a bone as if it were a homogeneous material. In fact, of course, it is not. Figure 12.1:2 shows a sketch of a long bone. It

TABLE 12.1:1 Mechanical Properties of Wet Compact Bone in Tension, Compression, and Torsion Parallel to Axis. Data Adopted from Yamada 1970

Bone	Horses	Cattle	Pigs	Human (20–39 yrs.)
Ultimate Tensile Strength (MPa)				
Femur	121 ± 1.8	113 ± 2.1	88 ± 1.5	124 ± 1.1
Tibia	113	132 ± 2.8	108 ± 3.9	174 ± 1.2
Humerus	102 ± 1.3	101 ± 0.7	88 ± 7.3	125 ± 0.8
Radius	120	135 ± 1.6	100 ± 3.4	152 ± 1.4
Ultimate Percentage Elongation				
Femur	0.75 ± 0.008	0.88 ± 0.020	0.68 ± 0.010	1.41
Tibia	0.70	0.78 ± 0.008	0.76 ± 0.028	1.50
Humerus	0.65 ± 0.005	0.76 ± 0.006	0.70 ± 0.033	1.43
Radius	0.71	0.79 ± 0.009	0.73 ± 0.032	1.50
Modulus of Elasticity in Tension (GPa)				
Femur	25.5	25.0	14.9	17.6
Tibia	23.8	24.5	17.2	18.4
Humerus	17.8	18.3	14.6	17.5
Radius	22.8	25.9	15.8	18.9
Ultimate Compressive Strength (MPa)				
Femur	145 ± 1.6	147 ± 1.1	100 ± 0.7	170 ± 4.3
Tibia	163	159 ± 1.4	106 ± 1.1	
Humerus	154	144 ± 1.3	102 ± 1.6	
Radius	156	152 ± 1.5	107 ± 1.6	
Ultimate Percentage Contraction				
Femur	2.4	1.7 ± 0.02	1.9 ± 0.02	1.85 ± 0.04
Tibia	2.2	1.8 ± 0.02	1.9 ± 0.02	
Humerus	2.0 ± 0.03	1.8 ± 0.02	1.9 ± 0.02	
Radius	2.3	1.8 ± 0.02	1.9 ± 0.02	
Modulus of Elasticity in Compression (GPa)				
Femur	9.4 ± 0.47	8.7	4.9	
Tibia	8.5		5.1	
Humerus	9.0		5.0	
Radius	8.4		5.3	
Ultimate Shear Strength (MPa)				
Femur	99 ± 1.5	91 ± 1.6	65 ± 1.9	54 ± 0.6
Tibia	89 ± 2.7	95 ± 2.0	71 ± 2.8	
Humerus	90 ± 1.7	86 ± 1.1	59 ± 2.0	
Radius	94 ± 3.3	93 ± 1.8	64 ± 3.2	
Torsional Modulus of Elasticity (GPa)				
Femur	16.3	16.8	13.5	3.2
Tibia	19.1	17.1	15.7	
Humerus	23.5	14.9	15.0	
Radius	15.8	14.3	8.4	

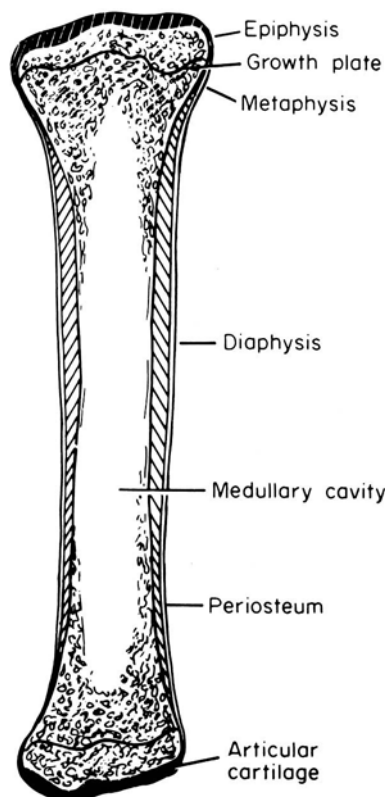


Figure 12.1:2 The parts of a long bone. From Rhinelander (1972). Reproduced by permission.

consists of a shaft (diaphysis) with an expansion (metaphysis) at each end. In an immature animal, each metaphysis is surmounted by an epiphysis, which is united to its metaphysis by a cartilaginous growth plate (epiphyseal plate). At the extremity of each epiphysis, a specialized covering of articular cartilage forms the gliding surface of the joint (articulation). The coefficient of dry friction between the articulate cartilages of a joint is very low (can be as low as 0.0026, see p. 410, about the lowest of any known solid material); hence the cartilage covering makes an efficient joint.

The growth plate, as its name indicates, is the place where calcification of cartilage takes place. At the cessation of growth, the epiphyses, composed of cancellous bone, become fused with the adjacent metaphyses. The outer shell of the metaphyses and epiphyses is a thin layer of cortical bone continuous with the compactum of the diaphysis.

The diaphysis is a hollow tube. Its walls are composed of dense cortex (compactum), which is thick throughout the extent of the diaphysis but

tapers off to become the thin shell of each metaphysis. The central space (medulla or medullary cavity) within the diaphysis contains the bone marrow.

Covering the entire external surface of the mature long bone, except for the articulation, is the periosteum. The inner layer of the periosteum contains the highly active cells that produce circumferential enlargement and remodeling of the growing long bone; hence it is called the osteogenic layer. After maturity, this layer consists chiefly of a capillary blood vessel network. The outer layer of the periosteum is fibrous and comprises almost the entire periosteum of a mature bone. In the event of injury to a mature bone, some of the resting cells of the inner periosteal layer become osteogenic.

Over most of the diaphysis, the periosteum is tenuous and loosely attached, and the blood vessels therein are capillary vessels. At the expanded ends of long bones, however, ligaments are attached firmly and can convey blood vessels of larger size. The same is true at the ridges along the diaphyses, where heavy fascial septa are attached.

Thus when we speak about the mechanical properties of bone, we must specify which part of the bone we are talking about. The figures quoted in Table 12.1:1 refer to the cortical region of the diaphysis, measured from specimens machined from the compactum, with a cross-sectional area of at least several mm^2 . Thus they represent the average mechanical properties of that part of the bone.

When examined microscopically, the bone material is seen to be a composite. Figure 12.1:3 shows Ham's (1969) sketch of the basic structure of compact bone. The basic unit is the Haversian system or osteon. In the center of an osteon is an artery or vein. These blood vessels are connected by transverse channels called Volkmann's canals. The rectangular pattern shown in Fig. 12.1:3 is an idealization; in actual bone they are more or less oblique.

About two-thirds of the weight of bone, or half of its volume, is inorganic material with a composition that corresponds fairly closely to the formula of hydroxyapatite, $3\text{Ca}_3(\text{PO}_4)_2 \cdot \text{Ca}(\text{OH})_2$, with small quantities of other ions. It is present as tiny crystals, often about 200 Å long, and with an average cross-section of 2500 Å² (about 50 × 50 Å) (Bourne, 1972). The rest of the bone is organic material, mainly collagen. The hydroxyapatite crystals are arranged along the length of the collagen fibrils.

Groups of collagen fibrils run parallel to each other to form fibers in the usual way. The arrangements of fibers differ in different types of bone. In woven-fibered bone the fibers are tangled. In other types of bone the fibers are laid down neatly in lamellae. The fibers in any one lamella are parallel to each other, but the fibers in successive lamellae are about at right angles to each other. As is seen in Fig. 12.1:3, the lamallae in osteones are arranged in concentric (nearly circular) cylindrical layers, whereas those near the surface of the bone are parallel to the surface (e.g., the outer circumferential lamellae).

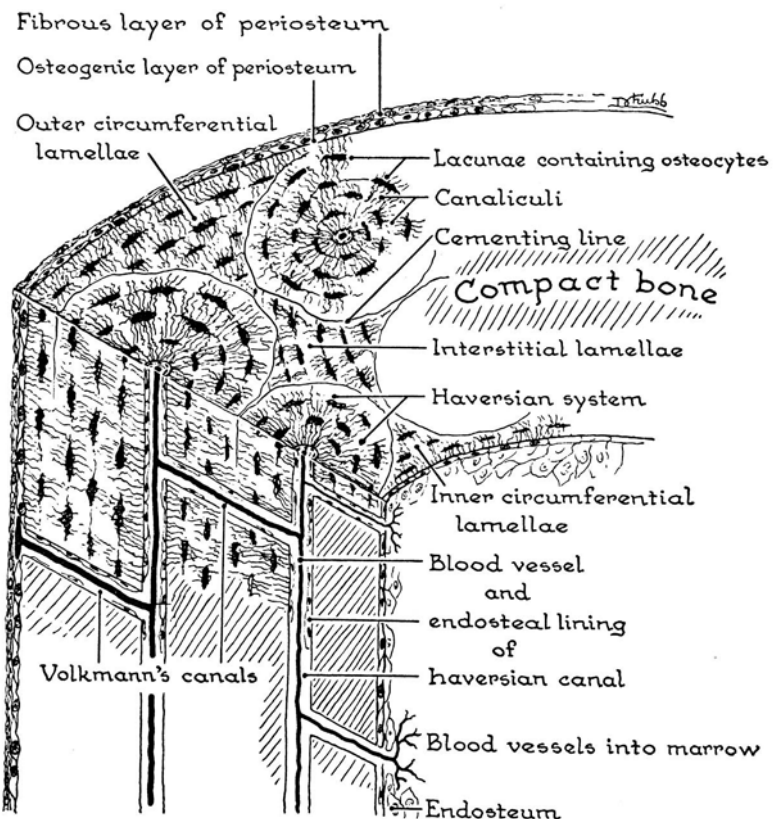


Figure 12.1:3 The basic structure of compact bone. From Ham (1969). Reproduced by permission.

Bone as a Composite Material

Thus bone material is a composite of collagen and hydroxyapatite. Apatite crystals are very stiff and strong. The Young's modulus of fluorapatite along the axis is about 165 GPa (24×10^6 lb in. $^{-2}$). This may be compared with the Young's modulus of steel, 200 GPa, aluminum, 6061 alloy, 70 GPa. Collagen does not obey Hooke's law exactly, but its tangent modulus is about 1.24 GPa (180 000 lb in. $^{-2}$). The Young's modulus of bone (18 GPa in tension in human femur) is intermediate between that of apatite and collagen. But as a good composite material, the bone's strength is higher than that of either apatite or collagen, because the softer component prevents the stiff one from brittle cracking, while the stiff component prevents the soft one from yielding.

The mechanical properties of a composite material (Young's modulus, shear modulus, viscoelastic properties, and especially the ultimate stress and strain at failure) depend not only on the composition, but also on the struc-

ture of the bone (geometric shape of the components, bond between fibers and matrix, and bonds at points of contact of the fibers). To explain its mechanical properties, a detailed mathematical model of bone would be very interesting and useful for practical purposes (see Problems 12.1–12.3). That such a model cannot be very simple can be seen from the fact that the strength of bone does correlate with the mass density of the bone; but not very strongly. Amtmann (1968, 1971), using Schmitt's (1968) extensive data on the distribution of strength of bone in the human femur, and Amtmann and Schmitt's (1968) data on the distribution of mass density in the same bone (determined by radiography), found that the correlation coefficient of strength and density is only 0.40–0.42. Thus one would have to consider the structural factors to obtain a full understanding of the strength of bone. Incidentally, Amtmann and Schmitt's data show that both density and strength are nonuniformly distributed in the human femur: the average density varies from 2.20 to 2.94 from the lightest to the heaviest spot, while the strength varies over a factor of 1.35 from the weakest place to the strongest place.

Problems

- 12.1 Assume that in a lamellar bone the collagen fibrils and apatite crystals are perfectly bonded parallel to each other. Derive the Young's modulus of the composite lamellae in uniaxial tension or compression in a direction parallel to the fibrils. Derive also the Young's modulus in the direction perpendicular to the fibrils, as well as the shear modulus parallel and perpendicular to the fibrils. Express the results in terms of the elastic moduli of the individual components and the ratio of the volumes of the collagen and apatite (see Currey, 1964).
- 12.2 Relax the perfect bond hypothesis of the previous problem. Introduce some model of bonding between the collagen and apatite to explore the effect of bonding on the mechanical properties of the composite material.
- 12.3 Use the results of Problems 12.1 and 12.2 to establish a model of an osteon. Then build up a model of a bone by a proper organization of the osteons. What additional experiments should be done to verify whether the model is satisfactory or not? A successful model will then be able to correlate the mechanical properties of the bone with the mass density and structure and composition of the bone, and will be useful in applications to surgery, medicine, nutrition, sports, etc. For some early attempts, which are not quite successful, see Currey (1964), Young (1957), and Knese (1958).

12.2 Bone as a Living Organ

The most remarkable fact about living bone is that it is living, and this is made most evident by the blood circulation. Blood transports materials to and from bone, and bone can change, grow, or be removed by resorption; and these processes are stress dependent.

That mechanical stresses modulate the change, growth, and resorption of bone has been known for a long time. An understressed bone can become weaker. An overstressed bone can also become weakened. There is a proper range of stresses that is optimal for the bone. Evidence for these biological effects of stresses are prevalent in orthopedic surgery and rehabilitation. Local stress concentration imposed by improper tightening of screws, nuts, and bolts in bone surgery, for example, may cause resorption, and result in loosening of these fasteners in the course of time.

Many authors, looking toward nature, feel that the evolution process has resulted in an optimum design of bone: optimum in the sense familiar to engineers designing light weight structures such as airplanes and space craft. This includes (a) the general shaping of the structure to minimize stresses while transmitting prescribed forces acting at specified points, (b) distribution of material to achieve a minimum weight (or volume, or some other pertinent criteria). Some well-known theories of optimum design include (a) the theory of uniform strength, that every part of the material be subjected to the same maximum stress (maximum normal stress if the material is brittle, maximum shear stress if the material is ductile) under a specific set of loading conditions, and (b) the theory of trajectorial architecture, which would put material only in the paths of transmission of forces, and leave voids elsewhere.

The idea of optimum design may be illustrated by a few examples. Let us consider the design of a thin-walled submarine container to enclose a volume V and to resist an external pressure p while maintaining the internal pressure at atmospheric. Any one of the shells sketched in Fig. 12.2:1(a) can be designed to meet this objective. If the same material is used for the construction of these shells, the spherical shell will be the lightest and most economical in the use of the material. The cylindrical shell will be at least twice as heavy. The egg shaped shell lies in between, while the biconcave shell will be the heaviest. Hence if the weight of the structure is the criterion, then the spherical shell is the optimal.

Next consider the design of a beam to support a load P over a span L ; Fig. 12.2:1(b). To design such a beam, we first compute the bending moment in the beam. Let the moment at station x be $M(x)$. Then the maximum bending stress at any station x can be computed from the formula $\sigma = Mc/I$, where c is the distance between the neutral axis and the outer fiber of the beam, and I is the area moment of inertia of the cross-section. For a specific material of construction, σ must be smaller than the permissible design stress (yield stress or ultimate failure stress). If the beam cross-section is uniform, the critical condition is reached only at one point: under the load P . Greater economy of material can be obtained by designing a beam of variable cross-section, with I/c varying with x in the same manner as $M(x)$. Then the stress will reach the critical condition in every cross-section simultaneously. The latter design is optimal in the sense of economy of material. Next, we can compare different shapes of beam cross-section. We

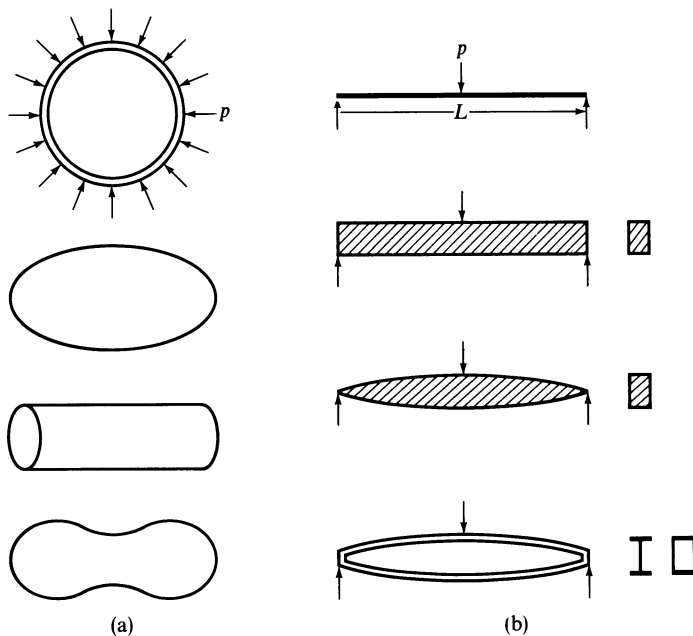


Figure 12.2:1 Examples of optimal design. (a) Shells resisting an external pressure. (b) Equally strong beams supporting a load P over a span L .

see that for the same value of I/c , it is most economical to concentrate the material at the outer flanges, as sketched in Fig. 12.2:1(b). In this sense, then, the last entry is the minimum weight design.

The design illustrated in the last drawing of part (b) of Fig. 12.2:1 is an example of “load trajectory” design. As illustrated in this figure, the upper flange is subjected to compression while the lower flange is subjected to tension. The compressive and tensile forces are transmitted along these “trajectories” (flanges). The significance of this remark will become evident when we consider bone structure below.

Note that it is imperative to state clearly the conditions under which an optimal design is sought. An optimal design for one set of design conditions may not be optimal under another set of design conditions.

For bone, Roux (1895, p. 157) formulated the *principle of functional adaptation*, which means the “adaptation of an organ to its function by practicing the latter,” and the *principle of maximum-minimum design*, which means that a maximum strength is to be achieved with a minimum of constructional material. He assumes that through the mechanism of hypertrophy and atrophy, bone has functionally adapted to the living conditions of animals and has achieved the maximum-minimum design. Considerable studies have been done since Roux’s formulation to show that this is true

(see, for example, Pauwels, 1965, Kummer, 1972). This has resulted in many beautiful illustrations that tell us how wonderful our bones are.

Let us quote one example. Roux (1895) suggests that spongy bone represents a trajectorial structure. Pauwels (1948) demonstrated that the architecture of substantia spongiosa is indeed trajectorial. Kummer's (1972) theoretical construction of a three-dimensional trajectorial system in a femur model is shown in Fig. 12.2:2, and it resembles the real bone structure quite closely.

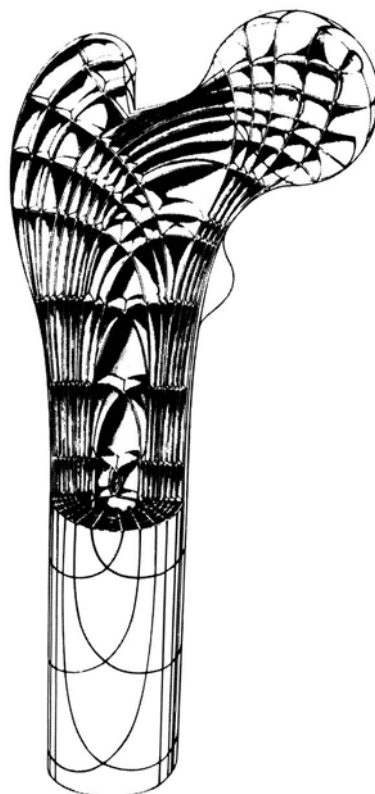


Figure 12.2:2 Theoretical construction of the three-dimensional trajectorial system in a femur model. From Kummer (1972), by permission.

12.3 Functional Adaptation of Bone

The most frequently used method to verify whether hypertrophy or atrophy has occurred in a bone due to its use or disuse is by means of x-ray, which measures the opacity of bone, which in turn is proportional to the mineral content of the bone. Another way is to measure wave transmission velocity

and vibration modes of the bone. Results obtained by these methods have generally supported the idea of functional adaptation.

Changes in bone may take place slowly (in months or years) due to the action of bone cells (osteoclasts for resorption; osteoblasts for apposition), or rapidly (in days) due to the uptake or output of mineral salts. These processes are illustrated in a sketch made by Kummer (1972); see Fig. 12.3:1.

Julius Wolff (1884) first advanced the idea that living bones change according to the stress and strain acting in them. Change in the external shape of bone is called *external or surface remodeling*. Changes in porosity, mineral content, x-ray opacity, and mass density of bone are called *internal remodeling*. Both types occur during normal growth. But they occur also in mature bone.

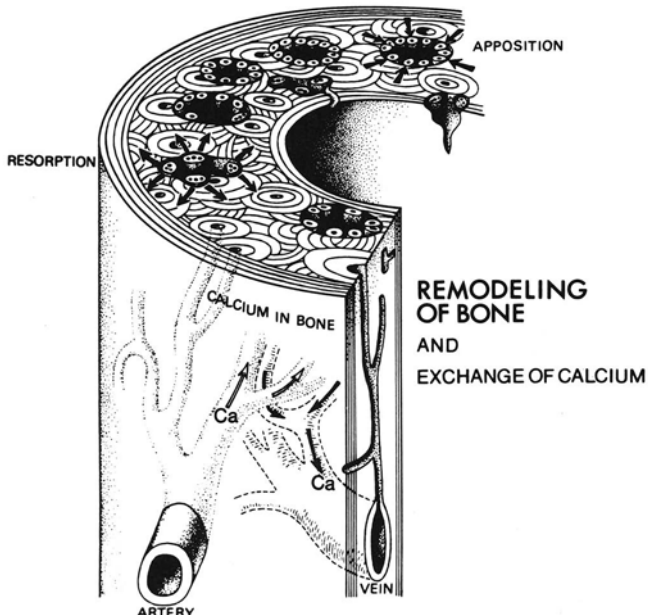


Figure 12.3:1 Conceptual drawing of the remodeling of bone by apposition, resorption, and calcium exchange. From Kummer (1972), by permission.

After Wolff, the phenomenon of stress-controlled bone development was described by Glücksmann (1938, 1939, 1942) and Frost (1964). Evans (1957) reviewed the literature and concluded that clinical and experimental evidence indicated that compressive stress stimulates the formation of new bone and is an important factor in fracture healing. Dietrick et al. (1948) conducted an experiment on remodeling in humans by immobilizing some volunteers from the waist down in plaster casts for periods of from 6 to 8 weeks. During this study their urine, feces, and blood were analyzed for organics such as creatine and inorganics such as calcium and phosphorous. Four days after the plaster

casts were removed the subjects resumed normal activity. The chemical analysis indicated that during the immobilization, their bodies suffered a net loss of bone calcium and phosphorous. After normal activity had been resumed, the mineral loss phenomenon was reversed and the body regained calcium and phosphorous. It took approximately 6 weeks to recover from the effects of this immobilization.

A similar net loss of calcium was reported by Mack et al. (1967) for astronauts subjected to weightlessness for periods of 4 days or more. Mack correlated this calcium loss with a decrease in the x-ray opacity of the bones. This loss of calcium can be minimized by asking the astronauts to perform some exercises that put stresses into the bones similar to those that occur in normal activity on earth.

Kazarian and von Gierke (1969) reported on immobilization studies with rhesus monkeys. Wonder et al. (1960) studied the mouse and the chicken in hypergravity. Hert et al. (1971) studied intermittent loading on rabbits. The results are the same: subnormal stresses cause loss of bone strength, radiographic opacity, and size. Hert et al. concluded further that intermittent stress is a morphogenetic stimulus to functional adaptation of bone, and that the effect of compressive stress is the same as that of tensile stress.

On the other hand, Pauwels (1948) and Amtmann (1968) observed the bone structure of humans and showed that the distribution of material and strength is related to the severity of stresses expected in normal activity.

The principle of remodeling is, of course, very important for orthopedic surgery, and many experiments have been done. Woo et al. (1976) and Torino et al. (1976) showed that remodeling due to rigid plate fixation in dogs occurs by thinning of the femoral diaphysis cortex rather than by induced osteoporosis in the cortex. In other words, it is primarily surface remodeling.

How can we put these concepts into a mathematical form so that bone modeling can be studied and predicted? Such a mathematical framework is needed because the stresses in bones in an animal in its normal activity and under experimental conditions are nonuniform in space, vary from one location to another, and are nonstationary in time, varying from one instant to next. To evaluate any experimental result we need a quantitative approach that cannot be done without mathematics.

Several proposed theories are yet to be validated against experiment. Cowin and Hegedus (1976) expressed the ideas as follows. Bone is considered to be constituted of three basic materials: the bone cells, the extracellular fluid, and the solid extracellular material called bone matrix. The bone matrix is porous. The extracellular fluid is in contact with blood plasma, which supplies the material necessary for the synthesis of bone matrix. Let ξ be the matrix volume fraction and γ be the local mass density of the bone matrix. Let ε_{ij} be the strain tensor. Then at a constant temperature, one assumes the existence of constitutive equations of the form

$$\dot{\xi} = \frac{1}{\gamma} c(\xi, \varepsilon_{ij}) \quad (1)$$

and

$$\dot{\sigma}_{ij} = \xi C_{ijkl}(\xi) \dot{\epsilon}_{kl}, \quad (2)$$

where the superposed dot indicates the material time rate, $\dot{\sigma}_{ij}$ is the stress tensor, $c(\xi, \epsilon_{ij})$ represents the rate at which bone matrix is generated by chemical reaction, and $\xi C_{ijkl}(\xi)$ is a tensor of rank four representing the elastic constants of the bone matrix. The elastic constants are assumed to depend on the volume fraction of the bone matrix. These equations may represent internal remodeling of the bone when the functions $c(\xi, \epsilon_{ij})$ and $C_{ijkl}(\xi)$ are determined.

For external remodeling, one needs to describe the rate at which bone material is added or taken away from the bone surface. Cowin and Hegedus (1976) suggested the following form. Let x_1, x_2, x_3 be a set of local coordinate axes with an origin located on the bone surface, with x_3 normal to the surface of the bone and x_1, x_2 tangent to it. Let the strains in the x_1x_2 plane be $\epsilon_{11}, \epsilon_{22}, \epsilon_{12}$. If external modeling is linearly proportional to the strain variation, then one might express the rate of increase of the surface in the x_3 direction in the form

$$U = k_{11}(\epsilon_{11} - \epsilon_{11}^0) + k_{22}(\epsilon_{22} - \epsilon_{22}^0) + k_{12}(\epsilon_{12} - \epsilon_{12}^0), \quad (3)$$

where k_{11}, k_{22}, k_{12} and $\epsilon_{11}^0, \epsilon_{22}^0, \epsilon_{12}^0$ are constants. If the right-hand side is positive, the surface grows by deposition of material. If the right-hand side is negative, the surface resorbs. But this equation is untenable, because it does not incorporate the idea that tensile stress and compressive stress have the same effect with regard to bone remodeling (Hert et al., 1971). Nor does it include remodeling due to surface traction (normal and shear stress acting on the surface) as is often found under orthopedic prosthesis (Woo et al., 1976). To include these effects we may assume

$$U = k_{ij}[\epsilon_{ij}^2 - (\epsilon_{ij}^0)^2], \quad (4)$$

where the indexes range over 1, 2, 3. The summation convention is used.

Although the validity of these equations remains to be shown and the material constants are yet to be determined, the simplicity of the concept is exhibited. With these constitutive equations, the stress and strain distribution in a bone can be determined by the methods of continuum mechanics. Then the remodeling can be predicted.

The Mechanism for the Control of Remodeling

Piezoelectricity has been proposed as a mechanism for bone to sense stress and cause remodeling. Fukada (1957, 1968) discovered piezoelectricity in bone and later identified it as due to collagen. Becker and Murray (1970) reported that an electric field is capable of activating the protein-synthesizing organelles in osteogenic cells of frogs. It is also known that the presence of an electric field near polymerizing tropocollagen will cause the fibers to orient

themselves perpendicular to the line of force. Bassett and Pawlick (1964) reported that if a metal plate is implanted adjacent to a living bone, a negative charge on the plate will induce the deposition of new bone material on the electrode. Thus it is possible that piezoelectricity lies behind the remodeling activities.

Biochemical activity of calcium is another possible mechanism. Justus and Luft (1970) have shown that straining the bone increases calcium concentration in the interstitial fluid. They showed that this is due to a change in the solubility of the hydroxyapatite crystals in response to stresses.

Problems

- 12.4** Consider a long bone of hollow circular cylindrical cross-section with inner radius R_i and outer radius R_o . Let the bone be subjected to an axial compressive load P . Assume that Eq. (3) applies. Show that the inner and outer radii will change according to

$$R_o(t) = R_o(0) + k_o a (1 - e^{-bt}),$$

$$R_i(t) = R_i(0) + k_i a (1 - e^{-bt}),$$

where a and b are constants

$$b = \frac{2P}{\pi E} \left\{ \frac{k_o R_o(0) + k_i R_i(0)}{[R_o^2(0) - R_i^2(0)]^2} \right\},$$

$$a = \frac{R_o^2(0) - R_i^2(0)}{2[k_o R_o(0) - k_i R_i(0)]} \left\{ 1 - \frac{\varepsilon_1^0 \pi E}{P} [R_o^2(0) - R_i^2(0)] \right\}.$$

The constants k_i and k_o are the values of k_{11} on the inner and outer radii, respec-

$$R_o(\infty) = R_o(0) + k_o a, \quad R_i(\infty) = R_i(0) - k_i a.$$

- 12.5** Discuss the preceding problem if the constitutive Eq. (4) applies.

- 12.6** A steel plate is attached to a bone by means of screws, thus inducing a compressive stress between the plate and the bone. Discuss the remodeling of the bone under the plate if (a) the screws are tightened uniformly so that compressive stress under the plate is uniform, or (b) one screw is given an extra turn or two so that a nonuniform compressive stress results.

- 12.7** Consider the interaction of the screw threads with the bone in the situations named in Problem 12.6. Discussion the remodeling of the bone around the screws.

- 12.8** A long bone is subject to a bending moment M . Discuss the remodeling of the bone under bending in the context of Eqs. (1), (2) and (4).

This discussion would be woefully amiss if we did not recall also that growth in general is modulated by endocrine. The endocrine STH (somato-

tropic or growth hormone) affects all growing tissues; it increases all cell division and all subsidiary processes, such as total protein synthesis, net protein synthesis, total turnover (likewise for lipid and carbohydrate metabolism), and tissue growth. The endocrine ACH (adrenal-cortical hormone) has the opposite effect; it affects all tissues and it decreases all cell division and subsidiary processes. The endocrine T₄ (thyroxine) also affects all tissues; it probably increases turnover, but information is very incomplete. Estrogens, on the other hand, selectively decrease cell division and subsidiary processes; they affect cartilage and lamellar bone. Furthermore, the normality of bone is significantly influenced by vitamins A, C, and D, and the calcium "tone" is modulated by calcitonin. Thus, bone is a complex biochemical entity. We have discussed only its mechanical aspects. The importance of the mechanical aspects is obvious: not only to intellectual speculation, but also to clinical applications in orthopedics. If we know these aspects well, then we can control bone remodeling through mechanical stresses that can be applied through exercises, either voluntarily or with the help of mechanical devices. Exercise is man's most basic approach to health.

12.4 Blood Circulation in Bone

The discussions of the preceding sections suggest the importance of blood circulation on the stress-dependent changes that take place in bone. Let us review the vascular system in bone in this section. Because of its hardness and opaqueness, it is not easy to investigate blood flow in bone. But by methods of injection (with ink, polymer, dye, radio-opaque or radioactive material), thin sectioning, calcium dissolution, microradiography, and electron microscopy, much has been learned about the vasculature in bone. A rich collection of interesting photographs can be found in Brookes (1971) and Rhinelander (1972). Figure 12.4:1 shows the vascular patterns in bone cortex sketched by Brookes (1971). Starting from the bottom of the figure, it is seen that the principal artery enters the bone through a distinct foramen. Within the medulla the artery branches into ascending and descending medullary arteries. These subdivide into arterioles that penetrate the endosteal surface to supply the diaphyseal cortex.

At the top of Fig. 12.4:1 can be seen the articular cartilage. Beneath it are the epiphyseal arteries. Then there is the growth cartilage, below which are three types of bone: the endochondral bone, the endosteal bone, and the periosteal bone. The orientations of vessels in these three types of bone are different (according to Brookes, 1971). In the endochondral bone the vessels point upward and outward; at mid-diaphyseal levels the vessels are transverse, while inferiorly they point downward and outward; that is, the cortical vessels have a radiate, fan-shaped disposition when viewed as a whole. This vascular pattern is evident in bone formed by periosteal apposition. The center of radiation of the vessels in periosteal bone corresponds with the site

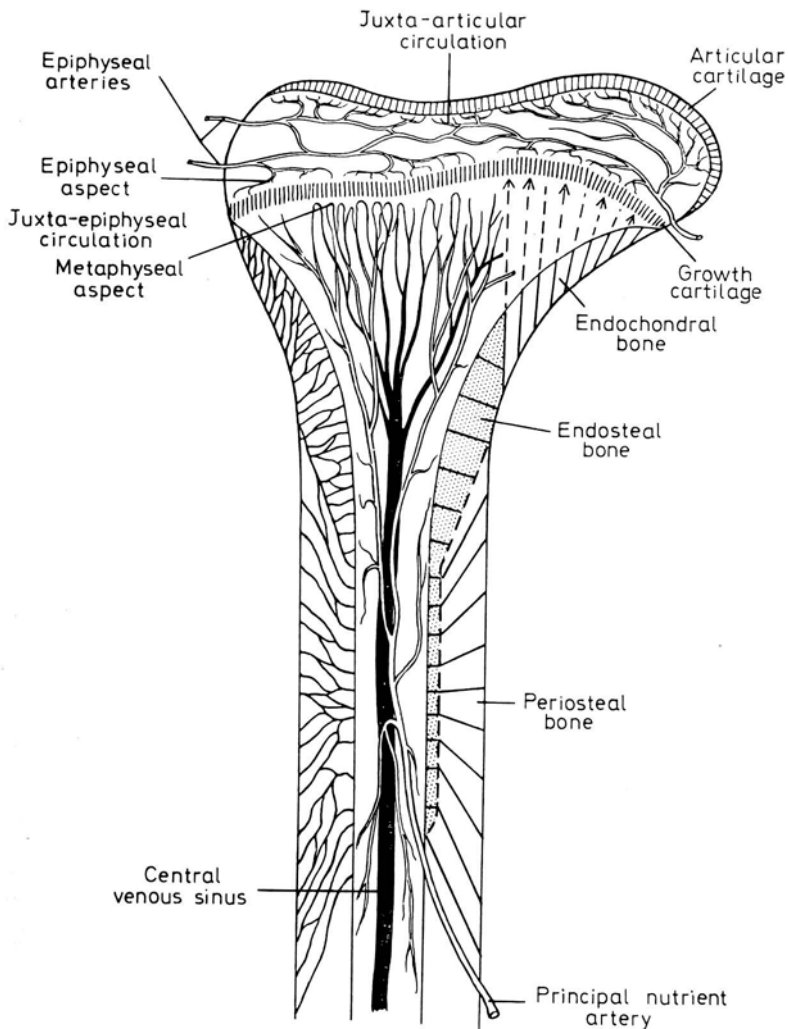


Figure 12.4:1 The three vascular patterns in bone cortex, corresponding to the three types of bone present. The left side shows vessels. The right side sketch shows an idealized pattern. From Brookes (1971), by permission.

of primary ossification of the shaft. The center of radiation of the vessels in endosteal bone lies outside of the shaft. It is emphasized that communicating canals are frequent, but these are by no means wholly transverse, nor so numerous as to obliterate the three primary patterns observed in the cortex of long bones.

A fuller view of the blood supply to a long bone is shown in Fig. 12.4:2. The top half is similar to Fig. 12.4:1, except that the venous sinusoids are

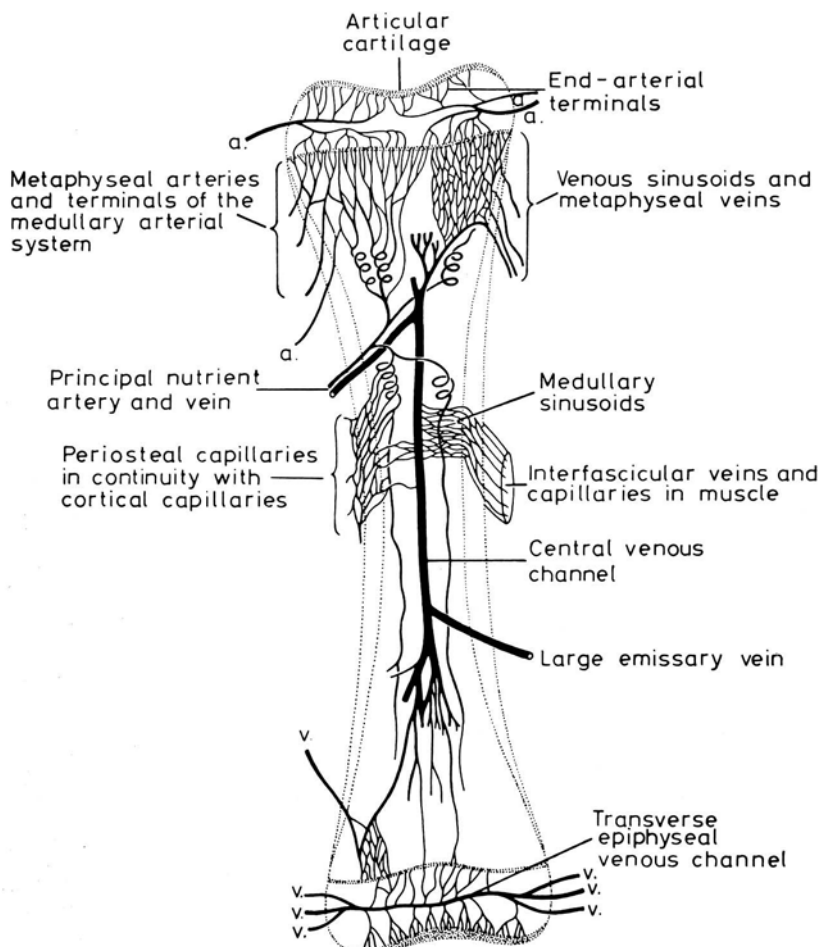


Figure 12.4:2 Vascular organization of a long bone in longitudinal section. From Brookes (1971), by permission.

added. The principal nutrient vein and its branches are shown more fully in Fig. 12.4:2. The numerous metaphyseal arteries are shown here to arise from periarticular plexuses, and to anastomose with terminal branches of the ascending and descending medullary arteries. In the middle part of the figure are shown the periosteal capillaries, which are present on all smooth diaphyseal surfaces where muscles are not firmly attached.

Anatomical variations are great between mammalian species, and between long bones in the same species. These sketches illustrate only the general concepts. The vascular patterns shown in Figs. 12.4:1 and 12.4:2 do not conform to the sketch shown in Fig. 12.1:3, which is a stylized traditional

view that has to be modified in its details as far as blood vessel pattern is concerned.

Hemodynamics of bone is difficult to study because of the smallness of the blood vessels and their inaccessibility for direct observation. Measurements have been made on the temperature distribution and temperature changes in bone; and indirect estimates of blood flow rate have been made under the assumption that heat transfer is proportional to blood flow. Perfusion with radioactive material and measurement of retained radioactivity in bone is another indirect approach. Some data are given in Brookes (1971). Direct measurements of flow and pressure are obviously needed.

12.5 Cartilage

Cartilage and bone are specialized connective tissues and consist of the same three tissue elements: cells embedded in an intercellular matrix, permeated by a system of fibers. In man during early fetal life, the greater part of the skeleton is cartilaginous, but eventually much of this is replaced by bone. In adult life, cartilage persists on the articulating surfaces of synovial joints, in the walls of the thorax, larynx, trachea, bronchi, nose, and ears, and as isolated small masses in the skull base.

The matrix in which the cartilage cells (chondrocytes) are embedded varies in appearance and in the nature of its contained fibers. Accordingly, cartilage is often classified into *hyaline cartilage* (from *hyalos*, meaning glass), *white fibrocartilage* (containing much collagen), and *yellow elastic fibrocartilage* (containing a rich elastin network). A densely *cellular cartilage*, with only fine partitions of matrix separating the cells, is normal in the fetus.

Costal, nasal, tracheo-bronchial and all temporary cartilages, as well as most articular cartilages, are of the hyaline variety. It has long been known that if the surface of articular cartilage is pierced by a round-bodied pin, after withdrawal of the pin, a longitudinal "split-line" remains, and that on any particular joint surface, the patterned arrangement of the split-lines is constant and distinctive. These split-lines follow the predominant direction of the collagen bundles in the tangential zone of the cartilage. The proportion of collagen in the matrix increases with age.

White fibrocartilage is found in intervertebral discs, articular discs, and the lining of bony grooves that lodge tendons. Yellow elastic fibrocartilage is found in the external ears, larynx, epiglottis, and the apices of the arytenoids.

The location of these cartilages suggests their function. The intervertebral disc bears the load imposed by the spine; it is elastic and makes the spine flexible. The cartilage at the ends of the ribs gives the ribs the desired mobility. The articular cartilage at the ends of long bones provides lubrication for the surfaces of the joints, and serves as a shock absorber to impact loads and as a load bearing surface in normal function. Sometimes it is its elasticity and rigidity that seems to be needed. In the bronchioles of man there is very

little cartilage; but in diving animals such as the seal there is a considerable amount of cartilage in the bronchioles: its function seems to be to keep the bronchioles from collapsing too soon when the animals dive deeply into the water. It is proposed that this is the mechanism with which these animals avoid nitrogen sickness. If a man dives too deeply into the water, the lung collapses in such a way that the bronchioles collapse before the alveoli do, so that gas is trapped in them, which has to be absorbed into the bloodstream. For a seal the alveoli can empty first, and nitrogen trapping is avoided.

A modern view of cartilage is that it is a complex tissue with a definite ultrastructural fibrous arrangement, biologically active, and rheologically complex. In the following discussion, we shall consider the viscoelasticity of articular cartilage, and its frictional behavior.

12.6 Viscoelastic Properties of Articular Cartilage

Cartilage is a viscoelastic material. It is rather porous, and the interstitium is filled with fluid. Under stress, fluid can move in and out of the tissue, (it flows in when the tissue is dilated, and out when it is compressed), and the mechanical properties of cartilage change with the fluid content. In fact, the movement of fluid under stress seems to be the principal way this avascular tissue gets its nutrients. Hence the stress-strain-history relationship is important not only to the understanding of the load-carrying qualities of cartilage, but also to the well-being of the tissue.

A simple method of demonstrating the viscoelasticity of cartilage is the indentation test, which can be done *in situ* to mimic physiological conditions. Time-dependent creep deformation can be seen. Upon unloading, an instantaneous recovery is followed by a time-dependent one. The recovery will not be complete if the test is done with the tissue exposed to air; but if the specimen is completely immersed in a solution bath, complete recovery can be achieved by fluid resorption during unloading.

A rigorous theoretical analysis of the indentation test is very difficult for cartilage, which obeys a nonlinear viscoelastic law and is subject to finite deformation. For ease of analysis and interpretation, it is better to do uniaxial loading or strip biaxial tests on flat plate-like specimens. (However, the preparation of test specimens is then quite difficult.) In the following we shall quote a report by Woo et al. (1979), which also contains references to vibration tests and theoretical analyses by other authors.

Articular cartilage specimens were taken from the humeral heads of bovine animals. This joint surface is large (about 9–10 cm in diameter) and is relatively flat, so that cartilage-bone plugs, 1.25 cm in diameter, can be cored. A die cutter with sharp razor blades formed into a standardized dumbbell shape was used to stamp each plug perpendicularly through the articular cartilage surface to the subchondral bone along the split line, or the zero-degree (0°) direction. The cartilage-bone plug was then placed on a

sledge microtome to obtain slices 250–325 μm thick. The specimen's test section has dimensions $1 \times 4.25 \times 0.25 - 0.325 \text{ mm}$.

An Instron testing machine coupled with a video dimensional analyzer (VDA) system was used for strain rate dependent and cyclic tests. A special solenoid device provided rapid stretch (up to 30 mm/s) for relaxation tests. This test equipment was not entirely satisfactory because it was found that stress relaxation in articular cartilage is very rapid. For example, comparing the load values recorded using a storage oscilloscope and that of a strip chart recorder, the differences in peak forces could be as much as 25%, although the time lag for the strip chart recorder was less than 250 ms. However, the mechanical vibration of the test system prevented the authors from using the oscilloscope data.

Test results are stated in terms of the stretch ratio, λ ,

$$\lambda = \frac{\text{deformed gage length}}{\text{initial gage length}},$$

the Green's strain, E ,

$$E = \frac{1}{2}(\lambda^2 - 1),$$

the Lagrangian stress, T ,

$$T = \frac{\text{force}}{\text{initial undeformed cross-sectional area}},$$

and the Kirchhoff stress, S ,

$$S = \frac{T}{\lambda}.$$

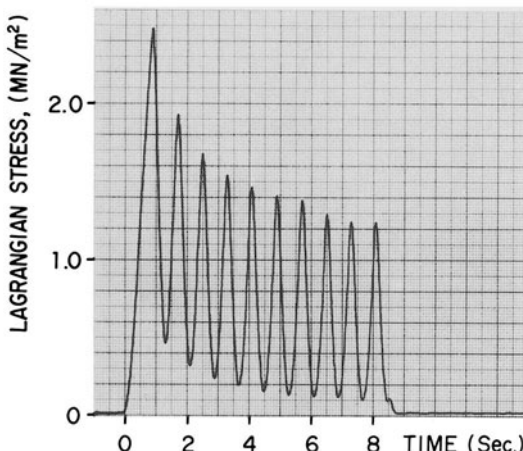


Figure 12.6:1 Stress response of bovine femoral articular cartilage subjected to cyclic stretching between $\lambda = 1.07-1.10$. Temp.: 37°C. Specimen immersed in saline. From Woo et al. (1979), by permission.

Tests specimens were immersed in normal saline solution at 37°C. Four specimens were subjected to cyclic tests at different strain rates varying from 0.04%/s to 4%/s, and it was found that the hysteresis loops and the peak stresses increased slightly with increased strain rates. Thus articular cartilage is moderately, though not highly, strain rate sensitive. Figure 12.6:1 shows the preconditioning behavior of cartilage when it is subjected to cyclic stretching between $\lambda = 1.07$ and 1.10. It is seen that after 10 cycles of stretching the stress-time curve tends asymptotically to a steady state cyclic response.

The results of uniaxial tensile stress relaxation studies are summarized in Fig. 12.6:2. The *experimental reduced relaxation function* is defined as $G(t) = T(t)/T(t \sim 250 \text{ ms})$. The true *reduced relaxation function* $T(t)/T(t = 0)$ cannot be obtained experimentally. At a small extension ($\lambda = 1.05$), the stress reached its relaxed state within 15 min. However, for higher extensions (λ between 1.16 and 1.29), the stress relaxation did not level after 100 min. These characteristics are similar to that which are shown in Fig. 7.5:4 in Chapter 7 for the mesentery. Different reduced relaxation functions are needed for the small stretch and moderate stretch regimes. However, as shown in Fig. 12.6:2, in each regime the reduced relaxation function depends on λ only to a small degree. By ignoring this dependence, Woo et al. (1979) used the quasi-linear model of viscoelasticity (Chapter 7, Sec. 7.6) to characterize the articular cartilage. In brief, this model assumes that the relaxation function, K , is dependent on both strain and time and can be written as

$$K(t) = G(t) * S^e[E(t)], \quad (1)$$

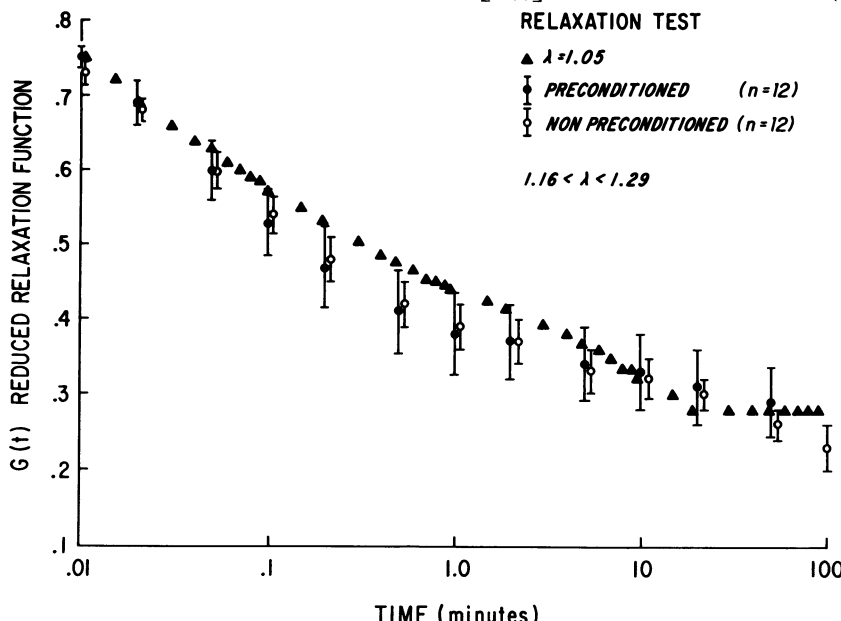


Figure 12.6:2 The reduced relaxation function of articular cartilage at a lower stretch ($\lambda = 1.05$) and at higher stretches, $\lambda = 1.16-1.29$. From Woo et al. (1979), by permission.

where S^e is the “elastic response” and $G(t)$ is the “reduced relaxation function” with $G(0) = 1$. The stress-strain-history integral takes the forms

$$\begin{aligned} S(t) &= \int_{-\infty}^t G(t - \tau) \dot{S}^e(\tau) d\tau \\ &= S^e[E(t)] - \int_0^t \frac{\partial G(t - \tau)}{\partial \tau} S^e(\tau) d\tau. \end{aligned} \quad (2)$$

Once the mechanical property functions in this model, $G(t)$ and $S^e[E(t)]$, are determined, the time dependent stress, $S(t)$, with known history of strain, $E(t)$, can be determined by Eq. (2).

Relaxation test data for a 0° mid-zone cartilage specimen are shown in Fig. 12.6:3, in which the experimental values for $G(t)$ were calculated using stress data normalized by an extrapolated value for the stress at $t = 0$. The form for $G(t)$ used in the model was taken to be Eq. (36) of Sec. 7.6:

$$G(t) = \left[1 + C \left\{ E_1 \left(\frac{t}{\tau_2} \right) - E_1 \left(\frac{t}{\tau_1} \right) \right\} \right] / \left[1 + C \log \left(\frac{\tau_2}{\tau_1} \right) \right], \quad (3)$$

where E_1 is the *exponential integral* function, and C , τ_1 , and τ_2 are material constants. C , τ_1 , and τ_2 were determined in the least square sense using a computer program based on the method of Powell (1965); the values found were $\tau_1 = 0.006$ s, $\tau_2 = 8.38$ s, and $C = 2.02$.

The cyclic stress data (Fig. 12.6:1) corresponding to a saw-tooth series of ramp extensions for the same specimen was used to determine the elastic

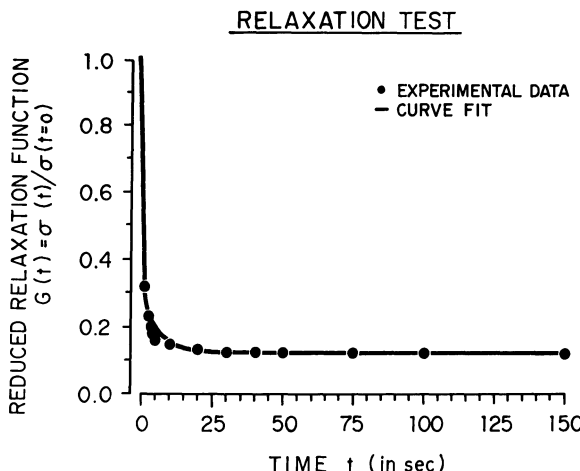


Figure 12.6:3 The experimental reduced relaxation function of articular cartilage compared with a theoretical expression given in Eq. (3) with the constants c , τ_1 , τ_2 determined empirically. From Woo et al. (1979), by permission.

response, $S^e\{E\}$. Here S^e was assumed to be a power series in E of the form

$$S^e = S^e\{E\} = \sum_{i=1}^n a_i E^i. \quad (4)$$

Substitution of Eq. (4) into Eq. (2) with $G(t)$ now known in the form of Eq. (3) yields a linear set of equations that can be solved for the constants, a_i . By numerical integration and least squares procedure, the constants found for $n = 2$ are $a_1 = 30 \text{ MN/m}^2$ and $a_2 = 56 \text{ MN/m}^2$. Figure 12.6:4 compares Kirchhoff stress-time curves measured experimentally and computed from the quasi-linear viscoelastic model. Similar agreement was obtained for a higher order of n .

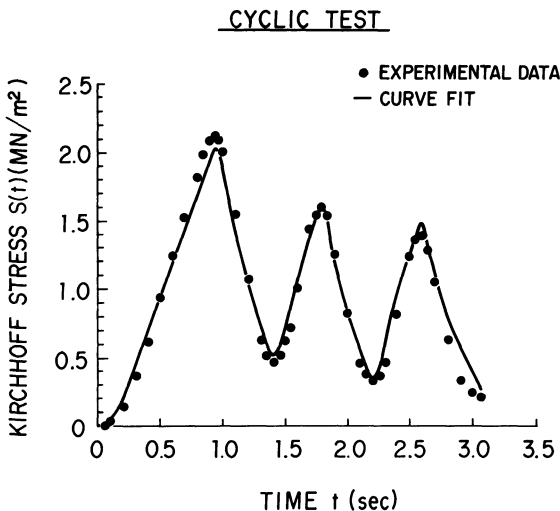


Figure 12.6:4 Comparison of experimental data on stress response to the first three cycles of loading and unloading as given in Fig. 12.6:1 with theoretical expressions given in Eqs. (1)–(4) with the constants $c, \tau_1, \tau_2, a_1, a_2$ determined empirically. From Woo et al. (1979), by permission.

The S^e so computed is considerably higher than the measured stress level at 250 ms when the specimen is subjected to a ramp stretching, indicating that a significant amount of stress relaxation has taken place in the first 250 ms. This method of determining the elastic response from cyclic stretching data is quite effective. The rapid relaxation of articular cartilage at very small time is believed to be caused by the fluid movement from the tissue when it is first subjected to stress.

A similar rapid stress relaxation was found by Mow et al. (1977), who tested articular cartilage plugs in compression. They attributed the rapid relaxation to the ease of extrusion of fluid in the tissue. Figure 12.6:5 shows the result of Mow et al. (1980) on the stress response to a ramp-step strain

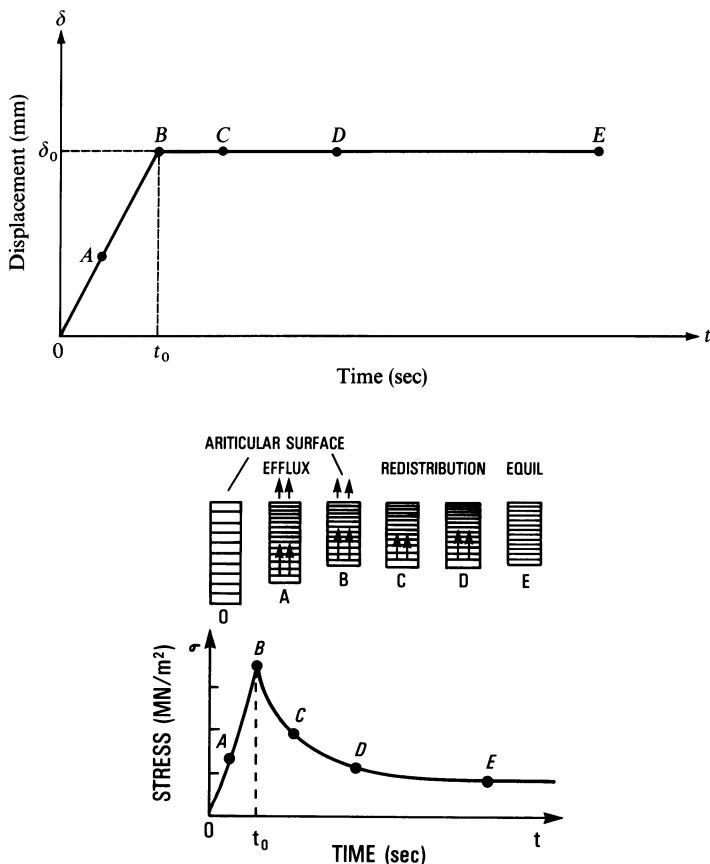


Figure 12.6:5 Top: Displacement, strain, and fluid movement in the cartilage in the free-draining confined-compression stress-relaxation experiment. O, A, B defines the compressive phase and B, C, D, E defines the stress relaxation phase. Bottom: The corresponding stress history. Middle diagrams: Horizontal lines depict the compressive strain field, and arrows indicate the fluid velocity. Stress relaxation times of the order of 1–5 s are usually observed. From Mow et al. (1980), by permission.

history in compression and their concept of dynamic strain distribution and fluid movement. A detailed theoretical analysis is given in their 1980 paper.

12.7 The Lubrication Quality of Articular Cartilage Surfaces

Articular cartilage, which is the bearing material lining the bone in synovial joints, exhibits unique and extraordinary lubricating properties. It possesses a “coefficient of friction” (the resistance to sliding between two surfaces divided by the normal force between the surfaces) that is many times less

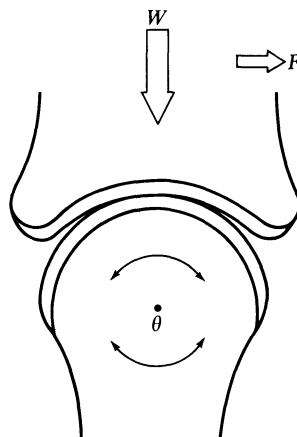


Figure 12.7:1 Schematic diagram of a joint friction experiment using an isolated animal synovial joint.

than man's best artificial material. It exhibits almost two orders of magnitude less friction than most oil lubricated metal on metal. Mature cartilage in man, with little or no regenerative ability, maintains a wear life of many decades.

Earlier experiments on the synovial joint tribology have usually taken either of two forms. One approach has sought to experimentally simulate intact synovial joint conditions *in vitro* by preserving the natural cartilage geometry, kinematics, and chemical environment. This approach is exemplified by Linn (1967) and is shown schematically in Fig. 12.7:1, where an excised intact joint, devoid of surrounding connective tissue, capsule or restraining ligaments, is tested *in vitro*. Figure 12.7:2 shows a diagrammatic sketch of another approach, in this case representative of the work of McCutchen (1959), where excised segments of articular cartilage are tested upon planar surfaces of another (man-made) material (usually glass). These experimental

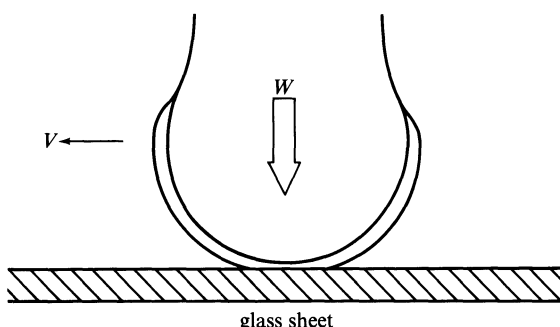


Figure 12.7:2 Concept of an experiment to measure the coefficient of friction between articular cartilage and glass.

approaches tend to complement one another, the intact joint tests being more physiologically representative of the *in vivo* situation, while the planar sliding studies are more tribologically definitive. They each have their limitations, however: the geometric and kinematic complexity of the intact tests inhibit parameter isolation, making analysis difficult, while the geometrically more tractable planar sliding studies lack the cartilage against cartilage interfacial contact condition.

Malcom (1976) presented an alternative approach that is much easier to analyze. Figure 12.7:3 shows a schematic diagram of the experimental specimen configuration used by Malcom. It consists essentially of an axisymmetric cylindrical cartilage annulus tested in contact with another conformationally matching layer of cartilage. The articular cartilage specimens are obtained from opposing, geometrically matched regions of bovine scapular and humeral joint surfaces. A specially designed electromechanical instrument generated specified mechanical and kinematic conditions by loading and rotating the cylindrical specimen and measuring the resultant cartilage frictional and deformational responses. Experimental monitoring and data recording were done on-line via a PDP 8/E computer. The specimen environment was regulated throughout the experiment by maintaining the car-

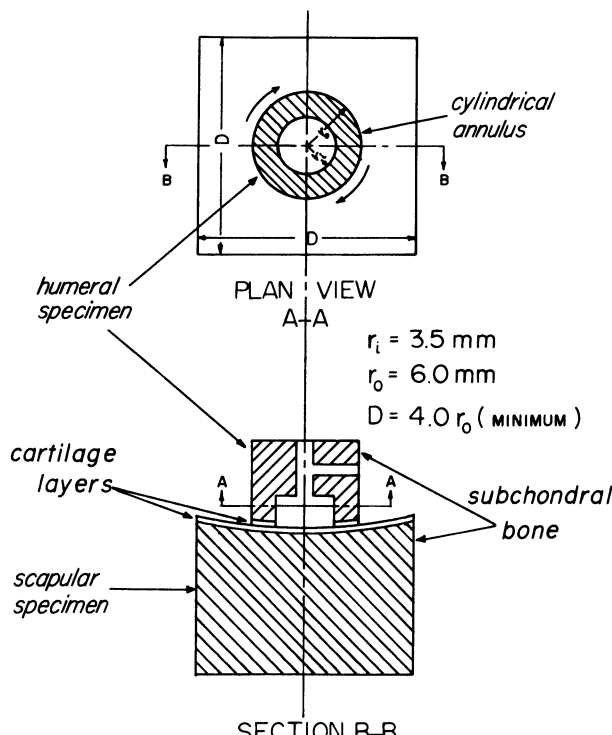


Figure 12.7:3 Sketch of the test specimen used by Malcom to measure the coefficient of friction between articular cartilage surfaces. From Malcom (1976), by permission.

tilage in a thermally controlled bath of whole bovine synovial fluid or buffered normal saline.

Figure 12.7:4 shows the experimentally obtained shear stress history on nine cartilage specimen pairs after they were suddenly loaded to a static normal stress of 204 kPa (2.04 kgf/cm^2) and were continuously rotated at 0.7 rad/s. The shear stress approached asymptotically a value lying in the range 1.5–2.8 kPa after 1000s of loading. Upon a sudden unloading to a normal stress of 53 kPa, the shear stress decreased and reached asymptotically a value in the range 0.4–0.8 kPa. The curves show the typical specimen response diversity when a group of different biological specimens are tested under identical conditions.

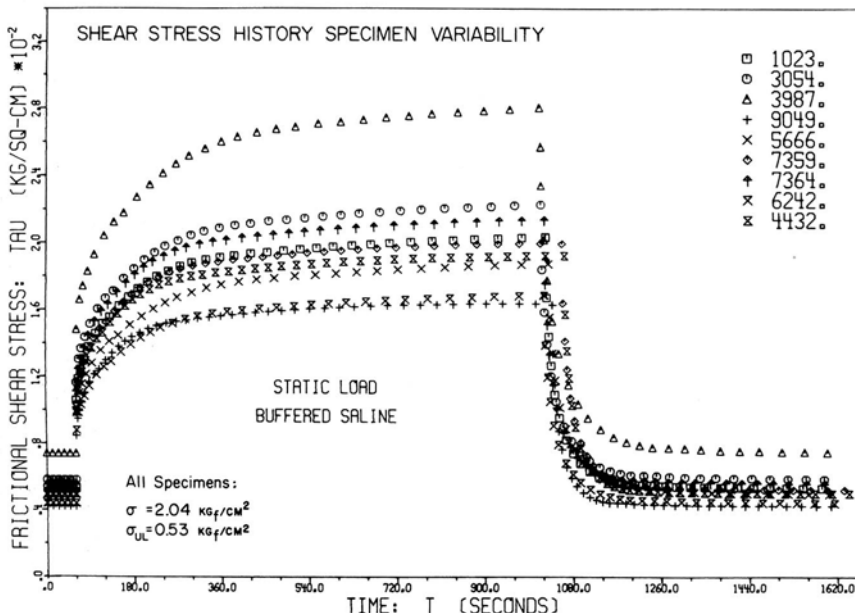


Figure 12.7:4 History of variation of the shear stress between two articular cartilage surfaces when they are subjected to a step loading and rotation, and at a later instant of time a step unloading to a lower level of normal stress and continued rotation. From Malcom (1976), by permission.

The gradual increase in friction after a step loading and rotation is accompanied by compression of the specimen and extrusion of interstitial fluid from the cartilage, as one could have predicted according to the results shown in Fig. 12.6:5 and discussed in the preceding section. Figure 12.7:5 shows the cartilage normal compression histories for the nine specimens, which were obtained simultaneously with the data in Fig. 12.7:4. The compressive strain is seen to be directly related to the increase in frictional shear between the cartilage surfaces.

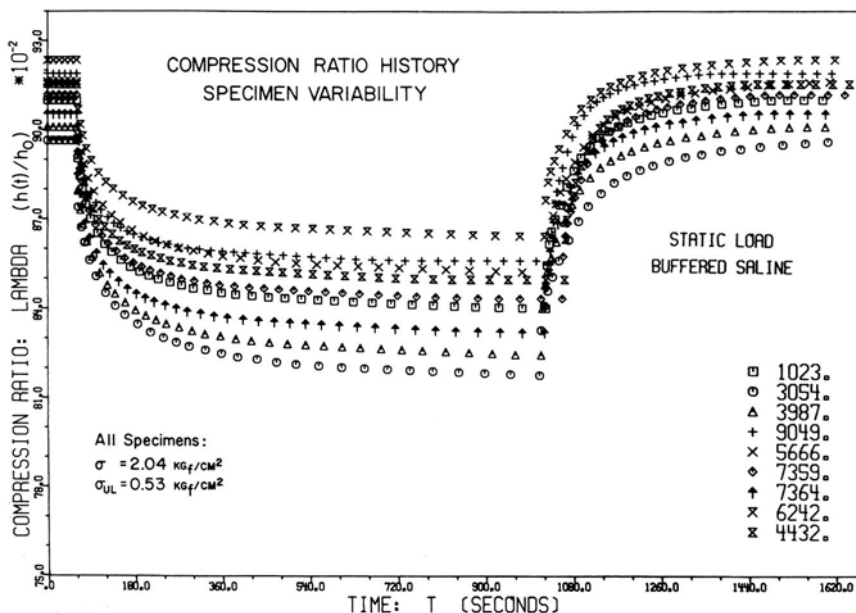


Figure 12.7:5 History of the change of thickness of articular cartilage specimens taken simultaneously with the shear stress record shown in Fig. 12.7:4. From Malcom (1976), by permission.

When tested in different rates of rotation, it was found that the asymptotic values of the shear stress (and therefore the coefficients of friction) are relatively insensitive to the sliding velocity within the range 1–400 mm/s. When the sliding velocity further decreases, the friction coefficient increases. At the static condition, a considerably larger coefficient of friction was measured. A summary of results for four of the loading conditions and lubricating bath combinations is shown in Fig. 12.7:6. The y axis represents the steady state friction coefficient, $\mu_\infty = \tau_\infty/\sigma$, where σ is the value of the static or dynamic (1 cycle/s square wave) normal stress, and τ_∞ is the asymptotic frictional shear stress. The actual curves shown are nonlinear regression line fits to the resultant experimental data (57 to 112 observations per curve). Note particularly the low magnitude of the friction coefficients that were obtained. For the least efficient lubrication mode of statically loaded cartilage in buffered isotonic saline lubricant, the mean friction coefficient ranged from 0.0065 to 0.030 at normal stresses of 70–370 kPa (0.70–3.7 kgf/cm²), respectively. The most efficient lubrication combination was cyclic dynamic loading in a whole bovine synovial fluid lubricating bath. Under these conditions, the data show a mean minimum friction coefficient of 0.0026 at a normal stress of 500 kPa and a maximum coefficient of 0.0038 at a maximum normal stress of 2 MPa. These values may be compared with other typical engineering values of μ of 0.5–2.0 or higher for clean metal surfaces, 0.3–0.5

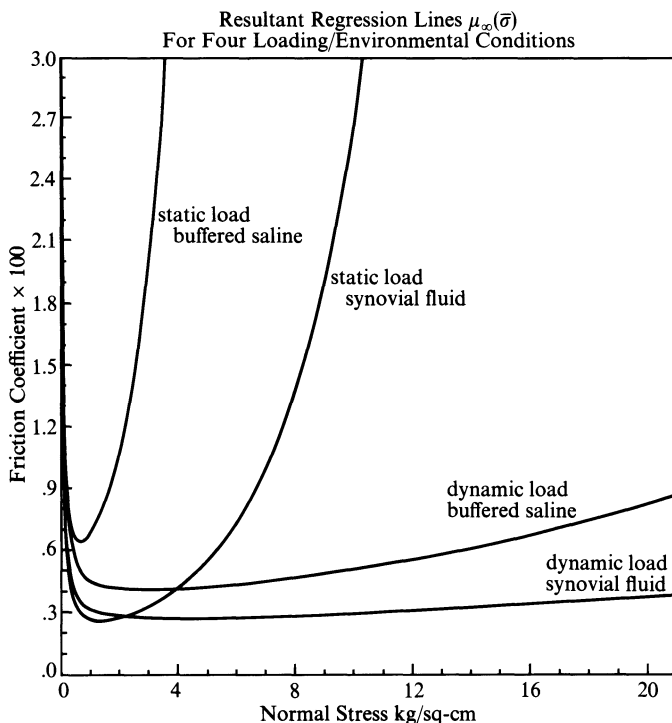


Figure 12.7:6 The mean values of the coefficient of friction between two articular cartilage surfaces as a function of the normal stress between the surfaces. The coefficient of friction depends on whether the measurements were made in a static or dynamic condition, and on the bathing fluid, whether it is buffered saline or synovial fluid. From Malcom (1976), by permission.

for oil lubricated metal, and 0.05–0.1 for teflon coated surfaces. The superiority of the synovial joint is truly striking.

A change of environmental factor can significantly change the coefficient of friction between articular cartilage surfaces. Especially noteworthy is the effect of hydrogen ion concentration in the bath. The cartilage's compressibility (for specimens with a porous boundary without impediment to fluid extrusion) suddenly increases when pH values become less than 5, and correspondingly the coefficient of friction between cartilage surfaces increases at pH less than 5. This finding is in conflict with the results of Linn and Radin (1968), which showed that deformation increased for pH ~ 5.5 and below, but the μ is maximum at pH 5.0. Malcom explained this difference in terms of a “ploughing” effect in Linn and Radin’s experiments and its absence in his.

Malcom’s experimental configuration permits a tribologically controlled study of articular cartilage lubrication, where long-term steady-state responses may be observed during static and dynamic loading conditions. While more rigorous control over the kinematic parameters is permitted by this approach,

the essential feature of articular cartilage sliding on articular cartilage is not sacrificed. The results are essentially in agreement with those of McCutchen (1959) and the synovial joint pendulum studies by Unsworth et al. (1975).

Why is articular joint so efficient in lubrication? There have been several theories which we now list:

Fluid Transport Effects. There is no doubt that cartilage supports load imposed on it by hydrostatic pressure of the fluid in the composite material, rather than by elastic recoil of the solid matrix material. Friction is low when the cartilage is filled with normal amount of fluid. Friction increases when fluid is squeezed out. McCutchen (1959) advocates that the synovial joint is so effective because the time required for the fluid to be squeezed out is so long, and the bone arrangement is such that the loading area between the bones in the joint shifts at such a rate that the cartilage remains effectively filled with synovial fluid. As soon as the load is removed the compressed cartilage rebounds quickly to absorb synovial fluid back into it. In this way, the entire cartilage remains effective as the animal moves.

Fluid Mechanical (Lubrication Layer) Effects. The synovial fluid is drawn between sliding surfaces by virtue of its viscosity, and the high pressure generated within it would support the load (MacConaill, 1932). By a reason which we have elaborated earlier in Chapter 5, Sec. 5.5, in connection with the lubrication layer theory for the red blood cells, the fluid layer in the synovial joint will have a lubrication effect. This effect is caused by the change in velocity profile in the lubrication layer. In addition, the rheological properties due to the high concentration of hyaluronic acid may also contribute to this mechanism by providing a high viscosity when the shear rate drops to zero and by shear thinning at higher shear rates (see Chapter 6, Sec. 6.7). Finally, the normal stress effects generated by the long chain polymer molecules will also help support the load (Ogston and Stanier, 1953).

Articular Cartilage Effects. There are two kinds. First, the cartilage deforms under loading so that it can redistribute the load as mechanical contact stresses and fluid pressure dictate (Dowson, 1967). Second, there could be a lubricating molecular species that interacts with the cartilage and acts as a boundary lubricant insulating and coating the surfaces (Radin et al., 1970).

Some of these theories overlap, or are, at times, contradictory. The final resolution awaits further research.

In diseased states, the lubrication quality of cartilage deteriorates. An experiment on sliding friction between a normal bovine cartilage annulus and a pathological human tibial plateau specimen showed that for both the osteoarthritic and the rheumatoid arthritic cases, there was a significant increase in the measured interfacial friction force. For the osteoarthritic case an average friction coefficient μ of 0.01–0.09 was measured across the normal force range for static and dynamic loading in a buffered saline environment.

Problems

- 12.9** An articular cartilage is a porous medium. In order to obtain some idea as to how it functions, consider the following idealized problem. Let a flat layer of a porous medium be of uniform thickness h_0 initially, and infinite in extent in the x, z plane, free on one surface ($y = h_0$), and attached to an infinite rigid base on the other surface ($y = 0$). Let this porous layer be loaded suddenly by a large rigid cylinder, parallel to z , of radius a ($a \gg h_0$), and with a total of force of W acting in the y direction. Under the load the porous layer will deform and fluid in the pores will move. Assume that the solid matrix material of the porous layer is linearly elastic and obeys Hooke's law. Assume that the fluid movement in the porous medium obeys Darcy's law:

$$\langle \mathbf{v}_f \rangle = -\frac{K}{\mu} (\nabla \langle p \rangle - \rho_f \mathbf{g})$$

where $\langle \mathbf{v}_f \rangle$ is the macroscopic velocity of the fluid, ρ_f is the density of the fluid, μ is the shear viscosity of the fluid, $\langle p \rangle$ is the macroscopic fluid pressure, \mathbf{g} is the gravitational acceleration, ∇ is the gradient operator, and K is a constant called the *permeability* of the porous medium. The cylinder and the base are assumed impermeable. The normal stress acting on the cylinder at the interface with the porous layer is equal to the sum of the stress in the matrix material and the fluid pressure. On the free surface of the layer there is nothing to prevent the fluid from moving in or out of the surface.

Write down the equations of conservation of mass and momentum. Assuming $a \gg h_0$, and derive an approximate equation that governs the thickness distribution h as a function of location x and time t . If the load W is applied as a step function, determine $h(x,t)$.

- 12.10** Generalize the investigation proposed in the preceding problem along the following lines. (a) The force imposed by the cylinder consists of a normal force W parallel to y and a shear force S parallel to x . (b) The matrix solid behaves like most biological solids with an elastic modulus proportional to the normal stress. See Sec. 7.5. (c) The cylinder is replaced by a sphere.

- 12.11** Discuss the applicability of Darcy's law to cartilage, and to other biological tissues. [Note: A special statistical formulation with application to soft tissues is given by Lew, H. S. and Fung, Y. C. (1970) *Int. J. Solids and Structures* **6**, 1323–1340.]

References

- Amtmann, E. (1968) *J. Biomech.* **1**, 271–277.
 Amtmann, E. (1971) *Ergebnisse der Anatomie und Entwicklungsgeschichte* **44**, 7–89.
 Amtmann, E. and Schmitt, H. P. (1968), *Z. Anat.* **127**, 25–41.
 Basset, C. A. L., and Pawlick, R. J. (1964) *Nature* **204**, 652–653.
 Becker, R. O., and Murray, D. G. (1970) *Clin. Orthopedics* **73**, 169–198.

- Bourne, G. H. (ed.) (1972) *The Biochemistry and Physiology of Bone*, 2nd edn. Vol. 1: *Structure*. Vol. 2: *Physiology and Pathology*. Vol. 3: *Development and Growth*. Academic, New York.
- Brannan, E. W., Rockwood, C. A., and Potts, P. (1963) *Aerospace Med.* **34**, 900–906.
- Brookes, M. (1971) *The Blood Supply of Bone. An Approach to Bone Biology*. Butterworths, London.
- Cowin, S. C., and Hegedus, D. M. (1976) *J. Elasticity* **6**, 313–325, 337–352.
- Cowin, S. C., and Nachlinger, R. R. (1978) *J. Elasticity* **8**, 285–295.
- Crowningshield, R. D. and Pope, M. H. (1974) *Ann. Biomed. Engineering* **2**, 217–225.
- Currey, J. D. (1964) *Biorheology* **2**, 1–10.
- Dietrick, J. E., Whedon, G., and Shorr, E. (1948) *Am. J. Med.* **4**, 3–36.
- Dowson, D. (1967) *Proc. Institution Mech. Eng. (London)* **181**, Part 3J, 45–54. Bound volume entitled *Lubrication and Wear in Living and Artificial Human Joints*.
- Evans, F. G. (1957) *Stress and Strain in Bones. Their Relation to Fractures and Osteogenesis*. C. C. Thomas, Springfield, Ill.
- Evans, F. G. (1969) *Artificial Limbs* **13**, 37–48.
- Evans, F. G. (1973) *Mechanical Properties of Bone*. Charles C Thomas, Springfield, Ill.
- Frost, H. M. (1964) *The Laws of Bone Structure*. Charles C Thomas, Springfield, Ill.
- Fukada, E. and Yasuda, I. (1957) *J. Physiol. Soc. Japan* **12**, 1158–1162.
- Fukada, E. (1968) *Biorheology* **5**, 199–208.
- Fung, Y. C. (1972) In *Biomechanics: Its Foundations and Objectives*, pp. 181–208. Prentice-Hall, Englewood Cliffs, N.J.
- Gjelsvik, A. (1973) *J. Biomech.* **6**, 69–77, 187–193.
- Glücksmann, A. (1938) *Anat. Record* **72**, 97–115.
- Glücksmann, A. (1939) *Anat. Record* **73**, 39–55.
- Glücksmann, A. (1942) The role of mechanical stress in bone formation in vitro. *J. of Anatomy* **76**, 231–239.
- Ham, A. W. (1969) *Histology*, 6th edn. Lippincott, Philadelphia.
- Hert, J. A., Liskova, M., and Landa J. (1971) *Folia Morphol.* **19**, 290–300, 301–317.
- Hert, J., Sklenska, A., and Liskova, M. (1971) *Folia Morphol.* **19**, 378–387.
- Justus, R. and Luft, J. H. (1970) *Calcified Tissue Res.* **5**, 222–235.
- Kazarian, L. E., and van Gierke, H. E. (1969) *Clin. Orthopedics* **65**, 67–75.
- Knese, K.-H. (1972) *Knochenstruktur als Verbundbau*. G. Thieme, Stuttgart.
- Kummer, B. K. F. (1972) In *Biomechanics: Its Foundations and Objectives*, Fung, Y. C., Perrone, N., and Anliker, M. (eds.). Prentice-Hall, Englewood Cliffs, N.J., pp. 237–271.
- Lanyon, L. B., and Baggott D. G. (1976) *J. Bone Joint Surg.* **58B**, 436–443.
- Linn, F. C. (1967) *J. Bone Joint Surg.* **49A**, 1079–1098.
- Linn, F. C., and Radin, E. L. (1968) *Arth. Rheum.* **11**(5), 674–682.
- MacConaill, M. A. (1932) *J. Anatomy* **66**, 210–227.
- Mack, P. B., LaChange, P. A., Vost, G. P., and Vogt, F. B. (1967) *Am. J. Roentgenol.* **100**, 503–511.
- Malcom, L. L. (1976) Frictional and deformational responses of articular cartilage

- interfaces to static and dynamic loading. Ph. D. thesis, Univ. of Calif., San Diego, La Jolla, Calif.
- Martin, B. (1972) The effects of geometric feedback in the development of osteoporosis. *J. Biomech.* **5**, 447–455.
- McCutchen, C. W. (1959) *Nature* **184**, 1284–1285.
- Mow, V. C., Lipschitz, H., and Glimcher, M. J. (1977) *Trans. Orthop. Res. Soc.* **2**, 75.
- Mow, V. C., Kuei, S. C., Lai, W. M., and Armstrong, C. G. (1980) *J. Biomech. Eng. Trans. ASME* **102**, 73–84.
- Ogston, A. G., and Stanier, J. E. (1953) *J. Physiol.* **119**, 244–252, and 253–258.
- Pauwels, F. (1948) *Z. Anat.* **114**, 129–166.
- Pauwels, F. (1950) *Z. Anat.* **115**, 327–351.
- Pauwels, F. (1965) *Gesammelte Abhandlungen zur funktionellen Anatomie des Bewegungsapparates*. Springer-Verlag, New York.
- Powell, M. J. D. (1965) *Computer J.* **7**, 303–307.
- Radin, E. L., Swann, D. A., and Weisser, P. A. (1970) *Nature*, **228**, 377.
- Reilly, D. T., and Burstein, A. H. (1974) *J. Bone Joint Surg.* **56A**, 1001–1022.
- Rhinelander, F. W. (1972) In *The Biochemistry and Physiology of Bone*, 2nd edn. Bourne, G. H. (ed.). Academic, New York, pp. 2–78.
- Roux, W. (1895) *Gasammelte Abhandlungen über Entwicklungsmechanik der Organismen*. I u. II. Engelmann, Leipzig.
- Schmitt, H. P. (1968) *Z. Anat.* **127**, 1–24.
- Torino, A. J., Davidson, C. L., Klopper, P. J., and Linclau, L. A. (1976) *J. Bone Joint Surg.* **58B**, 107–113.
- Torzilli, P. A., and Mow, V. C. (1972) *J. Biomech.* **9**, 541–522, 587–606.
- Unsworth, A., Dowson, D., and Wright, V. (1975) *J. Lub. Tech. Trans. ASME* **97**, 369–376.
- Woo, S. L. Y., Akeson, W. H., Coutts, R. D., Rutherford, L., Doty, D., Jemmott, G. F., and Amiel, D. (1976) *J. Bone Joint Surg.* **58A**, 190–195.
- Woo, S. L.-Y., Simon, B. R., Kuei, S. C., and Akeson, W. H. (1979) *J. Biomech. Eng., Trans. ASME* **102**, 85–90.
- Wolff, J. (1884) *Sitz. Ber. Preuss. Akad. d. Wiss. 22. Sitzg., physik. -math. Kl.*
- Wonder, C. C., Briney, S. R., Kral, M., and Skavstad, C. (1960) *Nature* **188**, 151–152.
- Yamada, H. (1970) *Strength of Biological Materials*. Williams and Wilkins, Baltimore.
- Young, J. Z. (1957) *The Life of Mammals*. Oxford University Press, London.

Author Index

- Abbot, B. C. 353, 381
Abderhalden, E. 100
Aberg, A. K. G. 381
Abramowitz, M. 237, 257
Adkins, J. E. 225, 253, 258
Aidley, D. J. 379, 381
Akeson, W. H. 415
Alexander, R. M. 257, 303, 304, 327
Almansi, E. 30, 246
Amiel, D. 415
Amtmann, E. 389, 394, 413
Andersson, G. 21
Anliker, M. 219, 270, 283, 294, 298, 414
Anthony, R. L. 259
Aristotle 2
Armeniades, C. D. 260
Armstrong, C. G. 415
Aroesty, J. 172
Arridge, R. G. C. 258, 260
Ashton, F. T. 358, 359, 381
Asmussen, E. 21
Axelsson, J. 381
Ayorinde, O. A. 277, 298
Azuma, T. 265, 266, 270, 273, 290, 291,
 298

Baer, E. 206, 207, 258, 259, 260
Baez, A. 298
Baez, S. 285, 286, 298

Baggott, D. G. 414
Balazs, E. A. 189, 190, 191, 192, 194
Barbee, J. H. 98, 146, 147, 148, 163, 172
Bassett, C. A. L. 396
Bauer, R. D. 241, 258, 270, 273, 299, 301
Bayliss, W. M. 360, 381
Becker, E. 234, 235, 258
Becker, R. O. 395, 413
Benis, A. M. 99, 172
Bennett, V. 131, 136
Bergel, D. H. 172, 237, 238, 258, 299,
 300, 325, 326, 327
Berne, R. M. 330, 333, 353
Bevan, J. A. 295, 299
Bevan, R. D. 299
Biggs, R. 91, 92, 98
Bingham, E. C. 77, 175
Biot, M. A. 240, 258
Blackshear, P. L. 98, 137
Blatz, P. J. 225, 258
Bodner, S. R. 234, 258
Bohr, D. F. 265, 299, 360, 379, 381
Boltzmann, L. 45
Bond, T. 103, 159
Borelli, G. A. 2, 4, 8
Born, M. 177
Bourne, G. H. 414, 415
Bouskela, E. 290, 299
Bowen, T. E., Jr. 350, 354
Boyle, R. 2, 4

- Bozler, E. 381
 Braasch, D. 172
 Brading, A. F. 381
 Brady, A. J. 348, 349, 350, 351, 354
 Brankov, G. 277, 299
 Brannan, E. W. 414
 Branton, D. 131, 136
 Braunwald, E. 354
 Brennen, C. 195
 Briney, S. R. 415
 Britten, A. 99
 Brokaw, C. J. 195
 Brookes, M. 397, 398, 399, 400, 414
 Brooks, D. E. 98
 Brutsaert, D. I. 354
 Bryant, C. A. 99, 137
 Buchtal, F. 226, 229, 258
 Bugliarello, G. 90, 98
 Bülbring, E. 360, 372, 381
 Burnstock, G. 356, 360, 381, 382
 Burstein, A. H. 384, 415
 Burton, A. C. 108, 134, 136, 138, 159,
 173, 265, 286, 299, 300
 Busse, R. 273, 301
 Butler, T. M. 382
- Canham, P. B. 108, 113, 136
 Caplan, S. R. 326, 327
 Carew, T. E. 299
 Carlson, F. D. 312, 327
 Caro, C. G. 168, 172, 299
 Casson, M. 63, 74, 98
 Cauchy, A. L. 25, 30, 246
 Chakrin, L. W. 178, 183, 194, 195
 Chang, P. C. 299
 Charm, S. E. 99
 Chen, H. Y. L. 221, 236, 258
 Chen, P. 109, 110, 111, 112, 137
 Chien, S. 63, 65, 82, 96, 99, 108, 130,
 137, 138, 159, 172
 Chu, B. M. 258
 Ciferri, A. 203, 258
 Clapeyron, B. P. E. 18
 Clarke, R. O. 173
 Clift, A. F. 187, 195
 Cokelet, G. R. 63, 64, 65, 67, 98, 99, 100,
 113, 137, 146, 147, 148, 163,
 172
 Collins, R. 241, 258
- Copley, A. L. 100, 137, 175, 298
 Coutts, R. D. 415
 Covell, J. W. 354
 Cowan, P. M. 212, 258
 Cowin, S. C. 394, 395, 414
 Cox, R. H. 299, 381
 Crew, H. 21
 Crowingshield, R. D. 384, 414
 Crystal, R. G. 295, 299
 Cunningham, E. 194
 Currey, J. D. 389, 414
- Dale, W. C. 206, 207, 258
 Daly, C. H. 259
 Davidson, C. L. 415
 Davies, R. E. 382
 Davis, S. 184, 185, 186, 194
 Davson, H. 360, 381
 Dawson, S. V. 259
 Delfs, E. 194
 Dellenback, R. J. 99, 137
 Demiray, H. J. 277, 299
 de Salvio, A. 21
 Descartes, R. 2, 4
 DeVries, A. 137
 Diamont, J. 206, 258
 Dietrick, J. E. 393, 414
 Dintenfass, L. 93, 94, 99, 113, 137
 Dobrin, P. B. 299, 381
 Döring, W. 234, 258
 Dorman, F. D. 98
 Doty, D. 415
 Dowson, D. 412, 414, 415
 Doyle, J. M. 299
 Duhamel, J. M. C. 37
 Dunn, F. 241, 258
- East, D. J. 16, 21
 Edman, K. A. P. 322, 343, 344, 345, 346,
 347, 348, 354
 Edmonds, P. D. 258
 Einstein, A. 181
 Ellis, D. 241, 260
 Engelmann, T. W. 360, 381
 Euler, L. 2, 4, 246
 Evans, E. 104, 105, 106, 107, 111, 112,
 125, 126, 127, 129, 130, 131, 133,
 135, 137, 138, 384

- Evans, F. G. 21, 260, 393, 414
Evans, J. W. 173
- Fahraeus, R. 80, 94, 146, 147, 162, 163,
 172
Fenn, W. P. 313, 316, 327
Feughelman, M. 203, 258
Fick, A. 3, 5
Fisher, G. M. 299
Fitz-Gerald, J. M. 169, 172
Flory, P. J. 212, 258
Flügge, W. 115, 118, 137
Föppl, O. 234, 235, 258
Ford, L. E. 325, 327
Forstrom, R. J. 98
Frank, O. 3, 5, 8, 10, 20, 270, 299
Frasher, W. G. 220, 259, 262, 263, 264,
 299, 300
Fremont, H. 137
Freundlich, H. 175
Frey-Wyssling, A. 194
Friedman, B. 260
Fronek, K. 61, 244, 258, 277, 300
Frost, H. M. 393, 414
Fry, D. L. 112, 137, 296, 299
Fry, W. J. 258
Fuchs, J. C. A. 301
Fukada, E. 395, 414
Fung, Y. C. 25, 47, 61, 99, 100, 102, 103,
 104, 105, 106, 107, 109, 110, 111,
 112, 113, 114, 124, 132, 137, 144,
 145, 150, 151, 152, 153, 154, 156,
 160, 161, 162, 163, 164, 165, 166,
 167, 172, 173, 202, 219, 220, 221,
 222, 224, 231, 234, 235, 236, 237,
 239, 242, 243, 244, 248, 249, 250,
 251, 252, 254, 256, 258, 259, 260,
 268, 270, 272, 273, 274, 275, 277,
 278, 279, 280, 286, 287, 288, 289,
 296, 299, 300, 301, 316, 327, 334,
 335, 337, 338, 339, 340, 347, 348,
 349, 350, 354, 361, 362, 363, 364,
 366, 368, 370, 373, 374, 375, 376,
 377, 378, 380, 381, 382, 414
- Gabe, I. T. 62, 99
Gabelnick, H. L. 194
Gaehtgens, P. 295, 300
- Galeski, A. 259
Galileo, G. 1, 2, 3, 4, 8, 21
Garrett, R. R. 212, 258
Garrick, E. 234, 259
Gathercole, L. J. 207, 258
Geiger, S. R. 353
Gibbs, D. A. 189, 190, 194
Gibson, T. 259
Gierke, H. E. von 394, 414
Gilbert, W. 7
Gilliland, E. R. 99, 100
Gjelsvik, A. 414
Glimcher, M. J. 415
Glover, F. A. 194
Glücksmann, A. 393, 414
Goldsmith, H. L. 81, 83, 84, 85, 86, 88,
 89, 90, 99, 100, 149, 150, 169,
 172, 173
Golenhofen, K. 360, 381
Goodwin, J. W. 98
Gordon, A. M. 314, 315, 327, 354
Gordon, A. R. 381
Gore, R. W. 284, 285, 300
Gou, P. E. 277, 300
Graustein, W. C. 137
Green, A. E. 225, 253, 258
Green, G. 30, 246
Greenfield, J. C. 301
Gregersen, M. I. 63, 99, 131, 137
Gross, J. F. 172
Guest, M. M. 159
Gumbel, E. J. 109, 110, 111, 137
Guth, E. 235, 259
Guyton, A. C. 360, 381
- Hales, S. 7, 9, 20
Ham, A. W. 387, 388, 414
Hamel, G. 30, 246
Hammerle, W. E. 99, 137
Handa, H. 300
Hardung, V. 237, 238, 259, 270, 300
Harkness, M. L. R. 212, 213, 214, 259,
 263, 300
Harkness, R. D. 212, 213, 214, 259, 263,
 300
Harkness, S. M. 259
Hartert, H. 92, 99
Harvey, E. N. 181, 194
Harvey, W. 2, 3, 4, 7, 8

- Hasegawa, M. 265, 266, 270, 290, 291, 298
 Hayashi, K. 273, 277, 300
 Haynes, R. H. 146, 172
 Hearle, J. W. S. 203, 259
 Hefner, L. L. 350, 354
 Hegedus, D. M. 394, 395, 414
 Heilbrunn, L. V. 182, 194
 Hert, J. A. 394, 395, 414
 Hill, A. V. 8, 10, 310, 311, 312, 313, 314, 316, 322, 323, 326, 327, 342, 343, 345, 346, 348, 350, 351, 360, 364, 381
 Hiltner, A. 259
 Histand, M. B. 298
 Hochmuth, R. M. 113, 125, 126, 127, 129, 130, 135, 137, 155, 172, 173
 Hoeber, T. W. 135, 137
 Holman, M. E. 382
 Hooke, R. 2, 4, 35
 Hoppin, F. G. 245, 259
 Houchin, D. W. 108, 137
 Hu, W. C. 241, 258
 Huddart, H. 379, 382
 Hunt, S. 379, 382
 Hunter, P. J. 325, 326, 327
 Huntsman, L. L. 354
 Huriyama, H. 382
 Huxley, A. F. 325, 326, 327, 354
 Huxley, H. E. 328
 Hyatt, R. E. 259
- Intaglietta, M. 286, 287, 300, 301
 Iwazumi, T. 328
- Jackson, S. F. 259
 Jaffrin, M. Y. 380, 382
 Jan, K. M. 137, 172
 Janicki, J. S. 259, 301
 Janssen, J. 3
 Janssen, Z. 3
 Jay, A. W. C. 158, 172
 Jemmott, G. F. 415
 Jennett, W. 172
 Jerrad, W. 286
 Jewell, B. R. 326, 328
 Johnson, E. A. 354
 Johnson, P. C. 159, 172, 285, 286, 300, 382
 Jones, A. W. 381
 Jorgensen, K. 21
 Julian, F. J. 325, 326, 327, 328, 354
 Justus, R. 394, 414
- Kaiser, E. 226, 229, 258
 Kastelic, J. 206, 259
 Kasyanov, V. 277, 300
 Katchalsky, A. 134, 137
 Kazarian, L. E. 394, 414
 Kedem, D. 137
 Keller, A. 258
 Kelvin, Lord (W. Thomson) 21, 45, 51
 Kenedi, R. M. 21, 226, 259
 Kenner, T. 270, 300, 301
 King, J. R. 110, 138
 King, R. G. 192, 193, 194
 Kirchhoff, G. 246
 Klibansky, C. 137
 Klopper, P. J. 415
 Knese, K. H. 389, 414
 Knets, I. 300
 Knopoff, L. 234, 259
 Kobayashi, A. S. 298
 Kohn, R. R. 258
 Komi, P. V. 21
 Korteweg, D. J. 3, 5
 Kot, P. 159, 172
 Kral, M. 415
 Kreuger, J. W. 328, 352
 Krogh, A. 8, 10
 Kuei, S. C. 193, 194, 415
 Kummer, B. K. F. 392, 393, 414
 Kurihara, S. 382
 Kuriyama, H. 360, 372, 381, 382
 Kurland, G. S. 99
 Kürum, K. 146
- Lachange, P. A. 414
 Lagrange, J. L. 246
 Lai, W. M. 193, 194, 415
 Lai-Fook, S. 240, 259
 Lamar, J. K. 188, 194
 Lamb, H. 3, 5
 Lamarck, C. de 7

- Lamé, G. 18, 35
Lampert, H. 298
Lanczos, C. 229, 259
Landa, J. 414
Landel, R. I. 225, 260
Langsjoen, P. H. 93, 94, 99
Lanir, Y. 242, 243, 244, 249, 250, 251, 259
Lanyon, L. B. 414
Laplace, M. 17, 19
Larcan, A. 99
Laszt, L. 270, 300
Lee, G. C. 259
Lee, J. S. 144, 150, 151, 152, 153, 154, 172, 173, 220, 259, 300
Levy, M. N. 330, 333, 353
Lew, H. S. 156, 173
Lighthill, M. J. 158, 168, 169, 173
Linclau, L. A. 415
Lindal, R. G. 138, 173
Lindholm, U. S. 258
Lindqvist, T. 99, 146, 163, 172
Lingard, P. S. 131, 138
Linn, F. C. 407, 411, 414
Lipschitz, H. 415
Liskova, M. 414
Litt, M. 178, 183, 194, 258
Llaurado, J. G. 299
Lowy, J. 381, 382
Luft, J. H. 396, 414
Lundberg, J. L. 99
Luse, S. A. 99, 137
Lutz, R. J. 177, 178, 182, 183, 184, 194
- MacConaill, M. A. 412, 414
Macfarlane, R. G. 91, 92, 98
Mack, P. B. 394, 414
Magaribuchi, T. 382
Malcolm, L. L. 408, 409, 410, 411, 414
Malpighi, M. 3, 4, 7, 8, 21
Marchesi, S. L. 138
Margetts, W. G. 100
Marlow, J. 84, 99
Marple, R. N. 113, 137, 172
Marquart, D. W. 279, 300
Marsh, B. S. 313, 316, 327
Martin, B. 415
Mashima, H. 360, 382
- Mason, S. G. 100, 149, 150, 173
Mason, W. P. 234, 259
Matsuda, T. 270, 298
Maxwell, J. C. 45, 51
McCutchon, C. W. 407, 412, 415
McDonald, D. A. 270, 300
McElhaney, J. H. 241, 259
Meiselman, H. J. 113, 137
Melnik, L. 137
Merati, J. K. 298
Merrill, E. W. 62, 63, 64, 65, 66, 99, 100
Merrillees, N. C. R. 382
Merz, J. T. 19, 21
Messmer, K. 93, 99, 100, 137, 172
Miller, D. I. 16, 21
Miller, L. H. 137
Mills, C. C. 98
Mohandas, N. 135, 137
Mommaerts, W. F. H. M. 312, 328, 353
Mooney, M. 225, 259
Moores, S. U. 382
Morgan, F. R. 226, 259
Mori, K. 300
Moritake, K. 273, 300
Mow, V. C. 193, 194, 405, 406, 415
Mulvany, M. J. 382
Munn, J. I. 108, 137
Murray, D. G. 395, 413
- Nachernson, A. 21
Nachlinger, R. R. 414
Needham, D. M. 382
Neubert, H. K. P. 233, 234, 235, 259
Neumann, F. 37
Newton, I. 23, 34
Nilsson, E. 322, 343, 344, 345, 346, 347, 348, 354
Noble, M. I. M. 326, 328, 350, 354
Nolan, A. C. 325, 328
Nomura, S. 259
Noordergraaf, A. 238, 260
Norris, C. H. 136, 138
North, A. C. T. 258
- Ogden, E. 298
Ogston, A. G. 174, 175, 189, 194, 415
Oka, S. 77, 78, 100

- Olmsted, M. 328
 Onogi, S. 298
 Ortengren, R. 14, 21
- Parmley, W. W. 321, 328, 343, 354
 Parnell, B. L. 108, 137
 Pascal, B. 23
 Pasch, T. 241, 258, 270, 299
 Patel, D. J. 240, 259, 277, 299, 300, 301
 Patitucci, P. 258, 277, 300, 341, 354, 361,
 362, 363, 364, 372, 373, 374, 375,
 376, 377, 378, 382
 Patterson, S. W. 333, 354
 Pauwels, F. 392, 394, 415
 Pawlick, R. J. 396, 413
 Payne, B. J. 195
 Peachey, L. D. 332, 354
 Pearson, K. 21
 Pedley, T. J. 172, 299
 Pegram, B. L. 299
 Perrone, N. 219, 299, 414
 Peters, R. H. 203, 259
 Phibbs, R. H. 90, 100
 Pinto, J. G. 220, 222, 259, 334, 335, 337,
 338, 339, 340, 341, 350, 354
 Piola, G. 246
 Piper, H. 354
 Plomb, E. P. 287, 300
 Podolsky, R. J. 325, 328
 Poiseuille, J. 2, 4, 34
 Polissar, M. J. 313, 328
 Pollack, G. H. 326, 328, 350, 352, 354
 Ponder, E. 108, 113, 132, 138
 Pope, M. H. 384, 414
 Potts, P. 414
 Powell, M. J. D. 415
 Price, J. M. 361, 362, 363, 364, 372, 373,
 374, 375, 376, 377, 378, 382
 Prosser, C. L. 360, 381
 Prothero, J. 159, 173
 Purdy, R. E. 299
- Rachev, A. 299
 Radin, E. L. 411, 412, 414, 415
 Rand, R. H. 134, 138
 Randall, J. T. 258
 Reilly, D. T. 384, 415
- Rhinelander, F. W. 397, 415
 Ridge, M. D. 226, 259
 Rivlin, R. S. 225, 259
 Roach, M. R. 265, 300
 Rockwood, C. A. 414
 Rodarte, J. R. 259
 Rosenquist, T. H. 173, 301
 Ross, J., Jr. 348, 349, 354
 Routbart, J. L. 234, 259
 Roux, W. 389, 392, 415
 Rowlands, S. 172
 Rundgren, A. 213, 214
 Rushmer, R. F. 297, 300
 Rutherford, L. 415
- Sack, H. S. 234, 259
 Saint Venant, B. de 30, 246
 Salzman, E. W. 99
 Santorio, S. 3, 4
 Sato, M. 300
 Saunders, D. W. 225, 259
 Scher, A. M. 353
 Schmid-Schoenbein, G. 61, 93, 113, 138,
 258, 296, 300
 Schmid-Schoenbein, H. 99, 100, 113, 118,
 137, 138, 172
 Schmidt-Nielsen, K. 113, 138
 Schmitt, H. P. 384, 389, 413, 415
 Schroter, R. C. 172, 299
 Schwan, H. P. 258
 Scott-Blair, G. W. 92, 100, 187, 194
 Seaman, G. V. F. 98
 Seed, W. A. 172, 299
 Segre, G. 149, 173
 Seifriz, W. 138
 Seraydarian, K. 328
 Seshadri, V. 173
 Sevilla, J. 90, 98
 Shah, J. S. 258
 Shapiro, A. H. 380, 382
 Sharma, M. G. 273, 300
 Shepherd, J. T. 295, 300
 Sherwood, T. K. 99
 Shettles, L. B. 194
 Shin, H. 99
 Shoenberg, C. F. 382
 Shorr, E. 414
 Siegman, M. J. 381, 382

- Siger, A. 312, 327
Silberberg, A. 149, 173
Simmons, R. M. 325, 326, 327, 328
Simon, B. R. 415
Singer, C. J. 2, 3, 4, 7, 21, 138
Skalak, R. 126, 128, 129, 133, 134, 135,
 137, 138, 159, 169, 172, 173
Skavgstad, C. 415
Skibo, L. 172
Sklenska, A. 414
Smoluchowski, M. von 181
Snyder, R. W. 277, 300
Sobin, P. 292, 293, 300
Sobin, S. S. 112, 138, 141, 142, 143, 173,
 197, 200, 288, 289, 299, 300, 301
Sollins, M. R. 325, 326, 328
Somlyo, A. P. 299, 358, 359, 381
Somlyo, A. V. 358, 359, 381
Sommer, J. R. 354
Sonnenblick, E. H. 321, 328, 343, 354
Spach, M. S. 353
Sparks, H. V., Jr. 299, 381
Sperelakis, N. 353
Stainsby, G. 298
Stanier, J. E. 174, 175, 189, 194, 415
Starling, E. H. 8, 10, 354, 360, 381
Steck, T. L. 131, 138
Steers, E. 138
Stegun, A. 237, 257
Stokes, G. G. 34, 73
Stoltz, J. F. 99
Stoychev, S. 299
Struik, D. J. 138
Su, C. 299
Sung, K. L. P. 137
Sutera, S. P. 113, 137, 150, 156, 157,
 158, 172, 173
Svanes, K. 162, 173
Swann, D. A. 415
- Tanaka, T. T. 268, 270, 272, 273, 274,
 275, 277, 301, 378, 382
Taylor, G. I. 113, 138, 188, 195
Taylor, M. 99
Theodorsen, T. 234, 259
Thoma, R. 89, 100
Thomson, W. (Lord Kelvin) 21, 45, 51
Thorson, J. 326, 328
- Thurston, G. B. 72, 100
Tillack, T. W. 138
Todhunter, I. 21
Tomita, T. 381
Tong, P. 132, 249, 250, 251, 258, 260
Torino, A. J. 394, 415
Torp, S. 260
Torzilli, P. A. 415
Tozeren, A. 137, 138
Treloar, L. R. G. 202, 260
Tremer, H. M. 138, 173, 301
Treviranus, G. R. 7
Tristram, G. R. 259
Tsang, W. C. O. 107, 108, 138
Tucker, W. K. 259
- Uekermann, U. 295, 300
Unsworth, A. 412, 415
Usami, S. 99, 137, 172
Uvelius, B. 382
- Vadas, E. B. 100
Vaishnav, R. N. 240, 259, 277, 299, 300,
 301
Valanis, K. C. 225, 260
Van Brocklin, J. D. 241, 260
van der Pol, B. 3, 5
Vanhoutte, P. M. 295, 300
Vawter, D. 244, 260
Verdugo, P. 354
Veronda, D. R. 225, 260
Viidik, A. 204, 205, 210, 211, 213, 214,
 226, 260
Vogt, F. B. 414
Voigt, W. 51
von Helmholtz, H. 2, 4, 5
Von Khreningen-Guggenberger, J. 188,
 195
Voss, G. O. 98
Vost, G. P. 414
- Wack, P. E. 259
Wagner, K. W. 234, 260
Wallner, A. 328
Wardell, J. R., Jr. 195
Warrell, D. A. 159, 173

- Warwick, R. 306, 307, 328
Waugh, R. 129, 131, 137, 138
Wayland, H. 159, 172, 258
Weber, E. H. 20
Weissenberg, K. 59
Weisser, P. A. 415
Wells, M. K. 298
Wells, R. E. 99, 113, 118, 138
Wertheim, M. G. 219, 226, 260
Werthessen, N. T. 379, 382
Wesley, R. L. R. 277, 294, 301
West, J. B. 173, 244, 260, 300
Westerhof, N. 238, 260
Westmann, R. A. 225, 260
Wetterer, E. 270, 273, 301
Whedon, G. 414
White, D. C. S. 326, 328
Whitmore, R. L. 100, 138
Wiederhielm, C. 290, 299
Williams, P. L. 306, 307, 328
Wilson, T. A. 240, 259, 260
Wolf, E. 177
Wolf, S. 379, 382
Wolff, H.S. 12, 21
Wolff, J. 393, 415
Wonder, C. C. 394, 415
Woo, S.-L.-Y. 394, 395, 401, 402, 403, 404, 415
Worthy, P. R. 137
Wright, V. 226, 259, 415
Wu, T. Y. 188, 195
Wylie, E. B. 270, 301

Yamada, H. 15, 16, 21, 384, 385, 415
Yasuda, I. 414
Yen, R. T. 100, 144, 145, 162, 163, 164, 165, 166, 167, 173
Yih, C. S. 193, 195
Yin, F. C. P. 366, 368, 370, 382
Yoshida, T. 360, 382
Young, J. 8, 21
Young, J. T. 301
Young, J. Z. 415
Young, T. 2, 4, 5, 6, 19

Zarda, P. R. 118, 123, 138
Zazt, L. 62, 99
Zener, C. 52
Zweifach, B. W. 113, 138, 162, 173, 286, 287, 296, 300, 301

Subject Index

- A-bands 305, 330
Abductin 201
ACH hormone 397
Actin 306, 307, 308
Active myocardium 342
Alignment of cells in flow 85
Alveolar sheet 141–146
Aorta, windkessel 20
Apparent viscosity of blood 82, 139, 157
 in the lung 145
 in a tube 146
Applicable deformation 119, 120, 121
Arteries (*see* Blood vessels)
Arterioles 284–286
Articular cartilage 386, 398
Articulation 386
- Back pain 14
Balloon, thin-walled 16
Bergel–Hunter approach 325
Biaxial loading 242–245
Biconcave shape, RBC 105
 effect of 105
 theory of 114
Bilayer 135
Bingham plastic 77, 97, 98
Biology, definition and history of 6, 7
- Biomechanics
 , applications of 10–12
 , definition of 1, 6
 , history of 1
 in health science 10
 , method in 12–13
 , scope of 10–12
Biorheology 175
Bioviscoelastic fluids 174 – 195
 , testing methods of 177 – 181
Bioviscoelastic solids 196–260
Blood
 , composition of 62
 , constituents of 62
 , constitutive equation of 70
 , yield stress of 64, 65
Blood clotting 91, 92
Blood flow
 boundary layer 79
 , entry condition of 79
 , laminar 72–80
 velocity profile 76, 86
 wall effect 89
 yielding stress effect 74–78, 79
Blood rheology
 , cell alignment in 85
 , cell deformation in 82, 83, 88
 , constitutive equation in 68 – 71

- Blood rheology [*cont.*] , flow rule in 70 , myocardial infarction in 94 , radial migration in 89, 90 , rouleaux in 80 , sedimentation in 94 , thixotropy in 71 , thrombosis in 93 , viscoelasticity in 71 , yield rule in 70, 71 , yield stress in 64
- Blood rouleaux 80, 81–84
- Blood vessels 261–301 , arteriole 284 , biaxial loading in 276 , capillary 286 , carotid artery 294 , collagen/elastin ratio of 262, 263 , creep in 274 , hysteresis in 274 , long term response of 295 , meaning of a_1 , a_2 , a_4 for 280, 281 , natural state of 261 , preconditioning of 262 , relaxation function of 271–174 , smooth muscle of 265, 295, 357, 358, 359 , strain energy functions for 277, 281, 282 , stress relaxation of 270–273 , stress-strain relation of 269, 276, 284, 286, 290, 291 , tangent modulus of 268 , uniaxial loading of 267 , vasa vasorum 262 viscoelasticity of 274–276 wall structure of 262–266 wave speed in 282, 283 , Young's modulus for 268, 269, 270
- Blood viscosity in capillaries 141–146, 150, 154 coefficients 69 , Fahraeus effect for 147, 148, 149 , Fahraeus-Lindqvist effect for 146, 149 , strain rate invariants for 69 , tubular pinch effect for 149
- Boltzman model 45, 46, 47
- Bolus flow 153
- Bone 383–400 anatomy 384, 386–389 collagen 387, 388 , as composite material 388, 389 , external remodeling of 393–395 , functional adaptation of 391–396 , growth of 389, 390, 391–396 , Haversian system of 387, 388 , hydroxyapatite in 387, 388 , internal remodeling of 393–395 , microcirculation in 397–400 , optimum design of 390 osteon 387, 388 , remodeling of 393–396 , resorption of 389, 390, 391–396 , structure of 386–389 , surface remodeling of 393, 395 , table of strength (deformation and moduli) for 385 , wet vs dry 384
- Boundary condition of blood flow 72, 80, 89
- Boundary layer of blood 79 of yielding 79
- Calcitonin 397
- Capillaries 286–290 , lung 287–288
- Capillary blood flow pressure distribution 153 , sheet flow of 141–146 , tube flow of 150–156
- Cartilage 400–413 , articular 401–412 , bronchial 401 , classification of 400 , coefficient of friction of 411 compression test 405–406 , cyclic loading of 405 , fluid movement in 405, 406, 410 , indentation test for 401 , low friction of 386, 406–412 lubrication 406–412 , preconditioning of 402 relaxation 403, 404 relaxation spectrum 404

- split line 400
stress-strain relation 405
, tension test for 401–405
, types of 400
, variable shear 409
, viscoelasticity of 401–406
- Casson's equation 65
Casson's plot, blood viscosity 64, 65, 67
Cauchy's formula 25
Cell deformation in flow 88
Cell membrane
, area dilatation of 125
, area modulus of 125, 126, 133
, bending of 123
, bending rigidity of 118
, constitutive equation for 133
cytoskeleton 136
elasticity 132–135
experiments 122, 123
, fluid mosaic model of 136
, model of 135
shear experiment 126
shear modulus 129, 134
spectrin 136
suction 127
tethering experiment 127
viscoelasticity of 129
viscoplasticity of 130
- Cell-tube interaction 150, 153, 154
Cervical mucus 187
Cerrolow 125
Circulation in bone 397–400
Coagulation of blood 91
Coefficient of thermal expansion 38
Coefficient of viscosity 34
Collagen 203–208
, critical temperature of 212
, fascicle 206
fibers 205, 206
fibrils 205
in blood vessels 262, 263
in bone 387, 388
in cervix 209
in ligaments 209
in pregnancy 212–214
in skin 209
in stress-strain relationship 210–211
in tendon 208
- molecules 204
, of tropocollagen type 204, 255
, post-partum 213, 214
structure in tissues 208, 209
- Collagen/elastin ratio 262, 263
Complementary energy 253–256
Complex modulus of elasticity 49,
179
of the Kelvin body 49, 50
of the Maxwell body 49
- Complex representation 48
Cone-plate viscometer, 59
Constitutive equation 13, 22, 32,
68–71
Continuum 22
Couette viscometer 58
Creep 41
in blood vessels 274
in heart muscle 340
Creep function 43, 46, 47, 227
, reduced 227
, tensorial 47
Cross-bridges in muscle 308
Cylinder shell
inflated 16
thick-walled 18
- Cytoskeleton 136
- δ_{ij} , Kronecker delta 29
 $\delta(t)$, unit impulse function 43
Damping, arteries 283
Deformability of red cells 112
Deformation 27
, applicable 119
, isochoric 119
Deformation gradient 31, 247
Dense bodies 358, 359
Depolarization waves 353
Diaphysis 386, 397, 398
Dilatancy 175, 176
Dimensional analysis 143
Dimension analyzer 60
Dirac delta function 43, 44
Discharge hematocrit 166
Displacement vector 28
Duhamel-Newman equation 37
Dynamic similarity 144

- Eagle-albumin solution 102
 EGTA 371
 Elastin 197–201
 Elasticity 35
 , anisotropic 35
 , measurements of 60, 61
 , table of constants for 37
 Endocrine 396, 397
 Endothelium
 , critical shear stress of 112
 , damage 296
 , leucocytes' action on 296
 Entry flow 79, 149, 162
 Epinephrine 371
 Epiphysis 386, 398
 Equations of equilibrium 26
 Equation of state 33
 Exponential integral 237, 257
 Extreme-value
 , statistical distribution 109
 , statistics 108
- Fading memory theory 324
 Fascicle 206, 207
 Fasciculi of muscle 305
 Fenn and Marsh equation 313, 316
 Fahraeus effect 147, 148, 163
 Fahraeus-Lindqvist effect 146
 , inversion of 156
 Fibers 203
 , crystallization of 203
 Fibrin 91
 Fibrinogen 62, 91
 First Course (Fung's) 25, 30, 39, 40, 69, 98
 Flow rate in tube 74
 , Casson fluid 77, 78
 , Newtonian fluid 74
 Flow separation 170
 Fluid
 , ideal 33
 , incompressible 33
 , Newtonian 33
 , non-Newtonian 38
 , nonviscous 32
 , Stokes 34
 , viscous 33
- Foot, analysis of the 15–16
 Fung's modified Hill's equation 347, 348
- Gas, ideal 33
 Gaussian curvature 120
 Generalized model of viscoelasticity
 51–56
 , Kelvin 51, 53–55
 , Maxwell 55
 , Voigt 51, 55
 , Zener's relaxation spectrum 52
- Ghost cells 84
 Green's strain 39
 Ground substance 208
 Growth plate 386, 398
 Growth, stress response, arteries 295
 Gumbel probability paper 110, 111
 Gumbel slope 109
- H-band 305, 307, 330
 Hair 203
 Harmonic oscillation 47
 , complex representation of 48
 , phase of 48
 Haversian system 387, 388
 Heart muscle
 , active 342
 , contractile element of 344–350
 , creep in 340
 , damage in testing of 352
 , depolarization waves in 353
 , elastic response of 336–339
 , Hill's equation for 346, 347, 348, 349
 , modified Hill's equation for 347, 348, 349
 , non-tetanization of 302
 , oscillations of 340
 , relaxation of 334–336
 , resting tension correction in 350
 , series element for 343, 344
 , stress-strain relation for 338, 339
 , structure of 330, 332
 , syncytium in 329
 , tubules in 331, 332
 , unstimulated, 333–342
 whole heart experiments for 351

- Hematocrit 63, 148
at branching point 161
, dynamic 160, 161
in tubes 165–167
in narrow tubes 159, 162
, optimal 95
- Hemorheology 175
- Hemostasis 92
- Herschel-Bulkley material 98
- Hill's equation 310
compared with that of Fenn and Marsh 313, 316
, derivation of 312
, illustration of 311
, modified 347, 348, 349
, nondimensional forms of 313, 314, 316
- Hill's three-element model 316–324, 343
, contractile element in 317, 344
, critique of 323, 350
, difficulties in 350, 351
, formulas for 318–319
, isometric-isotonic change over in 320
, parallel element in 317, 323, 342, 350, 351
, quick release in 319
, series element in 317, 321, 343, 344
, tension redevelopment in 322, 323
, velocity of contraction in 322
- Hookean solid 35
- Hooke's law 27, 35
- Hyaluronic acid 189
- Hydroxyapatite 387, 388
- Hyperelastic material 247
- Hysteresis 41
in blood vessels 274
- I-bands 305, 330
- Incompressible fluid 33, 34
- Incompressible material 248
- Incremental elasticity 238, 239, 240
- Interalveolar septa 141, 142
- Intercalated discs 329
- Internal friction 50, 51
- Invariants 39, 69
- Inversion
of the Fahraeus-Lindqvist effect 156
of the stress-strain relation 253–256
- Inward migration, red cell 90
- Isotropic tensor 34, 40
- Isotropy 34, 35
- Isochoric deformation 119
- Isotonic solution 102
- Kelvin model 41, 42, 45, 53, 54
- Kinematic similarity 144
- Kronecker delta 29
- Lamé constants 35
- Laplace, law of 17
- Leak-back 168
- Length-tension relation, muscle 315
- Lighthill theory 168, 169
- Ligaments 209
- Ligamentum nuchae 198
- Log decrement for arteries 283
- Loss modulus 179
- Lubrication layer theory 158, 159, 168–170
- Lubrication of joints 406–412
, coefficient of friction for 411
, compression of tissue in 410
, Malcolm's experiments on 408, 412
, osteoarthritic 412
, shear stress history of 409
- Lung 8, 141–146
- M-band 307, 330
- Material
, Hookean 27
, incompressible 248
, Kelvin 41, 44, 45, 54
, Maxwell 41, 44, 45, 55
, standard linear 41, 44, 45
, Voigt 41, 44, 45, 55
- Maxwell model 41, 42, 44, 45, 55
, generalized 55
- Medullary cavity 386, 387
- Meromyosin 308
- Metaphysis 386, 398
- Microcirculation
, discovery of 8
in bone, 397–400

- Microcirculation [cont.]**
 , pulmonary 8, 9
- Microrheology** 139
- Minute rhythm** 360
- Mitochondria** 329, 331
- Model design** 80
- Model of viscoelasticity**
 , Kelvin 41, 42, 54
 , Maxwell 41, 42, 55
 , standard linear 41, 42
 , Voigt 41, 42, 55
- Modified Hill's equation** 347, 348
- Moens-Korteweg equation** 282, 283
- Mohr's circle** 127
- Modulus, elasticity** 36
 , complex 49
 , Lamé 35
 rigidity 28
 , shear 28, 35, 36
 , table of 37
 , Young's 27, 36
- Motor unit, muscle** 310
- Mucus** 182–186
 , cervical 187
- Multi-unit smooth muscle** 357
- Muscle**
 , heart 329
 , skeletal 302
 , smooth 355
 spindles 310
 tone 310
- Myocardium (see Heart muscle)**
- Myofibrils, muscle** 305
- Myosin** 306, 307, 308
- Neurons, muscle** 309
- Newtonian fluid** 33
- Newton's rings** 175, 176
- Non-Newtonian fluid** 38
- No-slip condition** 40, 72
- Oka's Casson fluid flow** 77, 78
- Optimum design** 390, 392
 of bone 391, 392
 principle 391
 of Roux 391
- Osmotic swelling, RBC** 123
- Osteoarthritic joint** 191
 cartilage 412
 synovial fluid 191
- Osteon** 387, 388
- Oswald viscometer** 56
- Palpation** 19, 20
- Parameter identification** 279
- Particulate flow** 86
- Periosteum** 386, 387, 399
- Peripheral resistance** 20
- Phase angle** 48
- Phosphocreatine** 312
- Physiology, definition of** 7
- Pinnate muscle** 304
- Plasma expander** 94
- Plasma-rich layer at wall** 90, 155
- Plasma skimming** 149, 155, 162
- Platelets** 62
- Plug flow** 87
- Poise** 23, 24
- Poisson's ratio** 36
- Polissar equation** 313
- Polycarbonate sieves** 131
- Preconditioning** 211, 219, 220, 240
- Pressure in incompressible material** 248
- Pressure distribution** 33, 153
- Principal axes** 39, 40
- Prothrombin** 91
- Protoplasm** 181
- Pseudo-elasticity** 238–242, 248
 , definition of 240
 in arteries 277
 , strain rate effect on 241
- Pseudo strain energy** 248, 252
- Pulmonary blood flow** 141–146
- Pulmonary capillaries** 287–289
- Quasi-linear viscoelasticity** 226–228
- Red blood cells**
 , deformability of 101, 102, 112
 , deformation in flow of 88
 , deformation in tube flow of 155
 , dimensions of 104–112
 , geometry of 101, 102, 104

- in capillaries 103, 151, 152, 153
- in interference microscopy 105
- in isotonic solution 101
 - , internal viscosity of 113
 - , largest 110–112
 - , life span of 101
 - , 120 day life of 101
 - , model of 125
 - , osmotic swelling of 123
 - , shape of 104–112
- in sieves 131
 - , sphering of 105
 - , stress distribution for 114–117
 - , surface area of 10, 107
 - , tank treading of 121
 - , thickness equation for 104
 - , volume of 106, 107
- Red cell membrane** (*see Cell membrane*)
- Relative viscosity 139, 157
 - in lung 145
 - in tube 146
- Relaxation 41
 - , blood vessel 270–273
 - , cartilage 403, 404, 406, 410
 - , heart muscle 334, 335
 - in metals 52, 53
 - , mesentery 236, 237
 - , smooth muscle 369–370, 372–376
 - spectrum of arteries 275
- Relaxation function 44, 46, 226
 - , reduced 226, 228
 - , tensorial 47
- Relaxation spectrum 46, 232–234, 404
- Relaxation time 43, 45
- Resilin 201
- Return period 110
- Rheogoniometer 59
- Rheology 62, 175
- Rheometer 59
- Rheopexy 175, 176
- Rouleaux
 - formation 80, 81–84
 - deformation 84
- Saliva 186
- Sarcomeres 307
- Sarcosomes 329
- Sedimentation, red cell 94
- Semen 187
- Serum 62
- Shear 27
 - , simple 126
 - , pure 126, 128
- Shear rate 63
- Shear thickening 176
- Shear thinning 176
- Sheet flow in lung 141–146
- Shell, cylindrical 16, 19
- Shell, spherical 16, 19
- Shoveling, snow 14
- Sickle cells 83
- Silk 203
- Similarity laws 80, 144
- Simple fluid 180
- SI units 23
- Skeletal muscle** 302–328
 - , Bergel-Hunter approach to 325
 - , contractile element of 317
 - , crab chela 303
 - , Fenn and Marsh equation for 313, 316
 - , fading memory theory for 324
 - , functional arrangements of 303
 - , Hill's equation for 310
 - , length-tension relation for 315
 - , maximum velocity of contraction for 315
 - , new theory for 324
 - , parallel element in 317, 323
 - , pinnate 304
 - , Polissar equation for 313
 - , series element in 317, 321
 - , single twitch of 308
 - , structure of 305–307
 - , tetanization of 302, 309
 - , velocity of contraction of 311, 312, 313, 315, 322
 - , wave summation in 308
- Skin 248
 - , constitutive equation of 249, 252
- Sliding element theory 308
- Smooth muscles** 355–382
 - , actin in 358, 359
 - , bundles of 356
 - , cell dimensions of 356
 - , dense bodies of 358, 359
 - , electron micrographs of 358, 359
 - , extracellular space between 357

- Smooth muscles [cont.]**
 , minute rhythm of 360, 361–365
 , multi-unit 357
 , myosin filaments in 358, 359
 , rhythmic contraction of 360
 , spontaneous contraction of 360, 361
 , structure of 356, 358, 589
 , taenia coli 361–365, 371–379
 , types of 355
 , ureter 365–371, 379–380
 , visceral 357
- Solids**
 , Hookean 35, 38
 , non-Hookean 38
- Sound speed** 37
- Spectrin** 136
- Spectrum, relaxation** 46
- Spermatozoa** 188
- Spherical shell** 16
 , thick-walled 19
- Sphericity index, RBC** 108, 111
- Spindles, muscle** 310
- Split line, cartilage** 400
- Spontaneous contraction** 360, 361, 365.
 372–374
- Statistics, extreme value** 108
- STH hormone** 396, 397
- Stokes fluid** 34
- Stokes formula** 73, 179, 193
- Storage modulus** 179
- Strain** 26
 , Almansi 246
 , Cauchy 30
 , Eulerian 30
 , Green's 30, 39, 246
 , Hamel 30, 246
 , infinitesimal 30
 invariants 39, 69
 , Lagrangian 30
 , shear 27
 , St. Venant 30, 246
 symmetry 30
 tensor 30
- Strain energy function** 218, 247
 , pseudo 248
- Strain rate, tensor** 31, 32
- Streamline pattern** 152
- Stress** 22, 23, 25, 34
 , Cauchy 246, 248
 , Euler 246, 248
 , Kirchhoff 246, 247, 248
 , Lagrangian 246, 248
 , Piola 246, 248
- Stress analysis, RBC** 114–118
- Stress in a cylindrical shell** 17, 18
- Stress in a spherical shell** 17, 19
- Stress invariants** 39
- Stress rate** 47
- Stress relaxation (see Relaxation)**
- Stress-strain relation**
 for arteries 277
 for blood vessels 277
 for bone 383
 for cartilage 405
 for taenia coli 377
 for ureter 369
 for veins 292
 , interpretation of the 281
 , inversion of the 253 – 256
 , uniaxial 292
- Stretch ratio** 26, 39
- Summation convention** 26
- Surfaces, applicable** 120
- Syncytium** 329
- Synovial fluid** 175, 188–193
 , osteoarthritic 190, 191
- Synovial joint** 407–412
- Taenia coli** 361–365, 371–379
 , active tension in 364, 372–374
 , active/resting tension in 378
 , cyclic loading of 376
 , EGTA effect in 374
 , epinephrine effect in 374
 , frequency effect in 375
 , L_{\max} (definition) for 364
 , minute rhythm of 360–365, 372–374
 , relaxation of 372
 , relaxation function for 375
 , relaxation spectrum for 375, 376
 , resting 371, 378
 , spectrum of relaxation for 375, 376
 , spontaneous contraction of 360–365,
 372–374
 , step length change in 363, 372 – 374
 , step tension change in 363, 372–374
 , strain-rate effect in 375

- , stress-strain relation for 377
- , wave form of 361
- Temperature effect on elasticity 37
- Tendon 15, 16, 206, 208, 209
- Tensor 26, 34, 39, 40
- Tetanization 309
- Thermodynamics of deformation 214, 218
- Thermoelasticity 37, 214–218
- Thixotropy 71, 72, 175, 176
- Thrombosis 91
- Tone, muscle 310
- Traction 24
- Tube flow 72–80
 - , Newtonian 74
 - , non-Newtonian 74–80
- Tube hematocrit 167
- Tube, inflated 16, 19
- Tubular pinch effect 149
- Tubules 331, 332

- Unit-impulse function** 43, 45
- Unit-step function** 43
- Ureter 365–371, 379–380
 - , active tension of 366
 - , creep in 370, 371
 - , cyclic stretching of 367–369
 - , relaxation of 369, 370
 - , resting tension of 366
 - , stress-strain relation for 369

- VDA 60, 243, 244
- Veins 290–295
- Velocity profile 86
- Video dimension analyzer 60, 61, 243
- Visceral smooth muscle 357
- Viscoelasticity 41–56, 253
 - , applications of 50–53
 - , Boltzman theory of 45–47
 - models 41, 54–56
 - of blood 72
 - of blood vessels 274–276
 - of cervical mucus 187
 - of mucus 182–186
 - of saliva 186

- of semen 187
- , testing of 56–60
- Viscometers**
 - , capillary 57
 - , Couette 58
 - , cone-plate 59
 - , falling sphere 60
 - , oscillating rod 60
 - , Ostwald 56
 - , tuning fork 60
- Viscosity**
 - , apparent 139, 140
 - , coefficient of 34
 - , Newtonian 66
 - , non-Newtonian 63, 64, 66
 - of air 35
 - of blood 63, 64
 - of hemoglobin 113
 - of protoplasm 181
 - of water 35
 - , relative 139, 140
 - , temperature effect on 64
- Viscous fluid** (*see* Viscosity) 33
- Vitamin effect** 397
- Voigt model** 41, 42, 45, 55
- Volume change and I_1, I_2, I_3** 40
- Vorticity tensor** 32

- Wall effect** 89
- Waves**
 - , decay rate of 283
 - in arteries 282, 283
- Wave summation** 308, 309
- Weissenberg effect** 59
- Windkessel theory** 20, 21
- Wolff's law** 393

- Yield stress** 27
 - of blood 63–66

- Z-bands** 305, 330
- Zener's relaxation spectrum of metal** 52, 53